# Assessment of Factors Influencing Effective $CO_2$ Storage Capacity and Injectivity in Eastern Gas Shales

## Final Technical Report

Prepared for:
U.S. Department of Energy
National Energy Technology Laboratory
DOE Award Number: DE-FE0004633
Period of Performance: 10/01/2010 to 06/30/2013

Prepared by:
Michael Godec, Principal Investigator
Advanced Resources International, Inc.
4501 Fairfax Drive ▪ Suite 910 ▪ Arlington, Virginia 22203

Date:
October 23, 2013


4501 Fairfax Drive ▪ Suite 910 ▪ Arlington, Virginia 22203 ▪ Phone: (703) 528-8420 ▪ web: www.adv-res.com

## Disclaimer

This report was prepared as an account of work sponsored by an agency of the United States Government. Neither the United States Government nor any agency thereof, nor any of their employees, makes any warranty, express or implied, or assumes any legal liability or responsibility for the accuracy, completeness, or usefulness of any information, apparatus, product, or process disclosed, or represents that its use would not infringe privately owned rights. Reference herein to any specific commercial product, process, or service by trade name, trademark, manufacturer, or otherwise does not necessarily constitute or imply its endorsement, recommendation, or favoring by the United States Government or any agency thereof. The views and opinions of authors expressed herein do not necessarily state or reflect those of the United States Government or any agency thereof.

## Advanced Resources International, Inc.

The material in this Report is intended for general information only. Any use of this material in relation to any specific application should be based on independent examination and verification of its unrestricted applicability for such use and on a determination of suitability for the application by professionally qualified personnel. No license under any Advanced Resources International, Inc., patents or other proprietary interest is implied by the publication of this Report. Those making use of or relying upon the material assume all risks and liability arising from such use or reliance.

# ABSTRACT

Building upon advances in technology, production of natural gas from organic-rich shales is rapidly developing as a major hydrocarbon supply option in North America and around the world. The same technology advances that have facilitated this revolution – dense well spacing, horizontal drilling, and hydraulic fracturing – may help to facilitate enhanced gas recovery (EGR) and carbon dioxide ($CO_2$) storage in these formations. The potential storage of $CO_2$ in shales is attracting increasing interest, especially in Appalachian Basin states that have extensive shale deposits, but limited $CO_2$ storage capacity in conventional reservoirs.

The goal of this cooperative research project was to build upon previous and on-going work to assess key factors that could influence effective EGR, $CO_2$ storage capacity, and injectivity in selected Eastern gas shales, including the Devonian Marcellus Shale, the Devonian Ohio Shale, the Ordovician Utica and Point Pleasant shale and equivalent formations, and the late Devonian-age Antrim Shale.

The project had the following objectives: (1) Analyze and synthesize geologic information and reservoir data through collaboration with selected State geological surveys, universities, and oil and gas operators; (2) Improve reservoir models to perform reservoir simulations to better understand the shale characteristics that impact EGR, storage capacity and $CO_2$ injectivity in the targeted shales; (3) Analyze results of a targeted, highly monitored, small-scale $CO_2$ injection test and incorporate into ongoing characterization and simulation work; (4) Test and model a smart particle early warning concept that can potentially be used to inject water with uniquely labeled particles before the start of $CO_2$ injection; (5) Identify and evaluate potential constraints to economic $CO_2$ storage in gas shales, and propose development approaches that overcome these constraints; and (6) Complete new basin-level characterizations for the $CO_2$ storage capacity and injectivity potential of the targeted eastern shales.

In total, these Eastern gas shales cover an area of over 116 million acres, may contain an estimated 6,000 trillion cubic feet (Tcf) of gas in place, and have a maximum theoretical storage capacity of over 600 million metric tons. Not all of this gas in-place will be recoverable, and economics will further limit how much will be economic to produce using EGR techniques with $CO_2$ injection. Reservoir models were developed and simulations were conducted to characterize the potential for both $CO_2$ storage and EGR for the target gas shale formations. Based on that, engineering costing and cash flow analyses were used to estimate economic potential based on future natural gas prices and possible financial incentives.

The objective was to assume that EGR and $CO_2$ storage activities would commence consistent with the historical development practices. Alternative $CO_2$ injection/EGR scenarios were considered and compared to well production without $CO_2$ injection. These simulations were conducted for specific, defined model areas in each shale gas play. The resulting outputs were estimated recovery per typical well (per 80 acres), and the estimated $CO_2$ that would be injected and remain in the reservoir (i.e., not produced), and thus ultimately assumed to be stored.

The application of this approach aggregated to the entire area of the four shale gas plays concluded that they contain nearly 1,300 Tcf of both primary production and EGR potential, of which an estimated 460 Tcf could be economic to produce with reasonable gas prices and/or modest incentives. This could facilitate the storage of nearly 50 Gt of $CO_2$ in the Marcellus, Utica, Antrim, and Devonian Ohio shales.

# Table of Contents


| | |
|---|---|
| Volume 1 | Summary Report |
| Volume 2 | Basin-Level Characterization Of Enhanced Gas Recovery And $CO_2$ Storage Potential In The Marcellus Shale |
| Volume 3 | Basin-Level Characterization Of Enhanced Gas Recovery And $CO_2$ Storage Potential In The Utica Shale |
| Volume 4 | Basin-Level Characterization Of Enhanced Gas Recovery And $CO_2$ Storage Potential In The Antrim Shale |
| Volume 5 | Basin-Level Characterization Of Enhanced Gas Recovery And $CO_2$ Storage Potential In The Devonian Ohio Shale |
| Volume 6 | Analyses of the Targeted, Highly Monitored, Small-Scale $CO_2$ Injection Test In Kentucky |
| Volume 7 | Testing Innovative Technology for Monitoring $CO_2$ Flow Behavior |
| Volume 8 | Assessment of Technical and Economic Potential of Recovering Methane and Storing $CO_2$ in Eastern Gas Shales |

# Volume 1
# Summary Report

# Assessment of Factors Influencing Effective $CO_2$ Storage Capacity and Injectivity in Eastern Gas Shales

Prepared for:
U.S. Department of Energy
National Energy Technology Laboratory
DOE Award Number: DE-FE0004633

Prepared by:
Michael Godec, Principal Investigator
Advanced Resources International, Inc.
4501 Fairfax Drive ▪ Suite 910 ▪ Arlington, Virginia 22203

Date:
October 23, 2013

Advanced Resources International, Inc.

4501 Fairfax Drive ▪ Suite 910 ▪ Arlington, Virginia 22203 ▪ Phone: (703) 528-8420 ▪ web: www.adv-res.com

## Advanced Resources International, Inc.

# EXECUTIVE SUMMARY

Building upon advances in horizontal drilling and hydraulic fracturing technologies, production of natural gas from organic-rich gas shales is rapidly developing as a major hydrocarbon energy supply option in North America and around the world. Although known for decades, what "changed the game" was the recognition that one could "create a permeable reservoir" by using intensively stimulated horizontal wells. The same advances that have facilitated this revolution in production from gas shales and tight oil – dense well spacing, horizontal drilling, and hydraulic fracturing – may help to facilitate enhanced gas recovery (EGR) and carbon dioxide ($CO_2$) storage in these formations.

The potential storage of $CO_2$ in organic-rich gas shales is attracting increasing interest, especially in Appalachian Basin states that have extensive shale deposits, but limited $CO_2$ storage capacity in conventional porous reservoirs. It has been demonstrated in coal seams that $CO_2$ is preferentially adsorbed compared to methane. Gas shale reservoirs are expected to react similarly, and desorb methane while preferentially adsorbing $CO_2$. In addition, some component of the pore volume that contains "free" gas is expected to be available for $CO_2$ storage as non-adsorbed $CO_2$, especially where previous hydraulic fracturing has enhanced injectivity. Although still in the conceptual stage, $CO_2$ injection into organic-rich gas shales could provide dual benefits: an economic benefit from the incremental recovery of adsorbed methane, and an environmental benefit of secure $CO_2$ storage.

The goal of this cooperative research project was to build upon previous and on-going work to assess key factors that would influence effective $CO_2$ storage capacity and injectivity in selected Eastern gas shales. The most prolific and promising gas shale formations for $CO_2$ storage were selected as the focus for this project, including the Devonian Marcellus Shale in New York, Pennsylvania, West Virginia and eastern Ohio; the Devonian Ohio Shale in Kentucky; the Ordovician Utica and Point Pleasant shale and equivalent formations in New York, Pennsylvania, West Virginia and Ohio; and the late Devonian-age Antrim Shale in the Michigan Basin.

Specifically, the project had the following objectives:

- Analyze and synthesize geologic information and reservoir property data, through collaboration with selected State geological surveys, universities, and oil and gas operators.
- Improve reservoir models to perform detailed reservoir simulations to better understand the shale characteristics that impact storage capacity and $CO_2$ injectivity in these targeted Eastern shales.

- Analyze results of a targeted, highly monitored, small-scale $CO_2$ injection test in Kentucky and incorporate into ongoing characterization and simulation work.
- Test and model a smart particle early warning concept that can potentially be used to inject water with uniquely labeled particles before the start of $CO_2$ injection.
- Identify and evaluate potential constraints to economic $CO_2$ storage in gas shales, and propose development approaches that overcome these constraints.
- Complete new basin-level characterizations for the $CO_2$ storage capacity and injectivity potential of the targeted eastern shales considered.

Research on the potential for recovering methane and storing $CO_2$ in gas shales is significantly less advanced than that for coal seams. Ongoing reservoir characterization and reservoir simulation work is demonstrating that the basic concept that shales can store $CO_2$ based on trapping through adsorption on organic material (similar to coals), as well as with the natural fractures within the shales, is scientifically achievable. Still lacking, however, is sufficient testing of this concept with site-specific geologic and reservoir data and detailed reservoir simulation, verified by field tests, in a variety of gas shale settings.

In total, the Eastern gas shales considered in this assessment cover an area of nearly 182,000 square miles (over 116 million acres). These shales may contain an estimated 6,000 Tcf of gas in place, and have a maximum theoretical storage capacity of over 600 million metric tons. These results are summarized in **Table ES-1**.

Table ES-1. Estimated Total Gas in-Place and Theoretical Maximum $CO_2$ Storage Capacity for the Eastern Gas Shales Considered in this Study

| | Total Area | | Total Gas in Place | | Maximum Theoretical Storage Capacity | | |
|---|---|---|---|---|---|---|---|
| | Square Miles | Acres | Bcf/Sq. Mile | Trillion Cubic Feet | Trillion Cubic Feet | Billion Metric Tons | Million Metric Tons/Sq. Mile |
| Marcellus Shale | 41,274 | 26,415,006 | 31.5 | 1,299 | 3,356 | 171 | 4.15 |
| Utica Shale | 57,913 | 37,063,938 | 62.5 | 3,618 | 6,426 | 340 | 5.90 |
| Antrim Shale | 36,758 | 23,525,120 | 20.5 | 753 | 1,356 | 72 | 1.95 |
| Devonian Ohio Shale | 45,844 | 29,340,000 | 8.6 | 394 | 393 | 21 | 0.45 |
| TOTAL | 181,789 | 116,344,064 | | 6,063 | 11,530 | 604 | |

Clearly, not all of the gas in-place in these for shale plays will be recoverable, and economics will further limit of this gas in-place that will be economic to produce using EGR techniques with $CO_2$ injection. Thus, not all of the "maximum theoretical storage capacity" will be technically or economically accessible; as will the gas in-place be recoverable. Important, therefore, is a determination of what portion of this potential gas in-place is recoverable, and how much storage capacity is truly accessible.

Reservoir models were developed and simulations were conducted to characterize the potential for both $CO_2$ storage and EGR for the target gas shale formations. Based on that, engineering costing and cash flow analyses were used to estimate economic potential based on natural gas prices and possible financial incentives such as $CO_2$ emission reduction credits or carbon taxes.

Input parameters were developed for reservoir modelling, assumed to represent those parameters for a "typical well" defined for each of the model areas considered in each of the basins assessed. Based on the reservoir models, reservoir simulations were performed using ARI's proprietary COMET3 reservoir simulator. Where possible, history matching was done based on known production to "truth-test" the models to actual producing shale gas wells.

In each of the areas considered, the objective was to assume that EGR and $CO_2$ storage activities would commence consistent with the historical development practices in the basin. In the relatively immature (in terms of development) Marcellus and Utica Shales, the standard well drilling practice is a horizontal well completed with multi-stage massive hydraulic fractures, assumed to be at 80 acre spacing. The Antrim Shale, in contrast, a more mature play, with a long history of development, with most of the older wells (the primary target for enhanced gas recovery with $CO_2$ injection) drilled vertically, the simulations assumed vertically completed and stimulated wells, again drilled on 80-acre spacing. Relatively small (relative to today's practice), single-stage hydraulic stimulations were assumed, consistent with traditional practices in the Antrim shale.

For each area, several alternative $CO_2$ injection/EGR scenarios were considered in the simulations, and were compared to situation where the "typical well" would produce without $CO_2$ injection. These simulations were conducted for each of the model areas in each shale gas play assessed. The resulting key outputs were the estimated recovery per typical well (per 80 acres), and the estimated $CO_2$ that would be injected and remain in the reservoir (i.e., not produced), and thus ultimately assumed to be stored.

Based on the estimated average methane production per "typical" well, estimates of the total technical recovery potential for each area represented by that well were developed. Similarly, based on the estimated $CO_2$ stored per well, estimates for the total $CO_2$ storage potential for each area represented by the "typical" wells were also developed. Adjustments to

this overall potential were made based on assumptions of the total number of potential well sites that would in fact be accessible in each area, and the portion of those that would perform better than the "typical well."

The application of this approach concluded that nearly 1,300 Tcf of EGR potential is estimated to be associated with the injection of $CO_2$ into the four selected shale gas plays, of which, 460 Tcf could be economic with reasonable gas prices and/or modest incentives. This could facilitate the storage of nearly 50 Gt of $CO_2$. This is summarized in **Table ES-2**.

Table ES-2: Estimates of Technical and Economic Methane Recovery and $CO_2$ Storage Potential for the Eastern Gas Shales Assessed in this Study

| | Total Gas **in Place** (Trillion Cubic Feet) | Max. Theoretical Storage Capacity (Billion Metric Tons) | Technical EGR Production Potential (Trillion Cubic Feet) | "Economic" EGR Production Potential (Trillion Cubic Feet) | Technical $CO_2$ Storage Potential (Billion Metric Tons) | "Economic" $CO_2$ Storage Potential (Billion Metric Tons) |
|---|---|---|---|---|---|---|
| Marcellus Shale | 1,299 | 171 | 849 | 348 | 49 | 39 |
| Utica Shale | 3,618 | 340 | 344 | 104 | 10 | 8 |
| Antrim Shale | 753 | 72 | 16 | 8 | 1 | 1 |
| Devonian Ohio Shale | 394 | 21 | 69 | n.e. | 21 | 2 |
| TOTAL | 6,063 | 604 | 1,278 | 460 | 80 | 50 |

n.e. = not estimated

It is recommended that efforts build upon the results of this study to expand and focus reservoir characterization research in both gas and liquid-rich shale settings to evaluate alternative development and optimization strategies for these reservoirs, encompassing, both "primary" and "enhanced" or "improved" recovery, and, also providing for the long term storage of $CO_2$.

However, much about the mechanisms and potential for storing $CO_2$ and enhancing methane recovery in shales remains unknown. As a result, future research is necessary, and the results of this research could dramatically change the conclusions documented in this report. Numerous sources of uncertainty are identified, and recommendations for further work to refine and expand this analysis are focused on reducing or eliminating these uncertainties by acquiring additional reservoir and engineering data to improve the reservoir characterization, and industry input to investigate hypothetical development scenarios.

# Table of Contents

EXECUTIVE SUMMARY ..... II
1. INTRODUCTION ..... 1
**2.** PROJECT OBJECTIVES ..... 3
**3.** STATUS OF RD&D ON $CO_2$ STORAGE IN SHALES ..... 5
a. Eastern Kentucky Shale Gas Enhanced Recovery and $CO_2$ Storage Project (U.S.) ..... 5
b. New York State Research and Development Authority (U.S.) ..... 6
c. Stanford University (U.S.) ..... 6
d. University of Oklahoma (U.S.) ..... 6
e. U.S. DOE Industrial Carbon Management Initiative – Research on $CO_2$ Storage in Depleted Shale Gas Reservoirs ..... 6
f. Commonwealth Scientific and Industrial Research Organisation (Australia) ..... 7
g. Council for Geoscience (CGS), University of Pretoria in South Africa ..... 7
h. IEA Greenhouse Gas Research Programme (IEAGHG) (U.K.) ..... 8
i. Summary ..... 8
**4.** SUMMARY OF RESULTS OF TESTING OF INNOVATIVE TECHNOLOGY FOR MONITORING $CO_2$ FLOW BEHAVIOR ..... 10
**5.** REVIEW OF THE ANALYSES OF THE TARGETED, HIGHLY MONITORED, SMALL-SCALE $CO_2$ INJECTION TEST IN KENTUCKY ..... 12
a. Background ..... 12
b. Description of the Site for the Kentucky $CO_2$ Injection Test ..... 12
c. Overview of Injection Operations and Associated Monitoring ..... 15
d. Summary of Analyses Based on Data Provided to Date ..... 16
**6.** BASIN-LEVEL CHARACTERIZATION OF GAS RECOVERY AND $CO_2$ STORAGE POTENTIAL IN EASTERN GAS SHALES ..... 18
a. Marcellus Shale ..... 18
b. Utica Shale ..... 24
c. Antrim Shale ..... 28
d. Devonian Ohio Shale ..... 34
e. Summary ..... 37
**7.** ASSESSMENT OF TECHNICAL AND ECONOMIC POTENTIAL OF RECOVERING METHANE AND STORING $CO_2$ IN EASTERN GAS SHALES ..... 38
**8.** CONCLUSIONS AND RECOMMENDED NEXT STEPS ..... 45
**9.** REFERENCES ..... 47

# List of Figures

Figure 1. Synthetic Scheme of Fluorescent Fluoro-Polymer Functionalized Nanoparticles ..... 10
Figure 2. Proposed Test Well Configuration for Huff and Puff Injection Test. ..... 11
Figure 3. Final Location of Injection and Shallow Monitoring Well for the KY Injection Test ..... 13
Figure 4. Surface Features at the KY Injection Test Site ..... 14
Figure 5. Schematic of the SS#1 Kentucky Injection Test Well ..... 15
Figure 6. Simplified Stratigraphic Chart Showing Marcellus and Other Devonian Shale Formations of the Appalachian Basin ..... 18
Figure 7. Marcellus Study Area, Model Area Sub-Divisions, and Locations of Wells Used in the Analysis ..... 19
Figure 8. Utica/ Point Pleasant Study Area with Model Area Sub-Divisions ..... 25
Figure 9. Simplified Stratigraphic Column for Utica and Point Pleasant Shale Formations ..... 26
Figure 10: Antrim Shale Production in the Michigan BasinFigure 11: Stratigraphic Chart for Upper Devonian in Michigan Basin ..... 28
Figure 12: Antrim Shale Cross-Sections and Model Areas ..... 32
Figure 13. Distribution and Nomenclature of Devonian shales of Kentucky ..... 35
Figure 14. General Stratigraphic Nomenclature for the Shales of Kentucky ..... 35

# List of Tables

Table ES-1. Estimated Total Gas in-Place and Theoretical Maximum CO2 Storage Capacity for the Eastern Gas Shales Considered in this Study ..... iii
Table 1. Summary of Estimated Gas In-Place for Marcellus Model Areas ..... 21
Table 2. Estimated Theoretical Maximum $CO_2$ Storage Capacity for Marcellus Model Areas ..... 22
Table 3. Estimated Total Gas In-Place and Theoretical Maximum $CO_2$ Storage Capacity for Marcellus – Aggregated by State ..... 23
Table 4. Utica Point Pleasant; Summary of Total Gas In-Place, Resource Concentration and Total Theoretical Maximum $CO_2$ Storage Capacity by Model Area ..... 27
Table 5. Antrim Shale; Estimated Total Gas in-Place and Theoretical Maximum $CO_2$ Storage Capacity by Model Area ..... 33
Table 6. $CO_2$ Storage Capacity in the Devonian Black Shales of the Appalachian Basin ..... 37
Table 7. Estimated Total Gas in-Place and Theoretical Maximum $CO_2$ Storage Capacity for the Eastern Gas Shales Considered in this Study ..... 37
Table 8: Methane Recovery and $CO_2$ Storage Potential for the Marcellus Shale ..... 41
Table 9: Methane Recovery and $CO_2$ Storage Potential for the Utica Shale ..... 42
Table 10: Methane Recovery and $CO_2$ Storage Potential for the Antrim Shale ..... 43
Table 11: Estimates of Technical and Economic Methane Recovery and $CO_2$ Storage Potential for the Eastern Gas Shales Assessed in this Study ..... 44

# 1. INTRODUCTION

Building upon advances in horizontal drilling and hydraulic fracturing technologies, production of natural gas from organic-rich gas shales is rapidly developing as a major hydrocarbon energy supply option in North America and around the world. Although known for decades, what "changed the game" was the recognition that one could "create a permeable reservoir" by using intensively stimulated horizontal wells.

The proliferation of activity into new shale plays in the United States has increased annual shale gas (wet) production from 0.39 Tcf per year in 2000 to nearly 8.0 Tcf in 2011. Today, shale gas represents 34% of U.S. gas production (dry basis). The market has moved from tight gas supplies with huge price spikes during cold weather to low and stable prices, just because of the new supplies of shale gas (EIA, 2013a).

Proved natural gas reserves have grown from 34 Tcf in 2008 to nearly 132 Tcf in 2011, nearly a four-fold increase. The Appalachian basin states (PA, WV, KY, TN, NY, and OH) and Michigan (Antrim shale) contribute almost 34 Tcf (26% of this total).

Production of shale gas in the United States is expected to continue to increase. In its most recent Annual Energy Outlook (AEO) (2013 Early Release), the U.S. Energy Information Administration (EIA) predicts that U.S. shale gas production will grow by 113 percent from 2011 to 2040, with its contribution to total U.S. natural gas production increasing from 34 percent in 2011 to 50 percent in 2040 (EIA, 2013a).

A recent report sponsored by EIA (EIA, 2013b) and prepared by Advanced Resources assessed 95 shale basins and 137 shale formations in 41 countries (excluding the U.S.). Including information from Advanced Resources' proprietary data base of U.S. shale gas and shale oil resources, the assessment concluded that globally there are 7,795 Tcf of risked, technically recoverable shale gas resources, and 335 billion barrels of risked, technically recoverable shale oil resources.

The same advances that have facilitated this revolution in production from gas shales and tight oil – dense well spacing, horizontal drilling, and hydraulic fracturing – may help to facilitate enhanced gas recovery (EGR) and $CO_2$ storage in these formations.

The potential storage of $CO_2$ in organic-rich gas shales is attracting increasing technical interest, especially in Appalachian Basin states that have extensive shale deposits, but limited $CO_2$ storage capacity in conventional porous reservoirs. It has been demonstrated in coal seams that $CO_2$ is preferentially adsorbed compared to methane. Gas shale reservoirs are expected to react similarly, and desorb methane while preferentially adsorbing $CO_2$. In addition, some component of the pore volume that contains "free" gas is expected to be available for $CO_2$

storage as non-adsorbed $CO_2$, especially where previous hydraulic fracturing has enhanced injectivity. Although still in the conceptual stage, $CO_2$ injection into organic-rich gas shales could provide dual benefits: an economic benefit from the incremental recovery of desorbed methane, and an environmental benefit of secure $CO_2$ storage.

The low permeability and porosity typical of gas shale formations make $CO_2$ storage in shale challenging, especially when compared to other storage reservoirs such as depleted conventional oil and gas reservoirs and deep saline aquifers. Low porosity constrains the potential storage capacity, while low permeability constrains the injectivity of gas shales. Such constraints are counter-balanced by the great extent and thickness of candidate shale formations, plus the adsorptive capacity of gas shales for $CO_2$, which offers the potential to store $CO_2$ securely.

Potential $CO_2$ storage capacity of gas shales is just beginning to be rigorously assessed. Critical factors that will determine storage capacity and injectivity of $CO_2$ in gas shales are the volume and rate that methane can be desorbed and then produced from the shales, as well as the relative contribution of free gas from the gas-filled or, effective, pore volume. Consequently, understanding the $CO_2$ storage capacity of such shale formations requires a firm understanding the gas productive capacity of the shale.

The potential for storing $CO_2$ in shale, building on the current boom in shale gas development and production in the Appalachian Basin, can provide a basis for extending the emerging paradigm of shale gas production potential in the eastern U.S., and provide additional benefits of further enhancing gas recovery from shales via $CO_2$ injection, while providing a large potential opportunity for the secure, permanent storage of $CO_2$.

# 2. PROJECT OBJECTIVES

The goal of this cooperative research project was to build upon previous and on-going work to assess key factors that would influence effective $CO_2$ storage capacity and injectivity in selected gas shales within the Appalachian and Michigan basins. The most prolific and promising gas shale formations for $CO_2$ storage were selected as the focus for this project, including the Devonian Marcellus Shale in New York, Pennsylvania, West Virginia and eastern Ohio; the Devonian Ohio Shale in Kentucky; and the Ordovician Utica and Point Pleasant shale and equivalent formations in New York, Pennsylvania, West Virginia and Ohio. The late Devonian-age Antrim Shale in the Michigan Basin was also investigated because it has similar reservoir properties to the Appalachian Basin Devonian shale formations, and the existing production infrastructure, shallow depth, and its reservoir characteristics may make the Antrim particularly attractive for $CO_2$ storage.

Specifically, the project had the following objectives:

- Analyze and synthesize geologic information and reservoir property data, through collaboration with selected State geological surveys, universities, and oil and gas operators.
- Improve reservoir models to perform detailed reservoir simulations to better understand the shale characteristics that impact storage capacity and $CO_2$ injectivity in these targeted Eastern shales. (This simulation work was enhanced by the acquisition of proprietary data obtained from shale operators.)
- Analyze results of a targeted, highly monitored, small-scale $CO_2$ injection test in Kentucky and incorporate into ongoing characterization and simulation work.
- Test and model a smart particle early warning concept that can potentially be used to inject water with uniquely labeled particles before the start of $CO_2$ injection.
- Identify and evaluate potential constraints to economic $CO_2$ storage in gas shales, and propose development approaches that overcome these constraints.
- Complete new basin-level characterizations for the $CO_2$ storage capacity and injectivity potential of the targeted eastern shales considered.

Injecting $CO_2$ to enhance recovery and store $CO_2$ in liquids-rich (in contrast to gas-rich) shale reservoirs may also be conceivable. Some early reservoir simulation work on enhancing or improving recovery in liquids-rich shales has been performed to date on the Bakken Formation in the Williston Basin in the U.S. (Iwere, Heim, and Cherian, 2012) and plays in Western Canada (Clarkson and Pedersen, 2011). These efforts have used “typical” rock and fluid properties with numerical simulation models, not calibrated to historical well performance, resulting in recommended theoretical methods to improve recovery performance in liquid-rich

shales. Consequently, a sound basis for the evaluation of $CO_2$ injection for enhanced recovery and potential $CO_2$ storage in actual reservoir settings in emerging liquids-rich shale basins has yet to be established.

For this reason, this study only focused on issues associated with $CO_2$ storage and enhanced gas recovery in gas shales.

# 3. STATUS OF RD&D ON $CO_2$ STORAGE IN SHALES

The low permeability and porosity typical of gas shale formations make $CO_2$ storage in shale challenging, especially when compared to other storage reservoirs such as depleted conventional oil and gas reservoirs and deep saline aquifers. Low porosity constrains the potential storage capacity, while low permeability constrains the injectivity of gas shales. Such constraints are counter-balanced by the great extent and thickness of candidate shale formations, plus the strong adsorptive capacity of gas shales for $CO_2$, which offers the potential to store $CO_2$ securely. Potential $CO_2$ storage capacity of gas shales is just beginning to be rigorously assessed.

Beyond the research summarized in this report, a number of other research activities related to $CO_2$ storage in gas shales has been performed or is ongoing. A brief summary of these efforts is provided below. Additional details on the results of this research can be found by consulting the references.

## a. Eastern Kentucky Shale Gas Enhanced Recovery and $CO_2$ Storage Project (U.S.)

Led by the Kentucky Geological Survey (KGS), the goal of the "Eastern Kentucky Shale Gas Enhanced Recovery and $CO_2$ Storage Project" is to test and demonstrate injecting $CO_2$ into organic-rich, black gas shales for long-term storage and enhanced natural gas production. The main tasks of this project are to acquire data for reservoir simulation; use modeling to test and plan $CO_2$ injection; undertake site selection, construction, and injection for a small scale injection test; and assess the results of that test. $CO_2$ adsorption isotherms of gas shale samples and have been developed and relationships between $CO_2$ adsorption and methane desorption established for the Devonian Ohio Shale (Nuttall and others, 2005; ARI, 2010; DOE/NETL, 2006).

A targeted, highly monitored, small-scale $CO_2$ injection test in Kentucky was pursued. DOE/NETL provided support under the cooperative research project that is the subject of this report in the procurement of logging services for the test, analyses of the data collected during the test, as well as the incorporation of the data obtained from the test for improved and updated resource characterization and simulation work. This is described in more detail in Volume 6.

The KGS has developed initial volumetric estimates of the $CO_2$ storage capacity of the Carbonaceous (black) Devonian gas shales that underlie approximately two-thirds of the state of Kentucky in the U.S., and concluded that as much as 28 Gt could be stored in the deeper and thicker parts of these shales (Nuttall and others, 2005.). This is described in more detail in Volume 5.

## b. New York State Research and Development Authority (U.S.)

Several projects were conducted at the New York State Research and Development Authority (NYSERDA) to characterize potential of $CO_2$ storage in New York. One project characterized the geology of central New York for $CO_2$ storage and assessed the potential for EGR. Advanced Resources directed a project to assess gas shale formations for $CO_2$ storage and enhanced gas recovery potential throughout the state (NYSERDA, 2006; ARI, 2011)

## c. Stanford University (U.S.)

Researchers at Stanford University are investigating the feasibility of geologic $CO_2$ storage in shale reservoirs (DOE/NETL, 2011). The objective of this work is to conduct a series of multi-scale, multi-physics, interdisciplinary laboratory and theoretical studies to assess the feasibility of using depleted organic-rich shale reservoirs for large-scale $CO_2$ storage. Other objectives are to determine how the physical and chemical processes associated with $CO_2$ interaction with organic-rich shales affect: (1) the ability to inject $CO_2$ over a long period of time, (2) the ability to store $CO_2$ as a free phase, and (3) the ability of the shale to adsorb and permanently store $CO_2$.

## d. University of Oklahoma (U.S.)

Researchers at the University of Oklahoma have developed a methodology to assess the potential for $CO_2$ storage in organic rich gas shales, with a focus on the New Albany and Barnett shales. They found that pore volume estimation is a crucial step for storage assessment, particular in terms of the $CO_2$ that can be adsorbed. They also conclude that gas transport within the shales takes place in the presence of dynamic porosity and permeability fields, and it could be dominated by the adsorbed-phase transport (Kang and others, 2011). Experimental work to date demonstrates that the organic shale has the ability to store significant amounts of gas, due primarily to trapping of the adsorbed gas within the finely dispersed organic matter in the shale.

## e. U.S. DOE Industrial Carbon Management Initiative – Research on $CO_2$ Storage in Depleted Shale Gas Reservoirs

As part of its Regional University Alliance (RUA), Industrial Carbon Management Initiative, DOE/NETL is sponsoring research to characterize the potential to store $CO_2$ in and enhance gas recovery from shale gas wells that have been depleted through primary production. This activity involves experimental characterization of shale properties, reservoir simulation of $CO_2$ storage in and enhanced gas recovery from shales, and an initial, screening-level techno-economic assessment of the viability of those scenarios as might be applied in the Marcellus Shale (Dilmore, 2012).

Preliminary findings have shown that $CO_2$ sorption capacity in the Marcellus ranges from 1.6 to 10.3 cubic meters per metric ton. Organic rich facies have been shown to have the highest $CO_2$ and methane sorptive capacities, and are strongly related to TOC. $CO_2$/methane sorption ratios range from 1.32 to 4.2. Hysteresis is exhibited in shale permeability as a function of net stress, while porosity of shale to $CO_2$ decreases with increasing net stress.

In addition, NETL used the same procedure as KGS to estimate the $CO_2$ storage potential across the entire Marcellus shale formation in the Appalachian Basin in the eastern U.S. They estimated that the Marcellus shale has the potential to store from 17 to 166 Gt of $CO_2$ (DOE/NETL, 2010).

## f. Commonwealth Scientific and Industrial Research Organisation (Australia)

Researchers at CSIRO in Australia conducted diffusive transport and gas sorption experiments on one well-characterized shale sample (Muderong Shale, Australia) and different clay minerals to obtain information on the sealing integrity and the $CO_2$ storage potential of these materials. All measurements were performed under reservoir conditions relevant for $CO_2$ storage (temperature = 45–50 $^{o}$C; pressure < 20 MPa). Repeat diffusion experiments on one shale plug yielded increased effective diffusion coefficients and a decrease in the concentration of the bulk $CO_2$ volume. The $CO_2$ was believed to be dissolved in formation water, sorbed to mineral surfaces, or involved with geochemical reactions. For this shale sample, bulk volume $CO_2$ concentrations were found to be significantly greater within the experimental time frame when compared to coal and cemented sandstone. This high $CO_2$ storage potential could not fully be explained by $CO_2$ dissolution in water alone. Further gas sorption experiments were performed on crushed shale and various clay minerals, showing that high $CO_2$ sorption capacities are related to a combination of $CO_2$ dissolution in water and gas sorption on clay minerals (Busch and others, 2008).

## g. Council for Geoscience (CGS), University of Pretoria in South Africa

In collaboration with Sasol Petroleum International (SPI) and Chesapeake Energy, CGS is pursuing an assessment of the shale gas potential of the selected shale formations in the Karoo Basin in South Africa. The initial stages of this project involve preparation, sampling and logging of eight cores. Sampling was done in different intervals ranging from 1 meter where the shale displays a dark color to 10 meters when the shale is light. The samples were taken to an

analytical laboratory in the United States. Following the results of the gas content in the samples, future continuation of this project is expected.[1]

Part of this effort involves assessing the physicochemical properties of South African shales in the context of geological $CO_2$ storage, focusing on the $CO_2$ adsorption capacity of the carbonaceous shales of the Ecca Group in the Basin. This is being done by analyzing adsorption isotherms from a volumetric adsorption system to attempt to investigate how much $CO_2$ can be stored per molecule of methane recovered.

## h. IEA Greenhouse Gas Research Programme (IEAGHG) (U.K.)

IEAGHG sponsored a global assessment of the potential for $CO_2$ storage in gas shales, performed by Advanced Resources, which concluded that technical methane recovery potential from world's gas shale basins could be as much as 188 trillion cubic meters (6,634 trillion cubic feet) globally (not including consideration of the potential for enhanced gas recovery (EGR) realized as a result of $CO_2$ injection in shales), and could facilitate the potential storage of 740 Gt of $CO_2$ in gas shales (Godec, et al., 2013).

## i. Summary

Research on the potential for recovering methane and storing $CO_2$ in gas shales is significantly less advanced than that for coal seams. Ongoing reservoir characterization and reservoir simulation work is demonstrating that the basic concept that shales can store $CO_2$ based on trapping through adsorption on organic material (similar to coals), as well as with the natural fractures within the shales, is scientifically achievable. Still lacking, however, is sufficient testing of this concept with site-specific geologic and reservoir data and detailed reservoir simulation, verified by field tests, in a variety of gas shale settings.

Given this status, the key knowledge gaps and technical barriers identified include:

1. A lack of information on the available storage capacity in gas shales in all but a few, targeted settings.

2. A lack of geological and reservoir data for defining the favorable settings for injecting and storing $CO_2$ in shales, particularly the lack of data on shale depositional settings and reservoir properties. This is true for assessing both the production and $CO_2$ storage potential in shales.

---

[1] "Core logging and sampling methods in Karoo Basin Shale Gas Investigation," CGS website (http://www.geoscience.org.za/index.php?option=com_content&view=article&id=1294:core-logging-and-sampling-methods-in-karoo-basin-shale-gas-investigation&catid=124:projects-2010&Itemid=536)

3. Understanding the near-term and longer-term interactions between $CO_2$ and shales, particularly the mechanisms of swelling in the presence of $CO_2$, shrinkage with release of methane, and the physics of $CO_2$/methane exchange under reservoir conditions.

4. Formulating and testing alternative reliable, high volume $CO_2$ injection strategies and well designs.

5. Integrating $CO_2$ storage and enhanced recovery of methane in shales.

# 4. SUMMARY OF RESULTS OF TESTING OF INNOVATIVE TECHNOLOGY FOR MONITORING $CO_2$ FLOW BEHAVIOR

Original research conducted as part of this effort was performed by researchers at the Department of Earth and Atmospheric Sciences at Cornell University. They begin by acknowledging that storing $CO_2$ in shale depends on the diffusion of $CO_2$ into stagnant areas adjacent to the fractures into which the $CO_2$ is injected. Field tests could measure the rate of this diffusion and provide an early indication of the viability of storage. They designed and carried out laboratory experiments which illustrate how this can be done, developed models of the process, and used the models to design field tests that would be most effective in assessing the viability of storing $CO_2$ in shale.

One set of experiments and models involved the inter-diffusion of $CO_2$ and methane at atmospheric pressure. A second set involved the diffusion of a chemical tracer (trifluorotoluene, or TFT) and nanoparticles in hydrofluoroether (HFE), a supercritical $CO_2$ analogue.

In addition, two kinds of nanoparticles (**Figure 1)** were synthesized specifically for this purpose, with the process for the synthesis of these particles described. Super-critical $CO_2$-philic nanoparticles were synthesized and shown that they can be used in laboratory experiments to measure diffusional $CO_2$ sequestration into a matrix slit. The results of this work also show that these experiments can be successfully modeled.

Figure 1. Synthetic Scheme of Fluorescent Fluoro-Polymer Functionalized Nanoparticles

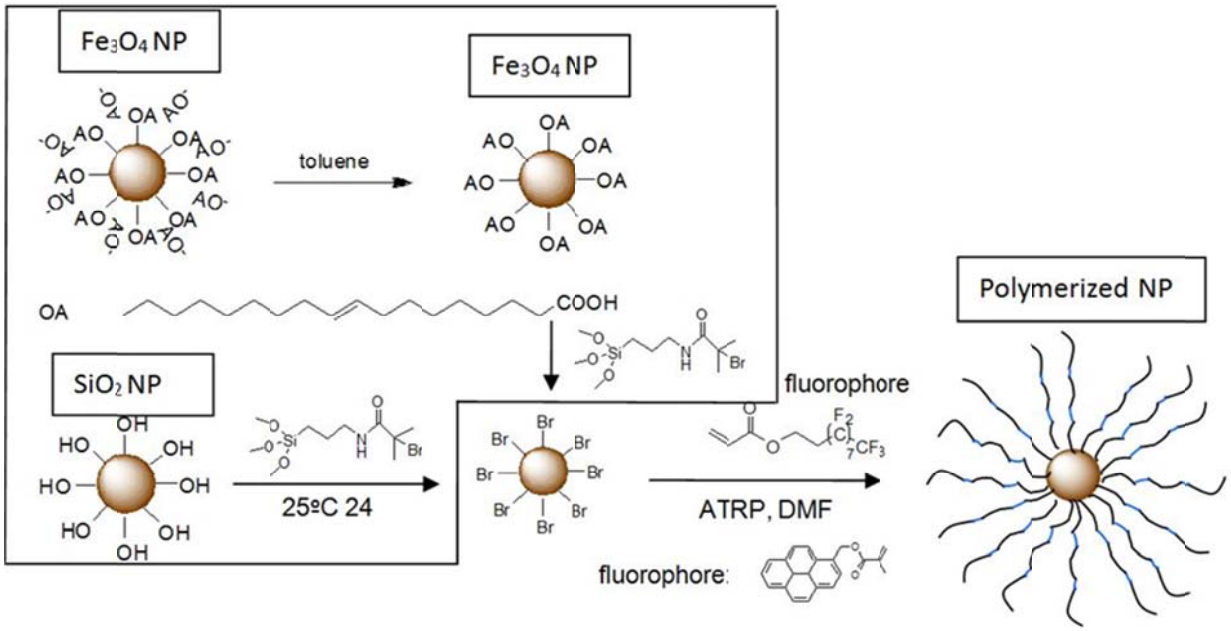

Using the same methods that were shown to be successful in the laboratory experiments, the diffusion constants of the gases, the TFT, and the nanoparticles tracers in supercritical $CO_2$ are estimated.

The researchers show how the insights gained from the laboratory experiments and models can be used to design field tests that can assess the viability of optimally storing $CO_2$ in shale. They show that successful sequestration could be achieved if the fractures are closely enough spaced. This can provide the parameters necessary for the effective design of field tests using the simple rule-of-thumb that the most information will be obtained for tests where the diffusional relaxation time of the fast-diffusing chemical tracer is approximately equal to the residence time of the injected fluid in the formation.

They demonstrated that the well spacing that is optimal for the kind of testing that could assess the potential for $CO_2$ storage is much smaller than the currently operational well separation. Based on a simplifying set of assumptions, they modeled a simple two-well test and a huff-puff test (**Figure 2**). The laboratory experiments and the models constructed show that field tests could provide a very useful early indication of the potential viability of storing $CO_2$ in shale.

Figure 2. Proposed Test Well Configuration for Huff and Puff Injection Test.

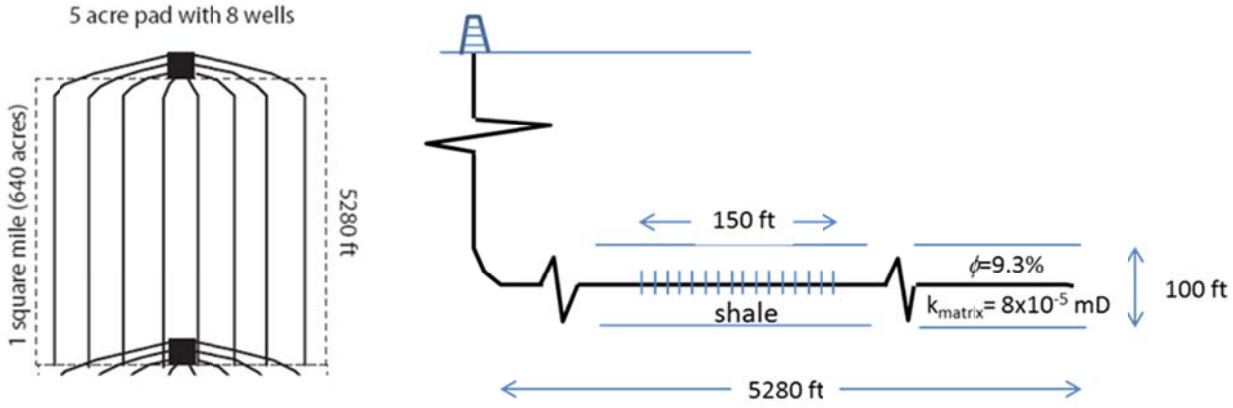


The particles synthesized, the laboratory experiments performed, and the modeling and field test designs developed show how gas-interdiffusion and chemical and nanoparticles tracers in supercritical $CO_2$ could provide an early indication of the viability of storing $CO_2$ in shale. However, they did not yet demonstrate that the nanoparticles or TFT will be inert tracers in shale, and the approximations made in the modeling may undermine some of the field test predictions. The laboratory experiments are subject to deficiencies that will not be present in field tests. For example, the flow in the forced and gravitational flow in the diffusion slit in the gas diffusion experiments will not be important in the field situation.

# 5. REVIEW OF THE ANALYSES OF THE TARGETED, HIGHLY MONITORED, SMALL-SCALE $CO_2$ INJECTION TEST IN KENTUCKY

## a. Background

Anticipating requirements to mitigate $CO_2$ emissions resulting from the use of coal in Kentucky, the State Legislature passed House Bill (HB) 1 in a 2007 special session. Among a variety of activities, HB 1 included funding to test the black shale for $CO_2$ enhanced gas recovery potential in Kentucky. The bill encouraged the Kentucky Geological Survey (KGS), the lead state agency on the effort, to partner with industry and other government bodies to share the cost of this important research. The Kentucky Consortium for Carbon Sequestration was formed to accomplish this goal.

Thus, the activity associated with the targeted, monitored, small-scale $CO_2$ injection test in Kentucky that is the subject of this report was funded by the State of Kentucky with funds appropriated under HB 1. This included costs for support for personnel from the University of Kentucky and the KGS, wellhead gas sampling, site pad clearing, construction, road improvements, deployment of downhole and surface readout monitors, running the casing hanger, slickline deployment of a downhole memory recording operation (MRO), rig services, tubing, packer, various rental of equipment, and $CO_2$ supply, storage, and handling.

NETL support to this effort involved the procurement of logging services for the test. Logging services included three logging runs: a baseline logging run prior to injection, a logging run during injection operations, and a logging run after injection operations were complete. Also included were analyses of data collected during the test.

## b. Description of the Site for the Kentucky $CO_2$ Injection Test

The original plan for the eastern Kentucky test was to perform $CO_2$ injection into one $CO_2$ injection well and three nearby wells that were to be monitored for $CO_2$ breakthrough. However, the owner of this site ultimately changed business plans and decided not to participate in the research project, withdrawing permission for the test to be conducted at the site. This caused the KGS to need to find a new site for the $CO_2$ injection test. A new site was secured in central Johnson County in eastern Kentucky (**Figure 3**).

Figure 3. Final Location of Injection and Shallow Monitoring Well for the KY Injection Test


Source: Kentucky Geological Survey

The surface layout of the test site is shown in **Figure 4**.

The well at the site was originally drilled and completed on May 27, 2002 to a depth of 1,910 feet. A standard set of open-hole nuclear logs was acquired at the time. In constructing the well, 1,808 feet of 4.5-inch casing was cemented into place and perforated across the Devonian Ohio Shale and Mississippian Berea sand intervals between 1,130 and 1,672 feet (**Figure 5**).

Figure 4. Surface Features at the KY Injection Test Site


Source: Kentucky Geological Survey

Figure 5. Schematic of the SS#1 Kentucky Injection Test Well

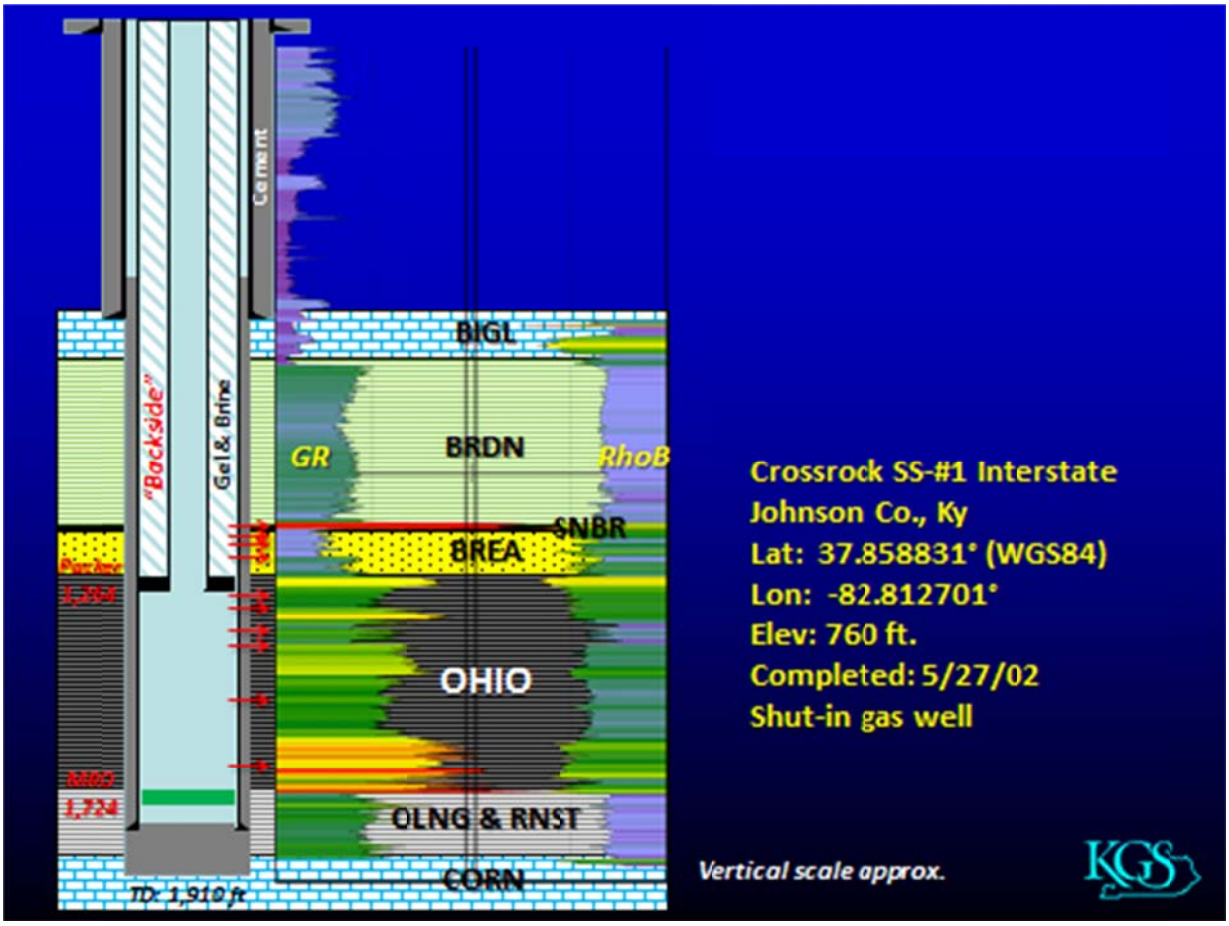


Source: Kentucky Geological Survey

## c. Overview of Injection Operations and Associated Monitoring

In the fall of 2011, acquisition of baseline logging was completed. The logging runs were conducted by Schlumberger Carbon Services. Initial baseline logging included the reservoir saturation tool (RST), PBMS (pressure & temperature), a Spinner log, and a multi-finder caliper (PMIT) log.

The $CO_2$ injection test took place in September 2012. KGS led the injection test; Crossrock Drilling, LLC provided well operations and services; Ferus Inc. provided $CO_2$ storage and supply services; Nabors Well Services provided the $CO_2$ pumping services, and Advanced Resources International (supported under this contract) oversaw logging operations and led the well test analysis and modeling activities. The injection target was the Ohio Devonian shale. The well was perforated with approximately seven shots (based on the original well log) from 1,274 feet to 1,672 feet. In total, 87 tons of $CO_2$ were injected over the three days.

Parker Energy Services/Schlumberger Carbon Services arrived on location at the end of injection to attempt a wire line injection spinner survey. Unfortunately, attempts to download the data collected as a part of this test were unsuccessful. A post-injection spinner survey was conducted during flow back operations.

A decision was then made to try increasing the pump rates. However, a shut in pressure of 590 psi was discovered on the casing annulus (i.e. the "backside annulus") above the packer. This pressure was roughly equivalent to the injection tubing's shut in pressure, suggesting communication between the injection tubing and the casing annulus. At this point, a decision was made to end the injection and proceed to flowing back the well.

Post injection logging and flow back operations were then started. Prior to the flow back, a post injection RST log was run. Post injection operations included well logging, flow back of the injection well, and compositional and volumetric monitoring of the vented gas. Pressure fall off data and temperatures were recorded after each of the three injection stages. The intention was to compare the results of the post injection sigma log to the pre-injection baseline sigma log. An anomalous drop in the capture cross section will indicate $CO_2$ buildup. Advanced Resources did not perform this comparative analysis; as of completion of this contract, Schlumberger had not provided their final analysis.

## d. Summary of Analyses Based on Data Provided to Date

The injection and pressure fall off and flow back data and the log results (spinner results and RST saturation profiles) were initially analyzed and used to model the $CO_2$ injection. The dataset was used to determine the nature of the pressure communication between the injection tubing and the casing annulus. Analyses were conducted using the PanSystem® Well Testing Analysis software.[2]

Unfortunately, inadequately accurate data were provided for some measurements. The data provided were read off of data plots; the more accurate original recorded data could not be provided. This, along with other unexplained data anomalies, made it difficult to develop conclusive analyses with regard to the test.

Nonetheless, based on the analyses that were performed, the following can be concluded and/or inferred from the injection pilot test:

- The level of effective permeability observed indicates that the black shale is more permeable than other representative samples.

[2] http://www.ep-solutions.com/Solutions/EPS/PanSystem.htm

- The presence of linear flow behavior (half-slope) on the log-log diagnostic plots indicates the presence of either a short infinite conductivty induced natural fracture or open natural fractures.

Alone, these observations are inconclusive. However, a combination of these circumstances suggests that for the duration of this test, there was communication between the Berea sand and the black shale. These are:

- The proximity of the lowermost and uppermost shale perforation and the fact they were most likely fracture stimulated at the same time
- The above average level of effective permeability and linear flow behavior determined from the well test analysis
- The observed annular pressure response.

# 6. BASIN-LEVEL CHARACTERIZATION OF GAS RECOVERY AND $CO_2$ STORAGE POTENTIAL IN EASTERN GAS SHALES

## a. Marcellus Shale

The Marcellus shale is the lowermost formation of the Middle Devonian-age Hamilton Group. The names "Marcellus Formation" and "Marcellus Shale" are often used interchangeably, although commonly the name "Marcellus Shale" refers to the most organic-rich zones, the black shale, at the base of the Marcellus Formation. The names and subdivisions of the Marcellus shale change across the states in which it exists. A simplified stratigraphic correlation chart for New York, Pennsylvania, West Virginia, and Ohio is shown in **Figure 6**, which illustrates the location of the Marcellus black shale above the top of the Onondaga limestone and equivalent formations.

Figure 6. Simplified Stratigraphic Chart Showing Marcellus and Other Devonian Shale Formations of the Appalachian Basin

| System/Series | Michigan Basin | Eastern Ohio | West Virginia | | Pennsylvania | | New York | |
|---|---|---|---|---|---|---|---|---|
| Late Devonian | Ellsworth/ Antrim Shale | West Falls Fm./ Java Fm./ Olentangy Sh. | West Falls Group/ Rhinestreet Shale/ Brailler Fm. (in part) | | West Falls Group/ Rhinestreet Shale/ Brailler Fm. (in part) | | West Falls Group/ Rhinestreet Shale | |
| | *Antrim - Lachine Mbr.* | | | | | | | |
| | *Antrim -Paxton Mbr.* | *Unconformity* | Sonyea Formation | | Sonyea Group | | Sonyea Group | |
| | *Antrim - Norwood Mbr.* | | | | | | | |
| | Squaw Bay Ls | | Gennessee Group *(Burket Shale in part)* | | Harrell Shale | | Gennessee Group | |
| | *Unconformity* | | | | Genesee/ Burket Sh. | | | |
| | | | Tully Limestone (in part) | | Tully Limestone (in part) | | Tully Limestone | |
| Middle Devonian | Traverse Group | | Hamilton Grp./ Millboro Shale | Hamilton Group & equivalents | Hamilton Group Undivided | Hamilton Group | Upper Hamilton Group Shale Fms. | Hamilton Group |
| | | | Mahantango Shale | | Mahantango Shale | | Skaneateles Shale | |
| | | | | | *Stafford Ls.* | | *Stafford Ls.* | |
| | | Hamilton Grp | | | *Upper Marcellus Shale* | | *Marcellus Shale - Oatka Creek* | |
| | | | | | *Purcell Ls.* | | *Cherry Valley Ls.* | |
| | Dundee Limestone | *Marcellus Shale* | *Marcellus Shale* | | *Lower Marcellus Shale* | | *Marcellus Shale - Union Springs* | |
| | Detroit River Grp | Onondaga Ls and equivalents | Onondaga Limestone | | Onondaga Limestone | | Onondaga Limestone | |
| Early Devonian | Bois Blanc Fm. | Bois Blanc Fm. & Oriskany Ss. | Needmore Shale/ Huntersville Chert/ Oriskany Ss. | | Needmore Shale/ Huntersville Chert/Bois Blanc & Oriskany Ss. | | Tristates Group/ Esopus Sh./ Oriskany Ss. | |
| | | Helderberg Limestone | Helderberg Limestone | | Helderberg Group | | Helderberg Group | |

**Figure 7** shows the study area outline, the nine "model areas" subdivisions assumed in the assessment, and the locations of 149 digital study wells used for this analysis. The well data set was compiled from public log data. Sixty-seven study wells had a complete log suite consisting of gamma-ray, density, and resistivity through the Marcellus. This subset of wells was used for calculating free methane gas in-place and estimating maximum $CO_2$ storage capacity as non-adsorbed ('free') $CO_2$.

Figure 7. Marcellus Study Area, Model Area Sub-Divisions, and Locations of Wells Used in the Analysis

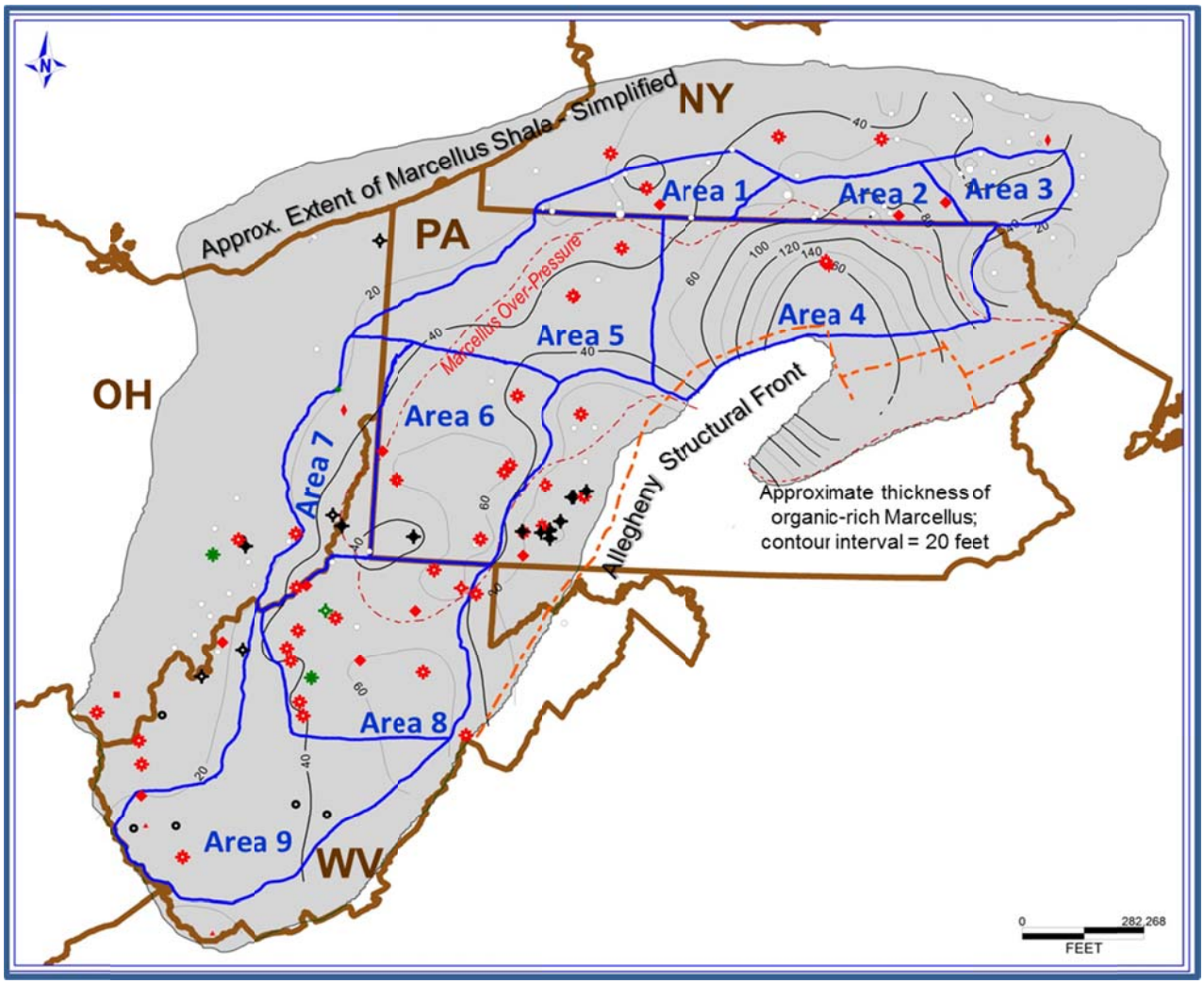

Total gas in-place and $CO_2$ storage capacity were extrapolated from the individual well log calculations for nine "model areas" indicated in **Figure 7**. The model areas are sub-divisions of the total Marcellus study area based on parameters such as depth and thickness of the Marcellus, reservoir pressure gradient, and computed TOC. For each model area, the average calculated gas in-place and storage capacity values per unit area were multiplied by the geographical area contained within the model area boundaries. Model area totals of Marcellus gas in-place and theoretical maximum $CO_2$ storage capacity were summed to determine state totals of gas in-place and maximum $CO_2$ storage capacity.

**Table 1** summarizes the estimated Marcellus gas in-place by model area, as well as for the total study area. The total Marcellus study area is 41,274 square miles, or 26,415,006 acres. Total Marcellus gas in-place is estimated to be 1,299 trillion cubic feet (Tcf), of which 562,509 Bcf is estimated to be adsorbed gas in-place and 736,407 Bcf is estimated to be free (non-adsorbed) gas in-place. Over the entire study area, the concentration of total Marcellus gas in-place ranges from 8.2 Bcf/mile$^2$ in Area 9 (south and south central West Virginia) to 64.6 Bcf/mile$^2$ in Area 4 (northeastern Pennsylvania where the Marcellus is thick and over-pressured). Averaged over the entire study area, Marcellus gas in-place is estimated to be 31.4 Bcf/ mile$^2$, with 13.6 Bcf/ mile$^2$ adsorbed gas in-place and 17.8 Bcf/mile$^2$ free gas in-place.

**Table 2** summarizes the theoretical maximum $CO_2$ storage capacity by model area, which assumes that all adsorbed and 'free' gas is replaced by injected $CO_2$. Actual $CO_2$ storage capacity in organic-rich shale is a fraction of the gas in-place volume, and strongly influenced by injection design and field operating parameters, reservoir production and depletion, in addition to intrinsic reservoir characteristics such as porosity, thickness, reservoir pressure and permeability. Theoretical maximum $CO_2$ storage capacity in the Marcellus for the entire study area is estimated to be 3,356 Tcf, approximately 2.6 times the total gas in-place. Maximum $CO_2$ storage as an adsorbed phase is estimated to be 1,935,171 Bcf and maximum $CO_2$ storage as a "free" or non-adsorbed phase is estimated to be 1,420,921 Bcf. **Table 3** presents the same information aggregated by state.

Table 1. Summary of Estimated Gas In-Place for Marcellus Model Areas

| Summary of Estimated Gas In-Place for Marcellus Model Areas | | | | | | | | |
|---|---|---|---|---|---|---|---|---|
| MODEL AREA | Area Description | Total Area, miles$^2$ | Adsorbed Gas In-Place, Bcf/ mile$^2$ | Free Gas In-Place, Bcf/ mile$^2$ | Total Adsorbed Gas in-Place, Bcf | Total Free Gas In-Place, Bcf | Estimated Total Gas In-Place, Bcf | *Estimated Theoretical Maximum $CO_2$ Storage, Bcf* |
| AREA 1 | West Central NY; Normal Pressure | 1,965 | 4.9 | 5.9 | 9,676 | 11,510 | 21,186 | *66,001* |
| AREA 2 | South Central NY; Normal Pressure | 1,820 | 17.0 | 15.8 | 30,913 | 28,752 | 59,665 | *190,467* |
| AREA 3 | East Central NY; Under Pressured | 1,679 | 7.0 | 6.4 | 11,827 | 10,803 | 22,631 | *80,530* |
| AREA 4 | Northeast PA; Over Pressured | 7,825 | 26.5 | 38.1 | 207,546 | 297,847 | 505,393 | *1,184,168* |
| AREA 5 | NW - North Central PA; Over Pressured | 5,705 | 12.9 | 20.5 | 73,319 | 117,163 | 190,482 | *476,823* |
| AREA 6 | SW - South Central PA; Normal to Over Pressured | 5,571 | 11.9 | 14.7 | 66,433 | 81,661 | 148,094 | *368,350* |
| AREA 7 | Eastern OH & WV Panhandle; Normal to Under-Pressured | 3,517 | 9.5 | 11.9 | 33,493 | 41,808 | 75,300 | *225,713* |
| AREA 8 | North & Central WV; Normal to Under-Pressured | 6,305 | 15.7 | 19.1 | 98,862 | 120,692 | 219,554 | *565,895* |
| AREA 9 | South & Southwest WV; Under Pressured | 6,887 | 4.4 | 3.8 | 30,440 | 26,172 | 56,612 | *198,147* |
| Marcellus Study Area Total | | 41,274 | 13.6 | 17.8 | 562,509 | 736,407 | 1,299 Tcf | *3,356 Tcf* |

Table 2. Estimated Theoretical Maximum $CO_2$ Storage Capacity for Marcellus Model Areas

| Estimated Theoretical Maximum $CO_2$ Storage Capacity for Marcellus Model Areas | | | | | | | |
|---|---|---|---|---|---|---|---|
| MODEL AREA | Area Description | Total Area, miles$^2$ | Adsorbed $CO_2$ Storage, Bcf/ mile$^2$ | Free (non-adsorbed) $CO_2$ Storage, Bcf/ mile$^2$ | Total Maximum Adsorbed $CO_2$ Storage, Bcf | Total Maximum Non-Adsorbed $CO_2$ Storage, Bcf | Theoretical Maximum $CO_2$ Storage Capacity, Bcf |
| AREA 1 | West Central NY; Normal Pressure | 1,965 | 17.9 | 15.7 | 35,121 | 30,880 | 66,001 |
| AREA 2 | South Central NY; Normal Pressure | 1,820 | 64.2 | 40.5 | 116,848 | 73,618 | 190,467 |
| AREA 3 | East Central NY; Under Pressured | 1,679 | 37.0 | 10.9 | 62,174 | 18,356 | 80,530 |
| AREA 4 | Northeast PA; Over Pressured | 7,825 | 88.1 | 63.2 | 689,581 | 494,587 | 1,184,168 |
| AREA 5 | NW - North Central PA; Over Pressured | 5,705 | 43.5 | 40.1 | 248,008 | 228,815 | 476,823 |
| AREA 6 | SW - South Central PA; Normal to Over Pressured | 5,571 | 39.6 | 26.5 | 220,437 | 147,913 | 368,350 |
| AREA 7 | Eastern OH & WV Panhandle; Normal to Under-Pressured | 3,517 | 35.1 | 29.1 | 123,292 | 102,421 | 225,713 |
| AREA 8 | North & Central WV; Normal to Under-Pressured | 6,305 | 52.6 | 37.1 | 331,770 | 234,185 | 565,895 |
| AREA 9 | South & Southwest WV; Under Pressured | 6,887 | 15.7 | 13.1 | 108,000 | 90,147 | 198,147 |
| Marcellus Study Area Total | | 41,274 | 39.1 | 28.7 | 1,935,171 | 1,420,921 | 3,356,093 |

Table 3. Estimated Total Gas In-Place and Theoretical Maximum $CO_2$ Storage Capacity for Marcellus – Aggregated by State

| | New York | Pennsylvania | West Virginia | Eastern Ohio & West Virginia Panhandle | Total Study Area |
|---|---|---|---|---|---|
| Potential $CO_2$ Storage Area, acres | 3,496,798 | 12,224,704 | 8,442,802 | 2,250,702 | 26,415,006 |
| Potential $CO_2$ Storage Area, mile$^2$ | 5,464 | 19,101 | 13,192 | 3,517 | 41,273 |
| Adsorbed Gas In-Place, Bcf | 52,416 | 347,299 | 129,302 | 33,493 | 562,509 |
| Non-Adsorbed, 'Free' Gas In-Place, Bcf | 51,065 | 496,670 | 146,864 | 41,808 | 736,407 |
| Total Gas In-Place, Bcf | 103,481 | 843,969 | 276,166 | 75,300 | 1,298,916 |
| Maximum $CO_2$ Storage, Adsorbed, million tonnes, Mt | 10,926 | 59,083 | 22,434 | 6,290 | 98,733 |
| Maximum $CO_2$ Storage, 'Free', million tonnes, Mt | 6,268 | 44,455 | 16,548 | 5,226 | 72,496 |
| Total $CO_2$ Storage Capacity, million tonnes, Mt | 17,194 | 103,538 | 38,982 | 11,516 | 171,229 |
| | | | | | |
| Total Maximum $CO_2$ Storage Capacity per Unit Area, Mt/ mile$^2$ | 3.15 | 5.42 | 2.95 | 3.27 | 4.15 |

## b. Utica Shale

The Utica Shale and Point Pleasant Formation comprise an Ordovician oil and gas play which extends through a majority of the Appalachian Basin, including New York, Quebec, Pennsylvania, Ohio, Maryland, and West Virginia - occupying an area nearly twice as large as the Marcellus shale. The Utica and Point Pleasant shale formations are located immediately above and in lateral facies in association with the top of the Trenton Limestone. In the deepest portion of the basin, the Utica Shale and equivalent formations occur at depths greater than 14,000 feet. The total Utica/ Point Pleasant study area selected for this analysis is 57,913 square miles, or, 37,063,938 acres.

Like that for the Marcellus, methane gas in-place is estimated for the Utica/ Point Pleasant from analysis of public well logs and other petrophysical data. Theoretical maximum $CO_2$ storage capacity for the Utica/ Point is estimated using $CO_2$ isotherms for the Utica obtained from recent wells in New York and Ohio. Eleven model areas were identified and a composite model well was characterized for each model area (**Figure 8**).

The complex stratigraphy of the Utica Shale and the underlying Point Pleasant Formation is simplified in this study for the reservoir model, **Figure 9**. The Utica is divided into two model layers, the “Upper Utica” and the “Basal Utica Shale”, a high gamma ray, low bulk density zone at the base for the Utica immediately overlying the Trenton Limestone or Trenton-equivalent formations. The Point Pleasant was also divided into two reservoir model layers, the “Upper (Shaley) Point Pleasant” and the carbonate-rich “Lower Point Pleasant”. The Point Pleasant in Ohio and West Virginia is approximately equivalent to the Flat Creek and Dolgeville members of the Utica Group in New York. The Basal Utica model layer is approximately equivalent to the “clay-rich” Indian Castle member of the Utica Group in New York, and the Upper Utica is approximately equivalent to the Upper Indian Castle in New York.

Figure 8. Utica/ Point Pleasant Study Area with Model Area Sub-Divisions

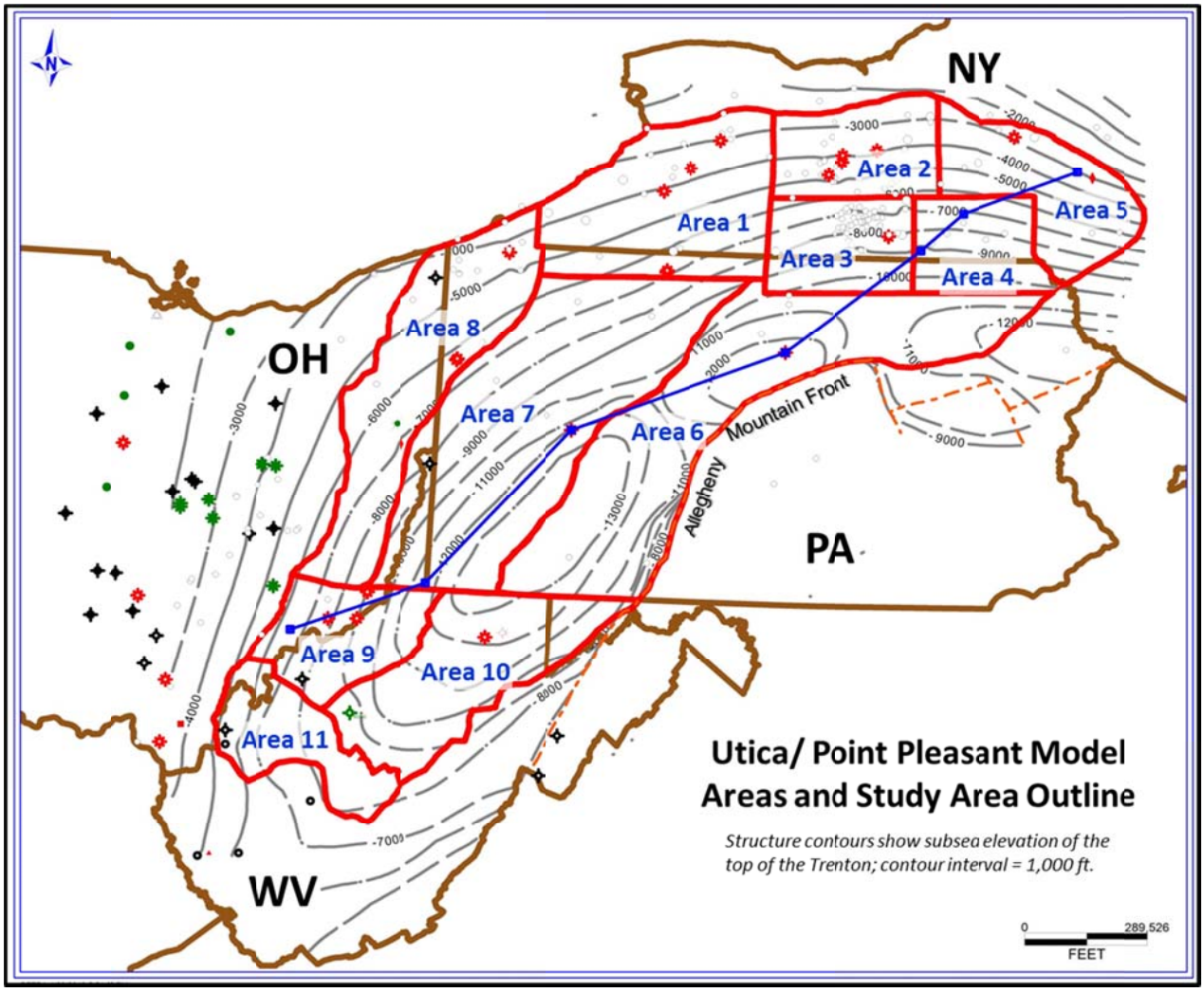

Figure 9. Simplified Stratigraphic Column for Utica and Point Pleasant Shale Formations

<table>
<tr><th rowspan="2">System/ Series<br>(N. American)</th><th colspan="2">West-Central</th><th>Central Basin</th><th>Eastern Basin</th></tr>
<tr><th>West-Central OH</th><th>Eastern OH</th><th>WV & PA</th><th>PA & NY</th></tr>
<tr><td rowspan="7">Upper Ordovician</td><td rowspan="2">Cincinnati Group</td><td>Queenston Shale</td><td>Juniata Fm.</td><td>Queenston Shale</td></tr>
<tr><td>Cincinnati Group</td><td rowspan="2">Reedsville Shale</td><td rowspan="2">Martinsburg Fm.</td><td rowspan="2">Lorraine Group</td></tr>
<tr><td>Kope Fm.</td><td>Kope Fm.</td></tr>
<tr><td>Utica Shale</td><td>Utica Shale</td><td>Utica Shale (in part)</td><td>Utica Shale</td></tr>
<tr><td rowspan="2">Pt. Pleasant</td><td rowspan="2">Pt. Pleasant</td><td>Pt. Pleasant equivalent (in part)</td><td>Pt. Pleasant equiv. (in part)</td></tr>
<tr><td rowspan="2">Trenton Limestone</td><td rowspan="2">Trenton Group</td></tr>
<tr><td rowspan="4">Middle Ordovician</td><td>Lexington Ls</td><td>Lexington Limestone</td></tr>
<tr><td colspan="2">Black River Group</td><td>Black River Group</td><td>Black River Group</td></tr>
<tr><td colspan="2">Wells Creek Fm.</td><td>Wells Creek equiv. (in part)</td><td rowspan="2">(Unconformity)</td></tr>
<tr><td colspan="2">(Unconformity)</td><td>(Unconformity)</td></tr>
<tr><td>Lower Ordovician</td><td colspan="2">Beekmantown/ Knox Dolomite</td><td>Beekmantown Grp.</td><td>Beekmantown/ Tribes Hill</td></tr>
</table>

Total Utica gas in-place (which includes both the Upper Utica and Basal Utica reservoir layers) is estimated to be 1,241 Tcf, of which 349 Tcf is estimated to be adsorbed gas in-place and 892 Tcf is estimated to be free (non-adsorbed) gas in-place. Total Point Pleasant gas in-place (which includes both the Upper Point Pleasant (shale-rich) and the Lower Point Pleasant (carbonate-rich) reservoir layers) is estimated to be 2,377 Tcf, of which 489 Tcf is estimated to be adsorbed gas in-place and 1,888 Tcf is estimated to be free (non-adsorbed) gas in-place. Averaged over the entire study area, the estimated concentration of gas in-place for the total Utica is 6.1 Bcf/mile$^2$ adsorbed and 15.8 Bcf/mile$^2$ non-adsorbed. For the total Point Pleasant, the estimated concentration of gas in-place, averaged over the entire study area is 10.3 Bcf/ mile$^2$ adsorbed and 39.8 Bcf/ mile$^2$ non-adsorbed.

**Table 4** provides a summary of gas in-place and maximum $CO_2$ storage capacity estimated for the total Utica and Point Pleasant shales.

.

Table 4. Utica Point Pleasant; Summary of Total Gas In-Place, Resource Concentration and Total Theoretical Maximum $CO_2$ Storage Capacity by Model Area

| MODEL AREA | Area Description | Potential $CO_2$ Storage Area, miles$^2$ | Potential $CO_2$ Storage Area, acres | Total Gas In-Place, Tcf | Theoretical Maximum $CO_2$ Storage, billion tonnes, Gt | Total Gas In-Place, Bcf/mile$^2$ | Maximum $CO_2$ Storage, Mt/ mile$^2$ | Total Gas In-Place, Bcf/ 80-acres | Maximum $CO_2$ Storage, Mt/ 80-acres |
|---|---|---|---|---|---|---|---|---|---|
| AREA 1 | Western NY & Northwest PA | 6,329 | 4,050,794 | 159.9 | 16.15 | 25.3 | 2.5 | 3.2 | 0.32 |
| AREA 2 | North Central NY | 3,114 | 1,992,915 | 19.1 | 1.99 | 6.1 | 0.6 | 0.8 | 0.08 |
| AREA 3 | South Central NY; North Central PA | 2,803 | 1,793,827 | 154.9 | 13.91 | 55.3 | 5.0 | 6.9 | 0.62 |
| AREA 4 | Southeast Central NY (Broome & Tioga Cos.) | 2,456 | 1,572,025 | 254.1 | 21.51 | 103.4 | 8.8 | 12.9 | 1.09 |
| AREA 5 | Northeast NY (Cortland, Madison, Otsego Cos.) | 3,831 | 2,451,694 | 312.8 | 33.89 | 81.6 | 8.9 | 10.2 | 1.11 |
| AREA 6 | Northeast PA; East Central PA | 10,590 | 6,777,578 | 1,046.3 | 92.8 | 98.8 | 8.8 | 12.4 | 1.10 |
| AREA 7 | West PA; WV Panhandle; East Central OH | 11,204 | 7,170,236 | 946.1 | 86.45 | 84.5 | 7.7 | 10.6 | 0.96 |
| AREA 8 | Northwest PA; Eastern OH | 6,459 | 4,133,518 | 358.7 | 39.1 | 55.5 | 6.1 | 6.9 | 0.76 |
| AREA 9 | Northwest WV; Southeast OH | 3,044 | 1,948,414 | 131.7 | 13.19 | 43.3 | 4.3 | 5.4 | 0.54 |
| AREA 10 | Central WV | 5,346 | 3,421,544 | 170.5 | 15.28 | 31.9 | 2.9 | 4.0 | 0.36 |
| AREA 11 | Southwest-South Central WV | 2,737 | 1,751,393 | 63.6 | 6.16 | 23.2 | 2.3 | 2/9 | 0.28 |
| Utica/ Point Pleasant Study Area Totals & Average | | 57,913 | 37,063,938 | 3,617.7 | 340.4 | 62.5 | 5.9 | 7.8 | 0.74 |

## c. Antrim Shale

The Antrim Shale is the most important unconventional gas reservoir in the Michigan Basin. Most current production from the Antrim is located in twelve northern counties south of the Antrim subcrop under glacial till. This is illustrated in **Figure 10**, which shows Antrim producing wells in the Michigan Basin, the depth to the top of the Antrim Shale, and location of the Antrim Shale subcrops in the northern counties. The shale produces from a depths ranging from 300 feet to 2,000 feet, where the Antrim is naturally fractured. Gas production targets are the fissile, organic-rich black shales in the Lachine and Norwood Members of the Antrim shown in the stratigraphic chart in **Figure 11**. These Lower Antrim members have very high total organic carbon (TOC), up to 20 percent, but low thermal maturity (0.4 % – 0.6 % Ro).

Figure 10: Antrim Shale Production in the Michigan Basin

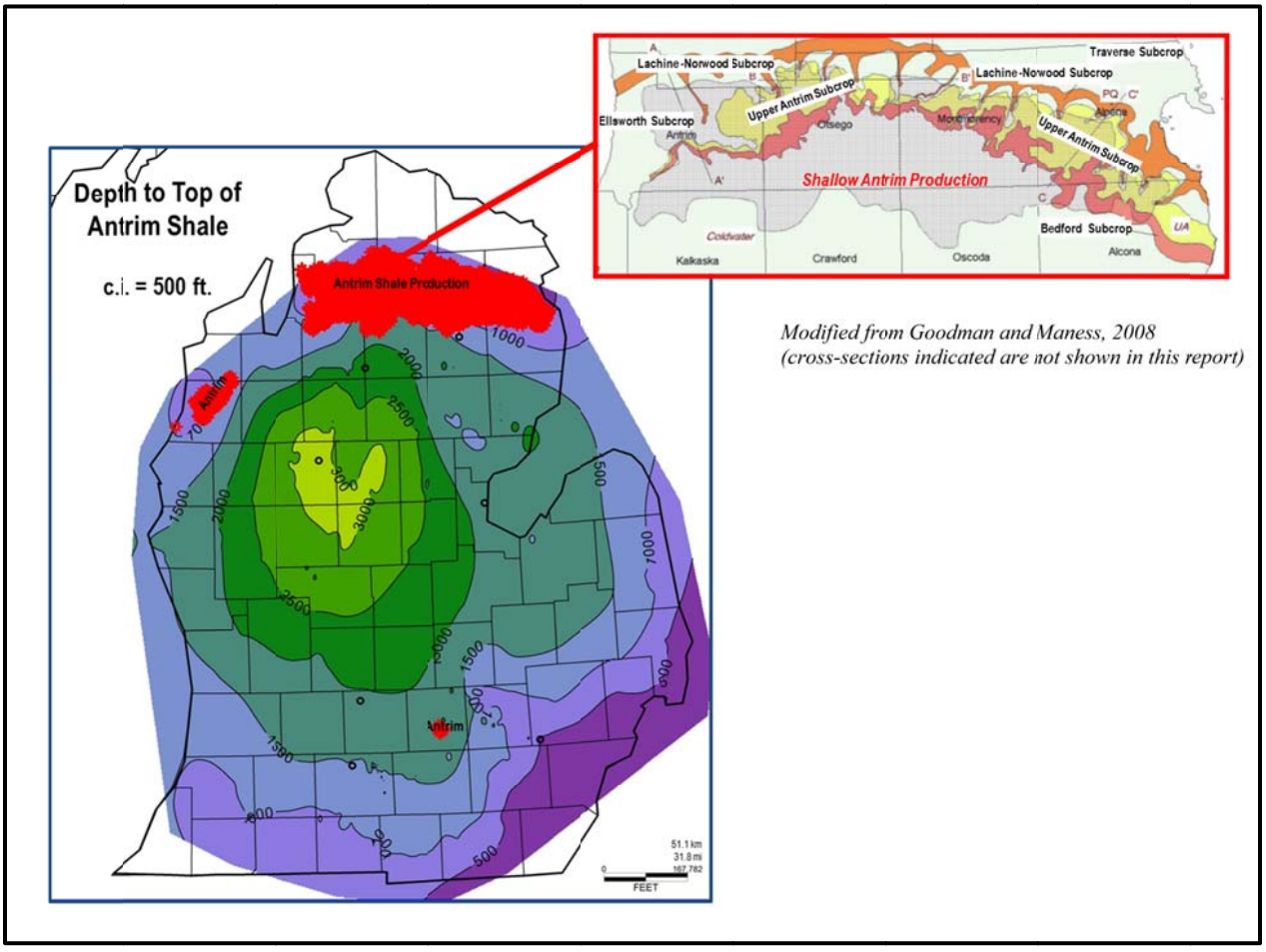

Figure 11: Stratigraphic Chart for Upper Devonian in Michigan Basin

| System/Series | Michigan Basin |
|---|---|
| Mississippian | Berea Sandstone |
| Upper Devonian | Ellsworth Shale/ Bedford Shale |
| | Ellsworth Shale/ Upper Antrim Shale |
| | *Antrim - Lachine Member.* |
| | *Antrim -Paxton Member.* |
| | *Antrim - Norwood Member* |
| | Squaw Bay Ls |
| Middle Devonian | *Unconformity* |
| | Traverse Group |
| | Dundee Limestone |
| | Detroit River Grp |
| Lower Devonian | Bois Blanc Fm. |

Antrim production in this area is predominately biogenic gas, which appears to be sourced by anaerobic bacteria consuming thermally immature organic material in the Lachine and Norwood Members. Fractures are necessary for production and the groundwater flow system from the northern Antrim subcrop appears to control the conditions for methanogenic bacteria activity.

Thermogenic gas production from the Antrim Shale occurs at depths greater than 2,000 feet. In the central Michigan Basin, the Antrim Shale may be in the oil generation window at depths greater than 2,500 feet. The primary source for the thermogenic gas in the Antrim appears to be underlying older Devonian and Ordovician shales, the gas having migrated into the Antrim via vertical fractures. Thermogenic gas production in the Antrim occurs to maximum depths of 2,600 feet in Crawford County and 3,200 feet in Missaukee County. The thermogenic Antrim gas play in the central basin is characterized as having significantly fewer fractures than the shallow biogenic gas play, as well as low fracture permeability and low productivity compared to the biogenic gas play.

The Antrim shale study area includes the entire Michigan Basin where the depth to the Antrim shale in the northern basin is below than depth of the Antrim subcrop beneath surface glacial deposits. Most of the Antrim shale gas production in the Michigan Basin occurs at very shallow depths, substantially less than the 2,500 feet, which is generally regarded as the minimum depth for $CO_2$ injection and storage as a dense phase fluid. Due to the very high kerogen content and low thermal maturity, the shallow Antrim is expected to behave much like coal with respect to $CO_2$ storage. Most of the $CO_2$ is expected to be strongly adsorbed on the kerogen in the Antrim as well as dissolved into any oil that might be present in the shale.

By including the entire Michigan Basin, the Antrim shale study area is much greater than the Antrim Shale production area that extends across portions of twelve counties in the northern basin. In addition to the Antrim biogenic gas play in the north, the study area includes the thermogenic gas play in the central basin area, and the southern perimeter of the basin where a hypothetical southern biogenic gas play is proposed. Very little Antrim gas production occurs in the thermogenic gas play of the central basin. The thermogenic gas is sourced from deeper Devonian and Ordovician shale and migrates to the Antrim via fractures and faults. Thermogenic gas production is thought to be limited by the paucity of fractures in the central basin compared to the pervasive fracturing of the Antrim in the northern basin.

For this analysis, Antrim shale gas in-place and theoretical maximum $CO_2$ storage capacity were estimated for the Antrim in the entire basin, although the reservoir simulation focused on the northern biogenic gas play where there is meaningful well performance data. Gas in-place and theoretical maximum $CO_2$ storage are estimated and reported separately for the northern and central basin Antrim. Gas in-place and $CO_2$ storage are estimated for the

southern basin using the Antrim shale production in the north as an analog. This is reported as only hypothetical $CO_2$ storage potential.

Threfore, three model areas were proposed for the Antrim Shale: 1) the northern shallow biogenic gas play area; 2) the thermogenic Antrim play area in the central Michigan Basin, and 3) a hypothetical southern shallow biogenic gas play on the southern rim of the basin. The three model areas are shown in **Figure 12.** Model well parameters for reservoir simulation are generalized based on published Antrim data and analyses and previous modeling of the Antrim shallow biogenic gas play conducted by Advanced Resources.

The northern shallow biogenic gas model area is the only model area of the three for which reservoir simulation of enhanced gas recovery and $CO_2$ injection and storage is practical. Only the northern shallow biogenic gas play has enough Antrim production data and known reservoir parameters to produce meaningful simulation results. The model area for the thermogenic Antrim gas play has very little Antrim production data, and little supporting data to estimate essential input parameters to the reservoir simulation.

For this analysis, gas in-place and theoretical maximum $CO_2$ storage capacity for the Lachine and Norwood members of the Antrim were estimated using basin-scale assumptions about reservoir properties and other inputs that are based on the available published data. The southern basin model area was assumed to have many of the same reservoir characteristics as the Antrim northern biogenic gas play model area, although biogenic gas production from shallow, highly fractured Antrim Shale has yet to be successfully established in the southern Michigan basin. $CO_2$ gas content in the produced gas stream is assumed to be 30 percent in the northern biogenic gas play (Model Area 1), zero percent for the thermogenic Antrim gas play (Model Area 2) and 10 percent for the hypothetical southern biogenic gas play (Model Area 3).

**Table 5** provides a summary for each model area of total gas in-place and total theoretical maximum $CO_2$ storage capacity. For each model area, the average calculated gas in-place and $CO_2$ storage capacity values per unit area are multiplied by the geographical area contained within the model area boundaries.

Figure 12: Antrim Shale Cross-Sections and Model Areas

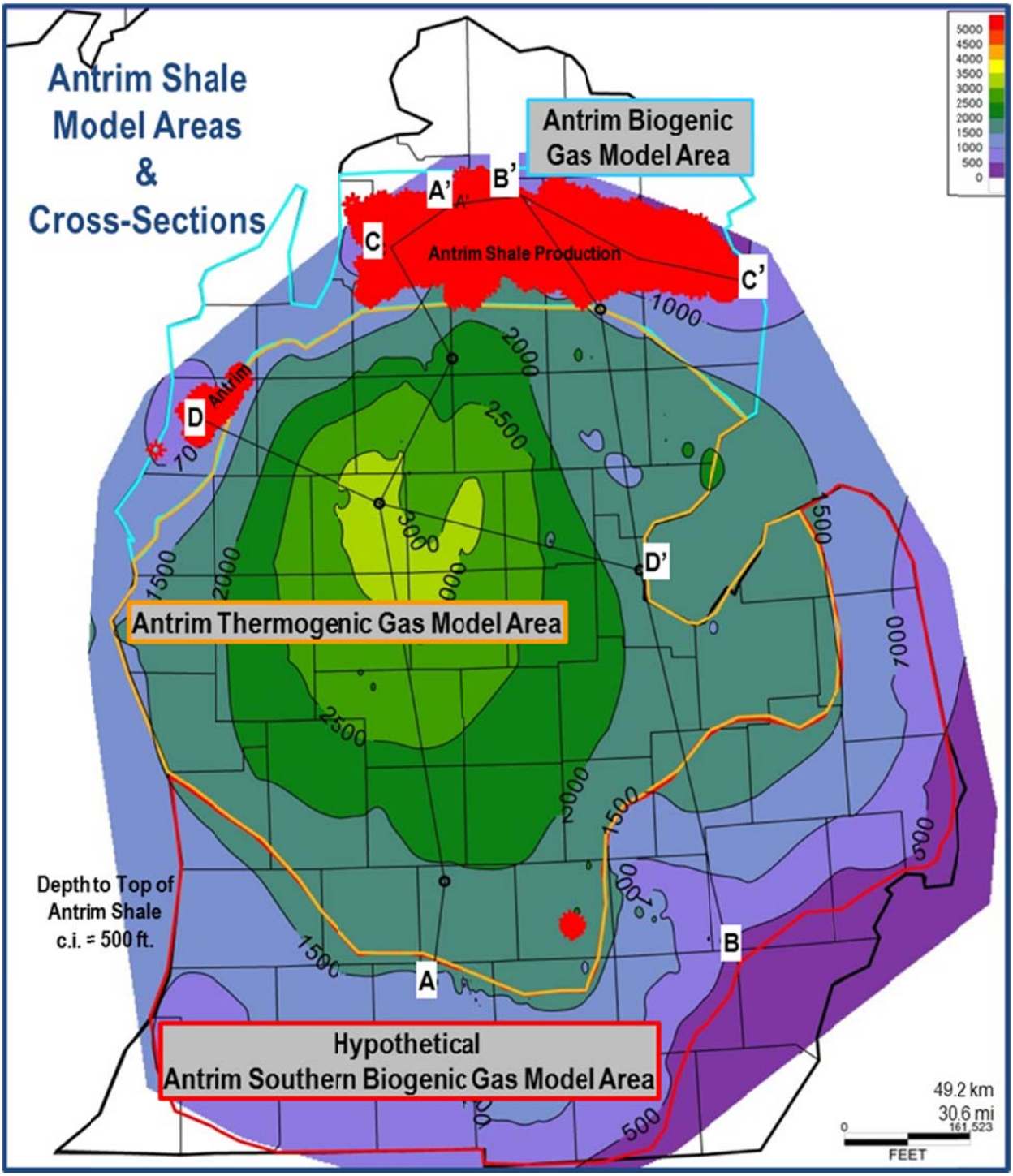

Table 5. Antrim Shale; Estimated Total Gas in-Place and Theoretical Maximum $CO_2$ Storage Capacity by Model Area

| Theoretical Maximum $CO_2$ Storage, Bcf/mi$^2$ | Model Area 1<br>Antrim Shale Shallow Biogenic Gas Play – Northern Basin | Model Area 2<br>Antrim Shale Deep Thermogenic Gas Play – Central Basin | Model Area 3<br>Hypothetical Shallow Biogenic Gas Play - Southern Basin |
|---|---|---|---|
| Total Area, mile$^2$ | 5,411 | 19,295 | 12,052 |
| TOTAL ANTRIM ADSORBED Gas in-Place, Bcf | 64,499 | 347,696 | 143,660 |
| TOTAL ANTRIM FREE Gas in-Place, Bcf | 16,179 | 134,293 | 46,400 |
| TOTAL ANTRIM Gas in-Place, Bcf | 80,678 | 481,989 | 190,060 |
| Theoretical Maximum $CO_2$ Storage, ADSORBED, MT | 6,710 | 36,082 | 14,944 |
| Theoretical Maximum $CO_2$ Storage, FREE, MT | 1,407 | 9,455 | 3,134 |
| Theoretical Maximum $CO_2$ Storage, ADSORBED + FREE, MT | 8,117 | 45,537 | 18,078 |

## d. Devonian Ohio Shale

Shales dominate the Middle and Late Devonian strata of the Appalachian Basin. Black, organic-rich units alternate with gray shales consisting mostly of quartz and clay minerals. The shale overlies strata that vary in age from Upper Ordovician through Middle Devonian. The shale ranges in thickness from outcrops in places along the crest of the Cincinnati Arch to more than 3,600 feet in West Virginia. In the gas productive areas of Kentucky, the shale is typically 200 to 1,600 feet thick. The shale ranges in depth from the outcropping on the western margin of the basin to more than 4,000 feet.

**Figure 13** shows the aerial limits of the nomenclature used for the Devonian shales in Kentucky; known variously as the New Albany (Illinois Basin), Chattanooga (central Kentucky, Cincinnati Arch area), and Ohio (Appalachian Basin) Shales. The Devonian shales of the Illinois Basin areas of western Kentucky and southwestern Indiana are correlative to similar shales of the Appalachian Basin (**Figure 14**).

The Ohio Shale consists of the Huron Member and the Cleveland Member in Ohio, and is correlated with the Chattanooga Shale in Kentucky and Tennessee, and the Dunkirk shale in New York. It has been suggested that equivalent units may extend into Alabama and Georgia.

Large volumes of natural gas may be technically recoverable from the Devonian shales of Kentucky, Ohio, and West Virginia. The USGS estimated a total area for the “Low Thermal Maturity” area as 45,844 square miles (29,340,000 acres). The technically recoverable gas from the Huron, Rhinestreet, Cleveland, and Marcellus intervals is estimated to range from 26 Tcf to 82 Tcf, depending on the success of new gas extraction technologies and practices. The total estimated in-place Devonian shale gas of the tri-state area has been estimated to be 394 Tcf (Kuuskraa, et al., 1985). While much of the resource is in the Huron shale interval, significant portions are located in other thinner, yet organically rich, shale units that have experienced less development to date.

Figure 13. Distribution and Nomenclature of Devonian shales of Kentucky

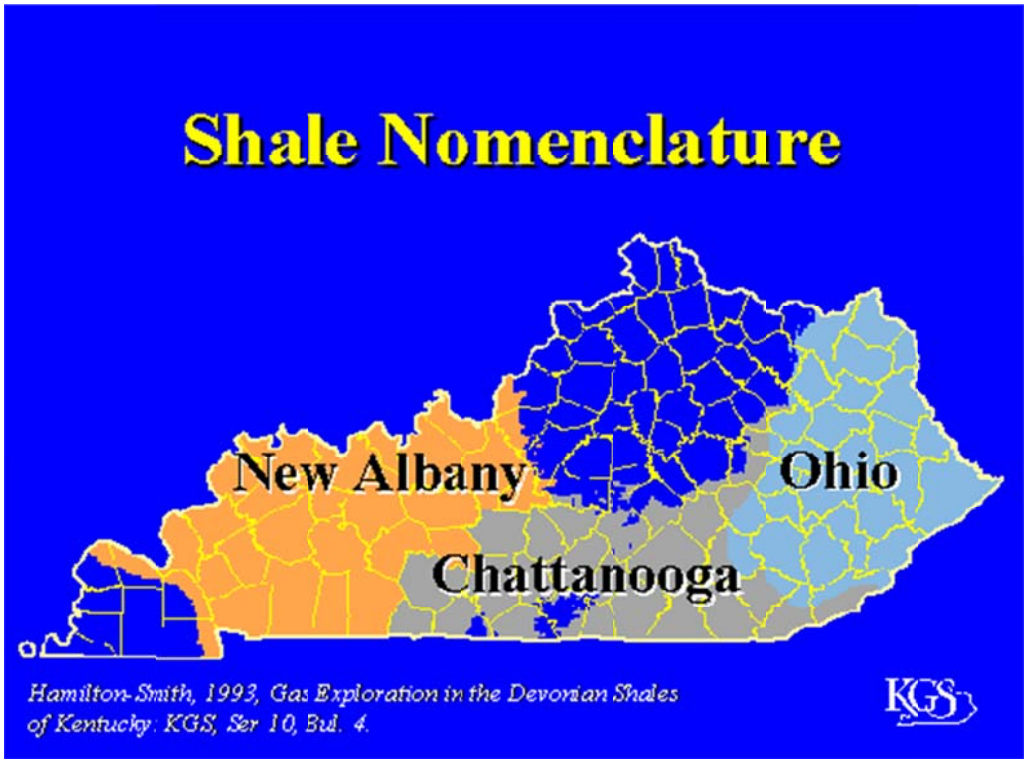


Figure 14. General Stratigraphic Nomenclature for the Shales of Kentucky

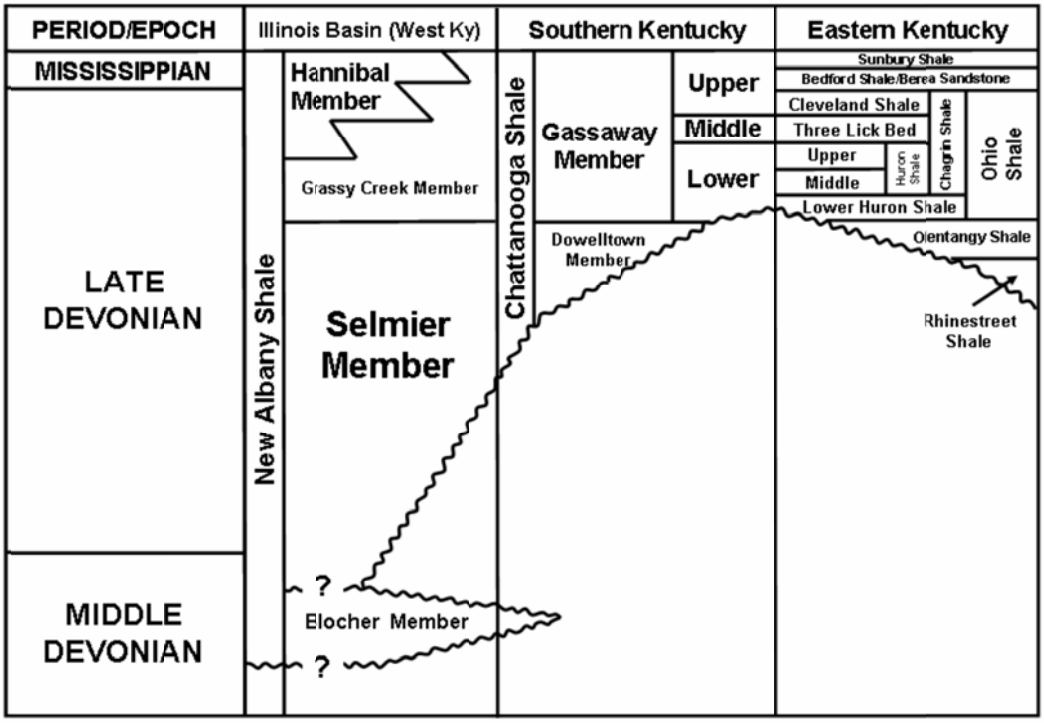


Source: Hamilton-Smith, 1993, p. 3.

Led by the Kentucky Geological Survey (KGS), the "Eastern Kentucky Shale Gas Enhanced Recovery and $CO_2$ Storage Project" was established to research and demonstrate injecting $CO_2$ into organic-rich, black gas shales for long-term storage and enhanced natural gas production in Kentucky. For this effort, the previous KGS work on the basin-level geologic characterization of the Devonian Ohio Black Shales in Kentucky is summarized. Initially, volumetric estimates were developed to indicate a $CO_2$ sequestration capacity of as much as 28 Gt total in the deeper and thicker parts of the Devonian shales in Kentucky. In the Big Sandy Gas Field area of eastern Kentucky, assuming a net thickness of shale with 4 percent or greater TOC, 6.8 Gt of $CO_2$ storage potential was estimated to exist in the five-county area. KGS researchers concluded that, discounting the uncertainties in reservoir volume and injection efficiency, the black shales of Kentucky could be a potentially large geologic sink for $CO_2$ (Nuttall and others, 2005).

Updating this previous work, as part of Phase I efforts of the Midwest Regional Carbon Sequestration Partnership (MRCSP)[3] research, an updated methodology was developed to assess the potential $CO_2$ storage capacity in the Devonian Ohio shales in a study area consisting of the central and northern Appalachian Basin and the Michigan Basin. In Phase II of the research, these estimates were updated by accounting for the variation of TOC of shale across the study area (thus allowing the $CO_2$ storage capacity to vary) and introducing an efficiency factor for displacement and storage (Nuttall, 2010).

Estimated storage capacity was estimated at various displacement efficiencies in the deeper (at least 1,000 feet deep) and thicker (at least 100 feet thick) black shales in the Appalachian Basin. Based on this, estimated $CO_2$ storage capacity ranged from 2.2 Gt at a 3 percent efficiency (analogous to the estimated efficiencies in saline aquifers), to as much as 30 Gt by assuming storage efficiencies analogous to those in continuous coals (up to 40 percent). A mid-range $CO_2$ storage capacity estimate of about 21 Gt was developed based on storage efficiency values of 28% (**Table 6**).

[3] http://www.dnr.state.oh.us/tabid/8290/Default.aspx

Table 6. $CO_2$ Storage Capacity in the Devonian Black Shales of the Appalachian Basin

| State | Estimated $CO_2$ Storage Capacity (billion tons) | | |
|---|---|---|---|
| | Efficiency Factor - 3% | Efficiency Factor - 28% | Efficiency Factor - 40% |
| Kentucky | 0.10 | 0.93 | 1.34 |
| Ohio | 0.51 | 4.78 | 6.82 |
| Pennsylvania | 0.80 | 7.46 | 10.66 |
| West Virginia | 0.82 | 7.61 | 10.87 |
| Total | 2.23 | 20.78 | 29.69 |

Source: Nuttall, 2010

No alternative or independent estimate was made of the $CO_2$ storage capacity in the Devonian shales of the central and northern Appalachian Basin and the Michigan Basin was made in this report.

## e. Summary

In total, the eastern gas shales considered in this assessment cover an area of near 182,000 square miles (over 116 million acres). These shales may contain an estimated 6,000 Tcf of gas in place, and have a maximum theoretical storage capacity of over 600 million metric tons. These results are summarized in **Table 7**.

Table 7. Estimated Total Gas in-Place and Theoretical Maximum $CO_2$ Storage Capacity for the Eastern Gas Shales Considered in this Study

| | Total Area | | Total Gas in Place | | Maximum Theoretical Storage Capacity | | |
|---|---|---|---|---|---|---|---|
| | Square Miles | Acres | Bcf/Sq. Mile | Trillion Cubic Feet | Trillion Cubic Feet | Billion Metric Tons | Million Metric Tons/Sq. Mile |
| Marcellus Shale | 41,274 | 26,415,006 | 31.5 | 1,299 | 3,356 | 171 | 4.15 |
| Utica Shale | 57,913 | 37,063,938 | 62.5 | 3,618 | 6,426 | 340 | 5.90 |
| Antrim Shale | 36,758 | 23,525,120 | 20.5 | 753 | 1,356 | 72 | 1.95 |
| Devonian Ohio Shale | 45,844 | 29,340,000 | 8.6 | 394 | 393 | 21 | 0.45 |
| TOTAL | 181,789 | 116,344,064 | | 6,063 | 11,530 | 604 | |

# 7. ASSESSMENT OF TECHNICAL AND ECONOMIC POTENTIAL OF RECOVERING METHANE AND STORING $CO_2$ IN EASTERN GAS SHALES

Clearly, not all of the gas in-place in these for shale plays will be recoverable, and economics will further limit the amount of this gas in-place that will be economic to produce using EGR techniques with $CO_2$ injection. Thus, not all of the "maximum theoretical storage capacity" will be technically or economically accessible. Important, therefore, is a determination of what portion of this potential gas in-place is recoverable, and how much storage capacity is truly accessible. Some critical questions that need to be addressed when understanding the economic potential for EGR from and $CO_2$ storage in gas shales include:

- What impact does the phasing of primary and EGR have on the effectiveness of $CO_2$ storage?
- What shale reservoir environment provides the best economics?
- Are greenfield or brownfield projects better?
- How sensitive are results to natural gas prices?
- How might incentives for $CO_2$ emission reduction impact the results?

In this assessment, the objective was to develop preliminary reservoir models and simulations to characterize the potential for both $CO_2$ storage and EGR for the target gas shale formations. Based on that, engineering costing and cash flow analyses were used to estimate economic potential based on natural gas prices and possible $CO_2$ emission reduction credits or carbon taxes.

Input parameters were developed for reservoir modelling, assumed to represent those parameters for a "typical well" defined for each of the model areas considered in each of the basins assessed. Based on the reservoir models, reservoir simulations were performed using ARI's proprietary COMET3 reservoir simulator. Where possible, history matching was done based on known production to "truth-test" the models to actual producing shale gas wells.

These reservoir simulations allowed for the estimation of $CO_2$ injection rates into gas shale reservoirs, the rate at which adsorbed methane is displaced from the shale by $CO_2$, the total volume of $CO_2$ stored, the initial dimensions of the $CO_2$ plume, and the disposition of the $CO_2$ in the reservoir over time. Potential constraints to economic EGR and $CO_2$ storage in gas shales were assessed -- particularly the low permeability and porosity -- with potential development and production options proposed that may help overcome these constraints. Engineering costing and cash flow analyses were performed to determine the impact on

economic viability of the phasing of primary production and EGR, natural gas prices, and potential $CO_2$ emission reduction credits or carbon taxes.

Finally, the results of these assessments were used to estimate the technical and economic potential for EGR and $CO_2$ storage in each of the targeted shale gas basins in this assessment.

In each of the areas considered, the objective was to assume that EGR and $CO_2$ storage activities would commence consistent with the historical development practices in the basin. In the relatively immature (in terms of development) Marcellus and Utica Shales, the standard well drilling practice is a horizontal well completed with multi-stage massive hydraulic fractures, assumed to be at 80 acre spacing. The Antrim Shale, in contrast, a more mature play, with a long history of development, with most of the older wells (the primary target for enhanced gas recovery with $CO_2$ injection) drilled vertically, the simulations assumed vertically completed and stimulated wells, again drilled on 80-acre spacing. Relatively small (relative to today's practice), single-stage hydraulic stimulations were assumed, consistent with traditional practices in the Antrim shale.

For each area, several alternative $CO_2$ injection/EGR scenarios were considered in the simulations, and compared to situation where the "typical well" would produce without $CO_2$ injection. These simulations were conducted for each of the model areas in each shale gas play assessed. The resulting key outputs were the estimated recovery per typical well (per 80 acres), and the estimated $CO_2$ that would be injected and remain in the reservoir (i.e., not produced), and thus ultimately assumed to be stored.

Based on the estimated average methane production per well, estimates of the total technical recovery potential for each area were then developed. Similarly, based on the estimated $CO_2$ stored per well, estimates for the total $CO_2$ storage potential for each area were also developed. Adjustments to this potential were made based on assumptions of the total number of potential well sites that would in fact be accessible, and the portion of those that would perform better than the "typical well"

Economic analyses were performed for selected areas within each shale gas play considered, resulting in the determination of those areas within each play where a portion of the resource, could be economic at a given gas prices to develop, perhaps with some assistance of relatively modest incentives. This then characterized the economic potential for EGR and $CO_2$ storage in each of the shale gas plays.

These results are summarized in **Table 8** for the Marcellus Shale, **Table 9** for the Utica Shale and **Table 10** for the Antrim Shale. Note that the criteria for economic viability varied in each of the three plays.

No independent assessment of the technical and economic recovery potential for EGR and $CO_2$ storage in the Devonian Ohio shale was performed for this assessment. However, estimates were developed of total technical potential for EGR, assuming a "typical" incremental recovery of 0.75 Bcf for well (comparable to the more marginal areas of the other plays assessed). Technical $CO_2$ storage capacity was assumed to be that corresponding to the 28% efficiency factor, while "economic" storage capacity was assumed to be that associated with the 3% efficiency factor.

Table 8: Methane Recovery and $CO_2$ Storage Potential for the Marcellus Shale

| | Total Area, Acres | Total Area, miles$^2$ | Estimated Total Gas In-Place, Bcf | Estimated Theoretical Maximum $CO_2$ Storage, Bcf | No. of Wells at 80-Acre Spacing | No. of Accessible, Feasible Well Sites | $CH_4$ Production per Well (Bcf) | $CO_2$ Stored per Well (Bcf) | Technical $CH_4$ Production Potential (Bcf) | Technical $CH_4$ Production Potential Better than Average(Bcf) | $CO_2$ Storage Potential (Bcf) | $CO_2$ Storage Potential (MMtonne) |
|---|---|---|---|---|---|---|---|---|---|---|---|---|
| Area 1 | 1,257,845 | 1,965 | 21,186 | 66,001 | 15,723 | 7,862 | 1.59 | 2.67 | 12,490 | 6,245 | 20,990 | 1,111 |
| Area 2 | 1,164,491 | 1,820 | 59,665 | 190,467 | 14,556 | 7,278 | 3.64 | 3.91 | 26,465 | 13,232 | 28,421 | 1,504 |
| Area 3 | 1,074,462 | 1,679 | 22,631 | 80,530 | 13,431 | 6,715 | 1.49 | 2.05 | 9,972 | 4,986 | 13,750 | 728 |
| Area 4 | 5,007,988 | 7,825 | 505,393 | 1,184,168 | 62,600 | 31,300 | 9.49 | 6.93 | 296,997 | 148,499 | 216,830 | 11,472 |
| Area 5 | 3,651,027 | 5,705 | 190,482 | 476,823 | 45,638 | 22,819 | 5.18 | 5.20 | 118,088 | 59,044 | 118,658 | 6,278 |
| Area 6 | 3,565,689 | 5,571 | 148,094 | 368,350 | 44,571 | 22,286 | 5.73 | 6.97 | 127,696 | 63,848 | 155,219 | 8,213 |
| Area 7 | 2,250,702 | 3,517 | 75,300 | 225,713 | 28,134 | 14,067 | 4.89 | 4.10 | 68,822 | 34,411 | 57,604 | 3,048 |
| Area 8 | 4,035,195 | 6,305 | 219,554 | 565,895 | 50,440 | 25,220 | 6.12 | 9.65 | 154,409 | 77,205 | 243,247 | 12,870 |
| Area 9 | 4,407,607 | 6,887 | 56,612 | 198,147 | 55,095 | 27,548 | 1.26 | 2.28 | 34,641 | 17,321 | 62,671 | 3,316 |
| | 26,415,006 | 41,274 | 1,298,917 | 3,356,094 | 330,188 | 165,094 | | | 849,581 | 424,791 | 917,390 | 48,539 |
| Economic Areas @ $5.00/Mcf -- 4, 5, 6, & 8 | | | | | | | | | 697,191 | 348,595 | 733,954 | 38,834 |
| | Assumes | 50% | of well sites are accessible | | | | | | | | | |
| | | 50% | of the accessible well sites are better than average | | | | | | | | | |

Table 9: Methane Recovery and $CO_2$ Storage Potential for the Utica Shale

| | Total Area, Acres | Total Area, miles$^2$ | Estimated Total Gas In-Place, Bcf | Estimated Theoretical Maximum $CO_2$ Storage, Bcf | No. of Wells at 80-Acre Spacing | No. of Accessible, Feasible Well Sites | $CH_4$ Production per Well (Bcf) | $CO_2$ Stored per Well (Bcf) | Technical $CH_4$ Production Potential (Bcf) | Technical $CH_4$ Production Potential Better than Average(Bcf) | $CO_2$ Storage Potential (Bcf) | $CO_2$ Storage Potential (MMtonne) |
|---|---|---|---|---|---|---|---|---|---|---|---|---|
| Area 1 | 4,050,794 | 6,329 | 159,900 | 16,150 | 50,635 | 25,317 | 3.02 | 3.06 | 76,522 | 38,261 | 77,535 | 4,102 |
| Area 2 | 1,992,915 | 3,114 | 19,100 | 1,990 | 24,911 | 12,456 | 1.85 | 2.38 | 23,012 | 11,506 | 29,613 | 1,567 |
| Area 3 | 1,793,827 | 2,803 | 154,900 | 13,910 | 22,423 | 11,211 | 2.89 | 0.65 | 32,387 | 16,193 | 7,231 | 383 |
| Area 4 | 1,572,025 | 2,456 | 254,100 | 21,510 | 19,650 | 9,825 | 2.13 | 0.16 | 20,928 | 10,464 | 1,572 | 83 |
| Area 5 | 2,451,694 | 3,831 | 312,800 | 33,890 | 30,646 | 15,323 | 6.50 | 4.29 | 99,638 | 49,819 | 65,736 | 3,478 |
| Area 6 | 6,777,578 | 10,590 | 1,046,300 | 92,800 | 84,720 | 42,360 | 0.75 | 0.01 | 31,770 | 15,885 | 628 | 33 |
| Area 7 | 7,170,236 | 11,204 | 946,100 | 86,450 | 89,628 | 44,814 | 0.17 | 0.00 | 7,618 | 3,809 | 34 | 2 |
| Area 8 | 4,133,518 | 6,459 | 358,700 | 39,100 | 51,669 | 25,834 | 1.21 | 0.06 | 31,260 | 15,630 | 1,576 | 83 |
| Area 9 | 1,948,414 | 3,044 | 131,700 | 13,190 | 24,355 | 12,178 | 0.69 | 0.02 | 8,448 | 4,224 | 210 | 11 |
| Area 11 | 3,421,544 | 5,346 | 170,500 | 15,280 | 42,769 | 21,385 | 0.17 | 0.00 | 3,662 | 1,831 | 96 | 5 |
| Area 12 | 1,751,393 | 2,737 | 63,600 | 6,160 | 21,892 | 10,946 | 0.81 | 0.06 | 8,825 | 4,413 | 646 | 34 |
| | 37,063,938 | 57,913 | 3,617,700 | 340,430 | 463,299 | 231,650 | | | 344,071 | 172,035 | 184,877 | 9,782 |
| | | | | | | | | | | | | |
| Economic Areas @ $7.50/Mcf -- 1,3,5 | | | | | | | | | 208,547 | 104,274 | 150,502 | 7,963 |
| | | | | | | | | | | | | |
| | Assumes | 50% | of well sites are accessible | | | | | | | | | |
| | | 50% | of the accessible well sites are better than average | | | | | | | | | |

Table 10: Methane Recovery and $CO_2$ Storage Potential for the Antrim Shale

| | Total Area, Acres | Total Area, miles$^2$ | Estimated Total Gas In-Place, Bcf | Estimated Theoretical Maximum $CO_2$ Storage, Bcf | No. of Wells at 80-Acre Spacing | No. of Accessible, Feasible Well Sites | $CH_4$ Production per Well (Bcf) | $CO_2$ Stored per Well (Bcf) | Technical $CH_4$ Production Potential (Bcf) | Technical $CH_4$ Production Potential Better than Average(Bcf) | $CO_2$ Storage Potential (Bcf) | $CO_2$ Storage Potential (MMtonne) |
|---|---|---|---|---|---|---|---|---|---|---|---|---|
| Area 1 | 3,462,962 | 5,411 | 80,678 | 8,117 | 43,287 | 21,644 | 0.74 | 1.58 | 16,016 | 8,008 | 17,098 | 905 |
| Area 2 | 12,349,068 | 19,295 | 481,989 | 45,537 | 154,363 | 77,182 | n.e. | n.e. | n.e. | n.e. | n.e. | n.e. |
| Area 3 | *7,713,139* | *12,052* | 190,060 | 18,078 | 96,414 | 48,207 | n.e. | n.e. | n.e. | n.e. | n.e. | n.e. |
| | 23,525,169 | 36,758 | 752,727 | 71,732 | 294,065 | 147,032 | | | 16,016 | 8,008 | 17,098 | 905 |

Thus, given these assumptions, it is estimated that nearly 1,300 Tcf of EGR associated with the injection of $CO_2$ into the four selected shale gas plays, of which, 460 Tcf could be economic with reasonable gas prices and/or modest incentives. This could facilitate the storage of nearly 50 Gt of $CO_2$. This is summarized in **Table 11**.

Table 11: Estimates of Technical and Economic Methane Recovery and $CO_2$ Storage Potential for the Eastern Gas Shales Assessed in this Study

| | Total Gas in Place (Trillion Cubic Feet) | Max. Theoretical Storage Capacity (Billion Metric Tons) | Technical EGR Production Potential (Trillion Cubic Feet) | "Economic" EGR Production Potential (Trillion Cubic Feet) | Technical $CO_2$ Storage Potential (Billion Metric Tons) | "Economic" $CO_2$ Storage Potential (Billion Metric Tons) |
|---|---|---|---|---|---|---|
| Marcellus Shale | 1,299 | 171 | 849 | 348 | 49 | 39 |
| Utica Shale | 3,618 | 340 | 344 | 104 | 10 | 8 |
| Antrim Shale | 753 | 72 | 16 | 8 | 1 | 1 |
| Devonian Ohio Shale | 394 | 21 | 69 | n.e. | 21 | 2 |
| TOTAL | 6,063 | 604 | 1,278 | 460 | 80 | 50 |

# 8. CONCLUSIONS AND RECOMMENDED NEXT STEPS

Building upon combined developments in horizontal drilling and hydraulic fracturing technologies, production of natural gas from organic-rich gas shales is rapidly developing as a major hydrocarbon energy supply option in the U.S., with activity in the Eastern gas shales leading the way. Eastern gas shales can also serve as potential storage formations for $CO_2$, though this has not been demonstrated on a field scale. The same technologies – horizontal drilling and hydraulic fracturing – that have contributed to the recent rapid increase in shale gas development and production may also open up the possibility of using shale formations as actual storage media for $CO_2$ by increasing permeability and injectivity, allowing storage to potentially be more cost effective.

The technical recovery potential for methane from the Eastern Gas Shales assessed in this effort is estimated to be nearly 1,300 Tcf. This could facilitate the potential storage of nearly 80 Gt of $CO_2$. Economically, an estimated 406 Tcf is recoverable, and could help in the storage of 50 Gt of $CO_2$.

It is recommended that efforts build upon the results of this study to expand and focus reservoir characterization research in both gas and liquid-rich shale settings to evaluate alternative development and optimization strategies for these reservoirs, encompassing, both "primary" and "enhanced" or "improved" recovery, and, also providing for the long term storage of $CO_2$.

Finally, much about the mechanisms and potential for storing $CO_2$ and enhancing methane recovery in shales remains unknown. As a result, future research is necessary, and the results of this research could dramatically change the conclusions documented in this report.

There are numerous sources of uncertainty given the current availability and quality of data. These include: (1) limited $CO_2$ and methane isotherm data, (2) lack of access to reservoir test data and sustained production data for calibration of the reservoir simulation, (3) representation of reservoir matrix and fracture properties in the reservoir simulation, and (4) fracture density and spacing, fracture permeability, dominant fracture trends. These uncertainties are not unique to EGR and $CO_2$ storage; they also apply in most areas to more traditional shale gas development and production as well.

Specific areas of recommended further research include the following:

- Obtaining additional isotherm data for all of the areas considered, and other shale plays, particularly $CO_2$ isotherms.

- Improve the representation of regional fracturing in the model characterization of reservoir permeability and porosity. This would incorporate the latest understanding of fracture density, fracture trends, fracture orientation, and in situ fracture widths.
- Obtain sustained production data and reservoir test data to calibrate reservoir simulation results and improve model representation of reservoir permeability.
- Further investigate potential limitations of reservoir depth on $CO_2$ storage.

Refining and expanding this analysis needs to focus on reducing or eliminating these uncertainties, acquiring additional reservoir and engineering data to improve the reservoir characterization, and incorporating industry input on possible development scenarios.

# 9. REFERENCES

Advanced Resources International (ARI). 2011. Geologic, Engineering, and Economic Evaluation of the $CO_2$ Sequestration Capacity of New York's Gas Shales: Final Report. Prepared for the New York State, Energy Research and Development Authority, December 2011

Advanced Resources International (ARI). 2010. Reservoir Modeling and Simulation of the Devonian Gas Shale of Eastern Kentucky for Enhanced Gas Recovery and $CO_2$ Storage, report prepared for the Kentucky Geological Survey, January, 2010

Busch, Andreas, Sascha Alles, Yves Gensterblum, Dirk Prinz, David N. Dewhurst, Mark D. Raven, Helge Stanjek, and Bernhard M. Krooss. 2008. "Carbon dioxide storage potential of shales," International Journal of Greenhouse Gas Control, Volume 2, pp. 297 – 308, 2008

Clarkson..R. and P.K. Pedersen. 2011. "Production Analysis of Western Canadian Unconventional Light Oil Plays," CSUG/SPE 149005 presented at Canadian Unconventional Resources Conference, Calgary, Alberta, Canada, 15–17 November 2011

Dilmore, Robert. 2012. "ICMI – $CO_2$ Storage in Depleted Shale Gas Reservoirs," presentation a the Coal Seq VIII Forum, Pittsburgh, PA, October 23, 2012

Hamilton-Smith, T., 1993, Gas exploration in the Devonian shales of Kentucky: Kentucky Geological Survey, ser. 11, Bulletin 4, 31 p.

Iwere, F.O., Robin N. Heim, and B.V. Cherian. 2012. "Numerical Simulation of Enhanced Oil Recovery in the Middle Bakken and Upper Three Forks Tight Oil Reservoirs of the Williston Basin," SPE Paper No. 154937 presented at the Americas Unconventional Resources Conference, Pittsburgh, PA USA, June 5-7,

Kuuskraa, V.A., K. Sedwick, and A.B. Yost II, A.B., "Technically Recoverable Devonian Shale Gas in Ohio, West Virginia, and Kentucky," SPE Paper No. 14503-MS presented at the SPE Eastern Regional Meeting, Morgantown, West Virginia, 6-8 November 1985.

New York State Energy Research and Development Authority (NYSERDA). 2006. Overview of $CO_2$ Sequestration Opportunities in New York State, August 2006

Nuttall, Brandon, 2010. Reassessment of $CO_2$ Sequestration Capacity and Enhanced Gas Recovery Potential of Middle and Upper Devonian Black Shales in the Appalachian Basin, MRCSP Phase II Topical Report, October 2005–October 2010, DOE Cooperative Agreement DE-FC26-05NT42589, OCDO Grant Agreement No. DC-05-13

Nuttall, Brandon; Cortland F. Eble; James A. Drahovzal, and Mark Bustin. 2005. *Analysis of Devonian Black Shales for Potential Carbon Dioxide Sequestration and Enhanced Natural Gas Production*, Report DE-FC26-02NT41442 prepared by the Kentucky Geological Survey, University of Kentucky, for the U.S. Department of Energy, National Energy Technology Laboratory, December 30, 2005

Seung Mo Kang, Ebrahim Fathi, Ray J. Ambrose, I. Yucel Akkutlu, and Richard F. Sigal. 2011. "Carbon Dioxide Storage Capacity of Organic-Rich Shales," SPE Journal, Volume 16, Number 4, December 2011, pp. 842-855, (SPE-134583-PA)

U.S. Department of Energy, National Energy Technology Laboratory (DOE/NETL), 2006. Analysis of Devonian Black Shale in Kentucky for Potential Carbon Dioxide Sequestration and Enhanced Natural Gas Production (DOE/NETL Fact Sheet), 3/2006

U.S. Department of Energy/National Energy Technology Laboratory (DOE/NETL). 2010. Impact of the Marcellus Shale Gas Play on Current and Future CCS Activities, August 2010

U.S. Department of Energy, National Energy Technology Laboratory (DOE/NETL). 2011. Interdisciplinary Investigation of $CO_2$ Sequestration in Depleted Shale Gas Formations (DOE/NETL Fact Sheet), April 2011)

U.S. Energy Information Administration (EIA). 2013a. Annual Energy Outlook 2013, May 2, 2013 (http://www.eia.gov/forecasts/aeo/index.cfm)

U.S. Energy Information Administration (EIA). 2013b.Technically Recoverable Shale Oil and Shale Gas Resources: An Assessment of 137 Shale Formations in 41 Countries Outside the United States, prepared by Advanced Resources International, June 10, 2013 (http://www.eia.gov/analysis/studies/worldshalegas/)

Yost, A.B., R.L. Mazza, and J.B. Gehr. 1993. $CO_2$/Sand Fracturing in Devonian Shales, SPE Paper No. 26925 prepared for the 1993 Eastern Regional Conference and Exhibition, Pittsburgh, PA, U.S.A., 2-4 November

# Volume 2
# Basin-Level Characterization Of Enhanced Gas Recovery And $CO_2$ Storage Potential In The Marcellus Shale

## Assessment of Factors Influencing Effective $CO_2$ Storage Capacity and Injectivity in Eastern Gas Shales

Prepared for:
U.S. Department of Energy
National Energy Technology Laboratory
DOE Award Number: DE-FE0004633

Prepared by:
Michael Godec, Principal Investigator
Advanced Resources International, Inc.
4501 Fairfax Drive, Suite 910
Arlington, VA 22203

Date:
October 23, 2013


4501 Fairfax Drive ▪ Suite 910 ▪ Arlington, Virginia 22203 ▪ Phone: (703) 528-8420 ▪ web: www.adv-res.com

## Advanced Resources International, Inc.

# Table of Contents

**1. INTRODUCTION** ..... 1
a. Background ..... 1
b. Project Objectives ..... 2
c. Objective of this Volume ..... 2
**2. SHALE GAS PRODUCTION AND $CO_2$ STORAGE POTENTIAL IN THE BASIN** ..... 3
a. Marcellus Production History and Development ..... 3
b. Marcellus Resource Potential ..... 4
c. Sources of $CO_2$ Emissions ..... 5
d. Potential Alternative Storage Horizons ..... 5
**3. GEOLOGIC CHARACTERIZATION** ..... 6
a. Geologic Setting ..... 6
b. Stratigraphy ..... 8
c. Marcellus Study Area ..... 9
d. Type Log and Stratigraphic Cross-Sections ..... 10
**4. RESERVOIR DATA** ..... 12
a. Adsorption Isotherms ..... 12
b. Total Organic Carbon ..... 12
c. X-Ray Diffraction Mineralogy ..... 13
d. Core Permeability ..... 13
**5. ESTIMATED GAS IN-PLACE AND THEORETICAL MAXIMUM $CO_2$ STORAGE CAPACITY** ..... 14
a. Overview of Calculated Gas In-Place and $CO_2$ Storage Capacity ..... 14
b. Well Log Analysis Methodology ..... 15
i. TOC Extrapolated from Density or Gamma Ray Logs ..... 15
ii. Porosity from Density Logs ..... 16
iii. Adsorbed Gas Content and Theoretical Maximum Adsorbed $CO_2$ Capacity ..... 16
iv. Free Gas In-Place and Theoretical Maximum $CO_2$ Storage Capacity ..... 17
v. Theoretical Maximum $CO_2$ Storage as 'Free' $CO_2$ (Non-Adsorbed) ..... 18
c. Marcellus Log Calculation Results ..... 19
d. Total Gas in-Place and $CO_2$ Storage Capacity ..... 19
i. Caveats and Assumptions Regarding this Assessment ..... 20
**6. DEFINITION OF MODEL AREAS FOR RESERVOIR MODELING IN THE BASIN** ..... 22
a. Rational for the Development of Model Areas ..... 22
b. Overview of Model Areas ..... 22
c. Sources of Data for Representative Wells in Each Model Area ..... 22
REFERENCES ..... 24
FIGURES ..... 28
TABLES ..... 48
APPENDICES ..... 60

# List of Figures

Figure 1. Map Showing Extent and Depth of Marcellus Shale, and Area of Reservoir 'Over-pressure' ..... 28
Figure 2. Ohio Annual Marcellus Gas Production, 1984 - 2012 ..... 29
Figure 3. New York Annual Marcellus Gas Production, 1984 – 2012 ..... 29
Figure 4. Annual Marcellus Gas Production by State, 2000 – 2012 ..... 29
Figure 5. Pennsylvania Annual Marcellus Gas Production, 2004 - 2011 ..... 30
Figure 6. Relative Contribution of Pennsylvania Marcellus Gas to Total Gas Production, 2004 – 2011 ..... 30
Figure 7. Pennsylvania Marcellus Annual Well Permits and Wells Drilled, 2004 - 2011 ..... 30
Figure 8. Relative Contribution of Marcellus Gas to Total West Virginia Gas Production, 2005 - ..... 31
Figure 9. West Virginia Annual Marcellus Gas Production, 2005 - 2012 ..... 31
Figure 10. Simplified Stratigraphic Chart Showing Marcellus and Other Devonian Shale Formations of the Appalachian Basin ..... 32
Figure 11. Schematic Cross-Section Illustrating a Shallow Onlap Depositional Model for Devonian Black Shales (source: NY State Museum) ..... 33
Figure 12. Schematic Map of Marcellus Shale Extent and Thermal Maturity ..... 34
Figure 13. Marcellus Study Area and Model Area Sub-Divisions ..... 35
Figure 14. Type Log of the Marcellus for North Central Pennsylvania ..... 36
Figure 15. Marcellus Regional Stratigraphic Cross-Sections ..... 37
Figure 16. Stratigraphic Cross-section A – A' ..... 38
Figure 17. Stratigraphic Cross-section B – B' ..... 39
Figure 18. Stratigraphic Cross-Section C – C' ..... 40
Figure 19. Marcellus Adsorption Isotherms ..... 41
Figure 20. Relationship of Langmuir Volume and TOC for Marcellus Methane Isotherms ..... 42
Figure 21. Relationship of Langmuir Volume and TOC for Marcellus $CO_2$ Isotherm ..... 42
Figure 22. Correlation of TOC and Bulk Density for Marcellus Core Samples ..... 43
Figure 23. Correlation of TOC and Bulk Density for Marcellus Drill Cuttings, New York ..... 44
Figure 24. Correlation of TOC and Gamma Ray for Marcellus Drill Cuttings, New York ..... 44
Figure 25. Crushed Sample Pressure-Decay Permeability, Marcellus Whole Core Samples ..... 45
Figure 26. Total Marcellus Gas in-Place by Model Area, Bcf/ 80-acres ..... 46
Figure 27. Total Marcellus Theoretical Maximum $CO_2$ Storage Capacity by Model Area, Mt/ 80-acres ..... 47

# List of Tables

Table 1. Resource Assessments for the Marcellus Shale in the Appalachian Basin ....48
Table 2. Summary of Adsorption Isotherm Data Obtained for the Marcellus ....49
Table 3. Summary of Marcellus X-Ray Diffraction Mineralogy ....50
Table 4. Marcellus TOC Extrapolated from Density and Gamma Ray Logs ....51
Table 5. Log Analysis Variables to Calculate Marcellus Porosity and Water Saturation ....52
Table 6. Summary and Description of Marcellus Model Areas ....53
Table 7. Model Layer Attributes for Lower Marcellus (Union Springs) ....54
Table 8. Model Layer Attributes for Upper Marcellus (Oatka Creek) ....55
Table 9. Model Layer Attributes for Purcell/ Cherry Valley Limestone ....56
Table 10. Summary of Estimated Gas In-Place for Marcellus Model Areas ....57
Table 11. Estimated Theoretical Maximum $CO_2$ Storage Capacity for Marcellus Model Areas ....58
Table 12. Estimated Total Gas In-Place and Theoretical Maximum $CO_2$ Storage Capacity for Marcellus – Aggregated by State ....59

# List of Appendices

Appendix 1. Lower Marcellus (Union Springs) – Mean Total Porosity ....60
Appendix 2. Lower Marcellus (Union Springs) - Mean Calculated Water Saturation ....61
Appendix 3. Lower Marcellus (Union Springs) - Mean Effective (Gas-filled) Porosity ....62
Appendix 4. Lower Marcellus (Union Springs) – Mean Calculated TOC ....63
Appendix 5. Upper Marcellus (Oatka Creek) – Mean Calculated Density Porosity ....64
Appendix 6. Upper Marcellus (Oatka Creek) – Mean Calculated Water Saturation ....65
Appendix 7. Upper Marcellus (Oatka Creek) – Mean Effective (Gas-Filled) Porosity ....66

# 1. INTRODUCTION

## a. Background

Organic-rich gas shales are recognized as sharing some of the same methane storage characteristics as coal seams. Natural gas is adsorbed on kerogen and clay surfaces in gas shales, similar to methane storage within coal seams. Gas is also stored as "free" (non-adsorbed) gas in fracture porosity and inter-granular microporosity, as well as in micropores commonly observed within the kerogen of thermally mature shale (intra-kerogen porosity). The relative amounts of adsorbed and "free" gas recovered during the producing life of a shale gas well are unknown.

The potential storage of $CO_2$ in organic-rich gas shales is attracting increasing interest, especially in Appalachian Basin states that have extensive shale deposits, but limited $CO_2$ storage capacity in conventional porous reservoirs. It has been demonstrated in coal seams that $CO_2$ is preferentially adsorbed at a ratio of two or more $CO_2$ molecules for every methane molecule displaced. Gas shale reservoirs are expected to react similarly and desorb methane while preferentially adsorbing $CO_2$. In addition, some component of the pore volume that contains "free" gas is expected to be available for $CO_2$ storage as non-adsorbed $CO_2$, especially where previous hydraulic fracturing has enhanced injectivity and reservoir pore space. Although still in the conceptual stage, $CO_2$ injection into organic-rich gas shales could provide dual benefits: an economic benefit from the incremental recovery of adsorbed methane, and an environmental benefit of secure $CO_2$ storage.

The goal of this cooperative research project is to build upon previous and on-going work to assess key factors that would influence effective $CO_2$ storage capacity and injectivity in selected gas shales within the Appalachian Basin. The Appalachian Basin is endowed with thick and extensive shale formations, ranging in age from the Ordovician through the Devonian. The most prolific and promising gas shale formations for $CO_2$ storage were selected as the focus for this project, including the Devonian Marcellus Shale in New York, Pennsylvania, West Virginia and eastern Ohio; the Devonian Ohio Shale in Kentucky; and the Ordovician Utica and Point Pleasant shale and equivalent formations in New York, Pennsylvania, West Virginia and Ohio. The late Devonian age Antrim Shale in the Michigan Basin was also investigated because it has similar reservoir properties to the Appalachian Basin Devonian shale formations, and the existing production infrastructure, shallow depth, and its reservoir characteristics may make the Antrim particularly attractive for $CO_2$ storage.

## b. Project Objectives

The low permeability and porosity typical of gas shale formations make $CO_2$ storage in shale challenging, especially when compared to other storage reservoirs such as depleted conventional oil and gas reservoirs and deep saline aquifers. Low porosity constrains the potential storage capacity, while low permeability constrains the injectivity of gas shales. Such constraints are counter-balanced by the great extent and thickness of candidate shale formations, plus the strong adsorptive capacity of gas shales for $CO_2$, which offers the potential to store $CO_2$ securely. Potential $CO_2$ storage capacity of gas shales is just beginning to be rigorously assessed. Critical factors that will determine the storage capacity and injectivity of $CO_2$ in gas shales are the volume and rate that methane can be desorbed and then produced from the shales, as well as the relative contribution of free gas from the gas-filled or, effective, pore volume. Consequently, understanding the $CO_2$ storage capacity of such shale formations requires a firm understanding the gas productive capacity of the shale.

## c. Objective of this Volume

This volume reports on the basin-level geologic characterization of the Marcellus Shale in New York, Pennsylvania, West Virginia and Ohio. The objective of the Marcellus geologic characterization is to estimate methane gas in-place and potential $CO_2$ storage capacity as both adsorbed $CO_2$ displacing methane, and as non-adsorbed $CO_2$ replacing free gas in the pore volume.

A second objective of the geologic characterization is to identify and characterize subareas within Marcellus Shale that have relatively distinct characteristics, to provide a consistent set of inputs to reservoir simulation.

# 2. SHALE GAS PRODUCTION AND $CO_2$ STORAGE POTENTIAL IN THE BASIN

Building upon advances in horizontal drilling and hydraulic fracturing technologies, organic-rich gas shale formations have rapidly developed into a major hydrocarbon supply option in North America. The same technologies that have contributed to the rapid development of shale gas production - horizontal drilling and massive hydraulic fracturing - may also afford the possibility of using shale formations for cost effective storage of $CO_2$. Storing $CO_2$ in shales may offer particular advantages. Unlike storage in saline aquifers, $CO_2$ injection into gas shale formations may enhance methane production, the revenues from which would help offset the costs of storage. In addition, most basins that contain shale gas resources cover large geographic areas, which may be populated with significant concentrations of anthropogenic $CO_2$ emissions. This is the case with the Marcellus Shale in the Appalachian Basin. The Appalachian Basin is approximately 300 miles (480 kilometers) wide and 600 miles (970 kilometers) long and contains thick, extensive gas shale formations: Marcellus, Utica, Ohio, and other Devonian gas shales. Moreover, the Appalachian Basin region hosts a large portion of the coal-fired power generation capacity in the United States.

## a. Marcellus Production History and Development

The Marcellus Shale is a regionally extensive Devonian natural gas play that spans much of the Appalachian Basin from New York State into Kentucky (**Figure 1**). Gas production from Devonian age shale formations dates back to 1821 from a hand dug well in Fredonia, New York (NYSERDA, 2007). Historical production uniquely attributable to the Marcellus is difficult to identify prior to 2004, when Range Resources completed the first successful horizontal Marcellus well (Range Resources, 2013). In New York and Ohio, historical gas production from the Marcellus dates back to the mid- 1980s, but the production volumes from vertical wells were low (**Figures 2** and **3**).

Annual gas production statistics for the Marcellus Shale are collected by various state agencies overseeing Marcellus Shale gas production in their state.[1] Total annual Marcellus production as compiled by the U. S. Energy Information Administration (EIA) increased from 2 billion cubic feet (Bcf) in 2008, to 76 Bcf in 2009, to 476 Bcf in 2010. Cumulative production of Marcellus Shale gas to date is estimated to be 2 Tcf. Marcellus proved reserves have also

[1] The Pennsylvania Department of Environmental Protection reports Marcellus production bi-annually since 2011; production data prior to 2010 are reported annually. The West Virginia Geological and Economic Survey compiles monthly Marcellus production volumes from data reported by the West Virginia Department of Environmental Protection. Marcellus production data for New York and Ohio are reported annually by the New York Department of Environmental Conservation and by the Ohio Department of Natural Resources, Division of Oil and Gas Resources.

increased dramatically - from 102 Bcf in 2008, to 4.5 trillion cubic feet (Tcf) in 2009, to 13.2 Tcf in 2010. (EIA, 2008, 2009, 2010)

**Figure 4** illustrates that most of the current Marcellus production in the Appalachian Basin occurs in Pennsylvania. Marcellus production in Pennsylvania has increased by orders of magnitude since 2010 **(Figure 5)** eclipsing the combined Marcellus production of New York, Ohio and West Virginia. The contribution of the Marcellus to total natural gas produced in Pennsylvania has grown from 1 percent in 2007 to 80 percent by 2011 (**Figure 6**). The annual number of drilling permits and Marcellus well completions in Pennsylvania has declined since reaching a peak in 2011 (**Figure 7**).

West Virginia is the second largest producer of Marcellus Shale gas (**Figure 4**). During the period 2005 to 2011, Marcellus gas production in West Virginia increased from less than 1 percent of total gas production to approximately 40 percent.(**Figures 8** and **9**). Marcellus production in Ohio appears to have peaked in 2010 and New York Marcellus production has declined sharply since 2008, attributed to indefinite moratoria in New York on new drilling permits and hydraulic fracturing. The Marcellus gas production decline observed in Ohio is attributed in part to the current industry focus on oil production from the Utica and Point Pleasant shales. In addition, the areal extent of the Marcellus shale in Ohio is limited compared to neighboring states. Despite declines in New York and Ohio, the annual Marcellus production in the Appalachian Basin overall is expected to continue to increase.

## b. Marcellus Resource Potential

In 2002, the United States Geological Survey (USGS) estimated the total undiscovered technically recoverable gas resource of the Appalachian Basin to be 70.2 Tcf (USGS, 2003). Only 2 Tcf of this undiscovered resource was believed to exist in the Marcellus shale, a volume that has been exceeded by total cumulative Marcellus production to date. The rapid expansion of Marcellus production, which followed the expanded application of technological advancements in horizontal well drilling and hydraulic fracturing, prompted a re-evaluation of Marcellus resources by the USGS and others. In 2011, the USGS revised its Marcellus resource assessment upward to 84 Tcf (Mean) undiscovered technically recoverable resources (USGS, 2011).[2] **Table 1** compares several recent resource assessments for the Marcellus. In most cases, the most recent Marcellus resource assessment represents a significant increase in undiscovered resources compared to the previous assessment. For example, the 2012 Potential Gas Committee assessment of undiscovered technically recoverable gas shale resources for the Appalachian Basin rose to 563 Tcf, representing a 148 percent increase from their 2010 assessment (PGC, 2013). The Pennsylvania State University Marcellus Outreach and Research

[2] USGS 2011 assessment of Marcellus undiscovered resources ranges from 42.9 Tcf (95 percent probability) to 144.1 Tcf (5 percent probability). 84 Tcf represents the mean case.

Center estimates 1,500 Tcf of gas-in-place for the Marcellus in Pennsylvania, of which nearly 500 Tcf is estimated to technically recoverable (Engelder, 2012).

## c. Sources of $CO_2$ Emissions

The Appalachian Basin encompasses all or a portion of nine states: Indiana, Kentucky, Maryland, Michigan, New Jersey, New York, Ohio, Pennsylvania, and West Virginia. This region generates approximately 30 percent of all U.S. electricity and 80 percent of the $CO_2$ emissions in the region are related to power generation. (DOE/NETL, 2012) In total, approximately 670 million metric tons (740 million tons) of $CO_2$ are emitted each year from these stationary sources. Emissions are highest along the Ohio River Valley and coastlines, where many power plants and industries are located. (Maps of $CO_2$ emissions in the Appalachian Basin region may be found in the United States' Department of Energy *2012 Carbon Utilization and Storage Atlas,* online at: http://www.netl.doe.gov/technologies/carbon_seq/refshelf/atlasIV/Atlas-IV-2012.pdf.)

## d. Potential Alternative Storage Horizons

In addition to hydraulically fractured organic-rich shales for long-term $CO_2$ storage, the Appalachian Basin contains several geologic targets that are potential candidate for $CO_2$ storage (DOE/NETL, 1999; 2004; 2005; Wickstrom, 2005). These include: (1) deep saline aquifers, (2) mature oil and gas fields, and (3) deep unmineable coal seams (DOE/NETL, 2012). Potential storage capacity ranges from 28 to 90 million metric tons of $CO_2$ in these targets in the onshore, with the potential of 164 to 658 billion metric tons more in offshore formations.

# 3. GEOLOGIC CHARACTERIZATION

Several organic-rich black shale formations occur in the Appalachian Basin, ranging in age from the late Ordovician through the middle to late Devonian. Devonian age shale formations such as the Ohio, Huron and Rhinestreet have long been development targets. The middle Devonian Marcellus shale is more widespread than the Ohio-Rhinestreet shale plays. The Marcellus shale is deeper, over-pressured in some areas, and extends farther east into areas with little or no previous drilling and gas production, thus offering a very large natural gas resource and extensive $CO_2$ storage potential.

Geological characterization of the Marcellus shale for this report builds upon the previous work by the United States Geological Survey (see Roen and Kepferle, eds., 1993), state geological surveys (see Avary and Patchen, 2008; Harper, 2008; Ohio Geological Survey; 1982 to present), the New York State Museum (see Smith and Leone, 2010a, b) as well as industry data and analyses that are becoming increasingly available (see Wrightstone, 2009 and Zagorski, et al, 2011).

For this report, methane gas in-place is estimated for the Marcellus from analysis of public well logs and other petrophysical data. Theoretical maximum $CO_2$ storage capacity for the Marcellus is estimated using $CO_2$ isotherms for the Marcellus obtained from a recent well in New York. Model areas are identified and a composite model well is characterized for each model area. Various model well parameters provide input for the Marcellus reservoir simulation using *COMET3*. Reservoir simulation will examine potential cumulative gas production, $CO_2$ storage, and enhanced gas recovery under various reservoir quality scenarios.

## a. Geologic Setting

The Marcellus Shale is Devonian aged black shale that extends throughout the Appalachian Basin from New York State into Kentucky (**Figure 1**). The Marcellus was deposited in a shallow continental sea basin in proto-north America associated with mid-phase building of the Appalachian Mountains. Basin subsidence and subsequent burial brought the Marcellus formation into the oil window, where the shales reached thermal maturity and generated hydrocarbons.

The Appalachian Basin developed in proto-north America in direct response to three episodes of mountain building that elevated the Appalachian Mountains (Faill, 1999; Quinlan & Beaumont, 1984). The thickening of Earth's crust by mountain building formed a depression called a foreland basin directly adjacent and parallel to the mountain chain (Ver Straeten and others, 2011; Dickinson, 1974; Allen et al., 1986; Klein, 1991; Castle, 2001). The basin was covered by a relatively shallow continental sea which was bounded to the north, east and west except for a small ocean access in the southwest (Ettensohn and Barron, 1981). Establishment of the Appalachian foreland basin initiated in the Ordovician during the early stages of the

mountain building sequence, and continued to grow through the Early Permian after mountain building had ceased (Faill, 1997). Erosion of the uplifted mountains provided the sedimentary input that filled the shallow continental sea basin with a thick succession of sedimentary rocks.

The Appalachian basin is host to several unique black-shale formations, including the Ohio Shale, Rhinestreet, Huron and Marcellus shales. Black shales are organic-rich shales consisting of silt- and clay-sized mineral grains that accumulate with organic matter (Swanson, 1961), and are considered to be a major primary source of hydrocarbon generation (Klemme and Ulmishek, 1991). The contribution and preservation of organic matter in marine sediments occurs when marine organisms die and settle on the basin floor in an oxygen- depleted environment. Aerobic decay is inhibited, allowing for the incorporation of organic material into sediments. The genesis of black shales is controlled primarily by sedimentation rates, high organic productivity, and the intensity of oxidation (Tourtelot, 1979; Suess, 1980; Emerson, 1985; Arthur and Sageman, 1994). While the depositional setting may vary, it is essential that the environment of deposition be anoxic to preserve organic matter for burial (Schieber, 2003; Arthur and Sageman, 2004).

Deposition of the Marcellus Shale occurred during two major transgressive-regressive depositional sequences (Griffing and Ver Straeten, 1991; Ver Straeten and others, 2011; Ettensohn and Barron, 1981; Ettensohn, 1998). Abundant marine life was nurtured in the shallow continental sea environment, and the remains of organisms descended to the basin floor after death (Ettensohn and Barron, 1981; Ettensohn, 1998). The organic enriched mud was preserved by the prevailing anoxic conditions. Rapid relative sea-level rise and restricted hydrologic conditions are thought to have been the major controls on oxygen depletion in the basin (Arthur and Sageman, 2004). Deltaic progradation in the upper Devonian transported an influx of clastic sediment that buried the Marcellus (Faill, 1999; Ettensohn, 1985a, 1985b). The sediment supply was fairly continuous until the final mountain building phase in the Early Permian interrupted deposition (Faill, 1997; Engelder and Lash, 2008). The associated tectonism caused the final stage of subsidence and greatly altered the basin structure (Quinlan and Beaumont, 1984; Faill, 1997).

The thermal maturation of hydrocarbons in the Devonian shale formations likely peaked between the Late Pennsylvanian and the Early Triassic, when the greatest depths in the basin where achieved (Ryder, no date; Rowan, 2006). Vitrinite reflectance data indicates high thermal maturation of the Marcellus shale, however thermal maturity varies regionally within the basin (Repetski and others, 2008; Rowan, 2006).

## b. Stratigraphy

The Marcellus shale is the lowermost formation of the Middle Devonian age Hamilton Group. The names “Marcellus Formation” and “Marcellus Shale” are often used interchangeably, although commonly the name ”Marcellus Shale” refers to the most organic-rich zones, the black shale, at the base of the Marcellus Formation. **Figure 10** is a simplified stratigraphic correlation chart for New York, Pennsylvania, West Virginia and Ohio showing the location of the Marcellus black shale above the top of the Onondaga limestone and equivalent formations (Smith, 2010; Wrightstone, 2009; Zagorski, 2011). The names and subdivisions of the Marcellus shale change across the study area, as indicated by **Figure 10**, which shows three divisions of the Marcellus Formation in New York. These include the Union Springs (lowermost member), Cherry Valley limestone (middle), and the Oatka Creek (upper member), which may be divided into the lower Oatka Creek black shale and the upper Oatka Creek gray shale. The Union Springs and Oatka Creek black shales have been the traditional target reservoirs for Marcellus gas production in New York. In New York’s southern tier counties, the Cherry Valley limestone is interbedded with thin shales, which appear on well logs to be organic-rich, comparable in density and gamma ray response to the Oatka Creek and Union Springs black shales. In some areas, the Cherry Valley appears likely to contribute to gas in-place and $CO_2$ storage capacity for the Marcellus.

In Pennsylvania, the middle Marcellus interval of interbedded carbonate and shale is called either the Purcell and/or the Cherry Valley limestone. The lowermost Marcellus unit below the Purcell/ Cherry Valley is commonly called the “Lower Marcellus”. The Marcellus unit immediately above the Cherry Valley is simply called the “Upper Marcellus”. In northern Pennsylvania the “Upper” Marcellus may be further divided into Marcellus “gray shale” and more organic-rich “Upper Marcellus shale” (see Wrightstone, 2009). In western West Virginia and eastern Ohio, **Figure 10** shows that upper and lower Marcellus zones can no longer be distinguished, and the entire high-gamma ray, organic-rich shale at the base of the Hamilton Group is simply called “Marcellus Shale”.

The Pennsylvania naming conventions for subdivisions of the Marcellus are applied in this report. The Marcellus subdivisions for this report include the “Lower Marcellus” (corresponding generally to the Union Springs in New York); the “Purcell/ Cherry Valley” limestone; and the “Upper Marcellus” (corresponding generally to the Oatka Creek shale in New York). Log calculations were made separately for the Lower Marcellus, Purcell/ Cherry Valley, and Upper Marcellus units.

The stratigraphic position of the Marcellus is immediately above the top of the Onondaga limestone in New York and facies-equivalent formations in Pennsylvania and West Virginia.[3] The depositional environment for the Marcellus and other organic-rich Devonian black shales has been reinterpreted by the New York State Museum (Smith, 2010) as shallow water marine (water depths less than 100 feet) in a foreland basin. Subaerially exposed land to the west was onlapped by a marine basin, which was undergoing active subsidence and deepening to east. Other Middle Devonian black shales similarly onlap and pinch out against limestones and subaerial unconformities to the west (Smith, 2010). This concept is illustrated in **Figure 11**, which is a schematic regional cross-section of the Marcellus created by the New York State Museum Reservoir Characterization Group to show the on-lapping relationships of the Marcellus and other middle Devonian black shales against a tectonic high to the west. The landward, shallow part of the marine basins accumulated the greatest amount of organic material, which became progressively diluted in deeper water due to the influx of siliciclastics and organic-lean mudstones from uplifted areas to the east. Restricted marine circulation and oxygen-depleted conditions apparently prevailed for long durations in the landward areas of the marine basins, allowing for the preservation of organic material in relatively shallow water (Smith, 2010).

## c. Marcellus Study Area

Previous geologic work by the USGS, USDOE, state geological surveys, and industry have characterized trends in thickness, total organic carbon content (TOC) , thermal maturity and reservoir pressure gradient for the Marcellus shale. These Marcellus trends are summarized on the maps provided in **Figure 1**, showing depth to the Marcellus, thickness, reservoir pressure trends, and in **Figure 12**, showing Marcellus thermal maturity trends. The depth of the top of the organic-rich lower Marcellus increases to the south and southwest to more than 8,500 feet The net thickness of organic rich Marcellus ranges from less than 20 feet in western New York, western Pennsylvania and southeastern Ohio to approximately 250 feet in northeastern Pennsylvania. Thermal maturity of the Marcellus shale, as indicated by calculated vitrinite reflectance, Ro, increases to the east and southeast with increasing depth and net thickness. A dotted line on **Figure 12** indicates calculated vitrinite reflectance, Ro, of 1.5 percent, the apparent 'dry gas window' boundary for the Marcellus. Marcellus thermal maturity increases with depth to as much as 4.0 percent Ro (Smith and Leone, 2010a).

Various criteria have been proposed for identifying the most prospective areas for Marcellus exploration. Such criteria variously include a combination of reservoir depth and net

[3] In Pennsylvania and West Virginia the Marcellus is interpreted as conformable with the underlying Onesquethaw Group, which consists of the Onondaga Limestone, Huntersville Chert and Needmore Shale (calcitic shale). The Onondaga Limestone, Huntersville Chert and Needmore Shale underlying the Marcellus are facies equivalent; the facies grading generally west to east from limestone in the western and central portions of the basin to chert and shale in the east (Wrightstone, 2009).

thickness, thermal maturity, organic carbon content, reservoir pressure, natural fracture intensity, and upper and lower boundary zones for hydraulic fracturing. For example, the New York State Museum defines an exploration fairway for the Marcellus shale in New York that has at least 50 feet net thickness of organic-rich shale (defined as TOC greater than approximately 1.5 – 2.0 percent); thermal maturity of the Marcellus in the gas generation window as indicated by calculated vitrinite reflectance of least 1.1 percent Ro; and subsurface depth of 3,000 feet or greater to protect potential potable aquifers (Smith and Leone, 2010b). To maximize potential $CO_2$ storage, 2,500 feet to 3,000-feet depth requirement also represents an approximate miscibility boundary for $CO_2$. Below this depth, reservoir pressure is expected to be adequate for injection of $CO_2$ as a dense, miscible fluid, thereby increasing the efficiency of enhanced gas recovery (EGR) and $CO_2$ storage.

**Figure 13** shows the study area outline, the locations of 149 digital study wells used for this analysis, and subdivisions of the study area for the purpose of reservoir simulation. The Marcellus Shale study area boundary is defined by minimum depth to the Marcellus of approximately 3,000 feet and thermal maturity of at least 1 percent calculated Ro indicating that the thermal maturity of the Marcellus shale is in the gas window. The total study area in **Figure 13** is 26,415,006 acres or 41,274 square miles.

The well data set is compiled from public log data obtained through the New York, Pennsylvania, West Virginia and Ohio geological surveys. Digital log data (LAS) files are not available from public data sources for many wells, so the raster logs available for these wells were digitized. All study wells contain at least a gamma ray log through the Marcellus, from which TOC can be extrapolated and adsorbed gas in-place estimated. Sixty-seven study wells have a complete log suite consisting of gamma-ray, density and resistivity through the Marcellus. This subset of wells is used for calculating free methane gas in-place and estimating maximum $CO_2$ storage capacity as non-adsorbed ('free') $CO_2$.

## d. Type Log and Stratigraphic Cross-Sections

**Figure 14** is a type log of the Marcellus from north central Pennsylvania showing the gamma-ray, resistivity, photoelectric (PE) log, bulk density, and density and neutron porosity logs. The bulk density curve is shaded in light blue where it indicates bulk density less than 2.5 gm/cc. The Marcellus was subdivided into three layers for the purpose of reservoir simulation: the Lower Marcellus (Union Springs), the Purcell/ Cherry Valley and the Upper Marcellus (Oatka Creek). In New York, the Oatka Creek may be further divided into the Oatka Creek "black shale" at the base and the Oatka Creek "grey shale". These subdivisions are illustrated in **Figure 14**; however for the reservoir simulation, the upper Marcellus above the Purcell/ Cherry Valley is treated as single model layer.

In some areas of the basin, the top of the Marcellus can be difficult to distinguish on well logs from the overlying Devonian shale. In western West Virginia and eastern Ohio, for

example, the top of the Marcellus can be difficult to distinguish from the base of the overlying Rhinestreet shale. For this analysis, the top of the Marcellus is generally picked below the Stafford limestone (or apparent equivalent) at the first indication of elevated porosity (indicated by bulk density less than 2.6 grams per cubic centimeter (g/cc) and/or apparent high organic content as indicated by elevated gamma ray (greater than 200 API units). Because the focus of this study is potential $CO_2$ storage in shale, the Marcellus top is picked to reasonably include as much favorable shale section as possible (based on the gamma ray and density logs). In areas where the top of the Marcellus appears to be ambiguous on logs, this approach may, in fact, include some of the overlying Devonian Shale formations such as the Skaneateles or the Mahantango shales.

**Figure 15** shows the location of three stratigraphic cross-sections.[4] The cross-sections are provided as **Figures 16, 17** and **18.** The stratigraphic cross-sections are flattened on the Upper Marcellus to show stratigraphic relationships within the Marcellus, and to better illustrate the facies relationship of the Marcellus black shale and the Onondaga limestone and equivalents. The logs displayed on the cross-sections are representative of the various model areas identified for reservoir simulation. The corresponding Marcellus model area(s) are indicated at the base of the log.

The cross-sections are derived from the data base of digital study wells and include digital log curves, as well as calculated density porosity and water saturation. The gamma ray curve is displayed in Track 1 on a scale of 0 to 500 API units. Gamma ray log values less than 50 API units are shaded in light blue. The caliper log is displayed in Track 1 on a scale of 6 to 16 inches. The deep-reading resistivity curve is displayed as a red dash line in Track 2 on a 4-k cycle logarithmic scale of 1 ohm-m to 10,000 ohm-m. TOC extrapolated from bulk density is displayed in Track 2 on a linear scale of 0 to 10 weight percent. TOC greater than 5 percent is shaded in gray. If the photoelectric factor curve (PE) is available that is also displayed in Track 2 on a linear scale of 0 to 5 barns/$cm^3$, with values in the vicinity of "5" indicative of limestone In Track 3; bulk density is displayed with a black dash curve and bulk density values less than 2.5 are shaded in green. The neutron porosity curve is displayed in red on Track 3. Neutron porosity is not corrected for lithology so will read high porosity values in shale. Computed density porosity is displayed in blue in Track 3. Density porosity is corrected for TOC content and lithology; the density porosity curve displayed in Track 3 is total porosity. Track 4 displays a computed fractional water saturation curve. The water saturation computation uses the Simandoux (1963) modification of the Archie water saturation algorithm. Calculated water saturation curve values less than 0.25 are shaded in light red. Calculated water saturation values between 0.5 and 0.75 are shaded in medium blue and water saturation values greater than 0.75 are shaded in dark blue.

[4] Note that the cross-sections are sized for 11x17 landscape page.

# 4. RESERVOIR DATA

This section summarizes various data used in the evaluation of gas in-place and $CO_2$ storage capacity. Marcellus core data obtained from the NYSM include TOC, core porosity and permeability, x-ray diffraction mineralogy, gas content from canister desorption tests, methane adsorption isotherms, and mechanical properties. Sidewall core samples from a well in Otsego County, New York were donated to the project as cost share contribution to obtain new methane and $CO_2$ adsorption isotherm data, as well as porosity, permeability, TOC, and mineralogy data. X-ray diffraction mineralogy data for the Marcellus are used to extrapolate a characteristic grain density for non-organic reservoir matrix. Using the available data plus cross-plots of bulk density and TOC from the cored wells, bulk density cut-off values are applied to identify zones with apparent high organic carbon content.

## a. Adsorption Isotherms

Methane and $CO_2$ adsorption isotherms for the Marcellus are available from three New York wells, a proprietary well in north central Pennsylvania, and a proprietary well in Washington County, Ohio. Methane isotherm data are available from the New York State Museum for the Beaver Meadows #1 and Oxford #1 wells in Chenango County. Methane isotherms for the Marcellus from the Ross #1 well in Otsego County were made available to the project courtesy of Gastem USA, Inc. The New York State Energy Research and Development Authority (NYSERDA) acquired $CO_2$ isotherm data for the Marcellus from the Ross #1 well. The Marcellus isotherm data are shown in **Figure 19.** **Table 2** summarizes the Marcellus adsorption isotherm data including TOC content of the samples and the Langmuir parameters. **Figure 20** and **Figure 21** are cross-plots of Langmuir volume and TOC for the methane (Figure 20) and $CO_2$ (Figure 21) isotherms.

## b. Total Organic Carbon

Total organic carbon measurements were available from the NYSM for the Marcellus cores from the Beaver Meadows #1 and Oxford #1 wells in Chenango County and for drill cuttings from various wells throughout the state. **Figure 22** is a cross-plot of TOC and bulk density from the whole core data, which shows that TOC of 3 percent corresponds to bulk density of approximately 2.625 g/cc. TOC was also extrapolated based on the correlation between TOC measured from Marcellus drill cuttings in New York wells and corresponding bulk density and gamma ray log readings.[5] These correlations are shown in **Figures 23** and **24**. In **Figure 23**, cuttings samples with average of TOC of 3 percent corresponds to log bulk density

[5] Marcellus TOC data provided by James Leone, New York State Museum Reservoir Characterization Group (NYSM), for the New York State Energy Research and Development Authority (NYSERDA) Contract No. 105000, *Geologic, Engineering and Economic Evaluation of the $CO_2$ Sequestration Capacity of New York's Gas Shales*.

of approximately 2.60 g/cc. **Figure 24** shows significant scatter in the correlation between gamma ray and TOC from cuttings; the density log is clearly a better choice for estimating TOC. However, when no density log is available, the gamma ray correlation in **Figure 24**, may provide a reasonable estimate of TOC, especially for the Lower Marcellus/ Union Springs.

## c. X-Ray Diffraction Mineralogy

X-ray diffraction mineralogy data are available from the NYSM for 21 Marcellus samples from the Beaver Meadows #1 and Oxford #1 cores in Chenango County. Two industry operators provided proprietary x-ray diffraction mineralogy data from two wells in northern Pennsylvania and two wells in southeast Ohio. **Table 3** shows average Marcellus x-ray diffraction mineralogy from these data. Mineralogy data for the Union Springs and Oatka Creek black shale samples were averaged to determine a characteristic mineralogy for Marcellus black shale, and to extrapolate matrix grain density that reflect the complex mineralogy . Dominant clay minerals in the Marcellus (not indicated in **Table 3**) are illite, illite-smectite, and chlorite.

## d. Core Permeability

Marcellus core porosity and permeability data were made available to the project from two proprietary wells in northwest Pennsylvania. **Figure 25** shows the correlation of crushed sample pulse decay permeability to total core porosity from these data. Crushed sample pulse decay permeability is unconfined permeability to air. The porosity- permeability relationship in **Figure 25** was used to extrapolate matrix permeability from calculated total porosity for use in the reservoir simulations.

# 5. ESTIMATED GAS IN-PLACE AND THEORETICAL MAXIMUM $CO_2$ STORAGE CAPACITY

## a. Overview of Calculated Gas In-Place and $CO_2$ Storage Capacity

Methane gas-in place is calculated from the digital well logs available for the study wells. The estimate of theoretical maximum $CO_2$ storage capacity is based on calculated gas in-place by assuming that 100 percent the methane in-place, either as adsorbed or "free" gas is replaced in the reservoir by injected $CO_2$. The net stored volume of injected $CO_2$ will be very small fraction of theoretical maximum capacity values. Reservoir simulation will provide a first approximation of what actual gas recovery factors and net volumes of injected $CO_2$ are likely to be for the Marcellus. The simulation results will provide an initial basis for planning future research and policy directions, and can be refined as more production data become available in the future and $CO_2$ injection tests are initiated.

Methane gas in-place for the Marcellus shale is assumed to have two components: 1) methane adsorbed on organic matter contained in the shale; and 2) non-adsorbed methane, or free gas, contained within void space in the shale. Such voids could include micro-fracture porosity; intergranular porosity between clastic grains and particles; dissolution seams; voids within the framework of component minerals; and microporosity commonly observed within the kerogen of thermally-mature, organic–rich shale (intra-kerogen porosity). Estimating gas in-place thus requires two steps to calculate the quantity of adsorbed gas and the quantity of free (non-adsorbed) gas. Similarly, $CO_2$ storage capacity is assumed to have two components: storage of an adsorbed $CO_2$ phase displacing methane, and storage of non-adsorbed $CO_2$ replacing methane in the gas-filled pore space, or "effective" porosity.

Digital logs for the study wells were used to calculate the following attributes for the Marcellus:

- Vertical thickness
- Total organic carbon, TOC
- Adsorbed gas content
- Adsorbed gas in-place
- Theoretical maximum $CO_2$ storage capacity by adsorption
- Total porosity
- Water saturation
- Effective (gas-filled) pore volume
- Estimated 'free' (non-adsorbed) methane gas in-place
- Theoretical maximum $CO_2$ storage capacity as 'free' $CO_2$ (non-adsorbed)

The log calculations were made using IHS Petra software. The adsorbed component of gas in-place and maximum $CO_2$ storage capacity were calculated for the adsorbed component using available methane and $CO_2$ adsorption isotherms. A volumetric approach was used to estimate non-adsorbed gas in-place within effective (gas-filled) porosity. The end result of the log calculations are estimates of total methane gas-in place in billion cubic feet per acre (Bcf/ac) for the Marcellus, and theoretical maximum $CO_2$ storage capacity including an adsorbed component and non-adsorbed component. Units of Bcf/ac were selected for ease of scaling the calculated results to estimate gas resource in-place or $CO_2$ storage capacity for any well spacing of interest, such as 40 or 80 acres, and for ease of converting to units of Bcf/sqare mile.

Maps were created for the various calculated Marcellus attributes including thickness, TOC, total and effective porosity, adsorbed and non-adsorbed ('free') methane gas in-place, and theoretical maximum $CO_2$ storage capacity as adsorbed and non-adsorbed. Example maps are included in the **Appendix** of this volume. Using these mapped values and calculations made for individual study wells, the Marcellus study area was subdivided into smaller "model areas". Each model area is represented by a model well, which is a composite of the calculated input parameters for the study wells within the model area. In most cases, the value for a model well parameters such as TOC, porosity, or water saturation is the average of all calculated values for the wells within the model area. In other cases, a single calculated value was selected as the parameter value for the model well because that single value appeared to best represent the model area – contributing to the best match of simulated model well gas production and historical Marcellus production for the model area. The methodology for log analysis and calculation of gas in-place is discussed in the following section. The model well attributes that were provided as inputs to the reservoir simulation are discussed in the next chapter.

## b. Well Log Analysis Methodology

### i. TOC Extrapolated from Density or Gamma Ray Logs

TOC was extrapolated three ways, and the results from each method were compared. TOC was extrapolated from the bulk density log using the method developed by Schmoker (1993, 1979) for Devonian shale of the western Appalachian Basin:

$$TOC_{calculated} = 55.822 *((\rho_{Shale}/\rho_{log})-1)$$

Where, $\rho_{Shale}$ = maximum bulk density of gray shale (low organic content) and $\rho_{log}$ = bulk density reading from the log. TOC was also extrapolated based on the correlation between TOC measured from Marcellus drill cuttings in New York wells and the corresponding bulk density and gamma ray log readings. **Table 4** compares average TOC estimated from each method for five wells in northern Pennsylvania, and shows that TOC values extrapolated from bulk density are very close for the two methods. TOC extrapolated from the gamma ray log deviated

from the density log methods. TOC calculated based on the correlation of bulk density to TOC measured from Marcellus drill cuttings was selected as the preferred extrapolation approach for this analysis. If no density log was available, TOC was extrapolated from the gamma ray log and used for further log analysis only if the results seemed reasonable compared to nearby data.

### ii. Porosity from Density Logs

Density porosity ($\phi_{density}$) corrected for TOC is calculated from bulk density using the following relationship:

$$\rho_{log} = \rho_{matrix}(1 - \phi_{density} - TOC_{calculated}) + \rho_{fluid}(\phi_{density}) + \rho_{TOC}(TOC_{calculated})$$

Where, $\rho_{matrix}$ = matrix grain density determined from x-ray diffraction mineralogy or whole core analysis; $\rho_{fluid}$ = density of formation water; $\rho_{TOC}$ = density of organic matter; and $\rho_{log}$ = bulk density reading from the log. The equation is rearranged to solve for porosity, as follows:

$$\phi_{density} = \{\rho_{matrix} - [\rho_{log} \; x \; (((\rho_{matrix} \; x \; TOC_{calculated})/ \rho_{TOC}) - TOC_{calculated} + 1)]\} / (\rho_{matrix} - \rho_{fluid})$$

### iii. Adsorbed Gas Content and Theoretical Maximum Adsorbed $CO_2$ Capacity

Adsorbed methane and $CO_2$ in units of standard cubic foot per ton (scf/ton) are calculated using Langmuir coefficients from the available isotherm data for the Marcellus and extrapolated reservoir pressure based on depth. A reservoir pressure gradient is assigned to each study well estimated from the map of Marcellus shale regional pressure trends published by Zagorski, et al., (2011). In this way, the Marcellus overpressured areas are incorporated into the calculations of adsorbed gas in-place and potential $CO_2$ storage.

Relevant Marcellus isotherm data are summarized in **Table 2.** Adsorbed gas content or theoretical adsorbed $CO_2$ content were calculated using the following algorithm:

$$V_{adsorbed} = (V_L \; x \; P_{res})/(P_L + P_{res})$$

Where, $V_{adsorbed}$ = adsorbed gas content; volume of adsorbed gas at a reservoir pressure, $P_{res}$; $V_L$ = Langmuir volume from adsorption isotherm; $P_L$ =average Langmuir pressure from adsorption isotherm data

For each Marcellus study well, Langmuir volume was extrapolated from calculated TOC. **Figure 20** shows the correlation of Langmuir volume to TOC for the Marcellus methane isotherms; **Figure 21** shows the relationship of Langmuir volume to TOC for Marcellus $CO_2$ isotherms. The average Langmuir pressure in **Table 2** was used as $P_L$. Reservoir temperature and pressure curves were created for each study well by applying a temperature and pressure

gradient to the true vertical log depth. If a temperature log was available for the Marcellus interval, the temperature log data were used instead of a calculated reservoir temperature. Applying the data shown in **Table 2**, **Figure 20** and **Figure 21**, the algorithms for calculating adsorbed gas content (scf/ ton) are the following:

$$V_{L\_CH4} = 22.1 \; x \; \text{TOC (wt. \%)}, \quad \text{and:}$$

$$\text{Adsorbed}_{CH4} = ((22.1 \text{ x TOC}) \; x \; P_{res})/(678.1 \text{ psia } x \; P_{res})$$

For theoretical adsorbed $CO_2$ content in the Marcellus, the algorithms are the following:

$$V_{L\_CO2} = 66.9 \; x \; \text{TOC (wt. \%)} \quad \text{so,}$$

$$\text{Adsorbed}_{CO2} = ((66.9 \text{ x TOC}) \; x \; P_{res})/(246.8 \text{ psia } x \; P_{res})$$

Adsorbed methane in-place or $CO_2$ in-place (scf/acre) is computed by multiplying the adsorbed gas content (scf/ton) obtained from the previous step by an estimated quantity of shale (tons/acre):

Tons shale = (thickness *x* area *x* shale density *x* conversion factor (g/cc to tons/acre-ft.))

This then results in:

Adsorbed Gas (or $CO_2$), M/ac. = (h x area x bulk density x Adsorbed gas content (scf/ton) x 1359.7)/ (1 x 103)

For each study well, tons of shale were computed for each acre-foot of reservoir thickness and multiplied by the computed curve of adsorbed gas content in scf/ton. This provided computed log curves for each study well of adsorbed methane in-place (Mcf/acre-ft.) and maximum adsorbed $CO_2$. The final step summed the calculated curves for each study well and converted the units to Bcf/sq. mile, yielding total adsorbed methane gas in-place and theoretical maximum adsorbed $CO_2$ storage capacity for each well.

### iv. Free Gas In-Place and Theoretical Maximum $CO_2$ Storage Capacity

Free gas in-place was estimated by computing an effective (gas-filled) porosity:

$$\phi_{effective} = \phi_{density} \; x \; (1 - S_w)$$

Where, $S_w$ = calculated water saturation (fraction). All water saturation is assumed to be immobile as bound water. Effective, or gas-filled, porosity is assumed to be the fraction of total porosity not occupied by water. Water saturation is calculated using the Simandoux modification of the Archie equation for shaley sandstones (Simandoux, 1963 in Asquith and Krygowski, 2004):

$$S_w = ((0.4 \; x \; R_w)/\phi^m) \; x \; \{[(V_{shale} / R_{shale})^2 + ( (5 \; x \; \phi^m)/(R_t \; x \; R_w))]^{1/n} - (V_{shale}/ R_{shale})\}$$

Where, $S_w$ = water saturation; $R_w$ = water resistivity at formation temperature; $\phi$ = porosity; m = Archie cementation exponent (common default = '2'); $V_{shale}$ = shale content; $R_{shale}$ = resistivity of the shale; $R_t$ = deep resistivity log reading; n = Archie saturation exponent. **Table 5** summarizes the variables used for calculating density porosity and water saturation.

For this analysis, a three-part linear solution to the Simandoux equation published by Crain (1986) was implemented in PETRA[6] to calculate a water saturation curve for each study well. Shale volume ($V_{shale}$) was computed from the gamma ray log. A linear shale index approach produced the most consistent results compared to other published methods for estimating shale volume from the gamma ray log:

$$V_{shale} = (GR_{log\ reading} - GR_{non\text{-}shale}) / (GR_{shale} - GR_{non\text{-}shale})$$

An effective (gas-filled) porosity curve was calculated for the Marcellus in each study well for the total reservoir thickness. Cross-plots of core porosity and permeability data from the Gastem Ross #1 well in Otsego County, NY were used to estimate a 'pay' cut-off of 3 percent effective porosity. This porosity cut-off establishes the net reservoir thickness for calculating both free methane gas in-place and maximum $CO_2$ storage capacity, non-adsorbed.

The total thickness of these porous zones constitutes the net reservoir thickness (the 'effective' reservoir thickness) for calculating free methane gas in-place. The volume of free gas in-place for each acre-foot of net reservoir thickness was computed:

$$\text{Free methane gas-in-place} = (43560 \times \phi_{effective}) / Bg_{CH4}$$

Where, $Bg_{CH4}$ (rcf/scf) = the appropriate formation volume factor for methane computed for each study well based on depth and extrapolated reservoir temperature and pressure. The result was a computed curve yielding for each study well free (non-adsorbed) methane gas in-place in units of Bcf per acre-ft. A final step summed the calculated curves for each study well and converted the units to Bcf/ac, yielding total non-adsorbed methane gas in-place for each well.

### v. Theoretical Maximum $CO_2$ Storage as 'Free' $CO_2$ (Non-Adsorbed)

The maximum capacity for $CO_2$ storage as 'free' gas (non-adsorbed $CO_2$) is estimated by assuming that all calculated methane gas in-place as 'free' gas is replaced by $CO_2$. Methane gas must be removed from the reservoir by production to make reservoir volume available for injected $CO_2$. The methane recovery factors for the Marcellus and Utica are unknown but are certain to be significantly less than 100 percent, hence computed $CO_2$ storage capacity as 'free', non-adsorbed $CO_2$ is a theoretical maximum.

[6] http://www.ihs.com/products/oil-gas-information/analysis-software/petra.aspx?tid=t6&ocid=pc468:energy:ppc:0001&gasc_id=1036335105&gasc_label=yESWCPW1wAQQgfCU7gM&gclid=CO_KpumD1bgCFVOe4Aoda0UAWg

Maximum $CO_2$ storage capacity as non-adsorbed $CO_2$ was computed for each acre-foot of net reservoir thickness by substituting the appropriate formation volume factor for $CO_2$ ($Bg_{CO2}$) at the extrapolated reservoir pressure and temperature for the depth. Similar to free methane gas in-place, the result was a computed log curve for each study well yielding non-adsorbed $CO_2$ replacing free methane gas in-place in units of Bcf per acre-ft. A final step summed the calculated curves for each study well and converted the units to Bcf/ac, yielding the theoretical maximum $CO_2$ storage capacity as free $CO_2$ for each well. Total maximum $CO_2$ storage capacity includes the theoretical maximum $CO_2$ storage capacity as 'free' $CO_2$, as well as the maximum $CO_2$ storage capacity as adsorbed $CO_2$.

## c. Marcellus Log Calculation Results

The individual well log analyses yielded various calculated reservoir values for the Marcellus, which were mapped to identify apparent variation in reservoir characteristics across the study area. Maps of calculated values were used to select model areas for reservoir simulation and representative study wells within each model area. Selected maps of calculated values are included in the **Appendix** of this volume. **Table 6** provides a description and summary of the Marcellus model areas. Model layer attribute tables were also prepared for each of the reservoir model layers – the Upper Marcellus/ Oatka Creek, the Purcell/ Cherry Valley and the Lower Marcellus/ Union Springs. **Tables 7, 8** and **9** summarize the model layer attributes that were incorporated into the reservoir simulation.

## d. Total Gas in-Place and $CO_2$ Storage Capacity

**Table 10** summarizes the estimated Marcellus gas in-place by model area, as well as for the total study area. The total Marcellus study area is 41,274 square miles, or 26,415,006 acres. Total Marcellus gas in-place is estimated to be 1,299 trillion cubic feet (Tcf), of which 562,509 Bcf is estimated to be adsorbed gas in-place and 736,407 Bcf is estimated to be free (non-adsorbed) gas in-place. Over the entire study area, the concentration of total Marcellus gas in-place ranges from 8.2 Bcf/mile$^2$ in Area 9 (south and south central West Virginia) to 64.6 Bcf/mile$^2$ in Area 4 (northeastern Pennsylvania where the Marcellus is thick and over-pressured). Averaged over the entire study area, Marcellus gas in-place is estimated to be 31.4 Bcf/ mile$^2$**,** with 13.6 Bcf/ mile$^2$ adsorbed gas in-place and 17.8 Bcf/mile$^2$ free gas in-place.

**Table 11** summarizes the theoretical maximum $CO_2$ storage capacity by model area, which assumes that all adsorbed and 'free' gas is replaced by injected $CO_2$. Actual $CO_2$ storage capacity in organic-rich shale is a fraction of the gas in-place volume, and strongly influenced by injection design and field operating parameters, reservoir production and depletion, in addition to intrinsic reservoir characteristics such as porosity, thickness, reservoir pressure and permeability. Theoretical maximum $CO_2$ storage capacity in the Marcellus for the entire study area is estimated to be 3,356 Tcf, approximately 2.6 times the total gas in-place. Maximum $CO_2$ storage as an adsorbed phase is estimated to be 1,935 Tcf and maximum $CO_2$ storage as a

"free" or non-adsorbed phase is estimated to be 1,420 Tcf. **Table 12** presents the same information aggregate by state.

### i. Caveats and Assumptions Regarding this Assessment

***Limited well data set.*** Publicly available digital log data is limited, especially for Pennsylvania. One hundred forty-nine wells provided the basis for this resource characterization, which is sparse data coverage for a study area of this size. In addition, not all wells had a full log suite consisting of gamma-ray, bulk density and resistivity. Some of the logs were affected by significant "wash out" in the Marcellus, possibly due to abundant natural fracturing. In such wells, the density log was often not useable across all or a portion of the Marcellus. Some wells only had a gamma ray-neutron log available. All log data were used to the extent possible, even if the log data set was incomplete.

***Limited data set of methane and $CO_2$ isotherms.*** Methane isotherms available to the project are from three Marcellus wells in New York and two wells in Pennsylvania. $CO_2$ isotherms for the Marcellus were available from a single well in New York.

***Single porosity algorithm applied.*** A single density-porosity algorithm was assumed to apply everywhere. For example, a single porosity algorithm was applied for both the Upper and Lower Marcellus throughout the entire Marcellus study area. Calculated density-porosity was corrected for organic content, but the correction may not be universally appropriate across the range of apparent organic carbon content, possibly over-correcting porosity for kerogen content in low-TOC zones.

***Simandoux water saturation algorithm with estimated Archie model parameters applied to the entire Marcellus.*** Similar to the porosity caveat, a single approach for calculation water saturation was applied to the entire Marcellus. Estimated and default Archie model parameters were used for saturation exponent, 'n', tortuosity exponent, 'a', and cementation factor, 'm', because no other data are available. Inputs to the Simandoux equation such as shale resistivity were estimated and applied uniformly across all sub-horizons throughout the study area. The Simandoux algorithm is expected to work best in zones where clay shale volume is in the range of 50 to 85 percent, defaulting to a pure Archie equation as clay shale volume approaches zero and possibly over-correcting (water saturation too low) when clay shale volume exceeds 80 to 90 percent. The input parameters selected appeared to produce the most consistent results over the widest area.

An operator in Pennsylvania and an operator in Ohio provided access to independent petrophysical evaluations of their Marcellus core, which allowed for comparison between the approach used for this project and a commercial petrophysical analysis of the Marcellus gas shale. In addition, a Schlumberger ELAN log representing an integrated petrophysical interpretation of the wireline logs for the EOG Resources Beaver Meadows #1 in Chenango

County, New York was available from the New York State Museum. All of these resources were used to compare and calibrate the analytical approach developed for this reservoir characterization.

***Immobile formation water assumed***. Calculated water saturation was assumed to be immobile, representing both clay-bound water and water immobilized by capillary forces in microporosity. Effective porosity was assumed to be equivalent to the gas-filled pore volume, which was computed by multiplying total porosity by (1- fractional water saturation) a computed petrophysical analysis of the EOG Resources Beaver Meadows #1 well in Chenango County, NY.

***Other Caveats.*** Recovery factors for adsorbed and free gas are likely different, but as a practical matter, it will likely be impossible to distinguish adsorbed gas and non-adsorbed gas in the production stream. For example, free gas contained within intra-kerogen microporosity might be expected to be produced along with desorbed gas. Intra-kerogen porosity is thought to be significant, especially in the high-TOC zones within the Lower Marcellus, so free gas might be an important component of total gas produced from the high TOC zones.

If sufficient injectivity can be introduced via natural and induced fractures, a component of injected $CO_2$ is expected to be stored as non-adsorbed $CO_2$ in microporosity. The percentage of pore volume occupied by free gas, which will become accessible to injected $CO_2$, is likely to be extremely small, although no data are available to make a quantitative estimate. In qualitative terms, sustained methane production from gas shale is expected to provide adsorption sites for $CO_2$, and sustained production of any free gas from intra-kerogen and intergranular porosity could provide additional pore volume for $CO_2$ storage in a non-adsorbed or free phase.

The effective or 'gas-filled' pore volume available for $CO_2$ storage may be very small compared to the actual effective pore volume drained by the production of free gas. Contributing factors might include reservoir compaction with gas withdrawal, and hysteresis effects on capillary entry pressure and relative permeability to $CO_2$. For future $CO_2$ storage, it may be important to estimate separate storage capacity factors for $CO_2$ storage as an adsorbed phase and $CO_2$ storage as a non-adsorbed, free phase.

# 6. DEFINITION OF MODEL AREAS FOR RESERVOIR MODELING IN THE BASIN

## a. Rational for the Development of Model Areas

Total gas in-place and $CO_2$ storage capacity were extrapolated from individual log calculations for selected study wells contained within the nine "model areas" indicated in **Figure 13**. The model areas are sub-divisions of the total Marcellus study area based on parameters such as depth and thickness of the Marcellus, reservoir pressure gradient, and computed TOC. For each model area, the average calculated gas in-place and storage capacity values per unit area are multiplied by the geographical area contained within the model area boundaries. Model area totals of Marcellus gas in-place and theoretical maximum $CO_2$ storage capacity were summed to determine totals of gas in-place and maximum $CO_2$ storage capacity by state. The model area totals are shown in **Tables 10** and **11**; the state totals are presented in **Table 12**, where the estimated $CO_2$ storage volumes are converted to units of million tonnes.

## b. Overview of Model Areas

The model areas in **Figure 13** are large, but are broadly distinguished based on differences in criteria such as the depth and thickness of the Marcellus, reservoir over-pressure and under-pressure, calculated TOC and adsorbed gas content, average effective (gas-filled) porosity and final calculated gas in-place. **Figure 26** summarizes the calculated gas in-place for each model area as a representative resource "concentration" expressed in units of Bcf/ 80 acres, which represents one eighth of the resource concentration expressed in units of Bcf/ mile$^2$. **Figure 27** shows the same map, but with the maximum $CO_2$ storage capacity of each model area converted to units of million tonnes/ 80 acres. These maps are intended to provide quick overviews of the gas potential and the maximum $CO_2$ storage capacity for typical spacing units in the model areas. The model areas are large, but are broadly distinguished based on differences in criteria such as the depth and thickness of the Marcellus, reservoir over-pressure and under-pressure, calculated TOC and adsorbed gas content, average effective (gas-filled) porosity, and final calculated gas in-place.

## c. Sources of Data for Representative Wells in Each Model Area

The most important data sources for each model area are the study wells contained in each area, along with the digital log data, rock samples, and sample analysis data available for each well. Initial contour maps of estimated gas in-place and $CO_2$ storage capacity were overlaid with the study well locations to select at least two representative wells for each model area. A composite model well was then created for each model area based on the attributes of the representative wells. In most cases, the attributes of the composite model well represent average attributes of all the study wells. In some cases, a single well was selected as the model well because it appeared to best represent the typical calculated attributes of the model

area. As a first approximation, various log-derived input parameters such as total porosity, thickness, permeability, and gas in-place were provided from the model well to the reservoir simulation. History matching of the simulation results with Marcellus production data available for the model area required some iterative adjustment of the model well parameters, as discussed in Volume 8. This was accomplished in some areas by selecting different representative wells from the subset of study wells. In some areas, the history match was improved by choosing a single value for an input such as porosity - from the range of calculated values for the wells within the model area – that provided the best simulation result.

# 7. REFERENCES

Allen, P. A., Homewood, P. and Williams, G.D. 1986. Foreland basins: an introduction. *In* Foreland Basins (Ed. by P.A. Allen & P. Homewood), Special Publication of the International Association of Sedimentologists, 8, 3-12.

Arthur, M. A., and Sageman, B. B. 1994. Marine black shales: A review of depositional mechanisms and significance of ancient deposits. Annual Review Earth and Planetary Science, v. 22, p. 499-551

Arthur, M. A., and Sageman, B. B. 2004. Sea-Level Control on Source-Rock Development: Perspectives from the Holocene Black Sea, the Mid-Cretaceous Western Interior Basin of North America, And The Late Devonian Appalachian Basin. The Deposition of Organic-Carbon-Rich Sediments: Models, Mechanisms, and Consequences SEPM Special Publication No. 82, p. 35-59.

Asquith, G. and Krygowski, D., 2004, *Basic Well Log Analysis*, second edition, American Association of Petroleum Geologists, Tulsa, 242 pp.

Avary, K.L and Patchen, D.G., 2008, Regional Geology of the Middle Devonian Marcellus Shale, Appalachian Basin, presentation at American Association of Petroleum Geologists Eastern Section Meeting, Pittsburgh, PA, October, 2008.

Castle, J.W. 2001. Appalachian basin stratigraphic response to convergent-margin structural evolution. Basin Research, 13, pp. 397-418.

Crain, E.R., 1986, *The Log Analysis Handbook*, Pennwell Publishing Co., Tulsa, 684 pp.

Dickinson, W. R. 1974. Plate tectonics and sedimentation. In:Tectonics and Sedimentation (Ed. by W.R. Dickinson), Special Publication of the Society of Economic Paleontologists and Mineralogists, 22, 1-27.

Emerson, S. 1985. Organic carbon preservation in marine sediments, *in* Sundquist, E.T., Broecker, W.S. (Eds.), The Carbon Cycle and Atmospheric CO2: Natural Variations Archean to Present. Geophysical Monograph, vol. 32, pp. 78– 87.

Energy Information Administration (EIA), 2012. Annual Energy Outlook 2012, Early Release Overview. Online: http://www.eia.gov/forecasts/aeo/er/pdf/0383er(2012).pdf. Accessed: March 2013.

Energy Information Administration (EIA), 2008 - 2010. U.S. Crude Oil, Natural Gas, and Natural Gas Liquids Reserves, 2008 through 2010, Annual Reports. Online: (http://www.eia.gov/naturalgas/crudeoilreserves/pdf/table_3.pdf)

Engelder, Terry, 2012. How Much Natural Gas Can The Marcellus Shale Produce? Marcellus Center for Outreach and Research. The Pennsylvania State University. Online: http://www.marcellus.psu.edu/news/PDFs/gasreserves_day.pdf. Accessed : March 2013

Engelder, T., and Lash, G. G. 2008. Marcellus Shale Play's Vast Resource Potential Creating Stir in Appalachia. The American Oil and Gas Reporter. May 2008. Online: http://www.wpsu.org/gasrush/assets/pdfs/Marcellus_Shale_Play_May08.pdf. Accessed: March 2013.

Ettensohn, F. R. 1985a. The Catskill Delta Complex and the Acadian Orogeny: a model. In Woodrow, D. L. and Sevon, W. D. (eds.) The Catskill Delta, Geological Society of America, Special Paper 201, p. 39-50.

Ettensohn, F.R. 1985b. Controls on development of Catskill Delta complex basin-facies. In Woodrow, D. L. and Sevon, W. D. (eds.) The Catskill Delta, Geological Society of America, Special Paper 201, p. 65-77.

Ettensohn, F.R. 1998. Compressional tectonic controls on Epicontinental black-shale deposition: Devonian-Mississippian examples from North America. Shales and mudstones. Stuttgart: E. Schweizerbart. pp. 109–128.

Ettensohn, F.R., and Barron, L.S., 1981, Depositional model for the DevonianMississippian black shales of North America: A paleoclimatic-paleogeographic approach, in Roberts, T.G., ed., GSA Cincinnati '81 Field Trip Guidebooks, v. II: Economic geology, structure: Falls Church, American Geological Institute, p. 344–361.

Faill, R. T. 1997. A Geologic History of the North-Central Appalachians; Part 2, the Appalachian Basin from the Silurian through the Carboniferous. American Journal of Science, V. 297, 7. Pp. 729-761. Online: http://www.ajsonline.org/content/297/7/729.abstract. Accessed: March 2013.

Faill, R. T. 1999. Geologic History of Pennsylvania: Paelozoic, in The Geology of Pennsylvania, (Shultz, C. H., ed. Pennsylvania Geological Survey and the Pittsburgh Geological Survey. pp. 419-434.

Griffing, D.H., and Ver Straeten, C.A. 1991. Stratigraphy and depositional environments of the lower part of the Marcellus Formation (Middle Devonian) in eastern New York State. In Ebert, J.R., ed., New York State Geological Association, 63rd Annual Meeting Guidebook, p. 205-249

Harper, J.A., 2008, The Marcellus Shale – an Old "New" Gas Reservoir in Pennsylvania, *Pennsylvania Geology*, v. 38, no. 1, pp. 2 – 12.

Klein, G. 1991. Geodynamics and geochemical aspects of sedimentary basin classification. Journal of African Earth Sciences, 13, pp. 1-11.

Klemme, H. D., and Ulmishek, G. F. 1991. Effective petroleum source rocks of the world: stratigraphic distribution and controlling depositional factors. *AAPG Bulletin,* 75: 1809-1851.

New York State Energy Research and Development Authority (NYSERDA). 2007. New York's Natural Gas and Resource Endowment: Past, Present and Potential. http://www.dec.ny.gov/docs/materials_minerals_pdf/nyserda2.pdf

Ohio Geological Survey, 1982 to present, Stratigraphic cross-section trending northwest-southeast (along dip) illustrating the Devonian Shale interval in eastern Ohio and west-central West Virginia, *based on* Gray, J.D. and others, 1982, *An integrated study of the Devonian-age black shales in eastern Ohio*: Ohio Department of Natural Resources, Division of Geological Survey.

Ohio Geological Survey, 1982 to present, Stratigraphic cross-section trending southwest-northeast (along dip) illustrating the Devonian Shale interval in eastern Ohio and west-central West Virginia, *based on* Gray, J.D. and others, 1982, *An integrated study of the Devonian-age black shales in eastern Ohio*: Ohio Department of Natural Resources, Division of Geological Survey.

Pennsylvania Department of Conservation and Natural Resources, present, *Pennsylvania Devonian Shales Cross-Sections A-A', C-C', and E-E'*: stratigraphic cross-sections showing the Middle and Upper Devonian.

Pennsylvania Department of Environmental Protection (DEP). 2012. *Well Permits Issued and Drilled 2012.* http://files.dep.state.pa.us/OilGas/BOGM/BOGMPortalFiles/OilGasReports/2012/2012Wellspermitted-drilled.pdf. 2012. Accessed February 2013.

Potential Gas Committee, 2008 - 2012. *Potential Supply of Natural Gas in the United States*, 2008 through 2012, Biennial reports.

Quinlan, G.M., and Beaumont,C. 1984. Appalachian thrusting, lithospheric flexure, and Paleozoic stratigraphy of the Eastern Interior of North America Canadian Journal of Earth Sciences, 21, 973-996.

Range Resources. 2013. Range Resources, Marcellus Division. Online: www.rangeresources.com/operations/marcellus-division.aspx. Accessed February 2013.

Repetski, J.E., Ryder, R.T., Weary, D. J., Harris, A.G., and Trippi, M.H., 2008, Thermal Maturity Patterns (CAI and $\%R_o$) in upper Ordovician and Devonian Rocks of the Appalachian Basin: A Major Revision of USGS Map I-917-E Using New Subsurface Collections, Scientific Investigations Map 3006, United States Geological Survey, 26 pp., maps. . Online: http://pubs.usgs.gov/sim/3006/SIM3006.pdf. Accessed: March 2013.

Roen, J.B. and Kepferle, R.C., eds., 1993, Petroleum geology of the Devonian and Mississippian black shale of eastern North America: U.S.

Rowan, E. L. 2006. Burial and Thermal History of the Central Appalachian Basin, Based on Three 2-D Models of Ohio, Pennsylvania, and West Virginia. USGS. Online: http://pubs.usgs.gov/of/2006/1019/2006-1019.pdf. Accessed: March 2013.

Ryder, R. T. No Date (ND). Appalachian Basin Province (067). U.S.G.S. Online:http://certmapper.cr.usgs.gov/data/noga95/prov67/text/prov67.pdf. Accessed: March 2013. (Marcellus Shale Advisory Commission, 2011; PA DEP, 2012).

Sageman, B.B., Murphy, A.E., Werne, J.P., Ver Straeten, C.A., Hollander, D.J., and Lyons, T.W. 2003. A tale of shales: The relative roles of production, decomposition, and dilution in the accumulation of organic-rich strata, Middle–Upper Devonian, Appalachian Basin: Chemical Geology, v. 195, pp. 229–273.

Schieber, J. 2003. Black Shales. In: Gerard V. Middleton et al. (eds.), Encyclopedia of Sediments and Sedimentary Rocks, Kluwer Scientific Publishers, pp. 83-85

Schmoker, J. W., 1993, Use of formation-density logs to determine organic-carbon content in Devonian shales of the western Appalachian Basin and an additional example based on the Bakken Formation of the Williston Basin, in J. B. Roen, and R. C. Kepferle, eds., *Petroleum Geology of the Devonian and Mississippian Black Shale of Eastern North America*, U. S. Geological Survey Bulletin 1909, U.S. Government Printing Office, p. J1-J14.

Schmoker, J. W., 1979, Determination of organic content of Appalachian Devonian shales from formation-density logs: American Association of Petroleum Geologists *Bulletin*, v. 63, p. 1504-1537.

Simandoux, P., 1963, Mesures dielectriques en milieu poreux, application a mesure des saturations en eau: Etude du Comportement des Massifs Argileux, *Revue de l'institut Francais du Petrole*, *Supplementary Issue*.

Smith, L. B, 2010, Shallow Transgressive Onlap Model for Ordovician and Devonian Organic-Rich Shales, New York State, presentation to American Association of Petroleum Geologists Eastern Section Meeting, Kalamazoo, MI, September 25 – 29, 2010.

Smith, L. B. and Leone, J., 2010a, Integrated Characterization of Utica and Marcellus Black Shale Gas Plays, New York State, presentation to American Association of Petroleum Geologists Annual Convention and Exhibition, New Orleans, Louisiana, April 11-14, 2010.

Smith, L. B. and Leone, J. 2010b, Tectonic and Depositional Setting of Ordovician Utica and Devonian Marcellus Black Shales, New York State, poster presentation, American Association of Petroleum Geologists Annual Convention and Exhibition, New Orleans, LA, April 11-14, 2010.

Suess, E. 1980. Particulate organic carbon flux in the oceans: surface productivity and oxygen utilization: Nature, v. 288, p. 260-263.

Swanson, V. E. 1961. Geology and geochemistry of uranium in marine black shales: U.S

Tourtelot, H. A. 1979. Black Shale: Its Deposition and Diagenesis. *Clays and Clay Minerals,* 27, 5, pp. 313-321.

U.S. Department of Energy (DOE). 1999, Carbon sequestration research and development: Office of Fossil Energy, Office of Science, Washington, D.C., December, 195 p.

U.S. Department of Energy/National Energy Technology Laboratory (DOE/NETL). 2004, Carbon sequestration technology roadmap and program plan: 24 p. <www.fe.doe.gov/programs/sequestration/publications/programplans/2004/SequestrationRoadmap4-29-04.pdf>.

U.S. Department of Energy/National Energy Technology Laboratory (DOE/NETL). 2005, Carbon sequestration, technology roadmap and program plan 2005: 26 p. http://www.fe.doe.gov/programs/sequestration/publications/programplans/2006/sequestration_roadmap_2005.pdf

U.S. Department of Energy/National Energy Technology Laboratory (DOE/NETL). 2012. The United States 2012 Carbon Utilization and Storage Atlas. Online: http://www.netl.doe.gov/technologies/carbon_seq/refshelf/atlasIV/Atlas-IV-2012.pdf. Accessed: March 2013.

United States Geological Survey (USGS), 1993, Petroleum Geology of the Devonian-Mississippian Black Shale of Eastern North America, Roen, J.B. and Kepferle, R. C., eds., U.S. Geological Survey bulletin: 1909, 434 pp.

United States Geological Survey (USGS), 2003. National Assessment of Oil and Gas Fact Sheet Assessment of Undiscovered Oil and Gas Resources of the Appalachian Basin Province, 2002. February 2003. Online: http://pubs.usgs.gov/fs/fs-009-03/fs-009-03-508.pdf. Accessed: March 2013.

United States Geological Survey (USGS), 2011. National Assessment of Undiscovered Oil and Gas Resources of the Devonian Marcellus Shale of the Appalachian Basin Province, 2011. August 2011. Online: http://pubs.usgs.gov/fs/2011/3092/pdf/fs2011-3092.pdf. Accessed: March 2013.

Ver Straeten, C., Baird, G., Brett, C., and Over, J. 2011. The Marcellus Subgroup of New York and Beyond: Stratigraphy, Sequences, Mudrocks, and Sedimentology. The Marcellus subgroups in its type area, Finger Lakes area of New York, and beyond. Field Trip Guide NYSGA 2011. Pp. 23-86. Online: http://www.nysm.nysed.gov/staffpubs/docs/20398.pdf. Accessed: March 2013.

Wickstrom, L.H., Venteris, E.R., and Harper, J.A., and 26 others, 2005, Characterization of geologic sequestration opportunities in the MRCSP region- Phase 1 task report: Ohio Department of Natural Resources, Division of Geological Survey Open File Report 2005-1, 152 p., accessed at <http://www.dnr.state.oh.us/portals/10/pdf/OpenFileReports/OFR_2005-1.pdf>.

Wrightstone, G.R., 2009, Marcellus Shale – Geologic Controls on Production, presentation, American Association of Petroleum Geologists Annual Convention and Exhibition, Denver, CO, June 7-10, 2009.

Zagorski, W. A., Bowman, D.C., Emery, M., Wrightstone, G.R., 2011, An overview of some key factors controlling well productivity in core areas of the Appalachian Basin Marcellus Shale Play.

# FIGURES

Figure 1. Map Showing Extent and Depth of Marcellus Shale, and Area of Reservoir 'Over-pressure'

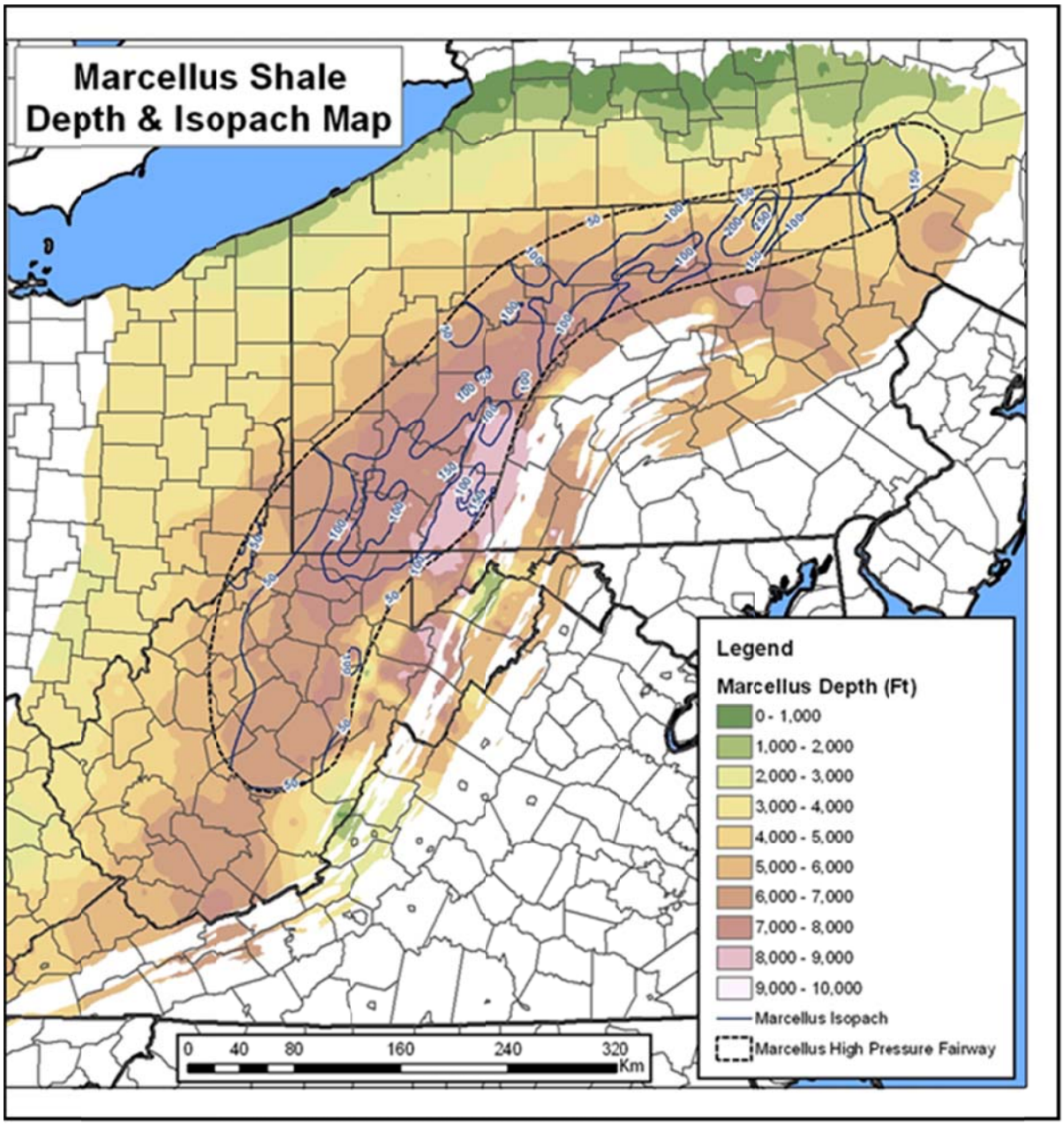


Compiled by Advanced Resources International. Sources: United States Geological Survey, Pennsylvania Department of Natural Resources, New York State Museum, Ohio Geological Survey, West Virginia Geological Survey.

Figure 2. Ohio Annual Marcellus Gas Production, 1984 - 2012

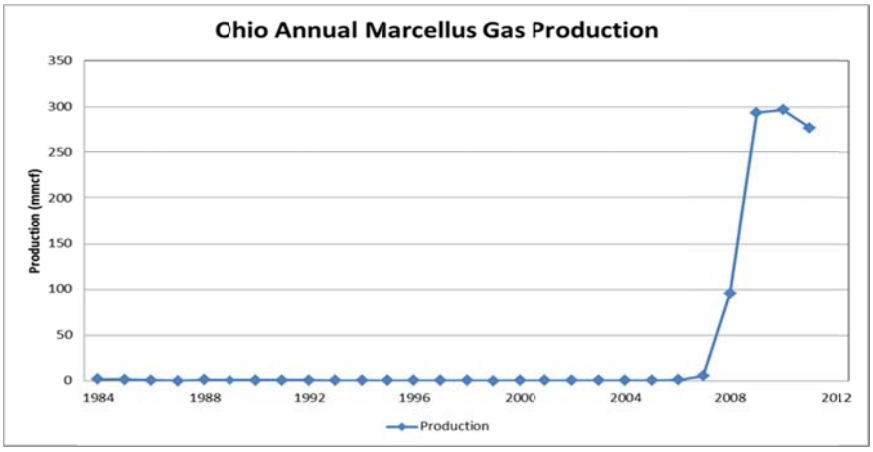


Figure 3. New York Annual Marcellus Gas Production, 1984 – 2012

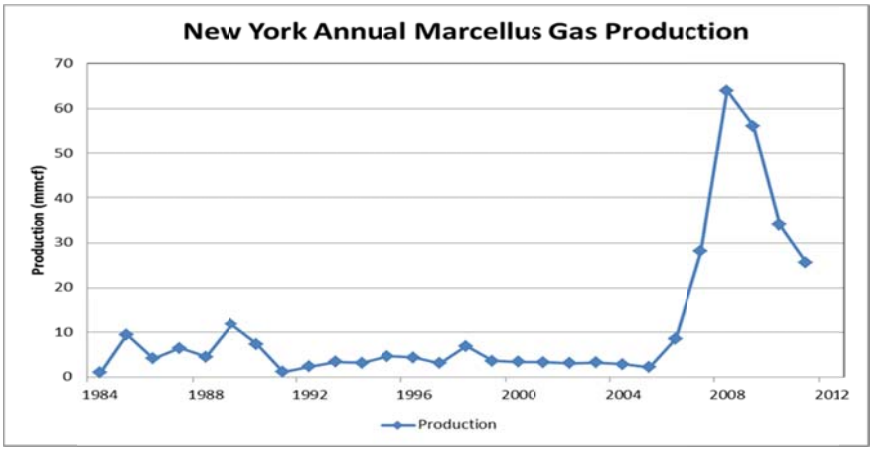


Figure 4. Annual Marcellus Gas Production by State, 2000 – 2012

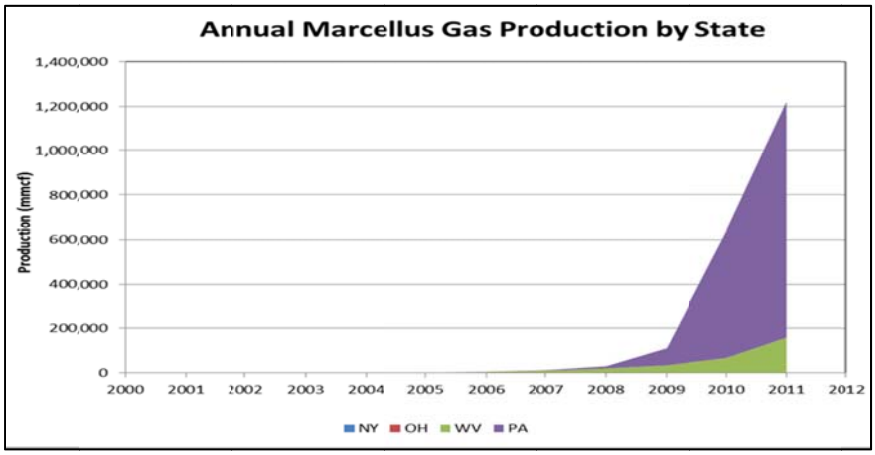

Figure 5. Pennsylvania Annual Marcellus Gas Production, 2004 - 2011

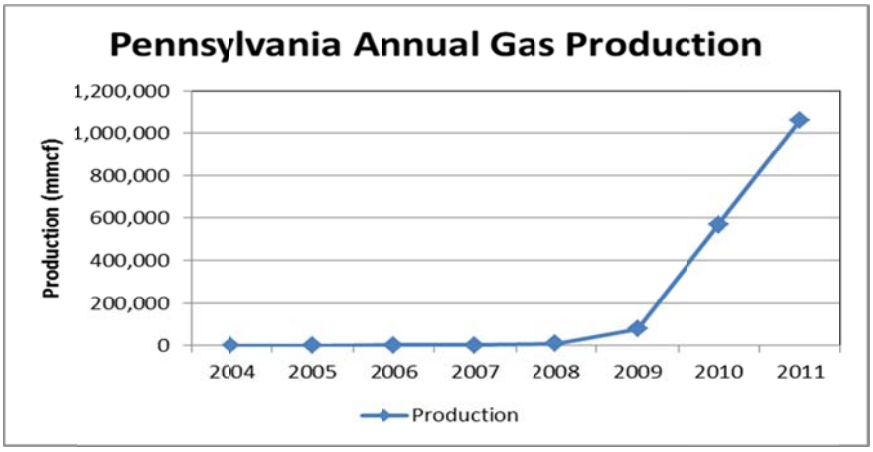


Figure 6. Relative Contribution of Pennsylvania Marcellus Gas to Total Gas Production, 2004 – 2011

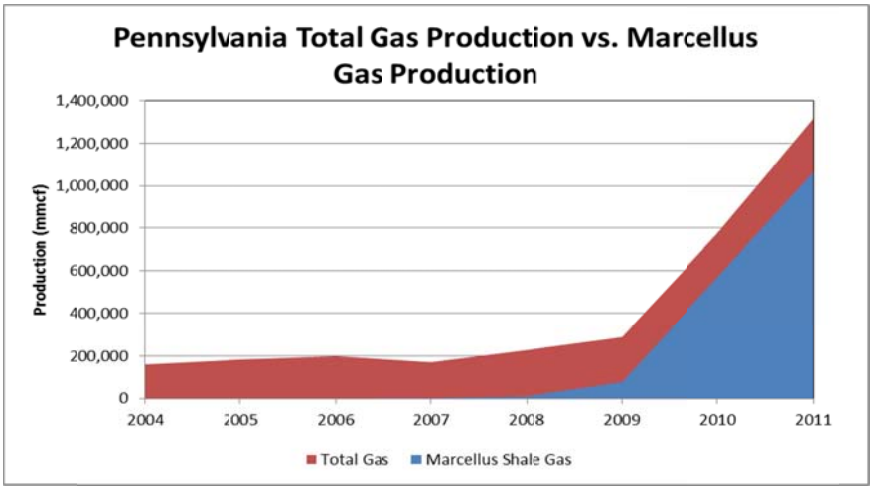


Figure 7. Pennsylvania Marcellus Annual Well Permits and Wells Drilled, 2004 - 2011

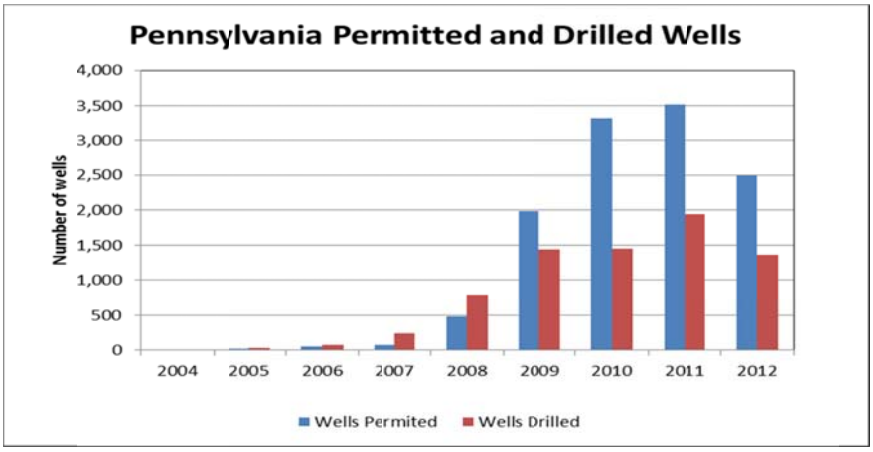

Figure 8. Relative Contribution of Marcellus Gas to Total West Virginia Gas Production, 2005 -

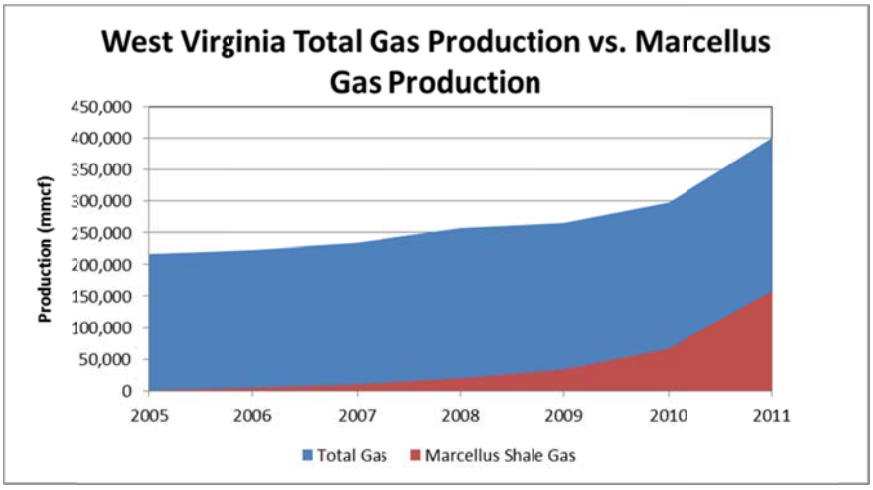


Figure 9. West Virginia Annual Marcellus Gas Production, 2005 - 2012

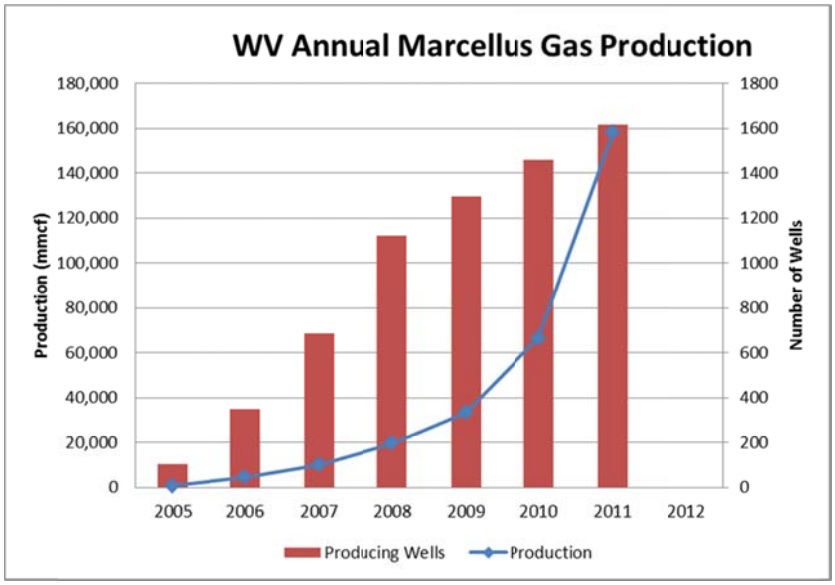

Figure 10. Simplified Stratigraphic Chart Showing Marcellus and Other Devonian Shale Formations of the Appalachian Basin

<table>
<tr><th>System/Series</th><th>Michigan Basin</th><th>Eastern Ohio</th><th colspan="2">West Virginia</th><th colspan="2">Pennsylvania</th><th colspan="2">New York</th></tr>
<tr><td rowspan="11">Late Devonian<br><br>Middle Devonian</td><td>Ellsworth/ Antrim Shale</td><td rowspan="2">West Falls Fm./ Java Fm./ Olentangy Sh.</td><td colspan="2" rowspan="2">West Falls Group/ Rhinestreet Shale/ Brailler Fm. (in part)</td><td colspan="2" rowspan="2">West Falls Group/ Rhinestreet Shale/ Brailler Fm. (in part)</td><td colspan="2" rowspan="2">West Falls Group/ Rhinestreet Shale</td></tr>
<tr><td>Antrim - Lachine Mbr.</td></tr>
<tr><td>Antrim -Paxton Mbr.</td><td rowspan="5">Unconformity</td><td colspan="2">Sonyea Formation</td><td colspan="2">Sonyea Group</td><td colspan="2">Sonyea Group</td></tr>
<tr><td>Antrim - Norwood Mbr.</td></tr>
<tr><td>Squaw Bay Ls</td><td colspan="2" rowspan="2">Gennessee Group<br>(Burket Shale in part)</td><td>Harrell Shale</td><td rowspan="2">Gennessee Group</td></tr>
<tr><td>Unconformity</td><td>Genesee/ Burket Sh.</td></tr>
<tr><td rowspan="5">Traverse Group</td><td colspan="2">Tully Limestone (in part)</td><td colspan="2">Tully Limestone (in part)</td><td colspan="2">Tully Limestone</td></tr>
<tr><td rowspan="4">Unconformity</td><td>Hamilton Grp./ Millboro Shale</td><td rowspan="4">Hamilton Group & equivalents</td><td>Hamilton Group Undivided</td><td rowspan="4">Hamilton Group</td><td>Upper Hamilton Group Shale Fms.</td><td rowspan="4">Hamilton Group</td></tr>
<tr><td rowspan="3">Mahantango Shale</td><td>Mahantango Shale</td><td>Skaneateles Shale</td></tr>
<tr><td>Stafford Ls.</td><td>Stafford Ls.</td></tr>
<tr><td>Hamilton Grp</td><td>Upper Marcellus Shale</td><td>Marcellus Shale - Oatka Creek</td></tr>
<tr><td>Dundee Limestone</td><td>Marcellus Shale</td><td>Marcellus Shale</td><td>Purcell Ls.</td><td>Cherry Valley Ls.</td></tr>
<tr><td>Detroit River Grp</td><td>Onondaga Ls and equivalents</td><td colspan="2">Onondaga Limestone</td><td>Lower Marcellus Shale</td><td>Marcellus Shale - Union Springs</td></tr>
<tr><td rowspan="2">Early Devonian</td><td>Bois Blanc Fm.</td><td>Bois Blanc Fm. & Oriskany Ss.</td><td colspan="2">Needmore Shale/ Huntersville Chert/ Oriskany Ss.</td><td colspan="2">Needmore Shale/ Huntersville Chert/Bois Blanc & Oriskany Ss.</td><td colspan="2">Tristates Group/ Esopus Sh./ Oriskany Ss.</td></tr>
<tr><td></td><td>Helderberg Limestone</td><td colspan="2">Helderberg Limestone</td><td colspan="2">Helderberg Group</td><td colspan="2">Helderberg Group</td></tr>
</table>

Source : Wickstrom and others, 2005.

Figure 11. Schematic Cross-Section Illustrating a Shallow Onlap Depositional Model for Devonian Black Shales (source: NY State Museum)

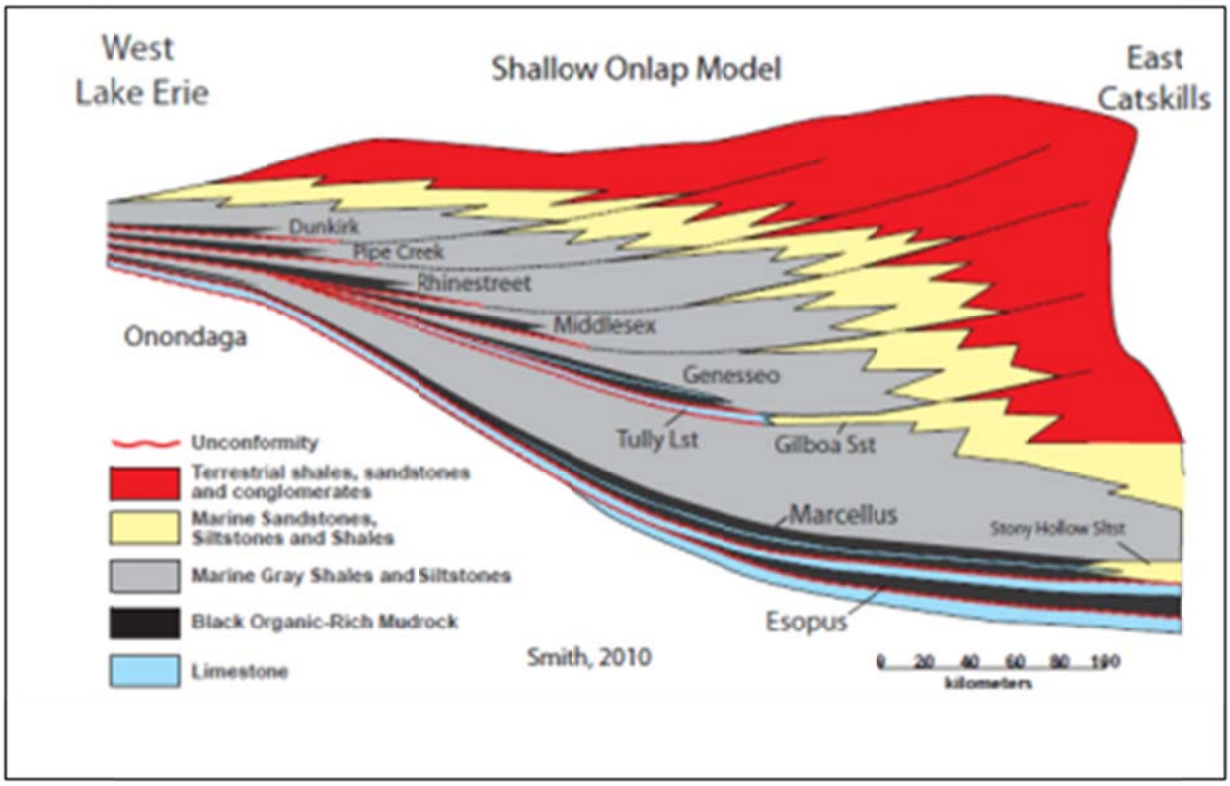

Figure 12. Schematic Map of Marcellus Shale Extent and Thermal Maturity

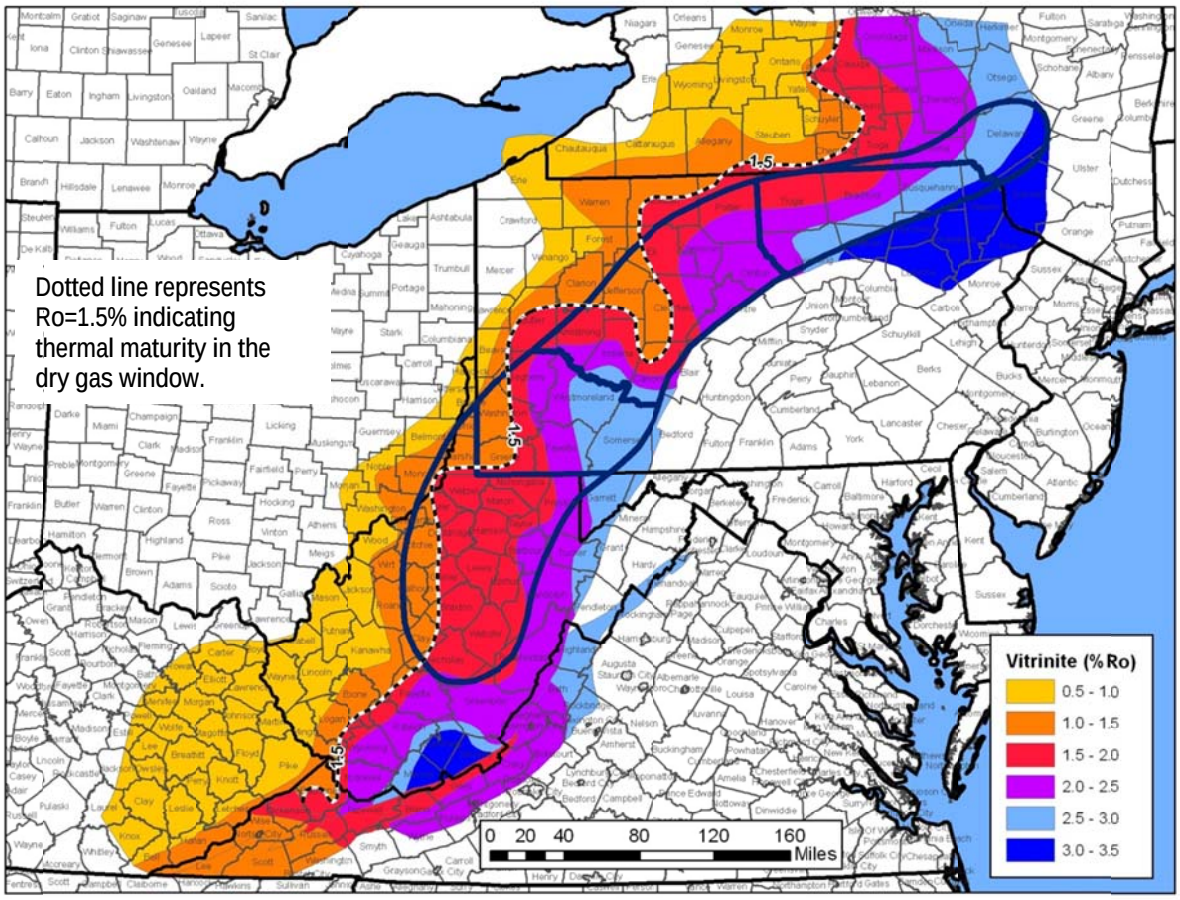


*Map compiled by Advanced Resources International. Source: USGS map SIM 300-6, Repetski, et al. 2008*

Figure 13. Marcellus Study Area and Model Area Sub-Divisions

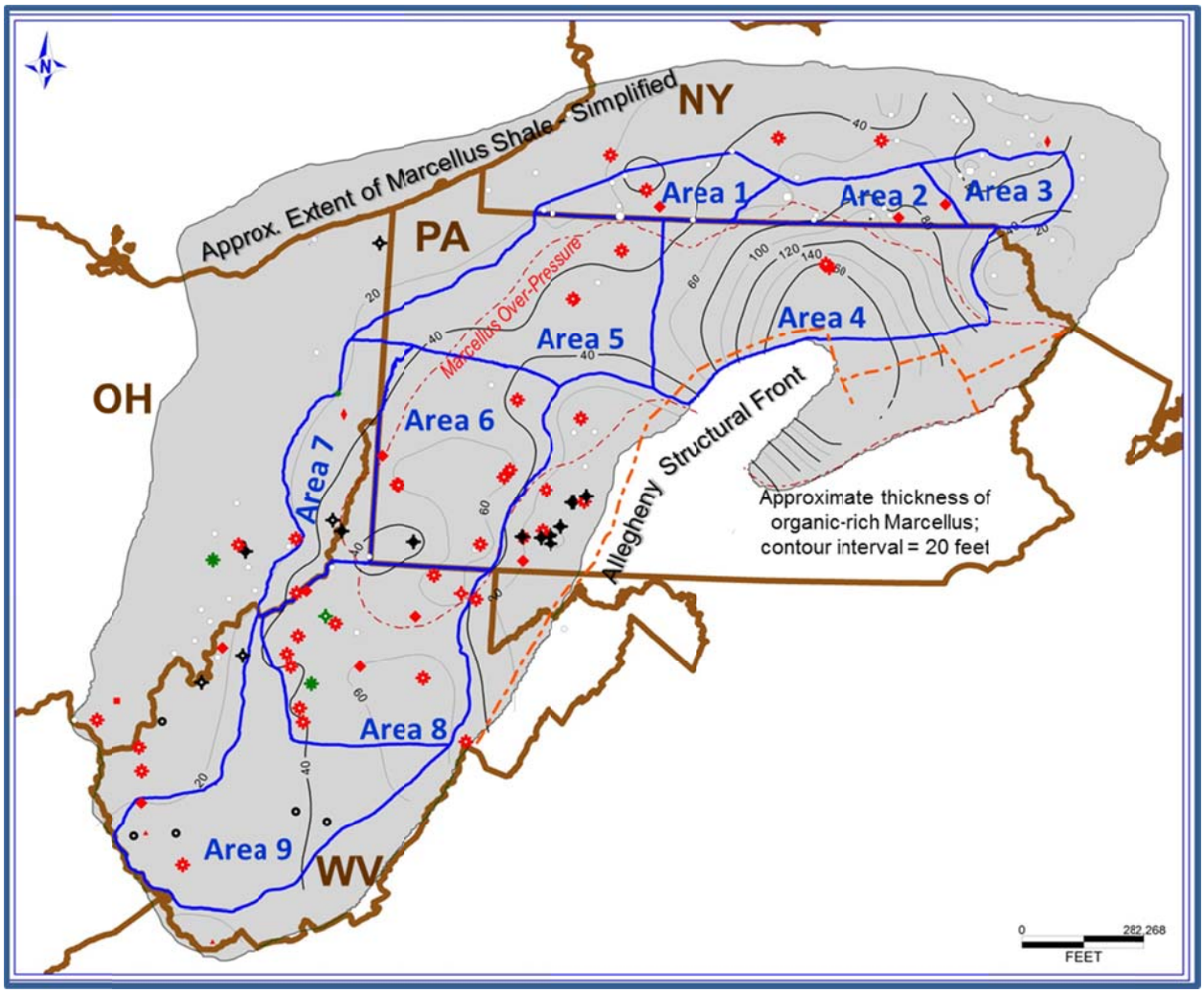

Figure 14. Type Log of the Marcellus for North Central Pennsylvania

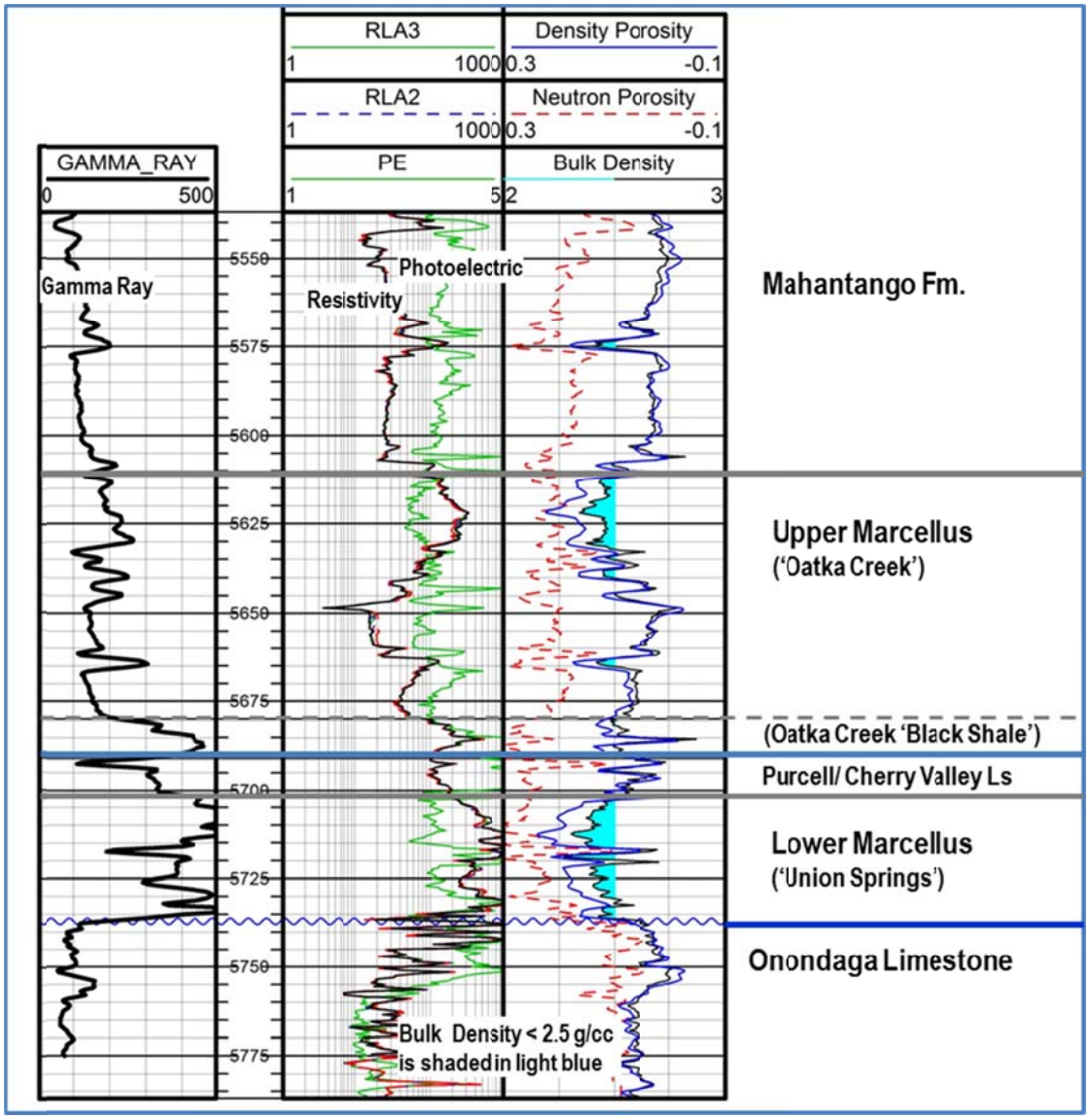

Figure 15. Marcellus Regional Stratigraphic Cross-Sections

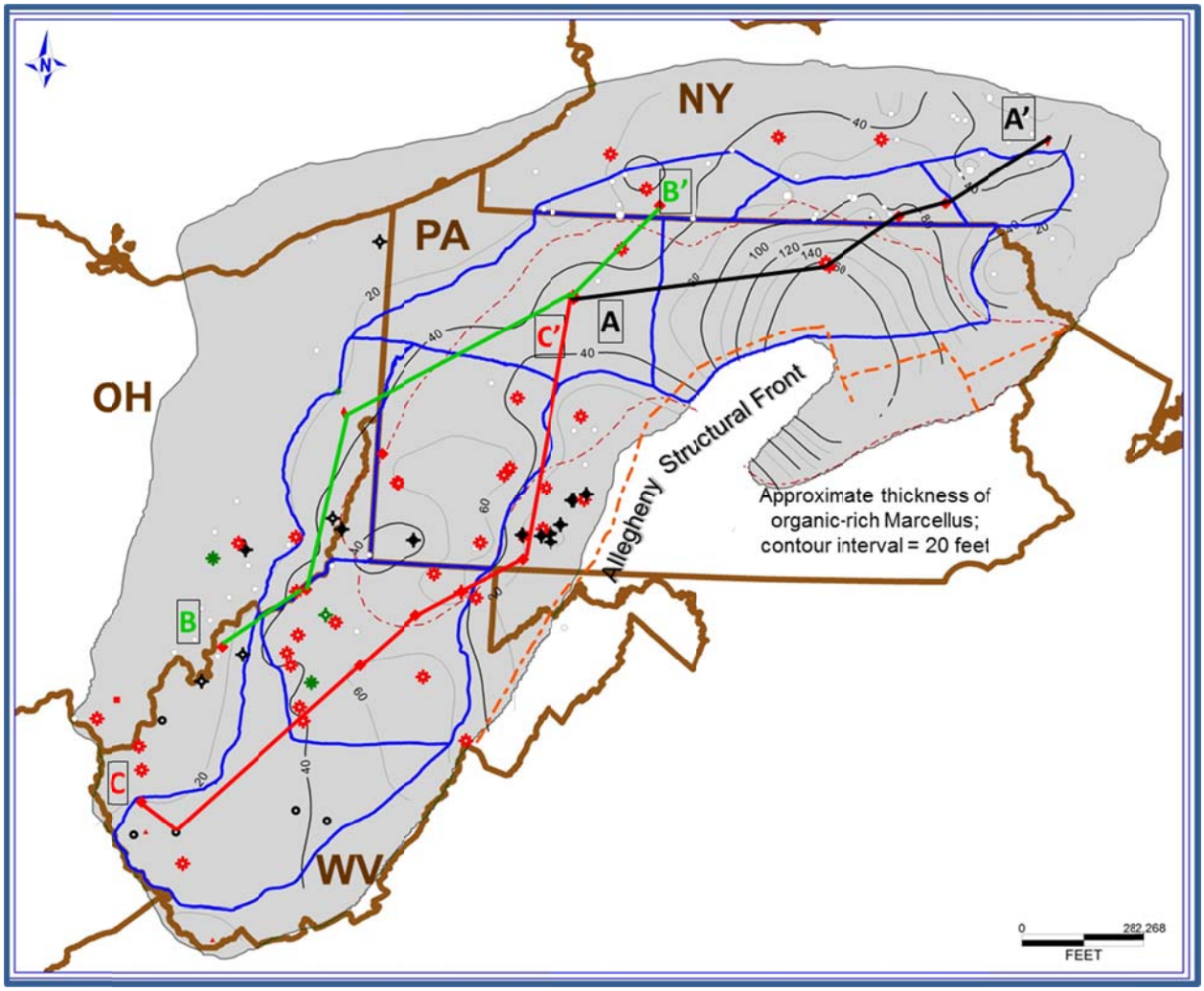

Figure 16. Stratigraphic Cross-section A – A'

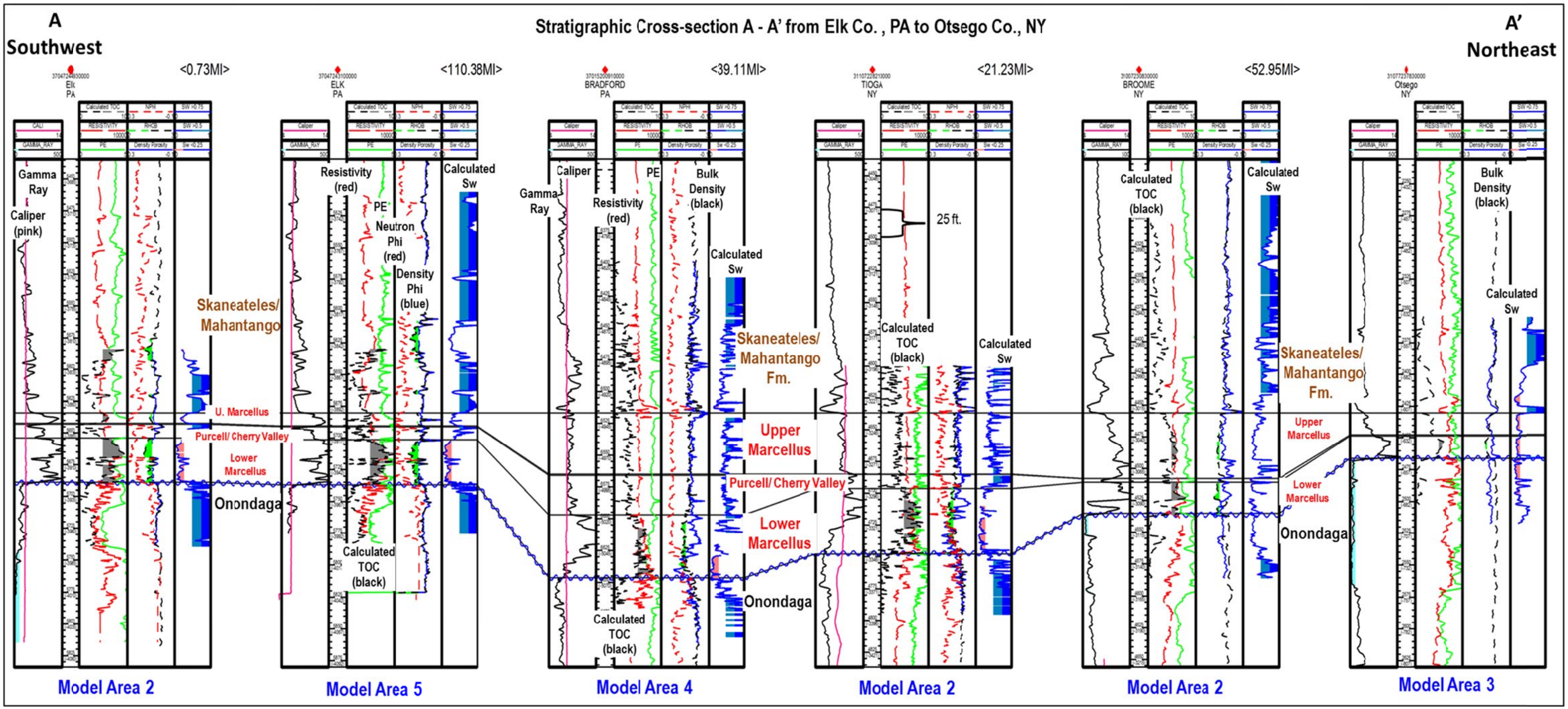

Figure 17. Stratigraphic Cross-section B – B'

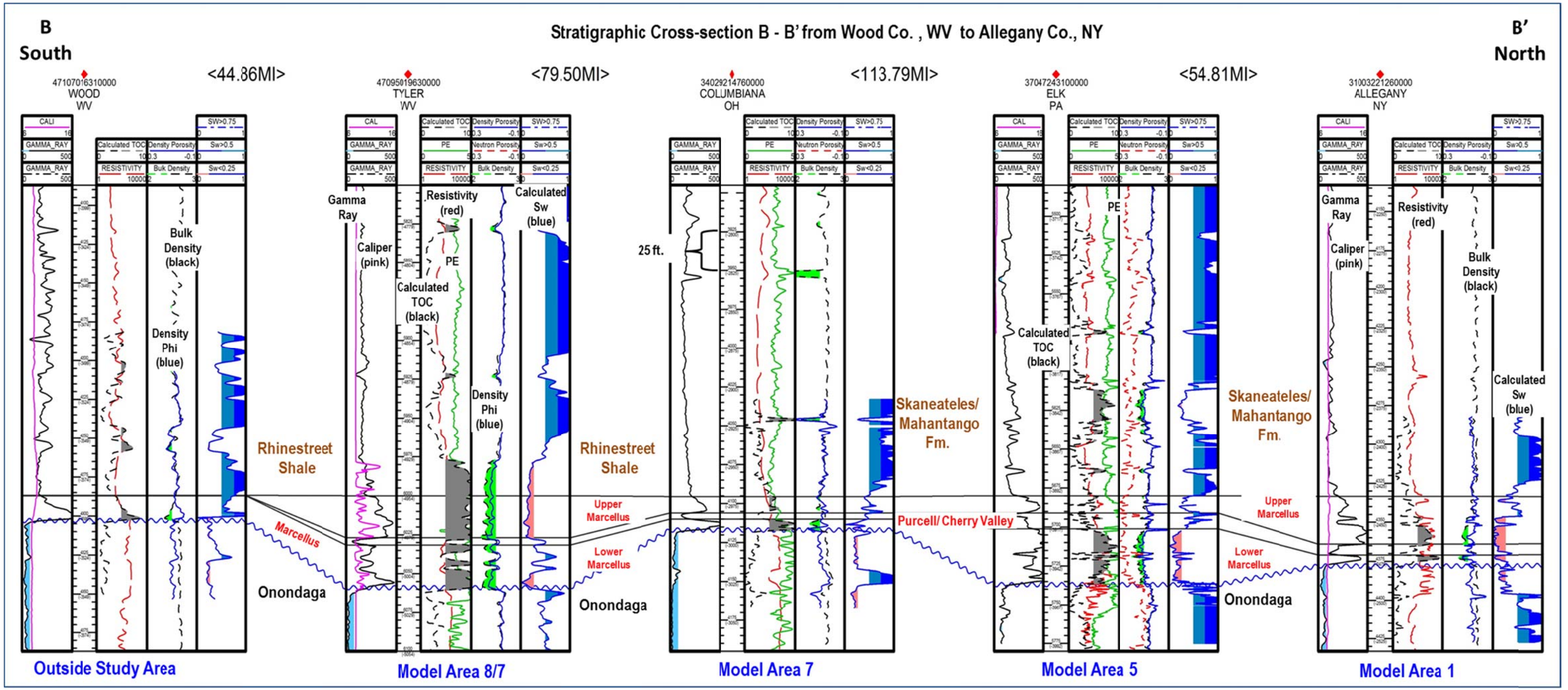

Figure 18. Stratigraphic Cross-Section C – C'

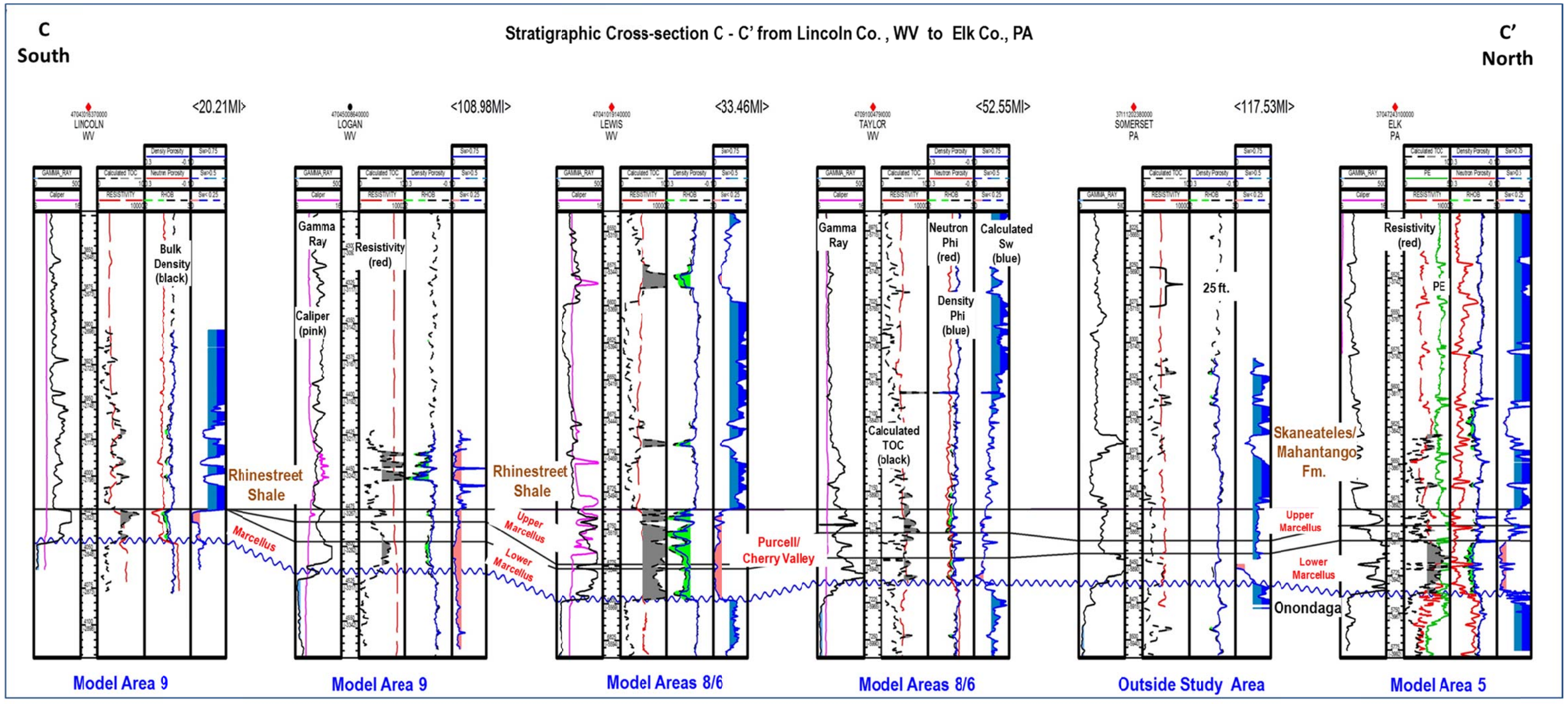

Figure 19. Marcellus Adsorption Isotherms

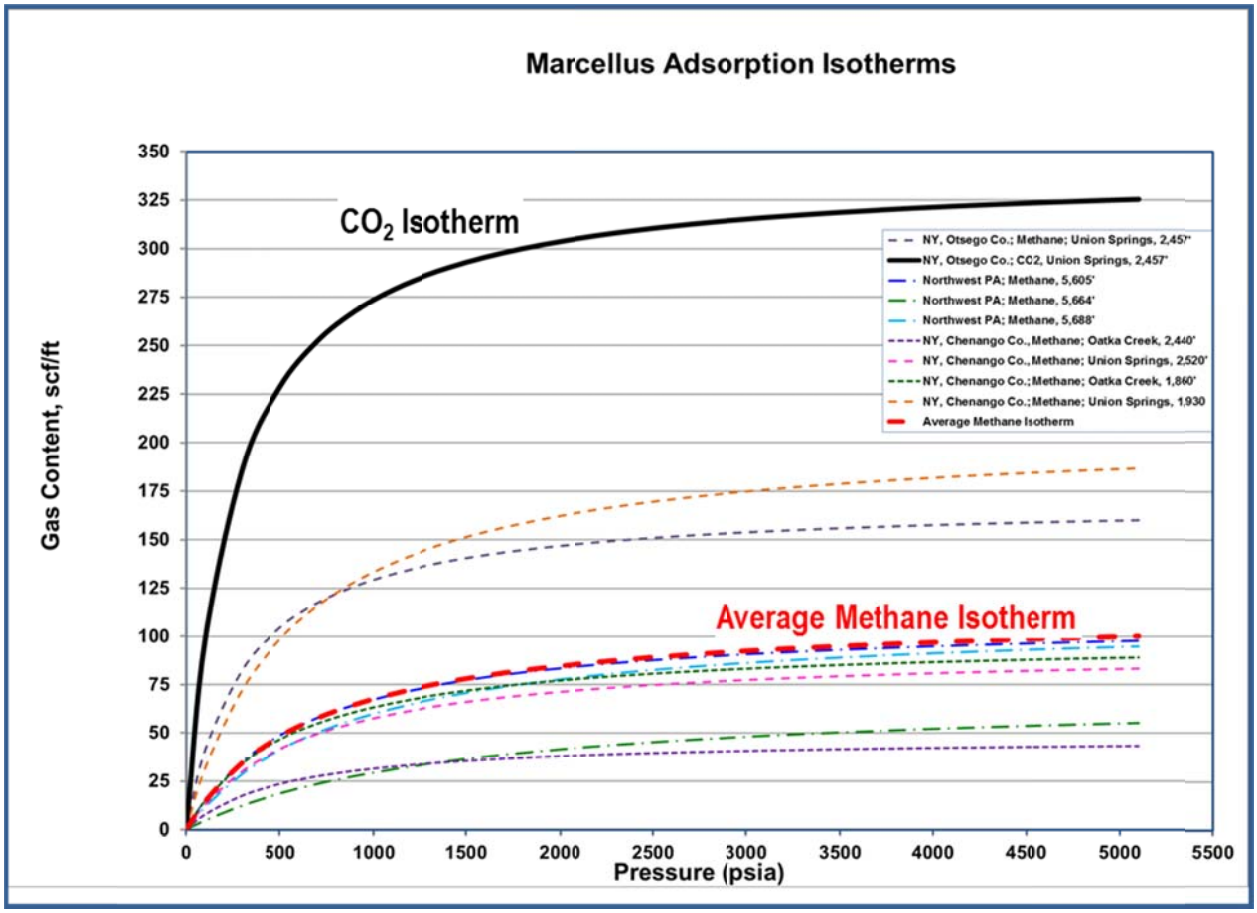

Figure 20. Relationship of Langmuir Volume and TOC for Marcellus Methane Isotherms

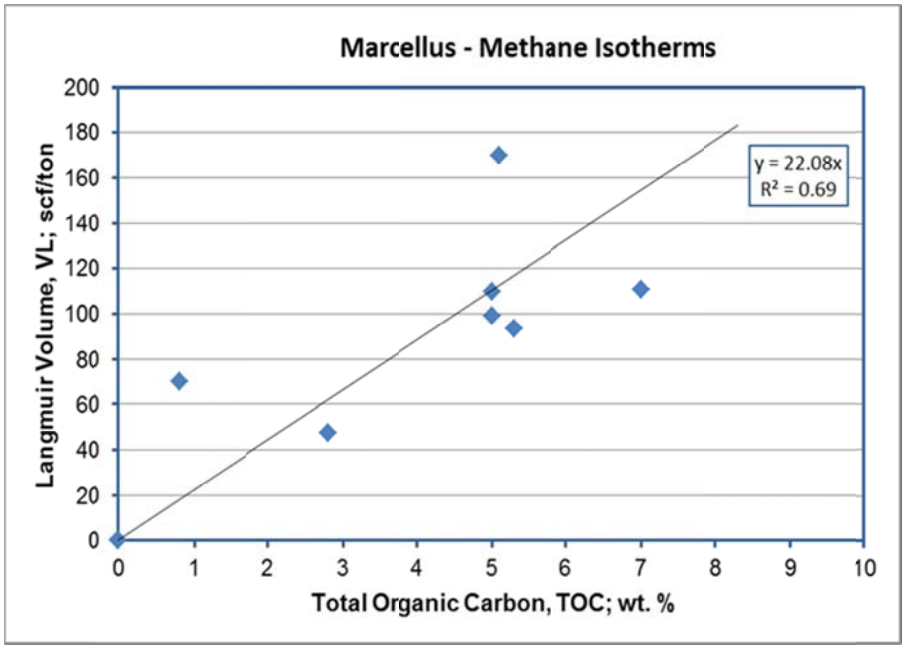


Figure 21. Relationship of Langmuir Volume and TOC for Marcellus $CO_2$ Isotherm

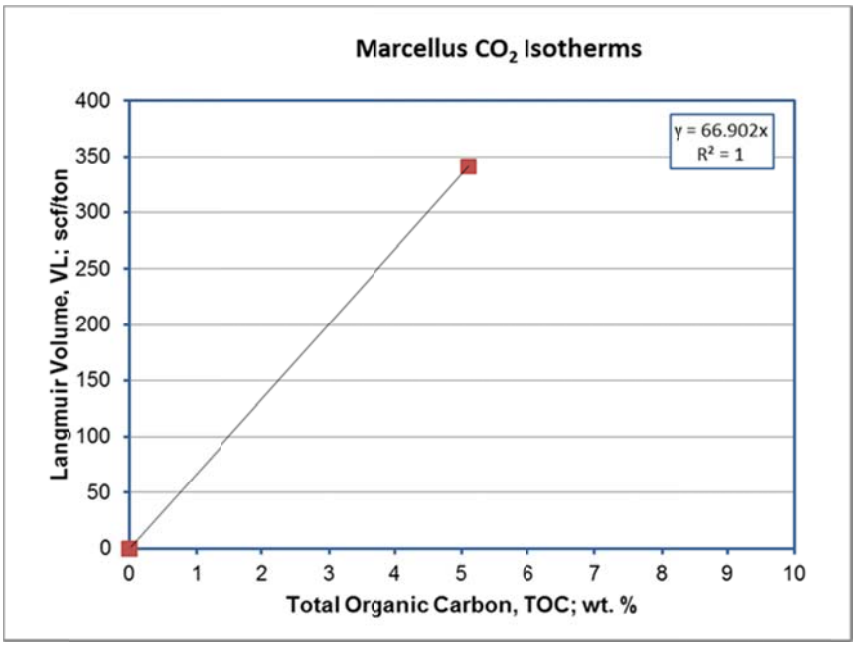

Figure 22. Correlation of TOC and Bulk Density for Marcellus Core Samples

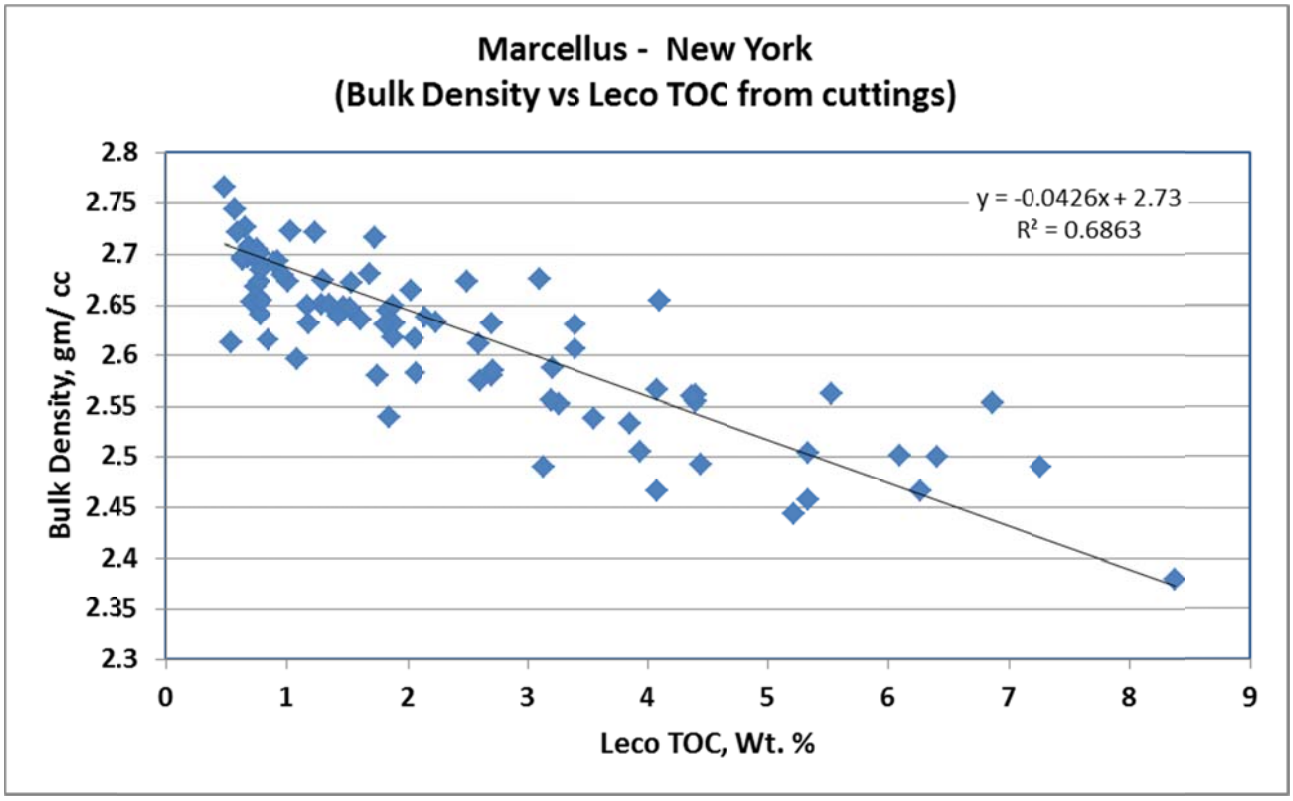

Figure 23. Correlation of TOC and Bulk Density for Marcellus Drill Cuttings, New York

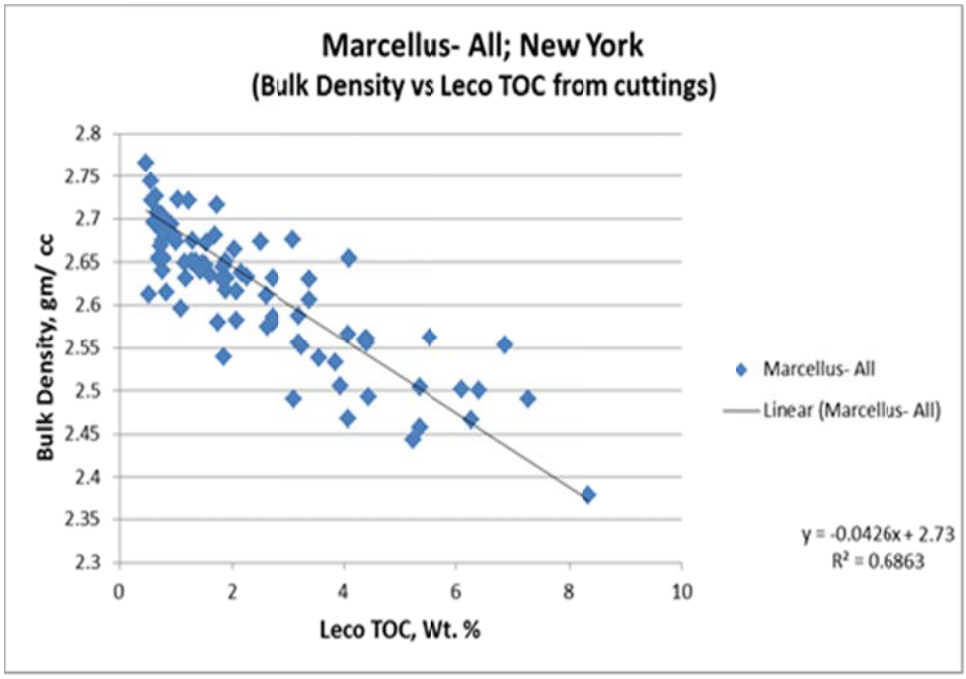


Figure 24. Correlation of TOC and Gamma Ray for Marcellus Drill Cuttings, New York

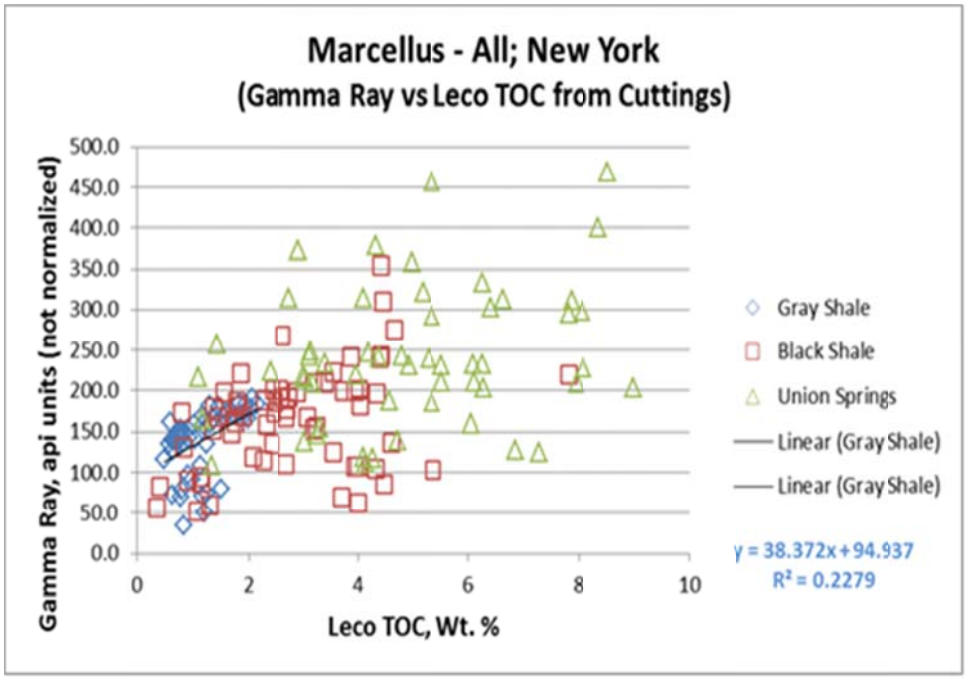

Figure 25. Crushed Sample Pressure-Decay Permeability, Marcellus Whole Core Samples

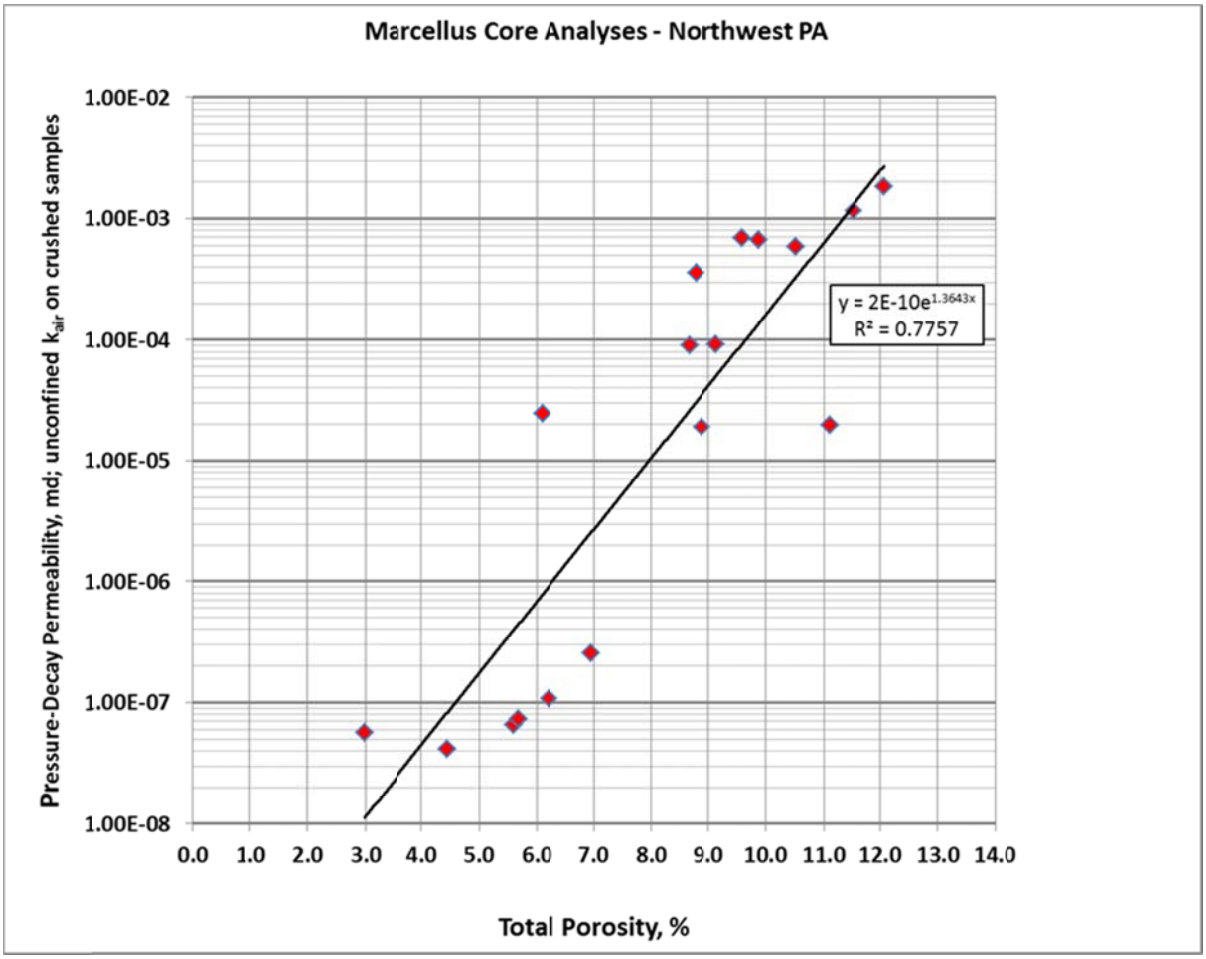

Figure 26. Total Marcellus Gas in-Place by Model Area, Bcf/ 80-acres

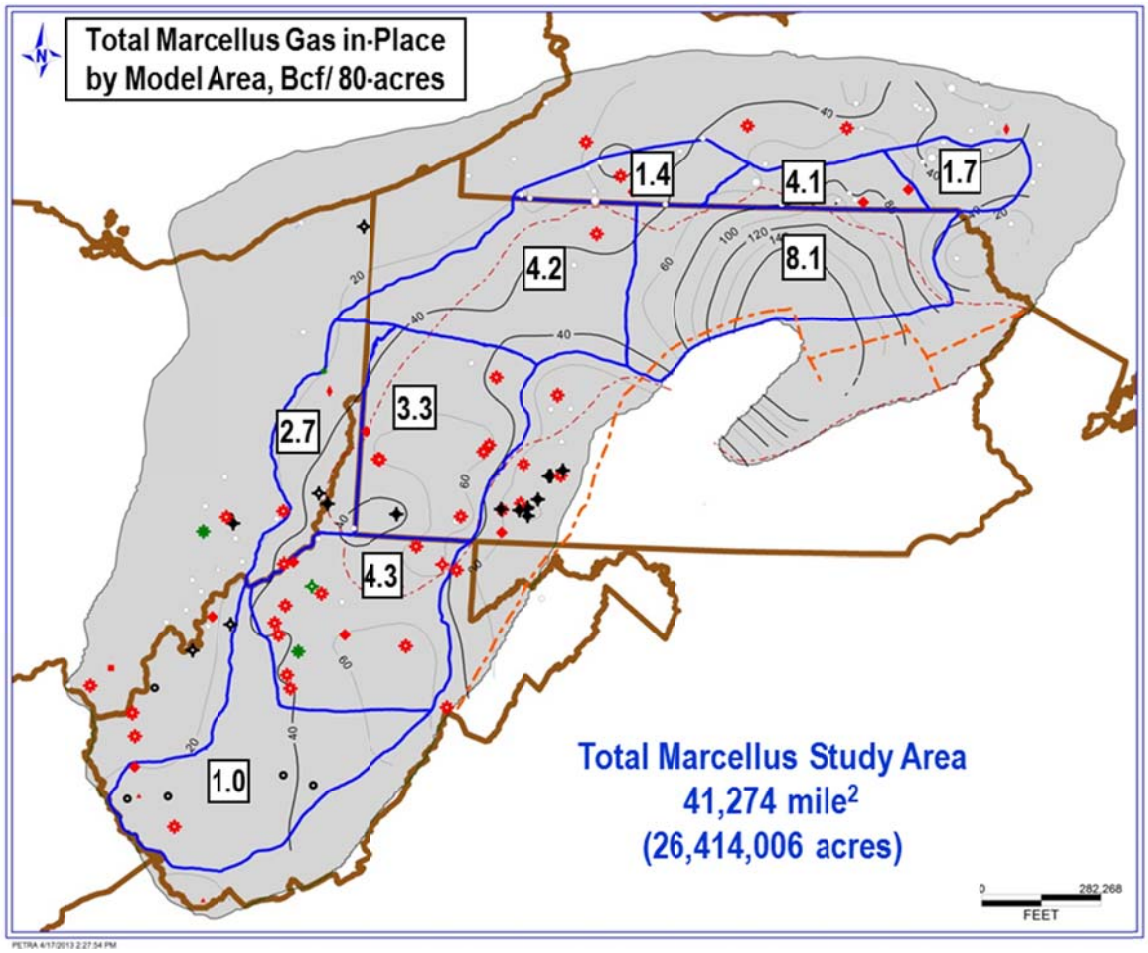

Figure 27. Total Marcellus Theoretical Maximum $CO_2$ Storage Capacity by Model Area, Mt/ 80-acres

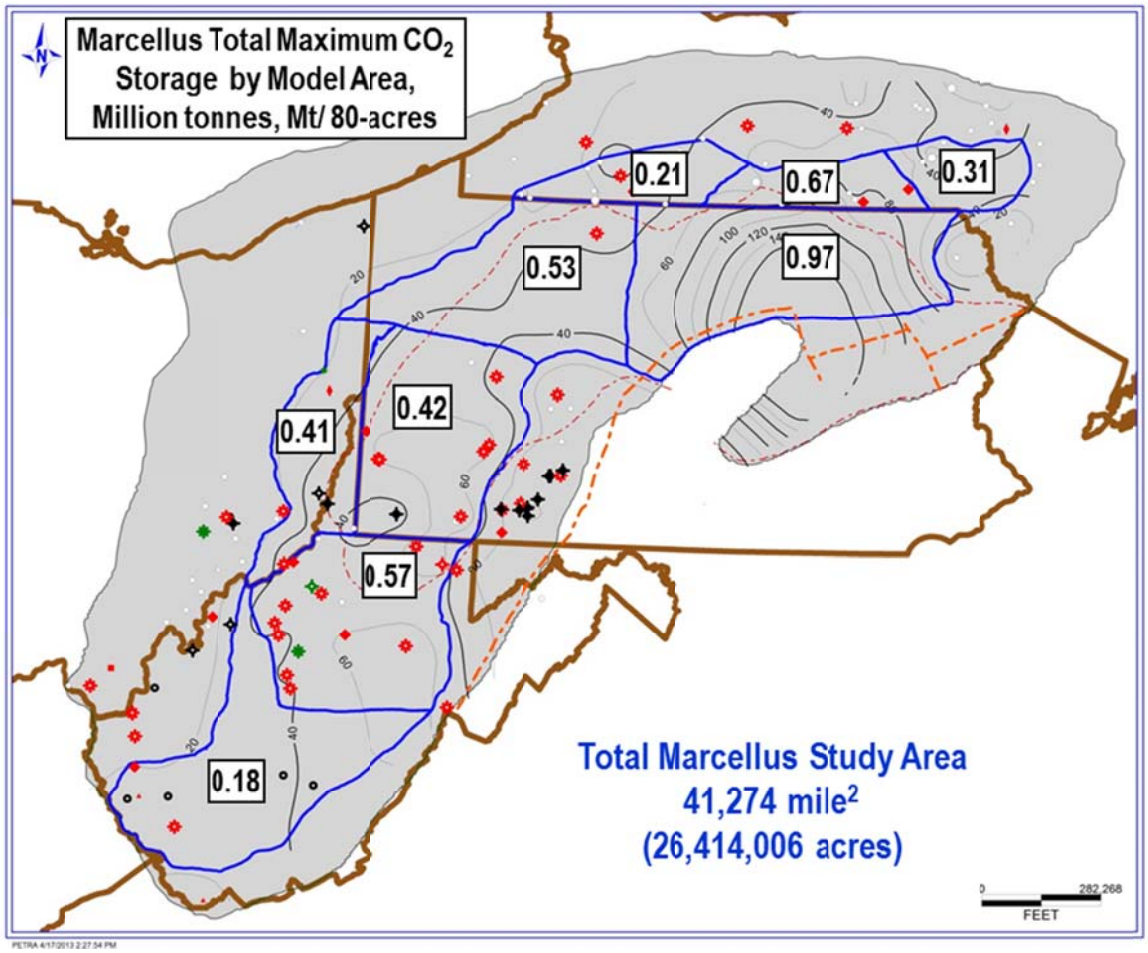

# TABLES

Table 1. Resource Assessments for the Marcellus Shale in the Appalachian Basin

| Marcellus Resource Assessments | | | | | | | |
|---|---|---|---|---|---|---|---|
| Source | Year | | | | | | Assessment |
| | 2002 | 2008 | 2009 | 2010 | 2011 | 2012 | |
| United States Geological Survey | 2 Tcf | - | - | - | 84 Tcf | - | Undiscovered technically recoverable resources; Mean Case |
| U.S. Energy Information Administration | - | 0.1 Tcf | 4.5 Tcf | 13 Tcf | - | 141 Tcf | Technically recoverable resources |
| Potential Gas Committee | - | 227 Tcf | - | 227 Tcf | - | 563 Tcf | Total Appalachian Basin recoverable resources; Most Likely Case |
| Pennsylvania State University | - | - | 489 Tcf | - | - | - | Technically recoverable resources; 1500 Tcf Gas in-place; PA only |

Sources: US. EIA, 2008 – 2010, U.S. Crude Oil, Natural Gas, and Natural Gas Liquids Reserves, 2008 through 2010, Annual Reports; U.S. EIA, 2012, Annual Energy Outlook 2012 Early Release Overview; Engelder, 2012, How much natural gas can the Marcellus shale produce? Pennsylvania State University Marcellus Research Center; Potential Gas Committee, 20018 – 2012, Potential Supply of Natural Gas in the United States, biennial report ; USGS, 2011, National Assessment of Undiscovered Oil and Gas Resources of the Devonian Marcellus Shale of the Appalachian Basin Province

Table 2. Summary of Adsorption Isotherm Data Obtained for the Marcellus

| Summary of Adsorption Isotherm Data Obtained for Marcellus | | | | | | | |
|---|---|---|---|---|---|---|---|
| Sample | Formation | Depth | Total Organic Carbon, TOC | Langmuir Volume (VL) - Methane | Langmuir Pressure (PL) - Methane | Langmuir Volume (VL) - $CO_2$ | Langmuir Pressure (PL) - $CO_2$ |
| | | ft | wt% | scf/ton | psia | scf/ton | psia |
| Beaver Meadow #1, Chenango, Co., NY | Marcellus - Oatka Creek | 1,860 | 5.00 | 99.0 | 565.0 | | |
| Beaver Meadow #1, Chenango, Co., NY | Marcellus - Union Springs | 1,930 | 8.30 | 207.0 | 552.0 | | |
| Oxford #1, Chenango, Co., NY | Marcellus - Oatka Creek | 2,440 | 2.80 | 47.5 | 508.0 | | |
| Oxford #1, Chenango, Co., NY | Marcellus - Union Springs | 2,520 | 5.30 | 93.6 | 626.4 | | |
| Otsego, Co., NY - proprietary | Marcellus - Union Springs | 2,457 | 5.10 | 169.8 | 313.3 | 341.2 | 246.8 |
| Northwest PA - proprietary | Marcellus | 5,605 | 5.00 | 110.0 | 633.2 | | |
| Northwest PA - proprietary | Marcellus | 5,664 | 0.80 | 70.1 | 1381.1 | | |
| Northwest PA - proprietary | Marcellus | 5,688 | 7.00 | 110.7 | 846.3 | | |
| | | | | Average Methane PL | 678.2 | Average $CO_2$ PL | 246.8 |

Table 3. Summary of Marcellus X-Ray Diffraction Mineralogy

| Marcellus X-Ray Diffraction Mineralogy | | | | | | | | | | |
|---|---|---|---|---|---|---|---|---|---|---|
| Data Source | Quartz | K-Feldspar | Plagioclase | Calcite | Dolomite | Fe-Dolomite | Siderite | Pyrite | Other[1] | Total Clay |
| NY | 39.0 | 0.6 | 3.7 | 22.4 | 0.6 | 1.4 | 0.3 | 8.1 | | 23.9 |
| PA | 33.0 | 0.6 | 3.8 | 22.7 | 2.8 | 0 | n.a. | 5.9 | 1.2 | 30.6 |
| OH | 29.4 | 5.2 | 3.1 | 3.3 | 2.7 | 0.5 | n.a. | 7.2 | 0.7 | 47.8 |
| [1]Other minerals include: fluorapatite , barite, gypsum and marcasite | | | | | | | | | | |

Table 4. Marcellus TOC Extrapolated from Density and Gamma Ray Logs

| Well | Upper Marcellus | | | Lower Marcellus | | |
|---|---|---|---|---|---|---|
| | TOC (Schmoker, 1993), % | TOC from Bulk Density, % | TOC from Gamma Ray, % | TOC (Schmoker, 1993), % | TOC from Bulk Density, % | TOC from Gamma Ray, % |
| Heartwood #1 37-083-53842 | No density log | No density log | 3.3 | No density log | No density log | 6.0 |
| FEI Fortuna Lutz #1V 37-015-20091 | 3.3 | 3.6 | 4.5 | 3.85 | 4.1 | 4.8 |
| J Foust #1H 37-015-20099 | 2.9 | 3.8 | 3.8 | 4.0 | 4.2 | 3.9 |
| Harper #5 H 37-015-20541 | 3.8 | 4.1 | 1.8 | 4.1 | 4.3 | 1.2 |
| Matoushek #1 37-127-20006 | 1.1 | 1.4 | 4.5 | 2.6 | 2.8 | 3.7 |

Table 5. Log Analysis Variables to Calculate Marcellus Porosity and Water Saturation

| Variable | Definition | Marcellus |
|---|---|---|
| $\rho_{Shale}$ | maximum bulk density of gray shale (low organic content), g/cc | 2.73 |
| $\rho_{matrix}$ | matrix grain density, g/cc | 2.77 |
| $\rho_{fluid}$ | density of formation water, g/cc | 1.10 |
| $\rho_{TOC}$ | density of organic matter, g/cc | 1.3 – 1.35 |
| $R_w$ | water resistivity at formation temperature, ohm-m | Variable based on temperature |
| $R_{shale}$ | shale resistivity, ohm-m | 25 - 50 |
| **a** | Archie tortuosity exponent | 1 *(common default)* |
| **m** | Archie cementation exponent | 2 *(common default)* |
| **n** | Archie saturation exponent | 2 *(common default)*<br>2.5 *(value used for Lower Marcellus)* |

Table 6. Summary and Description of Marcellus Model Areas

| Summary and Description of Marcellus Model Areas | | | | | | | | | |
|---|---|---|---|---|---|---|---|---|---|
| MODEL AREA | Area Description | Composite Model Well | Total Area, Acres | Total Area, miles$^2$ | Reservoir Pressure Gradient, psi/ft | Mean Reservoir Pressure, psia | Mean Reservoir Temperature, $^0$F | FVF for Methane, ft$^3$/ scf | FVF for $CO_2$, ft$^3$/ scf |
| AREA 1 | West Central NY; Normal Pressure | Allegany Co | 1,257,845 | 1,965 | 0.45 | 1,836 | 108.9 | 0.00719 | 0.00268 |
| AREA 2 | South Central NY; Normal Pressure | Tioga/ Broome Cos. | 1,164,491 | 1,820 | 0.45 | 2,084 | 112.7 | 0.00635 | 0.00248 |
| AREA 3 | East Central NY; Under Pressured | Chenango/ Otsego Cos. | 1,074,462 | 1,679 | 0.33 | 9,92 | 88.4 | 0.013525 | 0.00796 |
| AREA 4 | Northeast PA; Over Pressured | Bradford Co. | 5,007,988 | 7,825 | 0.64 | 4,053 | 138 | 0.003796 | 0.002286 |
| AREA 5 | NW - North Central PA; Over Pressured | Elk Co. | 3,651,027 | 5,705 | 0.56 | 3,197 | 128.5 | 0.004443 | 0.002275 |
| AREA 6 | SW - South Central PA; Normal to Over Pressured | Washington/ Fayette Cos. | 3,565,689 | 5,571 | 0.50 | 3,370 | 137 | 0.004358 | 0.002406 |
| AREA 7 | Eastern OH & WV Panhandle; Normal to Under-Pressured | Columbiana, OH; Tyler, WV | 2,250,702 | 3,517 | 0.41 | 2,079 | 120.9 | 0.006541 | 0.00267 |
| AREA 8 | North & Central WV; Normal to Under-Pressured | Tyler, Taylor, Lewis Cos. | 4,035,195 | 6,305 | 0.43 | 2,917 | 128.9 | 0.004977 | 0.002565 |
| AREA 9 | South & Southwest WV; Under Pressured | Lincoln Co. | 4,407,607 | 6,887 | 0.32 | 1,290 | 95 | 0.010223 | 0.002968 |
| Total Marcellus Study Area | | | 26,415,006 | 41,274 | | | | | |

Table 7. Model Layer Attributes for Lower Marcellus (Union Springs)

| Model Layer Attributes for Lower Marcellus (Union Springs) | | | | | | | | | |
|---|---|---|---|---|---|---|---|---|---|
| Model Area | Area Description | Average Depth, ft. | Thickness, ft. | Total Porosity, fraction | Matrix Permeability, md | Water Saturation, fraction | Calculated TOC, wt. % | Mean Adsorbed Gas Content, scf/ ton | Theoretical Max. Adsorbed $CO_2$, scf/ ton |
| AREA 1 | West Central NY; Normal Pressure | 3,649 | 15 | 0.072 | 3.69E-06 | 0.21 | 5.6 | 93.3 | 330.2 |
| AREA 2 | South Central NY; Normal Pressure | 4,695 | 33 | 0.079 | 9.59E-06 | 0.22 | 6.3 | 106.2 | 376.8 |
| AREA 3 | East Central NY; Under Pressured | 3,005 | 50 | 0.070 | 2.81E-06 | 0.26 | 5.5 | 75.3 | 294.6 |
| AREA 4 | Northeast PA; Over Pressured | 6,413 | 34 | 0.062 | 1.87E-06 | 0.19 | 5.6 | 107.0 | 353.1 |
| AREA 5 | NW - North Central PA; Over Pressured | 5,719 | 34 | 0.093 | 6.48E-05 | 0.18 | 6.8 | 123.6 | 422.3 |
| AREA 6 | SW - South Central PA; Normal to Over Pressured | 6,760 | 29 | 0.066 | 3.33E-06 | 0.51 | 4.1 | 77.9 | 261.8 |
| AREA 7 | Eastern OH & WV Panhandle; Normal to Under-Pressured | 5,080 | 9 | 0.115 | 5.62E-04 | 0.19 | 9.2 | 148.7 | 547.2 |
| AREA 8 | North & Central WV; Normal to Under-Pressured | 6,966 | 31 | 0.089 | 3.75E-05 | 0.24 | 6.7 | 120.0 | 413.3 |
| AREA 9 | South & Southwest WV; Under Pressured | 4,022 | 21 (Total Marcellus) | 0.084 | 1.9E-05 | 0.21 | 6.0 | 93.6 | 339.2 |

Table 8. Model Layer Attributes for Upper Marcellus (Oatka Creek)

| Model Layer Attributes for Upper Marcellus (Oatka Creek) | | | | | | | | | |
|---|---|---|---|---|---|---|---|---|---|
| Model Area | Area Description | Average Depth, ft. | Thickness, ft. | Total Porosity, fraction | Matrix Permeability, md | Water Saturation, fraction | Calculated TOC, wt. % | Mean Adsorbed Gas Content, scf/ ton | Theoretical Max. Adsorbed $CO_2$, scf/ ton |
| AREA 1 | West Central NY; Normal Pressure | 3,636 | 9 | 0.059 | 1.18E-06 | 0.10 | 5.1 | 81.4 | 297.8 |
| AREA 2 | South Central NY; Normal Pressure | 4,640 | 58 | 0.060 | 7.18E-07 | 0.57 | 4.7 | 74.5 | 278.1 |
| AREA 3 | East Central NY; Under Pressured | 2,439 | 10 | 0.070 | 2.81E-06 | 0.24 | 3.9 | 50.4 | 208.9 |
| AREA 4 | Northeast PA; Over Pressured | 6,281 | 43 | 0.044 | 7.88E-08 | 0.41 | 3.7 | 72.0 | 234.0 |
| AREA 5 | NW - North Central PA; Over Pressured | 5,696 | 11 | 0.058 | 5.46E-07 | 0.33 | 4.3 | 81.0 | 268.9 |
| AREA 6 | SW - South Central PA; Normal to Over Pressured | 6,714 | 26 | 0.065 | 1.42E-06 | 0.28 | 4.6 | 84.5 | 286.7 |
| AREA 7 | Eastern OH & WV Panhandle; Normal to Under-Pressured | 5,051 | 20 | 0.104 | 2.22E-04 | 0.26 | 7.1 | 118.8 | 426.9 |
| AREA 8 | North & Central WV; Normal to Under-Pressured | 6,933 | 13 | 0.076 | 6.37E-06 | 0.32 | 5.7 | 102.1 | 351.6 |
| AREA 9 | South & Southwest WV; Under Pressured | Absent | | | | | | | |

Table 9. Model Layer Attributes for Purcell/ Cherry Valley Limestone

| Model Layer Attributes for Purcell/ Cherry Valley Limestone | | | | | | | | | |
|---|---|---|---|---|---|---|---|---|---|
| Model Area | Area Description | Average Depth, ft. | Thickness, ft. | Total Porosity, fraction | Matrix Permeability, md | Water Saturation, fraction | Calculated TOC, wt. % | Mean Adsorbed Gas Content, scf/ ton | Theoretical Max. Adsorbed $CO_2$, scf/ ton |
| AREA 1 | West Central NY; Normal Pressure | 3,645 | 4 | 0.061 | 8.23E-07 | 0.16 | 2.5 | 40.3 | 147.4 |
| AREA 2 | South Central NY; Normal Pressure | 4,692 | 3 | 0.040 | 4.69E-08 | 0.53 | 3.4 | 58.3 | 200.4 |
| AREA 3 | East Central NY; Under Pressured | Absent | | | | | | | |
| AREA 4 | Northeast PA; Over Pressured | 6,324 | 89 | 0.05 | 1.83E-07 | 0.46 | 3.3 | 63.0 | 204.9 |
| AREA 5 | NW - North Central PA; Over Pressured | 5,707 | 12 | 0.043 | 7.06E-08 | 0.51 | 3.3 | 61.3 | 202.5 |
| AREA 6 | SW - South Central PA; Normal to Over Pressured | 6,740 | 20 | 0.036 | 1.23E-08 | 0.78 | 2.5 | 46.7 | 152.7 |
| AREA 7 | Eastern OH & WV Panhandle; Normal to Under-Pressured | 5,071 | 9 | 0.088 | 3.27E-05 | 0.44 | 4.9 | 83.1 | 291.5 |
| AREA 8 | North & Central WV; Normal to Under-Pressured | 6,946 | 20 | 0.062 | 9.43E-07 | 0.49 | 5.2 | 97.9 | 320.7 |
| AREA 9 | South & Southwest WV; Under Pressured | Absent | | | | | | | |

Table 10. Summary of Estimated Gas In-Place for Marcellus Model Areas

| Summary of Estimated Gas In-Place for Marcellus Model Areas | | | | | | | | |
|---|---|---|---|---|---|---|---|---|
| MODEL AREA | Area Description | Total Area, miles$^2$ | Adsorbed Gas In-Place, Bcf/ mile$^2$ | Free Gas In-Place, Bcf/ mile$^2$ | Total Adsorbed Gas in-Place, Bcf | Total Free Gas In-Place, Bcf | Estimated Total Gas In-Place, Bcf | *Estimated Theoretical Maximum $CO_2$ Storage, Bcf* |
| AREA 1 | West Central NY; Normal Pressure | 1,965 | 4.9 | 5.9 | 9,676 | 11,510 | 21,186 | *66,001* |
| AREA 2 | South Central NY; Normal Pressure | 1,820 | 17.0 | 15.8 | 30,913 | 28,752 | 59,665 | *190,467* |
| AREA 3 | East Central NY; Under Pressured | 1,679 | 7.0 | 6.4 | 11,827 | 10,803 | 22,631 | *80,530* |
| AREA 4 | Northeast PA; Over Pressured | 7,825 | 26.5 | 38.1 | 207,546 | 297,847 | 505,393 | *1,184,168* |
| AREA 5 | NW - North Central PA; Over Pressured | 5,705 | 12.9 | 20.5 | 73,319 | 117,163 | 190,482 | *476,823* |
| AREA 6 | SW - South Central PA; Normal to Over Pressured | 5,571 | 11.9 | 14.7 | 66,433 | 81,661 | 148,094 | *368,350* |
| AREA 7 | Eastern OH & WV Panhandle; Normal to Under-Pressured | 3,517 | 9.5 | 11.9 | 33,493 | 41,808 | 75,300 | *225,713* |
| AREA 8 | North & Central WV; Normal to Under-Pressured | 6,305 | 15.7 | 19.1 | 98,862 | 120,692 | 219,554 | *565,895* |
| AREA 9 | South & Southwest WV; Under Pressured | 6,887 | 4.4 | 3.8 | 30,440 | 26,172 | 56,612 | *198,147* |
| Marcellus Study Area Total | | 41,274 | 13.6 | 17.8 | 562,509 | 736,407 | 1,299 Tcf | *3,356 Tcf* |

Table 11. Estimated Theoretical Maximum $CO_2$ Storage Capacity for Marcellus Model Areas

| Estimated Theoretical Maximum $CO_2$ Storage Capacity for Marcellus Model Areas | | | | | | | |
|---|---|---|---|---|---|---|---|
| MODEL AREA | Area Description | Total Area, miles$^2$ | Adsorbed $CO_2$ Storage, Bcf/ mile$^2$ | Free (non-adsorbed) $CO_2$ Storage, Bcf/ mile$^2$ | Total Maximum Adsorbed $CO_2$ Storage, Bcf | Total Maximum Non-Adsorbed $CO_2$ Storage, Bcf | Theoretical Maximum $CO_2$ Storage Capacity, Bcf |
| AREA 1 | West Central NY; Normal Pressure | 1,965 | 17.9 | 15.7 | 35,121 | 30,880 | 66,001 |
| AREA 2 | South Central NY; Normal Pressure | 1,820 | 64.2 | 40.5 | 116,848 | 73,618 | 190,467 |
| AREA 3 | East Central NY; Under Pressured | 1,679 | 37.0 | 10.9 | 62,174 | 18,356 | 80,530 |
| AREA 4 | Northeast PA; Over Pressured | 7,825 | 88.1 | 63.2 | 689,581 | 494,587 | 1,184,168 |
| AREA 5 | NW - North Central PA; Over Pressured | 5,705 | 43.5 | 40.1 | 248,008 | 228,815 | 476,823 |
| AREA 6 | SW - South Central PA; Normal to Over Pressured | 5,571 | 39.6 | 26.5 | 220,437 | 147,913 | 368,350 |
| AREA 7 | Eastern OH & WV Panhandle; Normal to Under-Pressured | 3,517 | 35.1 | 29.1 | 123,292 | 102,421 | 225,713 |
| AREA 8 | North & Central WV; Normal to Under-Pressured | 6,305 | 52.6 | 37.1 | 331,770 | 234,185 | 565,895 |
| AREA 9 | South & Southwest WV; Under Pressured | 6,887 | 15.7 | 13.1 | 108,000 | 90,147 | 198,147 |
| Marcellus Study Area Total | | 41,274 | 39.1 | 28.7 | 1,935,171 | 1,420,921 | 3,356,093 |

Table 12. Estimated Total Gas In-Place and Theoretical Maximum $CO_2$ Storage Capacity for Marcellus – Aggregated by State

| | New York | Pennsylvania | West Virginia | Eastern Ohio & West Virginia Panhandle | Total Study Area |
|---|---|---|---|---|---|
| Potential $CO_2$ Storage Area, acres | 3,496,798 | 12,224,704 | 8,442,802 | 2,250,702 | 26,415,006 |
| Potential $CO_2$ Storage Area, mile$^2$ | 5,464 | 19,101 | 13,192 | 3,517 | 41,273 |
| Adsorbed Gas In-Place, Bcf | 52,416 | 347,299 | 129,302 | 33,493 | 562,509 |
| Non-Adsorbed, 'Free' Gas In-Place, Bcf | 51,065 | 496,670 | 146,864 | 41,808 | 736,407 |
| Total Gas In-Place, Bcf | 103,481 | 843,969 | 276,166 | 75,300 | 1,298,916 |
| Maximum $CO_2$ Storage, Adsorbed, million tonnes, Mt | 10,926 | 59,083 | 22,434 | 6,290 | 98,733 |
| Maximum $CO_2$ Storage, 'Free', million tonnes, Mt | 6,268 | 44,455 | 16,548 | 5,226 | 72,496 |
| Total $CO_2$ Storage Capacity, million tonnes, Mt | 17,194 | 103,538 | 38,982 | 11,516 | 171,229 |
| | | | | | |
| Total Maximum $CO_2$ Storage Capacity per Unit Area, Mt/ mile$^2$ | 3.15 | 5.42 | 2.95 | 3.27 | 4.15 |

# APPENDICES

## Appendix 1. Lower Marcellus (Union Springs) – Mean Total Porosity

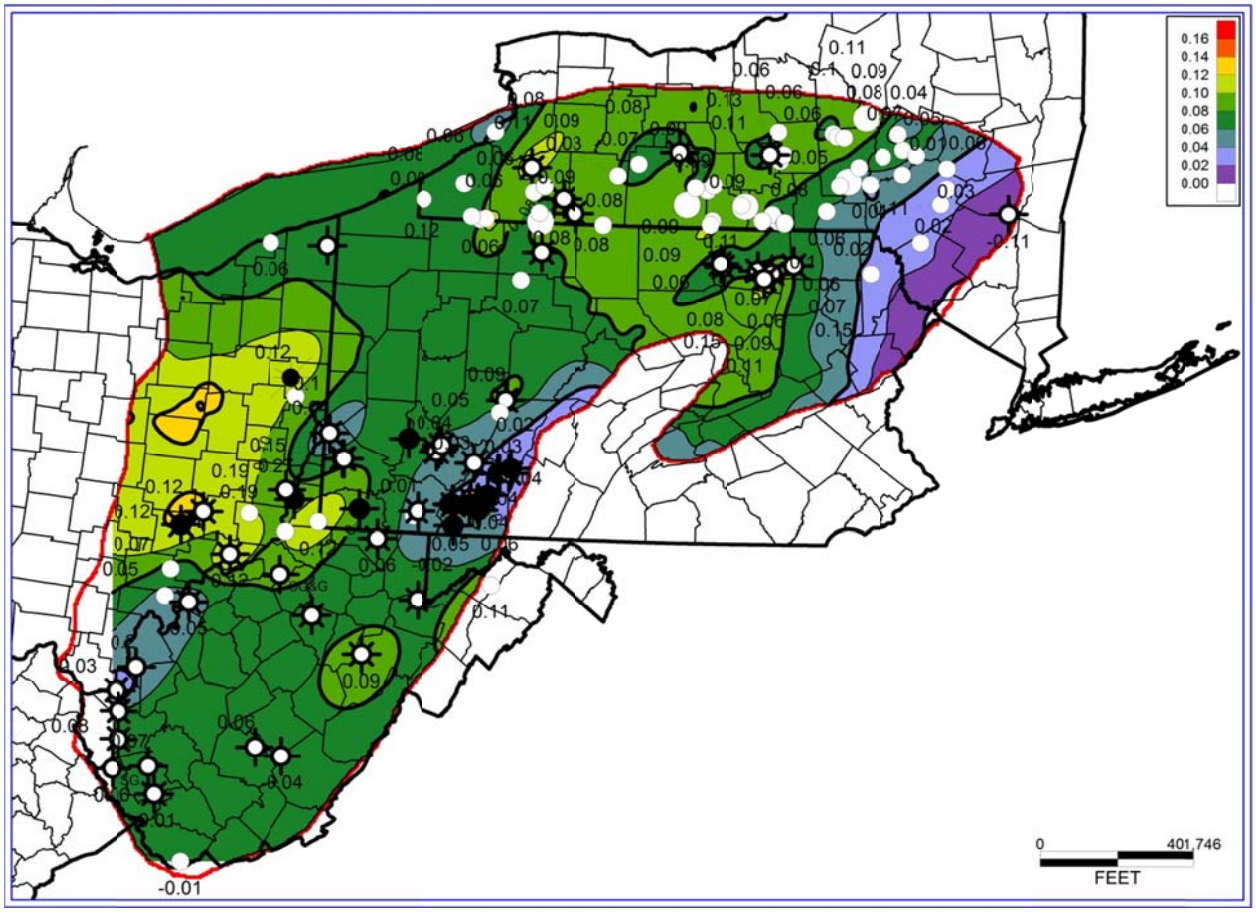

## Appendix 2. Lower Marcellus (Union Springs) - Mean Calculated Water Saturation

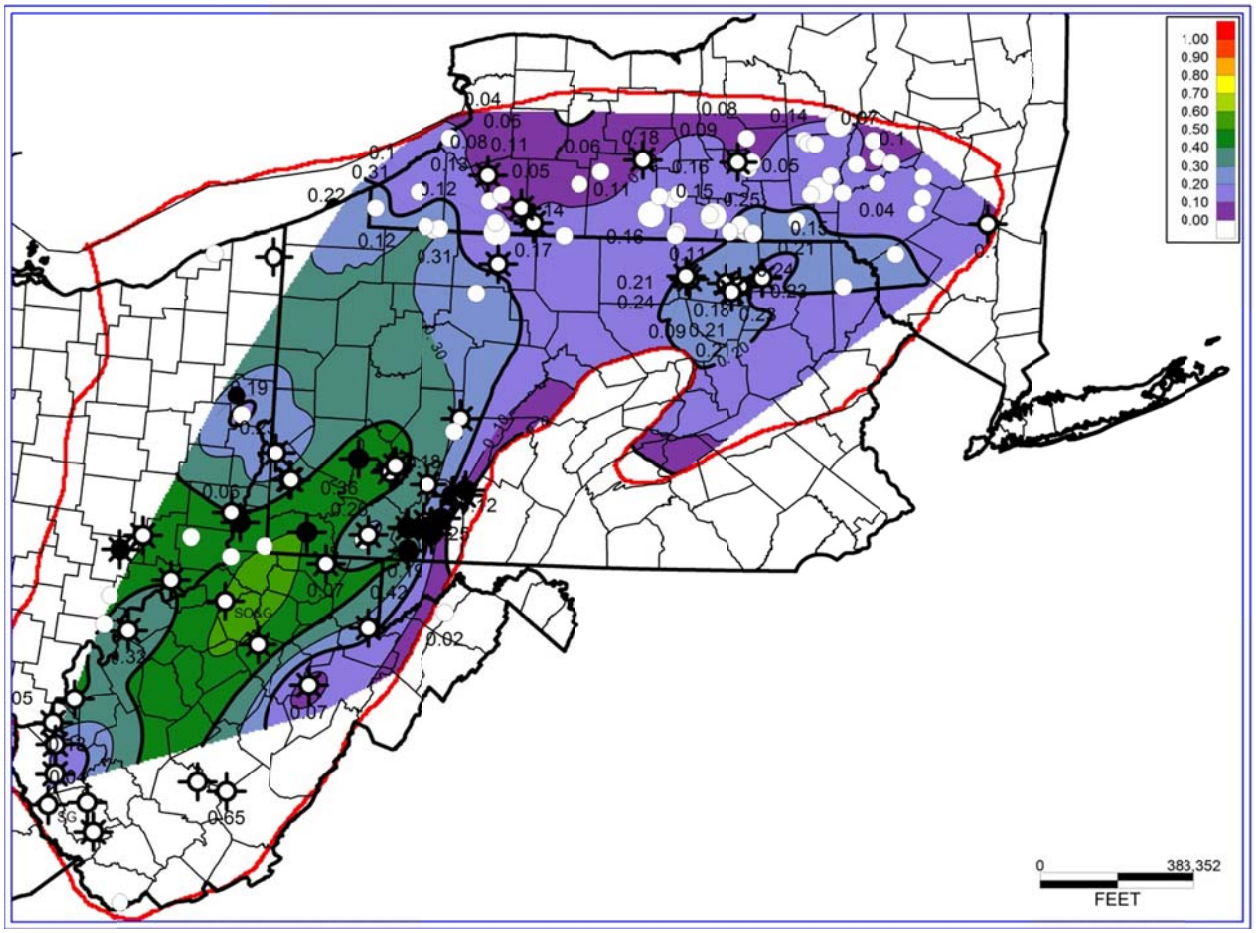

## Appendix 3. Lower Marcellus (Union Springs) - Mean Effective (Gas-filled) Porosity

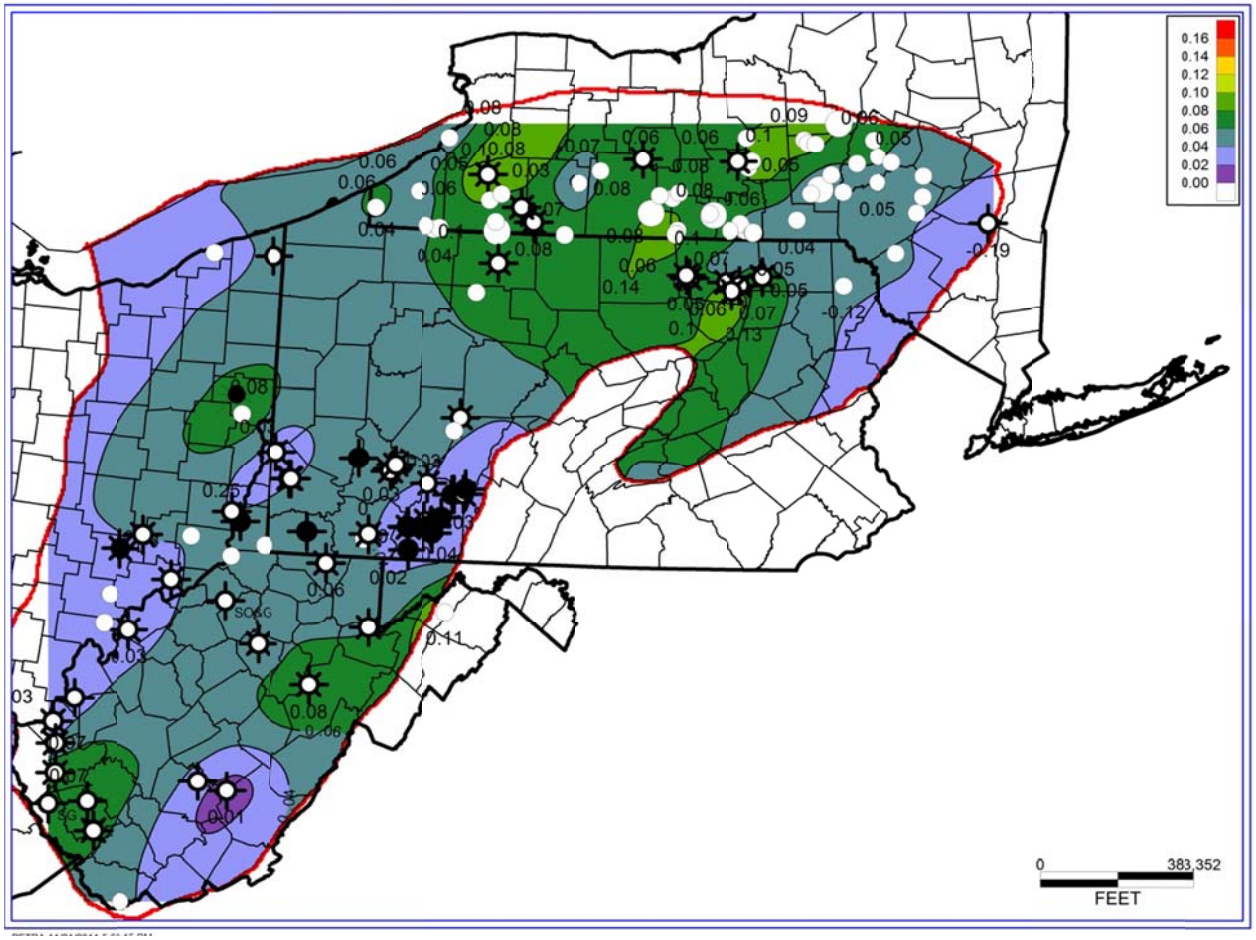

## Appendix 4. Lower Marcellus (Union Springs) – Mean Calculated TOC

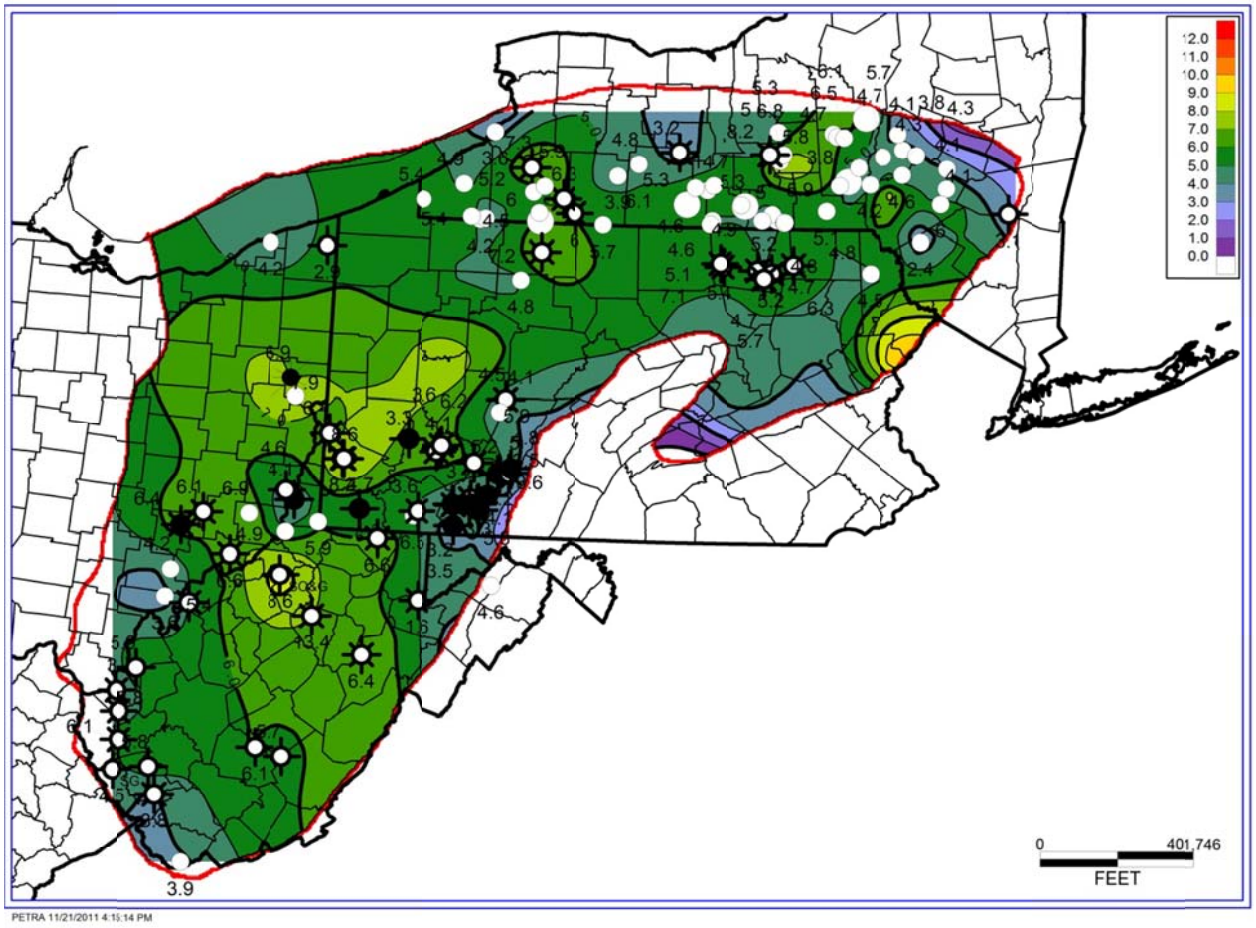

## Appendix 5. Upper Marcellus (Oatka Creek) – Mean Calculated Density Porosity

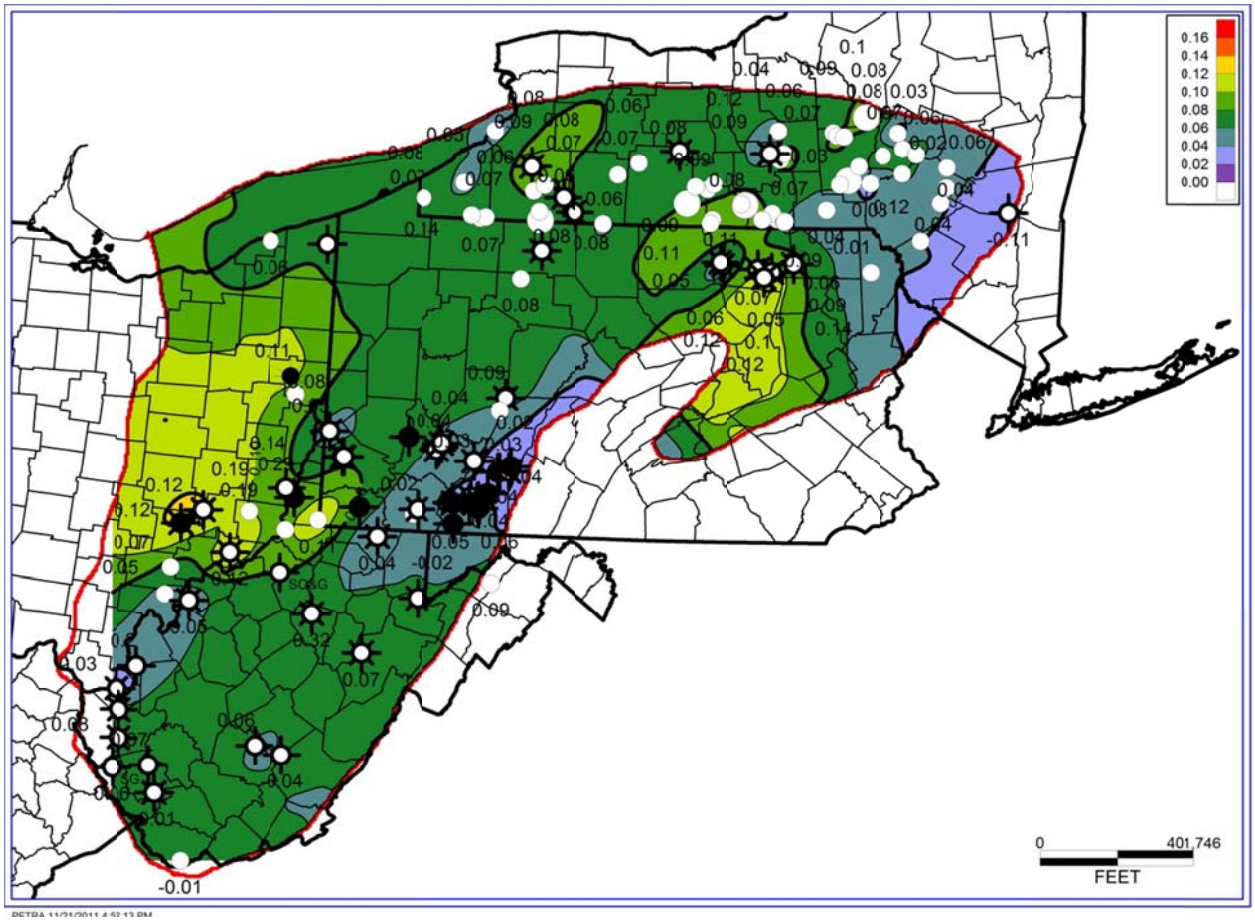

## Appendix 6. Upper Marcellus (Oatka Creek) – Mean Calculated Water Saturation

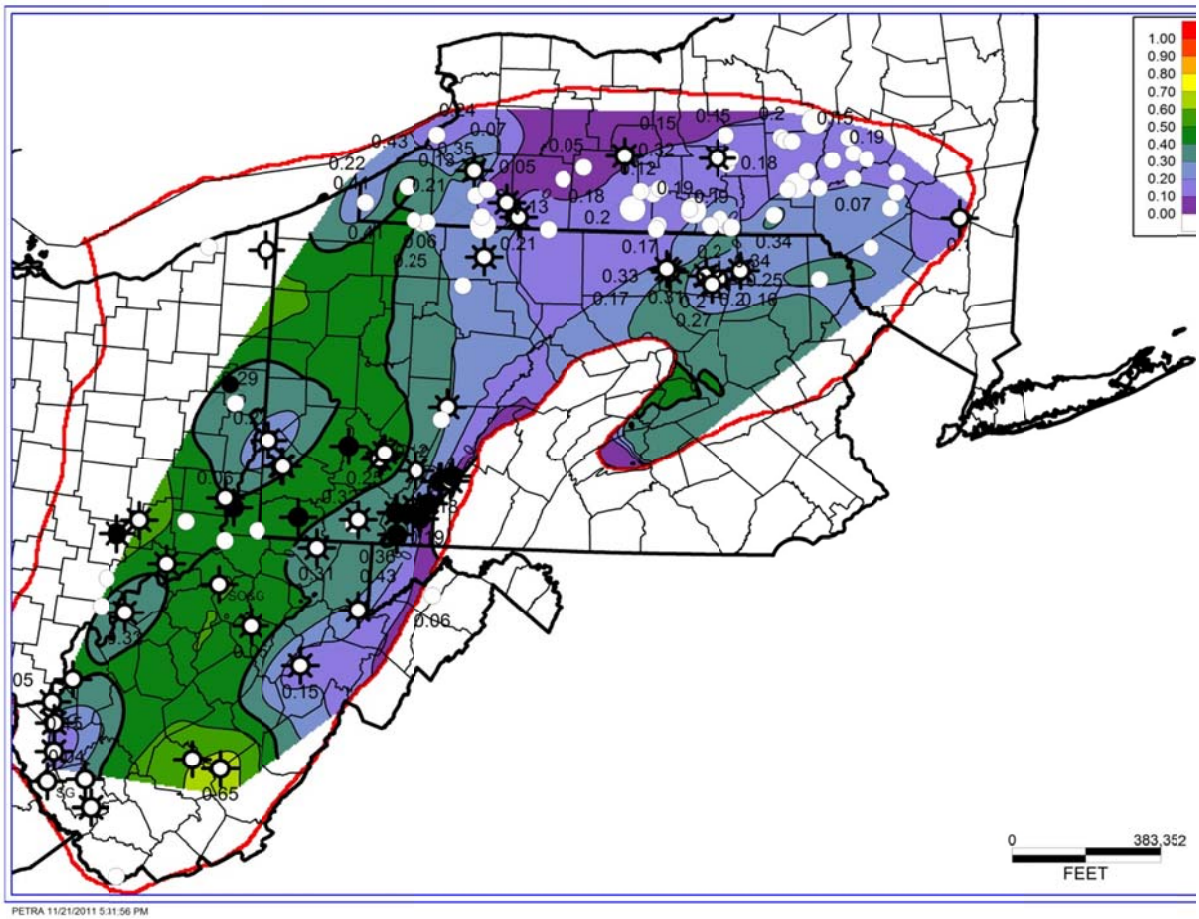

## Appendix 7. Upper Marcellus (Oatka Creek) – Mean Effective (Gas-Filled) Porosity

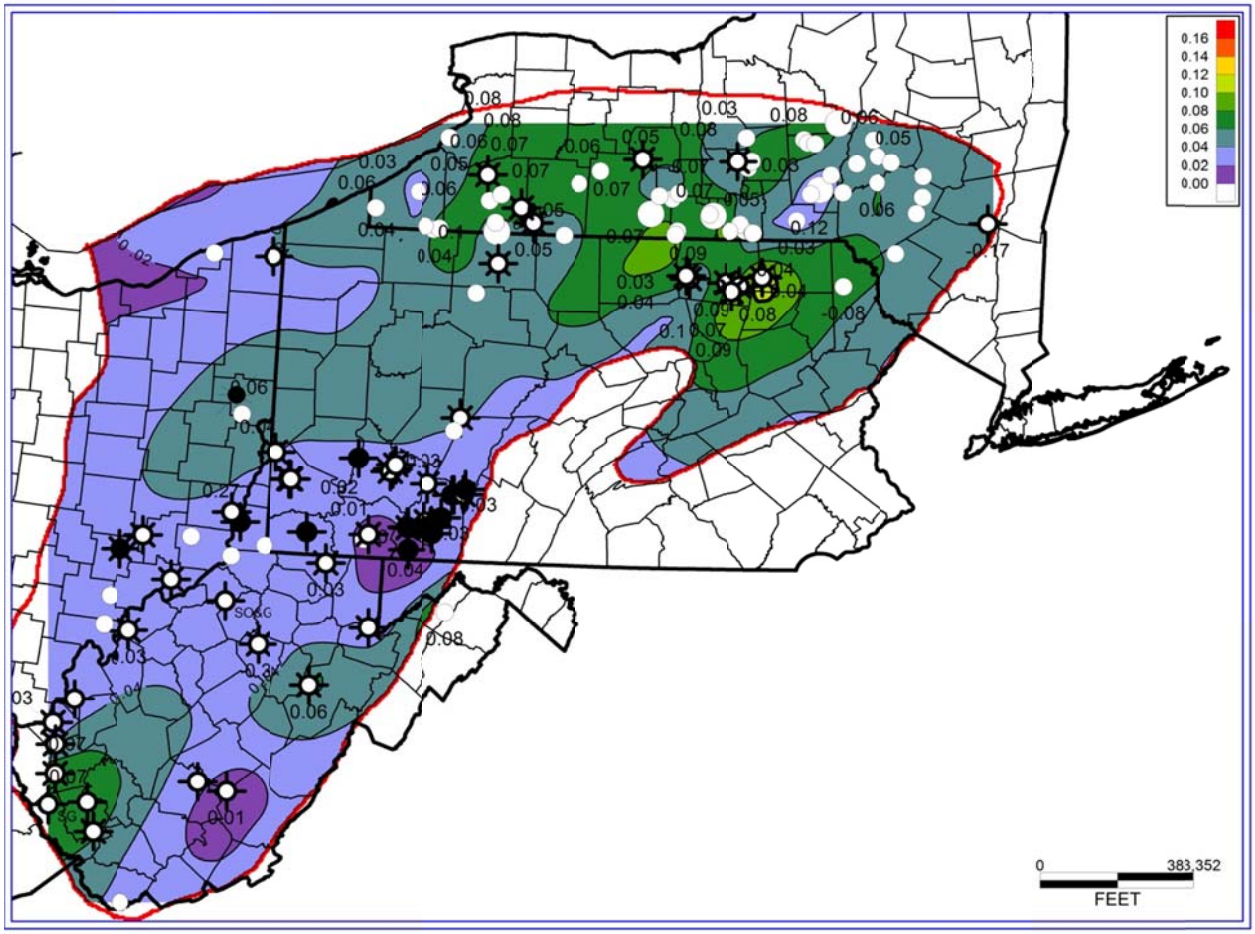

# Volume 3
# Basin-Level Characterization Of Enhanced Gas Recovery And $CO_2$ Storage Potential In The Utica Shale

## Assessment of Factors Influencing Effective $CO_2$ Storage Capacity and Injectivity in Eastern Gas Shales

Prepared for:
U.S. Department of Energy
National Energy Technology Laboratory
DOE Award Number: DE-FE0004633

Prepared by:
Michael Godec, Principal Investigator
Advanced Resources International, Inc.
4501 Fairfax Drive ▪ Suite 910 ▪ Arlington, Virginia 22203

Date:
October 23, 2013

Advanced Resources International, Inc.

4501 Fairfax Drive ▪ Suite 910 ▪ Arlington, Virginia 22203 ▪ Phone: (703) 528-8420 ▪ web: www.adv-res.com

## Advanced Resources International, Inc.

# Table of Contents

**1.** INTRODUCTION ..... 1
a. Background ..... 1
b. Project Objectives ..... 2
c. Objective of this Volume ..... 2
**2.** UTICA/ POINT PLEASANT SHALE GAS PRODUCTION AND $CO_2$ STORAGE POTENTIAL IN THE BASIN ..... 3
a. Utica/ Point Pleasant Production History and Development ..... 3
b. Utica/ Point Pleasant Resource Potential ..... 4
c. Sources of $CO_2$ Emissions ..... 4
**3.** GEOLOGIC CHARACTERIZATION ..... 5
a. Geologic Setting ..... 5
b. Stratigraphy ..... 6
c. Utica/ Point Pleasant Study Area ..... 7
d. Type Log and Stratigraphic Cross-Section ..... 8
**4.** RESERVOIR DATA ..... 10
a. Adsorption Isotherms ..... 10
b. Total Organic Carbon ..... 11
c. X-Ray Diffraction Mineralogy ..... 11
d. Core Porosity and Permeability ..... 12
**5.** ESTIMATED GAS IN-PLACE AND THEORETICAL MAXIMUM $CO_2$ STORAGE CAPACITY ..... 14
a. Overview of Calculated Gas In-Place and $CO_2$ Storage Capacity ..... 14
b. Well Log Analysis Methodology ..... 15
i. TOC Extrapolated from Density Logs ..... 15
ii. Porosity from Density Logs ..... 16
iii. Adsorbed Gas Content and Theoretical Maximum Adsorbed $CO_2$ Capacity ..... 16
iv. Free Gas In-Place and Theoretical Maximum $CO_2$ Storage Capacity ..... 18
v. Theoretical Maximum $CO_2$ Storage as 'Free' $CO_2$ (Non-Adsorbed) ..... 19
c. Utica Log Calculation Results ..... 20
d. Total Gas In-Place and Maximum $CO_2$ Storage Capacity ..... 20
i. Caveats and Assumptions Regarding this Assessment ..... 21
**6.** DEFINITION OF MODEL AREAS FOR RESERVOIR MODELING IN THE BASIN ..... 23
a. Rational for the Development of Model Areas ..... 23
b. Overview of Model Areas ..... 23
c. Sources of Data for Representative Wells in Each Model Area ..... 24
**7.** REFERENCES ..... 25
FIGURES ..... 29
TABLES ..... 48
APPENDICES ..... 62

# List of Figures

Figure 1. Map Showing Extent and Approximate Depth of Utica Shale ....29
Figure 2. Simplified Stratigraphic Column for Utica and Point Pleasant Shale Formations ....30
Figure 3. New York Utica Stratigraphy from the Mohawk Valley Outcrop ....31
Figure 4. Utica Thermal Maturity Boundaries ....32
Figure 5. Utica/ Point Pleasant Study Area with Model Area Sub-Divisions ....33
Figure 6. Utica/ Point Pleasant Type Log, Tioga County, New York ....34
Figure 7. Stratigraphic Cross-Section Showing Model Layers for Reservoir Simulation ....35
Figure 8. Methane Adsorption Isotherms for the Utica/ Point Pleasant ....36
Figure 9. $CO_2$ Adsorption Isotherms for the Utica/ Point Pleasant ....37
Figure 10. Cross-Plot Showing Correlation of TOC and Langmuir Volume for the Utica/ Point Pleasant Methane Isotherms ....38
Figure 11. Cross-Plot Showing Correlation of TOC and Langmuir Volume for the Utica/ Point Pleasant $CO_2$ Isotherms ....38
Figure 12. Cross-Plot Showing Correlation of TOC and Bulk Density for Utica, Point Pleasant and Trenton Data in Ohio and New York ....39
Figure 13. Utica and Point Pleasant Core Porosity and Permeability ....40
Figure 14. Impact of Net Effective Confining Stress on Measured Core Permeability ....41
Figure 15. Basal Utica Shale Reservoir Layer; Selected Model Well Parameters – Thickness, Average TOC, Average Total Porosity ....42
Figure 16. Upper (Shaley) Point Pleasant Reservoir Layer; Selected Model Well Parameters – Thickness, Average TOC, Average Total Porosity ....43
Figure 17. Basal Utica Shale Reservoir Layer – Total Estimated Gas in-Place, Bcf/square mile ....44
Figure 18. Upper (Shaley) Point Pleasant Reservoir Layer – Total Estimated Gas in-Place, Bcf/square mile ....45
Figure 19. Total Utica/ Point Pleasant; Gas in-Place by Model Area, Bcf/ 80-acres ....46
Figure 20. Total Utica/ Point Pleasant; Theoretical Maximum $CO_2$ Storage Capacity by Model Area, Mt/ 80-acres .46

# List of Tables

Table 1. Summary of Adsorption Isotherm Data Obtained for the Utica/ Point Pleasant ....48
Table 2. Summary of X-Ray Diffraction Mineralogy for the Utica/ Point Pleasant....49
Table 3. Utica and Point Pleasant Porosity-Permeability Relationships from Core Data ....49
Table 4. Adsorbed Gas Content Calculated from Isotherm Data and TOC....50
Table 5. Theoretical Maximum Adsorbed $CO_2$ Capacity from Isotherm Data and TOC....50
Table 6. Log Analysis Variables to Calculate Porosity and Water Saturation ....51
Table 7. Description and Summary of Model Areas for the Utica/ Point Pleasant ....52
Table 8. Model Layer Attributes for the Upper Utica Shale – Archie Water Saturation ....53
Table 9. Model Layer Attributes for the Basal Utica Shale – Simandoux Water Saturation ....54
Table 10. Model Layer Attributes for the Upper Point Pleasant – Simandoux Water Saturation ....55
Table 11. Model Layer Attributes for the Lower Point Pleasant – Archie Water Saturation ....56
Table 12. Utica Shale; Summary of Estimated Gas In-Place by Model Area....57
Table 13. Point Pleasant; Summary of Estimated Gas In-Place by Model Area ....58
Table 14. Utica Shale; Estimated Theoretical Maximum $CO_2$ Storage by Model Area ....59
Table 15. Point Pleasant; Estimated Theoretical Maximum $CO_2$ Storage by Model Area....60
Table 16. Utica/ Point Pleasant; Summary of Total Gas In-Place, Resource Concentration and Total Theoretical Maximum $CO_2$ Storage Capacity by Model Area....61
Appendix 1. Model Layer Attributes for the Upper Utica Shale; Water Saturation Calculated Using Simandoux ....63

# 1. INTRODUCTION

## a. Background

Organic-rich gas shales are recognized as sharing some of the same methane storage characteristics as coal seams. Natural gas is adsorbed on kerogen and clay surfaces in gas shales, similar to methane storage within coal seams. Gas is also stored as "free" (non-adsorbed) gas in fracture porosity and inter-granular microporosity, as well as in micropores commonly observed in within the kerogen of thermally mature shale (intra-kerogen porosity). The relative amounts of adsorbed and "free" gas recovered during the producing life of a shale gas well are unknown.

The potential storage of $CO_2$ in organic-rich gas shales is attracting increasing interest, especially in Appalachian Basin states that have extensive shale deposits, but limited $CO_2$ storage capacity in conventional porous reservoirs. It has been demonstrated in coal seams that $CO_2$ is preferentially adsorbed at a ratio of two or more $CO_2$ molecules for every methane molecule displaced. Gas shale reservoirs are expected to react similarly and desorb methane while preferentially adsorbing $CO_2$. In addition, some component of the pore volume that contains "free" gas is expected to be available for $CO_2$ storage as non-adsorbed $CO_2$, especially where previous hydraulic fracturing has enhanced injectivity and reservoir pore volume. Although still in the conceptual stage, $CO_2$ injection into organic-rich gas shales could provide dual benefits: an economic benefit from the incremental recovery of adsorbed methane and an environmental benefit of secure $CO_2$ storage.

The goal of this cooperative research project is to build upon previous and on-going work to assess key factors that would influence effective $CO_2$ storage capacity and injectivity in selected gas shales within the Appalachian Basin. The Appalachian Basin is endowed with thick and extensive shale formations, ranging in age from the Ordovician through the Devonian. The most prolific and promising gas shale formations for $CO_2$ storage were selected as the focus for this project including the Devonian Marcellus Shale in New York, Pennsylvania, West Virginia and eastern Ohio; the Devonian Ohio Shale in Kentucky; and the Ordovician Utica and Point Pleasant shale and equivalent formations in New York, Pennsylvania, West Virginia and Ohio. The late Devonian age Antrim Shale in the Michigan Basin was also investigated because it has similar reservoir properties to the Appalachian Basin Devonian shale formations, and the existing production infrastructure and shallow depth make the Antrim particularly attractive for $CO_2$ storage.

## b. Project Objectives

The low permeability and porosity typical of gas shale formations make $CO_2$ storage in shale challenging, especially when compared to other storage reservoirs such as depleted conventional oil and gas reservoirs and deep saline aquifers. Low porosity constrains the potential storage capacity, while low permeability constrains the injectivity of gas shales. Such constraints are counter-balanced by the great extent and thickness of candidate shale formations plus the strong adsorptive capacity of gas shales for $CO_2$, which offers the potential to store $CO_2$ securely. Potential $CO_2$ storage capacity of gas shales is just beginning to be rigorously assessed. Critical factors that will determine the storage capacity and injectivity of $CO_2$ in gas shales are the volume and rate that methane can be desorbed and then produced from the shales, as well as the relative contribution of free gas from the gas-filled or, effective, pore volume. Consequently, understanding the $CO_2$ storage capacity of such shale formations requires a firm understanding the gas productive capacity of the shale.

## c. Objective of this Volume

This volume reports on the basin-level geologic characterization of the Ordovician age Utica and Point Pleasant shale and equivalent formations in New York, Pennsylvania, West Virginia and Ohio. The objective of the Utica/ Point Pleasant geologic characterization is to estimate methane gas in-place and potential $CO_2$ storage capacity as both adsorbed $CO_2$ displacing methane, and as non-adsorbed $CO_2$ replacing free gas in the pore volume. The calculated gas in-place and calculated maximum $CO_2$ storage capacity provide points of comparison with the reservoir simulation results to estimate gas recovery factors and determine appropriate $CO_2$ injection rates.

A second objective of the geologic characterization is to select model areas based on expected capacity for gas production and $CO_2$ storage. Average reservoir characteristics of each model area are inputs to the reservoir simulation.

# 2. UTICA/ POINT PLEASANT SHALE GAS PRODUCTION AND $CO_2$ STORAGE POTENTIAL IN THE BASIN

Building upon advances in horizontal drilling and hydraulic fracturing technologies, organic-rich gas shale formations have rapidly developed into a major hydrocarbon supply option in North America. The same technologies that have contributed to the rapid development of shale gas production - horizontal drilling and massive hydraulic fracturing - may also afford the possibility of using shale formations for cost effective storage of $CO_2$. Storing $CO_2$ in shales may offer particular advantages. Unlike storage in saline aquifers, $CO_2$ injection into gas shale formations may enhance methane production, the revenues from which would help offset the costs of storage. In addition, most basins that contain shale gas resources cover large geographic areas, which may be populated with significant concentrations of anthropogenic $CO_2$ emissions. This is the case with the Utica and Point Pleasant shale formations in the Appalachian Basin. The Appalachian Basin is approximately 300 miles (480 kilometers) wide and 600 miles (970 kilometers) long and contains thick, extensive gas shale formations in addition to the Utica/ Point Pleasant – these include the Marcellus Shale, Ohio Shale, and other Devonian gas shales. The Appalachian Basin region also hosts a large portion of the coal-fired power generation capacity in the United States.

## a. Utica/ Point Pleasant Production History and Development

The Utica Shale and Point Pleasant Formation comprise an Ordovician oil and gas play which extends through a majority of the Appalachian Basin, including New York, Quebec, Pennsylvania, Ohio, Maryland, and West Virginia - occupying an area nearly twice as large as the Marcellus shale. The Utica and Point Pleasant shale formations are located immediately above and in lateral facies in association with the top of the Trenton Limestone. In the deepest portion of the basin, the Utica Shale and equivalent formations occur at depths greater than 14,000 feet. **Figure 1**, published by the Pennsylvania State University Marcellus Center for Outreach and Research, illustrates the depth and regional extent of the Utica Shale. Depth to the top of the Utica becomes shallow through central Ohio and eastern New York where the Utica outcrops. Another excellent resource for a comprehensive evaluation of the regional structural and stratigraphic context of the Utica Shale is the 2006 report by the Trenton-Black River Research Consortium, *A geologic play book for Trenton-Black River Appalachian Basin exploration* (Patchen and others, 2006).

The Utica has long been known as a source of hydrocarbons, but until recently, was not an economically viable hydrocarbon play in its own right. Technological advancements in horizontal drilling and multi-stage hydraulic fracturing have created a host of new opportunities for hydrocarbon production from the Utica and Point Pleasant shale. Large scale production of the Utica is in a nascent state, with the initiation of exploration and production in 2010. (Ohio Department of Natural Resources, 2012; Greenburg, 2012) The most active areas are located in

eastern Ohio and western Pennsylvania, with the first wells drilled and completed in late 2010. New York and Quebec have moratoria on hydraulic fracturing which has inhibited production and further exploration (Bertrand, 2012).

For 2012, Utica/ Point Pleasant production in Ohio was 635,900 barrels of oil and 12,837 million cubic feet (MMcf) of gas from 65 commercial producing wells. This is a significant increase from 2011 production of 46,300 barrels and 2,561 MMcf from 5 commercial producing wells. As of February 2013, 529 Utica/ Point Pleasant wells have been permitted in Ohio, and 242 have been drilled (ODNR, 2013). One noteworthy Utica well produced 1,523.4 MMcf of gas in 2011, 2% of the total gas produced in Ohio that year. In 2012, the most prolific Ohio Utica/ Point Pleasant gas well produced 1,657.5 MMcf and 9,800 barrels of oil. The most prolific Ohio Utica oil well in 2012 produced 46,900 barrels and 332.4 MMcf. In Pennsylvania, two Utica exploratory gas wells produced at rates of 4.4 MMcf/day for seven days and 3.9 MMcf/day for 6 days (Range Resources, 2012 and Marcellus Drilling News, 2012.)

## b. Utica/ Point Pleasant Resource Potential

An early commercial assessment of the Utica Shale estimates 155 trillion cubic feet (Tcf) gas in-place and 31 Tcf of technically recoverable gas resources (Boyer and others, 2011). The United States Geological Survey recently assessed undiscovered technically recoverable resources for the Utica of 39 Tcf of natural gas, 940 million barrels of oil, and 208 million barrels of natural gas liquids. (USGS, 2012). The U.S. Energy Information Administration's *2012 Annual Energy Outlook* estimates 16 Tcf of unproved, technically recoverable gas resources for the Utica Shale (EIA, 2012).

## c. Sources of $CO_2$ Emissions

The Appalachian Basin encompasses all or a portion of nine states: Indiana, Kentucky, Maryland, Michigan, New Jersey, New York, Ohio, Pennsylvania, and West Virginia. This region generates approximately 30 percent of all U.S. electricity and 80% of the $CO_2$ emissions in the region are related to power generation. In total, approximately 670 million metric tons or tonnes (740 million short tons) of $CO_2$ are emitted each year from these stationary sources. Emissions are highest along the Ohio River Valley and coastlines, where many power plants and industries are located. (Maps of $CO_2$ emissions in the Appalachian Basin region may be found in the United States' Department of Energy *2012 Carbon Utilization and Storage Atlas,* online at: http://www.netl.doe.gov/technologies/carbon_seq/refshelf/atlasIV/Atlas-IV-2012.pdf.)

# 3. GEOLOGIC CHARACTERIZATION

Geological characterization of the Utica and Point Pleasant shale formations for this report build upon previous work by the United States Geological Survey (see Ryder, 2008; Rowan, 2006), the United States Department of Energy (Patchen and others, 2006), state geological surveys (see Faill, 1999; Hansen, 1997; Wickstrom 1992 & ), the New York State Museum (see Martin, 2005; Smith and Leone) (2010, 2011) as well as industry data and analyses that are becoming increasingly available.

For this report, methane gas in-place is estimated for the Utica/ Point Pleasant from analysis of public well logs and other petrophysical data. Theoretical maximum $CO_2$ storage capacity for the Utica/ Point is estimated using $CO_2$ isotherms for the Utica obtained from recent wells in New York and Ohio. Eleven model areas are identified and a composite model well is characterized for each model area. Various model well parameters provide input for the Utica Point Pleasant reservoir simulation using *COMET3*. Reservoir simulation examines potential cumulative gas production, $CO_2$ storage, and enhanced gas recovery under various reservoir quality scenarios.

## a. Geologic Setting

The Utica and Point Pleasant shale formations were deposited as organic-rich mudstone and carbonate in a restricted marine basin associated with the onset of the Appalachian Mountains uplift (Faill, 1999; Quinlan & Beaumont, 1984). These organic-rich rock formations are a major source of hydrocarbons in the basin, and have become a major focus for shale gas extraction in the region (Cole and others, 1987; Wallace and Roen, 1989; Ryder, 2008; Wickstrom, 2013).

The Appalachian Basin developed during the late Ordovician in response to an early phase of Appalachian mountain building (Faill, 1997). This mountain building event initiated a major tectonic evolution of proto- North America, forming a subsiding foreland basin westward of the rising mountains (Martin, 2005; Allen and others, 1986; Castle, 2001). The basin was covered by a relatively shallow continental sea which was bounded on all sides except for a small ocean access in the southwest (Ettensohn and Barron, 1981). Extensive carbonate platforms were deposited concurrently with mountain growth, and sub-basins formed amid the platforms (Wickstrom and others, 2012). Erosion of the uplifted mountains to the east provided the sediment source that filled the subsiding marine basin (Martin, 2005; Smith and Leone, 2011; Faill, 1997).

The sediments that comprise the Point Pleasant and Utica formations were deposited on and around the broad Ordovician carbonate platforms (Wickstrom and others, 2012; Holland and Patzkowsky, 1996). Point Pleasant precursor sediments filled the large inter-platform sub-

basins, creating an interlayered carbonate and calcareous shale formation (Wickstrom, 2013). Subsequent sea-level rise submerged the carbonate platforms, and deposition of the Point Pleasant Formation graded into the widespread deposition of the Utica Shale (Martin, 2005; Joy and others, 2005). Restricted marine circulation produced anoxic conditions in the basin for the duration of deposition (Wickstrom and others, 1992). Oxygen depleted waters in conjunction with high organic productivity permitted the accumulation of organic-rich sediments, which sustained the deposition of black shales (Emerson, 1985; Arthur and Sageman, 1994).

## b. Stratigraphy

**Figure 2** is a simplified stratigraphic column for the Utica and Point Pleasant Formations in New York, Pennsylvania, West Virginia and Ohio. Actual stratigraphic relationships in the Utica and Point Pleasant are complex. The Utica Shale and Point Pleasant represent restricted shallow basin depositional facies in time-equivalent lateral facies relationship with carbonate platforms represented by the Trenton and Lexington Limestone and their equivalent members such as the Steuben Limestone in New York. In New York, three formations are recognized in Utica Group: the Flat Creek Formation at the base of the Utica; the middle Dolgeville Formation in lateral facies relationship with both the Flat Creek and the Trenton; and the Indian Castle Formation comprising the upper Utica. An excellent presentation of this stratigraphic concept was developed by Langhorne Smith and James Leone of the Reservoir Characterization Group at the New York State Museum (Smith and Leone, 2010, 2010a, 2010b). Their summary illustration of Utica stratigraphy in New York is provided in **Figure 3**. Figure 3 shows that the Flat Creek and Dolgeville members of the Utica in New York are time-equivalent to the Trenton Limestone members; the Indian Castle shale, and postdates the Trenton. Because of the lateral depositional facies changes in the Middle Ordovician, it can be challenging to discriminate, using well logs alone, what intervals might be “Trenton”, “shaley Trenton”, “members of Utica Group”, “Point Pleasant” or “Lexington Group”.

Further complicating the regional stratigraphy are apparent sub-basins within the Ordovician foreland basin, which experienced differential rates of sediment accumulation. Point Pleasant sub-basin(s) are recognized in Ohio, West Virginia and southwest Pennsylvania, and appear to have occurred along a northeast trend into New York. The Flat Creek and portions of the Dolgeville in New York are thought to be time equivalent to Point Pleasant in Ohio, and to have accumulated in similar sub-basins. Relying on subsurface well logs alone, it is very challenging to reconcile the intricacies of Utica stratigraphy in New York and northern Pennsylvania tier with the Utica/ Point Pleasant stratigraphy to the southwest in Ohio, West Virginia and southern Pennsylvania. Lacking a close distribution of subsurface well logs and detailed correlation to known stratigraphic “anchor” points, difficulties arise in many areas in discriminating “Trenton/ Lexington” facies and “Utica” and “Point Pleasant” facies. There is

further uncertainty in discriminating the top of the Utica on well logs from the base of the Lorraine and its time equivalent shale facies.

For the region-scale reservoir simulation presented in this analysis, an approach was needed to reduce the complexities of Utica/ Point Pleasant/ Trenton stratigraphy to a few recognizable and regionally-correlative geologic model layers for simulation of $CO_2$ injection and storage. Consequently, the Utica - Point Pleasant stratigraphic correlation chart in Figure 2 is greatly condensed. The lower members of the Utica Group in New York, the Flat Creek and Dolgeville, (inferred in northern Pennsylvania) are simply named "Point Pleasant equivalent formations" in Figure 2. The Indian Castle Formation in New York is simply called the Utica. Designation of geologic model layers for reservoir simulation is discussed below.

## c. Utica/ Point Pleasant Study Area

The boundary of the Utica Shale study area is defined by the Utica "wet gas" thermal maturity boundary (Rowan, 2006; Ohio DNR 2012), and by depth contours where depth to the Trenton Limestone is greater than 3,000 feet. The 3,000-foot depth boundary represents an approximate boundary for miscible injection of $CO_2$ into the overlying Utica shale. Below a subsurface depth of approximately 2,500 feet, reservoir pressure is expected to be adequate for injection of $CO_2$ as a dense phase fluid, thereby increasing the efficiency of enhanced gas recovery and $CO_2$ storage. **Figure 4** shows the approximate Utica thermal maturity boundaries and structure contours on top of the Trenton. The boundary of the Utica/ Point Pleasant study area is shown in **Figure 5**. Also shown on Figure 5 are the location of 261 original study wells with digitized gamma ray and bulk density logs through the Utica and Point Pleasant; the trace of a regional stratigraphic cross-section from Washington County, Ohio to Otsego County, New York; and the boundaries eleven model areas identified for reservoir simulation. The total Utica/ Point Pleasant study area encompasses 37,063,938 acres or 57,913 square miles.

The well data set is compiled from public log data obtained through the New York, Pennsylvania, West Virginia and Ohio geological surveys. Digital log data (LAS) files are not available from public data sources for many wells, so the raster logs available for selected wells were digitized. All study wells have at least a digital gamma ray log through the Utica, from which total organic carbon (TOC) could be extrapolated and adsorbed gas in-place estimated. The final focus of the study area included only wells located in the wet gas, dry gas, and over-mature thermal maturity windows, excluding wells located in the Utica/ Point Pleasant oil window. A final subset of 42 study wells was compiled which are located, at least, within the wet gas thermal maturity window and have a complete log suite through the Utica/ Point Pleasant consisting of gamma-ray, density and resistivity. This subset of 42 wells became the pool of study wells from which composite model wells were developed for each model area.

## d. Type Log and Stratigraphic Cross-Section

**Figure 6** is a type log of the Utica/ Point Pleasant showing gamma-ray, resistivity, photoelectric (PE) log, neutron and density porosity logs, calculated water saturation and calculated TOC. TOC is calculated from bulk density and is shaded grey where calculated TOC is greater than 2 percent. The gamma ray log is shaded light blue where less than 50 API units and shaded brown where greater than 150 API units. Density porosity is corrected for TOC and is shaded in green where the calculated porosity is greater than 3 percent. Calculated water saturation is shaded in blue where greater than 25 percent.

The Utica/ Point Pleasant is subdivided into four layers for the purpose of reservoir simulation: the "Upper" Utica Shale; the basal Utica Shale (a zone with high gamma ray and apparent greater organic content at the base of the Utica); the "clay-rich" or "shaley" Upper Point Pleasant and equivalent formations; and, the "carbonate-rich" Lower Point Pleasant and equivalents that overlie the Trenton. As previously discussed, this layering scheme represents a simplification of regional Utica/ Point Pleasant stratigraphy for the purpose of defining recognizable, regionally extensive layers for reservoir simulation.

Throughout the study area it is difficult to identify the top of the Utica Shale on well logs. The Utica is overlain by the Lorraine Group, the Martinsburg Formation or the Reedsville Shale, which together represent transition to a less-restricted, open marine deposition, plus an increasing influx of clastic material from highlands to the east. The transition from the carbonate shelf and restricted marine sub-basins of the Utica/ Point Pleasant to the more open marine environments represented by the Lorraine/ Martinsburg/ Reedsville formations is subtle and gradational. For this study, the top of the Utica was picked at a point on the well logs where the gamma ray log character appears increasingly thin bedded or laminar due to thin marine sandstones and carbonates, and where the neutron and density logs increasingly diverge - the neutron reading higher porosity in response to increased clay content and the density reading higher bulk density due to lower organic content.

**Figure 7** is a stratigraphic cross-section that extends southwest to northeast across the study area from Washington County, Ohio to Otsego County, New York. The cross-section is flattened on the top of an interval of high gamma ray, low bulk density shale at the base of the Utica, which immediately overlies either the Point Pleasant (where present), or the Trenton Limestone where the Point Pleasant is absent. The high gamma ray, low bulk density basal Utica shale appears to be a zone of high TOC compared to the rest of the Utica Shale above. This high TOC, basal Utica Shale is characterized in this analysis as one of four geologic model layers for reservoir simulation. The basal Utica zone is modeled as the target reservoir for Utica development in New York and northern Pennsylvania. The cross-section in Figure 7 shows that the basal Utica shale zone thickens to the northwest and thins significantly through West Virginia to southeast Ohio.

Where the basal Utica Shale becomes thin, the target reservoir layer shifts to the upper unit of the Point Pleasant, the so-called "shaley" Point Pleasant. The shaley or "upper" Point Pleasant interval is often washed-out on logs, with the caliper log indicating a severely enlarged well bore. This is presumed to be due to the presence of abundant natural fractures and possibly to reservoir over-pressure. The lower unit of the Point Pleasant, which often appears to have a gradational lower contact with underlying Trenton, is also called the "carbonate-rich" Point Pleasant. The gamma ray, neutron porosity, bulk density and photoelectric log all indicate an apparent increase in carbonate with respect to clay throughout the lower Point Pleasant, although the organic carbon content appears to remain elevated in interbedded shale layers.

# 4. RESERVOIR DATA

This section summarizes various data used in the evaluation of gas in-place and $CO_2$ storage capacity. Utica core data were obtained from wells on opposite sides of the study area in Otsego County, New York and Washington County, Ohio. Sidewall and whole core samples were donated by operators to the project to obtain new methane and $CO_2$ adsorption isotherm data, as well as core porosity, permeability, TOC, and X-ray diffraction, gas content from canister desorption tests, and mechanical properties. X-ray diffraction mineralogy data for the Utica/ Point Pleasant are used to extrapolate a characteristic grain density reservoir matrix. Using the available data plus cross-plots of bulk density and TOC from the cored wells, bulk density cut-off values are applied to identify zones with apparent high organic carbon content.

## a. Adsorption Isotherms

Methane and $CO_2$ adsorption isotherms for the Utica/ Point Pleasant are available from two wells, a well in Washington County, Ohio and from the Ross #1 well in Otsego County, New York. The New York State Energy Research and Development Authority (NYSERDA) acquired $CO_2$ isotherm data for the Utica from the Ross #1 well. The core data and core samples from Point Pleasant wells in Washington County, Ohio were donated by the operator. The methane isotherm data are shown in **Figure 8** and the $CO_2$ isotherm data are shown in **Figure 9**. **Table 1** summarizes characteristics and specific Langmuir parameters determined for each sample including depth, measured or computed TOC, and Langmuir volume and pressure.

Figures 8 and 9 and Table 1 illustrate interesting differences in the adsorptive capacity of the New York and Ohio samples. At equivalent pressure, the New York Utica samples adsorb about twice the gas as the Ohio Point Pleasant samples. The TOC content of all the samples in the data set is comparable. The data set is too small to know if this difference would persist with a larger population of samples. Thermal maturity of the samples sets are very different, with the New York Utica samples being over mature and the Ohio Point Pleasant samples in wet gas window. Different analytical techniques and lab protocols may contribute as well. There are too few data points to determine with confidence the significance of the different isotherm behavior; however, the regional variation in adsorption isotherms was incorporated into the estimation of adsorbed gas in-place and maximum $CO_2$ storage capacity from TOC. The New York isotherm data are used for estimating adsorbed gas in-place for New York and the northern tier of Pennsylvania from TOC. The Ohio data are used for southeast Ohio and southwest and south central West Virginia. The averaged isotherm data are used for the areas in between – central and southwest Pennsylvania, the West Virginia panhandle, and north central West Virginia. **Figure 10** is a cross-plot that correlates TOC and Langmuir volume for the Utica/ Point Pleasant methane isotherms. **Figure 11** shows the correlation of TOC and Langmuir Volume for the Utica/ Point Pleasant $CO_2$ isotherms.

## b. Total Organic Carbon

Total organic carbon measurements for Utica cuttings samples and bulk density data from logs were obtained from the New York State Museum Reservoir Characterization Group for 15 New York wells. TOC measurements from core and cuttings samples and bulk density data for seven Utica/ Point Pleasant wells were obtained from data available online from the Ohio Department of Natural Resources. In addition, TOC and bulk density data for Utica and Point Pleasant whole core and sidewall cores from two wells in Washington County, Ohio were provided to the project by an operator. All the TOC and corresponding bulk density data were carefully reviewed, quality-checked and correlated to evaluate the relationship between bulk density and TOC for the Utica/ Point Pleasant. It was determined that a single cross-plot of the best available Utica, Point Pleasant and Trenton data points provides the best extrapolation of TOC from bulk density. This relationship is shown in **Figure 12**. Unlike the Marcellus, no reasonable extrapolation of TOC can be made from the gamma-ray log for the Utica/ Point Pleasant.

Figure 12 shows some notable differences between the Ordovician Utica/ Point Pleasant and the Devonian Marcellus. Overall, measured TOC is much lower for the Utica/ Point Pleasant than for the Marcellus. Measured TOC for Utica/ Point Pleasant samples do not exceed 5 percent by weight, whereas many of the Marcellus samples had measured TOC greater than 10 to 12 percent. For the Marcellus, TOC of 3 percent corresponds to a bulk density of 2.60 grams per cubic centimeters (g/cc) (cuttings samples) to 2.625 g/cc (whole core samples). For the Utica/ Point Pleasant, Figure 12 shows that TOC of 3 percent corresponds to bulk density of approximately 2.58 g/cc. For the Utica, a bulk density cut-off of 2.60 g/cc on the density log corresponds to an estimate TOC of only 1.5 percent.

## c. X-Ray Diffraction Mineralogy

**Table 2** presents average x-ray diffraction mineralogy for the Utica/ Point Pleasant in New York and Ohio obtained from whole core and side wall core samples from wells in Otsego County, New York and Washington County, Ohio. Summary mineralogy data for the Utica in Quebec (Theriault, 2008) are provided for comparison. Table 2 shows distinct differences in mineralogy between the Utica and the Point Pleasant. The Point Pleasant and equivalent formations contain 33 to 59 percent calcite compared to about 20 percent for the Utica. The Utica contains approximately 25 percent quartz compared to 10 to 19 percent for the Point Pleasant. Clay content of the Utica is higher than the Point Pleasant. Table 2 indicates interesting regional variations in Utica/ Point Pleasant mineralogy, but the data set is too small to make conclusions about the significance. For example, average clay content of the Ohio samples for both the Utica and Point Pleasant is greater than the clay content of the New York samples. The potassium feldspar content of the Ohio samples is notably greater than for the

New York samples, but the New York samples are enriched in dolomite compared to the Ohio samples.

## d. Core Porosity and Permeability

Core porosity and permeability data for the Utica were provided to the project for three wells, a well in Otsego County, New York and two wells in Washington County, Ohio. The New York data are from sidewall cores. The Ohio data are from whole core plugs and sidewall cores. **Figure 13** shows the core porosity and permeability relationship for the core data. The porosity-permeability (phi-k) relationships are different for the Ohio and New York samples, with the New York samples showing lower permeability than the Ohio samples by an order of magnitude. The data set is too small to know why the porosity-permeability relationships are so different. They may represent real differences in rock properties or may be the result of different laboratory analytical techniques and sample preparation. There was no objective way to determine which phi-k correlation is "better" than the other, so both porosity-permeability correlations were incorporated into the regional analysis. The New York data were used to extrapolate air permeability for New York and the Pennsylvania northern tier. The Ohio data were used to extrapolate permeability for the central and southern portions of the study area from central Pennsylvania to southeast Ohio and central West Virginia. **Table 3** compares air permeability extrapolated from a range of porosity values using the two porosity-permeability relationships shown in Figure 13.

Permeability of the Utica/ Point Pleasant core samples is at least an order of magnitude greater than the permeability of Marcellus core samples of equal porosity. The explanation for this is unknown. It may be due to lower clay content of Utica/ Pleasant samples compared to the Marcellus, which would imply that the Utica/ Point Pleasant has a larger grain size than the Marcellus. Larger grain size for the Utica/ Point Pleasant, even on a microscopic scale, would result in larger pores and pore openings and greater permeability.

The Utica Point Pleasant also has significantly lower porosity than the Marcellus. One contributing factor may be the low TOC content of the Utica/ Point Pleasant compared to the Marcellus. Microporosity within this organic material or, intra-kerogen porosity, can be significant in gas shale and may develop due thermal maturation and gas expulsion from the kerogen. The average TOC content of Utica is less than half the average TOC content of the Marcellus, so the intra-kerogen porosity component of total porosity will be less for the Utica/ Point Pleasant.

**Figure 14** shows pulse decay air permeability for Utica/ Point Pleasant core plug samples from one of the cored wells in Washington County, Ohio. The pulse decay permeability data show the reduction of measured permeability as net confining stress is increased. The data shown in Figure 14 are used to determine a scaling factor to extrapolate in

situ reservoir permeability from the unconfined porosity-permeability relationships shown in Figure 13 and Table 3.

# 5. ESTIMATED GAS IN-PLACE AND THEORETICAL MAXIMUM $CO_2$ STORAGE CAPACITY

## a. Overview of Calculated Gas In-Place and $CO_2$ Storage Capacity

Methane gas-in place is calculated from the digital well logs available for 42 study wells. The estimate of theoretical maximum $CO_2$ storage capacity is based on calculated gas in-place by assuming that 100 percent of the methane in-place, either as adsorbed or "free" gas is replaced in the reservoir by injected $CO_2$. The net stored volume of injected $CO_2$ will be a very small fraction of theoretical maximum capacity values. This fraction will be estimated based on the simulation results reported in Volume 8.

Methane gas in-place for the Utica and Point Pleasant is assumed to have two components: 1) methane adsorbed on organic matter contained in the shale; and 2) non-adsorbed methane, or free gas, contained within void space in the shale. Such voids could include micro-fracture porosity; intergranular porosity between clastic grains and particles; dissolution seams; voids within the framework of component minerals; and microporosity commonly observed within the kerogen of thermally-mature, organic–rich shale (intra-kerogen porosity). Estimating gas in-place thus requires two steps to calculate the quantity of adsorbed gas and the quantity of free (non-adsorbed) gas. Similarly, $CO_2$ storage capacity is assumed to have two components: storage as an adsorbed $CO_2$ phase displacing methane; and storage of non-adsorbed $CO_2$ replacing methane in the gas-filled pore space, or "effective" porosity.

Digital logs for 42 study wells were used to calculate the following attributes for the Utica/ Point Pleasant model layers:

- Vertical thickness
- Total organic carbon, TOC
- Adsorbed gas content
- Adsorbed gas in-place
- Theoretical maximum $CO_2$ storage capacity by adsorption
- Total porosity from density log
- Water saturation
- Effective (gas-filled) pore volume
- Estimated 'free' (non-adsorbed) methane gas in-place

- Theoretical maximum $CO_2$ storage capacity as 'free' $CO_2$ (non-adsorbed)

The log calculations were made using IHS Petra software.[1] The adsorbed component of gas in-place and maximum $CO_2$ storage capacity were calculated using available methane and $CO_2$ adsorption isotherms. A volumetric approach was used to estimate non-adsorbed gas in-place contained within the effective (gas-filled) porosity. The end result of the log calculations are estimates of total methane gas-in place in billion cubic feet per acre (Bcf/ac), and theoretical maximum $CO_2$ storage capacity including an adsorbed component and non-adsorbed component. Units of Bcf/ac were selected for ease of scaling the calculated results to estimate gas resource in-place, or $CO_2$ storage capacity, for any well spacing of interest, such as 40 or 80 acres, and for ease of converting to units of Bcf/square mile.

The Utica/ Point Pleasant study area was subdivided into smaller "model areas" based on log characteristics observed in cross-sections and the log calculations made for individual study wells. Each model area is represented by a model well, which is a composite of the calculated parameters for the study wells within the model area. In most cases, the value for a model well parameter such as TOC, porosity, or water saturation, is the average of all calculated values for the wells within the model area. In other cases, a single calculated value is selected as the parameter value for the model well because that single value appears to best represent the model area. The methodology for log analysis and calculation of gas in-place is discussed in the following section. The model well attributes that were provided as inputs to the reservoir simulation are discussed in the next chapter and provided in **Table 8** for the Upper Utica Shale reservoir layer; **Table 9** for the Basal Utica Shale reservoir layer; **Table 10** for the Upper Point Pleasant reservoir layer, and **Table 11** for the Lower Point Pleasant layer.

## b. Well Log Analysis Methodology

### i. TOC Extrapolated from Density Logs

Total organic carbon (TOC) is calculated based on the correlation of bulk density to TOC measured from Utica /Point Pleasant drill cuttings and core shown in Figure 12.

$$TOC_{calculated} = (( 2.732 - \rho_{log})/.052)$$

[1] http://www.ihs.com/products/oil-gas-information/analysis-software/petra.aspx?tid=t6&ocid=pc468:energy:ppc:0001&gasc_id=1036335105&gasc_label=yESWCPW1wAQQgfCU7gM&gclid=CO_KpumD1bgCFVOe4Aoda0UAWg

### ii. Porosity from Density Logs

Density porosity ($\phi_{density}$) corrected for TOC is calculated from bulk density using the following relationship:

$$\rho_{log} = \rho_{matrix}(1 - \phi_{density} - TOC_{calculated}) + \rho_{fluid}(\phi_{density}) + \rho_{TOC}(TOC_{calculated})$$

Where, $\rho_{matrix}$ = matrix grain density determined from x-ray diffraction mineralogy or whole core analysis; $\rho_{fluid}$ = density of formation water; $\rho_{TOC}$ = density of organic matter; and $\rho_{log}$ = bulk density reading from the log. The equation is rearranged to solve for porosity.[2]

### iii. Adsorbed Gas Content and Theoretical Maximum Adsorbed $CO_2$ Capacity

Adsorbed methane and $CO_2$ in units of standard cubic foot per ton (scf/ton) are calculated using Langmuir coefficients from the available isotherm data for the Utica/ Point Pleasant and estimated reservoir pressure based on depth. A reservoir pressure gradient was estimated for each model area. The operators who provided Utica core samples and data for the wells in Washington County, OH and Otsego County, NY also provided information that the Utica in Otsego County is normally pressured and the Utica/ Point Pleasant in Washington County is overpressured with a gradient of approximately 0.60. Based on these points of information, reservoir pressure gradients are estimated for the other model areas. Because reservoir pressure is a key parameter for estimating adsorbed gas content and theoretical maximum adsorbed $CO_2$ storage, the estimated pressure gradients for the Utica model areas are a significant source of uncertainty in the final estimates of gas in-place and maximum storage capacity.

Relevant isotherm data are summarized in Table 1. Adsorbed gas content or theoretical adsorbed $CO_2$ content are calculated using the following algorithm:

$$V_{adsorbed} = (V_L \times P_{res})/(P_L + P_{res})$$

Where, $V_{adsorbed}$ = adsorbed gas content; volume of adsorbed gas at a reservoir pressure, $P_{res}$; $V_L$ = Langmuir volume from adsorption isotherm; $P_L$ =average Langmuir pressure from adsorption isotherm data

For each study well, Langmuir volume is extrapolated from calculated TOC. Figure 10 shows the correlation of Langmuir volume to TOC for the Utica/ Point Pleasant methane isotherms; Figure 11 shows the relationship of Langmuir volume to TOC for the $CO_2$ isotherms.

---

[2] $\phi_{density} = \{\rho_{matrix} - [\rho_{log} \times (((\rho_{matrix} \times TOC_{calculated})/\rho_{TOC}) - TOC_{calculated} + 1)]\} / (\rho_{matrix} - \rho_{fluid})$

The average Langmuir pressure in Table 1 was used as $P_L$. Reservoir temperature and pressure curves were created for each study well by applying a regional temperature gradient and the estimated reservoir pressure gradient to the vertical log depth. If a temperature log was available for the Utica/ Point Pleasant, the temperature log data were used instead of the extrapolated reservoir temperature. Applying the data shown in Table 1, Figure 10 and Figure 11, the algorithms for calculating adsorbed gas content (scf/ ton) are as follows:

For the thermally "overmature" areas of NY and PA, the average isotherms from the NY samples were used to compute adsorbed gas content and maximum adsorbed $CO_2$ content:

$$V_{L\_CH4} = 34.8 \; x \; TOC, \quad and:$$

$$Adsorbed_{CH4} = ((34.8 \times TOC) \; x \; P_{res})/(579 \; psia + P_{res})$$

$$V_{L\_CO2} = 68.4 \; x \; TOC, \quad and:$$

$$Adsorbed_{CO2} = ((68.4 \times TOC) \; x \; P_{res})/(476 \; psia + P_{res})$$

For the areas of eastern OH and western WV in the thermal maturity "wet gas" window, the average isotherms from the OH samples were used to compute adsorbed gas content and maximum adsorbed $CO_2$ content:

$$V_{L\_CH4} = 16.2 \; x \; TOC, \quad and:$$

$$Adsorbed_{CH4} = ((16.2 \times TOC) \; x \; P_{res})/(1{,}410 \; psia + P_{res})$$

$$V_{L\_CO2} = 22.6 \; x \; TOC, \quad and:$$

$$Adsorbed_{CO2} = ((22.6 \times TOC) \; x \; P_{res})/(533 \; psia + P_{res})$$

For the remaining portions of the study area in the "dry gas" window, including western NY and PA and central WV, the isotherms of the NY and OH samples were combined to create a composite isotherm:

$$V_{L\_CH4} = 22.1 \; x \; TOC, \quad and:$$

$$Adsorbed_{CH4} = ((22.1 \times TOC) \; x \; P_{res})/(1{,}078 \; psia + P_{res})$$

$$V_{L\_CO2} = 37.1 \; x \; TOC, \quad and:$$

$$Adsorbed_{CO2} = ((37.1 \times TOC) \; x \; P_{res})/(510 \; psia + P_{res})$$

These algorithms and average values for Langmuir pressure and Langmuir volume are also summarized in Tables 4 and 5.

Adsorbed methane in-place or $CO_2$ in-place (scf/acre) is computed by multiplying the adsorbed gas content (scf/ton) obtained from the previous step by an estimated quantity of shale (tons/acre):

Tons shale = (thickness *x* area *x* shale density *x* conversion factor (g/cc to tons/acre-ft.))[3]

For calculated study well, tons of shale were computed for each acre-foot of reservoir thickness and multiplied by the computed curve of adsorbed gas content in scf/ton. This provided computed log curves for each study well of adsorbed methane in-place (Mcf/acre-ft.) and maximum adsorbed CO2. The final step summed the calculated curves for each study well and converted the units to Bcf/sq. mile, yielding total adsorbed methane gas in-place and theoretical maximum adsorbed CO2 storage capacity for each well.

### iv. Free Gas In-Place and Theoretical Maximum $CO_2$ Storage Capacity

Free gas in-place was estimated by computing an effective (gas-filled) porosity:

$$\phi_{effective} = \phi_{density} \; x \; (1 - S_w)$$

Where, $S_w$ = calculated water saturation (fraction). All water saturation is assumed to be immobile as bound water. Effective, or gas-filled, porosity is assumed to be the fraction of total porosity not occupied by water. Water saturation is calculated using the Archie equation for water saturation, as well as the Simandoux modification of the Archie equation for shaley sandstones (Simandoux, 1963 in Asquith and Krygowski, 2004):

$$S_w = ((0.4 \; x \; R_w)/\phi^m) \; x \; \{[(V_{shale} / R_{shale})^2 + ( (5 \; x \; \phi^m)/(R_t \; x \; R_w))]^{1/n} - (V_{shale}/ R_{shale})\}$$

Where, $S_w$ = water saturation; $R_w$ = water resistivity at formation temperature; $\phi$ = porosity; m = Archie cementation exponent (common default = '2'); $V_{shale}$ = shale content; $R_{shale}$ = resistivity of the shale; $R_t$ = deep resistivity log reading; n = Archie saturation exponent. Table 6 summarizes the variables used for calculating density porosity and water saturation.

For this analysis, a three-part linear solution to the Simandoux equation published by Crain (1986) is implemented in PETRA to calculate a water saturation curve for each study well. Shale volume ($V_{shale}$) was computed from the gamma ray log. A linear shale index approach produced the most consistent results compared to other published methods for estimating shale volume from the gamma ray log:

$$V_{shale} = (GR_{\text{log reading}} - GR_{\text{non-shale}}) / (GR_{\text{shale}} - GR_{\text{non-shale}})$$

An effective (gas-filled) porosity curve was calculated for the Utica/ Point Pleasant in each study well for the total reservoir thickness. The total thickness of these porous zones constitutes the net reservoir thickness (the 'effective' reservoir thickness) for calculating free

[3] Adsorbed Gas (or $CO_2$), M/ac. = (h *x* area *x* bulk density *x* Adsorbed gas content(scf/ton) x 1359.7)/ (1 x $10^3$)

methane gas in-place. The volume of free gas in-place for each acre-foot of net reservoir thickness was computed:

$$\text{Free methane gas-in-place} = (43{,}560 \times \phi_{effective}) / Bg_{CH4}$$

Where, $Bg_{CH4}$ (rcf/scf) = the appropriate formation volume factor for methane computed for each study well based on depth and extrapolated reservoir temperature and pressure. The result was a computed curve yielding for each study well free (non-adsorbed) methane gas in-place in units of Bcf per acre-ft. A final step summed the calculated curves for each study well and converted the units to Bcf/ac, yielding total non-adsorbed methane gas in-place for each well.

Calculated water saturation has a large effect of the ultimate gas in place. The Archie equation for water saturation and the Simandoux equation yield very different results. The Simandoux equation is used to calculate effective (gas-filled) porosity for two of the reservoir model layers, the Basal Utica Shale and the "Shaley" Upper Point Pleasant layer. The unmodified Archie equation is used to calculate water saturation in the Upper Utica Shale reservoir layer and in the Lower Point Pleasant (carbonate –rich). The Archie equation appears to yield more reasonable results for these two model layers - the Lower Point Pleasant layer, because of less shale content and more carbonate, and the Upper Utica Shale layer, because of very low porosity. Appendix 1 is a table of model layer attributes for the Upper Utica layer in which the water saturation is calculated using Simandoux. This table can be compared to Table 8, in which water saturation is calculated using the Archie equation; these calculated data are used to estimate gas in-place for the Upper Utica layer. In Table 8, the average water saturation for the model areas ranges from 0.54 to 0.96; in Appendix 1, the average water saturation (calculated using Simandoux) ranges from 0.23 to 0.69.

### v. Theoretical Maximum $CO_2$ Storage as 'Free' $CO_2$ (Non-Adsorbed)

The maximum capacity for $CO_2$ storage as 'free' gas (non-adsorbed $CO_2$) is estimated by assuming that all calculated methane gas in-place as 'free' gas is replaced by $CO_2$. Methane gas must be removed from the reservoir by production to make reservoir volume available for injected $CO_2$. The methane recovery factors for the Utica/ Point Pleasant are unknown but are certain to be significantly less than 100 percent, hence computed $CO_2$ storage capacity as 'free', non-adsorbed $CO_2$ is a theoretical maximum.

Maximum $CO_2$ storage capacity as non-adsorbed $CO_2$ was computed for each acre-foot of net reservoir thickness by substituting the appropriate formation volume factor for $CO_2$ ($Bg_{CO2}$) at the extrapolated reservoir pressure and temperature for the depth. Similar to free methane gas in-place, the result was a computed log curve for each study well yielding non-adsorbed $CO_2$ replacing free methane gas in-place in units of Bcf per acre-ft. A final step summed the calculated curves for each study well and converted the units to Bcf/ac, yielding the

theoretical maximum $CO_2$ storage capacity as free $CO_2$ for each well. Total maximum $CO_2$ storage capacity includes the theoretical maximum $CO_2$ storage capacity as 'free' $CO_2$, as well as the maximum $CO_2$ storage capacity as adsorbed $CO_2$.

## c. Utica Log Calculation Results

The well log analyses for individual study wells were aggregated to create a composite model well for each of eleven model areas. The model areas boundaries are shown in Figure 5. Table 7 provides a description of the Utica/ Point Pleasant model areas and a summary of estimated model area parameters for calculating gas in-place and maximum $CO_2$ storage capacity. Included in Table 7 are the area in acres and miles$^2$, the estimated reservoir pressure gradient, extrapolated mean reservoir pressure and temperature, and estimated formation volume factor for methane and $CO_2$. Tables 8, 9, 10 and 11 summarize the model well attributes for each model area that are incorporated into the reservoir simulation for each reservoir layer. The model well attributes provided in these tables include: the average depth of the layer, thickness, average total porosity, average permeability, average calculated water saturation, average TOC, adsorbed gas content (scf/ton) and maximum adsorbed $CO_2$ storage capacity (scf/ton). Table 8 summarizes the model well attributes for the Upper Utica reservoir layer. The model well attributes for the Basal Utica Shale are summarized in Table 9. Table 10 contains the model well attributes for the Upper Point Pleasant layer (shale-rich Point Pleasant) and Table 11 contains the model well attributes for the Lower Point Pleasant reservoir layer, the carbonate-rich Point Pleasant.

## d. Total Gas In-Place and Maximum $CO_2$ Storage Capacity

Table 12 shows the calculated Utica gas in-place by model area, as well as for the total study area. Gas in-place for the two Utica reservoir layers are shown separately so that the gas in-place from the Upper Utica layer can be compared to the gas in-place calculated for the Basal Utica model layer. Table 13 shows the calculated Point Pleasant gas in-place by model area, as well as total gas in-place for the entire study area. For the two Point Pleasant reservoir layers, Table 13 lists the calculated gas in-place separately for each layer. The total Utica/ Point Pleasant study area is 57,913 square miles or, 37,063,938 acres.

Total Utica gas in-place (which includes both the "Upper Utica" and "Basal Utica Shale" reservoir layers) is estimated to be 1,241 trillion cubic feet (Tcf), of which 349 Tcf is estimated to be adsorbed gas in-place and 892 Tcf is estimated to be free (non-adsorbed) gas in-place. Total Point Pleasant gas in-place (which includes both the Upper Point Pleasant (shale-rich) and the Lower Point Pleasant (carbonate-rich) reservoir layers) is estimated to be 2,377 Tcf, of which 489 Tcf is estimated to be adsorbed gas in-place and 1,888 Tcf is estimated to be free (non-adsorbed) gas in-place. Averaged over the entire study area, the estimated concentration of gas in-place for the total Utica is 6.1 Bcf/square mile adsorbed and 15.8 Bcf/square mile non-

adsorbed. For the total Point Pleasant, the estimated concentration of gas in-place, averaged over the entire study area is 10.3 Bcf adsorbed and 39.8 Bcf non-adsorbed.

**Tables 14 and 15** summarize the theoretical maximum $CO_2$ storage capacity by model area, which assumes that all adsorbed and 'free' gas is replaced by injected $CO_2$. Actual $CO_2$ storage capacity is estimated via the reservoir simulation reported in Volume 8. Actual $CO_2$ storage capacity in organic-rich shale is expected to be a small fraction of the gas in-place volume, and strongly influenced by injection design and field operating parameters, reservoir production and depletion, in addition to intrinsic reservoir characteristics such as porosity, thickness, reservoir pressure and permeability. Maximum $CO_2$ storage capacity for the Utica (which includes both the Upper Utica and Basal Utica Shale reservoir layers) is estimated to be 2,275 Tcf, about 1.8 times the estimated Utica gas in-place. Total adsorbed $CO_2$ storage is estimated to be 758 Tcf; total $CO_2$ storage as a free, non-adsorbed phase is estimated to be 1,516 Tcf. Maximum $CO_2$ storage capacity for the Point Pleasant and equivalent formation is estimated to be 4,278 Tcf, of which 1,060 Tcf is estimated to be adsorbed gas, and 3,218 Tcf estimated to be stored as a free, non-adsorbed phase. Maximum $CO_2$ storage capacity of the Point Pleasant is estimated to be 1.8 times the gas in place.

### i. Caveats and Assumptions Regarding this Assessment

***Limited well data set.*** Publicly available digital log data is limited, especially for Pennsylvania. Only 42 wells have a full log suite consisting of gamma-ray, bulk density and resistivity, which is sparse data coverage for a study area of this size. Some of the logs were affected by significant "wash out" in the Point Pleasant, possibly due to abundant natural fracturing. In such wells, the density log was not useable across all or a portion of the Utica/ Point Pleasant. Some wells only had a gamma ray-neutron log available. All log data were used to the extent possible, even if the log data set was incomplete.

***Limited data set of methane and $CO_2$ isotherms.*** Methane isotherms available to the project are from one well in New York and two wells in Ohio. $CO_2$ isotherms for the Marcellus were available from a single well in New York.

***Single porosity algorithm applied.*** A single density porosity algorithm was assumed to apply everywhere. For example, a single porosity algorithm was applied for both the Utica and Point Pleasant throughout the entire study area. Calculated density porosity was corrected for organic content, but the correction may not be universally appropriate across the range of apparent organic carbon content, possibly over-correcting porosity for kerogen content in zones with very low TOC.

***Simandoux water saturation algorithm with estimated Archie model parameters applied to the entire Utica/ Point Pleasant.*** Similar to the porosity caveat, a single approach for calculation water saturation was applied to the entire Utica/ Point Pleasant. Estimated and default Archie model parameters were used for saturation exponent, 'n', tortuosity exponent, 'a', and cementation factor, 'm', because no other data were available. Inputs to the Simandoux equation such as shale resistivity were estimated and applied uniformly across all sub-horizons throughout the study area. The Simandoux algorithm is expected to work best in zones where clay shale volume is in the range of 50 to 85 percent, defaulting to a pure Archie equation as clay shale volume approaches zero and possibly over-correcting (water saturation too low) when clay shale volume exceeds 80 to 90 percent. The input parameters selected appeared to produce the most consistent results over the widest area.

***Immobile formation water assumed***. Calculated water saturation is assumed to be immobile, representing both clay-bound water and water immobilized by capillary forces in microporosity. Effective porosity is assumed to be equivalent to the gas-filled pore volume, which is computed by multiplying total porosity by (1- fractional water saturation).

***Other Caveats.*** Recovery factors for adsorbed and free gas are likely different, but as a practical matter, it will likely be impossible to distinguish adsorbed gas and non-adsorbed gas in the production stream. For example, free gas contained within intra-kerogen microporosity might be expected to be produced along with desorbed gas. Similarly, it may be impossible to determine what component of injected $CO_2$ is adsorbed, and what component is stored as a non-adsorbed free phase. Sustained methane production from gas shale is expected to provide adsorption sites for $CO_2$, and sustained production of any free gas from intra-kerogen and intergranular porosity could provide additional pore volume for $CO_2$ storage in a non-adsorbed or free phase. The percentage of pore volume currently occupied by free gas, which will become accessible to injected $CO_2$, is likely to be extremely small, although no data are available to make a quantitative estimate.

The effective or 'gas-filled' pore volume available for $CO_2$ storage may be miniscule compared to the actual effective pore volume drained by the production of free gas. Contributing factors might include reservoir compaction with gas withdrawal, and hysteresis effects on capillary entry pressure and relative permeability to $CO_2$. For future $CO_2$ storage, it may be important to estimate separate storage capacity factors for $CO_2$ storage as an adsorbed phase (expected to be comparatively "large") and $CO_2$ storage as a non-adsorbed, free phase (expected to be comparatively "very small").

# 6. DEFINITION OF MODEL AREAS FOR RESERVOIR MODELING IN THE BASIN

## a. Rational for the Development of Model Areas

Total gas in-place and $CO_2$ storage capacity are extrapolated from individual log calculations for selected study wells contained within the eleven "model areas" indicated in Figure 5. The model areas are sub-divisions of the total Utica/ Point Pleasant study area based on parameters such as depth and thickness of the Utica, reservoir pressure gradient, and computed TOC, and average porosity. As an example, **Figure 15** is a map of the study area that shows selected model well parameters – thickness, TOC, and average porosity for the Basal Utica Shale reservoir layer in each model area. Figure 15 shows that the Basal Utica Shale layer is thickest in the northeast in Model Areas 4 and 5 and thins to the south and southwest. Average porosity and average TOC are also greater in the northeast. **Figure 16** is a similar map for the Upper Point Pleasant showing selected model well parameters – thickness, TOC and average porosity. The average calculated porosity for the Upper Point Pleasant model wells is approximately 4 percent; thickness of the Upper Point Pleasant is more than double the thickness of the Basal Utica Shale reservoir layer. **Figure 17** is a base map of the model areas showing the estimated resource concentration for the Basal Utica Shale reservoir layer in Bcf/square mile. **Figure 18** is a similar base map of the model areas that summarizes the estimated gas in-place concentration for the Upper (Shaley) Point Pleasant reservoir layer in Bcf / square mile.

## b. Overview of Model Areas

The eleven Utica/ Point Pleasant model areas in are very large, but despite their size, the model areas are broadly distinguished by differences such as the depth and thickness of the individual Utica and Point Pleasant layers, reservoir pressure, calculated TOC, adsorbed gas content, average effective (gas-filled) porosity and final calculated gas in-place. **Table 16** provides a summary, by model area, of total gas in-place, resource concentration, and total theoretical maximum $CO_2$ storage capacity for the Utica plus the Point Pleasant. For each model area, the average calculated gas in-place and storage capacity values per unit area are multiplied by the geographical area contained within the model area boundaries. Theoretical maximum $CO_2$ storage capacity is converted from Bcf to units of million tonnes (Mt). **Table 16** expresses the calculated gas in-place for each model area as a representative resource "concentration" in units of Bcf/ 80 acres, which represents one eighth of the resource concentration expressed in units of Bcf/ square mile. **Table 16** similarly shows total maximum $CO_2$ storage capacity for each model area, converting to units of Mt/square mile and Mt/ 80 acres. **Figure 19** compares the total Utica/ Point Pleasant resource concentration of the model areas, expressed in units of Bcf/ 80 acres. **Figure 20** compares the total Utica/ Point Pleasant maximum $CO_2$ storage capacity of the model areas, expressed in units of Mt/80 acres.

## c. Sources of Data for Representative Wells in Each Model Area

The most important data sources for each model area are the study wells contained in each area, along with the digital log data, rock samples, and sample analysis data available for each well. Initial calculations of gas in-place and CO2 storage capacity were overlaid with the model area boundaries to select representative wells for each model area. A composite model well was then created for each model area based on the attributes of the representative wells. In most cases, the attributes of the composite model well represent average attributes of the study wells within the model area. In some cases, a single well was selected as the model well because it appeared to best represent the typical calculated attributes of the model area. Log-derived parameters from the composite model wells such as total porosity, thickness, permeability, and gas in-place were provided to the reservoir simulation for each model area.

# 7. REFERENCES

Allen, P. A., Homewood, P. and Williams, G.D. 1986. Foreland basins: an introduction. *In* Foreland Basins (Ed. by P.A. Allen & P. Homewood), Special Publication of the International Association of Sedimentologists, 8, 3-12.

Arthur, M. A., and Sageman, B. B. 1994. Marine black shales: A review of depositional mechanisms and significance of ancient deposits. Annual Review Earth and Planetary Science, v. 22, p. 499-551

Asquith, G. and Krygowski, D., 2004, *Basic Well Log Analysis*, second edition, American Association of Petroleum Geologists, Tulsa, 242 pp.

Bertrand, P. 2012. Quebec Installs Outright Moratorium on Hydraulic Fracturing. International Business Times. 4 April, 2012. http://www.ibtimes.com/quebec-installs-outright-moratorium-hydraulic-fracturing-433930. Accessed: February 2013.

Boyer, C., Clark, B., Jochen, V., Lewis, R., and Miller, C. K. 2011. Shale Gas: A Global Resource. Oilfield Review. Autumn, 2011. V 23, no. 3. P. 28-39. Online: http://www.slbalumni.com/~/media/Files/resources/oilfield_review/ors11/aut11/03_shale_gas.pdf. Accessed: April 2013.

Castle, J.W. 2001. Appalachian basin stratigraphic response to convergent-margin structural evolution. Basin Research, 13, pp. 397-418.

Cole, G. A., Drozd, R. J., Sedivy, R. A., and Halpern, H. I. 1987. Organic geochemistry and oil-source correlations, Paleozoic of Ohio: AAPG Bulletin, v. 71, no. 7, p. 788-809.

Crain, E.R., 1986, The Log Analysis Handbook, Pennwell Publishing Co., Tulsa, 684 pp

Emerson, S. 1985. Organic carbon preservation in marine sediments, in Sundquist, E.T., Broecker, W.S. (Eds.), The Carbon Cycle and Atmospheric CO2: Natural Variations Archean to Present. Geophysical Monograph, vol. 32, pp. 78– 87.

Ettensohn, F.R., and Barron, L.S., 1981, Depositional model for the Devonian Mississippian black shales of North America: A paleoclimatic-paleogeographic approach, in Roberts, T.G., ed., GSA Cincinnati '81 Field Trip Guidebooks, v. II: Economic geology, structure: Falls Church, American Geological Institute, p. 344–361.

Faill, R. T. 1997. A Geologic History of the North-Central Appalachians; Part 2, the Appalachian Basin from the Silurian through the Carboniferous. American Journal of Science, V. 297, 7. Pp. 729-761. Online: http://www.ajsonline.org/content/297/7/729.abstract. Accessed: March 2013.

Faill, R. T. 1999. Geologic History of Pennsylvania: Paelozoic, in The Geology of Pennsylvania, (Shultz, C. H., ed. Pennsylvania Geological Survey and the Pittsburgh Geological Survey. pp. 419-434.

Greenburg, J. 2012. The Fledgling Utica in The Utica Playbook 2012. Hart Energy. Pp.62-76.

Hansen, M. C. 1997. The Geology of Ohio—The Ordovician. The Ohio Division of Geological Survey. pp.1-7. Online: http://jrscience.wcp.muohio.edu/downloads/Ordoviciangeology.pdf. Accessed: April 2013.

Holland, S.M., and Patzkowsky, M.E. 1996. Sequence stratigraphy and long-term paleoceanographic change in the Middle and Upper Ordovician of the eastern United States, in Witzke, B.J., et al., eds., Paleozoic sequence stratigraphy: Views from the North American craton: Geological Society of America Special Paper 306, p. 117–129.

Institute for Energy Research, 2012. Utica Shale Fact Sheet. Institute for Energy Research. http://www.instituteforenergyresearch.org/wp-content/uploads/2012/10/Utica-Fact-Sheet.pdf. Accessed: February 2013.

Joy, M.P., Mitchell, C.E., and Adhya, S. 2000. Evidence of a tectonically driven sequence succession in the Middle Ordovician Taconic foredeep. Geology, v. 28, no. 8; p. 727-730.

Leone, J.R. and Smith, L., 2010, An in-depth Study of the Beaver Meadow and 74-NY-5 Cores from the Ordovician Utica and Devonian Marcellus Shales, New York State, presentation at American Association of Petroleum Geologists Eastern Section Meeting, Kalamazoo, MI, September 25 – 29, 2010.

Marcellus Drilling News. 2012. Seneca Resources Targets Utica Shale – in Western PA. http://marcellusdrilling.com/2012/11/seneca-resources-targets-utica-shale-in-western-pa/. Accessed: February 2013.

Martin, J. P. 2005. Utica Shale Deposition in The Taconic Foreland Basin: Evolution And The Potential For Natural Gas Production. GSA Sectional Meeting March 14-16th, 2005. Geological Society of America Abstracts with Programs, Vol. 37, No. 1, p. 5. https://gsa.confex.com/gsa/2005NE/finalprogram/abstract_83485.htm

McClain, T. 2012. Sequence Stratigraphic Interpretation of the Utica Shale and Associated Late Ordovician Strata, Eastern Ohio and Western Pennsylvania. AAPG. Online: http://www.searchanddiscovery.com/documents/2012/50613mcclain/ndx_mcclain.pdf. Accessed: April 2013.

Ohio Department of Natural Resources Geological Survey. 2012. The Utica-Point Pleasant Shale Play of Ohio. Presentation. 2012 http://www.ohiodnr.com/portals/10/energy/Utica Point Pleasant_presentation.pdf. Accessed: February 2013.

Ohio Department of Natural Resources (ODNR), 2013. Oil and Natural Gas Well and Shale Development Resources. http://www.ohiodnr.com/oil/shale/tabid/23174/Default.aspx. Accessed: February 2013.

Patchen, Douglas G., John B. Hickman, David C. Harris, James A. Drahovzal, Paul D. Lake, Langhorne B. Smith, Richard Nyahay, Rose Schulze, Ronald A. Riley, Mark T. Baranoski, Larry H. Wickstrom, Christopher D. Laughrey, Jaime Kostelnik, John A. Harper, Katharine Lee Avary, John Bocan, Michael Ed. Hohn and Ronald McDowell, A Geologic Play Book for Trenton-Black River Appalachian Basin Exploration: Final Report, DOE Award Number: DE-FC26-03NT41856, June 28, 2006

Pennsylvania State University, Marcellus Center for Outreach and Research. 2012. Utica Shale Depth Map. http://www.marcellus.psu.edu/images/UticaDepth.gif. Accessed: February 2013.

Quinlan, G.M., and Beaumont, C. 1984. Appalachian thrusting, lithospheric flexure, and Paleozoic stratigraphy of the Eastern Interior of North America Canadian Journal of Earth Sciences, 21, 973-996.

Range Resources, 2012. Range Resources Corporation Company Presentation. p. 51. Available online. Accessed: February 2013.

Repetski, J.E., Ryder, R.T., Weary, D. J., Harris, A.G., and Trippi, M.H., 2008, Thermal Maturity Patterns (CAI and %Ro) in upper Ordovician and Devonian Rocks of the Appalachian Basin: A Major Revision of USGS Map I-917-E Using New Subsurface Collections, Scientific Investigations Map 3006, United States Geological Survey, 26 pp., maps. . Online: http://pubs.usgs.gov/sim/3006/SIM3006.pdf. Accessed: March 2013.

Rowan, E. L., 2006. Burial and Thermal History of the Central Appalachian Basin, Based on Three 2-D Models of Ohio, Pennsylvania, and West Virginia. USGS. Online: http://pubs.usgs.gov/of/2006/1019/2006-1019.pdf. Accessed: March 2013.

Ryder, R. T., 2008. Assessment of Appalachian Basin Oil and Gas Resources: Utica-Lower Paleozoic Total Petroleum System. USGS Open-File Report 2008–1287. Online: http://pubs.usgs.gov/of/2008/1287/ofr2008-12872.pdf. Accessed: April 2013.

Simandoux, P., 1963, Mesures dielectriques en milieu poreux, application a mesure des saturations en eau: Etude du Comportement des Massifs Argileux, Revue de l'institut Francais du Petrole, Supplementary Issue.

Smith, L. and Leone, J., 2011, Tectonic and Depositional Setting of Marcellus and Utica Black Shales, New York State. AAPG poster. New York State Museum. Online: http://esogis.nysm.nysed.gov/Talks/2011_AAPG_Tectonic_Depositional_Setting_Marcellus_Utica_Black_Shales_New_York.pdf. Accessed: April 2013.

Smith, L. B, 2010, Shallow Transgressive Onlap Model for Ordovician and Devonian Organic-Rich Shales, New York State, presentation to American Association of Petroleum Geologists Eastern Section Meeting, Kalamazoo, MI, September 25 – 29, 2010.

Smith, L. B. and Leone, J., 2010a, Integrated Characterization of Utica and Marcellus Black Shale Gas Plays, New York State, presentation to American Association of Petroleum Geologists Annual Convention and Exhibition, New Orleans, Louisiana, April 11-14, 2010.

Smith, L. B. and Leone, J. 2010b, Tectonic and Depositional Setting of Ordovician Utica and Devonian Marcellus Black Shales, New York State, poster presentation, American Association of Petroleum Geologists Annual Convention and Exhibition, New Orleans, LA, April 11-14, 2010.

Theriault, R., 2008, Regional Geochemical Evaluation of the Ordovician Utica Shale Gas Play in Quebec, presentation to American Association of Petroleum Geologists Eastern Section Meeting, Pittsburgh, PA, September, 2008.

United States Geological Survey, 2012. Assessment of Appalachian Basin Oil and Gas Resources: Utica-Lower Paleozoic Total Petroleum System. U.S. Geological Survey Report 2008-1287. Online: http://pubs.usgs.gov/of/2008/1287/ofr2008-12872.pdf. Accessed: April 2013.

United States Geological Survey, 2012. Assessment of Undiscovered Oil and Gas Resources of the Ordovician Utica Shale of the Appalachian Basin Province, 2012. United States Geological Survey. http://pubs.usgs.gov/fs/2012/3116/FS12-3116.pdf. Accessed: February 2013.

United States Energy Information Administration, 2012. Annual Energy Outlook 2012, Early Release Overview. Online: http://www.eia.gov/forecasts/aeo/er/pdf/0383er(2012).pdf. Accessed: March 2013.

United States Energy Information Administration, 2011. Technology drives natural gas production growth from shale gas formations. U.S. Energy Information Administration. Today in Energy. 2011. http://www.eia.gov/todayinenergy/detail.cfm?id=2170#. Accessed: February 2013.

Wallace, L. G., and Roen, J. B. 1989. Petroleum source rock potential of the Upper Ordovician black shale sequence, northern Appalachian Basin: U.S. Geological Survey Open File Report 89-488, 66 p. Online: http://pubs.usgs.gov/of/1989/0488/report.pdf. Accessed: April 2013.

Wickstrom, L. H. 2013. Utica-Point Pleasant Play is a Star. Shale Experts. Online: http://www.shaleexperts.com/articles/Wickstrom-Utica-Point-Pleasant-Play-is-a-Star_999956694. Accessed: April 2013.

Wickstrom, L. H., Riley, R. A., Erenpreiss, M. S., and Perry, C. J. 2012. Geologic Overview and Activity Update for the Utica-Point Pleasant Shale Play in Ohio. AAPG Poster presentation. Online: http://www.ohiodnr.com/portals/10/pdf/Posters/Wickstrom_CenterPanel1_AAPG2012.pdf. Accessed: April 2013.

Wickstrom, L. H., Gray, J.D., and Stieglitz, R.D. 1992. Stratigraphy, structure, and production history of the Trenton Limestone (Ordovician) and adjacent strata in northwestern Ohio; Ohio Division of Geological Survey, Report of Investigations No. 143, 78 p., 1 pl.

# FIGURES

Figure 1. Map Showing Extent and Approximate Depth of Utica Shale

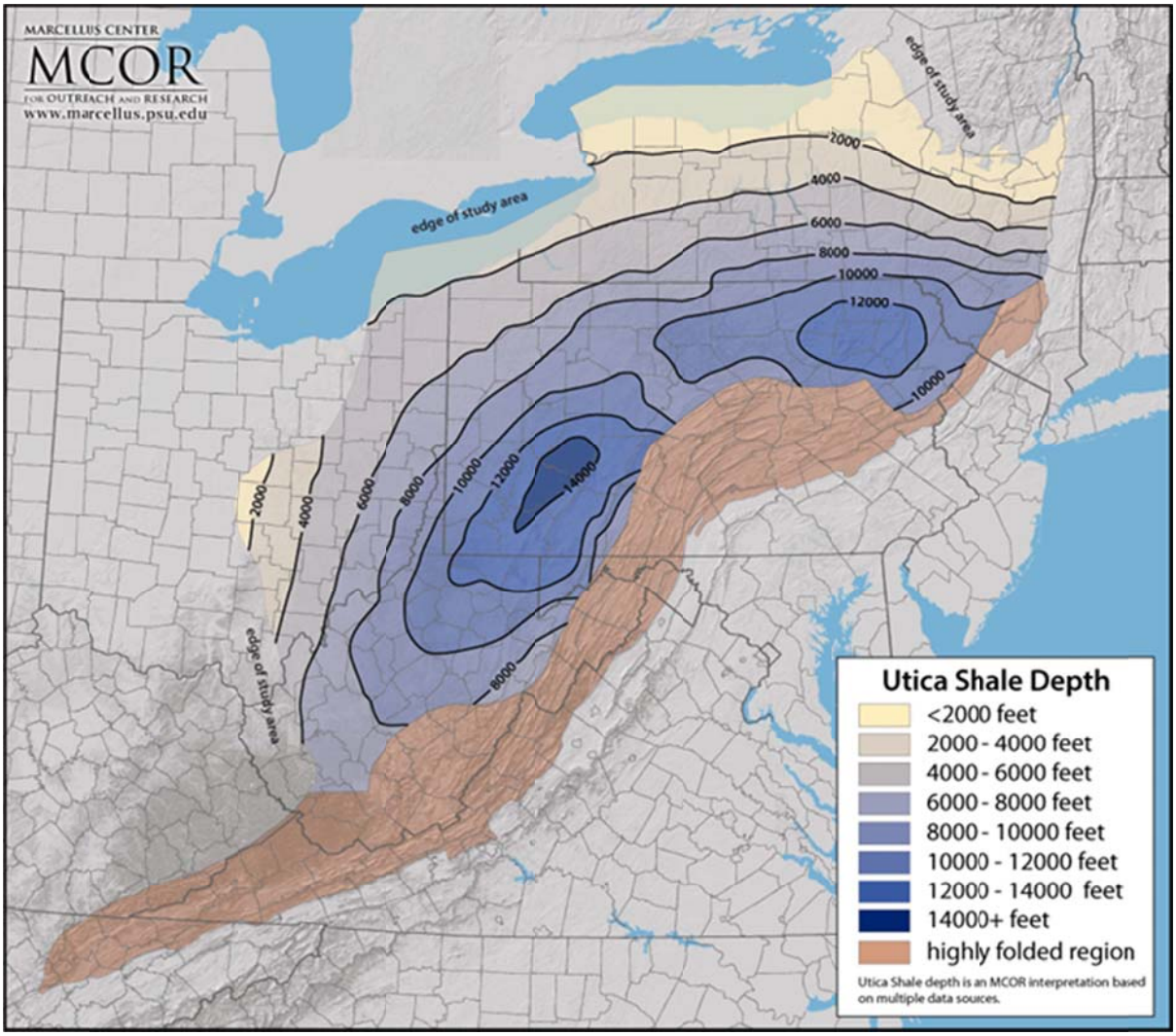

Figure 2. Simplified Stratigraphic Column for Utica and Point Pleasant Shale Formations

<table>
<tr><th rowspan="2">System/ Series<br>(N. American)</th><th colspan="2">West-Central</th><th>Central Basin</th><th>Eastern Basin</th></tr>
<tr><th>West-Central OH</th><th>Eastern OH</th><th>WV & PA</th><th>PA & NY</th></tr>
<tr><td rowspan="8">Upper Ordovician</td><td rowspan="2">Cincinnati Group</td><td>Queenston Shale</td><td>Juniata Fm.</td><td>Queenston Shale</td></tr>
<tr><td>Cincinnati Group</td><td rowspan="2">Reedsville Shale</td><td rowspan="2">Martinsburg Fm.</td><td rowspan="2">Lorraine Group</td></tr>
<tr><td>Kope Fm.</td><td>Kope Fm.</td></tr>
<tr><td>Utica Shale</td><td>Utica Shale</td><td>Utica Shale (in part)</td><td>Utica Shale</td></tr>
<tr><td rowspan="2">Pt. Pleasant</td><td rowspan="2">Pt. Pleasant</td><td>Pt. Pleasant equivalent (in part)</td><td>Pt. Pleasant equiv. (in part)</td></tr>
<tr><td rowspan="2">Trenton Limestone</td><td rowspan="2">Trenton Group</td></tr>
<tr><td>Lexington Ls</td><td>Lexington Limestone</td></tr>
<tr><td rowspan="3">Middle Ordovician</td><td colspan="2">Black River Group</td><td>Black River Group</td><td>Black River Group</td></tr>
<tr><td colspan="2">Wells Creek Fm.</td><td>Wells Creek equiv. (in part)</td><td rowspan="2">(Unconformity)</td></tr>
<tr><td colspan="2">(Unconformity)</td><td>(Unconformity)</td></tr>
<tr><td>Lower Ordovician</td><td colspan="2">Beekmantown/ Knox Dolomite</td><td>Beekmantown Grp.</td><td>Beekmantown/ Tribes Hill</td></tr>
</table>

Figure 3. New York Utica Stratigraphy from the Mohawk Valley Outcrop

(source Smith and Leone, 2010b)

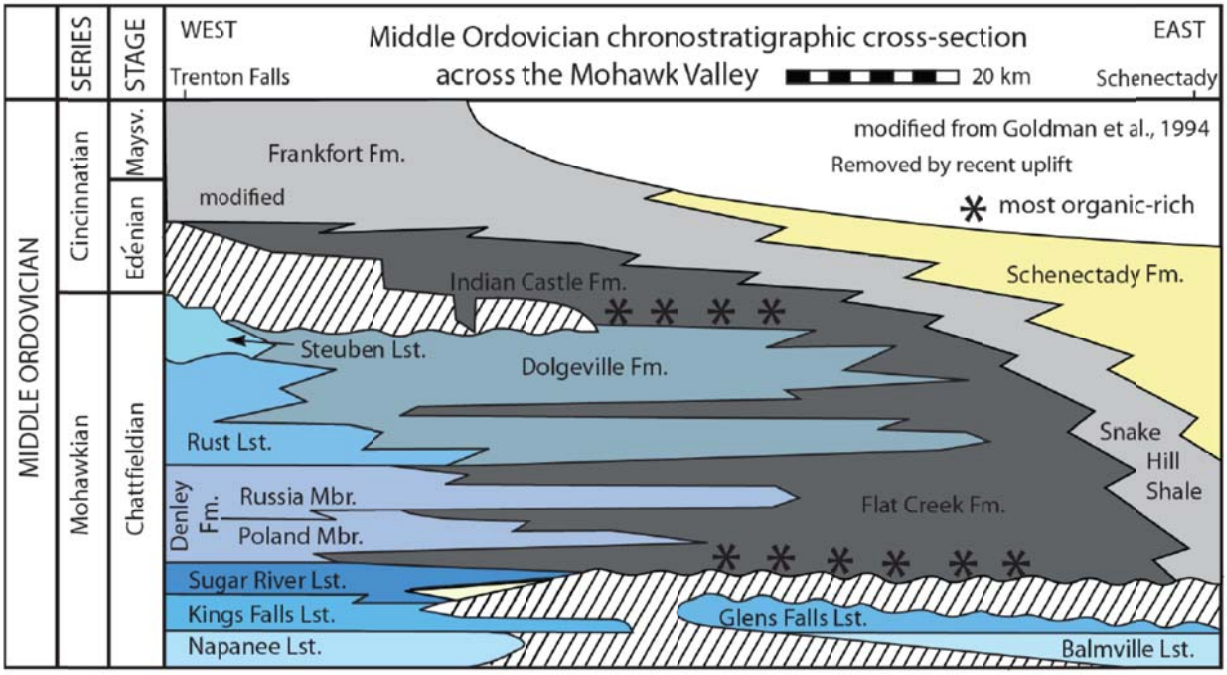

Figure 4. Utica Thermal Maturity Boundaries

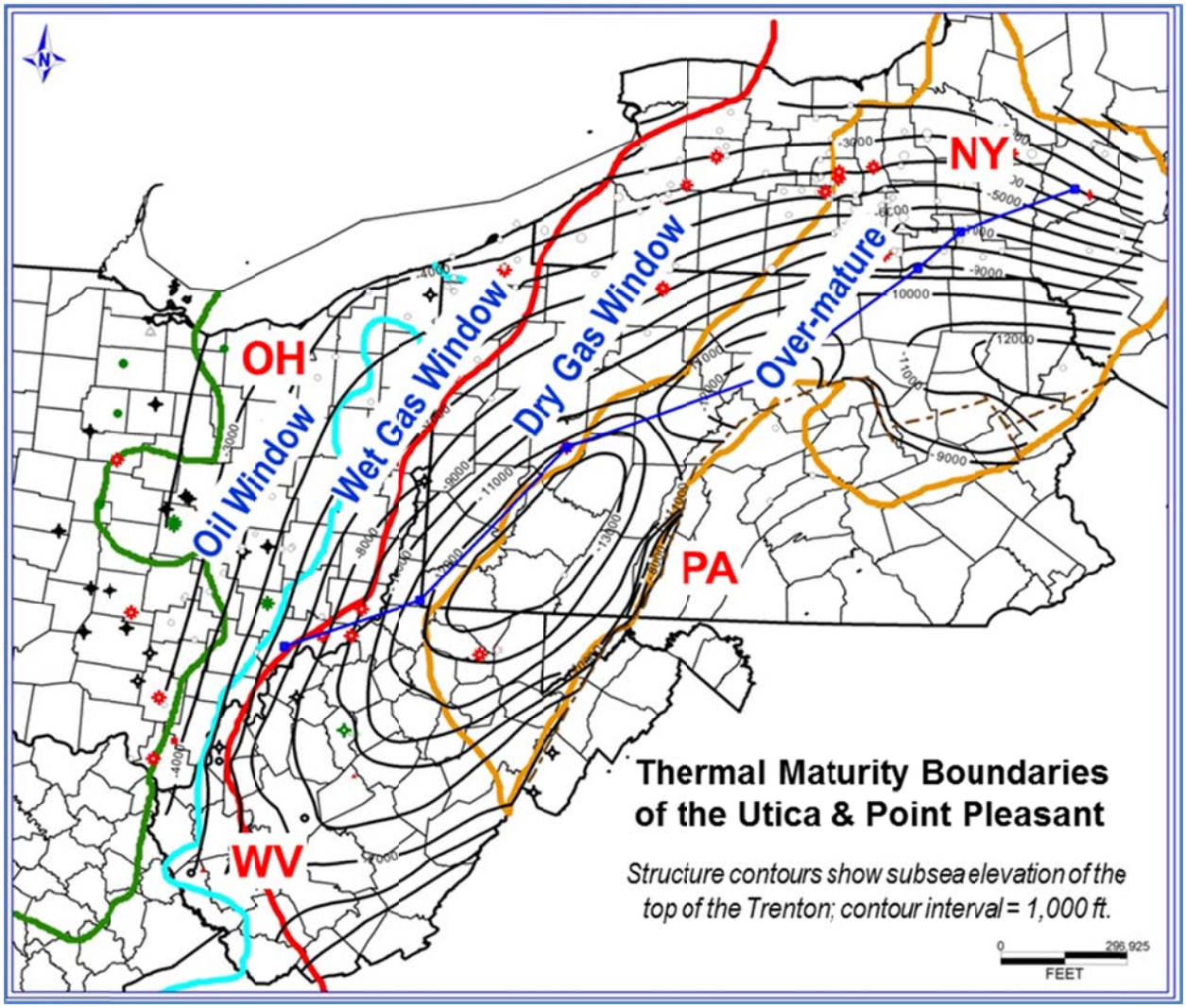

Figure 5. Utica/ Point Pleasant Study Area with Model Area Sub-Divisions

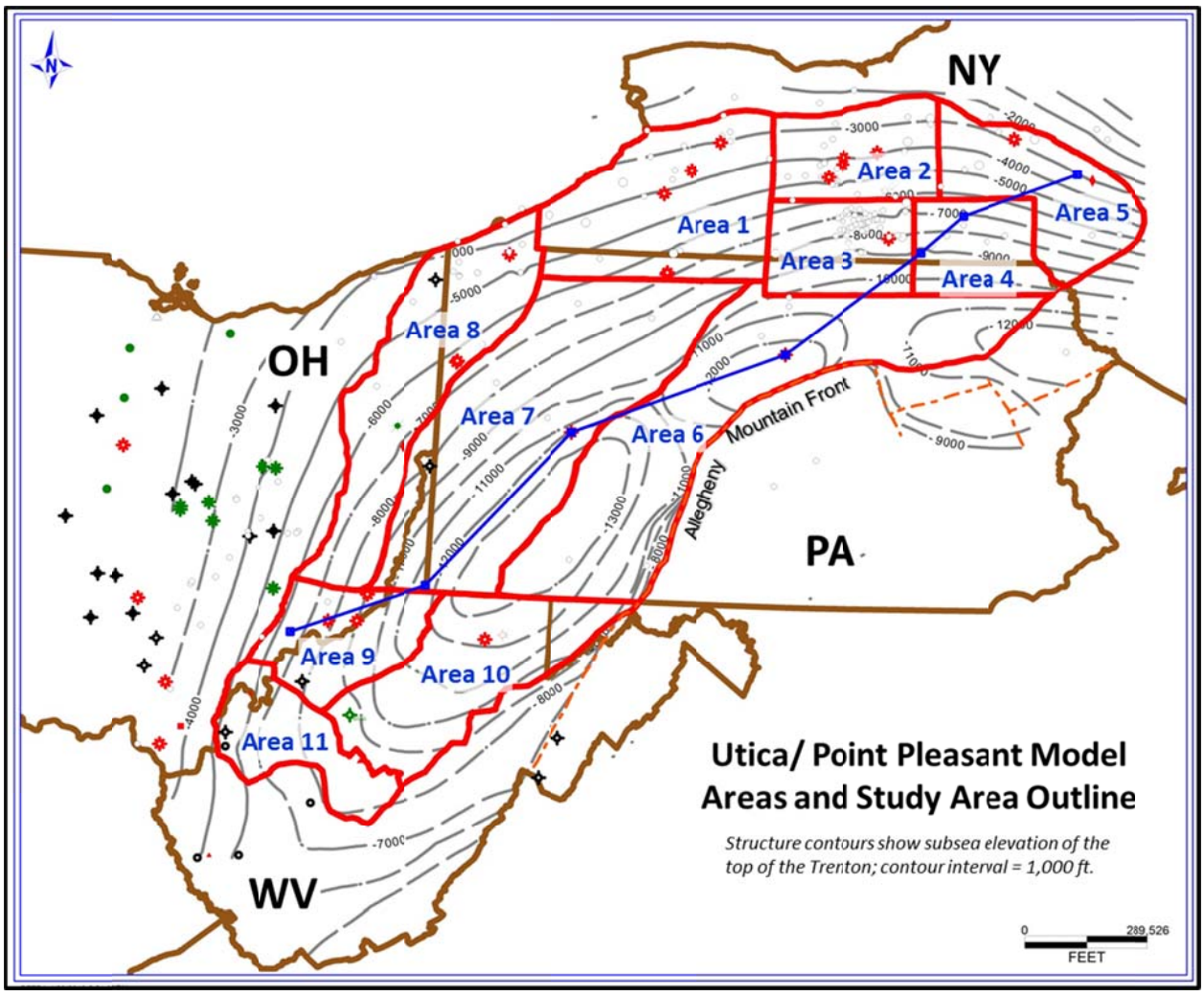

Figure 6. Utica/ Point Pleasant Type Log, Tioga County, New York

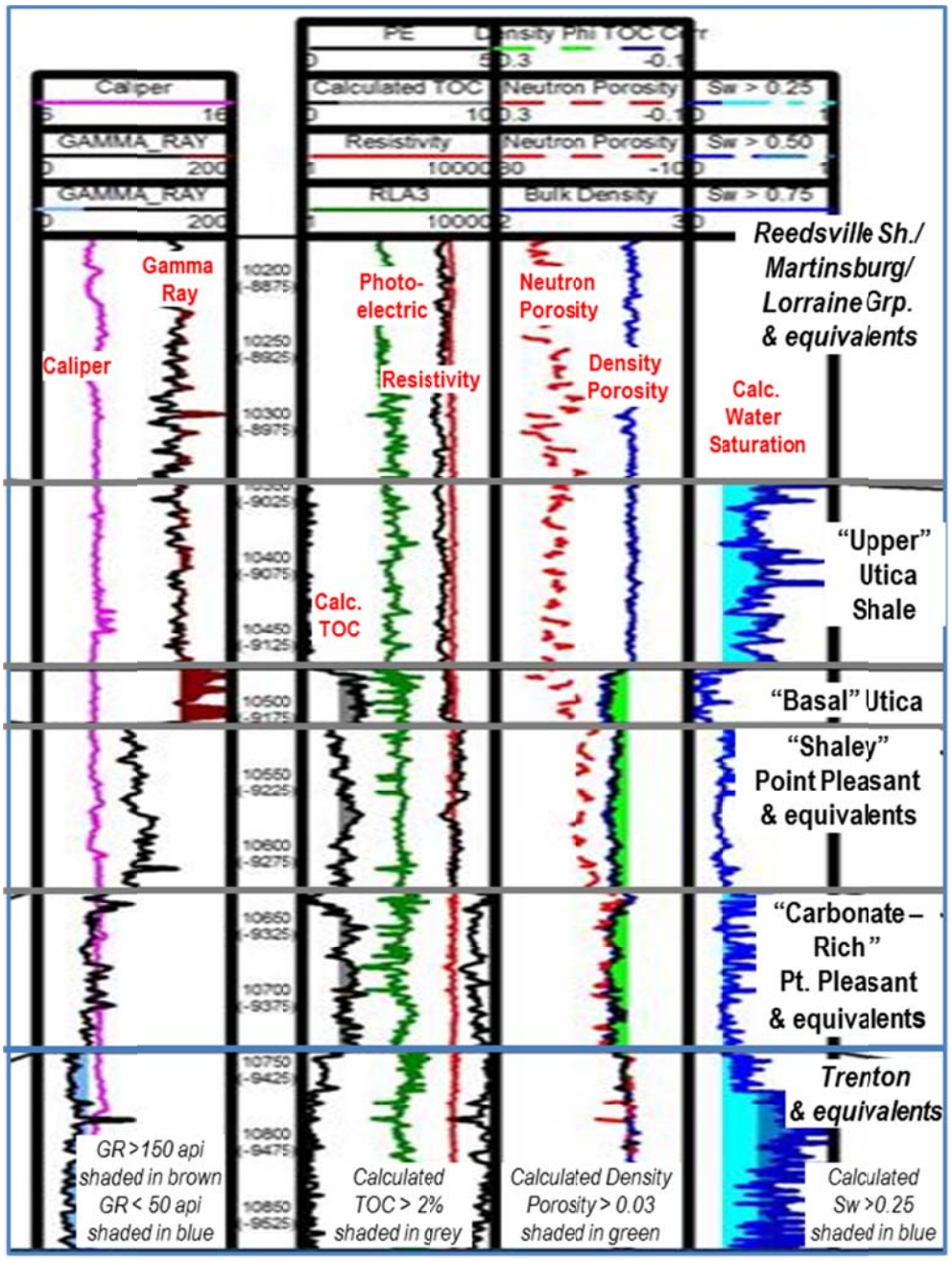

Figure 7. Stratigraphic Cross-Section Showing Model Layers for Reservoir Simulation

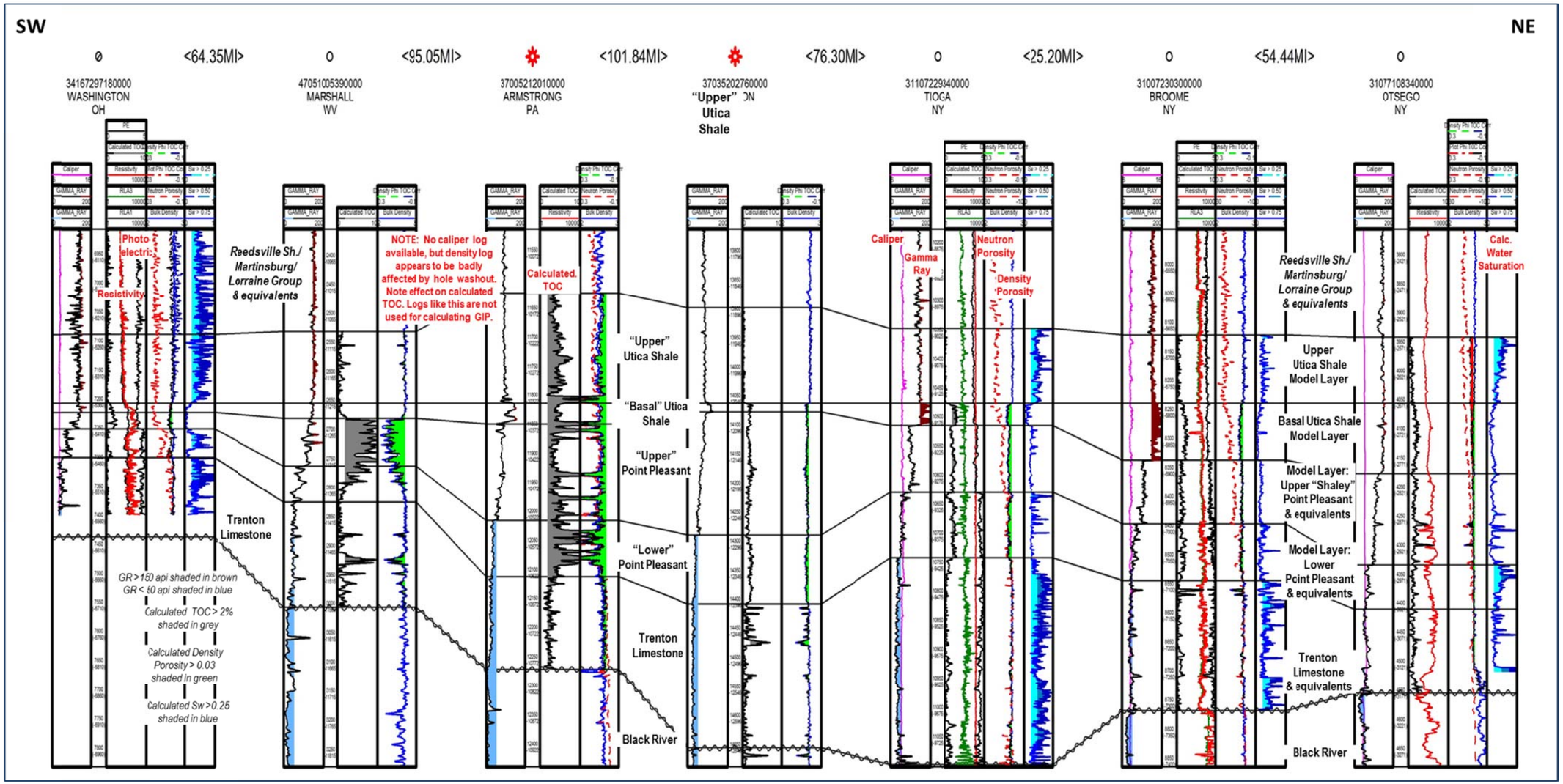

Figure 8. Methane Adsorption Isotherms for the Utica/ Point Pleasant

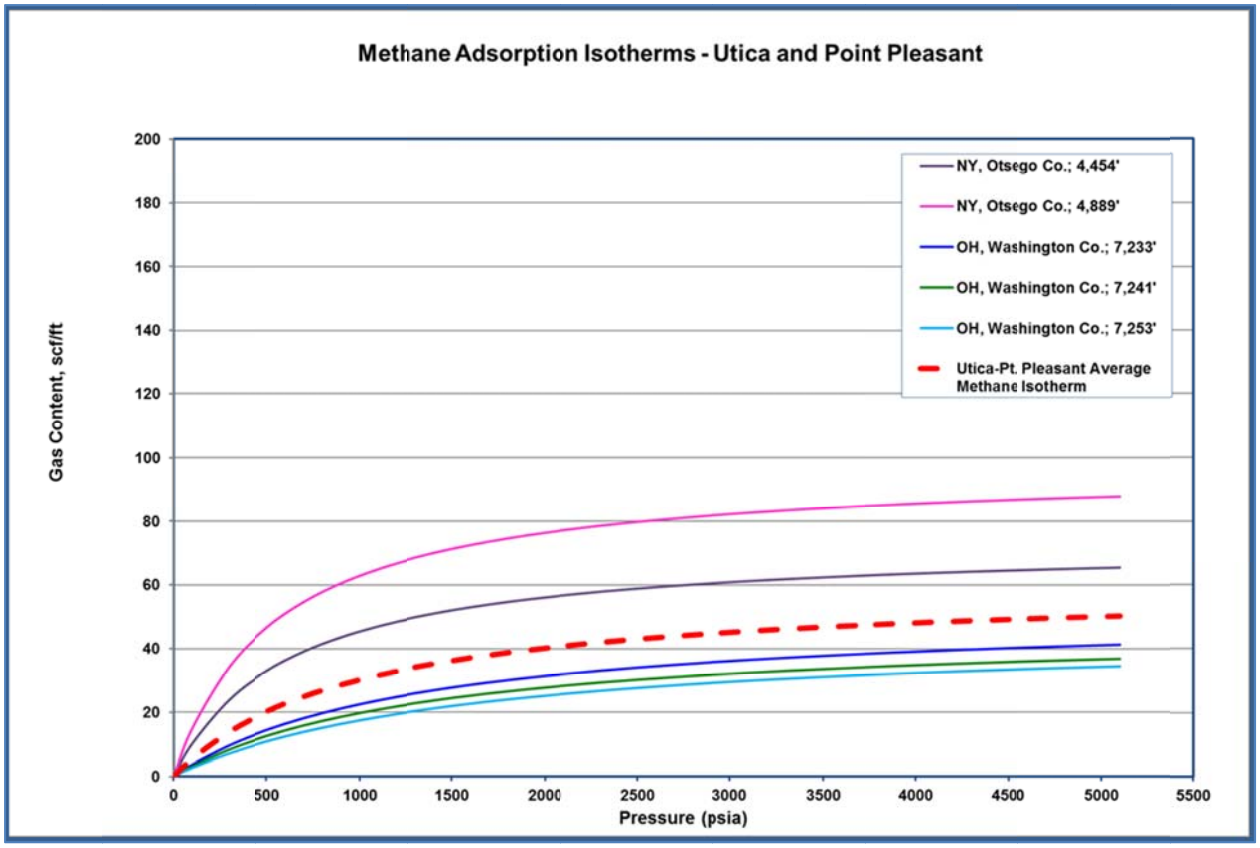

Figure 9. $CO_2$ Adsorption Isotherms for the Utica/ Point Pleasant

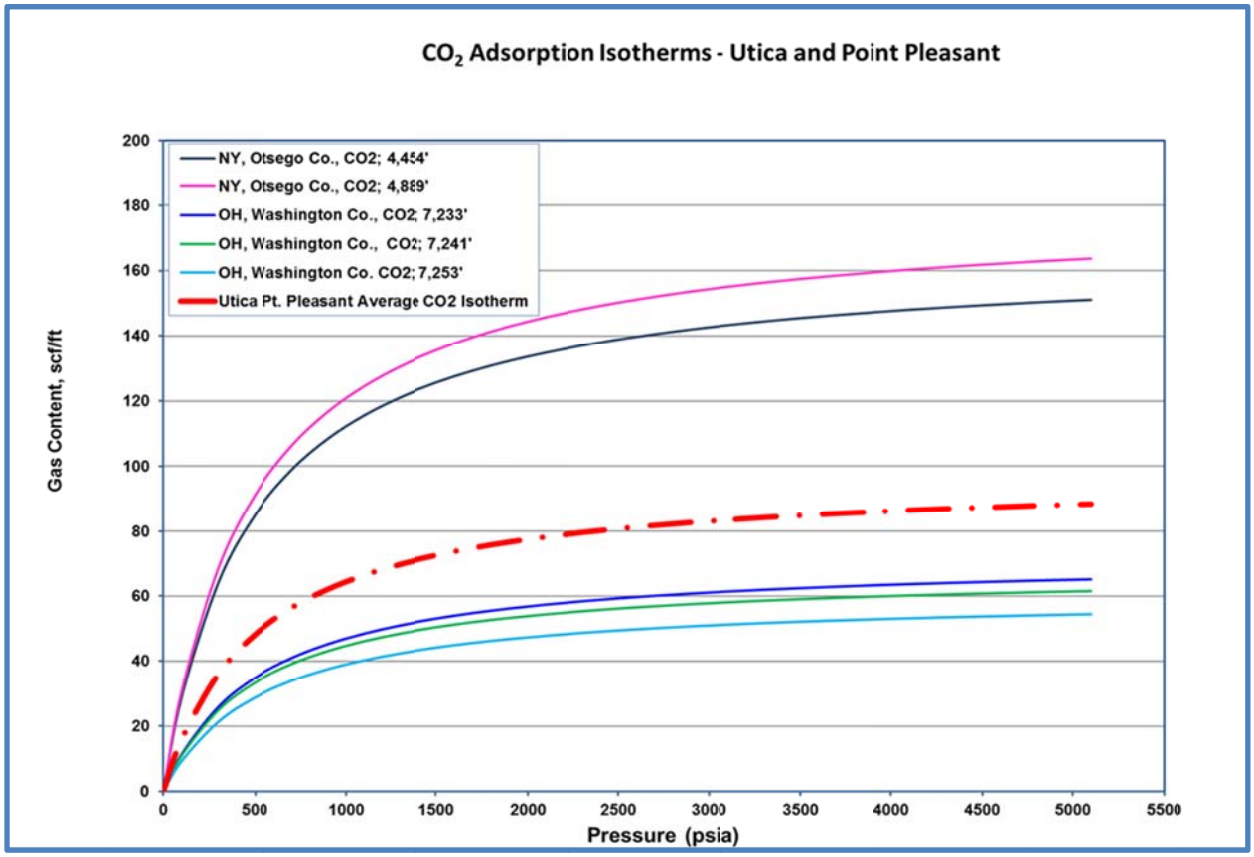

Figure 10. Cross-Plot Showing Correlation of TOC and Langmuir Volume for the Utica/ Point Pleasant Methane Isotherms

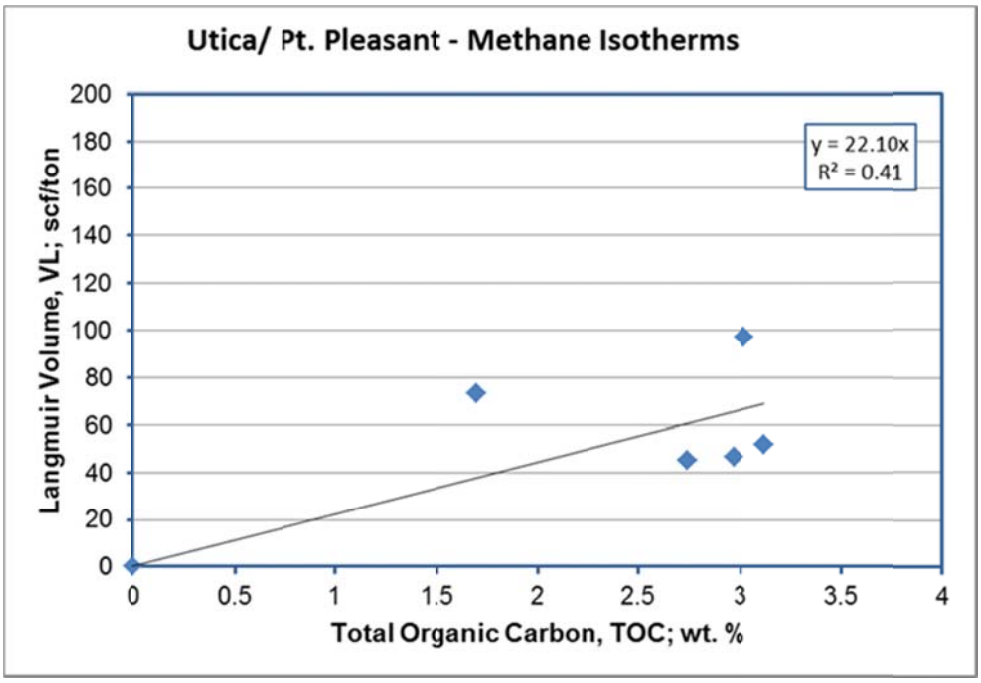


Figure 11. Cross-Plot Showing Correlation of TOC and Langmuir Volume for the Utica/ Point Pleasant $CO_2$ Isotherms

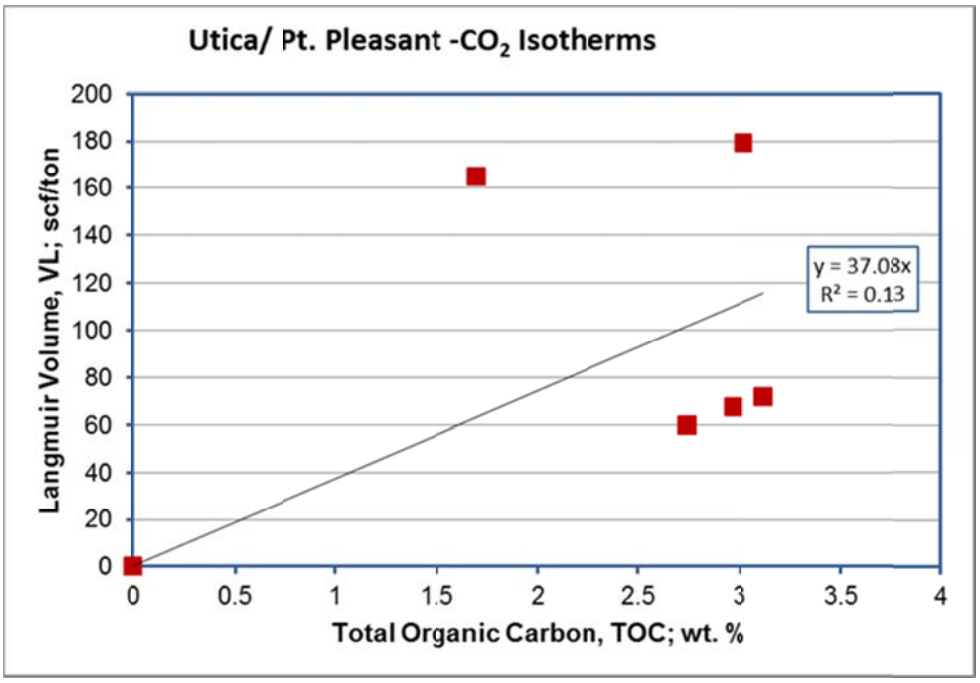

Figure 12. Cross-Plot Showing Correlation of TOC and Bulk Density for Utica, Point Pleasant and Trenton Data in Ohio and New York

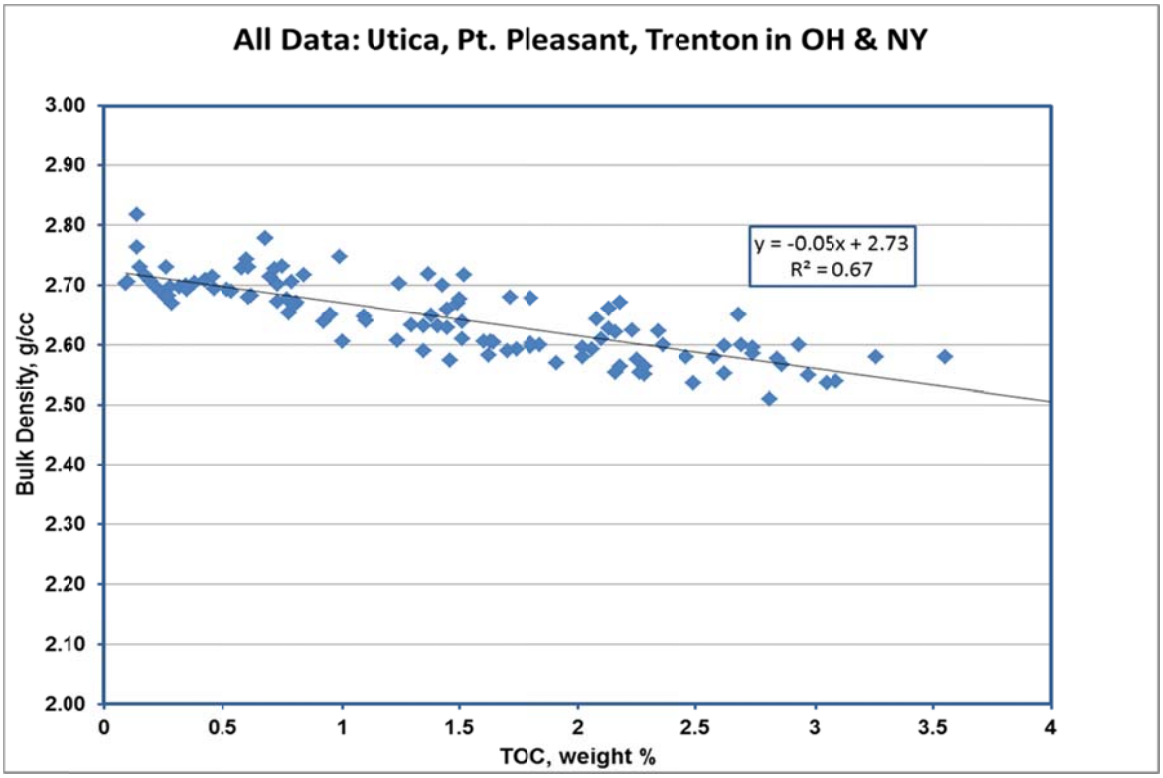

Figure 13. Utica and Point Pleasant Core Porosity and Permeability

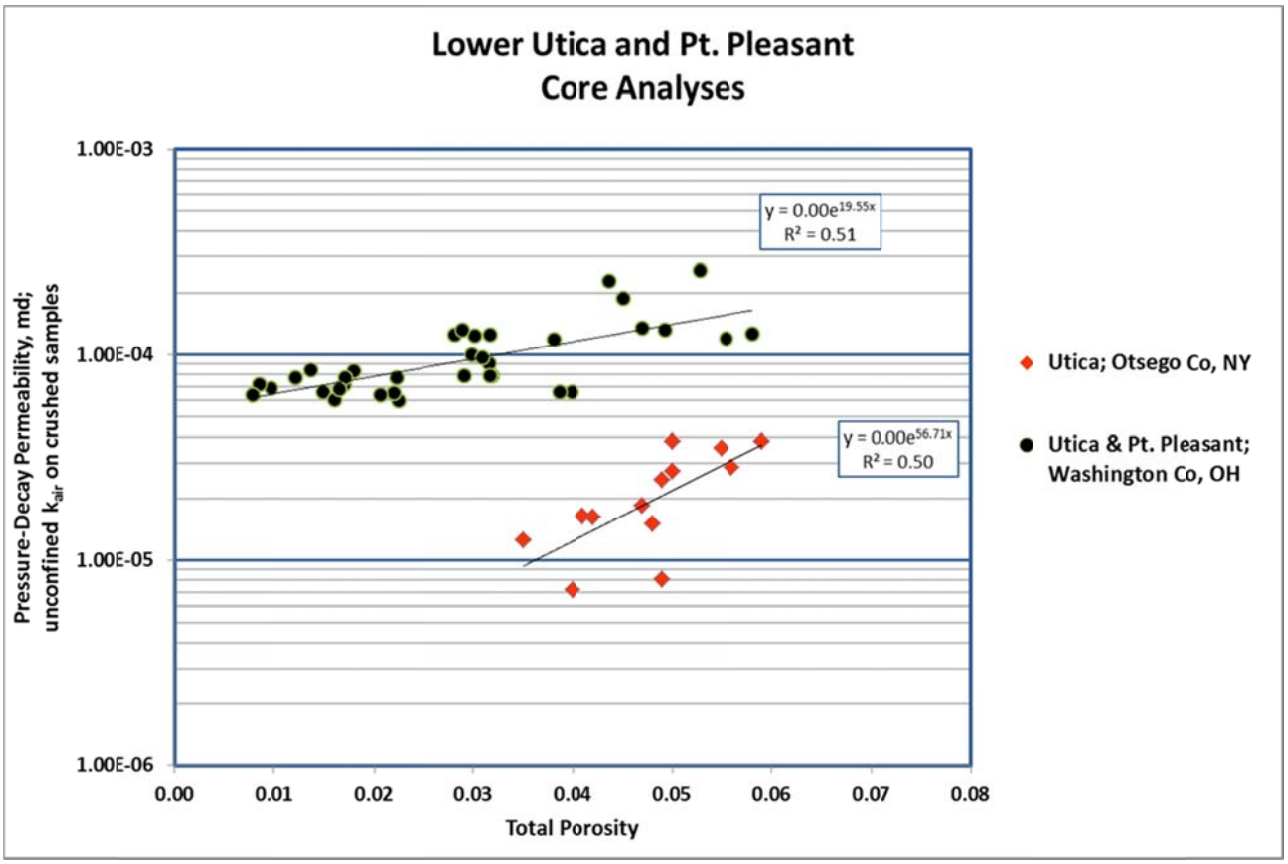

Figure 14. Impact of Net Effective Confining Stress on Measured Core Permeability

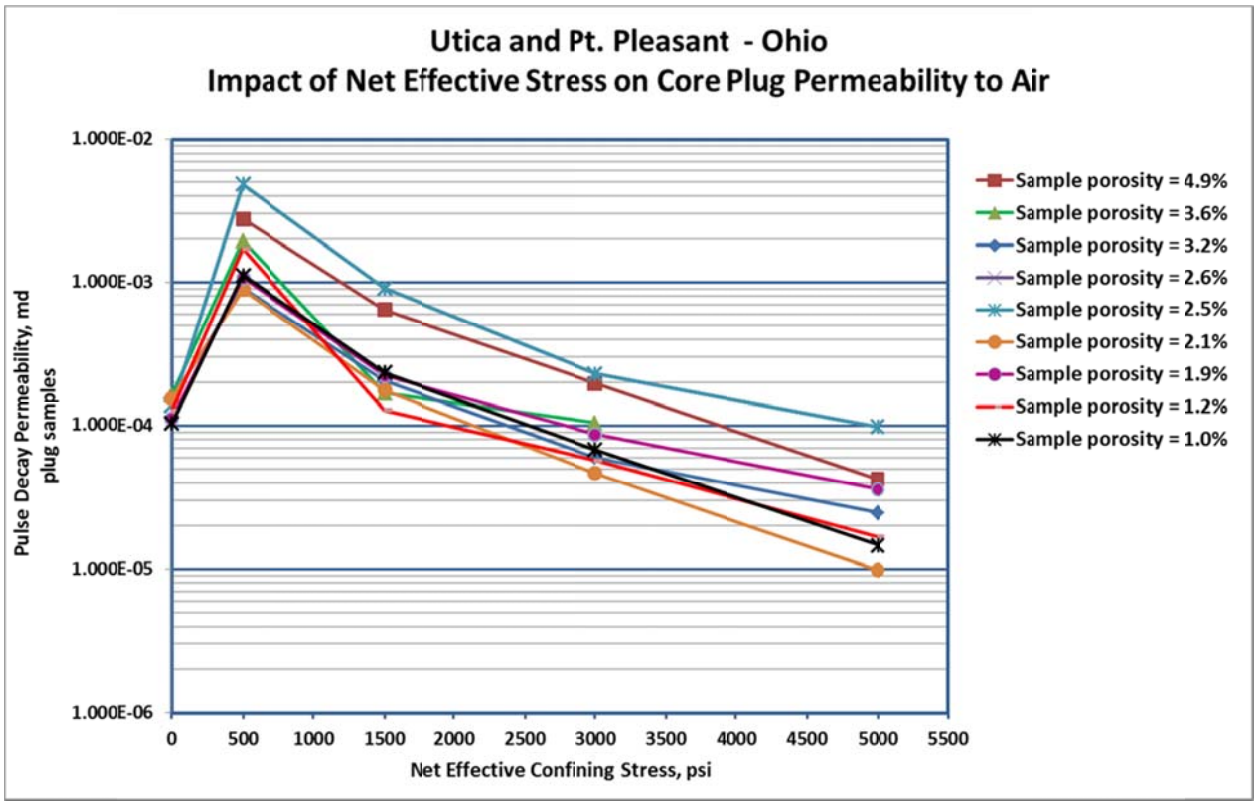

Figure 15. Basal Utica Shale Reservoir Layer; Selected Model Well Parameters – Thickness, Average TOC, Average Total Porosity

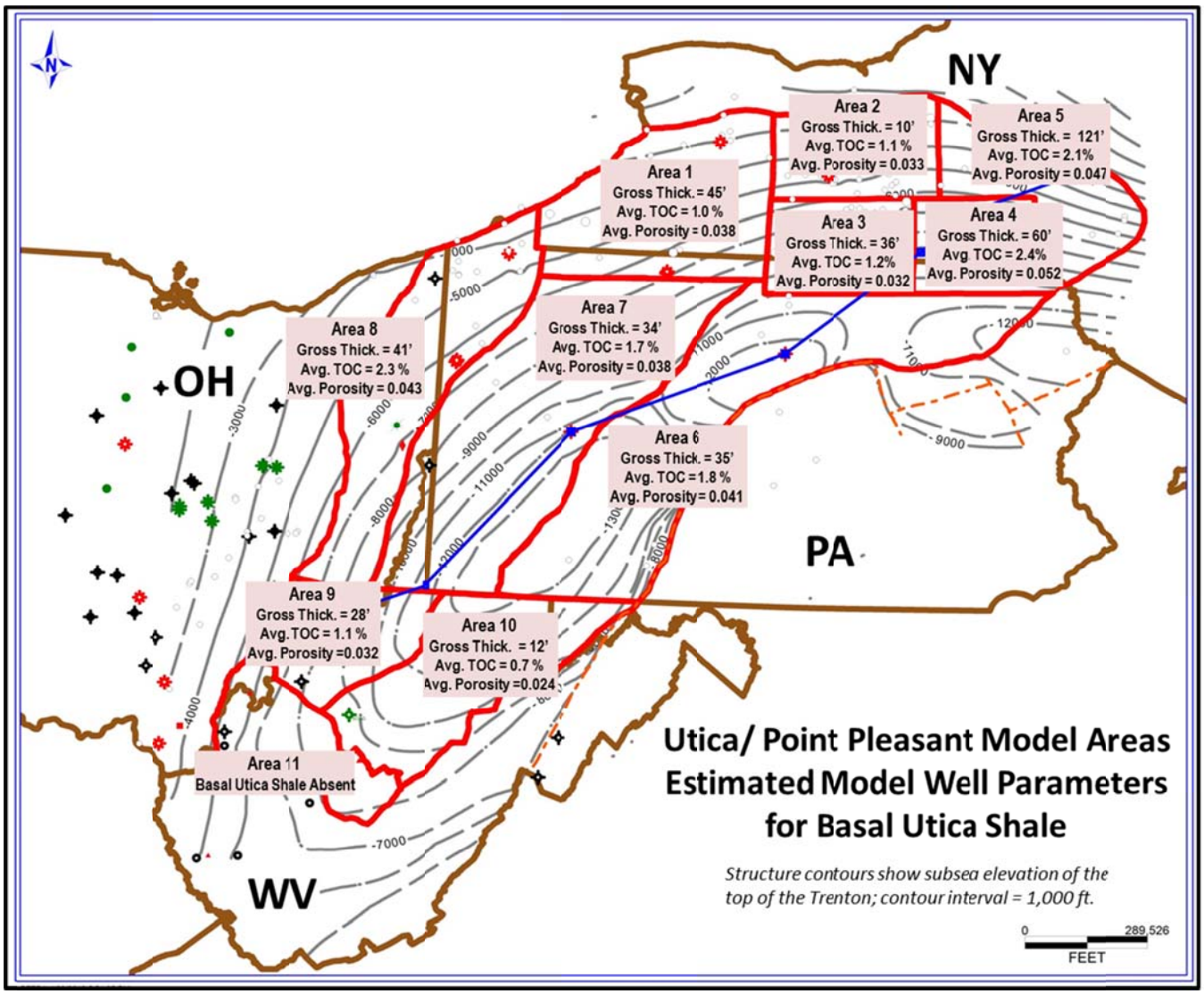

Figure 16. Upper (Shaley) Point Pleasant Reservoir Layer; Selected Model Well Parameters – Thickness, Average TOC, Average Total Porosity

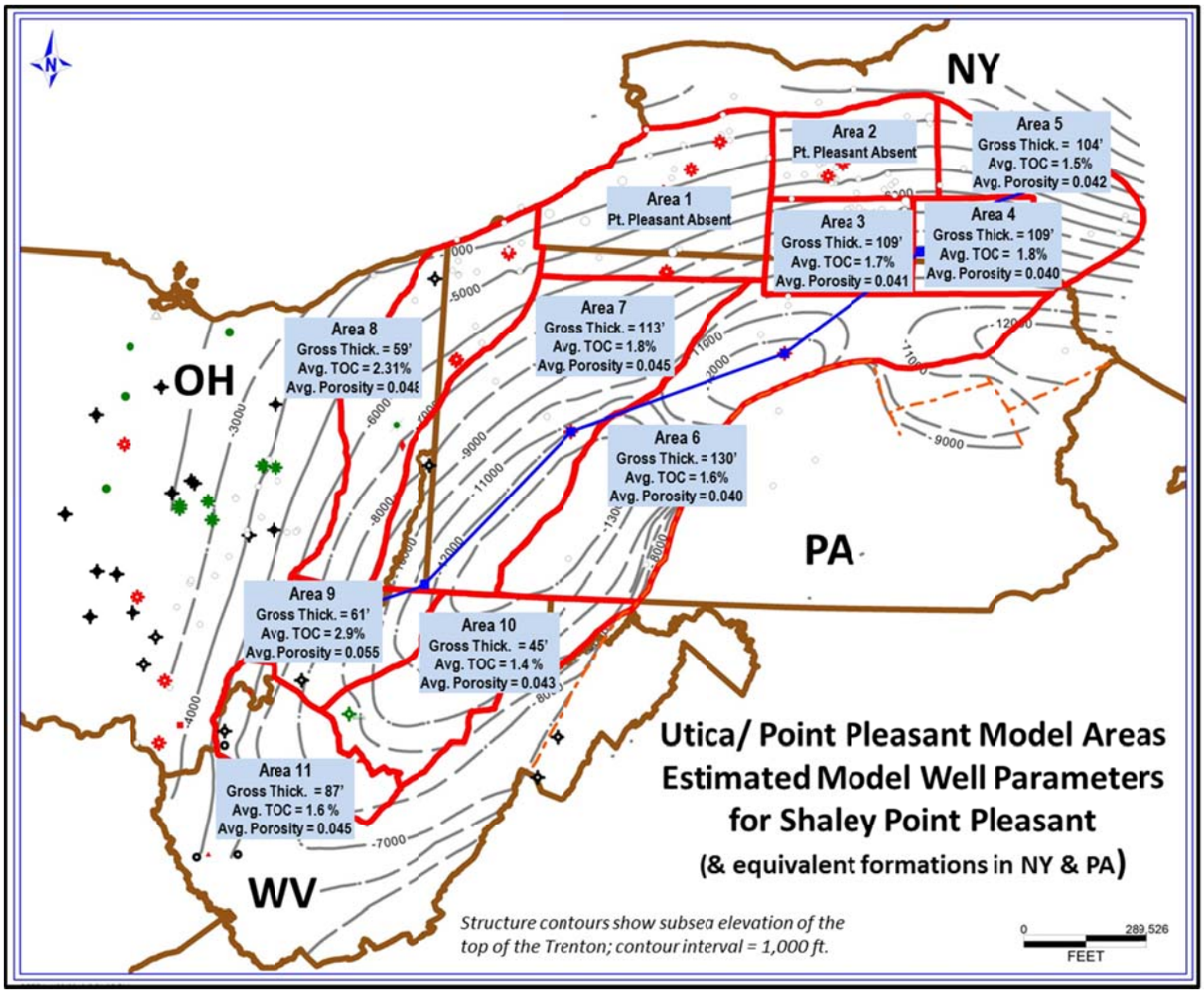

Figure 17. Basal Utica Shale Reservoir Layer – Total Estimated Gas in-Place, Bcf/square mile

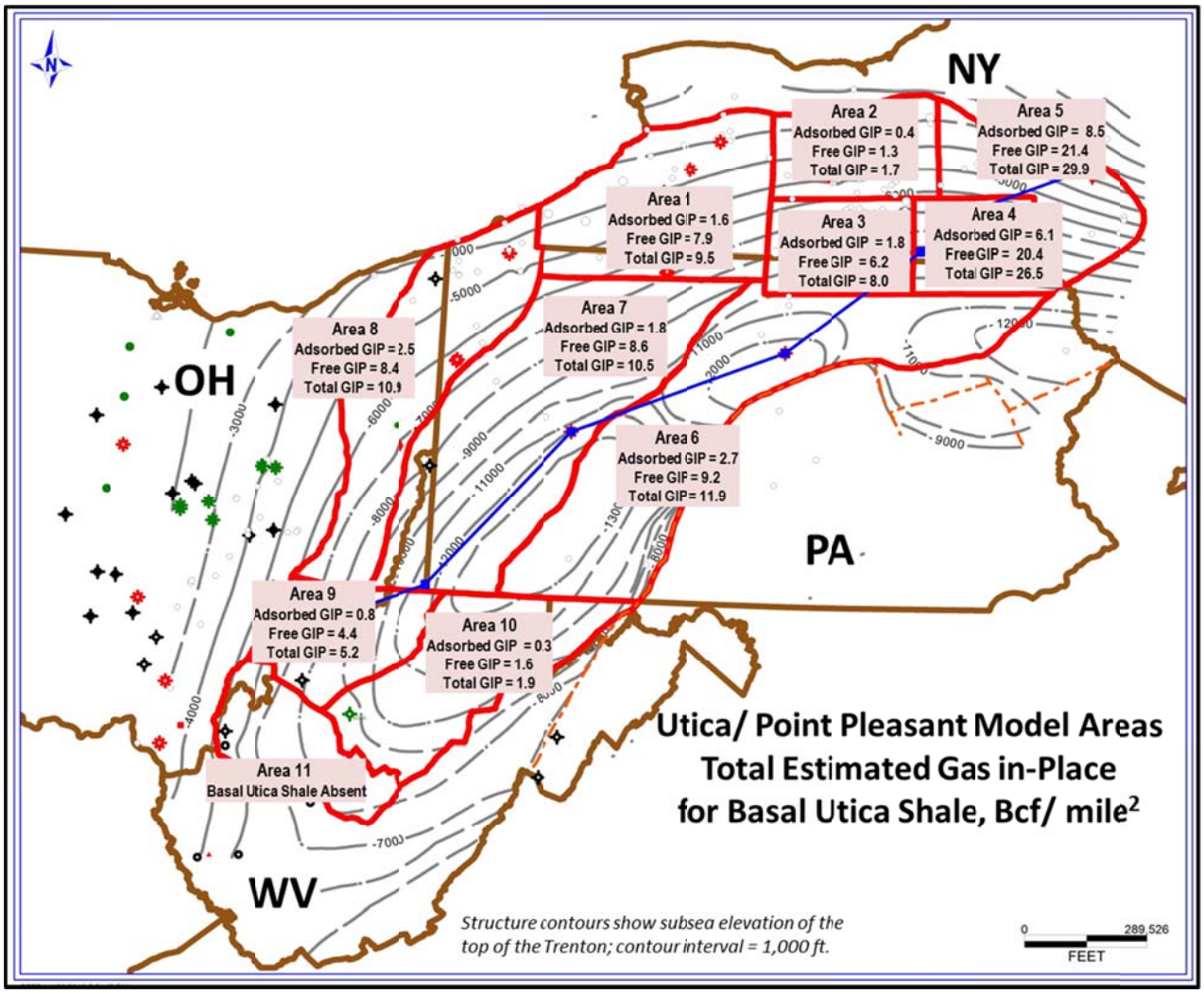

Figure 18. Upper (Shaley) Point Pleasant Reservoir Layer – Total Estimated Gas in-Place, Bcf/square mile

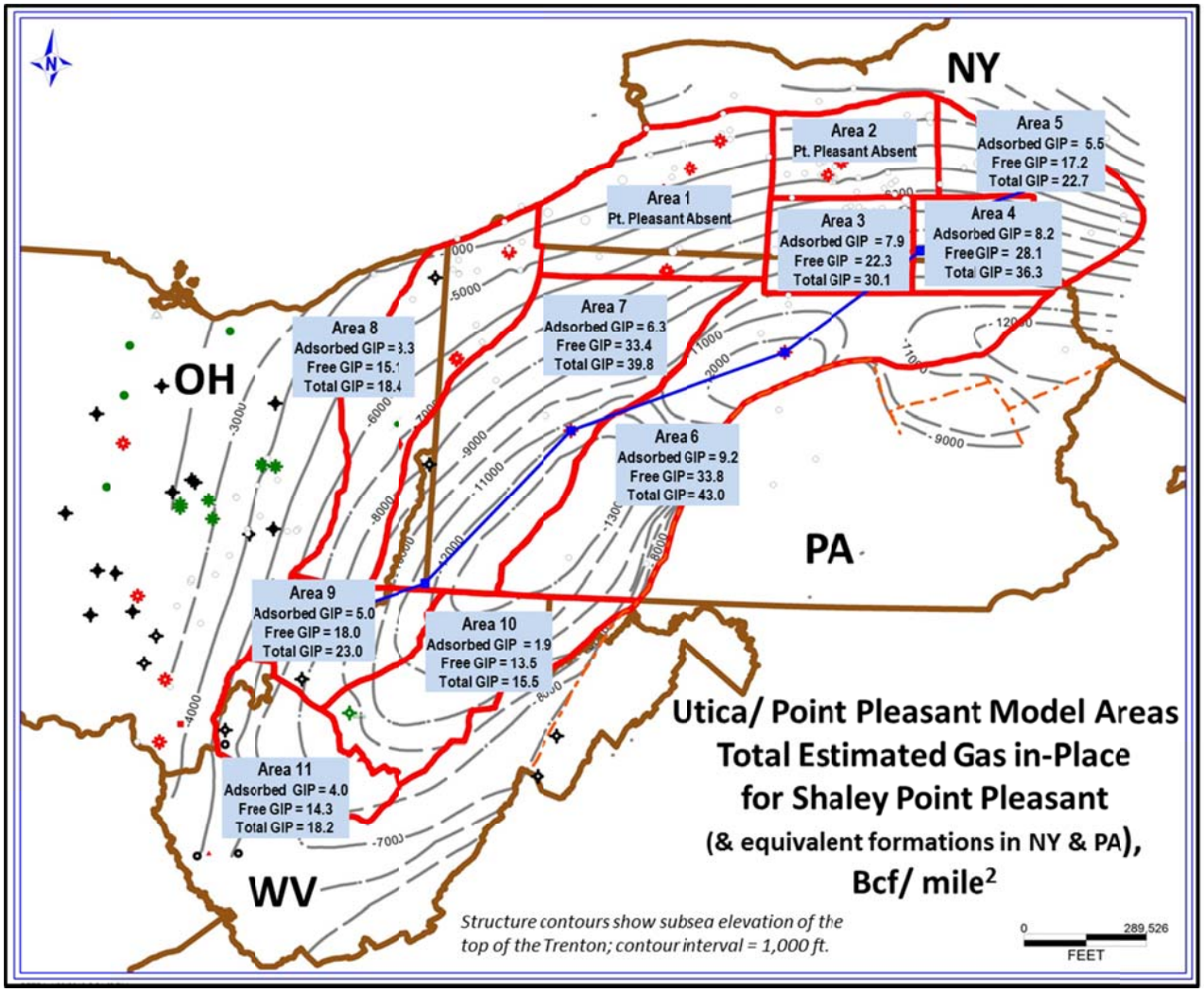

Figure 19. Total Utica/ Point Pleasant; Gas in-Place by Model Area, Bcf/ 80-acres

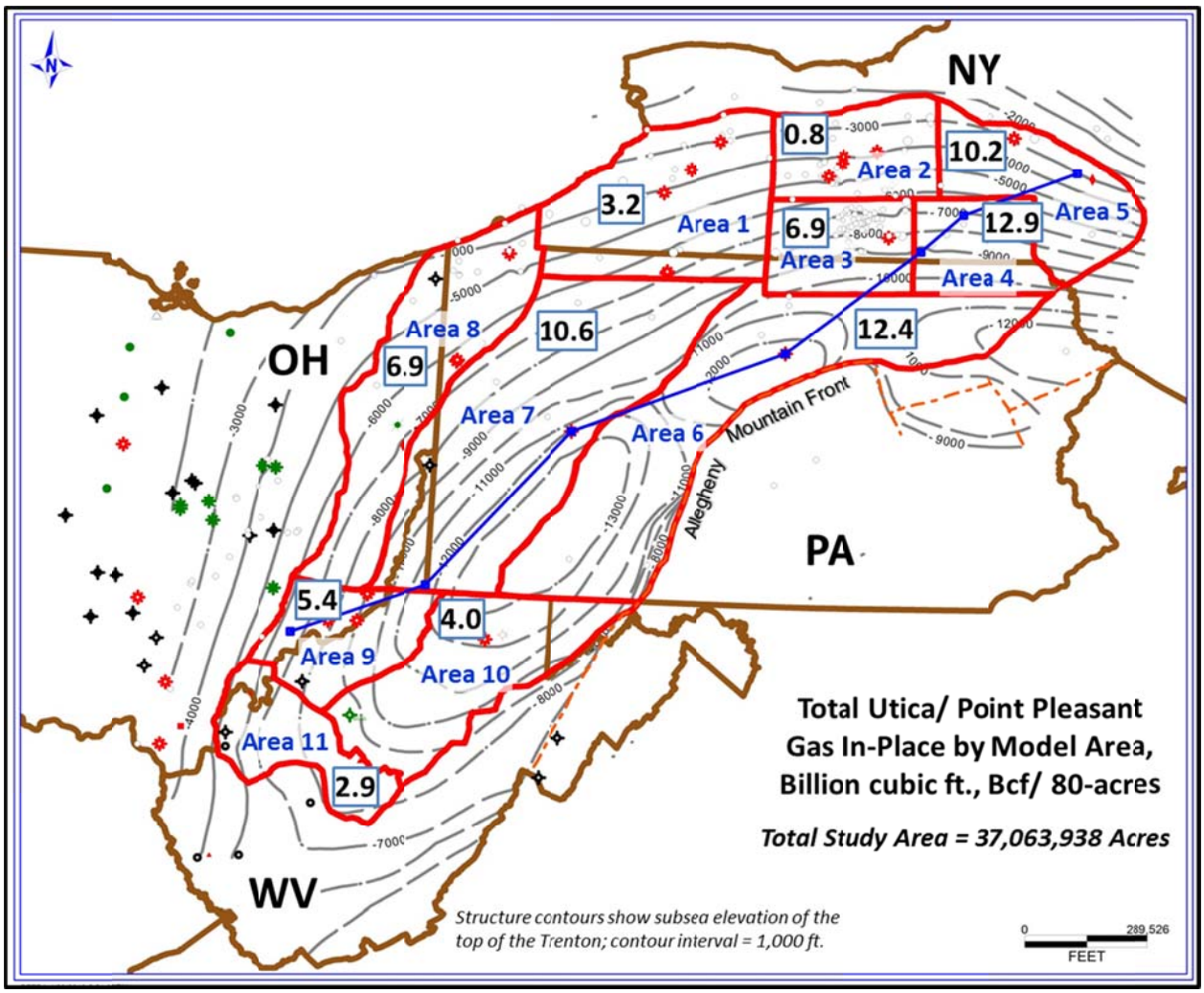

Figure 20. Total Utica/ Point Pleasant; Theoretical Maximum $CO_2$ Storage Capacity by Model Area, Mt/ 80-acres

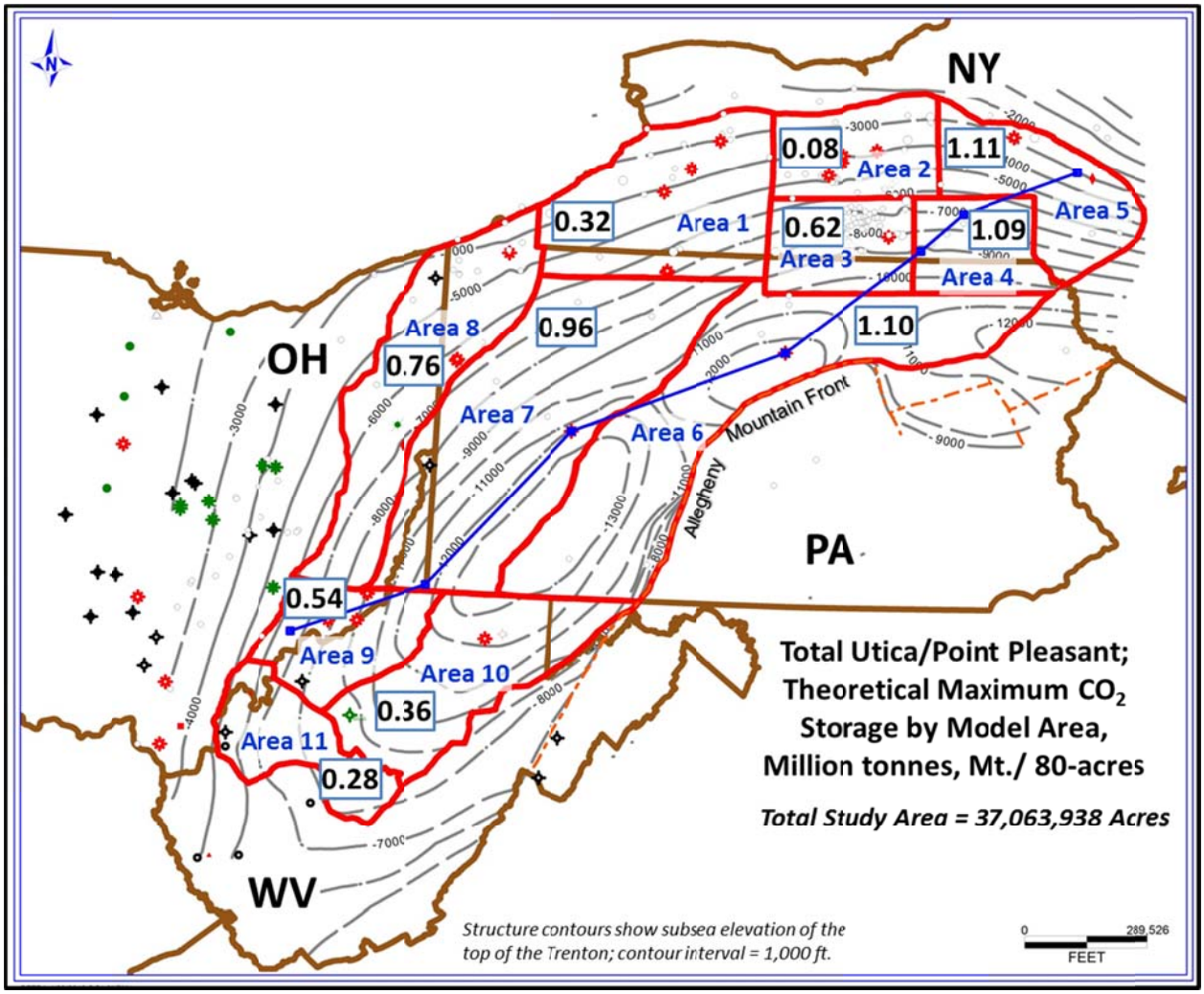

# TABLES

Table 1. Summary of Adsorption Isotherm Data Obtained for the Utica/ Point Pleasant

| Sample | Formations | Depth, ft. | TOC, wt. % | Methane Langmuir Volume (VL) scf/ ton | Methane Langmuir Pressure (PL) psia | CO2 Langmuir Volume (VL) scf/ton | CO2 Langmuir Pressure (PL) psia |
|---|---|---|---|---|---|---|---|
| Washington Co., OH | Point Pleasant-Shaley | 7,232 | 3.12 | 51.7 | 1294.6 | 72.0 | 533.6 |
| Washington Co., OH | Point Pleasant-Shaley | 7,241 | 2.97 | 46.6 | 1356.4 | 67.6 | 516.4 |
| Washington Co., OH | Point Pleasant – Carbonate-Rich | 7,253 | 2.74 | 45.1 | 1578.7 | 60.1 | 548.0 |
| Otsego Co., NY | Utica - Indian Castle clay-rich | 4,454 | 1.70 | 73.3 | 613.4 | 165.0 | 470.0 |
| Otsego Co., NY | Flat Creek (Point Pleasant Equivalent) | 4,889 | 3.02 | 97.2 | 545.2 | 179.2 | 482.3 |
| | | | | Average Methane PL | 1,077.7 | Average CO2 PL | 510.1 |

Table 2. Summary of X-Ray Diffraction Mineralogy for the Utica/ Point Pleasant

| Data Source | Quartz | K-Feldspar | Plagioclase | Calcite | Dolomite | Fe-Dolomite | Pyrite | Other[1] | Total Clay |
|---|---|---|---|---|---|---|---|---|---|
| Utica - NY (Indian Castle) | 25.7 | 0.2 | 11.8 | 23.0 | 7.1 | 0 | 1.2 | | 30.3 |
| Point Pleasant equivalent - NY (Flat Creek) | 9.8 | 0.7 | 1.6 | 59.0 | 0 | 8.1 | 0.1 | | 20.0 |
| Utica - Quebec | 10.0 | 0.5 | 4.5 | 50.0 | 5.0 | | 0 | | 25.0 |
| Utica - OH | 23.9 | 4.5 | 7.0 | 19.3 | 2.1 | 2.2 | 2.1 | 0.8 | 37.9 |
| Point Pleasant - OH | 18.6 | 5.4 | 3.4 | 32.9 | 2.1 | 0.9 | 2.3 | 0.3 | 34.1 |

[1]Other minerals: fluorapatite

Table 3. Utica and Point Pleasant Porosity-Permeability Relationships from Core Data

| Core Porosity | Southern PA, OH, WV | NY, PA |
|---|---|---|
| | Permeability to air, $k_{air}$, md | Permeability to air, $k_{air}$, md |
| 0.08 | 2.39 E-04 | 9.34 E-05 |
| 0.07 | 1.97 E-04 | 5.30 E-05 |
| 0.06 | 1.62 E-04 | 3.00 E-05 |
| 0.05 | 1.33 E-04 | 1.70 E-05 |
| 0.04 | 1.09 E-04 | 9.66 E-06 |
| 0.03 | 8.99 E-05 | 5.48 E-06 |
| 0.02 | 7.39 E-05 | 3.11 E-06 |
| 0.01 | 6.08 E-05 | 1.76 E-06 |
| 0.005 | 5.51E-05 | 1.33 E-06 |

Table 4. Adsorbed Gas Content Calculated from Isotherm Data and TOC

| Estimating Adsorbed Gas Content from Isotherm Data and Total Organic Carbon (TOC) | | | | |
|---|---|---|---|---|
| Samples | Average Langmuir Pressure, $P_L$, psia | Langmuir Volume, $V_L$, scf/ton | Adsorbed Gas Content, scf/ton | Approximate Thermal Maturity Area |
| NY Methane Isotherm Data | 579 | $V_L$ = 34.8 x TOC | =((34.8 x TOC) x Reservoir Pressure)/ (579+Res Press) | Over mature: central and east-central NY; central& northeast PA |
| Eastern OH Isotherm Data | 1,410 | $V_L$ = 16.2 x TOC | =((16.2 x TOC) x Reservoir Pressure)/ (1,410+Res Press) | West Gas Window: eastern OH & western WV |
| Composite Methane Isotherm Data (NY & OH) | 1,078 | $V_L$ = 22.1 x TOC | =((22.1 x TOC) x Reservoir Pressure)/ (1,078+Res Press) | Dry Gas Window: western NY, western PA; central WV and WV panhandle |

Table 5. Theoretical Maximum Adsorbed $CO_2$ Capacity from Isotherm Data and TOC

| Estimating Theoretical Maximum Adsorbed $CO_2$ Content from Isotherm Data and Total Organic Carbon (TOC) | | | | |
|---|---|---|---|---|
| Samples | Average Langmuir Pressure, $P_L$, psia | Langmuir Volume, $V_L$, scf/ton | Adsorbed Gas Content, scf/ton | Approximate Thermal Maturity Area |
| NY $CO_2$ Isotherm Data | 476 | $V_L$ = 68.4 x TOC | =((68.4 x TOC) x Reservoir Pressure)/ (476+Res Press) | Over mature: central and east-central NY; central& northeast PA |
| Eastern OH $CO_2$ Isotherm Data | 533 | $V_L$ = 22.6 x TOC | =((22.6 x TOC) x Reservoir Pressure)/ (533+Res Press) | West Gas Window: eastern OH & western WV |
| Composite $CO_2$ Isotherm Data (NY & OH) | 510 | $V_L$ = 37.1 x TOC | =((37.1 x TOC) x Reservoir Pressure)/ (510+Res Press) | Dry Gas Window: western NY, western PA; central WV and WV panhandle |

Table 6. Log Analysis Variables to Calculate Porosity and Water Saturation

| Variable | Definition | Utica/ Point Pleasant |
|---|---|---|
| $\rho_{Shale}$ | maximum bulk density of gray shale (low organic content), g/cc | 2.73 |
| $\rho_{matrix}$ | matrix grain density, g/cc | 2.75 |
| $\rho_{fluid}$ | density of formation water, g/cc | 1.10 |
| $\rho_{TOC}$ | density of organic matter, g/cc | 1.3 |
| $R_w$ | water resistivity at formation temperature, ohm-m | Variable based on temperature |
| $R_{shale}$ | shale resistivity, ohm-m | 50 |
| **a** | Archie tortuosity exponent | 1 *(common default)* |
| **m** | Archie cementation exponent | 2.15 |
| **n** | Archie saturation exponent | 2 *(common default)* |

Table 7. Description and Summary of Model Areas for the Utica/ Point Pleasant

| Description and Summary of Utica Shale/ Point Pleasant Model Areas | | | | | | | | |
|---|---|---|---|---|---|---|---|---|
| MODEL AREA | Area Description | Total Area, Acres | Total Area, miles$^2$ | Estimated Reservoir Pressure Gradient, psi/ft | Mean Reservoir Pressure, psia | Mean Reservoir Temperature, $^0$F | FVF for Methane, ft$^3$/ scf | FVF for $CO_2$, ft$^3$/ scf |
| AREA 1 | Western NY & Northwest PA | 4,050,794 | 6,329 | 0.46 | 2,720 | 131 | 0.00458 | 0.00237 |
| AREA 2 | North Central NY | 1,992,915 | 3,114 | 0.53 | 2,928 | 126 | 0.00476 | 0.00234 |
| AREA 3 | South Central NY; North Central PA | 1,793,827 | 2,803 | 0.53 | 4,812 | 178 | 0.00370 | 0.00227 |
| AREA 4 | Southeast Central NY (Broome & Tioga Cos.) | 1,572,025 | 2,456 | 0.63 | 5,968 | 184 | 0.00328 | 0.00216 |
| AREA 5 | Northeast NY (Cortland, Madison, Otsego Cos.) | 2,451,694 | 3,831 | 0.44 | 2,224 | 119 | 0.00505 | 0.00239 |
| AREA 6 | Northeast PA; East Central PA | 6,777,578 | 10,590 | 0.63 | 7,717 | 250 | 0.00316 | 0.00203 |
| AREA 7 | West PA; WV Panhandle; East Central OH | 7,170,236 | 11,204 | 0.60 | 6,621 | 208 | 0.00313 | 0.00208 |
| AREA 8 | Northwest PA; Eastern OH | 4,133,518 | 6,459 | 0.53 | 3,547 | 143 | 0.00425 | 0.00238 |
| AREA 9 | Northwest WV; Southeast OH | 1,948,414 | 3,044 | 0.53 | 4,738 | 176 | 0.00373 | 0.00230 |
| AREA 10 | Central WV | 3,421,544 | 5,346 | 0.53 | 6,406 | 222 | 0.00306 | 0.00203 |
| AREA 11 | Southwest- South Central WV | 1,751,393 | 2,737 | 0.53 | 4,083 | 158 | 0.00397 | 0.00244 |
| Utica/ Point Pleasant Study Area Total | | 37,063,938 | 57,913 | | | | | |

Table 8. Model Layer Attributes for the Upper Utica Shale – Archie Water Saturation

| Model Layer Attributes for Upper Utica Shale | | | | | | | | | |
|---|---|---|---|---|---|---|---|---|---|
| Model Area | Area Description | Average Depth, ft. | Thickness, ft. | Total Porosity, fraction | Matrix Permeability, md | Water Saturation, fraction* | Calculated TOC, wt. % | Mean Adsorbed Gas Content, scf/ ton | Theoretical Max. Adsorbed $CO_2$, scf/ ton |
| AREA 1 | Western NY & Northwest PA | 5,710 | 172 | 0.029 | 5.18E-06 | 0.65 | 0.9 | 13.6 | 26.8 |
| AREA 2 | North Central NY | 5,421 | 104 | 0.027 | 4.62E-06 | 0.87 | 0.6 | 9.3 | 18.3 |
| AREA 3 | South Central NY; North Central PA | 8,953 | 127 | 0.026 | 4.37E-06 | 0.80 | 0.5 | 8.5 | 15.7 |
| AREA 4 | Southeast Central NY (Broome & Tioga Cos.) | 9,297 | 116 | 0.020 | 3.11E-06 | 0.54 | 0.4 | 7.5 | 13.7 |
| AREA 5 | Northeast NY (Cortland, Madison, Otsego Cos.) | 4,734 | 199 | 0.031 | 5.80E-06 | 0.68 | 1.1 | 16.6 | 33.7 |
| AREA 6 | Northeast PA; East Central PA | 12,077 | 137 | 0.027 | 4.62E-06 | 0.73 | 0.8 | 14.9 | 26.8 |
| AREA 7 | West PA; WV Panhandle; East Central OH | 10,907 | 155 | 0.025 | 8.15E-05 | 0.73 | 0.70 | 9.4 | 24.1 |
| AREA 8 | Northwest PA; Eastern OH | 6,544 | 107 | 0.031 | 9.17E-05 | 0.73 | 1.3 | 15.0 | 42.1 |
| AREA 9 | Northwest WV; Southeast OH | 8,807 | 105 | 0.023 | 7.84E-05 | 0.96 | 0.5 | 5.8 | 15.5 |
| AREA 10 | Central WV | 11,991 | 84 | 0.020 | 7.39E-05 | 0.73 | 1.0 | 13.0 | 33.6 |
| AREA 11 | Southwest- South Central WV | 7,661 | 43 | 0.033 | 9.53E-05 | 0.60 | 0.8 | 10.1 | 27.7 |

** Archie water saturation algorithm used to compute water saturation for the Upper Utica Shale model layer.*

Table 9. Model Layer Attributes for the Basal Utica Shale – Simandoux Water Saturation

| Model Layer Attributes for Organic-Rich Basal Utica Shale | | | | | | | | | |
|---|---|---|---|---|---|---|---|---|---|
| Model Area | Area Description | Average Depth, ft. | Thickness, ft. | Total Porosity, fraction | Matrix Permeability, md | Water Saturation, fraction* | Calculated TOC, wt. % | Mean Adsorbed Gas Content, scf/ ton | Theoretical Max. Adsorbed $CO_2$, scf/ ton |
| AREA 1 | Western NY & Northwest PA | 5,882 | 45 | 0.038 | 8.63E-06 | 0.25 | 1.0 | 15.7 | 31.0 |
| AREA 2 | North Central NY | 5,525 | 10 | 0.033 | 6.50E-06 | 0.28 | 1.1 | 17.3 | 33.9 |
| AREA 3 | South Central NY; North Central PA | 9,080 | 36 | 0.032 | 6.14E-06 | 0.29 | 1.2 | 22.1 | 41.1 |
| AREA 4 | Southeast Central NY (Broome & Tioga Cos.) | 9,413 | 60 | 0.052 | 1.91E-05 | 0.22 | 2.4 | 45.6 | 83.2 |
| AREA 5 | Northeast NY (Cortland, Madison, Otsego Cos.) | 4,933 | 121 | 0.047 | 1.44E-05 | 0.32 | 2.1 | 30.8 | 62.5 |
| AREA 6 | Northeast PA; East Central PA | 12,214 | 35 | 0.041 | 1.02E-05 | 0.25 | 1.8 | 34.7 | 62.3 |
| AREA 7 | West PA; WV Panhandle; East Central OH | 11,062 | 34 | 0.038 | 1.05E-04 | 0.25 | 1.7 | 23.2 | 59.9 |
| AREA 8 | Northwest PA; Eastern OH | 6,651 | 41 | 0.043 | 1.16E-04 | 0.27 | 2.3 | 26.8 | 74.9 |
| AREA 9 | Northwest WV; Southeast OH | 8,912 | 28 | 0.032 | 9.35E-05 | 0.35 | 1.1 | 13.2 | 35.3 |
| AREA 10 | Central WV | 12,075 | 12 | 0.024 | 7.99E-05 | 0.38 | 0.7 | 9.7 | 25.1 |
| AREA 11 | Southwest-South Central WV | Absent | | | | | | | |
| **Simandoux water saturation algorithm used for the basal Utica Shale model layer; corrects the Archie equation for shale.* | | | | | | | | | |

Table 10. Model Layer Attributes for the Upper Point Pleasant – Simandoux Water Saturation

| Model Layer Attributes for Shale - Rich Point Pleasant (Upper Point Pleasant) and Equivalent Formations | | | | | | | | | |
|---|---|---|---|---|---|---|---|---|---|
| Model Area | Area Description | Average Depth, ft. | Thickness, ft. | Total Porosity, fraction | Matrix Permeability, md | Water Saturation, fraction* | Calculated TOC, wt. % | Mean Adsorbed Gas Content, scf/ ton | Theoretical Max. Adsorbed $CO_2$, scf/ ton |
| AREA 1 | Western NY & Northwest PA | Absent | | | | | | | |
| AREA 2 | North Central NY | Absent | | | | | | | |
| AREA 3 | South Central NY; North Central PA | 9,116 | 109 | 0.041 | 1.02E-05 | 0.34 | 1.7 | 31.4 | 58.4 |
| AREA 4 | Southeast Central NY (Broome & Tioga Cos.) | 9,473 | 109 | 0.040 | 9.66E-06 | 0.23 | 1.8 | 33.1 | 60.4 |
| AREA 5 | Northeast NY (Cortland, Madison, Otsego Cos.) | 5,054 | 104 | 0.042 | 1.08E-05 | 0.29 | 1.5 | 22.9 | 46.5 |
| AREA 6 | Northeast PA; East Central PA | 12,249 | 130 | 0.040 | 9.66E-06 | 0.26 | 1.6 | 30.8 | 55.3 |
| AREA 7 | West PA; WV Panhandle; East Central OH | 11,096 | 113 | 0.045 | 1.20E-04 | 0.26 | 1.8 | 24.6 | 63.4 |
| AREA 8 | Northwest PA; Eastern OH | 6,692 | 59 | 0.048 | 1.28E-04 | 0.20 | 2.1 | 24.6 | 68.9 |
| AREA 9 | Northwest WV; Southeast OH | 8,940 | 61 | 0.055 | 1.47E-04 | 0.28 | 2.9 | 36.6 | 98.2 |
| AREA 10 | Central WV | 12,087 | 45 | 0.043 | 1.16E-04 | 0.24 | 1.4 | 18.5 | 47.8 |
| AREA 11 | Southwest- South Central WV | 7,704 | 87 | 0.049 | 1.30E-04 | 0.52 | 1.6 | 19.6 | 53.5 |
| **Simandoux water saturation algorithm for the Upper (shaley) Point Pleasant model layer; corrects the Archie equation for shale.* | | | | | | | | | |

Table 11. Model Layer Attributes for the Lower Point Pleasant – Archie Water Saturation

| Model Layer Attributes for Carbonate - Rich Point Pleasant (Lower Point Pleasant) and Equivalent Formations | | | | | | | | | |
|---|---|---|---|---|---|---|---|---|---|
| Model Area | Area Description | Average Depth, ft. | Thickness, ft. | Total Porosity, fraction | Matrix Permeability, md | Water Saturation, fraction* | Calculated TOC, wt. % | Mean Adsorbed Gas Content, scf/ ton | Theoretical Max. Adsorbed $CO_2$, scf/ ton |
| AREA 1 | Western NY & Northwest PA | Absent | | | | | | | |
| AREA 2 | North Central NY | Absent | | | | | | | |
| AREA 3 | South Central NY; North Central PA | 9,225 | 51 | 0.037 | 8.15E-06 | 0.52 | 1.4 | 24.4 | 45.3 |
| AREA 4 | Southeast Central NY (Broome & Tioga Cos.) | 9,582 | 107 | 0.037 | 8.15E-06 | 0.37 | 1.7 | 31.8 | 58.0 |
| AREA 5 | Northeast NY (Cortland, Madison, Otsego Cos.) | 5,158 | 89 | 0.034 | 6.88E-06 | 0.54 | 1.0 | 15.2 | 30.8 |
| AREA 6 | Northeast PA; East Central PA | 12,379 | 99 | 0.045 | 1.28E-05 | 0.43 | 1.9 | 36.3 | 65.1 |
| AREA 7 | West PA; WV Panhandle; East Central OH | 11,209 | 87 | 0.046 | 1.23E-04 | 0.43 | 1.5 | 19.6 | 50.6 |
| AREA 8 | Northwest PA; Eastern OH | 6,751 | 79 | 0.046 | 1.23E-04 | 0.43 | 1.5 | 17.0 | 47.7 |
| AREA 9 | Northwest WV; Southeast OH | 9,001 | 53 | 0.044 | 1.18E-04 | 0.42 | 1.6 | 20.5 | 55.0 |
| AREA 10 | Central WV | 12,132 | 34 | 0.035 | 9.91E-05 | 0.33 | 0.4 | 5.2 | 13.4 |
| AREA 11 | Southwest- South Central WV | Absent | | | | | | | |
| ** Archie water saturation algorithm used for the Lower Point Pleasant model layer.* | | | | | | | | | |

Table 12. Utica Shale; Summary of Estimated Gas In-Place by Model Area

| Model Area | Area Description | Total Area, miles$^2$ | Model Layer | Adsorbed Gas In-Place, Bcf/ mile$^2$ | Free Gas In-Place, Bcf/ mile$^2$ | Total Adsorbed Gas in-Place, Bcf | Total Free Gas In-Place, Bcf | Model Area Total Gas In-Place, Bcf |
|---|---|---|---|---|---|---|---|---|
| AREA 1 | Western NY & Northwest PA | 6,329 | *Upper Utica Shale* | *5.4* | *10.4* | *34,255* | *65,663* | *99,919* |
| | | | Basal Utica Shale (High TOC) | 1.6 | 7.9 | 10,295 | 49,729 | 60,025 |
| AREA 2 | North Central NY | 3,114 | *Upper Utica Shale* | *2.3* | *2.1* | *7,115* | *6,651* | *13,766* |
| | | | Basal Utica Shale (High TOC) | 0.4 | 1.3 | 1,195 | 4,152 | 5,347 |
| AREA 3 | South Central NY; North Central PA | 2,803 | *Upper Utica Shale* | *2.5* | *4.9* | *7,082* | *13,807* | *20,889* |
| | | | Basal Utica Shale (High TOC) | 1.8 | 6.2 | 5,170 | 17,246 | 22,416 |
| AREA 4 | Southeast Central NY | 2,456 | *Upper Utica Shale* | *2.1* | *9.0* | *5,046* | *22,138* | *27,184* |
| | | | Basal Utica Shale (High TOC) | 6.1 | 20.4 | 15,104 | 50,085 | 65,189 |
| AREA 5 | Northeast NY | 3,831 | *Upper Utica Shale* | *7.7* | *10.6* | *29,315* | *40,423* | *69,738* |
| | | | Basal Utica Shale (High TOC) | 8.5 | 21.4 | 32,544 | 82,144 | 114,688 |
| AREA 6 | Northeast PA; East Central PA | 10,590 | *Upper Utica Shale* | *4.6* | *8.6* | *49,201* | *91,466* | *140,666* |
| | | | Basal Utica Shale (High TOC) | 2.7 | 9.2 | 29,023 | 97,783 | 126,806 |
| AREA 7 | West PA; WV Pan handle; East Central OH | 11,204 | *Upper Utica Shale* | *3.4* | *9.3* | *37,661* | *104,661* | *142,322* |
| | | | Basal Utica Shale (High TOC) | 1.8 | 8.6 | 20,568 | 96,725 | 117,293 |
| AREA 8 | Northwest PA; Eastern OH | 6,459 | *Upper Utica Shale* | *3.7* | *5.9* | *24,016* | *37,844* | *61,860* |
| | | | Basal Utica Shale (High TOC) | 2.5 | 8.4 | 16,148 | 54,391 | 70,539 |
| AREA 9 | Northwest WV; Southeast OH | 3,044 | *Upper Utica Shale* | *1.4* | *0.8* | *4,360* | *2,412* | *6,772* |
| | | | Basal Utica Shale (High TOC) | 0.8 | 4.4 | 2,580 | 13,367 | 15,946 |
| AREA 10 | Central WV | 5,346 | *Upper Utica Shale* | *2.6* | *4.1* | *13,971* | *22,076* | *36,046* |
| | | | Basal Utica Shale (High TOC) | 0.3 | 1.6 | 1,450 | 8,649 | 10,099 |
| AREA 11 | Southwest-South Central WV | 2,737 | *Upper Utica Shale* | *1.0* | *4.0* | *2,787* | *10,917* | *13,704* |
| | | | Basal Utica Shale (High TOC) | Absent | | | | |
| Utica Shale Study Area Totals | | 57,913 | *Upper Utica Shale* | *3.7* | *7.2* | *214,808* | *418,057* | *632,865* |
| | | | Basal Utica Shale (High TOC) | 2.4 | 8.6 | 134,078 | 474,271 | 608,349 |

Table 13. Point Pleasant; Summary of Estimated Gas In-Place by Model Area

| Model Area | Area Description | Total Area, miles$^2$ | Model Layer | Adsorbed Gas In-Place, Bcf/ mile$^2$ | Free Gas In-Place, Bcf/ mile$^2$ | Total Adsorbed Gas in-Place, Bcf | Total Free Gas In-Place, Bcf | Model Area Total Gas In-Place, Bcf |
|---|---|---|---|---|---|---|---|---|
| AREA 1 | Western NY & Northwest PA | 6,329 | Pt. Pleasant - Shaley (Upper) | Absent | | | | |
| | | | *Pt. Pleasant Carbonate (Lower)* | *Absent* | | | | |
| AREA 2 | North Central NY | 3,114 | Pt. Pleasant - Shaley (Upper) | Absent | | | | |
| | | | *Pt. Pleasant Carbonate (Lower)* | *Absent* | | | | |
| AREA 3 | South Central NY; North Central PA | 2,803 | Pt. Pleasant - Shaley (Upper) | 7.9 | 22.3 | 22,007 | 62,417 | 84,425 |
| | | | *Pt. Pleasant Carbonate (Lower)* | *2.9* | *6.8* | *8,035* | *19,113* | *27,148* |
| AREA 4 | Southeast Central NY | 2,456 | Pt. Pleasant - Shaley (Upper) | 8.2 | 28.1 | 20,202 | 69,065 | 89,267 |
| | | | *Pt. Pleasant Carbonate (Lower)* | *7.8* | *21.7* | *19,176* | *53,238* | *72,414* |
| AREA 5 | Northeast NY | 3,831 | Pt. Pleasant - Shaley (Upper) | 5.5 | 17.2 | 21,036 | 65,793 | 86,829 |
| | | | *Pt. Pleasant Carbonate (Lower)* | *3.1* | *7.7* | *11,991* | *29,522* | *41,512* |
| AREA 6 | Northeast PA; East Central PA | 10,590 | Pt. Pleasant - Shaley (Upper) | 9.2 | 33.8 | 97,326 | 358,366 | 455,692 |
| | | | *Pt. Pleasant Carbonate (Lower)* | *8.2* | *22.3* | *86,787* | *236,348* | *323,135* |
| AREA 7 | West PA; WV Pan handle; East Central OH | 11,204 | Pt. Pleasant - Shaley (Upper) | 6.3 | 33.4 | 70,993 | 374,503 | 445,496 |
| | | | *Pt. Pleasant Carbonate (Lower)* | *3.9* | *17.6* | *43,794* | *197,244* | *241,038* |
| AREA 8 | Northwest PA; Eastern OH | 6,459 | Pt. Pleasant - Shaley (Upper) | 3.3 | 15.1 | 21,463 | 97,341 | 118,805 |
| | | | *Pt. Pleasant Carbonate (Lower)* | *3.0* | *13.6* | *19,671* | *87,798* | *107,469* |
| AREA 9 | Northwest WV; Southeast OH | 3,044 | Pt. Pleasant - Shaley (Upper) | 5.0 | 18.0 | 15,132 | 54,781 | 69,913 |
| | | | *Pt. Pleasant Carbonate (Lower)* | *2.5* | *10.3* | *7,614* | *31,445* | *39,059* |
| AREA 10 | Central WV | 5,346 | Pt. Pleasant - Shaley (Upper) | 1.9 | 13.5 | 10,390 | 72,409 | 82,798 |
| | | | *Pt. Pleasant Carbonate (Lower)* | *0.4* | *7.4* | *2,220* | *39,384* | *41,603* |
| AREA 11 | Southwest-South Central WV | 2,737 | Pt. Pleasant - Shaley (Upper) | 4.0 | 14.3 | 10,815 | 39,091 | 49,906 |
| | | | *Pt. Pleasant Carbonate (Lower)* | Absent | | | | |
| Point Pleasant Study Area Totals | | 57,913 | Pt. Pleasant - Shaley (Upper) | 6.0 | 24.6 | 289,363 | 1,193,766 | 1,483,129 |
| | | | *Pt. Pleasant Carbonate (Lower)* | *4.3* | *15.2* | *199,288* | *694,091* | *893,379* |

Table 14. Utica Shale; Estimated Theoretical Maximum $CO_2$ Storage by Model Area

| Model Area | Area Description | Total Area, miles$^2$ | Model Layer | Adsorbed $CO_2$ Storage, Bcf/ mile$^2$ | Free $CO_2$ Storage Bcf/ mile$^2$ | Total Adsorbed $CO_2$ Storage, Bcf | Total Free $CO_2$ Storage, Bcf | Model Area Total Maximum $CO_2$ Storage, Bcf |
|---|---|---|---|---|---|---|---|---|
| AREA 1 | Western NY & Northwest PA | 6,329 | *Upper Utica Shale* | *10.7* | *20.1* | *67,617* | *126,915* | *194,532* |
| | | | Basal Utica Shale (High TOC) | 3.2 | 15.2 | 20,322 | 96,118 | 116,440 |
| AREA 2 | North Central NY | 3,114 | *Upper Utica Shale* | *4.5* | *4.3* | *13,918* | *13,526* | *27,443* |
| | | | Basal Utica Shale (High TOC) | 0.8 | 2.7 | 2,338 | 8,445 | 10,738 |
| AREA 3 | South Central NY; North Central PA | 2,803 | *Upper Utica Shale* | *4.7* | *8.0* | *13,158* | *22,552* | *35,710* |
| | | | Basal Utica Shale (High TOC) | 3.4 | 10.1 | 9,606 | 28,170 | 37,775 |
| AREA 4 | Southeast Central NY | 2,456 | *Upper Utica Shale* | *3.8* | *13.7* | *9,213* | *33,586* | *42,799* |
| | | | Basal Utica Shale (High TOC) | 11.2 | 30.9 | 27,579 | 75,985 | 103,564 |
| AREA 5 | Northeast NY | 3,831 | *Upper Utica Shale* | *15.5* | *22.3* | *59,437* | *85,325* | *144,762* |
| | | | Basal Utica Shale (High TOC) | 17.2 | 45.3 | 65,985 | 173,391 | 239,376 |
| AREA 6 | Northeast PA; East Central PA | 10,590 | *Upper Utica Shale* | *8.3* | *13.5* | *88,298* | *142,912* | *231,210* |
| | | | Basal Utica Shale (High TOC) | 4.9 | 14.4 | 52,087 | 152,783 | 204,869 |
| AREA 7 | West PA; WV Pan handle; East Central OH | 11,204 | *Upper Utica Shale* | *8.7* | *14.0* | *97,133* | *157,142* | *254,275* |
| | | | Basal Utica Shale (High TOC) | 4.7 | 13.0 | 53,047 | 145,227 | 198,274 |
| AREA 8 | Northwest PA; Eastern OH | 6,459 | *Upper Utica Shale* | *10.4* | *10.5* | *67,201* | *67,526* | *134,727* |
| | | | Basal Utica Shale (High TOC) | 7.0 | 15.0 | 45,186 | 97,050 | 142,236 |
| AREA 9 | Northwest WV; Southeast OH | 3,044 | *Upper Utica Shale* | *3.8* | *1.3* | *11,697* | *3,899* | *15,596* |
| | | | Basal Utica Shale (High TOC) | 2.3 | 7.1 | 6,921 | 21,611 | 28,532 |
| AREA 10 | Central WV | 5,346 | *Upper Utica Shale* | *6.8* | *6.2* | *36,158* | *33,359* | *69,517* |
| | | | Basal Utica Shale (High TOC) | 0.7 | 2.4 | 3,753 | 13,070 | 16,823 |
| AREA 11 | Southwest-South Central WV | 2,737 | *Upper Utica Shale* | *2.8* | *6.5* | *7,632* | *17,757* | *25,389* |
| | | | Basal Utica Shale (High TOC) | Absent | | | | |
| Utica Shale Study Area Totals | | 57,913 | *Upper Utica Shale* | *8.1* | *12.2* | *471,462* | *704,500* | *1,175,963* |
| | | | Basal Utica Shale (High TOC) | 5.2 | 14.7 | 286,823 | 811,850 | 1,098,672 |

Table 15. Point Pleasant; Estimated Theoretical Maximum $CO_2$ Storage by Model Area

| Model Area | Area Description | Total Area, miles$^2$ | Model Layer | Adsorbed $CO_2$ Storage, Bcf/ mile$^2$ | Free $CO_2$ Storage Bcf/ mile$^2$ | Total Adsorbed $CO_2$ Storage, Bcf | Total Free $CO_2$ Storage, Bcf | Model Area Total Maximum $CO_2$ Storage, Bcf |
|---|---|---|---|---|---|---|---|---|
| AREA 1 | Western NY & Northwest PA | 6,329 | Pt. Pleasant - Shaley (Upper) | Absent | | | | |
| | | | *Pt. Pleasant Carbonate (Lower)* | *Absent* | | | | |
| AREA 2 | North Central NY | 3,114 | Pt. Pleasant - Shaley (Upper) | Absent | | | | |
| | | | *Pt. Pleasant Carbonate (Lower)* | *Absent* | | | | |
| AREA 3 | South Central NY; North Central PA | 2,803 | Pt. Pleasant - Shaley (Upper) | 14.6 | 36.4 | 40.887 | 101,955 | 142,842 |
| | | | *Pt. Pleasant Carbonate (Lower)* | *5.3* | *13.0* | *14,928* | *36,424* | *51,352* |
| AREA 4 | Southeast Central NY | 2,456 | Pt. Pleasant - Shaley (Upper) | 15.0 | 42.7 | 36,887 | 104,780 | 141,667 |
| | | | *Pt. Pleasant Carbonate (Lower)* | *14.3* | *37.0* | *35,015* | *90,945* | *125,959* |
| AREA 5 | Northeast NY | 3,831 | Pt. Pleasant - Shaley (Upper) | 11.1 | 36.3 | 42,650 | 138,879 | 181,529 |
| | | | *Pt. Pleasant Carbonate (Lower)* | *6.3* | *16.3* | *24,312* | *62,315* | *86,627* |
| AREA 6 | Northeast PA; East Central PA | 10,590 | Pt. Pleasant - Shaley (Upper) | 16.5 | 52.9 | 174,665 | 559,935 | 734,601 |
| | | | *Pt. Pleasant Carbonate (Lower)* | *14.7* | *43.4* | *155,752* | *459,988* | *615,740* |
| AREA 7 | West PA; WV Pan handle; East Central OH | 11,204 | Pt. Pleasant - Shaley (Upper) | 16.3 | 50.2 | 183,102 | 562,294 | 745,396 |
| | | | *Pt. Pleasant Carbonate (Lower)* | *10.1* | *31.5* | *112,953* | *353,301* | *466,254* |
| AREA 8 | Northwest PA; Eastern OH | 6,459 | Pt. Pleasant - Shaley (Upper) | 9.3 | 26.9 | 60,058 | 173,687 | 233,745 |
| | | | *Pt. Pleasant Carbonate (Lower)* | *8.5* | *28.9* | *55,043* | *186,890* | *241,933* |
| AREA 9 | Northwest WV; Southeast OH | 3,044 | Pt. Pleasant - Shaley (Upper) | 13.3 | 29.1 | 40,597 | 88,567 | 129,164 |
| | | | *Pt. Pleasant Carbonate (Lower)* | *6.7* | *19.8* | *20,427* | *60,135* | *80,562* |
| AREA 10 | Central WV | 5,346 | Pt. Pleasant - Shaley (Upper) | 5.0 | 20.5 | 26,890 | 109,417 | 136,307 |
| | | | *Pt. Pleasant Carbonate (Lower)* | *1.1* | *12.3* | *5,745* | *65,731* | *71,475* |
| AREA 11 | Southwest-South Central WV | 2,737 | Pt. Pleasant - Shaley (Upper) | 10.8 | 23.2 | 29,621 | 63,580 | 93,201 |
| | | | *Pt. Pleasant Carbonate (Lower)* | Absent | | | | |
| Point Pleasant Study Area Totals | | 57,913 | Pt. Pleasant - Shaley (Upper) | 13.1 | 39.3 | 635,356 | 1,903,095 | 2,538,452 |
| | | | *Pt. Pleasant Carbonate (Lower)* | *9.3* | *28.8* | *424,174* | *1,315,729* | *1,739,903* |

Table 16. Utica/ Point Pleasant; Summary of Total Gas In-Place, Resource Concentration and Total Theoretical Maximum $CO_2$ Storage Capacity by Model Area

| MODEL AREA | Area Description | Potential $CO_2$ Storage Area, miles$^2$ | Potential $CO_2$ Storage Area, acres | Total Gas In-Place, Tcf | Theoretical Maximum $CO_2$ Storage, billion tonnes, Gt | Total Gas In-Place, Bcf/mile$^2$ | Maximum $CO_2$ Storage, Mt/ mile$^2$ | Total Gas In-Place, Bcf/ 80-acres | Maximum $CO_2$ Storage, Mt/ 80-acres |
|---|---|---|---|---|---|---|---|---|---|
| AREA 1 | Western NY & Northwest PA | 6,329 | 4,050,794 | 159.9 | 16.15 | 25.3 | 2.5 | 3.2 | 0.32 |
| AREA 2 | North Central NY | 3,114 | 1,992,915 | 19.1 | 1.99 | 6.1 | 0.6 | 0.8 | 0.08 |
| AREA 3 | South Central NY; North Central PA | 2,803 | 1,793,827 | 154.9 | 13.91 | 55.3 | 5.0 | 6.9 | 0.62 |
| AREA 4 | Southeast Central NY (Broome & Tioga Cos.) | 2,456 | 1,572,025 | 254.1 | 21.51 | 103.4 | 8.8 | 12.9 | 1.09 |
| AREA 5 | Northeast NY (Cortland, Madison, Otsego Cos.) | 3,831 | 2,451,694 | 312.8 | 33.89 | 81.6 | 8.9 | 10.2 | 1.11 |
| AREA 6 | Northeast PA; East Central PA | 10,590 | 6,777,578 | 1,046.3 | 92.8 | 98.8 | 8.8 | 12.4 | 1.10 |
| AREA 7 | West PA; WV Panhandle; East Central OH | 11,204 | 7,170,236 | 946.1 | 86.45 | 84.5 | 7.7 | 10.6 | 0.96 |
| AREA 8 | Northwest PA; Eastern OH | 6,459 | 4,133,518 | 358.7 | 39.1 | 55.5 | 6.1 | 6.9 | 0.76 |
| AREA 9 | Northwest WV; Southeast OH | 3,044 | 1,948,414 | 131.7 | 13.19 | 43.3 | 4.3 | 5.4 | 0.54 |
| AREA 10 | Central WV | 5,346 | 3,421,544 | 170.5 | 15.28 | 31.9 | 2.9 | 4.0 | 0.36 |
| AREA 11 | Southwest-South Central WV | 2,737 | 1,751,393 | 63.6 | 6.16 | 23.2 | 2.3 | 2/9 | 0.28 |
| Utica/ Point Pleasant Study Area Totals & Average | | 57,913 | 37,063,938 | 3,617.7 | 340.4 | 62.5 | 5.9 | 7.8 | 0.74 |

# APPENDICES

Appendix 1. Model Layer Attributes for the Upper Utica Shale; Water Saturation Calculated Using Simandoux

| Model Layer Attributes for Upper Utica Shale | | | | | | | | | |
|---|---|---|---|---|---|---|---|---|---|
| Model Area | Area Description | Average Depth, ft. | Thickness, ft. | Total Porosity, fraction | Matrix Permeability, md | Water Saturation, fraction* | Calculated TOC, wt. % | Mean Adsorbed Gas Content, scf/ ton | Theoretical Max. Adsorbed $CO_2$, scf/ ton |
| AREA 1 | Western NY & Northwest PA | 5,710 | 172 | 0.029 | 5.18E-06 | 0.43 | 0.9 | 13.6 | 26.8 |
| AREA 2 | North Central NY | 5,421 | 104 | 0.027 | 4.62E-06 | 0.42 | 0.6 | 9.3 | 18.3 |
| AREA 3 | South Central NY; North Central PA | 8,953 | 127 | 0.026 | 4.37E-06 | 0.42 | 0.5 | 8.5 | 15.7 |
| AREA 4 | Southeast Central NY (Broome & Tioga Cos.) | 9,297 | 116 | 0.020 | 3.11E-06 | 0.23 | 0.4 | 7.5 | 13.7 |
| AREA 5 | Northeast NY (Cortland, Madison, Otsego Cos.) | 4,734 | 199 | 0.031 | 5.80E-06 | 0.33 | 1.1 | 16.6 | 33.7 |
| AREA 6 | Northeast PA; East Central PA | 12,077 | 137 | 0.027 | 4.62E-06 | 0.38 | 0.8 | 14.9 | 26.8 |
| AREA 7 | West PA; WV Panhandle; East Central OH | 10,907 | 155 | 0.025 | 8.15E-05 | 0.38 | 0.70 | 9.4 | 24.1 |
| AREA 8 | Northwest PA; Eastern OH | 6,544 | 107 | 0.031 | 9.17E-05 | 0.40 | 1.3 | 15.0 | 42.1 |
| AREA 9 | Northwest WV; Southeast OH | 8,807 | 105 | 0.023 | 7.84E-05 | 0.69 | 0.5 | 5.8 | 15.5 |
| AREA 10 | Central WV | 11,991 | 84 | 0.020 | 7.39E-05 | 0.42 | 1.0 | 13.0 | 33.6 |
| AREA 11 | Southwest- South Central WV | 7,661 | 43 | 0.033 | 9.53E-05 | 0.31 | 0.8 | 10.1 | 27.7 |

* *Simandoux algorithm used to compute water saturation for the Upper Utica Shale model layer. Average calculated water saturation appears to be too low, resulting in high gas in-place.*

# Volume 4
# Basin-Level Characterization Of Enhanced Gas Recovery And $CO_2$ Storage Potential In The Antrim Shale

## Assessment of Factors Influencing Effective $CO_2$ Storage Capacity and Injectivity in Eastern Gas Shales

Prepared for:
U.S. Department of Energy
National Energy Technology Laboratory
DOE Award Number: DE-FE0004633

Prepared by:
Michael Godec, Principal Investigator
Advanced Resources International, Inc.
4501 Fairfax Drive ▪ Suite 910 ▪ Arlington, Virginia 22203

Date:
October 23, 2013


4501 Fairfax Drive ▪ Suite 910 ▪ Arlington, Virginia 22203 ▪ Phone: (703) 528-8420 ▪ web: www.adv-res.com

## Advanced Resources International, Inc.

# Table of Contents

**1. INTRODUCTION** ..... 1
a. Background ..... 1
b. Project Objectives ..... 1
c. Objective of this Volume ..... 2
**2. SHALE GAS PRODUCTION POTENTIAL IN THE BASIN** ..... 3
a. Development and Production History ..... 4
b. Reserves and Resource Potential ..... 4
c. Sources of $CO_2$ Emissions and Potential Alternative Storage Horizons ..... 5
d. Potential Benefits for Storing $CO_2$ in the Basin's Gas Shales ..... 5
**3. GEOLOGIC CHARACTERIZATION** ..... 6
a. Geologic Setting ..... 6
b. Stratigraphy ..... 7
c. Study Area ..... 8
d. Study Wells and Cross-Sections ..... 8
**4. RESERVOIR DATA USED** ..... 10
a. Adsorption Isotherms ..... 10
b. Total Organic Carbon ..... 10
c. X-Ray Diffraction Mineralogy ..... 10
d. Core Porosity and Permeability ..... 11
**5. ESTIMATED GAS IN-PLACE AND THEORETICAL MAXIMUM $CO_2$ STORAGE CAPACITY** ..... 12
a. Overview of Calculated Volumetric Gas In-Place and $CO_2$ Storage Capacity ..... 12
b. Well Log Analysis Methodology ..... 13
i. TOC Extrapolated from Density Logs ..... 13
ii. Porosity from Density Logs ..... 14
iii. Adsorbed Gas In-Place and Theoretical Maximum Adsorbed $CO_2$ Storage Capacity ..... 14
iv. Free Gas In-Place and Theoretical Maximum $CO_2$ Storage Capacity ..... 14
c. Antrim Log Calculation Results ..... 15
d. Total Gas In-Place and Maximum $CO_2$ Storage Capacity ..... 15
e. Comparing Estimates of Total Gas in-Place ..... 17
**6. DEFINITION OF MODEL AREAS FOR RESERVOIR MODELING IN THE BASIN** ..... 18
a. Overview and Rationale for Antrim Model Areas ..... 18
**7. REFERENCES** ..... 19
FIGURES ..... 23
TABLES ..... 33

# List of Figures

Figure 1: Antrim Shale Production in the Michigan Basin ....23
Figure 2: Stratigraphic Chart for Upper Devonian in Michigan Basin ....24
Figure 3: Antrim Shale – Total Annual Gas Production, 1968 - 2012 ....25
Figure 4: Antrim Shale Cross-Sections and Model Areas ....26
Figure 5: Antrim Shale Cross-Section A-A' ....27
Figure 6: Antrim Shale Cross-Section B-B' ....29
Figure 7: Antrim Shale Cross-Section C-C' ....29
Figure 8: Antrim Shale Cross-Section D-D' ....30
Figure 9: Summary of Antrim Shale Estimated Gas in-Place ....31
Figure 10: Summary of Antrim Shale Estimated Maximum $CO_2$ Storage Capacity ....32

# List of Tables

Table 1. Summary of Methane Adsorption Isotherm Data for the Antrim ....33
Table 2. Routine Core Analysis Data for the Antrim Shale, Otsego County, MI ....33
Table 3. Correlation of Total Gas Content (scf/ton) and Total Organic Carbon (TOC) for the Antrim Shale ....34
Table 4. Description and Summary of Antrim Model Areas ....34
Table 5. Model Layer Attributes for the Lachine and Norwood Members of the Antrim Shale ....35
Table 6. Antrim Shale; Summary of Estimated Gas In-Place ....36
Table 7. Antrim Shale; Summary of Estimated Theoretical Maximum $CO_2$ Storage Capacity ....37
Table 8. Antrim Shale; Estimated Total Gas in-Place and Theoretical Maximum CO2 Storage Capacity by Model Area ....38

# 1. INTRODUCTION

## a. Background

The potential storage of $CO_2$ in organic-rich gas shales is attracting increasing technical interest, especially in the Appalachian and Michigan Basin, which have extensive shale deposits, but limited $CO_2$ storage capacity in conventional porous reservoirs. Two $CO_2$ storage-mechanisms are expected for organic-rich gas shales, as an adsorbed phase on organic material in the reservoir, and as "free" or, non-adsorbed phase, in intergranular and fracture porosity. Coal beds preferentially adsorb $CO_2$ over methane, at a ratio of two or more $CO_2$ molecules for every methane molecule displaced. Organic-rich gas shale reservoirs are expected to react similarly and desorb methane while preferentially adsorbing $CO_2$. In addition, some component of the pore volume that contains methane as "free" gas is expected to be available for $CO_2$ storage as a non-adsorbed phase, especially where previous hydraulic fracturing has enhanced injectivity. Although still in the conceptual stage, $CO_2$ injection into organic-rich gas shales could provide dual benefits: an economic benefit from enhanced gas recovery and an environmental benefit of secure $CO_2$ storage.

## b. Project Objectives

The goal of this cooperative research project is to build upon previous and on-going work to assess key factors that would influence effective $CO_2$ storage capacity and injectivity in selected gas shales within the Appalachian and Michigan Basins The most promising gas shale formations for $CO_2$ storage in the Appalachian Basin include the Devonian Marcellus Shale in New York, Pennsylvania, West Virginia and eastern Ohio; the Devonian Ohio Shale in Kentucky; and the Ordovician Utica and Point Pleasant shale and equivalent formations in New York, Pennsylvania, West Virginia and Ohio.

In the Michigan Basin, the Devonian age Antrim Shale has similar features to the Marcellus, which make it attractive for potential $CO_2$ storage. These include two organic-rich shale members, the Lachine and Norwood, with net thickness, TOC and porosity comparable to the Marcellus; a pervasive network of natural fractures; demonstrated effectiveness of both vertical and horizontal drilling and hydraulic fracturing; and substantial production infrastructure in place. The Michigan Antrim Shale also has unique features expected to affect $CO_2$ storage. These include commercial production at very shallow depths (less than 2,000 feet); surface water recharge saturating the natural fracture system; a thermally immature reservoir that produces biogenic methane, and $CO_2$ at shallow depths, and thermogenic methane in the deep basin.

## c. Objective of this Volume

The Antrim Shale is one of the ten largest gas fields in North America. Gas production from the Antrim began in the 1940s and peaked in 1998 at about 548 million cubic feet per day (MMcfd). In 2012, total Antrim production in the Michigan Basin was approximately 164 MMcfd. By any measure, the Antrim Shale in the Michigan Basin is a mature gas play, and offers an excellent "test" case for the benefits of $CO_2$ injection and storage for enhanced gas recovery in a mature, producing unconventional gas play. Consequently, the Antrim Shale analysis presented in this volume is focused on reservoir simulation of $CO_2$ injection and storage in a gas shale play for which the key reservoir parameters are widely known. Previous published studies and analyses plus several well logs were reviewed to characterize "model wells" or "model reservoir layers" for the Antrim reservoir simulation. A general geologic description of the Antrim gas shale plays and "model layers" was developed.

# 2. SHALE GAS PRODUCTION POTENTIAL IN THE BASIN

The Antrim Shale is the most important unconventional gas reservoir in the Michigan Basin. Most current production from the Antrim is located in twelve northern counties south of the Antrim subcrop under glacial till. This is illustrated in **Figure 1**, which shows Antrim producing wells in the Michigan Basin, the depth to the top of the Antrim Shale, and location of the Antrim Shale subcrops in the northern counties. The shale produces from a depths ranging from 300 to 2,000 feet, where the Antrim is naturally fractured. Gas production targets are the fissile, organic-rich black shales in the Lachine and Norwood Members of the Antrim shown in the stratigraphic chart in **Figure 2**. These Lower Antrim members have very high total organic carbon (TOC), up to 20 percent, but low thermal maturity (0.4 % – 0.6 % Ro).

Antrim production in this area is predominately biogenic gas, which appears to be sourced by anaerobic bacteria consuming thermally immature organic material in the Lachine and Norwood Members. Fractures are necessary for production and the ground water flow system from the northern Antrim subcrop appears to control the conditions for methanogenic bacteria activity. There is a gentle regional dip southward from northern basin margin. Small anticlines trend northeast and northwest. The dominant fracture trends are northeast and northwest for near-vertical fractures. A third fracture set with lower angle dip also trends northeast. Glacial melt water from retreating glaciers infiltrated the fractures and established conditions in the organic-rich rock to support methanogenesis.

A steep salinity gradient in formation water occurs downdip from Antrim subcrop. Moving basinward from the subcrop, increasing salinity and an apparent reduction in fracture permeability creates a “depth floor” for biogenic Antrim production of about 2,000 feet. At the downdip edge of the biogenic gas play, biogenic Antrim gas mixes with thermogenic gas migrating up from the deep basin (Matson, 2011; Goodman and Maness, 2008, Waldron and others, 2007).

Thermogenic gas production from the Antrim Shale occurs at depths greater than 2,000 feet. In the central Michigan Basin, the Antrim Shale may be in the oil generation window at depths greater than 2,500 feet (East and others, 2012). The primary source for the thermogenic gas in the Antrim appears to be underlying older Devonian and Ordovician shales, the gas having migrated into the Antrim via vertical fractures. Thermogenic gas production in the Antrim occurs to maximum depths of 2,600 feet in Crawford County and 3,200 feet in Missaukee County. The thermogenic Antrim gas play in the central basin is characterized as having significantly fewer fractures than the shallow biogenic gas play, as well as low fracture permeability and low productivity compared to the biogenic gas play.

## a. Development and Production History

First gas production from the Antrim Shale began in the 1940s. Commercial scale development commenced in the late 1980s, supported by the financial incentives contained in the non-conventional fuels (Section 29) tax credit. Approximately 10,000 Antrim Shale wells have been completed, most in a twelve-county area of northern Lower Michigan. Annual Antrim Shale production peaked in 1998 (**Figure 3**) at approximately 200 billion cubic feet (Bcf). Annual Antrim production dropped precipitously from 131 Bcf in 2008 to less than 100 Bcf in 2011, and to approximately 60 Bcf in 2012. (Oil and Gas Journal, 2012) Cumulative Antrim Shale production is 3.1 trillion cubic feet (Tcf) since 1968 (Oliver and others, 1989). Drilling permits have similarly declined from 1,446 in 2006 to less than 50 in 2011, as companies have redirected exploration and development expenditures to more promising shale plays.

Production "sweet spots" appear to be linked with fracture intensity, and production trends follow the major fracture orientations. Recent geochemical analyses indicate that microbial communities in the Antrim are currently generating gas, or have done so in the recent past. A significant gradient in gas composition occurs from the outcrop to the central basin, which is the result of a continuum of mainly biogenic gas updip, mixing of biogenic and thermogenic, and finally predominately thermogenic gas basinward. Produced gas is predominately methane and $CO_2$ in the north with propane and ethane content increasing to the south (Goodman and Maness, 2008).

## b. Reserves and Resource Potential

Previous estimates of the resource in-place for the Antrim Shale in the Lower Michigan Basin are variously stated as 16 Bcf/ sq. mile (Decker, Hill and Wicks, 1993), 16 Bcf/ sq. mile to more than 32 Bcf/ sq. mile (Oil and Gas Journal, 1994) and up to 76 Tcf gas in-place (USGS, 1995). Considerable uncertainty in estimating Antrim gas in-place is derived from the difficulty of obtaining an accurate pore volume, as well as adequately assessing adsorbed gas.

Total remaining undiscovered resources for the Antrim were estimated by Curtis, 2002 to be 40.6 Tcf. Recent estimates of remaining undeveloped, technically recoverable resources range from 20 Tcf (Energy Information Administration, 2011) to 6 Tcf (Potential Gas Committee 2009). The United States Geological Survey, USGS, estimates 7.5 Tcf of undiscovered technically recoverable Antrim Shale resources. Remaining proved reserves for the Antrim Shale are estimated to be 2.3 Tcf. (Energy Information Administration, 2011)

## c. Sources of $CO_2$ Emissions and Potential Alternative Storage Horizons

A significant source of $CO_2$ emissions in the Michigan Basin is the Antrim produced gas, which contains a variable mixture of thermogenic and biogenic methane and biogenic $CO_2$. The biogenic methane is produced by the biodegradation of organic matter in the shale by distinct communities of methanogenic bacteria that are adapted to specific salinity conditions and organic substrates. $CO_2$ is produced by competing anaerobic microbial communities that favor the hydro-geochemical conditions that develop over time in the Antrim reservoir as production wells are dewatered and gas production increases. (Martini and others, 2009; Waldron and others, 2007) For this reason, $CO_2$ content in Antrim produced gas is initially low, 0.1% to 4%, but steadily increases to as much as 30% of produced gas during the productive life of a well (Goodman and Maness, 2008).

Antrim gas processing plants currently vent about 1 million tons[1] of $CO_2$ annually. More than 650,000 tons of Antrim $CO_2$ have been used for enhanced oil recovery projects in Silurian age pinnacle reef fields in northern Lower Michigan. The Midwest Region Carbon Sequestration Partnership (MRCSP) estimates that 8,500 million metric tons of $CO_2$ could be utilized for $CO_2$-EOR and ultimate storage in the northern Niagaran pinnacle reef trend (Goodman and Maness, 2008; Gupta and others, 2012). Potential horizons for $CO_2$ storage in saline aquifers include the Bois Blanc Formation, a sandstone formation, and the Bass Islands Formation, a dolomite. In 2008 and 2009, the MRCSP injected 60,000 metric tons of $CO_2$ into the Devonian-age Bois Blanc and Bass Islands saline aquifer formations, located at depths of between the deeper Niagaran pinnacle reefs and the Antrim Shale (MRCSP, 2010).

## d. Potential Benefits for Storing $CO_2$ in the Basin's Gas Shales

The Antrim Shale offers a unique potential advantage for $CO_2$ storage. The biogenic shale play in the northern Michigan Basin is a mature play. Significant volumes of gas have already been produced, so large scale $CO_2$ injection might provide an immediate enhanced gas recovery benefit. Operators would not need to wait several years for the reservoir to become sufficiently depleted before injecting $CO_2$. Substantial infrastructure is already present in the Antrim gas fields, including $CO_2$ compressors, pipelines, injection systems and thousands of existing wells that might be repurposed for injection and monitoring. In addition, the Antrim shale occurs at very shallow depths, which reduces drilling and monitoring costs. Adsorption of $CO_2$ on organic matter is expected to be the dominant $CO_2$ storage mechanism in the Antrim shale due to the very high organic carbon content of the Antrim. Adsorption-dominant $CO_2$ storage in the Antrim is expected to behave more like secure $CO_2$ storage in coal.

[1] U.S. short tons

# 3. GEOLOGIC CHARACTERIZATION

## a. Geologic Setting

The Michigan Basin is a structural sag basin that formed during the late Cambrian to Early Ordovician. Development of the Michigan Basin is thought to be linked to the protracted tectonic history of the Appalachian Mountains, although the specific processes that initiated and sustained basin formation are not fully understood (Catacosinos and others, 1990; Fisher and others, 1988; Gutschick and Sandberg, 1991; Howell and van der Pluijm, 1990). The Michigan Basin experienced episodes of subsidence throughout the Paleozoic, and was sporadically joined with the Appalachian Basin. At times, the Michigan Basin was independent of the greater Appalachian Basin, although the sediments and resulting stratigraphy of both basins remained closely associated (Nurmi, 1984; Catacosinos and Daniels, 1986).

The Antrim Shale was deposited during the late Devonian in a shallow water, oxygen-depleted marine setting. Organic-rich mud was sourced from the eroding Appalachian highlands, and is thought to have accumulated during a period of 12 million years following an episode of basin subsidence. Prevailing anoxic conditions inhibited the aerobic decay of organic matter, which allowed the preservation of organic material in the sediments. The Antrim Shale is correlative to the Devonian black shale of the eastern Appalachian Basin (the Ohio Shale, for example). Black shale formation ended in the latest Devonian in response to lowered sea levels, which swamped the Antrim with an influx of coarse grained sediment (Gutschick and Sandberg, 1991; Harell and others, 1991 Oliver and others, 1989; GRI, 1994; Asseez, 1969).

Burial of the Antrim Shale began with the deposition of the Berea Sandstone and continued with subsequent deltaic sediments. The maximum depth of burial of the Antrim occurred during the Permian and is believed to have been 3,000 to 4,000 feet deeper than the present day. This positions the Antrim Shale in the Michigan Basin within the oil generation thermal maturity window. (Gutschick and Sandberg, 1991; Wang and others, 1994; Cercone and Pollack, 1991; Cercone, 1984). Apparent thermal maturity of most of the Antrim Shale is low (0.4 % to 0.6% Ro) and varies across the basin according to present day depth. The deep Antrim in the central Michigan Basin displays the greatest thermal maturity, while the shallow, peripheral occurrences are immature (East and others, 2012). The gas produced in the shallow areas of the Antrim is predominately biogenic. The biogenic gas may be Pleistocene in age or younger, generated since the last glaciation (Dolton and Quinn, 1996). A mix of biogenic and thermogenic Antrim gas production occurs at the down dip edge of the shallow biogenic gas play, but sources of the thermogenic gas are deeper Devonian and Ordovician shale formations (Walter, 1994; Martini and others, 1994a, 1994b).

## b. Stratigraphy

**Figure 2** shows a simplified stratigraphic chart of the Upper Devonian in the Michigan Basin. The Antrim Shale formation is divided into four members. The uppermost member is the unnamed "Upper Antrim", black shale that becomes interbedded with gray shale and limestone to the west. The Upper Antrim shale member is considered equivalent to the Huron member of the Ohio Shale in the Appalachian Basin (Roen, 1993)

The Lachine member is fissile, organic-rich black shale below the Upper Antrim. The Lachine ranges in thickness from less than 50 to 150 feet, and is a target for gas production. Below the Lachine is the Paxton member, grey calcareous shale of variable thickness interbedded with thin argillaceous (clay-rich) limestone. The Norwood member is the basal unit of the Antrim, ranging in thickness from 20 to 50 feet. Like the Lachine, the Norwood is an organic-rich, fissile black shale. It contains a layer of carbonate concretions at the base and may be underlain by a thin limestone.

The Antrim Shale overlies the Traverse Group, a sequence of marine limestones and shales that ranges up to 500 feet thick. Portions of the Traverse Group are considered equivalent to the Middle Devonian Hamilton Group in the Appalachian Basin, while some upper formations of the Traverse Group are of Upper Devonian age (Ells, 1979). In outcrop, the Traverse Group is divided into multiple formations; the uppermost formation of the Traverse Group is the Squaw Bay Limestone. The contact between the Antrim Shale and the Squaw Bay Limestone is not exposed in outcrop, so the exact nature of the contact between the Antrim and underlying Traverse Group is not known. The contact between the Antrim and the Traverse Group may be transitional in part, where the Squaw Bay Limestone is present in the basin, and unconformable in part, where the Squaw Bay Limestone is absent (Ells, 1979). In the subsurface, the Traverse Group is commonly divided into three intervals: the Traverse Formation (predominately shaley with thin limestones), the Traverse Limestone (predominately limestone with thin shales), and the basal Bell Shale, which is absent in the southern Michigan Basin (Lilienthal, 1974).

To the west and east in the Michigan Basin, the Antrim Shale is overlain by and in facies relationship with the Ellsworth and Bedford Shales. In the western Michigan Basin, the Upper Antrim intertongues with the Ellsworth Shale, a gray-green silty shale containing minor beds of siltstone and sandstone. In the eastern Michigan Basin, the Antrim is overlain by and intertongues with the Bedford Shale, a bluish gray silty shale that becomes increasingly sandy in its upper part to the east (USGS, 2013). In the central part of the Michigan Basin, the Upper Antrim can be difficult to distinguish in the subsurface from the overlying Ellsworth/ Bedford shales. This is generally accomplished by relating stratigraphic changes observed in well cuttings to gamma ray log signature (Ells, 1979).

## c. Study Area

The Antrim Shale study area includes the entire Michigan Basin where the depth to Antrim shale in the northern basin is below the depth of the Antrim subcrop beneath surface glacial deposits. Most of the Antrim Shale gas production in the Michigan Basin occurs at very shallow depths, substantially less than the 2,500 feet, which is generally regarded as the minimum depth for $CO_2$ injection and storage as a dense phase fluid. Due to the very high kerogen content and low thermal maturity, the shallow Antrim is expected to behave much like coal with respect to $CO_2$ storage. Most of the $CO_2$ is expected to be strongly adsorbed on the kerogen in the Antrim, as well as dissolved into any oil that might be present in the shale.

By including the entire Michigan Basin, the Antrim Shale study area is much greater than the Antrim Shale production area that extends across portions of twelve counties in the northern basin. In addition to the Antrim biogenic gas play in the north, the study area includes the thermogenic gas play in the central basin area, and the southern perimeter of the basin where a hypothetical southern biogenic gas play is proposed. Very little Antrim gas production occurs in the thermogenic gas play of the central basin. The thermogenic gas is sourced from deeper Devonian and Ordovician shale and migrates to the Antrim via fractures and faults. Thermogenic gas production is thought to be limited by the paucity of fractures in the central basin compared to the pervasive fracturing of the Antrim in the northern basin.

For this analysis, Antrim Shale gas in-place and theoretical maximum $CO_2$ storage capacity were estimated for the Antrim in the entire basin, although reservoir simulation will focus on the northern biogenic gas play where there is meaningful well performance data. Gas in-place and theoretical maximum $CO_2$ storage are estimated and reported separately for the northern and central basin Antrim. Gas in-place and $CO_2$ storage are estimated for the southern basin using the Antrim shale production in the north as an analog. This is reported as only hypothetical $CO_2$ storage potential.

## d. Study Wells and Cross-Sections

Raster log images were acquired for sixteen wells distributed throughout the Michigan Basin to construct regional stratigraphic cross-sections through the Antrim Shale. Most of the raster logs are gamma ray-neutron and neutron-density logs. The lines of cross-section are shown on **Figure 4**. Two south-to-north cross-sections are provided as **Figure 5** and **Figure 6**. Two west-to-east cross-sections are provided as **Figures 7** and **8**.

The cross-sections show correlation of the Antrim Shale members across the basin. The stratigraphic cross-sections are flattened on the top of the Paxton because the Paxton can be picked more reliably from well logs than the top of the Antrim. The resulting cross sections show

that the Antrim shale members are continuous across the basin and thicken toward the basin center.

In the Ellsworth and Bedford shale, immediately overlying the Antrim typical gamma-ray values are less than 200 api units and bulk density is about 2.5 grams per cubic centimeter (g/cc). The Upper Antrim is picked on well logs where the gamma-ray increases sharply, and bulk density values drop to consistently less than 2.5 g/cc. The organic-rich Lachine and Norwood members of the Antrim are the targets for gas production and $CO_2$ storage. These shales are distinctive with exceptionally high gamma-ray and very low bulk density of 2.30 or lower. Depending upon the scaling of the gamma-ray log, raster images of the gamma-ray may show the curve "wrapping" at least once and frequently twice, indicating that the gamma-ray values may be greater than 500 to 600 api units. The corresponding bulk density for the most radioactive zones is frequently less than 2.25 g/cc.

The Upper Antrim is not included as a target for $CO_2$ storage in the reservoir simulation conducted for this analysis because almost all reported Antrim production is from the Lachine and Norwood. **Figure 5** through **Figure 8** show that the Upper Antrim appears organic-rich compared to the overlying Ellsworth/ Bedford shale, and may provide additional enhanced gas recovery and $CO_2$ storage potential. The cross-section figures show that the thickness of the Lachine and Norwood members varies across basin. The Lachine ranges from 45 feet thick near the basin margins to more than 150 feet thick in the center of the basin. The Norwood ranges in thickness from less than 20 feet towards the edges of the basin to more than 50 feet in the central basin. This estimate of gas in-place and $CO_2$ storage capacity assumes an average thickness of 90 feet is assumed for the Lachine and 30 feet for the Norwood.

# 4. RESERVOIR DATA USED

This section summarizes various reservoir data used to estimate gas in-place and theoretical maximum storage capacity. The data are summarized from published sources; no new Antrim core data were obtained.

## a. Adsorption Isotherms

Very little published methane isotherm data are available for the Antrim Shale in the Michigan Basin. **Table 1** summarizes the available methane adsorption isotherm data obtained for this analysis. The average Langmuir volume for all three samples in Table 1 is 122.1 standard cubic feet per ton (scf/ton) and the average Langmuir pressure is 711.2 psia. The average Langmuir parameters in Table 1 are applied to both the Lachine and Norwood Antrim Shale members to estimate adsorbed gas content.

No Antrim $CO_2$ adsorption isotherm data were available for this analysis. The Midwest Regional Carbon Sequestration Partnership published an initial estimate of theoretical $CO_2$ storage capacity for the Antrim and Ohio Shales, which applies $CO_2$ adsorption isotherms obtained for the Ohio Shale in the Appalachian Basin to the Antrim (Wickstrom and others, 2005). For this analysis, we estimate that $CO_2$ is preferentially adsorbed by a factor of 2, so assumed a Langmuir volume for $CO_2$ that is two times the Langmuir volume for methane shown in Table 1. The average $CO_2$ Langmuir volume assumed for the Antrim samples in Table 1 is 244.1 scf/ton.

## b. Total Organic Carbon

Total organic carbon content of the Antrim Shale is reported to range up to 20 percent. Decker, Hill and Wicks (1993) measured TOC on sidewall core samples from three Antrim wells in the northern Michigan Basin and report TOC values that range from 1 percent to 15 percent. Lancaster and Hill (1993) measured TOC values for Antrim samples from a well in Otsego County. They report TOC values for the Lachine of 5.2 percent and 11.6 percent; 3.2 percent TOC for the Paxton; and 17.7 percent TOC for the Norwood. Jarvie (2008) reports TOC and gas content data for twelve Antrim samples. For these samples, TOC ranges from 1 percent to 19 percent and associated gas content ranges from approximately 20 scf/ton to more than 160 scf/ton. Frantz and others (1994) report that typical TOC for the Lachine in the northern Michigan Basin ranges from 5 to 12 percent and from 10 to 16 percent for the Norwood.

## c. X-Ray Diffraction Mineralogy

Decker, Hill and Wicks (1993), present average mineralogy data for the Antrim. The Antrim mineral components are presented as volume percentages that sum to 100 percent of the

mineral fraction of the rock. In addition to the mineral fraction, the total rock volume of the Antrim would include kerogen (reported to range from 1 percent to 19 percent of total rock volume) and total porosity (which would account for about 7 percent to 10 percent of total rock volume). As reported by Decker, et al (1993) the mineral component of the Antrim Shale is comprised of quartz, 50 percent; plagioclase (feldspar), 3 percent; dolomite, 3 percent; pyrite, 10 percent; illite, 9 percent; and muscovite (mica), 25 percent.

## d. Core Porosity and Permeability

Very little Antrim core porosity data are reported in the literature. Lancaster and Hill (1993) report routine core analysis results for Lachine, Paxton and Norwood samples, for a single well in Otsego County. These data are provided in **Table 2**; the helium porosity values reported are total porosity. Total porosity values for the Lachine and Norwood samples in Table 2 range from 7.9 percent to 9.5 percent. The average total porosity for the Lachine and Norwood samples is 8.8 percent. The extrapolated gas-filled porosity for the Lachine and Norwood members ranges from less than 0.5 percent to 6.4 percent. The average extrapolated gas-filled porosity is 3.4 percent for the Lachine and Norwood combined. These data support the Antrim gas-filled porosity of 3 to 5 percent that is widely reported and used for Antrim reservoir simulation (Zuber and others, 1994; Frantz and others, 1994; Kuuskraa and others, 1992). No new Antrim permeability data were obtained for this report. Very little permeability data are publically available. The fracture permeability values reported for the Antrim appear to vary substantially, from 0.004 millidarcies (mD) to more than 1000 mD. The matrix permeability is assumed to be extremely low. For example, Zuber and others (1994) report matrix permeability for the Antrim of $2 \times 10^{-8}$ millidarcies.

# 5. ESTIMATED GAS IN-PLACE AND THEORETICAL MAXIMUM $CO_2$ STORAGE CAPACITY

Gas storage mechanisms recognized for the Antrim Shale include adsorption and storage as free gas in fracture porosity and intergranular microporosity. Two approaches can be used to estimate total gas in-place for the Antrim. The first approach is based on measurement of total *in situ* gas content from canister desorption and degassing. Cross plots of gas content and measured TOC and bulk density of the canister samples show a strong correlation between TOC and gas content, and an inverse relationship between bulk density and TOC content. Decker, Hill and Wicks (1993) and Jarvie (2008) each present empirical correlations of TOC and gas content, which could be applied for estimating total gas in-place in the Antrim. These data are compared in **Table 3**. The TOC, density and gas content correlation provided by Jarvie, (2008) predicts total *in situ* gas content that ranges from 17 percent to 33 percent higher than predicted total gas content using the Decker, Hill and Wicks (1993) correlation. This empirical approach does not estimate the adsorbed and free gas components separately, so does not capture the free gas component in fracture porosity.

A second approach estimates adsorbed gas content from adsorption isotherm data and uses a volumetric calculation to estimate free gas in gas-filled matrix and fracture porosity. For the Antrim, the disadvantage of this approach is the lack of adsorption isotherm data, core porosity and saturation data, and useable porosity and resistivity logs, which preclude a rigorous volumetric calculation. However, for an initial approximation of gas in-place, enough published data are available to make reasonable estimates of key reservoir parameters for a volumetric calculation. $CO_2$ adsorption isotherms are estimated based on published methane isotherm data by applying a multiplier to the Langmuir volume parameter for the methane isotherms that captures the preferential adsorption of $CO_2$ on coal and organic gas shale over methane. The chief advantage of a volumetric approach is that it provides an estimate of the relative amount of adsorbed gas in-place to free gas in-place.

This analysis uses both approaches to estimate gas in-place for the Antrim. The bulk density/ total gas content correlations provided by Decker, et al. and by Jarvie are used to estimate gas in-place based on estimated average bulk density values for the Antrim. Enough published core data and Langmuir isotherm data were found to provide reasonable inputs for a volumetric based estimation of gas in-place and theoretical $CO_2$ storage capacity.

## a. Overview of Calculated Volumetric Gas In-Place and $CO_2$ Storage Capacity

Volumetric gas in-place and theoretical maximum $CO_2$ storage capacity for the Lachine and Norwood members of the Antrim are estimated using basin-scale assumptions about

average reservoir properties and other inputs that are based on available published data. Gas in-place and $CO_2$ storage capacity were not calculated for individual wells and then aggregated to a regional estimate. Instead, a single calculation was made for each of three large, basin-scale model areas by applying average or representative reservoir variables. The calculation results are intended to provide a first approximation or "screening- level" estimate of potential gas in-place and theoretical $CO_2$ storage capacity for the Antrim.

The estimate of theoretical maximum $CO_2$ storage capacity is based on calculated gas in-place by assuming that 100 percent of the methane in-place, either as adsorbed or "free" gas, is replaced in the reservoir by injected $CO_2$. The net stored volume of injected $CO_2$ will be a very small fraction of theoretical maximum capacity values. The reservoir simulation reported in this volume provides a first approximation of what actual gas recovery factors and net volumes of injected $CO_2$ are likely to be for the Antrim.

Methane gas in-place for the Antrim is assumed to have two components: 1) methane adsorbed on organic matter contained in the shale, and 2) non-adsorbed methane, or free gas, contained within void space in the shale. Such voids could include micro-fracture porosity; intergranular porosity between clastic grains and particles; dissolution seams; voids within the framework of component minerals; and microporosity commonly observed within the kerogen of thermally-mature, organic–rich shale (intra-kerogen porosity). Estimating gas in-place thus requires two steps to calculate the quantity of adsorbed gas and the quantity of free (non-adsorbed) gas. Similarly, $CO_2$ storage capacity is assumed to have two components: storage as an adsorbed $CO_2$ phase displacing methane and storage of non-adsorbed $CO_2$ replacing methane in the gas-filled pore space, or "effective" porosity.

## b. Well Log Analysis Methodology

Conventional well log analysis methodologies were investigated for this analysis and were ultimately abandoned as impractical for the time and resources available. Two obstacles were a lack of digital log data and a general lack of resistivity logs, which precluded calculating water and hydrocarbon saturations and gas-filled porosity for individual wells..

### i. TOC Extrapolated from Density Logs

Total organic carbon was not extrapolated from well logs for this analysis. Single representative TOC values were assumed for the Lachine and for the Norwood from published data. Bulk density logs for several of the sixteen Antrim raster logs obtained for this analysis were examined to determine typical bulk density values for the Lachine and Norwood. Representative bulk density values were assigned to the Lachine and to the Norwood, and these bulk density values were input to published correlations of bulk density and gas content (Jarvie, 2008; Decker et al, 1993) to estimate gas content and to compute gas in-place.

### ii. Porosity from Density Logs

Porosity was not calculated from well logs for this analysis. Average values for total porosity and gas-filled porosity were assumed based on the data presented in Tables 1 and 2 and in various references cited previously in this report. Based on the published Antrim core data summarized in Table 2, total porosity of 0.09 was assumed for the Antrim. Gas saturation was assumed to be 39 percent providing an average gas-filled porosity of 0.035. Average gas filled porosity of 0.035 is assumed for calculating free gas in-place

### iii. Adsorbed Gas In-Place and Theoretical Maximum Adsorbed $CO_2$ Storage Capacity

Adsorbed methane and $CO_2$ in units of standard cubic foot per ton (scf/ton) were calculated using Langmuir coefficients from the available isotherm data for the Antrim Shale plus estimated reservoir pressure based on depth. A reservoir pressure gradient was estimated for each model area. A reservoir pressure gradient of 0.31 psia per foot was assumed for the shallow Antrim producing area in the northern basin. A normally pressured reservoir was assumed for the thermogenic gas play in the central basin. Relevant isotherm data are summarized in **Table 1.** Adsorbed gas content or theoretical adsorbed $CO_2$ content were calculated using the following algorithm:

$$V_{adsorbed} = (V_L \, x \, P_{res})/(P_L + P_{res})$$

Where, $V_{adsorbed}$ = adsorbed gas content; volume of adsorbed gas at a reservoir pressure, $P_{res}$; $V_L$ = Langmuir volume from adsorption isotherm; $P_L$ =average Langmuir pressure from adsorption isotherm data.

Adsorbed methane in-place or $CO_2$ in-place (scf/acre) is computed by multiplying the adsorbed gas content (scf/ton) obtained from the previous step by an estimated quantity of shale (tons/acre):

Tons shale = (thickness *x* area *x* shale density *x* conversion factor (g/cc to tons/acre-ft.))[2]

### iv. Free Gas In-Place and Theoretical Maximum $CO_2$ Storage Capacity

Free gas in-place was estimated by assuming an effective (gas-filled) porosity of 0.035.

Water saturation was not independently calculated. The total thicknesses of the Lachine and Norwood were assumed as the effective reservoir thickness for calculating free methane

[2] Adsorbed Gas (or $CO_2$), M/ac. = (h *x* area *x* bulk density *x* Adsorbed gas content(scf/ton) x 1359.7)/ (1 x $10^3$)

gas in-place. The volume of free gas in-place for each acre-foot of net reservoir thickness was computed:

Free methane gas-in-place= (43,560 x $\phi_{effective}$) /$Bg_{CH4}$

Where, $Bg_{CH4}$ (rcf/scf) = the appropriate formation volume factor for methane computed for each study area based on average depth and extrapolated reservoir temperature and pressure.

The maximum capacity for $CO_2$ storage as 'free' gas (non-adsorbed $CO_2$) is estimated by assuming that all calculated methane gas in-place as 'free' gas is replaced by $CO_2$. Methane gas must be removed from the reservoir by production to make reservoir volume available for injected $CO_2$. Methane recovery factors for the Antrim will be determined by the reservoir simulation, but are certain to be only a tiny fraction of the gas-filled pore volume hence, computed $CO_2$ storage capacity as 'free', non-adsorbed $CO_2$ is a theoretical maximum. Maximum $CO_2$ storage capacity as non-adsorbed $CO_2$ was computed for each acre-foot of net reservoir thickness by substituting the appropriate formation volume factor for $CO_2$ ($BgCO_2$) at the extrapolated reservoir pressure and temperature for the depth.

## c. Antrim Log Calculation Results

**Table 4** provides a description of the Antrim model areas and a summary of estimated model area parameters for calculating gas in-place and maximum $CO_2$ storage capacity. Included in Table 4 are the model areas in acres and square miles, estimated reservoir pressure gradient, extrapolated mean reservoir pressure and temperature, and estimated formation volume factor for methane and $CO_2$. **Table 5** summarizes average model well attributes for each model area that will be incorporated into the reservoir simulation. The model well attributes provided in these tables include: the average depth of the layer, thickness, average total porosity, average permeability, average calculated water saturation, average TOC, average bulk density, adsorbed gas content (scf/ton) and maximum adsorbed $CO_2$ storage capacity (scf/ton).

## d. Total Gas In-Place and Maximum $CO_2$ Storage Capacity

**Table 6** shows the calculated Antrim gas in-place by model area. Gas in-place for the Lachine and Norwood model layers are listed separately. Gas in-place is expressed as a resource concentration in units of billion cubic feet (Bcf) per square mile, and million cubic feet (MMcf) per 80 acres. **Table 7** shows theoretical maximum $CO_2$ storage capacity by model area expressed in units of billion cubic feet (Bcf) per square mile, million tonnes (MT) per square mile, and MT per 80 acres. **Table 8** shows estimated total gas in-place and total estimated theoretical $CO_2$ storage capacity by model area. **Figure 9** summarizes the estimated total gas

in-place and estimated total resource concentration for each of the three model areas. **Figure 10** summarizes the estimated theoretical maximum $CO_2$ storage capacity for each model area.

Total gas in-place for the northern Antrim biogenic gas play (Model Area 1), is estimated to be 80.7 trillion cubic feet (Tcf), of which 64.5 Tcf (80 percent) is estimated to be adsorbed gas in-place and 16.2 Tcf (20 percent) is estimated to be free (non-adsorbed) gas in-place. Total gas in-place for the Antrim thermogenic gas play in the central basin is 482.0 Tcf, of which 347.7 Tcf (72 percent) is estimated to be adsorbed and 134.3 Tcf (28 percent) is estimated to be free gas. The hypothetical shallow Antrim play in the southern basin (Model Area 3) is estimated to have potential gas in-place of 190.1 Tcf, of which 143.7 TCF (75 percent) is estimated to be adsorbed and 46.4 Tcf (25 percent) is estimated to be free gas.

The estimated resource concentration for Model Area 1 is 14.9 Bcf/ $mi^2$, of which 11.9 Bcf/$mi^2$ is adsorbed and 3.0 Bcf/$mi^2$ is free gas. For an 80-acre production area, the estimated gas in-place is 1,864 million cubic feet (MMcf), of which 1,490 MMcf/ 80-acres is adsorbed gas and 374 MMcf/80-acres is free gas. The estimated resource concentration for Model Area 2, the thermogenic Antrim gas play, is 25.0 Bcf/ $mi^2$, of which 18.0 Bcf/$mi^2$ is adsorbed and 7.0 Bcf/$mi^2$ is free gas. For an 80-acre production area, the estimated gas in-place would be 3,123 MMcf, of which 2,252 MMcf/ 80-acres is estimated to be adsorbed gas and 871 MMcf/80-acres is estimated to be free gas. For the hypothetical Antrim biogenic gas play in the south, the estimated resource concentration is 15.8 Bcf/$mi^2$. The $CO_2$ content in the produced gas of hypothetical Model Area 3 is assumed to be 10 percent, compared to 30 percent $CO_2$ content assumed for Model Area. This results in a slightly higher resource concentration for the hypothetical southern biogenic gas play.

Theoretical maximum $CO_2$ storage capacity for the northern Antrim biogenic gas play (Model Area 1), is estimated to be 8.1 billion tonnes (GT), of which 6.7 GT (83 percent) of $CO_2$ is estimated to be stored as an adsorbed phase, and 1.4 GT (17 percent) to be stored as a non-adsorbed phase replacing free gas. Theoretical maximum $CO_2$ storage capacity for the Antrim thermogenic gas play in the central basin is 45.5 GT, of which 36.1 GT (79 percent) is estimated to be adsorbed storage capacity and 9.4 GT (21 percent) is estimated to be non-adsorbed $CO_2$ replacing free gas. The maximum CO2 storage capacity of the hypothetical shallow Antrim play in the southern basin (Model Area 3) is estimated to be 18.1 GT, of which 15.0 GT (83 percent ) is estimated to be potential $CO_2$ storage as an adsorbed phase, and 3.1 GT (17 percent) as potential $CO_2$ storage as a non-adsorbed phase replacing free gas.

Expressed in terms of areal $CO_2$ storage capacity, the theoretical maximum $CO_2$ storage capacity for Model Area 1 is 1.50 million tonnes per square mile, MT/ $mi^2$, of which 1.24 MT/$mi^2$ would be adsorbed and 0.26 MT/$mi^2$ would be non-adsorbed $CO_2$ replacing free gas. For an 80-acre production area in Model Area 1, the theoretical maximum $CO_2$ storage capacity would

be 0.19 million tonnes (MT), of which 0.16 MT/ 80-acres would be an adsorbed phase and 0.03 MT/ 80 acres would be a non-adsorbed phase replacing free gas. The estimated maximum $CO_2$ storage capacity for Model Area 2, the thermogenic Antrim gas play, is 2.36 MT/ $mi^2$, of which 1.87 MT/$mi^2$ would be adsorbed and 0.49 MT/$mi^2$ would be a free, non-adsorbed phase. For an 80-acre Antrim production area in the central basin, the potential maximum $CO_2$ storage capacity would be 0.29 MT/ 80-acres, of which 0.23 MT/ 80-acres would be adsorbed and 0.06 MT/80-acres would be non-adsorbed $CO_2$ replacing free gas. For the hypothetical Antrim biogenic gas play in the south, the theoretical maximum $CO_2$ storage capacity per unit area is assumed to be the same as for the current Antrim biogenic gas play in the northern basin.

## e. Comparing Estimates of Total Gas in-Place

In this section, gas in-place is estimated for the Antrim biogenic gas play (Model Area 1) using correlations of TOC and bulk density, and bulk density to total gas content published by Decker, Hill and Wicks, 1993, as well as a later correlation of total gas content and bulk density published by Jarvie, 2008. Total gas content estimated from these two methods is compared to the total gas in-place estimated using the volumetric approach discussed above.

**Table 5** shows the average TOC assumed for the Lachine and Norwood members of 8 percent and 11 percent, respectively, which are based on core data published in Lancaster and Hill, 1993. An average bulk density for the Lachine and Norwood is extrapolated from TOC, using the correlation of TOC and bulk density provided in Table 3 (from Decker, Hill and Wicks, 1993). From the data in Table 3, an average bulk density of 2.36 g/cc is extrapolated for the Lachine and 2.27 g/cc is extrapolated for the Norwood. For the Lachine, an average bulk density of 2.36 corresponds to a total gas content of 60.2 scf/ ton using Decker, Hill and Wicks, 1993, or to a gas content of 76 scf/ton using Jarvie, 2008. For the Norwood, average bulk density of 2.27 g/cc corresponds to total gas content of 77.6 scf/ton using Decker and others, and 100.4 scf/ton using Jarvie, 2008. Total gas in place, in units of Bcf/ square mile are calculated for the Antrim using these gas content values for the Lachine and Norwood.

The volumetric approach discussed in this analysis estimates total methane gas in-place of 14.9 Bcf/square mile for the Antrim biogenic gas play, if gas content is assumed to be 70 percent methane and 30 percent $CO_2$. If the gas content is assumed to be 100 percent methane, the volumetric approach presented in this analysis estimates total methane gas in-place is 16.2 Bcf/$mi^2$. Using the total gas content correlation assumed by the Decker, et al, 1993, and assuming 100 percent methane content, identical thickness and areal extent, this analysis predicts total methane gas in-place of 15.7 Bcf/square mile for the Antrim biogenic gas play model area. Using the total gas content and bulk density correlation published by Jarvie, 2008, this analysis predicts total methane gas in-place of 20.0 Bcf/square mile.

# 6. DEFINITION OF MODEL AREAS FOR RESERVOIR MODELING IN THE BASIN

## a. Overview and Rationale for Antrim Model Areas

Three model areas are proposed for the Antrim Shale: 1.) the northern shallow biogenic gas play area; 2.) the thermogenic Antrim play area in the central Michigan Basin, and 3.) a hypothetical southern shallow biogenic gas play on the southern rim of the basin. The three model areas are shown in **Figure 4.** Model well parameters for reservoir simulation are generalized based on published Antrim data and analyses and previous modeling of the Antrim shallow biogenic gas play conducted by Advanced Resources.

The northern shallow biogenic gas model area is the only model area of the three for which reservoir simulation of enhanced gas recovery and $CO_2$ injection and storage is practical. Only the northern shallow biogenic gas play has enough Antrim production data and known reservoir parameters to produce meaningful simulation results. The model area for the thermogenic Antrim gas play has very little Antrim production data, and little supporting data to estimate essential input parameters to the reservoir simulation. $CO_2$ injection and storage and enhanced gas recovery in the southern shallow gas model area is completely hypothetical.

For this analysis, gas in-place and theoretical maximum $CO_2$ storage capacity for the Lachine and Norwood members of the Antrim are estimated using basin-scale assumptions about reservoir properties and other inputs that are based on the available published data. The southern basin model area is assumed to have many of the same reservoir characteristics as the Antrim northern biogenic gas play model area, although biogenic gas production from shallow, highly fractured Antrim Shale has yet to be successfully established in the southern Michigan basin. $CO_2$ gas content in the produced gas stream is assumed to be 30 percent in the northern biogenic gas play (Model Area 1), zero percent for the thermogenic Antrim gas play (Model Area 2) and 10 percent for the hypothetical southern biogenic gas play (Model Area 3).

**Table 8** provides a summary for each model area of total gas in-place and total theoretical maximum $CO_2$ storage capacity. For each model area, the average calculated gas in-place and $CO_2$ storage capacity values per unit area are multiplied by the geographical area contained within the model area boundaries. Theoretical maximum $CO_2$ storage capacity is converted from Bcf to units of million tonnes (MT).

# 7. REFERENCES

Azeez, A.O., 1969, Paleogeography of the Lower Mississippian rocks of the Michigan Basin: American Association of Petroleum Geologists Bulletin v. 53, no. 1, p. 127-135.

Catacosinos, P. A., and Daniels, P. A., Jr., 1986, Stratigraphy of middle Proterozoic to Middle Ordovician formations of the Michigan Basin, in Catacosinos, P. A., and Daniels, P. A., Jr., eds., Early sedimentary evolution of the Michigan Basin: Geological Society of America, Special Paper 256, p. 53–71.

Catacosinos, P. A., and Daniels, P. A., Jr., and Harrison III, W. B. 1990. Structure, Stratigraphy, and Petroleum Geology of the Michigan Basin: Chapter 30: Part II. Selected Analog Interior Cratonic Basins: Analog Basin, *in* Interior Cratonic Basins. AAPG Memoir 51. P. 561-601.

Cercone, K. R. 1984. Thermal history of Michigan basin: American Association of Petroleum Geologists Bulletin v. 68, no. 2, p. 130-136.

Cercone, K.R., and Pollack, H.N., 1991. Thermal maturity of the Michigan basin, in Catacosinos, P.A., and Daniels, P, A., eds, Early sedimentary evolution of the Michigan basin: Geological Society of America Special Paper 256, p. 1-11.

Curtis, J. B, 2002, Fractured shale gas systems, American Association of Petroleum Geologists *Bulletin, vol. 86, no. 11., p. 1921-1938.*

Decker, A.D., Hill, D.G., Wicks, D.E., 1993, Log-based gas content and resource estimates for the Antrim Shale, Michigan Basin, Society of Petroleum Engineers, SPE 25910.

Dellapenna, T. M. , 1991, Sedimentological, structural, and organic geochemical controls on natural gas occurrence in the Antrim Formation in Otsego County, Michigan: Western Michigan University, Kalamazoo, MI, Master's thesis, 147 pp.

East, J. A., Swezey, C. S., Repetski, J. E., and Hayba, D. O. 2012. Thermal Maturity Map of Devonian Shale in Illinois, Michigan, and Appalachian Basins of North America. USGS Scientific Investigations Map 3214. Online: http://pubs.usgs.gov/sim/3214/pdf/sim3214.pdf. Accessed: April 2013.

Ells, G.E., 1979, *Stratigraphic cross sections extending from Devonian Antrim Shale to Mississippian Sunbury Shale in the Michigan basin*: Michigan Geological Survey Report of Investigation 22, 186 p.

Fisher, J. H., Barratt, M. W., Droste, J. B., and Shaver, R. H., 1988, Michigan Basin, in The Geology of North America, v. D-2, Sedimentary Cover—North American Craton: U.S.: Geological Society of America, p. 361–382.

Frantz, J. H., Tatum, C.L. and five others, 1994, Evaluating the Optimal Norwood Deepening Method in the Antrim Shale, Society of Petroleum Engineers Eastern Region Meeting, November 1994, Charleston, WV, SPE 29171-MS.

Gas Research Institute. 1994. Gas Potential of the New Albany Shale (Devonian and Mississippian) in the Illinois Basin. Final Report for the Gas Research Institute by the Illinois Basin Consortium cooperative research

project. Contract No. 5090-213-1975. January 1994. Online: http://www.sitterdrilling.com/docs/Gas_Research_Institute.pdf. Accessed: April 2013.

Goodman, W. R. and Maness, T. R., 2008, Michigan's Antrim gas shale play – a two-decade template for successful Devonian gas shale development, American Association of Petroleum Geologists Annual Convention, San Antonio, TX, April 20-23, 2008.

Gupta, N., Cumming, L., Kelley, M., Paul, D., Mishra, S., Gerst, M., Place, M., 2012, Monitoring and Modeling $CO_2$ Behavior in Multiple Oil Bearing Carbonate Reefs for a Large Scale Demonstration in Northern Michigan, 11th International Conference on Greenhouse Gas Control Technologies; Kyoto, Japan, November 2012.

Gutschick, R. A., and Sandberg, C. A. 1991. Late Devonian history of Michigan Basin. GSA Special Papers 1991, v. 256, p. 181-202.

Harell, J. A., Hatfield, C. B., Gunn, G. R. 1991. Mississippian system of the Michigan basin; stratigraphy, sedimentology, and economic geology, in Catacosinos, P.A., and Daniels, P.A., eds, Early sedimentary evolution of the Michigan basin: Geological Society of America Special Paper 256, p. 202-220.

Howell, P. D., and van der Pluijm, B. A. 1990. Early history of the Michigan Basin: Subsidence and Appalachian tectonics. Geology, v. 18, pp. 1195 – 1198.

Howell, P. D., and van der Pluijm, B. A. 1999. Structural sequences and styles of subsidence in the Michigan basin. GSA Bulletin, v. 111, n 7, p. 974-991.

Kuuskraa, V.A., Wicks, D.E., Thurber, J.L., 1992, Geologic and reservoir mechanisms controlling gas recovery from the Antrim Shale, Society of Petroleum Engineers, SPE 24883.

Lancaster, D.E., and Hill, D.G., 1993, A multi-laboratory comparison of isotherm measurements on Antrim Shale samples, Otsego County, MI, Society of Core Analysts (SCA) Conference Paper Number 9303.

Lilienthal, R. T., 1974, *Subsurface Geology of Barry County, Michigan*: Michigan Geological Survey Report of Investigation 15, 18 pp.

Martini, A.M., Kirk, M., Petsh, S., McIntosh, J., 2009, Geochemical and microbial investigation of methanogenesis in the Upper Devonian shales: progress report. Research Partnership to Secure Energy America (RPSEA), Sugarland, TX.. Available online: http://www.rpsea.org/attachments/contentmanagers/429/Shale_Gas_Sourcing_-_Thermo-Biogenic_Kirk_Petsch_and_McIntosh.pdf

Martini, A.M., Budai, J. M., Walter, L.M., and Richard, J.A. 1994a. Methane and water sources in an unconventional Paleozoic gas reservoir: stable isotopic constraints: Geological Society of America Abstracts with Programs, v. 26, no. 7, p. A-323.

Martini, A.M., Budai, J.M., and Walter, L.M. 1994b. Formation fluid and gas sources highlighted by chemical and isotopic tracers: implications for migration pathways in the Antrim Shale, Northern Michigan basin, *in* Advances in Antrim Shale Technology, Workshop, December 13, 1994, sponsored by Gas Research Institute in Cooperation with the Michigan Section of the Society of Petroleum Engineers, Mt. Pleasant, Michigan, p.1-2.

Matson, M. M., 2010, The origin of natural fractures in the Antrim Shale. Michigan, American Association of Petroleum Geologists, Eastern Section Meeting, Kalamazoo, MI, September 25-29, 2010.

Matthews, R.D., 1993, Review and revision of the Devonian-Mississippian stratigraphy in the Michigan basin, in Roen, J.B., and Kepferle, R.C. (eds), Petroleum geology of the Devonian and Mississippian black shale of eastern North America: U.S. Geological Survey Bulletin 1909, p. D1-D85.

Midwest Regional Carbon Sequestration Partnership, 2010, Michigan Basin Carbon Dioxide Storage Validation Phase Field Experiment, Fact Sheet. Available online at: http://addap.tk/userdata/Fact%20Sheets/Michigan.pdf

Nurmi, R. D. 1984. Basin Analysis and Petroleum Potential of Michigan Basin: Deposition and Subsidence History from Middle Ordovician (Trenton Formation) to Early Devonian. AAPG Bulletin 1984, v 68, p 1925. Online: http://archives.datapages.com/data/bulletns/1984-85/data/pg/0068/0012/1900/1925b.htm. Accessed: April 2013.

Oil and Gas Journal Online, 2012, GlobalData: Michigan's Antrim shale gas production drops, in *Oil and Gas Journal Online*, August 30, 2012.

Oil and Gas Journal Online, 1994, Antrim gas play, production expanding in Michigan, *Oil and Gas Journal Archives Online*, May 30, 1994.

Oliver, S. J. P., Coates, J. M., Kuuskraa, V. A., Kelafant, J. R., and Brandenburg, C. F. 1989. The Antrim Shale of the Michigan Basin: An Active Devonian Shale Gas Play.. Society of Petroleum Engineers. Online: http://www.pe.tamu.edu/wattenbarger/public_html/Selected_papers/--Shale%20Gas/SPE19104.pdf. Accessed: February 2013.

Potential Gas Committee, 2009, *Potential Supply of Natural Gas in the United States,* Colorado School of Mines, December 2009.

Reszka, Carl R., 1991, The Michigan basin, in Sloss, L.L. (ed), The Geology of North America, v. P-2, Economic Geology, U.S.: Decade of North American Geology, Geological Society of America, p. 287-300.

Ryder, R.T., 1996, *Fracture patterns and their origins in the Upper Devonian Antrim Shale gas reservoir of the Michigan basin; a review,* United States Geological Survey, Open File Report 96-23, 33 pp.

Smith, R. A. 1912. The occurrence of oil and gas in Michigan: Mich. Geological and Biological Survey, Publication 14, Geol. Series 11.

United States Energy Information Administration, 2011, Review of Emerging Resources: U.S. Shale Gas and Oil Plays, U.S. Department of Energy, Energy Information Administration, Online: www.eia.gov/analysis/studies/usshalegas/pdf/usshaleplays.pdf. Accessed: April, 2013.

United States Energy Information Administration, 2007 - 2010, *U.S. Crude Oil, Natural Gas, and Natural Gas Liquids Reserves, 2007 – 2010, Annual Report. Online:* www.eia.gov/naturalgas/crudeoilreserves/pdf/table_13.pdf. Accessed: April 2013.

United States Geological Survey, 2013, Mineral Resources Online Spatial Data: http://mrdata.usgs.gov/geology/state/, Accessed August 7, 2013.

United States Geological Survey, 2005, Assessment of Undiscovered Oil and Gas Resources of the U.S. Portion of the Michigan Basin, USGS National Assessment of Oil and Gas Resources *Fact Sheet,* online: Online: http://pubs.usgs.gov/fs/2005/3070/2005-3070.pdf

Waldron, P.J., Petsch, S.T., Martini, A.M., Nuslein, K., 2 007, Salinity constraints on subsurface archaeal diversity and methanogenesis in sedimentary rock rich in organic matter, Applied and Environmental Microbiology, vol. 73, no. 13, p. 4171-4179.

Walter, L.M., and the Antrim Shale working group, University of Michigan. 1994. Project Overview: Regional hydrogeochemistry of the Antrim Shale, in Advances in Antrim Shale Technology, Workshop, December 13,1994, sponsored by Gas Research Institute in Cooperation with the Michigan Section SPE, Mt. Pleasant, Michigan, unpaged; 3 pages text plus figures.

Walton, I. and McLennan, J., 2013, The role of natural fractures in shale gas production, chapter 16 *in Effective and Sustainable Hydraulic Fracturing*, ed. A. P Bunger, J. McLennan, R. Jeffrey, p. 327 – 356, open access publication available from InTech, www.intechopen.com/books/.

Wang, H. F., Crowley, K. D., and Nadon, G. C. 1994, Thermal History of the Michigan Basin from Apatite Fission-Track Analysis and Vitrinite Reflectance, *in* Ortoleva, P. J., ed., Basin Compartments and Seals. AAPG Memoir 61, p. 167-177.

Wickstrom, L.H. and 28 others, 2005, Characterization of Geologic Sequestration Opportunities in the MRCSP Region, Phase 1 Task Report for Period of Performance October 2003 – September 2005, Midwest Region Carbon Sequestration Partnership, U.S. Department of Energy Cooperative Agreement DE-PS26-05NT42255, 152 pp.

Zuber, M. D., Frantz, J.H., Gatens, J.M., 1994, Reservoir characterization and production forecasting for Antrim Shale wells: an integrated reservoir analysis methodology, Society of Petroleum Engineers Annual Technical Conference, New Orleans, LA, September 25- 28, 1994, SPE 28606.

# FIGURES

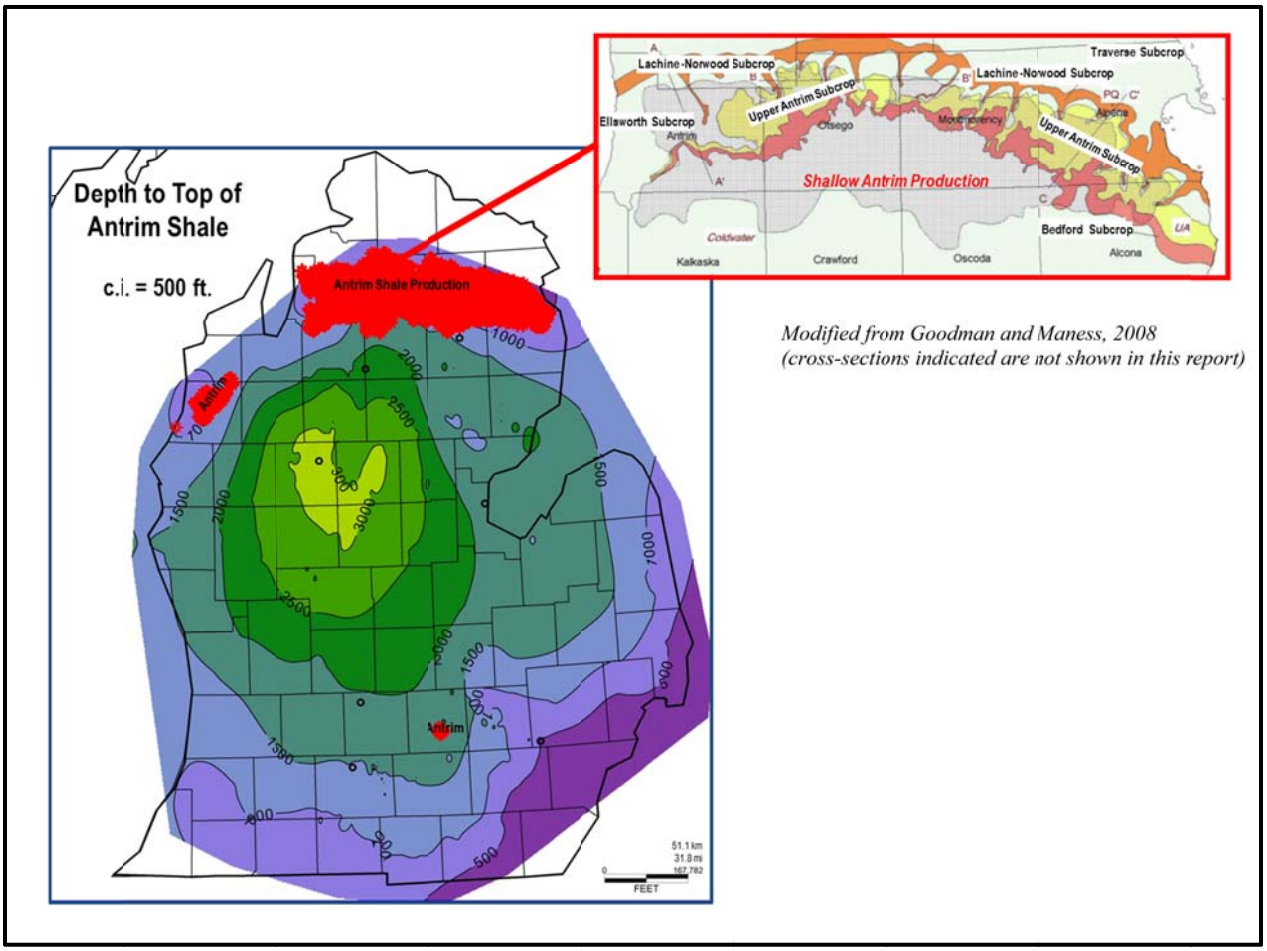


Figure 1: Antrim Shale Production in the Michigan Basin

| System/Series | Michigan Basin |
|---|---|
| Mississippian | Berea Sandstone |
| Upper Devonian | Ellsworth Shale/ Bedford Shale |
| | Ellsworth Shale/ Upper Antrim Shale |
| | *Antrim - Lachine Member.* |
| | *Antrim -Paxton Member.* |
| | *Antrim - Norwood Member* |
| | Squaw Bay Ls |
| Middle Devonian | *Unconformity* |
| | Traverse Group |
| | Dundee Limestone |
| | Detroit River Grp |
| Lower Devonian | Bois Blanc Fm. |

Figure 2: Stratigraphic Chart for Upper Devonian in Michigan Basin

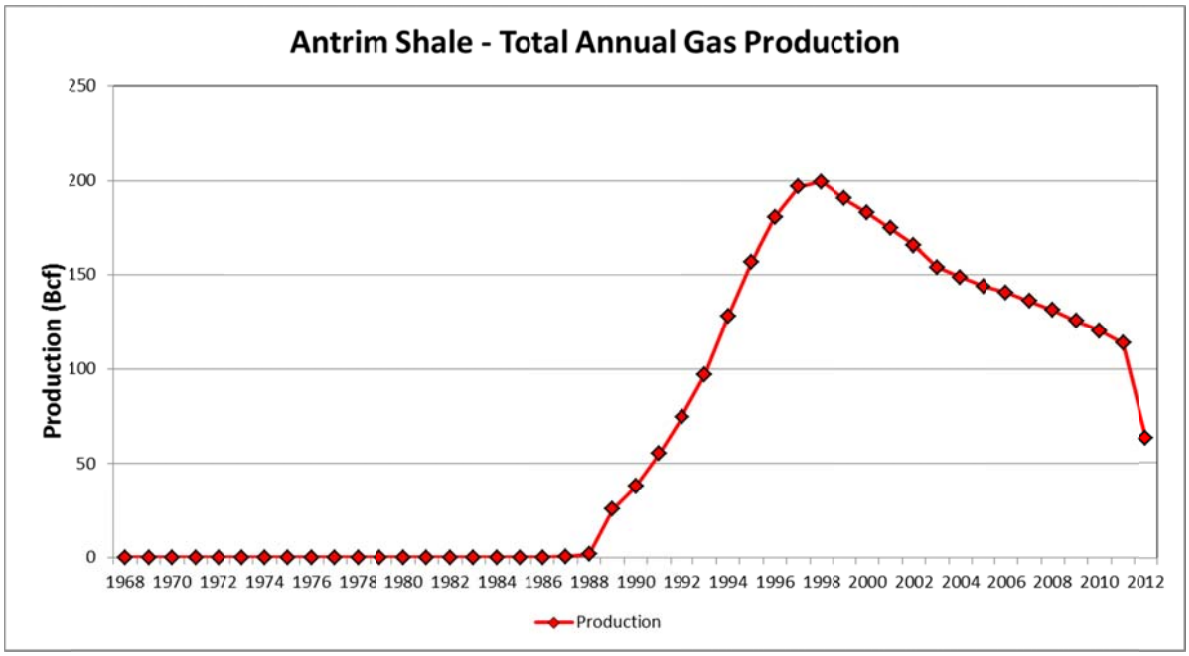


Figure 3: Antrim Shale – Total Annual Gas Production, 1968 - 2012

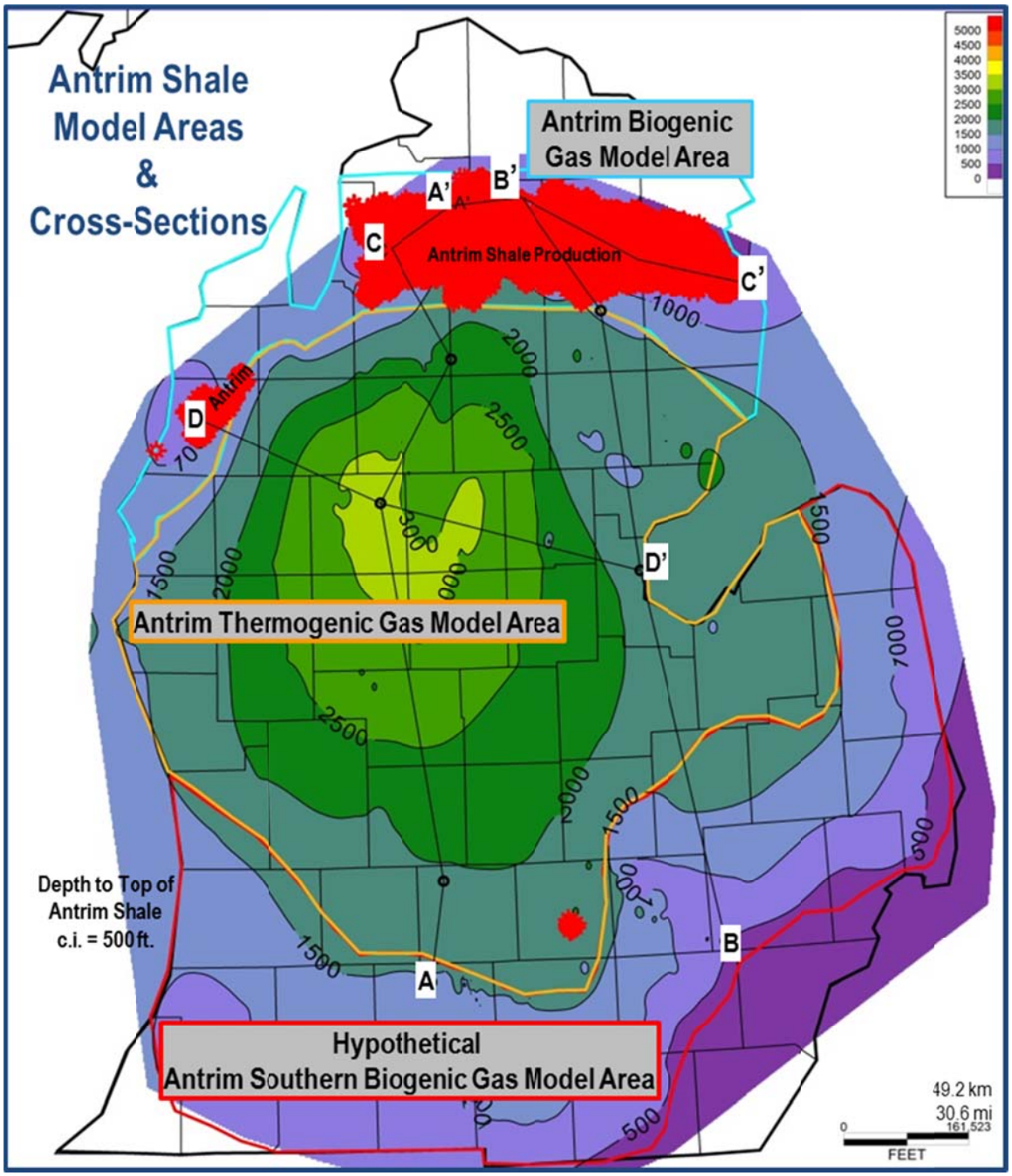


Figure 4: Antrim Shale Cross-Sections and Model Areas

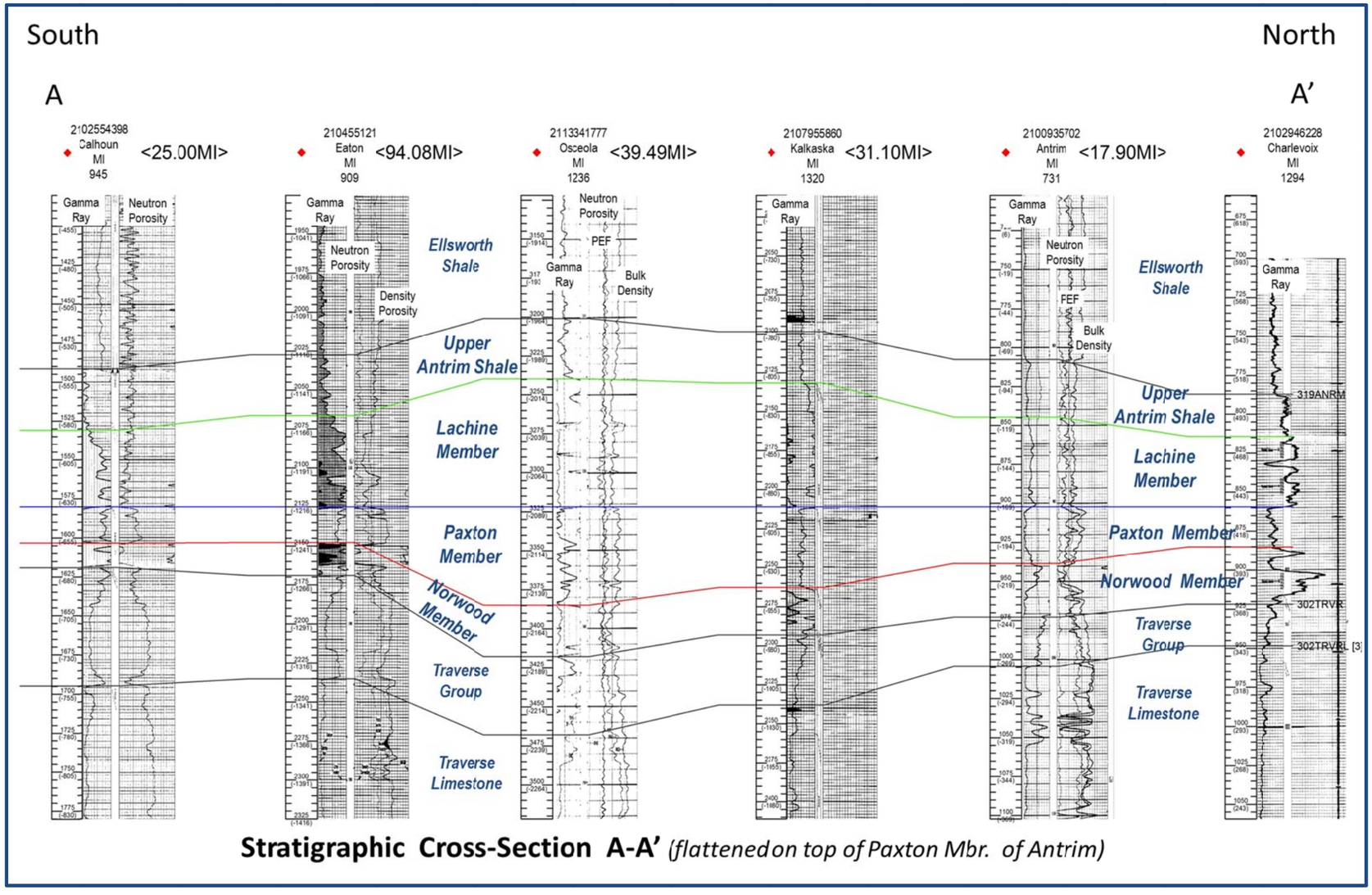


Figure 5: Antrim Shale Cross-Section A-A'

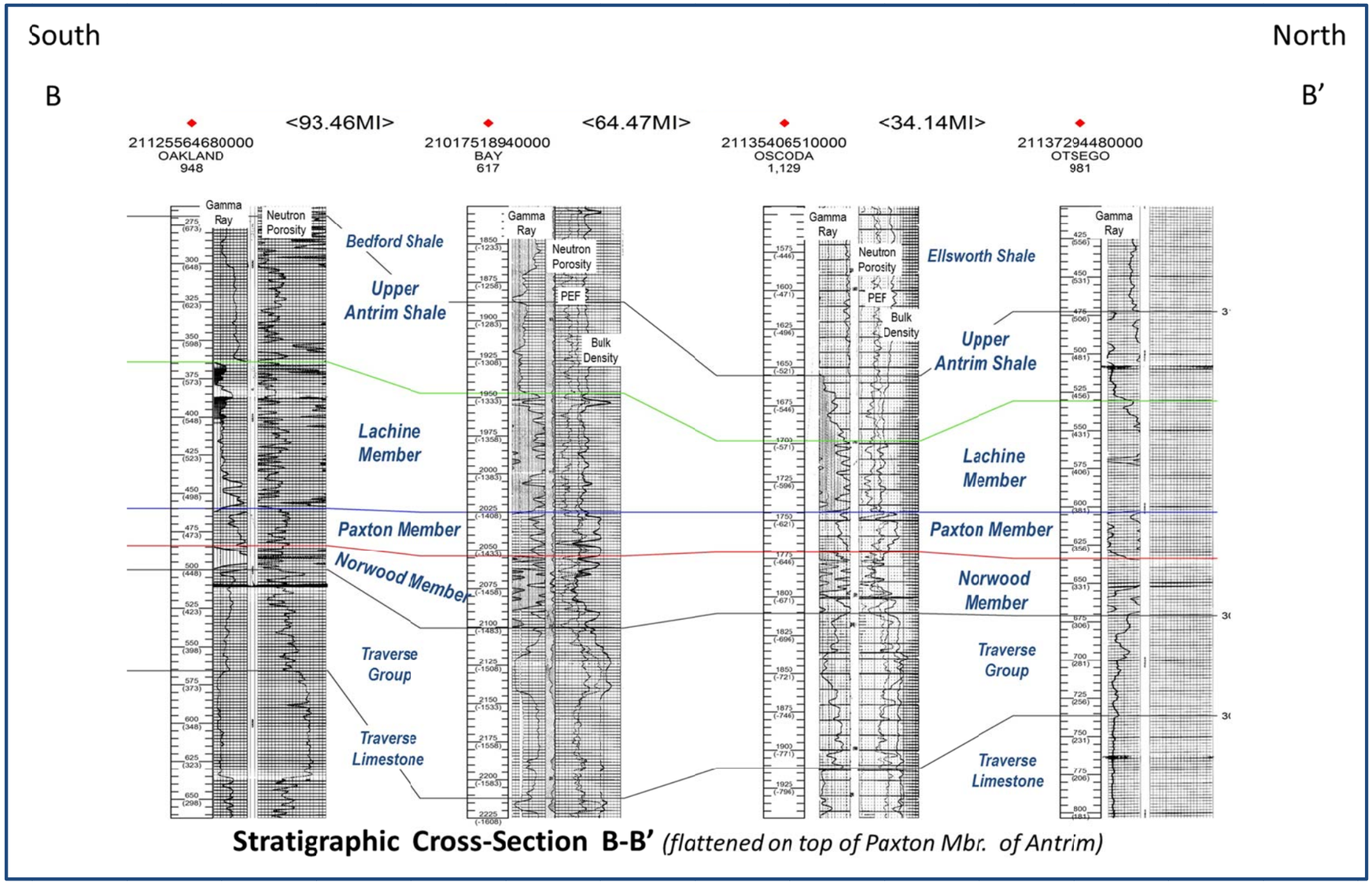


**Stratigraphic Cross-Section B-B'** *(flattened on top of Paxton Mbr. of Antrim)*

Figure 6: Antrim Shale Cross-Section B-B'

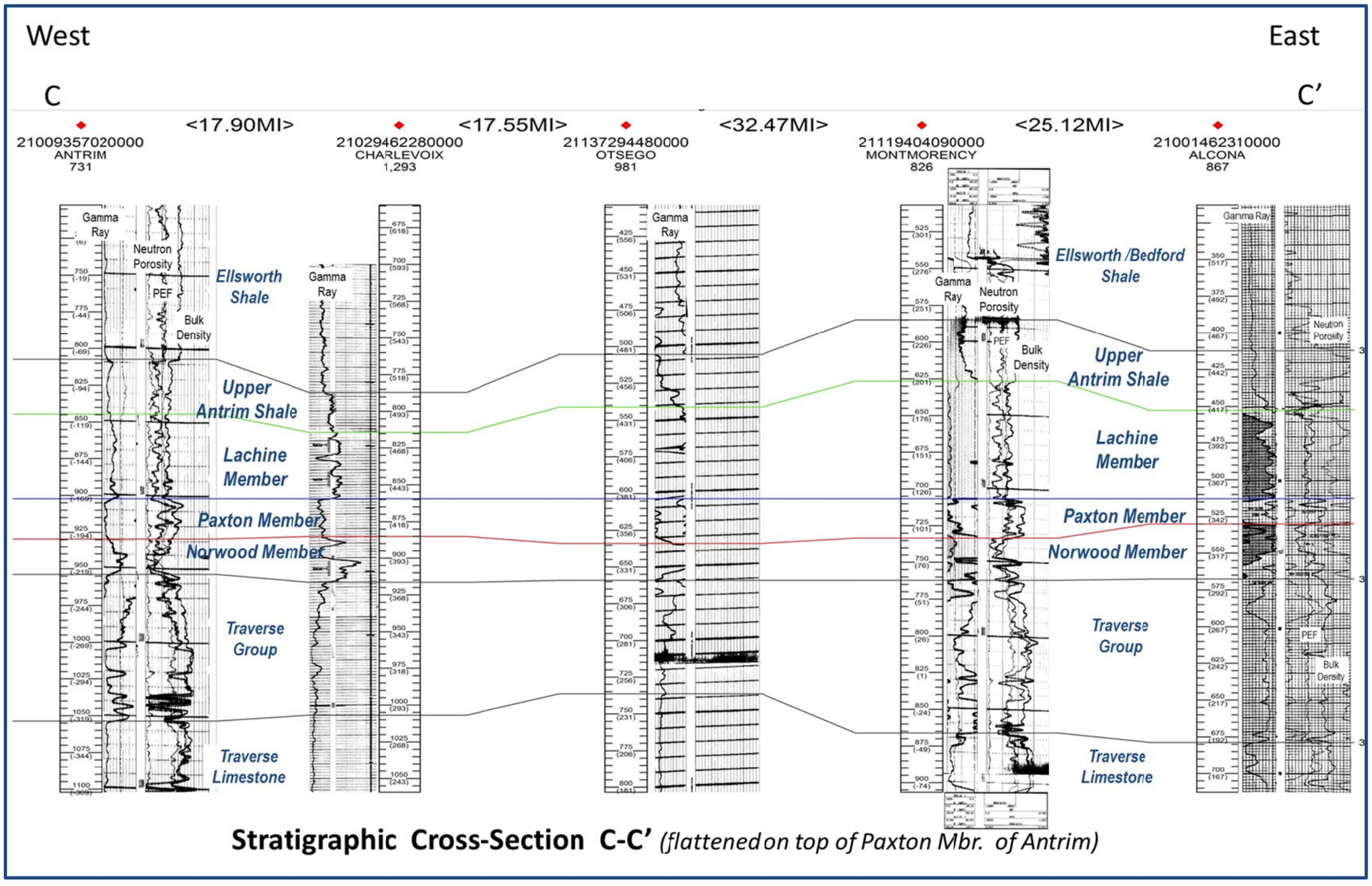


**Stratigraphic Cross-Section C-C'** *(flattened on top of Paxton Mbr. of Antrim)*

Figure 7: Antrim Shale Cross-Section C-C'

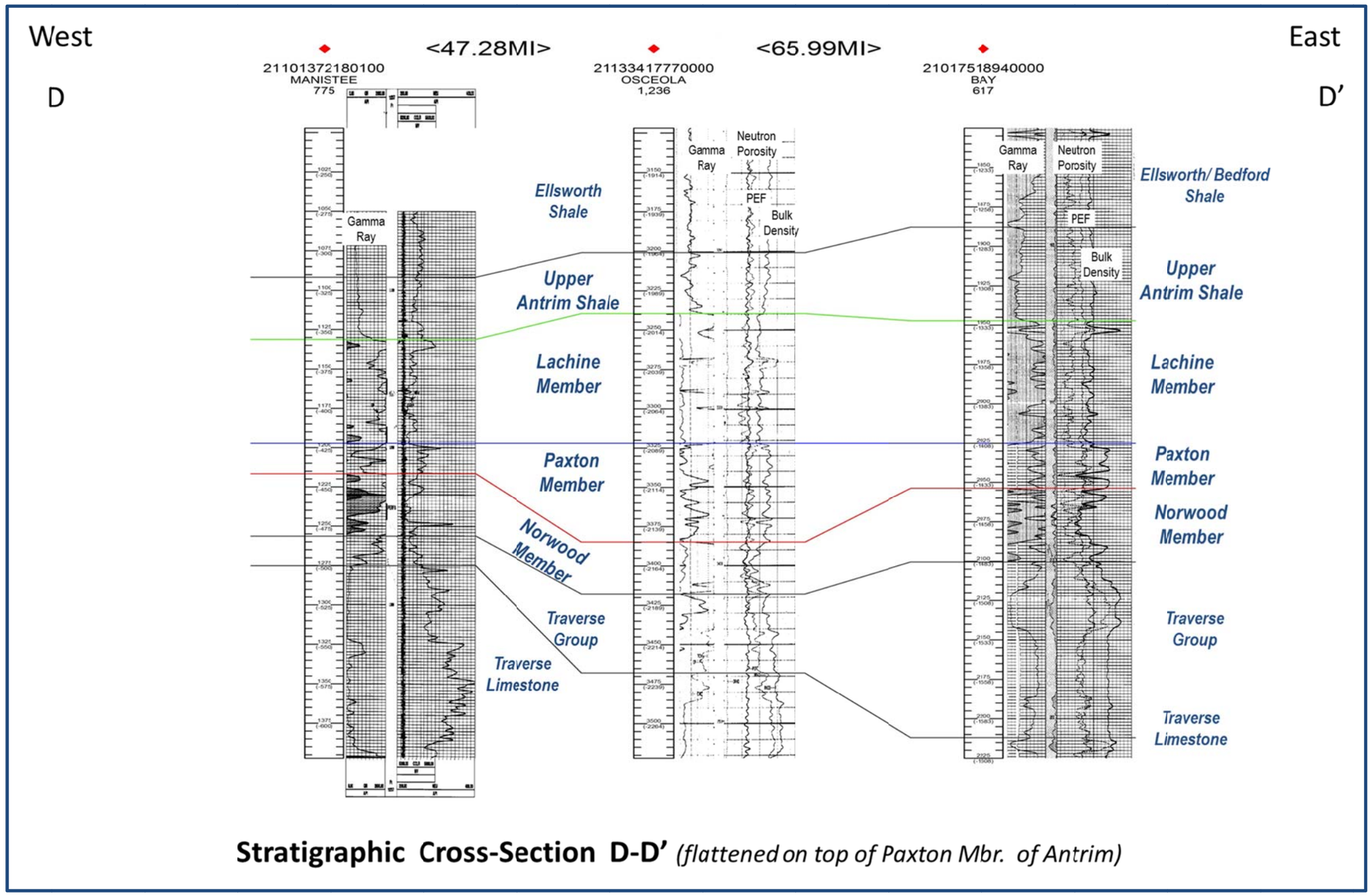


**Stratigraphic Cross-Section D-D'** *(flattened on top of Paxton Mbr. of Antrim)*

Figure 8: Antrim Shale Cross-Section D-D'

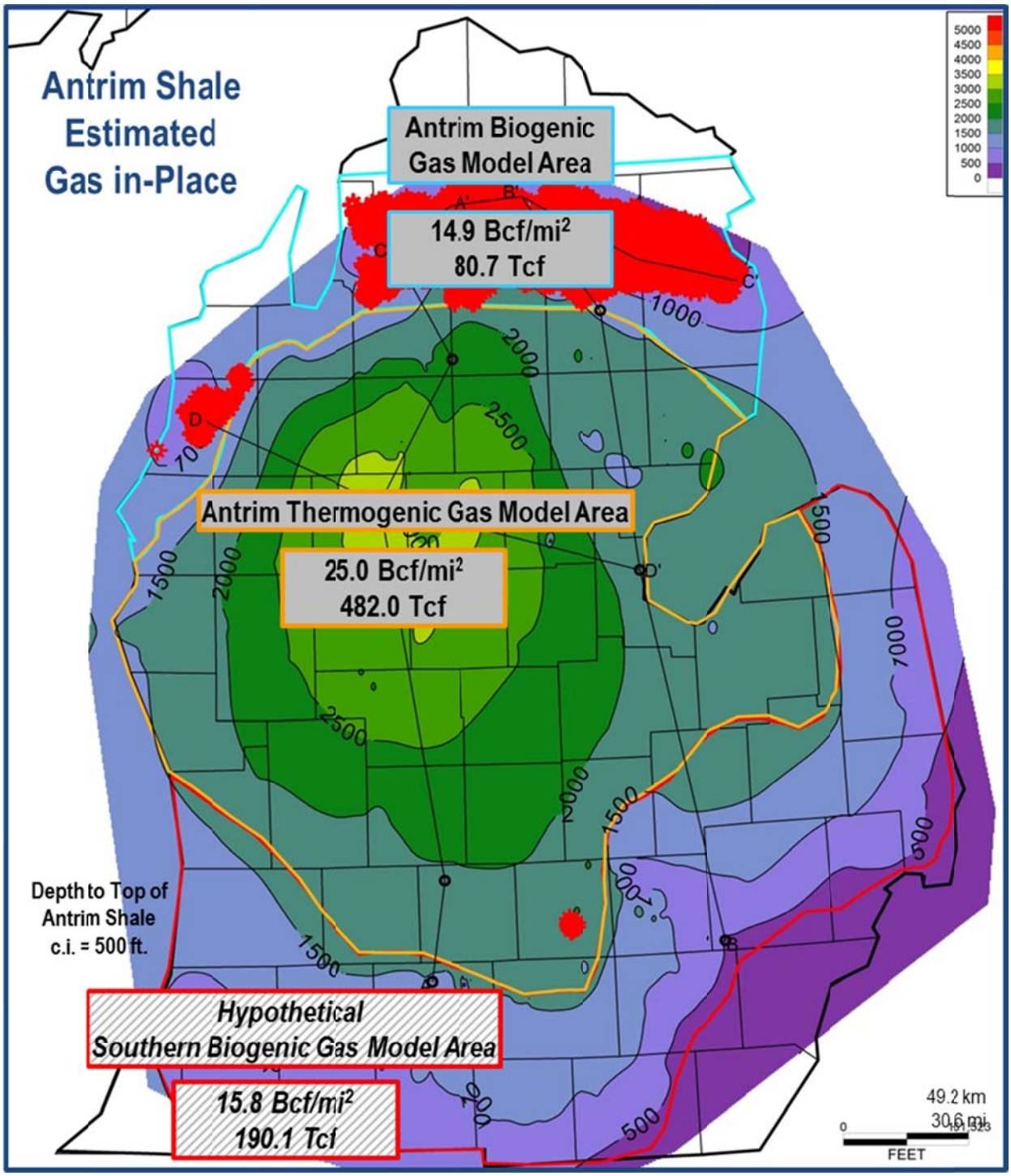


Figure 9: Summary of Antrim Shale Estimated Gas in-Place

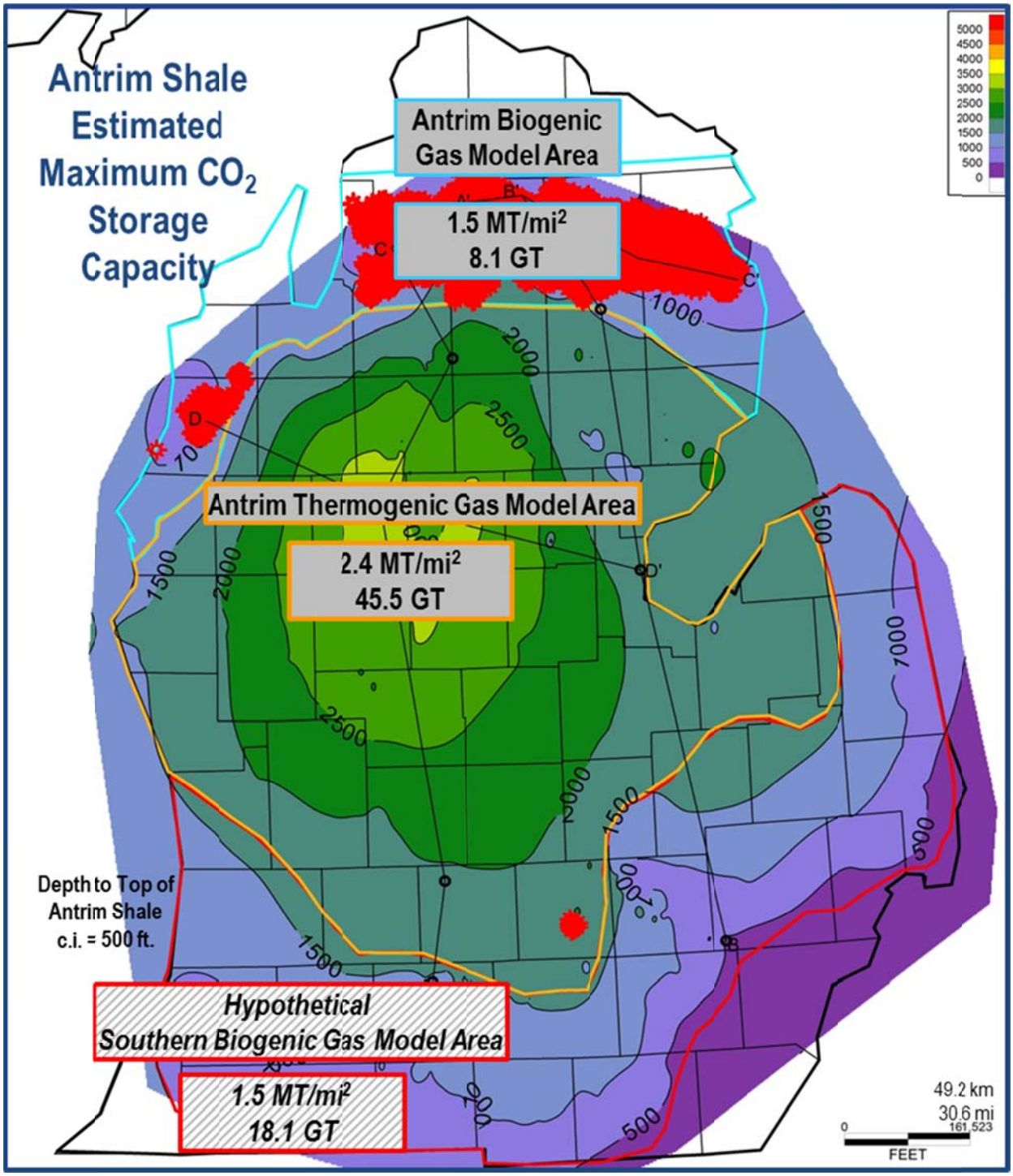


Figure 10: Summary of Antrim Shale Estimated Maximum $CO_2$ Storage Capacity

# TABLES

Table 1. Summary of Methane Adsorption Isotherm Data for the Antrim

| Interval | He Porosity, fraction | Langmuir Volume, VL, (scf/ton) | Langmuir Pressure, PL, (psia) | Source |
|---|---|---|---|---|
| Lachine | 0.074 (total porosity) | 122.8 | 654.8 | Nomeco Bagley East B3-11 Well, Otsego Co., MI Sample depth 1,360.6' – 1,361', reported in Lancaster and Hill, 1993 |
| Lachine | 0.090 (total porosity) | 145.6 | 749.3 | Nomeco Bagley East B3-11 Well, Otsego Co., MI Sample depth 1,360.6' – 1,361', reported in Lancaster and Hill, 1993 |
| Antrim (not differentiated) | 0.03 (gas-filled porosity) | 97.8 | 729.5 | Zuber, Frantz and Gatens, 1994. |
| Average | | 122.1 | 711.2 | |

Table 2. Routine Core Analysis Data for the Antrim Shale, Otsego County, MI

| Sample Depth, ft. | Antrim Shale Member | Helium Porosity, fraction | Water Saturation, % | Oil Saturation, % | Extrapolated Gas-Filled Porosity, fraction (this analysis) |
|---|---|---|---|---|---|
| 1,357 | Lachine | 0.092 | 44.7 | 13.5 | 0.038 |
| 1,370 | Lachine | 0.095 | 20.0 | 38.5 | 0.039 |
| 1,421 | Lachine | 0.083 | 22.1 | 67.2 | 0.009 |
| 1,428 | Lachine | 0.088 | 27.2 | 17.3 | 0.049 |
| 1,443 | Paxton | 0.106 | 32.0 | 57.2 | 0.011 |
| 1,472 | Paxton | 0.114 | 24.7 | 59.3 | 0.018 |
| 1,480 | Norwood | 0.091 | 28.7 | 1.5 | 0.064 |
| 1,486 | Norwood | 0.079 | 38.0 | 14.0 | 0.038 |
| 1,494 | Norwood | 0.090 | 50.7 | 46.7 | 0.002 |
| Average Lachine and Norwood | | 0.088 | 33.1 | 28.4 | 0.034 |
| Source: Lancaster and Hill, 1993 | | | | | |

Table 3. Correlation of Total Gas Content (scf/ton) and Total Organic Carbon (TOC) for the Antrim Shale

| Correlation of Bulk Density to TOC and Antrim Total Gas Content to TOC from SPE 25910 (Decker, Hill & Wicks, 1993) | | | | Correlation of Antrim Total Gas Content to TOC from Jarvie, 2008 |
|---|---|---|---|---|
| Bulk Density, g/cc | TOC, wt. % | Total Gas Content, scf/ton | | Total Gas Content, scf/ton |
| 2.06 | 18 | 118.4 | | 157.6 |
| 2.12 | 16 | 106.7 | | 141.2 |
| 2.18 | 14 | 95.1 | | 124.9 |
| 2.24 | 12 | 83.4 | | 108.6 |
| 2.30 | 10 | 71.8 | | 92.3 |
| 2.36 | 8 | 60.2 | | 76.0 |
| 2.42 | 6 | 48.5 | | 59.6 |
| 2.48 | 4 | 36.9 | | 43.3 |

Table 4. Description and Summary of Antrim Model Areas

| Description and Summary of Antrim Model Areas | | | | | | | | | |
|---|---|---|---|---|---|---|---|---|---|
| MODEL AREA | Area Description | Total Area, Acres | Total Area, $miles^2$ | Estimated Reservoir Pressure Gradient, psi/ft. | Estimated $CO_2$ Content in Gas Stream, fraction | Est. Reservoir Pressure, psia | Est. Reservoir Temperature, $^0F$ | Est. FVF for Methane, $ft^3/scf$ | Est. FVF for $CO_2$, $ft^3/scf$ |
| AREA 1 | Antrim Shale Shallow Biogenic Gas Play – Northern Basin | 3,462,962 | 5,411 | 0.31 | 0.30 | 500 | 70 | 0.02748 | 0.02353 |
| AREA 2 | Antrim Shale Deep Thermogenic Gas Play – Central Basin | 12,349,068 | 19,295 | 0.43 | 0 | 1,100 | 85 | 0.01686 | 0.01251 |
| AREA 3 | Hypothetical Shallow Biogenic Gas Play in Southern Basin | *7,713,139* | *12,052* | *0.31* | *0.10* | *500* | *70* | *0.02748* | *0.02353* |
| Total for Areas 1 and 2 | | 15,812,030 | 24,706 | | | | | | |

Table 5. Model Layer Attributes for the Lachine and Norwood Members of the Antrim Shale

| Attribute | Lachine | Norwood |
|---|---|---|
| Thickness, ft. | 90 | 30 |
| Total Porosity, fraction | 0.09 | .09 |
| Matrix Permeability, mD | 2.00E-8 | 2.00E-8 |
| Average Total Oil + Water Saturation, fraction | 0.61 | 0.61 |
| Gas- Filled Porosity, Fraction | 0.035 | 0.035 |
| Average Bulk Density, g/cc | 2.36 | 2.27 |
| Average TOC, % | 8.0 | 11.0 |
| Methane Isotherm Average Langmuir Volume, $V_L$, scf/ton | 122.1 | 122.1 |
| $CO_2$ Isotherm Average Langmuir Volume, $V_L$, scf/ton | 244.2 | 244.2 |
| Average Langmuir Pressure, $P_L$, psia | 711.2 | 711.2 |
| Adsorbed Gas Content, scf/ton (Area 1; Biogenic Gas Play, Northern Basin) | 48.3 | 50.5 |
| Adsorbed Gas Content, scf/ton (Area 2; Thermogenic Gas Play, Central Basin) | 73.5 | 74.8 |
| Maximum Adsorbed $CO_2$ Content, scf/ton (Area 1; Biogenic Gas Play, Northern Basin) | 96.5 | 101.1 |
| Maximum Adsorbed $CO_2$ Content, scf/ton (Area 2; Thermogenic Gas Play, Central Basin) | 147.0 | 149.7 |

Table 6. Antrim Shale; Summary of Estimated Gas In-Place

| Gas in-Place, Bcf/mi$^2$ | Model Area 1<br>Antrim Shale Shallow Biogenic Gas Play – Northern Basin | Model Area 2<br>Antrim Shale Deep Thermogenic Gas Play – Central Basin | Model Area 3<br>Hypothetical Shallow Biogenic Gas Play - Southern Basin |
|---|---|---|---|
| LACHINE Adsorbed Gas in-Place, Bcf/mi$^2$ | 8.92 | 13.58 | 8.92 |
| LACHINE Free Gas in-Place, Bcf/mi$^2$ | 2.24 | 5.22 | 2.88 |
| NORWOOD Adsorbed Gas in-Place, Bcf/mi$^2$ | 2.99 | 4.44 | 2.99 |
| NORWOOD Free Gas in-Place, Bcf/mi$^2$ | 0.75 | 1.74 | 0.96 |
| TOTAL ADSORBED Gas in-Place, Bcf/mi$^2$ | 11.92 | 18.02 | 11.92 |
| TOTAL FREE Gas in-Place, Bcf/mi$^2$ | 2.99 | 6.96 | 3.85 |
| TOTAL ANTRIM Gas in-Place, Bcf/mi$^2$ | 14.91 | 24.98 | 15.76 |
| TOTAL ADSORBED Gas in-Place, MMcf/ 80-acres | 1,490 | 2,252 | 1,490 |
| TOTAL FREE Gas in-Place, MMcf/ 80-acres | 374 | 871 | 374 |
| TOTAL ANTRIM Gas in-Place, MMcf/ 80-acres | 1,864 | 3,123 | 1,864 |

Table 7. Antrim Shale; Summary of Estimated Theoretical Maximum $CO_2$ Storage Capacity

| Theoretical Maximum $CO_2$ Storage, Bcf/mi$^2$ | Model Area 1 | Model Area 2 | Model Area 3 |
|---|---|---|---|
| | Antrim Shale Shallow Biogenic Gas Play – Northern Basin | Antrim Shale Deep Thermogenic Gas Play – Central Basin | Hypothetical Shallow Biogenic Gas Play - Southern Basin |
| LACHINE Max Adsorbed $CO_2$ Storage, Bcf/mi$^2$ | 17.84 | 27.16 | 17.84 |
| LACHINE Max Free $CO_2$ Storage, Bcf/mi$^2$ | 3.74 | 7.04 | 3.74 |
| NORWOOD Max Adsorbed $CO_2$ Storage, Bcf/mi$^2$ | 5.99 | 8.87 | 5.99 |
| NORWOOD Max Free $CO_2$ Storage, Bcf/mi$^2$ | 1.25 | 2.35 | 1.25 |
| TOTAL ADSORBED $CO_2$ Storage, Bcf/mi$^2$ | 23.83 | 36.03 | 23.83 |
| TOTAL FREE $CO_2$ Storage, Bcf/mi$^2$ | 4.99 | 9.39 | 4.99 |
| TOTAL ANTRIM Theoretical Max $CO_2$ Storage, Bcf/mi$^2$ | 28.82 | 45.42 | 28.82 |
| TOTAL ADSORBED $CO_2$ Storage, MT/mi$^2$ | 1.24 | 1.87 | 1.24 |
| TOTAL FREE $CO_2$ Storage, MT/mi$^2$ | 0.26 | 0.49 | 0.26 |
| TOTAL ANTRIM Theoretical Max $CO_2$ Storage, MT/mi$^2$ | 1.50 | 2.36 | 1.50 |
| TOTAL ADSORBED $CO_2$ Storage, MT/ 80-acres | 0.155 | 0.234 | 0.155 |
| TOTAL FREE $CO_2$ Storage, MT/80-acres | 0.032 | 0.061 | 0.032 |
| TOTAL ANTRIM Theoretical Max $CO_2$ Storage, MT/80-acres | 0.187 | 0.295 | 0.187 |

Table 8. Antrim Shale; Estimated Total Gas in-Place and Theoretical Maximum CO2 Storage Capacity by Model Area

| Theoretical Maximum $CO_2$ Storage, Bcf/mi$^2$ | Model Area 1<br>Antrim Shale Shallow Biogenic Gas Play – Northern Basin | Model Area 2<br>Antrim Shale Deep Thermogenic Gas Play – Central Basin | Model Area 3<br>Hypothetical Shallow Biogenic Gas Play - Southern Basin |
|---|---|---|---|
| Total Area, square mile | 5,411 | 19,295 | 12,052 |
| TOTAL ANTRIM ADSORBED Gas in-Place, Bcf | 64,499 | 347,696 | 143,660 |
| TOTAL ANTRIM FREE Gas in-Place, Bcf | 16,179 | 134,293 | 46,400 |
| TOTAL ANTRIM Gas in-Place, Bcf | 80,678 | 481,989 | 190,060 |
| Theoretical Maximum $CO_2$ Storage, ADSORBED, MT | 6,710 | 36,082 | 14,944 |
| Theoretical Maximum $CO_2$ Storage, FREE, MT | 1,407 | 9,455 | 3,134 |
| Theoretical Maximum $CO_2$ Storage, ADSORBED + FREE, MT | 8,117 | 45,537 | 18,078 |

# Volume 5
# Basin-Level Characterization Of Enhanced Gas Recovery And $CO_2$ Storage Potential In The Devonian Ohio Shale

## Assessment of Factors Influencing Effective $CO_2$ Storage Capacity and Injectivity in Eastern Gas Shales

Prepared for:
U.S. Department of Energy
National Energy Technology Laboratory
DOE Award Number: DE-FE0004633

Prepared by:
Michael Godec, Principal Investigator
Advanced Resources International, Inc.
4501 Fairfax Drive ▪ Suite 910 ▪ Arlington, Virginia 22203

Date:
October 23, 2013

Advanced Resources International, Inc.

4501 Fairfax Drive ▪ Suite 910 ▪ Arlington, Virginia 22203 ▪ Phone: (703) 528-8420 ▪ web: www.adv-res.com

## Advanced Resources International, Inc.

# Table of Contents

**1.** INTRODUCTION ..... 1
a. Background ..... 1
b. Project Objectives ..... 2
c. Objective of this Volume ..... 2
**2.** OVERVIEW OF HISTORICAL PRODUCTION ..... 3
**3.** GEOLOGICAL OVERVIEW ..... 5
**4.** RESEARCH ON ENHANCED GAS RECOVERY AND $CO_2$ STORAGE IN DEVONIAN OHIO SHALES ..... 8
**5.** DEVONIAN OHIO SHALE $CO_2$ STORAGE POTENTIAL ..... 9
**6.** INPUT DATA RESERVOIR SIMULATION ..... 11
**7.** REFERENCES ..... 14

# List of Figures

Figure 1. Kentucky Devonian Shale Gas Production Data ..... 4
Figure 2. Distribution and Nomenclature of Devonian shales of Kentucky ..... 6
Figure 3. General Stratigraphic Nomenclature for the Shales of Kentucky ..... 6
Figure 4. Nomenclature of Mississippian and Devonian Shales of Eastern Kentucky ..... 7
Figure 5: Stratigraphic Cross Section of the Study Area ..... 12
Figure 6: Methane and Carbon Dioxide Isotherms for Devonian Gas Shale ..... 13

# List of Tables

Table 1. $CO_2$ Storage Capacity in the Devonian Black Shales of the Appalachian Basin ..... 10

# 1. INTRODUCTION

## a. Background

Organic-rich gas shales are recognized as sharing some of the same methane storage characteristics as coal seams. Natural gas is adsorbed on kerogen and clay surfaces in gas shales, similar to methane storage within coal seams. Gas is also stored as "free" (non-adsorbed) gas in fracture porosity and inter-granular microporosity, as well as in micropores commonly observed within the kerogen of thermally mature shale (intra-kerogen porosity). The relative amounts of adsorbed and "free" gas recovered during the producing life of a shale gas well are unknown.

The potential storage of $CO_2$ in organic-rich gas shales is attracting increasing technical interest, especially in the Appalachian and Michigan Basin states that have extensive shale deposits, but limited $CO_2$ storage capacity in conventional porous reservoirs. It has been demonstrated in coal seams that $CO_2$ is preferentially adsorbed at a ratio of two or more $CO_2$ molecules for every methane molecule displaced. Gas shale reservoirs are expected to react similarly and desorb methane while preferentially adsorbing $CO_2$. In addition, some component of the pore volume that contains "free" gas is expected to be available for $CO_2$ storage as non-adsorbed $CO_2$, especially where previous hydraulic fracturing has enhanced injectivity. Although still in the conceptual stage, $CO_2$ injection into organic-rich gas shales could provide dual benefits: an economic benefit from the incremental recovery of adsorbed methane, and an environmental benefit of secure $CO_2$ storage.

The goal of this cooperative research project is to build upon previous and on-going work to assess key factors that would influence effective $CO_2$ storage capacity and injectivity in selected gas shales within the Appalachian and Michigan Basins. The Appalachian Basin is endowed with thick and extensive shale formations ranging in age from the Ordovician through the Devonian. The most prolific and promising gas shale formations for $CO_2$ storage were selected as the focus for this project, including the Devonian Marcellus Shale in New York, Pennsylvania, West Virginia and eastern Ohio; the Devonian Ohio Shale in Kentucky; and the Ordovician Utica and Point Pleasant shale and equivalent formations in New York, Pennsylvania, West Virginia and Ohio. The late Devonian-age Antrim Shale in the Michigan Basin was also investigated because it has similar reservoir properties to the Appalachian Basin Devonian shale formations, and the existing production infrastructure, shallow depth, and its reservoir characteristics may make the Antrim particularly attractive for $CO_2$ storage.

## b. Project Objectives

The low permeability and porosity typical of gas shale formations make $CO_2$ storage in shale challenging, especially when compared to other storage reservoirs such as depleted conventional oil and gas reservoirs and deep saline aquifers. Low porosity constrains the potential storage capacity, while low permeability constrains the injectivity of gas shales. Such constraints are counter-balanced by the great extent and thickness of candidate shale formations, plus the strong adsorptive capacity of gas shales for $CO_2$, which offers the potential to store $CO_2$ securely. Potential $CO_2$ storage capacity of gas shales is just beginning to be rigorously assessed. Critical factors that will determine the storage capacity and injectivity of $CO_2$ in gas shales are the volume and rate that methane can be desorbed and then produced from the shales, as well as the relative contribution of free gas from the gas-filled or, effective, pore volume. Consequently, understanding the $CO_2$ storage capacity of such shale formations requires a firm understanding the gas productive capacity of the shale.

## c. Objective of this Volume

This volume reports on the basin-level geologic characterization of the Devonian Ohio shale in Kentucky. The objective of this geologic characterization is to estimate methane gas in-place and potential $CO_2$ storage capacity as both adsorbed $CO_2$ displacing methane, and as non-adsorbed $CO_2$ replacing free gas in the pore volume.

However, unlike the work for the Marcellus, Utica, and Antrim shales reported in Volumes 2 through 4, this volume summarizes the results of previous work, and does not represent a new attempt at estimating the potential.

# 2. OVERVIEW OF HISTORICAL PRODUCTION[1]

Shale gas was discovered in eastern Kentucky around 1892, with the drilling of wells along Beaver Creek in Floyd County. Today, more than 6,000 shale gas wells are producing between 50 and 70 billion cubic feet (Bcf) of gas annually in Kentucky. Many of these wells are located in the Big Sandy gas field of Floyd, Knott, Letcher, Martin, and Pike Counties.

Modern drilling records of the Ohio Shale for the state of Ohio were first recorded during the 1950s, although reported production data prior to the mid 1980s is limited (ODNR, 2011). The recorded production history of the Ohio Shale dates back to the mid- 1980s in Ohio and West Virginia. The volume of gas produced from the shale has remained relatively low with respect to each state's total production.

A greater production contribution from the Ohio shales has been realized in Kentucky. **Figure 1** displays annual historical production from Devonian shales in Kentucky dating back to 1923, and illustrates a jump in production in the 1990s through mid-2000s. However, the production from the shale in many wells is comingled with other sources. Nonetheless, this suggests that drilling and production activity in the Devonian Shales has increased over time. According to a 1970s DOE report, up to 60% of gas at the time was produced from wells with a Devonian Shale source (Ray, 1975). However, this figure has likely evolved, and the utility of production data for Kentucky are mostly qualitative.

[1] *Note on Data Sources*: Annual statistics for gas production were collected from the Ohio Department of Natural Resources, the West Virginia Department of Environmental Protection, and the Kentucky Geological Survey. Well production is reported monthly to the West Virginia Department of Environmental Protection, and data are disclosed back to 1985. Ohio production statistics are reported annually beginning in 1984. Kentucky gas production data is sparse, but provides a historical production trend from shales from 1923 to 1984, and 1994 to 2008. Reported production data commonly include comingled sources of gas, so likely represent an upper limit of production from the Devonian shales.

Figure 1. Kentucky Devonian Shale Gas Production Data

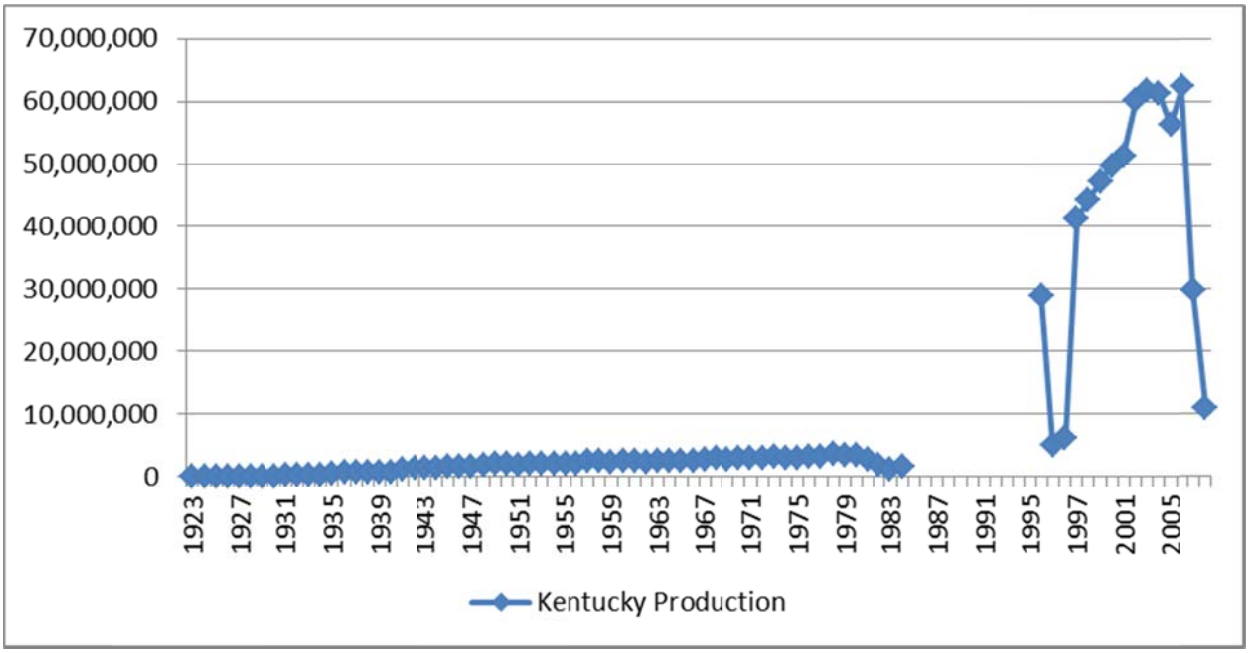


Note: Historical data from 1923 to 1984. Includes production from wells that are comingled with other sources

`

# 3. GEOLOGICAL OVERVIEW

Shales dominate the Middle and Late Devonian strata of the Appalachian Basin. Black, organic-rich units alternate with gray shales consisting mostly of quartz and clay minerals. The shale overlies strata that vary in age from Upper Ordovician through Middle Devonian. The shale ranges in thickness from outcrops in places along the crest of the Cincinnati Arch to more than 3,600 feet in West Virginia. In the gas productive areas of Kentucky, the shale is typically 200 to 1,600 feet thick. The shale ranges in depth from the outcropping on the western margin of the basin to more than 4,000 feet.

**Figure 2** shows the aerial limits of the nomenclature used for the Devonian shales in Kentucky; known variously as the New Albany (Illinois Basin), Chattanooga (central Kentucky, Cincinnati Arch area), and Ohio (Appalachian Basin) Shales.

The Ohio Shale is an Upper Devonian aged black shale that outcrops in central Ohio and extends through eastern Kentucky, south-western West Virginia, and eastern and central Tennessee (Schwietering, 1979; Roen, 1980). The Devonian shales of the Illinois Basin areas of western Kentucky and southwestern Indiana are correlative to similar shales of the Appalachian Basin (**Figure 3**).

The Ohio Shale of eastern Kentucky – the focus of this assessment -- is typically subdivided into seven recognizable units (**Figure 4**): Cleveland Shale; Three Lick Bed; Upper, Middle, and Lower Huron; Olentangy; and Rhinestreet. In the subsurface, these units have been differentiated based on gamma ray and density differences that are essentially related to the organic-matter content of the shale.

The Ohio Shale consists of the Huron Member and the Cleveland Member in Ohio, and is correlated with the Chattanooga Shale in Kentucky and Tennessee, and the Dunkirk shale in New York (Roen, 1980). It has been suggested that equivalent units may extend into Alabama and Georgia (Conant and Swanson, 1961; Glover, 1959; Roen, 1980).

The Devonian Ohio black shales have long been known to contain hydrocarbons. Some wells in Ohio have produced oil and gas for use as far back as 1870s (Hoover, 1960; Janssens and de Witt, 1976). The quantity of original gas-in-place is not well defined for these reservoirs; some have suggested that the upper Devonian shales may be as productive as the underlying Marcellus (Spencer, 2011; Thompson, 2010).

Figure 2. Distribution and Nomenclature of Devonian shales of Kentucky

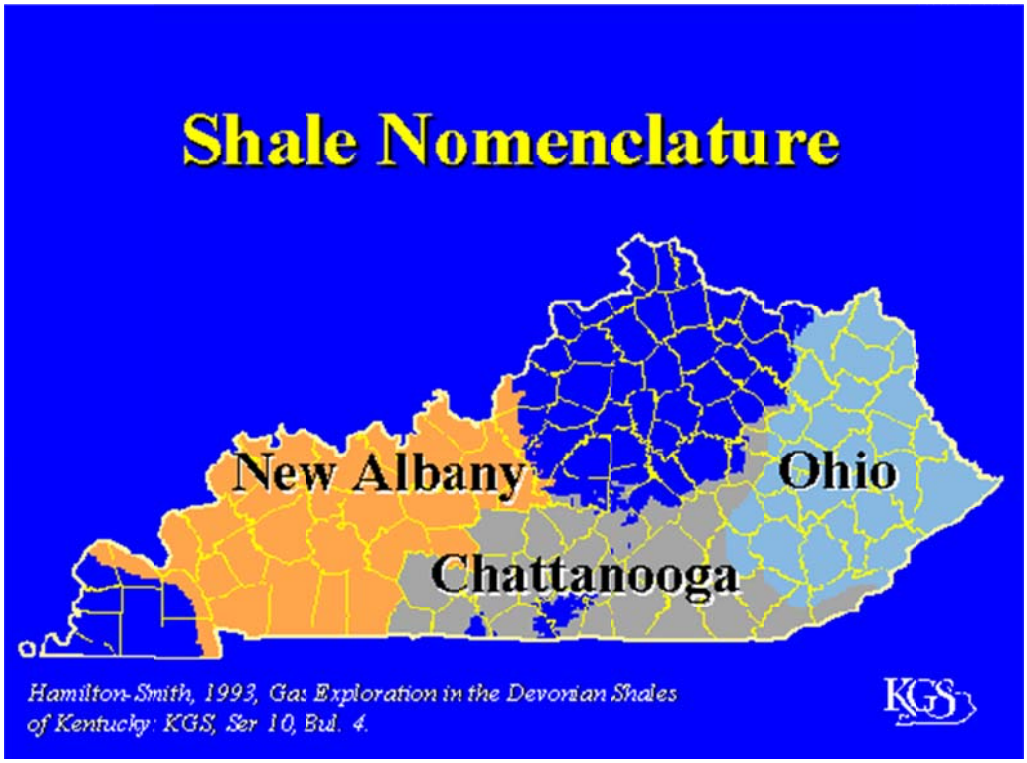


Figure 3. General Stratigraphic Nomenclature for the Shales of Kentucky

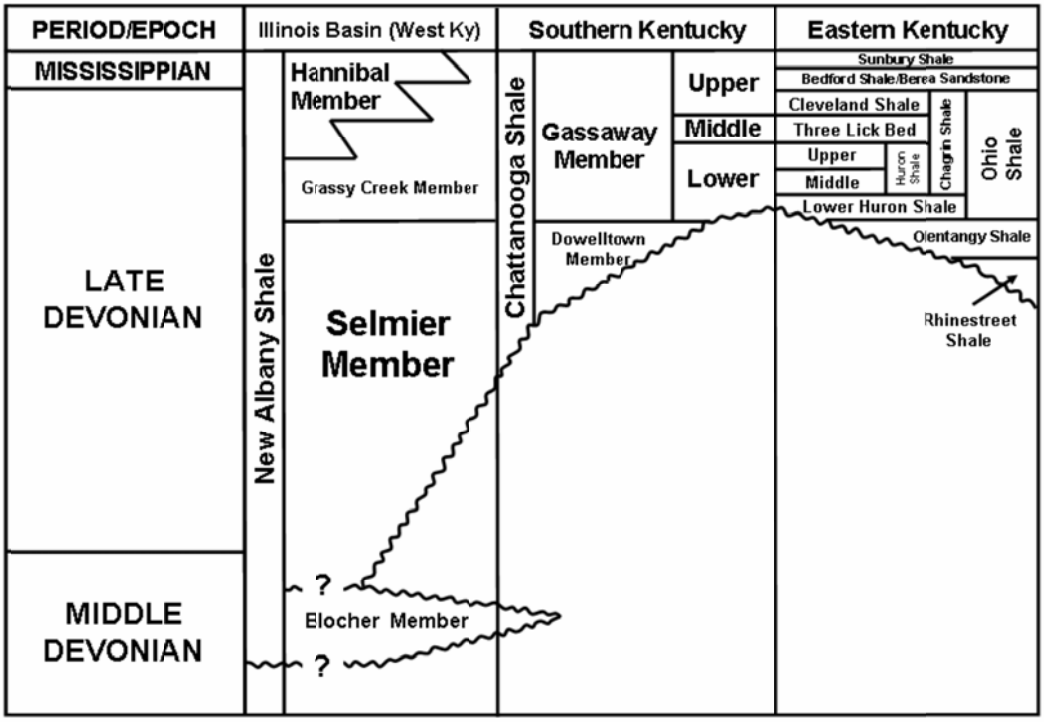


Source: Hamilton-Smith, 1993, p. 3.

Figure 4. Nomenclature of Mississippian and Devonian Shales of Eastern Kentucky

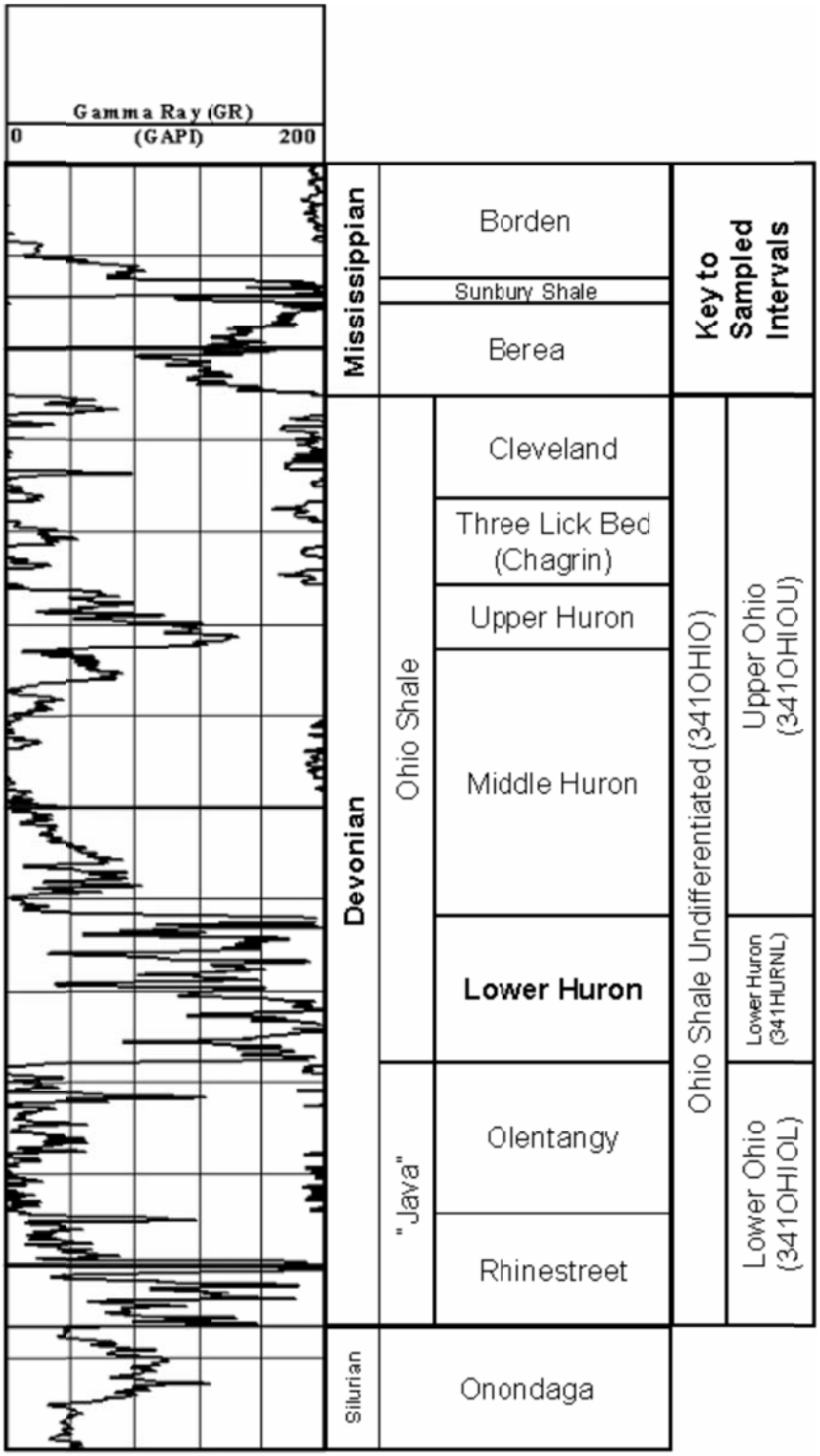


Source: Nuttall and others, 2005

# 4. RESEARCH ON ENHANCED GAS RECOVERY AND $CO_2$ STORAGE IN DEVONIAN OHIO SHALES

In 1993, the U.S. Department of Energy (DOE) conducted five $CO_2$/sand fracs in the Devonian Ohio Shale in eastern Kentucky to compare the effectiveness of cryogenic with hydraulic and nitrogen ($N_2$) stimulations (Yost and others, 1993). The study concluded that $CO_2$ fracs clean up faster and demonstrate higher flow rates than conventional stimulations. Subsurface assessment of storage opportunities suggests the black shale is both an effective seal (in deeper reservoirs) and a potential target for $CO_2$ storage.

Led by the Kentucky Geological Survey (KGS), the "Eastern Kentucky Shale Gas Enhanced Recovery and $CO_2$ Storage Project"[2] was established to research and demonstrate injecting $CO_2$ into organic-rich, black gas shales for long-term storage and enhanced natural gas production in Kentucky. The main tasks of this effort were to acquire data for reservoir simulation; use the modeling to test and plan $CO_2$ injection; undertake site selection, construction, and injection for a small scale injection test; and assess the results of that test. $CO_2$ adsorption isotherms of gas shale samples and have been developed and relationships between $CO_2$ adsorption and methane desorption established for the Devonian Ohio.

In 2005, Nuttall and others (2005) concluded $CO_2$ is preferentially adsorbed with respect to methane at an average volumetric ratio of 5:1; and thus, preferential adsorption may contribute to the enhancement of methane production. A new study was initiated to identify candidate wells, conduct reservoir modeling to design a test protocol, and conduct a pressure transient test simulating recompletion of a well to acquire data to improve understanding of enhancing production from gas shales (Nuttall and others, 2005; ARI, 2010; DOE/NETL, 2006).

Anticipating requirements to mitigate $CO_2$ emissions resulting from the use of coal in Kentucky, the Kentucky State Legislature passed House Bill (HB) 1 in a 2007 special session. This bill authorized funding for research by KGS in the areas of $CO_2$ enhanced oil recovery, $CO_2$ enhanced gas recovery, and permanent geologic storage of $CO_2$.[3]

Among a variety of activities, HB 1 included a mandate and funding to test the black shale for $CO_2$ enhanced gas recovery potential in Kentucky. The bill encouraged the KGS, the lead state agency on the effort, to partner with industry and other government bodies to share the cost of this important research. The Kentucky Consortium for Carbon Sequestration was formed to accomplish this goal.

---

[2] https://www.uky.edu/KGS/kyccs/ekyshale.htm
[3] http://www.uky.edu/KGS/kyccs/

# 5. DEVONIAN OHIO SHALE $CO_2$ STORAGE POTENTIAL

The Kentucky Geological Survey, as part of its shale characterization work, used drill cuttings from the KGS Well Sample and Core Library to develop both $CO_2$ and methane adsorption isotherms for the Devonian Ohio shale. Sidewall core samples were acquired to investigate $CO_2$ displacement of methane. An elemental capture spectroscopy log was used to investigate possible correlations between adsorption capacity and mineralogy.

Researchers concluded that average random vitrinite reflectance (Ro) data range from 0.78 to 1.59 (upper oil to wet gas and condensate hydrocarbon maturity range). Total organic carbon (TOC) content determined from acid-washed samples ranges from 0.69 to 14 percent. $CO_2$ adsorption capacities at 400 pounds per square inch (psia) were determined to range from 14 standard cubic feet per ton (scf/ton) in less organic-rich zones to more than 136 scf/ton in more organic-rich zones. A direct linear correlation between TOC and the adsorptive capacity of the shale was demonstrated, with the $CO_2$ adsorption capacity increasing with increasing organic carbon content (Nuttall and others, 2005).

Based on this initial work, volumetric estimates were developed to indicate a $CO_2$ sequestration capacity of as much as 28 billion metric tons (Gigatonnes, or Gt) in the deeper and thicker parts of the Devonian shales in Kentucky. In the Big Sandy Gas Field area of eastern Kentucky, assuming a net thickness of shale with 4 percent or greater TOC, 6.8 Gt of $CO_2$ storage potential was estimated to exist in the five-county area. KGS researchers concluded that, discounting the uncertainties in reservoir volume and injection efficiency, the black shales of Kentucky could be a potentially large geologic sink for $CO_2$.

Updating this previous work, as part of Phase I efforts of the Midwest Regional Carbon Sequestration Partnership (MRCSP)[4] research, an updated methodology was developed to assess the potential $CO_2$ storage capacity in the Devonian Ohio shales in a study area consisting of the central and northern Appalachian Basin and the Michigan Basin. In Phase II of the research, these estimates were updated by accounting for the variation of TOC of shale across the study area (thus allowing the $CO_2$ storage capacity to vary) and introducing an efficiency factor for displacement and storage (Nuttall, 2010).

[4] http://www.dnr.state.oh.us/tabid/8290/Default.aspx

Estimated storage capacity was estimated at various displacement efficiencies in the deeper (at least 1,000 feet deep) and thicker (at least 100 feet thick) black shales in the Appalachian Basin. Based on this, estimated $CO_2$ storage capacity ranged from 2.2 Gt at a 3 percent efficiency (analogous to the estimated efficiencies in saline aquifers), to as much as 30 Gt by assuming storage efficiencies analogous to those in continuous coals (up to 40 percent). A mid-range $CO_2$ storage capacity estimate of about 21 Gt was developed based on storage efficiency values of 28% (**Table 1**).

Table 1. $CO_2$ Storage Capacity in the Devonian Black Shales of the Appalachian Basin

| | Estimated $CO_2$ Storage Capacity (billion tons) | | |
|---|---|---|---|
| State | Efficiency Factor - 3% | Efficiency Factor - 28% | Efficiency Factor - 40% |
| Kentucky | 0.10 | 0.93 | 1.34 |
| Ohio | 0.51 | 4.78 | 6.82 |
| Pennsylvania | 0.80 | 7.46 | 10.66 |
| West Virginia | 0.82 | 7.61 | 10.87 |
| Total | 2.23 | 20.78 | 29.69 |

Source: Nuttall, 2010

No alternative or independent estimate was made of the $CO_2$ storage capacity in the Devonian Ohio shales.

# 6. INPUT DATA RESERVOIR SIMULATION

Based on the early characterization work by KGS, very preliminary efforts were undertaking to perform reservoir modeling and history matching of the Devonian Gas Shale Play in eastern Kentucky, and assess its potential for $CO_2$ enhanced gas recovery and carbon storage potential (ARI, 2010). In this work, a geologic model of the shale was compiled from mineralogical, petrographic, core, production, and wireline data. ARI's *COMET3* multi-phase, dual porosity simulator was used to investigate $CO_2$ injection into the shale for enhanced gas recovery and $CO_2$ storage.

To accomplish this, a subset of wells surrounding the potential injection site was selected for further study. These eight wells cover approximately 5,300 acres of productive shale. The reservoir was subdivided into the Upper Ohio and Lower Huron members. To capture geological heterogeneity, gas production rates for these wells served as a proxy to characterize permeability using geostatistical methods. Well production was history matched applying an automated process. Several $CO_2$ injection scenarios spanning huff-n-puff to continuous injection assessed to evaluate the enhanced gas recovery and the $CO_2$ storage capacity of these shales.

For this effort, an attempt was made to update this work, based on the revised characterization work performed under the MRCSP Phase 2 efforts summarized above, as well incorporating any key findings resulting from the small scale $CO_2$ injection pilot described in Volume 6.

Originally, a reservoir model was built assuming the stratigraphy of the three key study wells is shown in cross section in **Figure 5**. Production data sets from seven wells were selected for geo-statistical modeling and history matching. Monthly production data by well is publicly available only for Kentucky wells completed since 1997. Wells completed after 1997 were selected that produce from the shale interval only and have at least 60 months of publicly available production data. History matched gas production data served as proxies for characterizing the fracture permeability using geo-statistical methods.

Nine methane and sixteen carbon dioxide isotherms were measured on twelve wells located close to the study area, as presented in **Figure 6**.

Figure 5: Stratigraphic Cross Section of the Study Area

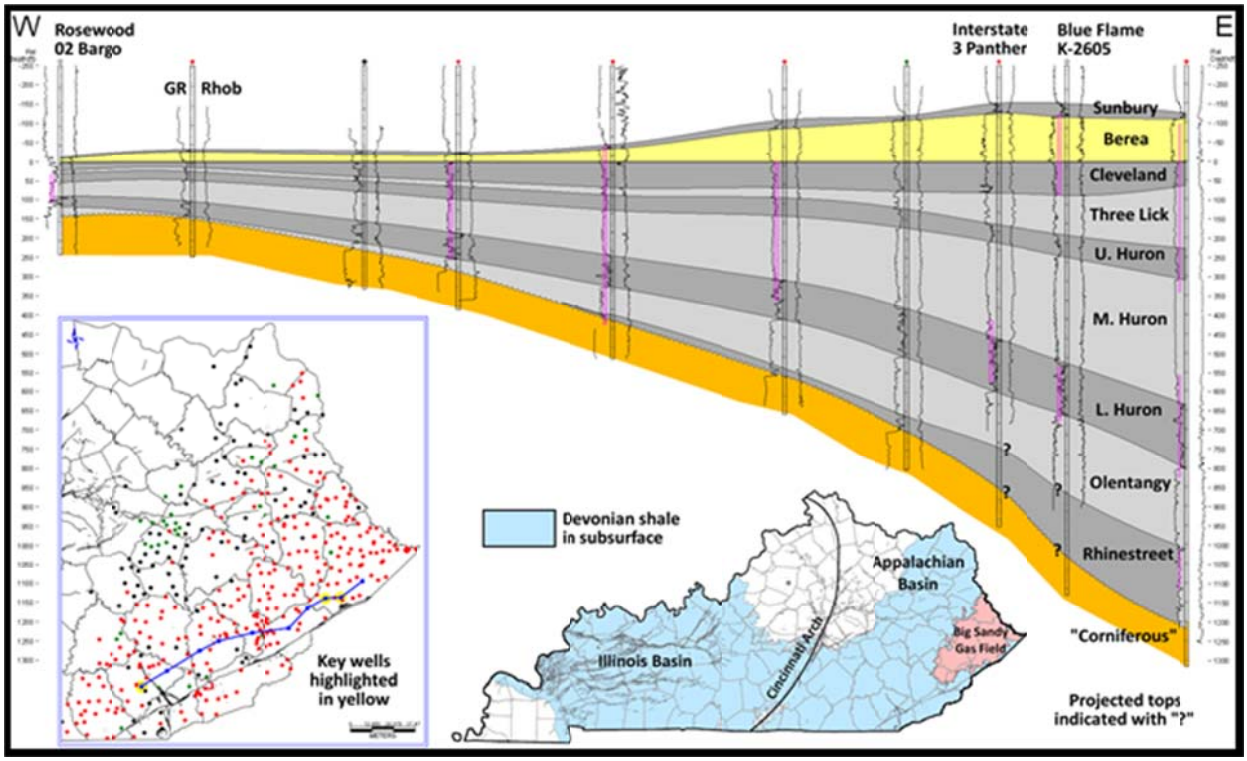


Uses the top of the Cleveland shale member of the Ohio shale, showing key wells. Dots on inset with location of cross section indicate wells for which digital wire-line log data are available for the shale interval

Figure 6: Methane and Carbon Dioxide Isotherms for Devonian Gas Shale

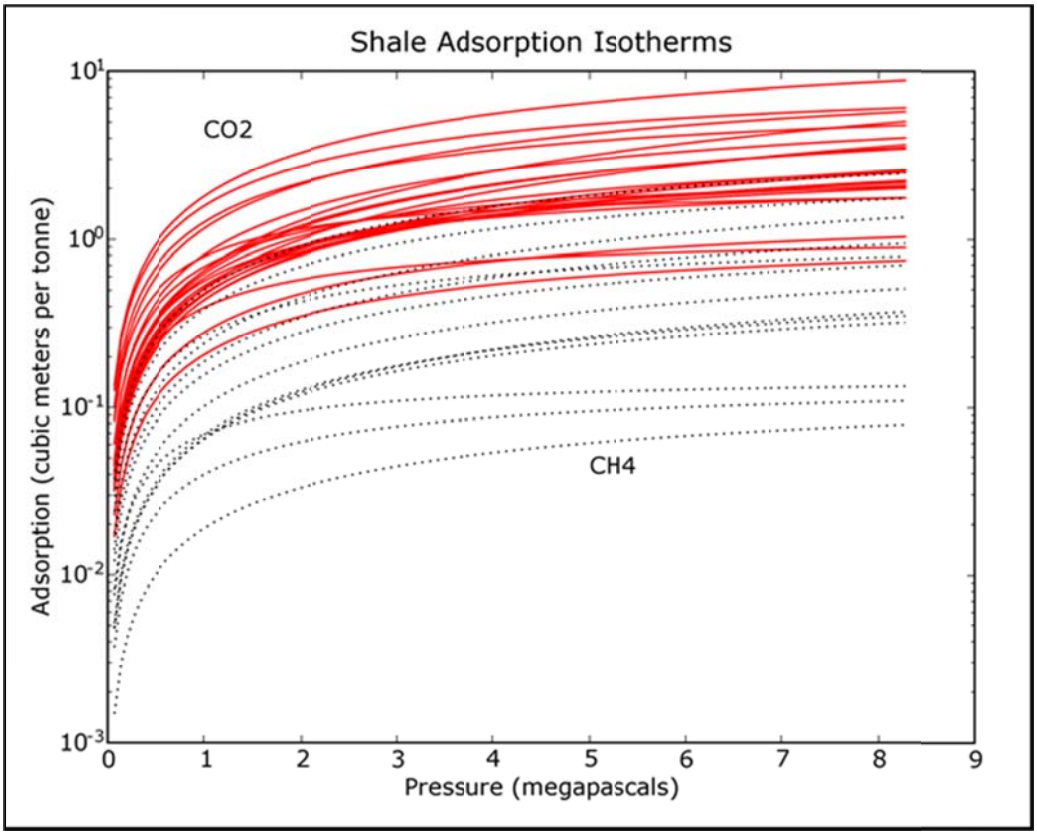

# 7. REFERENCES

Advanced Resources International (ARI). 2010. Reservoir Modeling and Simulation of the Devonian Gas Shale of Eastern Kentucky for Enhanced Gas Recovery and $CO_2$ Storage, report prepared for the Kentucky Geological Survey, January, 2010

Conant, L. C., and Swanson, V. E., 1961, Chattanooga shale and related rocks of central Tennessee and nearby areas: U.S. Geol. Survey Prof. Paper 357, 91 p.

U.S. Department of Energy, National Energy Technology Laboratory (DOE/NETL), 2006. Analysis of Devonian Black Shale in Kentucky for Potential Carbon Dioxide Sequestration and Enhanced Natural Gas Production (DOE/NETL Fact Sheet), 3/2006

Glover, Lynn. 1959. Stratigraphy and uranium content of the Chattanooga shale in northeastern Alabama, northwestern Georgia, and eastern Tennessee, USGS Bulletin: 1087-E

Hamilton-Smith, T., 1993, Gas exploration in the Devonian shales of Kentucky: Kentucky Geological Survey, ser. 11, Bulletin 4, 31 p.

Hoover, K. V. 1960. Devonian-Mississippian Shale Sequence in Ohio. Ohio Geological Information Circular no. 27. Online: http://www.netl.doe.gov/kmd/cds/disk7/disk1/EGS%5CDevonian-Mississipian%20Shale%20Sequence%20in%20Ohio.pdf. Accessed: March 2013.

Janssens, A., and de Witt Jr., W. 1976. Potential natural gas resources in the Devonian shales in Ohio: Ohio Geological Survey note 3.

Nuttall, Brandon, 2010. Reassessment of $CO_2$ Sequestration Capacity and Enhanced Gas Recovery Potential of Middle and Upper Devonian Black Shales in the Appalachian Basin, MRCSP Phase II Topical Report, October 2005–October 2010, DOE Cooperative Agreement DE-FC26-05NT42589, OCDO Grant Agreement No. DC-05-13

Nuttall, Brandon; Cortland F. Eble; James A. Drahovzal, and Mark Bustin. 2005. *Analysis of Devonian Black Shales for Potential Carbon Dioxide Sequestration and Enhanced Natural Gas Production*, Report DE-FC26-02NT41442 prepared by the Kentucky Geological Survey, University of Kentucky, for the U.S. Department of Energy, National Energy Technology Laboratory, December 30, 2005

Ohio Department of Natural Resources, (ODNR), 2011. Ohio Oil and Gas Summary. Ohio Department of Natural Resources: Division of Oil and Gas Resources Management. Online: http://ohiodnr.com/portals/11/publications/pdf/oilgas11.pdf. Accessed: March 2013.

Ray, E. O. 1975.Devonian Shale Development in Eastern Kentucky, in Natural Gas from Unconventional Geologic Sources. Board on Mineral Resources Commission on Natural Resources. U.S. Department of Energy. Online: http://www.netl.doe.gov/kmd/cds/disk7/disk1/EGS%5CDevonian%20Shale%20Development%20in%20Eastern%20Kentucky.pdf. Accessed: March 2013.

Roen, J. B. 1980. Stratigraphy of the Devonian Chattanooga and Ohio Shales And Equivalents In The Appalachian Basin: An Example of Long-Range Subsurface Correlation Using Gamma-Ray Logs. U.S. Department of Energy. http://www.netl.doe.gov/kmd/cds/disk7/disk1/EGS/Stratigraphy%20of%20the%20Devonian%20Chattanooga%20%26%20Ohio%20Shales%20%26%20Equ.pdf. Accessed: March 2013.

Schwietering, J. F. 1979. Devonian Shales of Ohio and their Eastern and Southern Equivalents. West Virginia Geological and Economic Survey for the Department of Energy contract EY-76-C-05-5199. Online: http://www.netl.doe.gov/kmd/cds/disk7/disk1/EGS%5CDevonian%20Shales%20of%20Ohio%20and%20Their%20Eastern%20and%20Southern%20Equiv.pdf. Accessed: March 2013.

Spencer, S. 2011. Upper Devonian may hold as much gas as Marcellus Shale: Range executive. Platts. 28 September, 2011. Online: http://www.platts.com/RSSFeedDetailedNews/RSSFeed/NaturalGas/6531422. Accessed: March 2013.

Thompson, D. 2010. Other Shale Formations in region have natural gas potential. Sun Gazette, Pennsylvania. 19 December, 2010. Online:http://www.sungazette.com/page/content.detail/id/557848/Other-shale-formations-in-region-have-natural-gas-potential.html. Accessed: March 2013.

Yost, A.B., R.L. Mazza, and J.B. Gehr. 1993. $CO_2$/Sand Fracturing in Devonian Shales, SPE Paper No. 26925 prepared for the 1993 Eastern Regional Conference and Exhibition, Pittsburgh, PA, U.S.A., 2-4 November

# Volume 6
# Analyses of the Targeted, Highly Monitored, Small-Scale $CO_2$ Injection Test In Kentucky

## Assessment of Factors Influencing Effective $CO_2$ Storage Capacity and Injectivity in Eastern Gas Shales

Prepared for:
U.S. Department of Energy
National Energy Technology Laboratory
DOE Award Number: DE-FE0004633

Prepared by:
Michael Godec, Principal Investigator
Advanced Resources International, Inc.
4501 Fairfax Drive ▪ Suite 910 ▪ Arlington, Virginia 22203

Date:
October 23, 2013


4501 Fairfax Drive ▪ Suite 910 ▪ Arlington, Virginia 22203 ▪ Phone: (703) 528-8420 ▪ web: www.adv-res.com

## Advanced Resources International, Inc.

# Table of Contents

**1.** INTRODUCTION ..... 1
a. Background ..... 1
i. Motivation for this test – House Bill 1 of 2007 ..... 2
ii. Role of NETL Support ..... 2
**2.** DESCRIPTION OF THE TEST SITE ..... 4
**3.** BASELINE LOGGING PRIOR TO INJECTION ..... 9
a. Description of Baseline Logging Activities ..... 9
b. Assessment of Baseline Logging Results ..... 10
**4.** MONITORING DURING THE SS#1 KENTUCKY CO2 INJECTION TEST ..... 13
**5.** POST-INJECTION LOGGING OF THE SS#1 KENTUCKY CO2 INJECTION TEST WELL ..... 17
**6.** PRELIMINARY ANALYSIS OF RESULTS OF THE SS#1 KENTUCKY CO2 INJECTION TEST ..... 20
**7.** WELL TEST ANALYSIS OF THE SS#1 KENTUCKY CO2 INJECTION TEST ..... 25
**8.** WELL TEST ANALYSIS OF THE SS#1 KENTUCKY CO2 INJECTION TEST...ERROR! BOOKMARK NOT DEFINED.

# List of Figures

Figure 1. Preliminary planned test (TEST) and monitor (MON) well locations for the KY injection test. Test well location included shallow monitoring well offset about 3 meters (10 feet) from test the well. However, the proposed monitor well to the southeast of the test well was discovered to have been abandoned and was not locatable.....5

Figure 2. Final location of injection and shallow monitoring well for the KY injection test, relative to two nearby wells used for characterizing the subsurface at the test site. .....6

Figure 3. Review of surface features near the injection and shallow monitoring well at the KY injection test site. .....7

Figure 4. Portion of the open-hole lithodensity log showing annotations interpreted to indicate locations of perforations in the well at the KY CO2 injection test site.....8

Figure 5. Tool used for multi-finger caliper (PMIT) logging .....9

Figure 6. Summary of multi-arm caliper and spinner surveys with respect to original gamma ray (GR) and gamma ray traces acquired during multiple spinner runs.....11

Figure 7. Results of the baseline logging run performed with the Spinner and Reservoir Saturation Tool .....12

Figure 8. Schematic of the SS#1 Kentucky Injection Test Well .....13

Figure 9. Backside annulus pressure measured on September 12 .....16

Figure 10. Field connection of the Bloodhound unit, along with the Bloodhound and gas sampling equipment in the truck. .....18

Figure 11. Monitored pressure and temperature data in the injection well (SS#1), the nearby shallow offset well (SS#1a) and two farther offset wells (SS#2 and SS#2); with the inset showing the pressure during the three CO2 injection cycles.....21

Figure 12. Monitored temperature data in the injection well (SS#1), the nearby shallow offset well (SS#1a) and two farther offset wells (SS#2 and SS#2) from the surface Datatraps.....22

Figure 13. Monitored temperature data in the injection well (SS#1), the nearby shallow offset well (SS#1a) and two farther offset wells (SS#2 and SS#2) for each of the three CO2 injection cycles.....23

Figure 14. Pressure fall off data over the three injection stages .....24

# 1. INTRODUCTION

## a. Background

Building upon advances in horizontal drilling and hydraulic fracturing technologies, production of natural gas from organic-rich gas shale formations is rapidly developing as a major hydrocarbon energy supply option in North America and around the world. Gas shale formations may also represent potential targets for the geologic storage of $CO_2$ based on trapping through adsorption on organic material, although this has not been demonstrated on a field scale. The same technologies – horizontal drilling and hydraulic fracturing – contributing to the recent rapid development of shale gas also open up the possibility of using shale formations as storage media for $CO_2$ by increasing permeability and injectivity, allowing storage to potentially be more cost effective.

Organic-rich gas shales are recognized as sharing some of the same methane storage characteristics as coal seams. Natural gas is adsorbed on kerogen and clay surfaces in gas shales, similar to methane storage within coal seams. Gas is also stored as "free" (non-adsorbed) gas in fracture porosity and inter-granular micro-porosity, as well as in the micro-pores commonly observed in the kerogen of thermally mature shale (intra-kerogen porosity). The relative amounts of adsorbed and "free" gas recovered during the producing life of a shale gas well are unknown, and are very likely to be dependent on the specific characteristics of the shale formation.

Of the various options for $CO_2$ storage, storing $CO_2$ in shales has particular advantages. Relative to storage in saline aquifers, $CO_2$ injection can enhance methane production, the revenues from which can help offset the costs of storage. Another benefit is that the risk of leakage is low, as the in-place methane has proven that adsorption, retention and seal have been effective for millions of years. Finally, gas shales are widespread; and significant concentrations of large $CO_2$ emission sources exists in the eastern United States, where finding suitable geologic storage sites has proven difficult.

Although still at a conceptual stage, $CO_2$ storage in gas shales is attracting increasing interest in the eastern United States, which is endowed with extensive shale deposits, but limited $CO_2$ storage capacity in conventional porous reservoirs (DOE/NETL, 2010).

In particular, shales dominate the Middle and Late Devonian strata of the Appalachian Basin. Black, organic-rich units alternate with gray shales consisting mostly of quartz and clay minerals. The shale overlies strata that vary in age from Upper Ordovician through Middle Devonian. The shale ranges in thickness from outcrops in places along the crest of the Cincinnati Arch to more than 3,600 feet in West Virginia. In the gas productive areas of

Kentucky, the shale is typically 200 to 1,600 feet thick. The shale ranges in depth from the outcropping on the western margin of the basin to more than 4,000 feet.

Shale gas production was discovered in eastern Kentucky around 1892 with the drilling of wells along Beaver Creek in Floyd County. Today, more than 6,000 shale gas wells are producing between 50 and 70 billion cubic feet (Bcf) of gas annually in Kentucky. Many of these wells are located in the Big Sandy gas field of Floyd, Knott, Letcher, Martin, and Pike Counties.

## b. Motivation for this Test – House Bill 1 of 2007

In 2005, a study of adsorption in the Ohio Shale in Kentucky concluded $CO_2$ is preferentially adsorbed with respect to methane at an average volumetric ratio of 5:1 (Nuttall, et al, 2005); and thus, preferential adsorption may contribute to the enhancement of methane production. A new study was initiated to identify candidate wells, conduct reservoir modeling to design a test protocol, and conduct a pressure transient test simulating recompletion of a well to acquire data to improve understanding of enhancing production from gas shales.

Anticipating requirements to mitigate $CO_2$ emissions resulting from the use of coal in Kentucky, the Kentucky State Legislature passed House Bill (HB) 1 in a 2007 special session. This bill authorized funding for research by the Kentucky Geological Survey (KGS) in the areas of $CO_2$ enhanced oil recovery, $CO_2$ enhanced gas recovery, and permanent geologic storage of $CO_2$.[1]

Among a variety of activities, HB 1 included a mandate and funding to test the black shale for $CO_2$ enhanced gas recovery potential in Kentucky. The bill encouraged the KGS, the lead state agency on the effort, to partner with industry and other government bodies to share the cost of this important research. The Kentucky Consortium for Carbon Sequestration was formed to accomplish this goal.

## c. Role of NETL Support

Thus, the activity associated with the targeted, monitored, small-scale $CO_2$ injection test in Kentucky that is the subject of this report was funded by the State of Kentucky with funds appropriated under HB 1. This included costs for support for personnel from the University of Kentucky and the KGS, wellhead gas sampling, site pad clearing, construction, road improvements, deployment of downhole and surface readout monitors, running the casing hanger, slickline deployment of a downhole memory recording operation (MRO), rig services, tubing, packer, various rental of equipment, and $CO_2$ supply, storage, and handling.

[1] http://www.uky.edu/KGS/kyccs/

NETL support to this effort involved the procurement of logging services for the test. Logging services included three logging runs: a baseline logging run prior to injection, a logging run during injection operations, and a logging run after injection operations were complete. Support under this contract also included analyses of the data collected during the test, as well as the incorporation of the data obtained from the test for improved and updated resource characterization and simulation work pertaining to the characterization of the enhanced gas recovery and $CO_2$ storage potential of the Ohio Devonian shale resource in Kentucky.

The primary objective of this report is to document the activities associated with the test and the analyses of data collected during the test.

# 2. DESCRIPTION OF THE TEST SITE

The original plan was for the eastern Kentucky test was to perform $CO_2$ injection into one $CO_2$ injection well and three nearby wells that were to be monitored for $CO_2$ breakthrough. For this test, the plan was to continuously inject approximately 300 to 500 metric tonnes of $CO_2$, where the $CO_2$ would displace natural gas toward surrounding wells, especially those wells that offset the injector in the direction of the major regional natural fracture system. These nearby wells would be continuously monitored for gas composition, ambient temperature, flowing pressure, volume, and rate.

At the time of the original project proposal, access had been granted from the owner of the surface and mineral rights at a site in Pike County, Kentucky. For this site, initial environmental reviews had been performed, approval for the test had been obtained from appropriate Kentucky state regulatory officials, and plans for the test were underway, planned for the spring of 2011.

However, the owner of this site ultimately changed business plans and decided not to participate in the research project, withdrawing permission for the test to be conducted at the site. This caused the KGS to need to find a new site for the $CO_2$ injection test. A new site was secured in central Johnson County in eastern Kentucky, agreements were finalized for access to the new site, a new Environmental Questionnaire was submitted to DOE/NETL and was reviewed and approved, and approval for the test was also obtained from appropriate Kentucky state regulatory officials.

The well made available for the test is the Interstate Natural Gas Company SS#1 Fee well, located off Sulfur Spring Road, north of Paintsville, Johnson County, in eastern Kentucky. The location of the well site for the test, and the originally planned site configuration, is shown in **Figure 1**. However, the proposed monitor well to the southeast of the test well was discovered to have been abandoned and was not locatable. Thus, the final well configuration for the test is shown in **Figure 2**. The proposed project area is predominantly rural and has had significant historical oil and gas drilling and coal mining activity. The injection well is located on a reclaimed surface coal mine site (**Figure 3**).

Figure 1. Preliminary planned test (TEST) and monitor (MON) well locations for the KY injection test. Test well location included shallow monitoring well offset about 3 meters (10 feet) from test the well. However, the proposed monitor well to the southeast of the test well was discovered to have been abandoned and was not locatable.

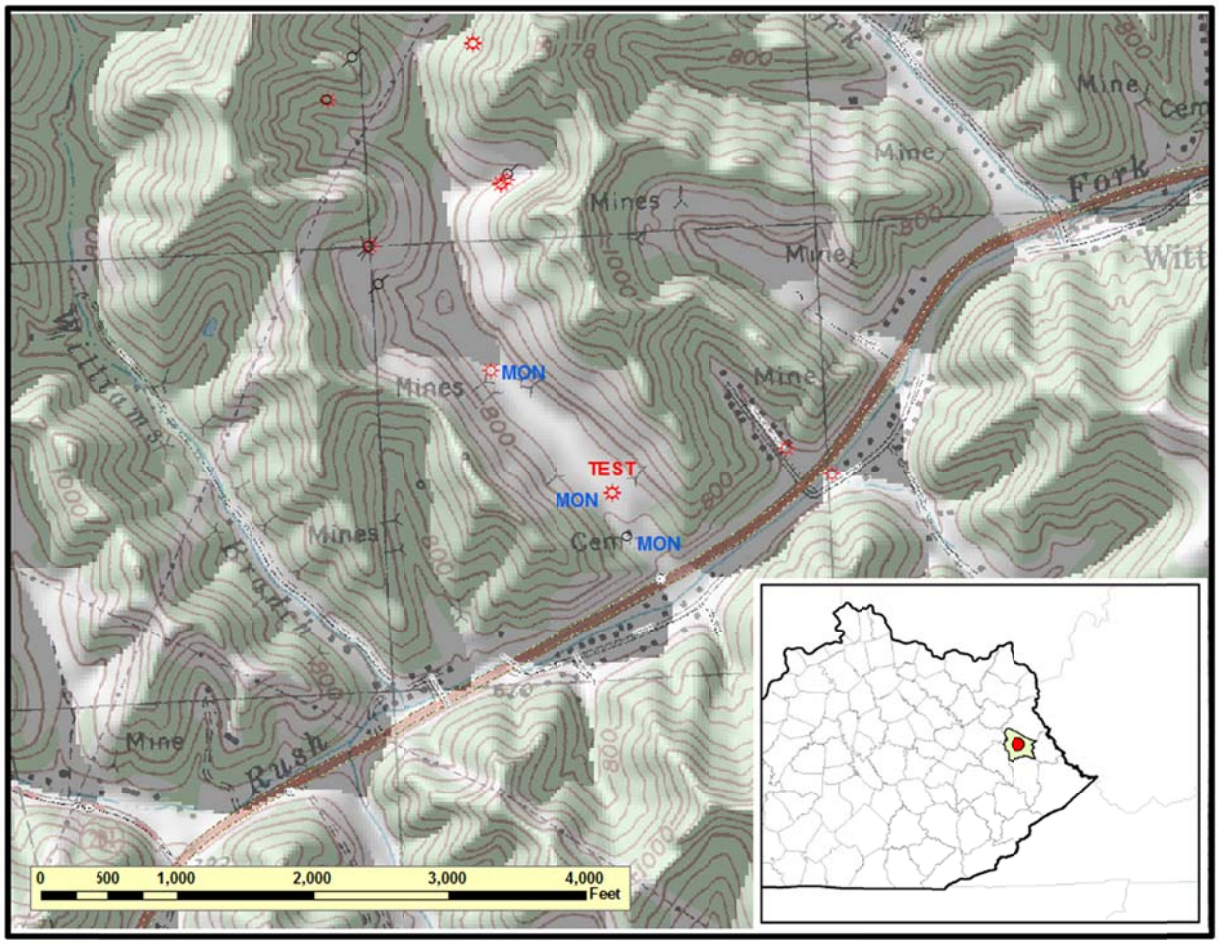


Source: Kentucky Geological Survey

Figure 2. Final location of injection and shallow monitoring well for the KY injection test, relative to two nearby wells used for characterizing the subsurface at the test site.


Source: Kentucky Geological Survey

Figure 3. Review of surface features near the injection and shallow monitoring well at the KY injection test site.


Source: Kentucky Geological Survey

The well was originally drilled and completed on May 27, 2002 to a depth of 1,910 feet. A standard set of open-hole nuclear logs was acquired at the time. In constructing the well, 1,808 feet of 4.5-inch casing was cemented into place and perforated across the Devonian Ohio Shale and Mississippian Berea sand intervals between 1,130 and 1,672 feet.

While no record is available describing the placement of the perforations or the manner (pump rate, breakdown pressures, etc.) of the original fracture stimulation, hand written arrows at irregular intervals were noted on the lithodensity logs on file with the State of Kentucky (**Figure 4**). These annotations were assumed to indicate the position of perforations duly noted at depths (in feet) of 1,672, 1,603, 1,520, 1,401, 1,369, 1,312, 1,274, 1,204, 1,171, 1,144, and 1,126.

Figure 4. Portion of the open-hole lithodensity log showing annotations interpreted to indicate locations of perforations in the well at the KY CO2 injection test site.

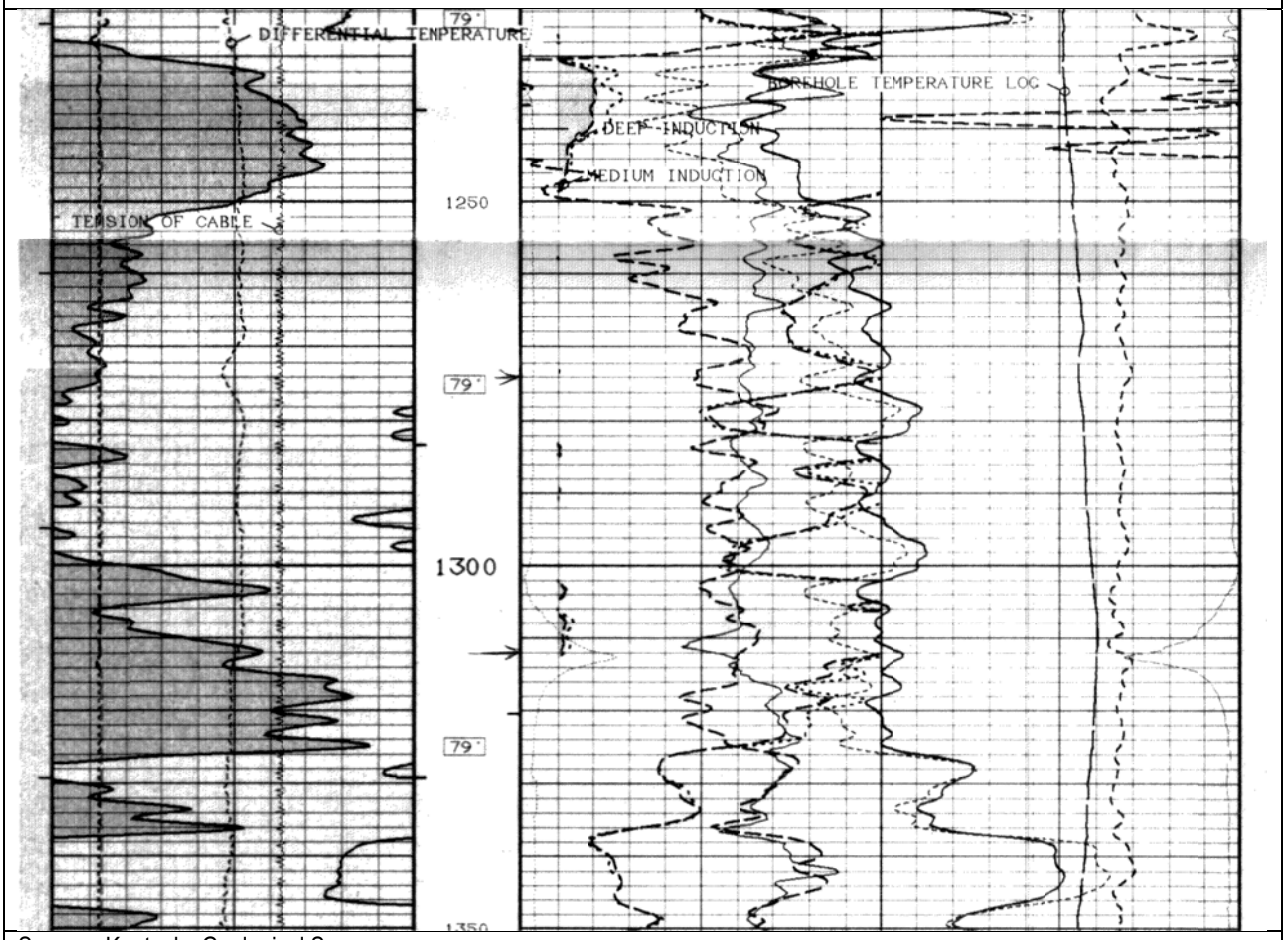


Source: Kentucky Geological Survey

# 3. BASELINE LOGGING PRIOR TO INJECTION

## a. Description of Baseline Logging Activities

In the fall of 2011, baseline logging was completed. The logging runs were conducted by Schlumberger Carbon Services. Initial baseline logging included the reservoir saturation tool (RST), PBMS (pressure & temperature), a Spinner log, and a multi-finger caliper (PMIT) log (**Figure 5**). DOE/NETL paid for the logging runs, with all other activities paid by the State of Kentucky.

Figure 5. Tool used for multi-finger caliper (PMIT) logging


Source: Kentucky Geological Survey

The multi-finger micro-caliper was run to determine the existence of perforations; a total of nine indentations and projections were identified. A spinner log was run over the perforated interval in three down and three up passes at different speeds; open perforations were identified at depths between 1,311 and 1,142 feet across the Upper Cleveland Member of the Ohio Shale and Berea formations. Initial reservoir characterization data were acquired with two runs of the RST in lithology and sigma capture cross section modes.

## b. Assessment of Baseline Logging Results

Multiple spinner surveys were run in up and down passes at 30, 60, and 90 minutes per foot over the interval from 1,100 feet to 1,700 feet. The gamma ray trace from the open-hole log suite was digitized by the KGS and was overlaid with the gamma ray traces from the three upward runs of the spinner tool. To facilitate comparison of the original gamma ray to the newly acquired data, the plot of the original trace was shifted left by 68.8 API units, the average difference between the average of the traces recorded during the spinner runs and the original gamma ray. Correspondence of the various gamma ray traces is very good.

**Figure 6** presents a summary of the perforations detected by the multi-arm caliper compared to the inferred perforation depths and the spinner surveys.

The multi-arm caliper tool detected indentations in the casing at 1,142, 1,203, 1,274, 1,311, 1,368.5, 1,514.5, and 1,666 feet (Figure 6, yellow circles) that correspond to the inferred perforation depths. Additionally, two projections into the casing were detected at depths of 1,123 and 1,170 feet. These projections correspond to the depths of two inferred perforations. Down passes of the spinner indicate flow (spinner curve deflections) from the inferred (but not detected) perforation at 1,603 and the perforation at 1,514.5. The spinner tool was set on stations at depths of 1,120, 1,138, 1,165, 1,198, 1,269, 1,308, 1,320, 1,363, 1,397, 1,515, 1,598, 1,660, and 1,670. No flow was reliably detected at stations below 1,320 feet. The spinner flow data for the three up passes are depicted on Figure 6.

The results of the baseline logging run performed with the Spinner and RST are shown in **Figure 7**.

Figure 6. Summary of multi-arm caliper and spinner surveys with respect to original gamma ray (GR) and gamma ray traces acquired during multiple spinner runs.

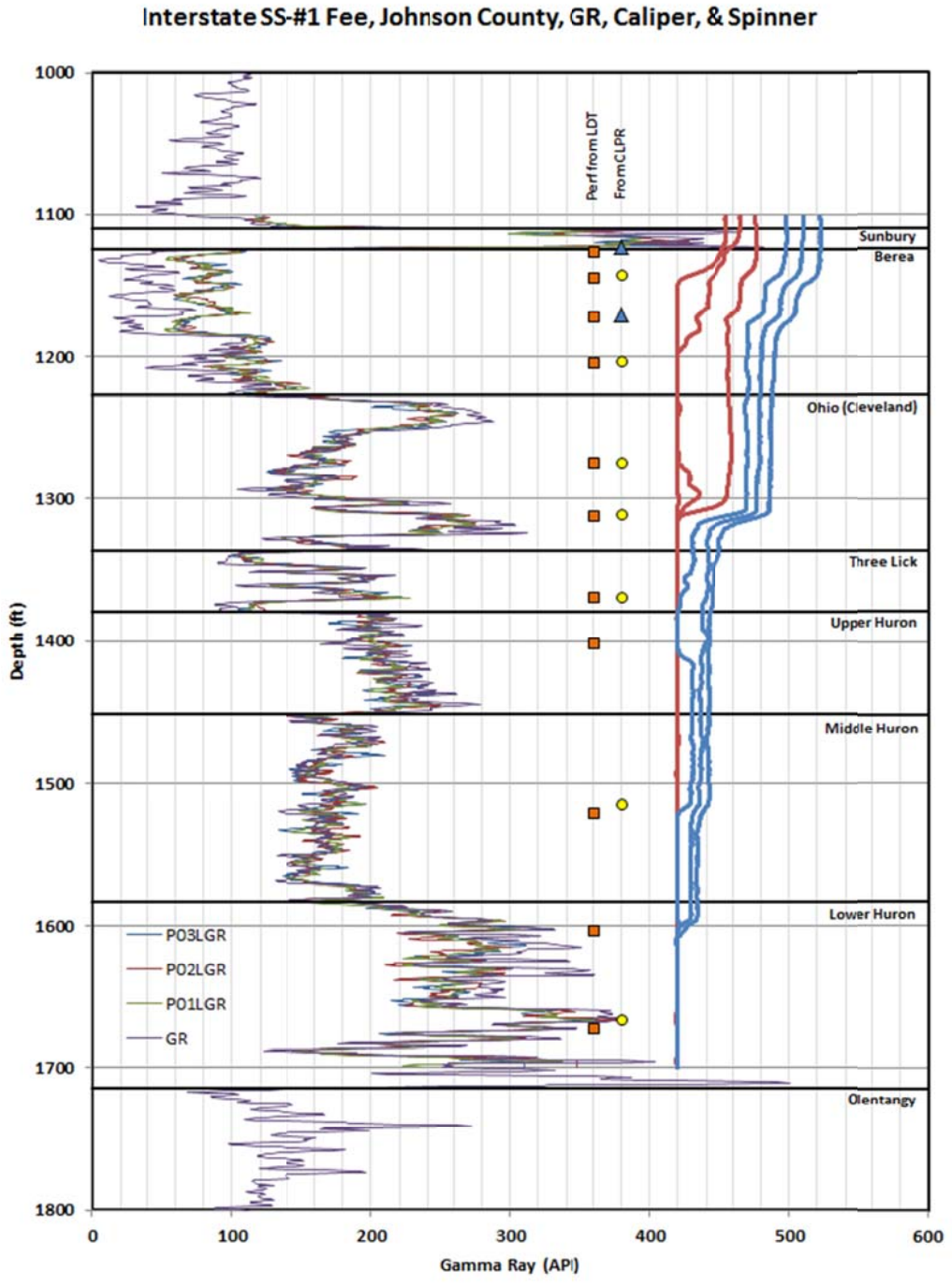


Source: Kentucky Geological Survey

Figure 7. Results of the Baseline Logging Run Performed with the Spinner and Reservoir Saturation Tool

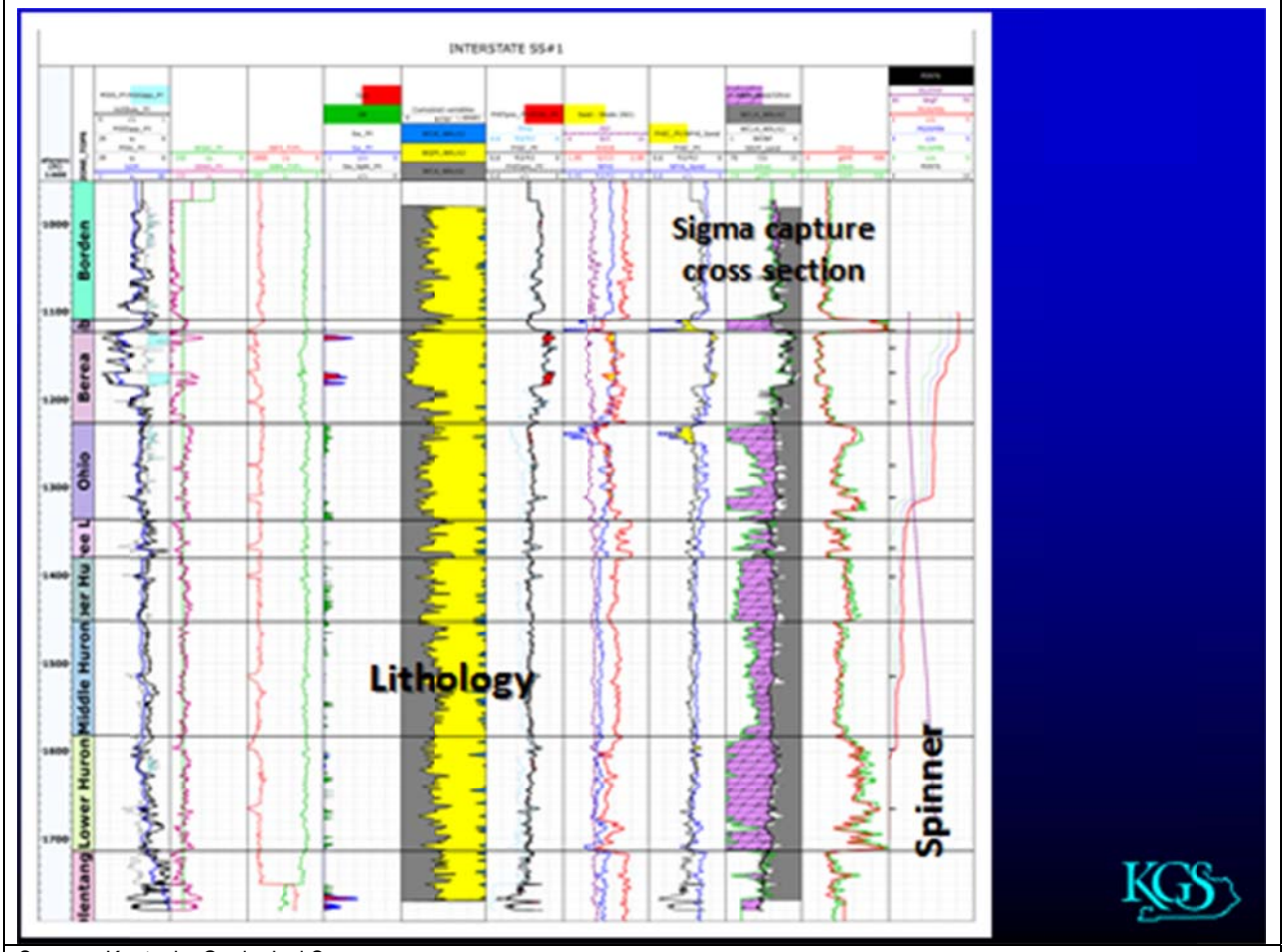


Source: Kentucky Geological Survey

# 4. MONITORING DURING THE SS#1 KENTUCKY CO2 INJECTION TEST

The $CO_2$ injection test took place in late September 2012. KGS led the injection test, Crossrock Drilling, LLC provided well operations and services, Ferus Inc. provided $CO_2$ storage and supply services, Nabors Well Services provided the $CO_2$ pumping services, and Advanced Resources International (supported under this contract) oversaw logging operations and led the well test analysis and modeling activities.

The injection target was the Devonian Ohio shale. The well was perforated with approximately seven shots (based on the original well log) from 1,274 feet to 1,672 feet. Perforations were present in the well casing above the tubing/packer, which was set at 1,264 feet. There were four perforations in the Berea (sandstone) and Sudbury Formations from 1,126 feet to 1,204 feet, which were not a target for injection.

A schematic of the test well is shown in **Figure 8**.

Figure 8. Schematic of the SS#1 Kentucky Injection Test Well

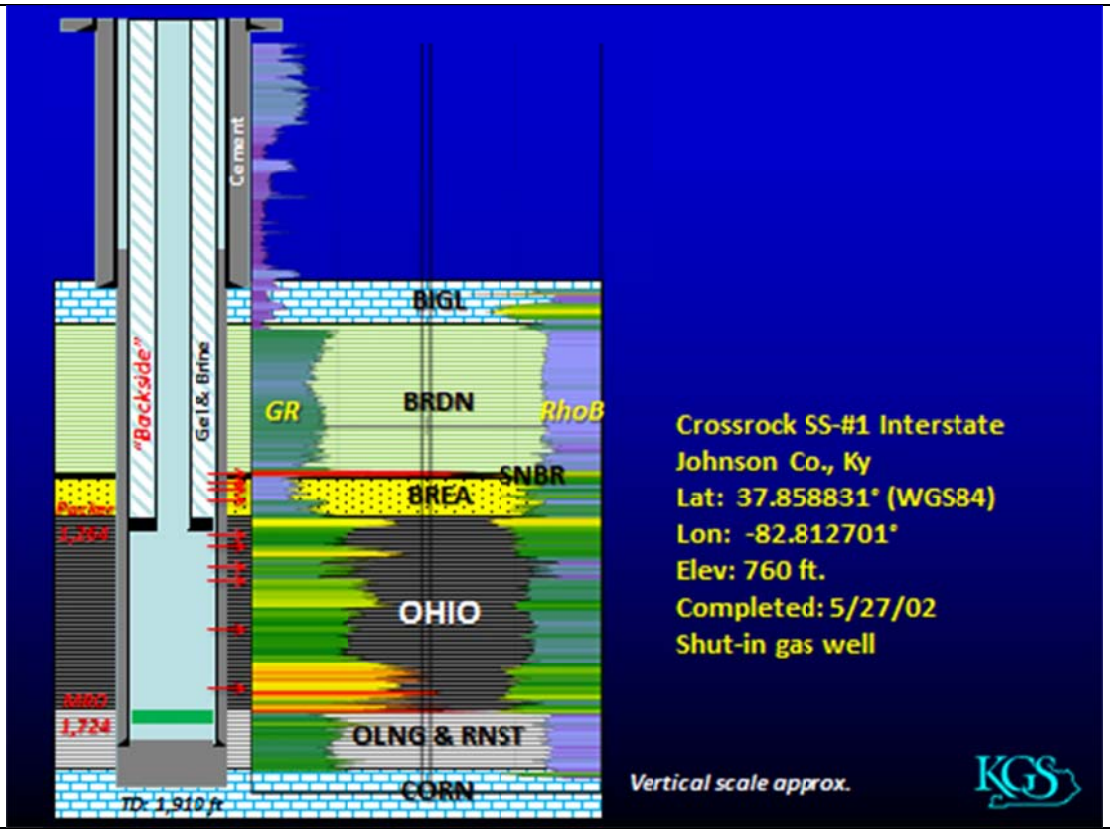


Source: Kentucky Geological Survey

The casing annulus was filled with gel and KCl brine. During injection and flow back operations, tubing pressures and temperature (wellhead) were recorded using Datatrap memory gauges. Downhole pressures and temperatures were recorded on digital memory gauges (set beneath the bottom perforation at 1,710 feet). Baseline shut-in pressure of the well was about 300 pounds per square inch (psi). The SS#1 casing annulus pressure was monitored with an analog pressure gauge. The shallow nearby offset well (SS#1a) and two farther offset wells (SS#2 and SS#2) were also equipped with surface memory pressure/temperature Datatrap gauges.

The first tool went into the well to clean the well and check for obstructions. The junk basket encountered fluid in the well at 1,754 feet, which was deep enough to access the zones of interest for logging. Logging depths were calibrated using an open-hole gamma-ray log from May of 2002.

The logging began with the 56-arm caliper tool. It was run from a depth of 1,785 feet to 1,000 feet to confirm the presence and depths of the well's perforations. Perforations were found and matched those from previous well logs. The full-bore spinner tool was run in both directions through the perforated section from 1,790 feet up to 1,100 feet to check flow across the perforations. Passes were made at 30, 60, and 90 feet per minute. Additional stationary checks were made at perforation depths of 1,120, 1,138, 1,165, 1,198, 1,269, 1,308, 1,320, 1,363, 1,397, 1,515, 1,598, 1,660, and 1,670 feet to check individual flow. After the spinner log was completed, Schlumberger requested work stoppage due to darkness on the well site.

$CO_2$ injection operations began on September 6, where 21 tons of $CO_2$ were pumped at 600 to 650 standard cubic feet per minute (scf/min) (3 barrels per minute) or 2.5 tons per hour. Shut in pressure at end of operations in the afternoon was 840 psi and by the morning of September 7, the shut in pressure had dropped to 580 psi.

Operations continued on September 7. Surface pressure had an initial rise from the shut in pressure of 580 psi to about 840 psi and slowly climbed to 890 psi. About 22 tons of $CO_2$ were pumped on September 7, pumping at 2.5 tons per hour. Injection operations were shut down in the afternoon. $CO_2$ injection operations re-started on Monday, September 10. $CO_2$ rates of 650 to 700 scf/min were maintained at pressures similar to those on September 6 and 7. Also on September 10, an injection survey and a step rate test were conducted to evaluate pressures at higher pumping rates.

In total, 87 tons of $CO_2$ was injected over the three days.

Parker Energy Services/Schlumberger Carbon Services arrived on location on September 10 to attempt a wire line injection spinner survey. The purpose of the spinner survey was to identify those perforations that were accepting the $CO_2$ volume and to determine the

relative percentages of $CO_2$ going into the flowing perfs. The spinner survey program included 4 passes, at rates of 30 feet per minute (ft/min), 60 ft/min, 90 ft/min and 120 ft/min pass. The spinner tool string (gamma ray detector, memory readout spinner tool and temperature/pressure probes) was run in at 11 a.m. The $CO_2$ injection rate was held steady throughout the spinner survey (at about 2.5 tons per hour rate at a pressure of about 850 psi). The survey was completed around 2:30 p.m., and Schlumberger attempted to download the data from the tool's memory card. Unfortunately, while the card apparently showed that data were recorded, it gave an error message when they tried to download it. Subsequent efforts to download the data at Schlumberger's shop were unsuccessful. A post-injection spinner survey was conducted during flow back operations.

At end of operations on September 10, after Schlumberger rigged down, a decision was made to try increasing the pump rates. With times approximate, observations made of flow data from displays in the Nabors van were as follows:

- 3:20 p.m.: 4th gear (pump truck) – pressure to 940 psi
- 3:22 p.m.: 5th gear – pressure to 950 psi, surface injection rate to 1.4 Mcf/min
- 3:26 p.m.: 6th gear – pressure to 960 psi, surface injection rate to 1.5 Mcf/min
- 3:29 p.m.: pressure to 970 psi
- 3:30 p.m.: 7th gear – pressure to 980 psi, pumping rate 1.5 Mcf/min, rate and pressure stayed steady for about 10 minutes when the volume of usable $CO_2$ ran out. This is equivalent to about 5.7 tons per hour.

On September 12, a shut in pressure of 590 psi was discovered on the casing annulus (i.e., the "backside annulus") above the packer (**Figure 9**). This pressure was roughly equivalent to the injection tubing's shut in pressure, suggesting communication between the injection tubing and the casing annulus. Potential causes of the communication that were hypothesized included packer failure, communication between formations through induced fractures (the well was fracture stimulated using nitrogen), or entry into the annulus of gas produced from the Berea or Sunbury formations.

A decision was made to end the injection and proceed to flowing back the well.

Figure 9. Backside annulus pressure measured on September 12


Source: Kentucky Geological Survey

# 5. POST-INJECTION LOGGING OF THE SS#1 KENTUCKY $CO_2$ INJECTION TEST WELL

On September 25, post injection logging and flow back operations were started on the SS#1. Prior to the flow back, a post injection RST log was run. The RST, a pulsed neutron tool, was run in "Sigma" mode, which measures the neutron capture cross section of the formation. The capture cross section is defined as the relative ability of the formation (and pore fluids) to "capture" or absorb free thermal neutrons. Chlorine has a high capture cross section and $CO_2$ has a low capture cross section. The intention was to compare the results of the post injection sigma log to the pre-injection baseline sigma log. An anomalous drop in the capture cross section will indicate $CO_2$ buildup. Advanced Resources did not perform this comparative analysis, and as of completion of this report, Schlumberger has not provided a final analysis.

At 10:45 a.m., the top ball valve was opened for the RST logging run. The surface data logger indicated the tubing pressure was 370 psia. After the RST run was complete, the top valve was closed about 1:00 p.m. and the lubricator vented.

For monitoring flow back, a meter run was constructed of 2-inch tubing connected to a full-port ball valve on the well head. The meter run included a NuFlo™ Scanner® 2000 microEFM digital flow meter and a gas expansion chamber with fittings for an iBall Instruments Bloodhound™ gas analyzer (**Figure 10**). The flow meter recorded flow volumes and temperature across a restrictive choke plate. Initial calculations based on Halliburton formulae (1985, p. 60) (Halliburton, 1985) suggested an estimated 0.25-inch diameter choke orifice. Based on experience of field personnel with the supply company providing the meter, a 1.375-inch choke size was selected. The Bloodhound™ gas analyzer is a self-contained unit often used in oilfield mud logging applications for the detection of methane, ethane, propane, isobutane, normal-butane, oxygen, $CO_2$, and hydrogen sulfide to document gas shows and detect potentially unsafe drilling conditions. An expansion chamber to prevent over pressuring the gas supply to the Bloodhound unit was installed at the end of the meter run. In retrospective, this position may have contributed to atmospheric contamination of the measured gas compositions. The Bloodhound™ unit was plumbed to a valve assembly and small canister gas samples were acquired for more complete analysis by Isotech® Laboratories.

Figure 10. Field connection of the Bloodhound unit, along with the Bloodhound and gas sampling equipment in the truck.

Source: Kentucky Geological Survey

A spinner survey was conducted at the start of the flow back operations. Due to the failure of the injection phase spinner survey and the termination of the injection after September 10, this was the only way to determine which perforations flowed $CO_2$ (and, by assumption, which perforations accepted the $CO_2$ during injection). The top valve was opened for the spinner survey at 2 p.m. At 2:34 p.m., the well was opened to start flow back for the spinner run and the first IsoTech isotube sample was collected as soon as the Bloodhound unit detected gas. The tubing pressure was noted to be 364 psi at 3:00 p.m. and read the same at 3:06 p.m., while pressure readout on the spinner tool showed 30 psi. A check of the ball valve for the tubing pressure Datatrap showed that it had been closed at some time during rigging in and out. The valve was reopened at 3:17 p.m. and read 28 psi, matching Schlumberger's readout.

The spinner survey program included four passes, a 30 ft/min, 60 ft/min, 90 ft/min and 120 ft/min pass. During the spinner run, at 4:00 p.m., flowing tubing pressure (Datatrap) was 23 psi and the backside annulus pressure 350 psi. At 4:00 p.m., the flowback was halted to allow Schlumberger to rig out. At 5:12 p.m., the tubing pressure in the SS-#1 had built up to 244 psi and the backside annulus was still 350 psi, but seemed to be dropping slightly. At 5:46 p.m., the tubing pressure was 256 psi and the backside pressure read lower, maybe 340 psi. This further suggested the presence of communication between the backside annulus and the injection tubing. Flowback was resumed at 6 p.m.

The initial flow back $CO_2$ concentration levels were around 9.8% and dropped to 6.6% by the end of the spinner flow test. Horizon collected five isotubes from the flow test and two additional isotubes once the well was opened for the remainder of the flow back operation on September 25. The gas readings reached a peak of just over 3,200 units. On September 26, the Bloodhound reported total gas units of 2,017 to 2,140 and $CO_2$ concentrations at 6.08% to 6.18%. The well was flowing steadily at 22 to 23 psi and had a backside annulus pressure of 300 psi (declining to 290 psi by the end of the day). Two isotube samples were collected on September 26. On September 27, the Bloodhound reported total gas units at 1,820 units and $CO_2$ concentration at 5.61%. One isotube sample was collected on both September 27 and 28. The final flowing tubing pressure on the data logger on the SS-#1 was 18.7 psi.. Horizon rigged down on September 28.

# 6. PRELIMINARY ANALYSIS OF RESULTS OF THE SS#1 KENTUCKY $CO_2$ INJECTION TEST

Pressure and temperature data were collected before, during and after the injection of $CO_2$. Pressure and temperature was monitored in the injection well (SS#1), the nearby shallow offset well (SS#1a) and two farther offset wells (SS#2 and SS#2) equipped with surface memory pressure/temperature Datatrap gauges. Pressure and temperature data for all the wells is shown in **Figure 11**, with the inset showing the pressure during the three $CO_2$ injection cycles.

More detailed temperature data for all the wells is shown in **Figure 12**, with the temperatures during each of the three injection cycles shown in **Figure 13**. It should be noted that these data are the temperature records from the surface Datatraps. With that in mind, they record the daily temperature fluctuations induced by day time heating of the exposed (and un-insulated) well head.

Pressure fall off data were recorded after each of the three injection stages, and are shown in **Figure 14.**

Post injection operations included well logging, flow back of the injection well, and compositional and volumetric monitoring of the vented gas. Schlumberger Carbon Services conducted the well logging and Horizon Well Logging operated the Bloodhound instrument for monitoring changing gas content during the flow back. Horizon also took gas samples for compositional and isotopic analysis at IsoTech. The $CO_2$ venting line was equipped with an orifice meter to monitor and digitally record injection volumes.

Figure 11. Monitored pressure and temperature data in the injection well (SS#1), the nearby shallow offset well (SS#1a) and two farther offset wells (SS#2 and SS#2); with the inset showing the pressure during the three CO2 injection cycles

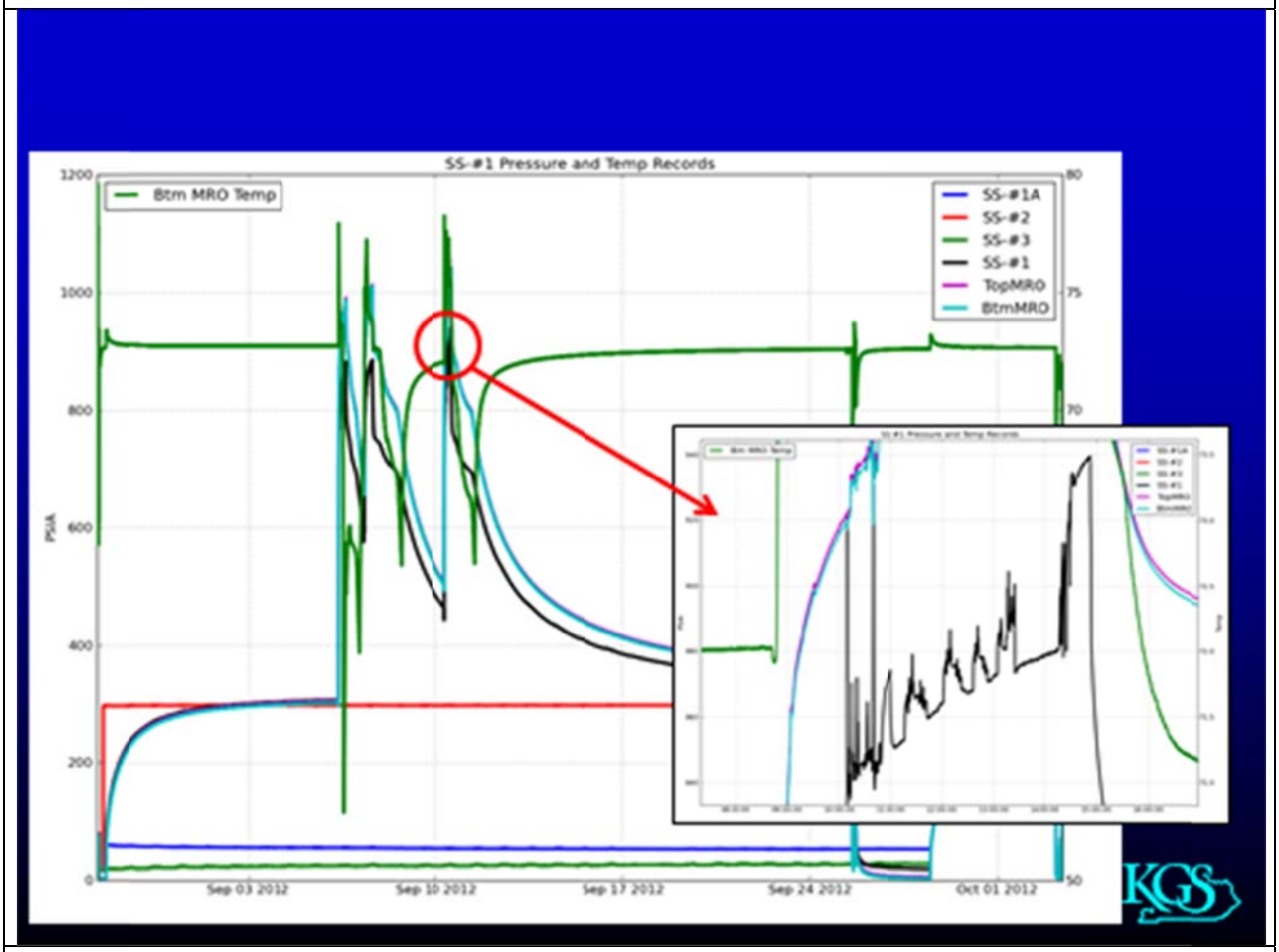


Source: Kentucky Geological Survey

Figure 12. Monitored temperature data in the injection well (SS#1), the nearby shallow offset well (SS#1a) and two farther offset wells (SS#2 and SS#2) from the surface Datatraps.

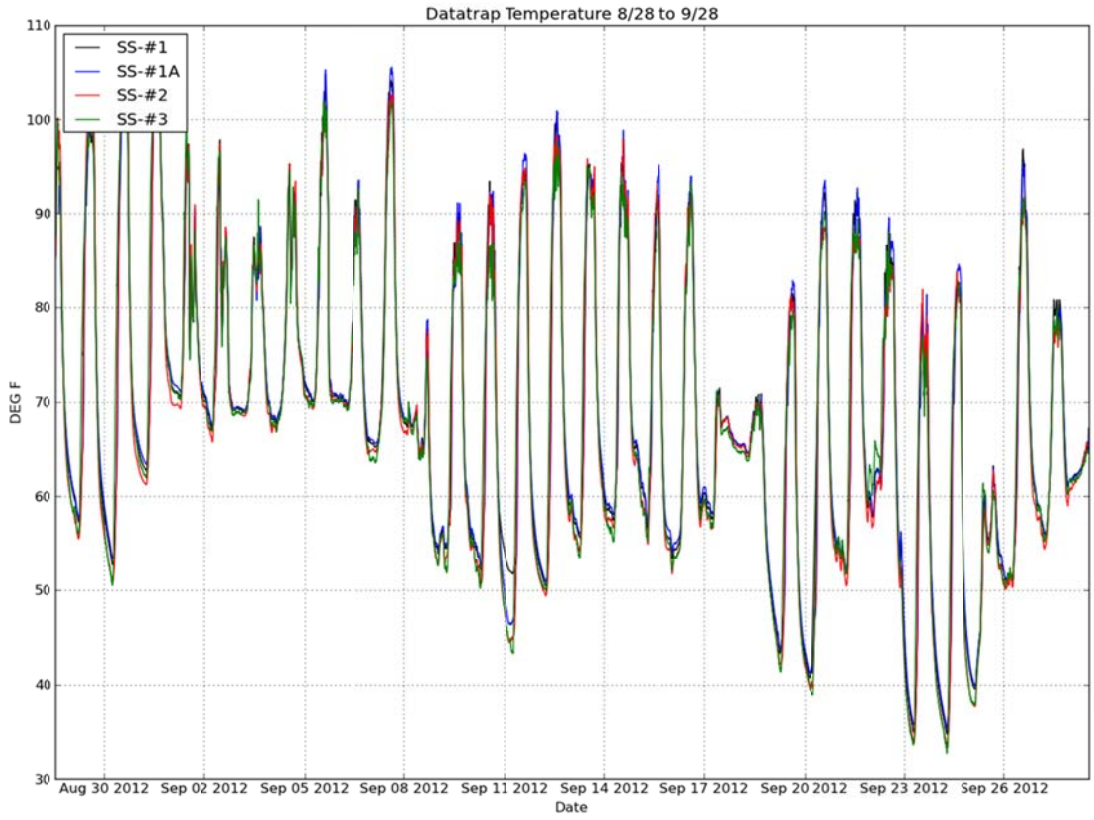


Source: Kentucky Geological Survey

Figure 13. Monitored temperature data in the injection well (SS#1), the nearby shallow offset well (SS#1a) and two farther offset wells (SS#2 and SS#2) for each of the three CO2 injection cycles

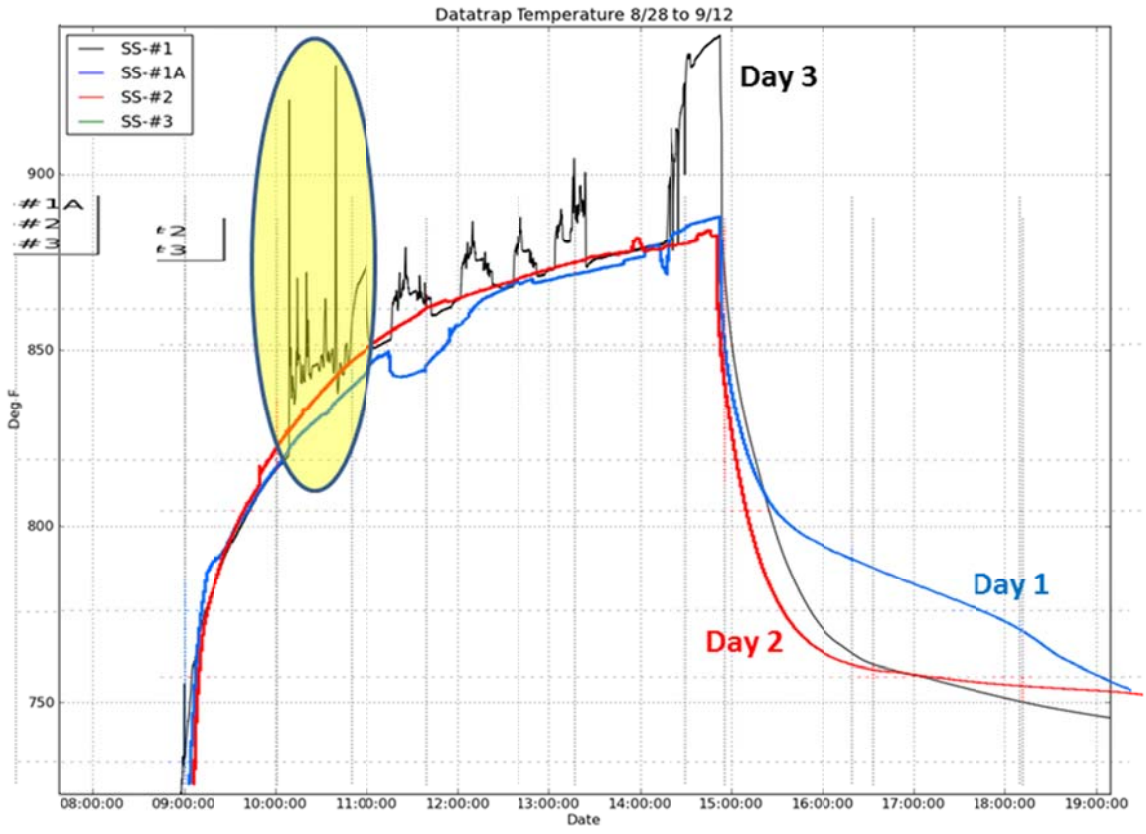


Source: Kentucky Geological Survey

Figure 14. Pressure fall off data over the three injection stages

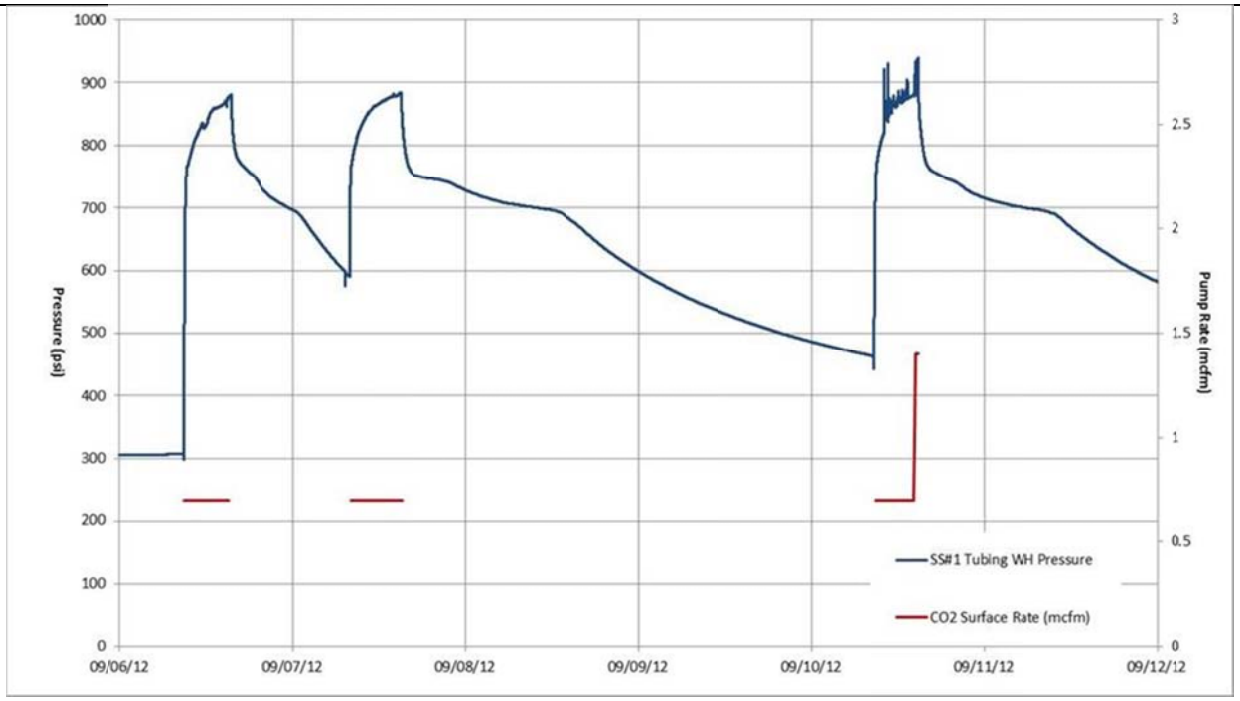


Source: Kentucky Geological Survey

# 7. WELL TEST ANALYSIS OF THE SS#1 KENTUCKY $CO_2$ INJECTION TEST

Text The injection and pressure fall off and flow back data and the log results (spinner results and RST saturation profiles) were initially analyzed and used to model the $CO_2$ injection. The dataset was used to determine the nature of the pressure communication between the injection tubing and the casing annulus.

Analyses were conducted using the PanSystem® Well Testing Analysis software.[2] The pressure data gathered during the $CO_2$ injection test was used to set up a radial, homogenous well test model. An infinite acting radial homogeneous model was assumed for this analysis.

In concert with the collected bottomhole pressure and injection data, key reservoir parameters constraining the numerical analysis centered around the detemination of initial pressure and temperature (for determining gas properties), which were taken from the bottomhole pressure gauge data. To arrive at an estimate of effective permeability, reservoir thickness was determined from the geophysical well log. As there were numerous perforations across the shale, the height of the shale spanning these performations was input into the model.

Next, offset core data from a nearby well from from an older, Eastern Gas Shales Study were used as a proxy to estimate the effective porosity of the black shale at the test well site. This offset well yielded the closest and most representative information applicable to the test site. Finally, the wellbore radius was input into the model, completing the items neceessary to compute the stimulation effectiveness (skin factor) of the black shale.

In addition, measured injection rate data consistent with the wellhead pressure data observed over the three injection periods was not available. Three separate data sheets were provided with both wellhead data and various measurements which are presumed to be sourced from the pumping unit. However, the data provided on each sheet is inconsistent. As no dates are provided, the sheets were matched to their respective periods based on the injection pressure profile. However, one of the data sheets cannot be matched to an injection period using this method. The remaining two data sheets can be matched to respective injection periods, but provide two kinds of rate data. In one case, calculated rate data is provided and in the other case, measured rate data is presented in barrels per minute. When converted to cubic feet per minute, the rate suggests an unreasonably high injection volume. The inconsistencies and variations in the provided data introduce doubt that it would be reliable in an injectivity test analysis.

[2] http://www.ep-solutions.com/Solutions/EPS/PanSystem.htm

Nonetheless, combined diagnostic plots and separate diagnostics were plotted for the three injection periods and subsequent falloff periods. The three injection periods exhibited similar early time behavior but diverged through the late-time period of the test. A Pan System Auto Match of the injection data on the semi-log curve was matched to the pressure response from each injection period.

During pressure falloff, none of the periods exhibit behavior consistent with a traditional injection falloff test due to pressure anomalies exhibited at approximately 750 and 690 psi, which are unexplained and corrupt our ability to properly analyze the data. As a result, extrapolated reservoir pressure estimates are significantly higher than the reservoir pressure measured before injection began. Therefore, no reliable results could be discerned from the falloff periods. However, a qualitative analysis of the very early time falloff does behave similarly to that of a formation with either natural fractures or one that has been artificial stimulated, indicating a heightened level of stimulation most likely due to hydraulic fracturing.

A review (skin vs flow rate analysis) of the impact of non-Darcy flow characteristics exhibited little differentiation between the three injection periods. This type of analysis should discern the impact of flow related skin (that is, the apparent skin factor should increase with rate). However, the dataset suffered from a lack of field collected injection data and the provided data was essentially the same value for each injection period. As a result the periods plot as a cloud and represent the average flow rate.

Thus, based on these analyses, the following can be concluded and/or inferred:

- The level of effective permeability observed indicates that the black shale is more permeable than other representative samples.
- The presence of linear flow behavior (half-slope) on the log-log diagnostic plots indicates the presence of either a short infinite conductivty induced natural fracture or open natural fractures.

Alone, these observations are inconclusive. However, a combination of these circumstances suggests that for the duration of this test, there was communication between the Berea sand and the black shale. These are:

- The proximity of the lowermost and uppermost shale perforation and the fact they were most likely fracture stimulated at the same time,
- The above average level of effective permeability and linear flow behavior determined from the well test analysis, and
- The observed annular pressure response.

Detailed document of the input paramters, assumptions and results from the PanSystem analyses are provided in **Appendix A**.

# 8. REFERENCES

Halliburton Services, 1985, Halliburton technical data Section 240 — Calculations and formulae: Houston, Texas, various pages.

Nuttall, Brandon; Cortland F. Eble; James A. Drahovzal, and Mark Bustin, Analysis of Devonian Black Shales for Potential Carbon Dioxide Sequestration and Enhanced Natural Gas Production, Report DE-FC26-02NT41442 prepared by the Kentucky Geological Survey, University of Kentucky, for the U.S. Department of Energy, National Energy Technology Laboratory, December 30, 2005.

U.S. Department of Energy/National Energy Technology Laboratory, Impact of the Marcellus Shale Gas Play on Current and Future CCS Activities, August 2010 (http://www.netl.doe.gov/technologies/carbon_seq/refshelf/Marcellus_CCS.pdf)

# APPENDIX A
# PAN SYSTEM REPORT SUMMARY

## Analysis of Injection-Falloff Test for Kentucky Geological Survey
## Well Interstate SS #1
## Shale interval from 1,274 to 1,672 feet
## September 2012

Title Page ..... 28
Input Data ..... 4
Reservoir Description ..... 4
Layer Parameters Data ..... 4
Well Parameters Data ..... 4
Fluid Parameters Data ..... 5
Layer 1 Correlations ..... 5
Boundary Geometry ..... 5
Layer Boundaries Data ..... 5
Model Parameters ..... 6
Rate Changes ..... 6
Test Overview ..... 7
Period #1 Analysis ..... 8
Local Results ..... 8
Line Details ..... 8
Local Results ..... 9
Line Details ..... 10
Period #2 Analysis ..... 11
Local Results ..... 11
Line Details ..... 11
Local Results ..... 12
Line Details ..... 13
Period #3 Analysis ..... 14
Local Results ..... 14
Line Details ..... 14
Local Results ..... 15
Line Details ..... 16
Combined Injection Analysis ..... 17
Local Results ..... 17
Line Details ..... 17
Local Results ..... 18
Line Details ..... 18

| | |
|---|---|
| Analyst name | George J. Koperna, Jr. |
| Company | CrossRock Drilling, LLC |
| Well | Interstate SS #1 |
| Field | Paintsville Quad |
| Date | 9/25/12 |
| Rig Name/Number | |
| Test | Ohio Shale |
| Depth Reference - MSL | Ground Level |
| Gauge Type | Digital memory |
| Gauge Number | |
| Gauge Depth - Measured | 1710 feet |
| Gauge Depth - Vertical | 1710 feet |
| Producing Formation Top | |
| Producing Formation Bottom | |
| Perforated interval Top | 1274 feet |
| Perforated interval Bottom | 1672 feet |

Analyst Notes:

In September 2012, a small scale $CO_2$ injection test was performed on Crossrock Drilling's Interstate SS #1 in Johnson County, Kentucky to observe and analyze potential for enhanced gas recovery in shale reservoirs. The Interstate SS #1 is a 1,910 foot vertical well and the injection target was the perforated Ohio shale interval between 1,274 feet and 1,672 feet. Approximately 100 tons of $CO_2$ were injected in three sessions between September 6 and September 10. Downhole memory gauges were deployed to record continuous pressure data to analyze both injection and falloff behavior in the well.

An infinite acting radial homogeneous model was used for this analysis. Combined diagnostic plots and separate diagnostics were plotted for the three injection periods and subsequent falloff periods. The three injection periods exhibited similar early time behavior but diverged through the late-time period of the test. A Pan System Auto Match of the injection data on the semi-log curve was matched to the pressure response from each injection period.

During pressure falloff, none of the periods exhibit behavior consistent with a traditional injection falloff test due to pressure anomalies exhibited at approximately 750 and 690 psi, which are unexplained and corrupt our ability to properly analyze the data. As a result, extrapolated reservoir pressure estimates are significantly higher than the reservoir pressure measured before injection began. Therefore, no reliable results could be discerned from the falloff periods. However, a qualitative analysis of the very early time falloff does behave similarly to that of a formation with either natural fractures or one that has been artificial stimulated.

The reservoir parameters are presented below are based on the analysis of the three injection periods:

| | |
|---|---|
| Permeability (k) range | 0.12 mD to 0.17 mD |
| Skin (S) range | -1.26 to 0.25 |

A review (skin vs flow rate analysis) of the impact of non-Darcy flow characteristics exhibited little differentiation between the three injection periods. This type of analysis should discern the impact of flow related skin (that is, the apparent ski factor should increase with rate). However, the dataset suffered from a lack of field collected injection data and the provided data was essentially the same value for each injection period. As a result the periods plot as a cloud and represent the average flow rate.

# Input Data

## Reservoir Description

Fluid type : Gas
Well orientation : Vertical
Number of wells : 1
Number of layers : 1

## Layer Parameters Data

| | Layer 1 |
|---|---|
| Formation thickness (ft) | 446.0000 |
| Average formation porosity | 0.0400 |
| Water saturation | 0.0000 |
| Gas saturation | 1.0000 |
| Formation compressibility (psi-1) | 1.0000e-4 |
| Total system compressibility (psi-1) | 5.4228e-3 |
| | |
| Layer pressure (psia) | 400.000000 |
| Temperature (deg F) | 70.000000 |

## Well Parameters Data

| | Interstate SS 1 |
|---|---|
| Well radius (ft) | 0.1875 |
| Distance from observation to active well (ft) | 0.000000 |
| Wellbore storage coefficient (bbl/psi) | 0.0400 |
| Storage Amplitude (psi) | 0.000000 |
| Storage Time Constant (hr) | 0.000000 |
| Second Wellbore Storage (bbl/psi) | 0.000000 |
| Time Change for Second Storage (hr) | 0.000000 |
| Well offset - x direction (ft) | 0.0000 |
| Well offset - y direction (ft) | 0.0000 |

## Fluid Parameters Data

| | Layer 1 |
|---|---|
| Gas gravity (sp grav) | 1.519160 |
| Water-Gas ratio (STB/MMscf) | 0.000000 |
| Water salinity (ppm) | 0.000000 |
| Check Pressure (psia) | 200.000000 |
| Check Temperature (deg F) | 70.000000 |
| Gas density (lb/ft3) | 1.64349 |
| Initial gas viscosity (cp) | 0.0163262 |
| Gas formation volume factor (ft3/scf) | 0.07059 |
| Water density (lb/ft3) | 62.4009 |
| Water viscosity (cp) | 0.96995 |
| Water formation volume factor (RB/STB) | 0.99945 |
| Initial Z-factor | 0.94151 |
| Initial Gas compressibility (psi-1) | 5.3228e-3 |
| Water compressibility (psi-1) | 3.2896e-6 |

## Layer 1 Correlations

Ug Correlation : Carr et al
Ug Correlation : Hall Correlation

## Boundary Geometry

## Layer Boundaries Data

Layer 1 Boundary Type : Infinitely acting

| | Layer 1 |
|---|---|
| L1 (ft) | 0.000000 |
| L2 (ft) | 0.000000 |
| L3 (ft) | 0.000000 |
| L4 (ft) | 0.000000 |
| Drainage area (acres) | 0.000000 |
| Dietz shape factor | 0.000000 |

## Model Parameters

Layer 1 Model Data
Layer 1 Model Type : Radial homogeneous

| | Layer 1 |
|---|---|
| Permeability (md) | 0.142609 |
| Skin factor (Well 1) | -0.740608 |
| Rate dependent skin coefficient (D) (1/(Mscf/day)) | 0.0000 |

## Rate Changes

Rate Change Data

| Time Hours | Pressure psia | Rate MMscf/day |
|---|---|---|
| 8.901987 | 304.505700 | 0.000000 |
| 15.427514 | 880.017300 | -1.008000 |
| 31.802294 | 590.058900 | 0.000000 |
| 38.913600 | 882.592000 | -1.008000 |
| 104.796728 | 460.033200 | 0.000000 |
| 110.881614 | 939.658600 | -1.039000 |
| 155.675000 | 531.862000 | 0.000000 |

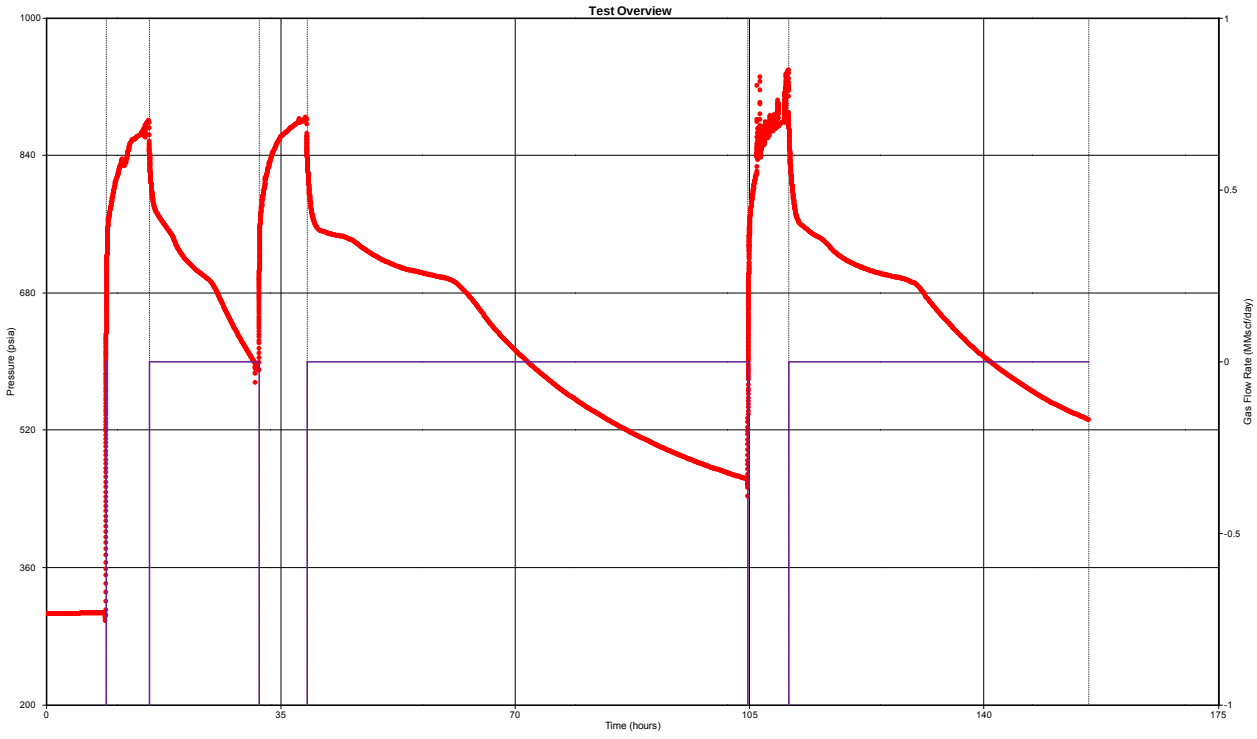


**Test Overview**

# Period #1 Analysis

## Injection #1

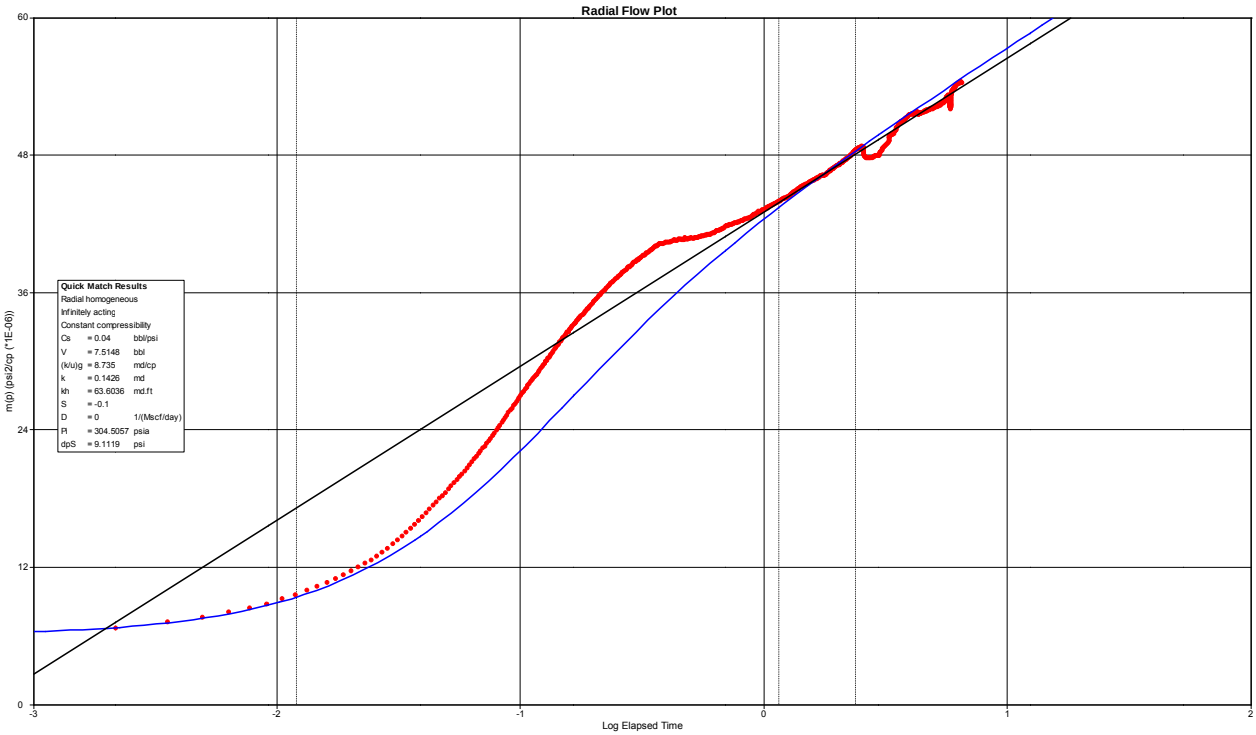


**Radial Flow Plot**

## Local Results

Radial Flow Plot Model Results
Radial homogeneous - Infinitely acting
Classic Wellbore Storage

| | Value |
|---|---|
| Permeability (md) | 0.145512 |
| Permeability-thickness (md.ft) | 64.898213 |
| Radius of investigation (ft) | 15.015263 |
| Flow efficiency | 1.025880 |
| dP skin (constant rate) (psi) | 9.544148 |
| Skin factor | -0.106898 |

## Line Details

Radial Flow Plot Line Details
Line type : Radial flow
Slope : 13.4637
Intercept : 43.0266
Coefficient of Determination : 0.994513

| | Radial flow |
|---|---|
| m(p) at dt = 1 hr (psi2/cp (*1E-06)) | 43.026559 |
| Pressure at dt = 1 hour (psia) | 787.771904 |

Number of Intersections = 0

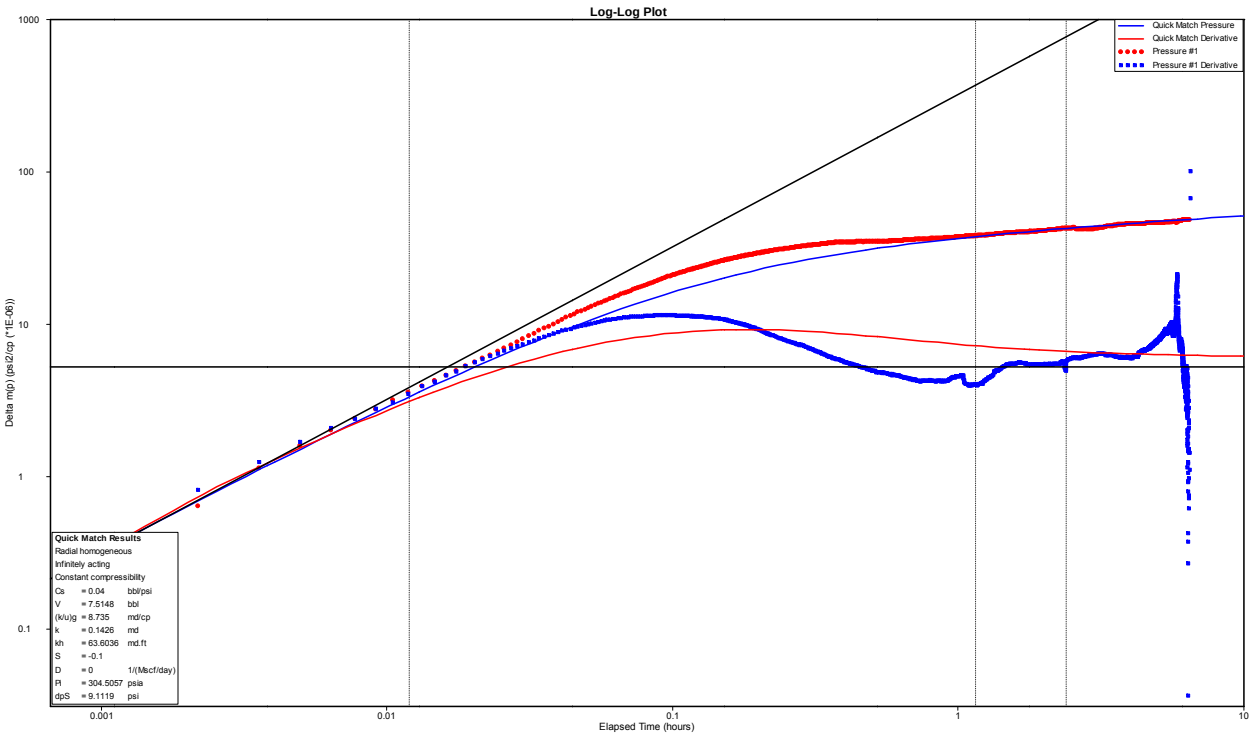


**Log-Log Plot**

## Local Results

Log-Log Plot Model Results
Radial homogeneous - Infinitely acting
Classic Wellbore Storage

| | Value |
|---|---|
| Wellbore storage coefficient (bbl/psi) | 0.045401 |
| Apparent wellbore volume (bbl) | 8.529586 |
| Permeability (md) | 0.16299 |
| Permeability-thickness (md.ft) | 72.693700 |
| Skin factor | 0.247806 |

## Line Details

Log-Log Plot Line Details

| | |
|---|---|
| Line type : | Wellbore storage |
| Slope : | 1 |
| Intercept : | 321.792 |
| Coefficient of Determination : | Not Used |
| Line type : | Radial flow |
| Slope : | 0 |
| Intercept : | 5.22019 |
| Coefficient of Determination : | Not Used |
| Number of Intersections = | 0 |

## Falloff #1

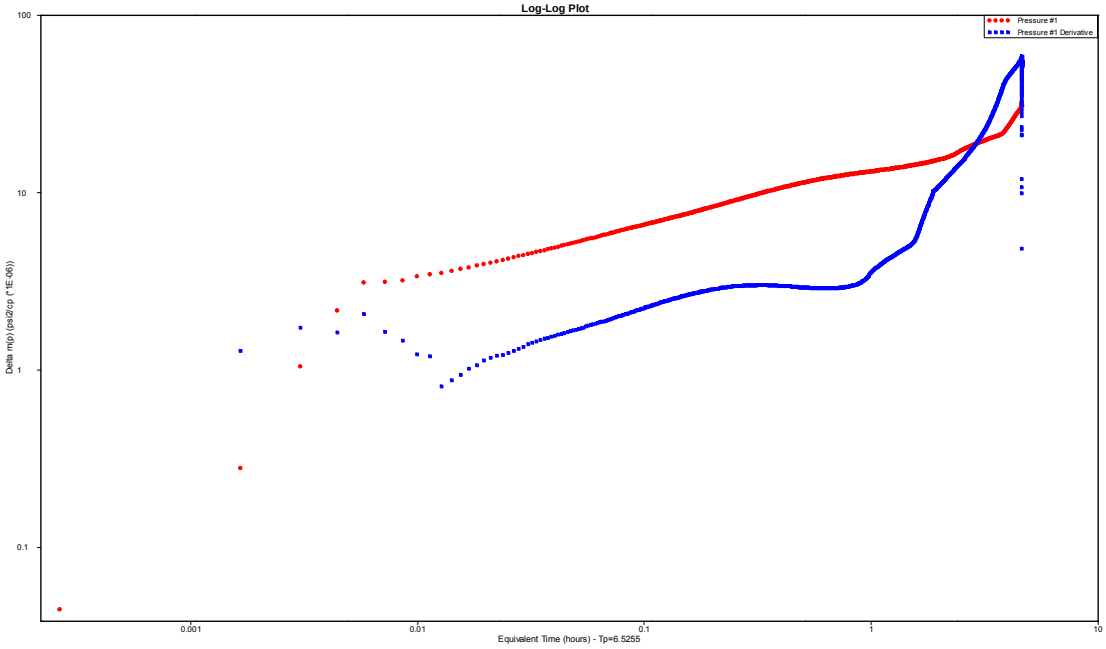


**Log-Log Plot**

# Period #2 Analysis

## Injection #2

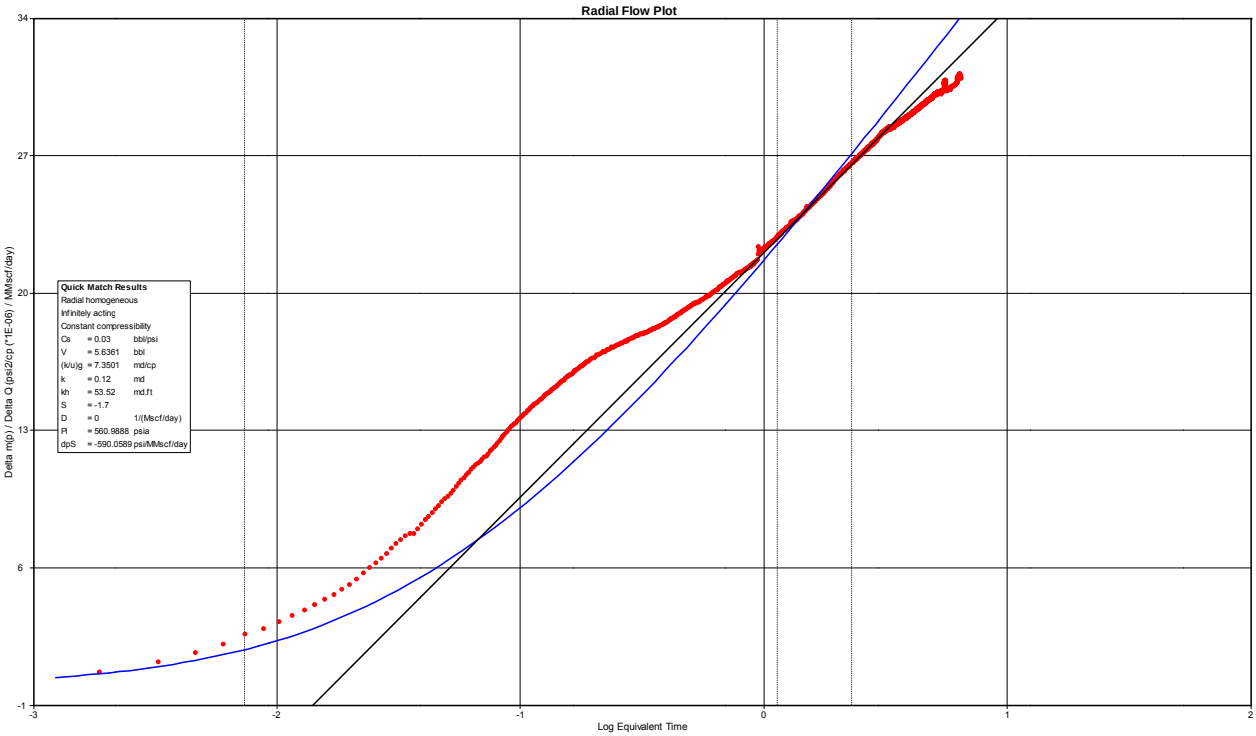


**Radial Flow Plot**

## Local Results

Radial Flow Plot Model Results
Radial homogeneous - Infinitely acting
Classic Wellbore Storage

| | Value |
|---|---|
| Permeability (md) | 0.156231 |
| Permeability-thickness (md.ft) | 69.679150 |
| Pcalc (psia) | 567.504732 |
| Radius of investigation (ft) | 16.241971 |
| dP skin (GAS - variable rate) (psi/MMscf/day) | -202.900304 |
| Skin factor | -1.262356 |

## Line Details

Radial Flow Plot Line Details
Line type : Radial flow
Slope : 12.4404
Intercept : 22.0764
Coefficient of Determination : 0.998459
Number of Intersections = 0

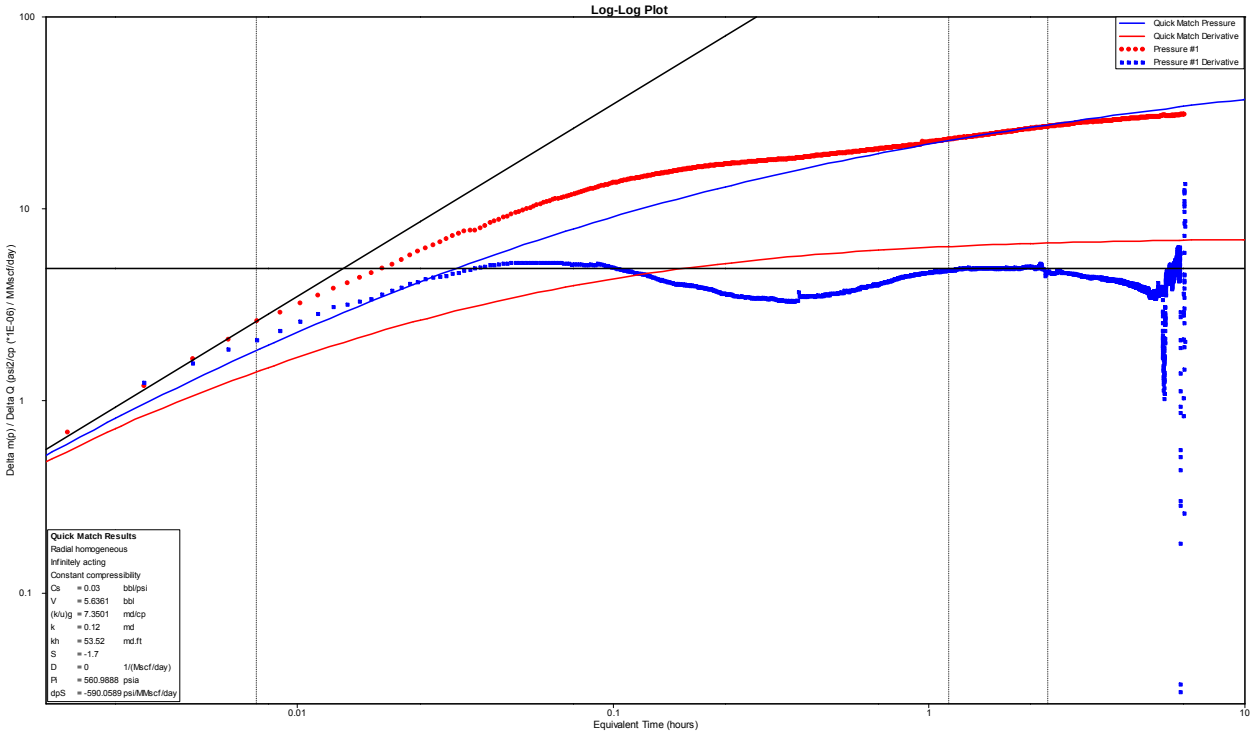


**Log-Log Plot**

## Local Results

Log-Log Plot Model Results
Radial homogeneous - Infinitely acting
Classic Wellbore Storage

| | Value |
|---|---|
| Wellbore storage coefficient (bbl/psi) | 0.041137 |
| Apparent wellbore volume (bbl) | 7.728397 |
| Permeability (md) | 0.1726 |
| Permeability-thickness (md.ft) | 76.979705 |
| Skin factor | -1.071923 |

## Line Details

Log-Log Plot Line Details
Line type : Wellbore storage
Slope : 1
Intercept : 352.333
Coefficient of Determination : Not Used
Line type : Radial flow
Slope : 0
Intercept : 4.89042
Coefficient of Determination : Not Used
Number of Intersections = 0

## Falloff #2

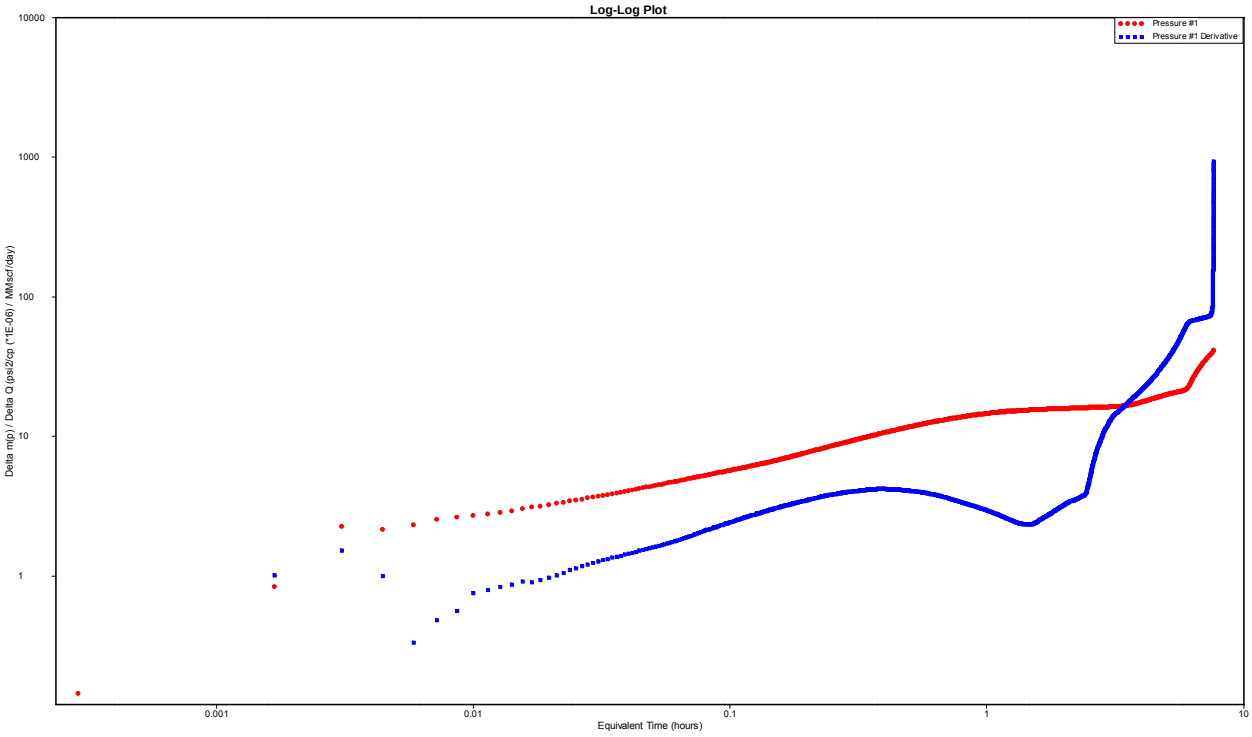


**Log-Log Plot**

# Period #3 Analysis

## Injection #3

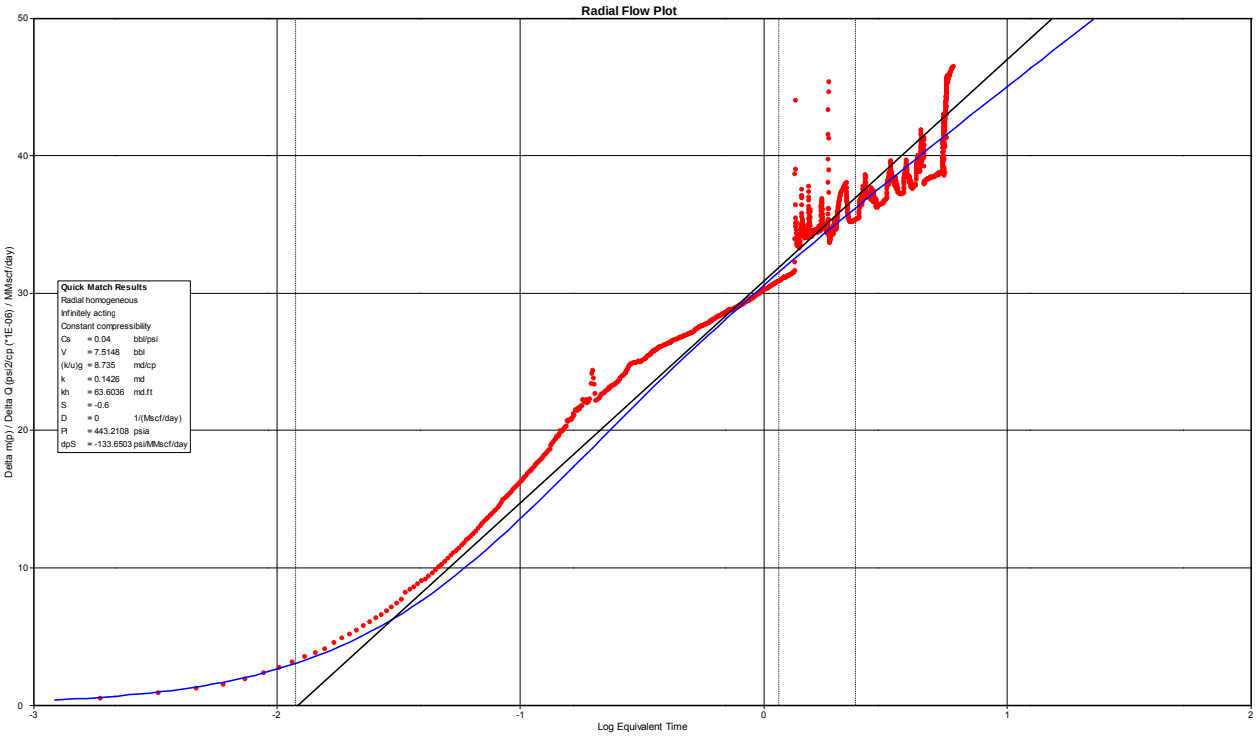


**Radial Flow Plot**

## Local Results

Radial Flow Plot Model Results
Radial homogeneous - Infinitely acting
Classic Wellbore Storage

| | Value |
|---|---|
| Permeability (md) | 0.120392 |
| Permeability-thickness (md.ft) | 53.695050 |
| Pcalc (psia) | 440.100906 |
| Radius of investigation (ft) | 13.188694 |
| dP skin (GAS - variable rate) (psi/MMscf/day) | -378.538950 |
| Skin factor | -0.972968 |

## Line Details

Radial Flow Plot Line Details
Line type : Radial flow
Slope : 16.1437
Intercept : 30.8791
Coefficient of Determination : 0.523004
Number of Intersections = 0

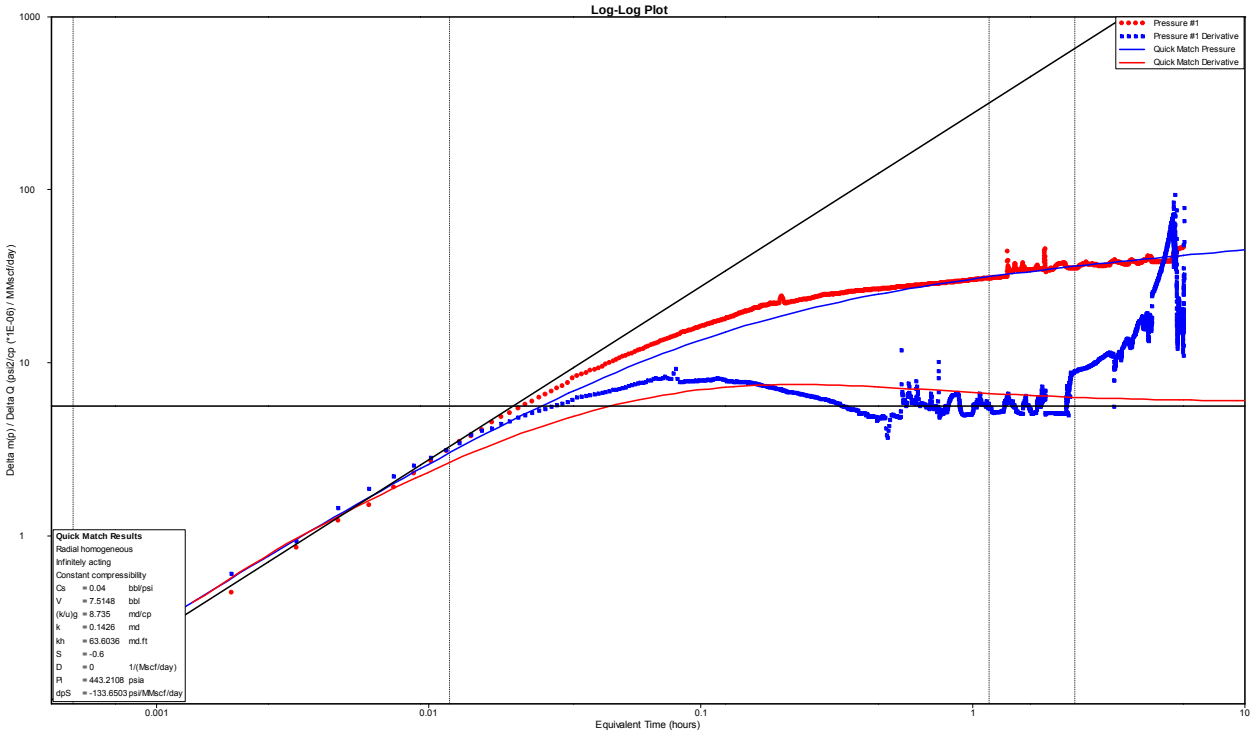


**Log-Log Plot**

## Local Results

Log-Log Plot Model Results
Radial homogeneous - Infinitely acting
Classic Wellbore Storage

| | Value |
|---|---|
| Wellbore storage coefficient (bbl/psi) | 0.052261 |
| Apparent wellbore volume (bbl) | 9.818416 |
| Permeability (md) | 0.1489 |
| Permeability-thickness (md.ft) | 66.409352 |
| Skin factor | -0.498413 |

## Line Details

Log-Log Plot Line Details
Line type : Wellbore storage
Slope : 1
Intercept : 277.333
Coefficient of Determination : Not Used
Line type : Radial flow
Slope : 0
Intercept : 5.66882
Coefficient of Determination : Not Used
Number of Intersections = 0

## Falloff #3

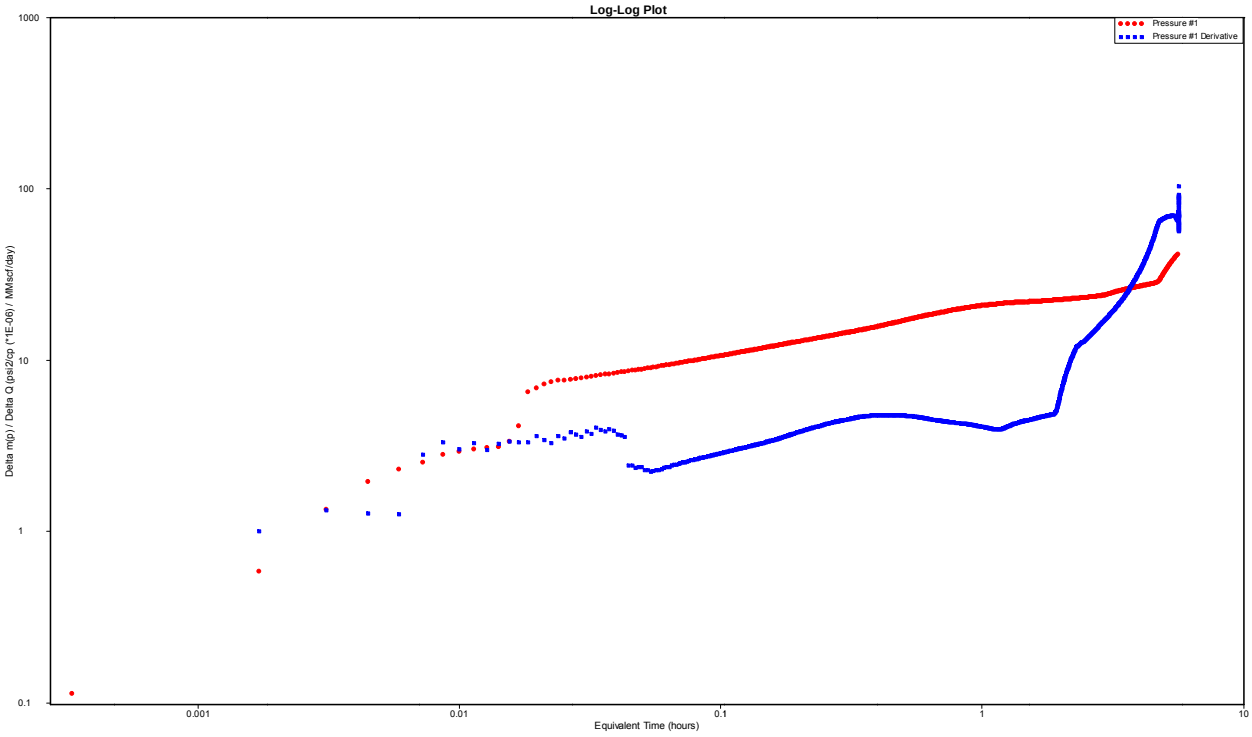


**Log-Log Plot**

# Combined Injection Analysis

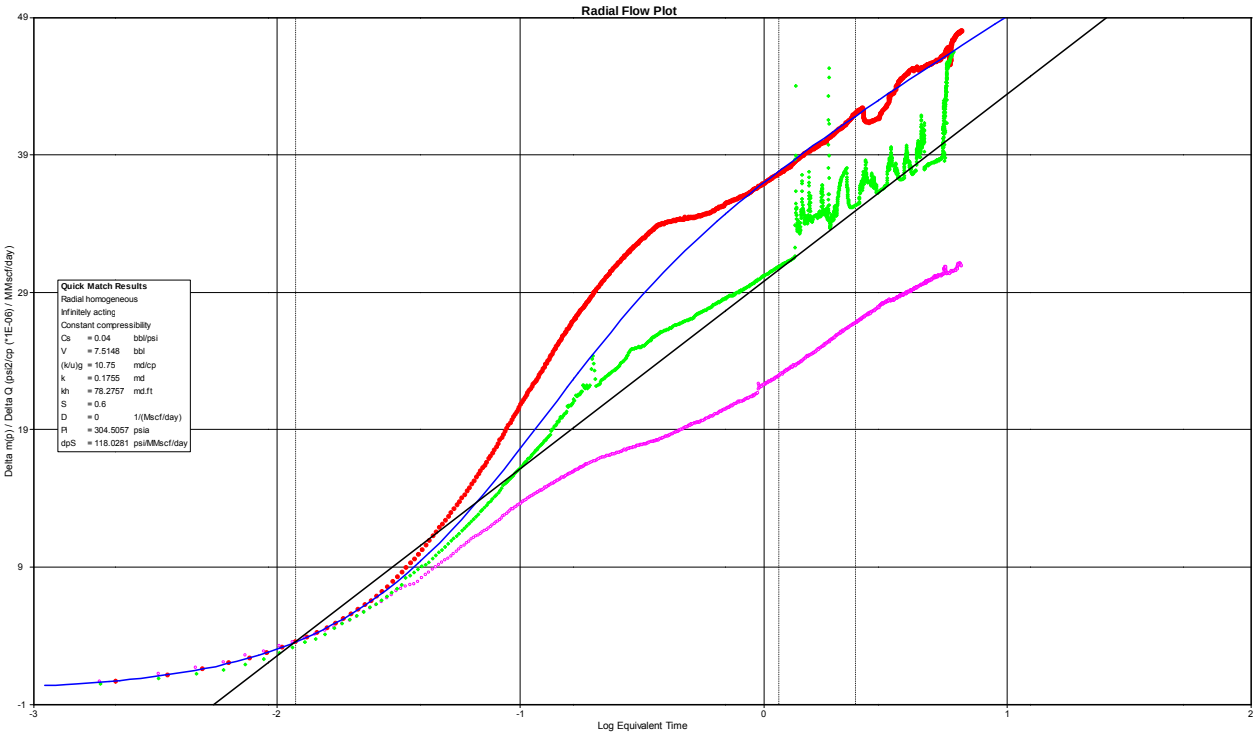


**Radial Flow Plot**

## Local Results

Radial Flow Plot Model Results
Radial homogeneous - Infinitely acting
Classic Wellbore Storage

| | Value |
|---|---|
| Permeability (md) | 0.142609 |
| Permeability-thickness (md.ft) | 63.603662 |
| Skin factor | -0.740608 |

## Line Details

Radial Flow Plot Line Details
Line type : Radial flow
Slope : 13.6287
Intercept : 29.8215
Coefficient of Determination : 0.036916
Number of Intersections = 0

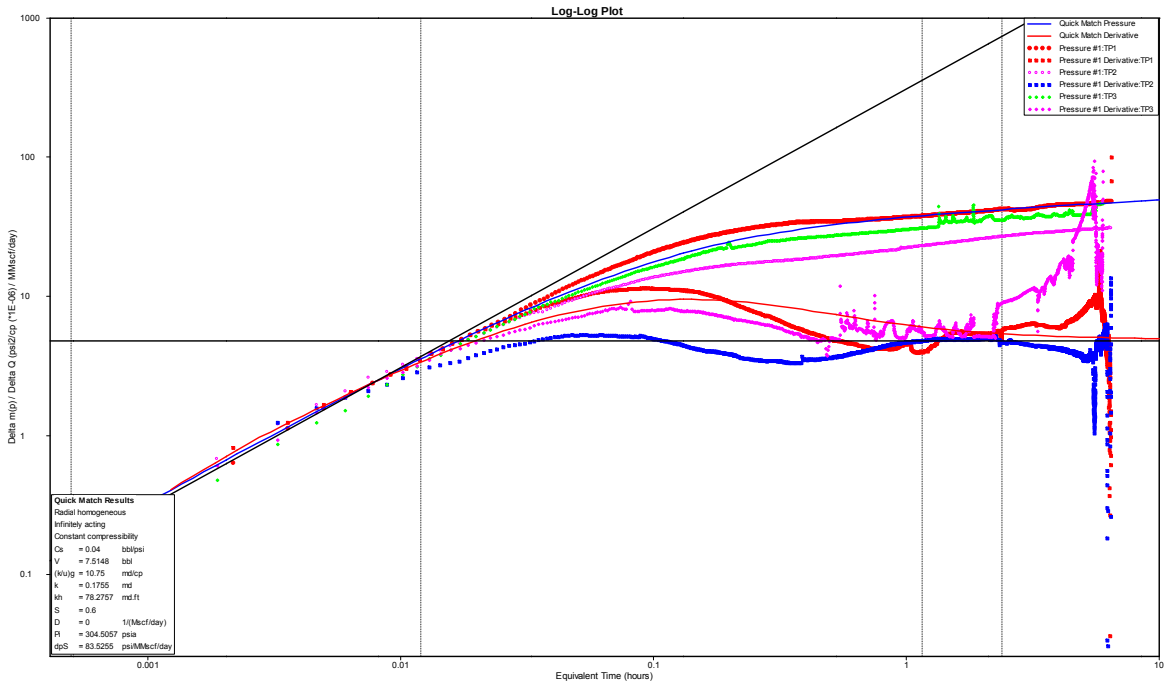


**Log-Log Plot**

## Local Results

Log-Log Plot Model Results
Radial homogeneous - Infinitely acting
Classic Wellbore Storage

| | Value |
|---|---|
| Wellbore storage coefficient (bbl/psi) | 0.04701 |
| Apparent wellbore volume (bbl) | 8.831824 |
| Permeability (md) | 0.175506 |
| Permeability-thickness (md.ft) | 78.275571 |

## Line Details

Log-Log Plot Line Details
Line type : Wellbore storage
Slope : 1
Intercept : 308.313
Coefficient of Determination : Not Used
Line type : Radial flow
Slope : 0
Intercept : 4.80946
Coefficient of Determination : Not Used
Number of Intersections = 0

# Volume 7
# Testing Innovative Technology for Monitoring $CO_2$ Flow Behavior

## Assessment of Factors Influencing Effective $CO_2$ Storage Capacity and Injectivity in Eastern Gas Shales

Prepared for:
U.S. Department of Energy
National Energy Technology Laboratory
DOE Award Number: DE-FE0004633

Prepared by:
Michael Godec
Advanced Resources International, Inc.
Arlington, Virginia
and
Cornell University
Department of Earth and Atmospheric Sciences
Ithaca, NY
L. M. Cathles (PI)
Russell Zhao (experiments)
Timothy Gao (modeling)
Chris Ober, Yisheng Xu, Lin Chen (particle synthesis)

Date:
October 23, 2013


4501 Fairfax Drive ▪ Suite 910 ▪ Arlington, Virginia 22203 ▪ Phone: (703) 528-8420 ▪ web: www.adv-res.com

## Advanced Resources International, Inc.

# ABSTRACT

Sequestering carbon dioxide ($CO_2$) in shale depends on the diffusion of $CO_2$ into stagnant areas adjacent to the fractures into which the $CO_2$ is injected. Field tests could measure the rate that this diffusion takes place and provide an early indication of the viability of sequestration. We have designed and carried out laboratory experiments which illustrate how this can be done, developed models of the process, and used the models to design the kinds of field tests that would be most effective in assessing the viability of sequestering $CO_2$ in shale. One set of experiments and models involves the inter-diffusion of $CO_2$ and $CH_4$ at atmospheric pressure. A second set involves the diffusion of a chemical tracer (trifluorotoluene, or TFT) and nanoparticles in hydrofluoroether (HFE), a supercritical $CO_2$ analogue. Two kinds of nanoparticles were synthesized for this purpose. The synthesis of these particles is described in detail. Using the same methods that were shown to be successful in the laboratory experiments, the diffusion constants of the gases, the TFT, and the nanoparticles tracers in supercritical $CO_2$ are estimated. We then show how the insights gained from the laboratory experiments and models can be used to design field tests can that assess the viability of sequestering $CO_2$ in shale in an optimum fashion. Successful sequestration could be achieved if the fractures are closely enough spaced. Well tests with well spacing of ~10 m could predict the viability of sequestration. Design of a single well huff-puff test could provide the needed information, but evaluation of this possibility requires models that do not make the simplifying assumptions currently made in our models.

# Table of Contents

ABSTRACT ..... II
**1.** INTRODUCTION ..... 1
**2.** SYNTHESIS OF $SCCO_2$-PHILIC NANOPARTICLE TRACERS ..... 4
a. Introduction ..... 4
b. Materials ..... 5
c. Methods ..... 5
d. Equipment ..... 8
i. Measuring particle size ..... 8
ii. Particle images: ..... 8
iii. Thermogravimetric analysis ..... 8
iv. Determining particle concentration ..... 8
v. Solubility ..... 8
e. Particle Synthesis ..... 9
i. Particle preparation ..... 9
ii. Making the particles fluorescent ..... 10
f. Characterization ..... 12
**3.** DUAL TRACER DIFFUSION EXPERIMENTS ..... 18
a. Introduction ..... 18
b. Gas diffusion experiments ..... 18
c. Analogue supercritical $CO_2$ dual tracer diffusion experiments ..... 20
i. Experimental materials ..... 20
ii. Apparatus design ..... 20
iii. Fabrication ..... 21
iv. Tracer Detection ..... 23
v. Data Interpretation ..... 24
vi. Experimental Results and interpretation ..... 28
vii. Conclusion ..... 30
**4.** STREAMLINE MODELING ..... 31
a. Modeling laboratory experiments ..... 31
b. Modeling field tests ..... 32
c. Field test design ..... 36
i. Test design based on a simple rule-of-thumb ..... 36
d. Test design based on a model that integrates flow and matrix diffusion ..... 38
i. The simplifying assumption of the coupled model ..... 38
ii. Shale properties ..... 39
iii. Results ..... 40
e. Summary and Discussion ..... 45
**5.** DISCUSSION AND OVERALL CONCLUSIONS ..... 46
**6.** ACKNOWLEDGEMENTS ..... 47
**7.** REFERENCES ..... 47

# List of Figures

Figure 1. Synthetic scheme of fluorescent fluoro-polymer functionalized nanoparticles. ....9
Figure 2. Fluorescent intensity versus concentration for $Fe_3O_4$ nanoparticle. ....11
Figure 3. Fluorescent intensity versus concentration for $SiO_2$ nanoparticles. ....12
Figure 4. Hydrodynamic size distributions of $Fe_3O_4$ and $SiO_2$ NPs as measured by DLS. ....13
Figure 5. TEM images of $Fe_3O_4$ and $SiO_2$ NPs ....13
Figure 6. SEM images of $Fe_3O_4$ NPs. (a) shows the bare $Fe_3O_4$ NPs, and (b) the polymerized $Fe_3O_4$ NPs. ....15
Figure 7. TGA images for $Fe_3O_4$ (left) and $SiO_2$ (right) nanoparticles. ....15
Figure 8. IR characterizations of $Fe_3O_4$ (left) and $SiO_2$ (right) NPs coated at different steps. ....16
Figure 9. Twenty milligrams of nanoparticles are dispersed in a 30mL pressure cell containing, depending on pressure and temperature, different phases of $CO_2$. ....17
Figure 10. Hele-Shaw modified flow cell used for gaseous diffusion experiments. ....19
Figure 11. Experiment schematic. ....21
Figure 12. A: Glass cell 1 before bonding. B: Glass cell 2 before bonding. See figure 11, 12 for dimensions. ....22
Figure 13. A. Protection of tubing after it is bonded with the glass cell. B. Close up of the clean bonding between polished glass surface and PDMS. ....22
Figure 14. Glass apparatus encased in PDMS. Vacuum grease is applied at each connection to prevent any potential evaporation. ....22
Figure 15. The glass diffusion system in operation in the lab. ....23
Figure 16. Measured fluorescence of silica nanoparticles dispersed in HFE together with TFT. ....24
Figure 17. Fluorescence calibration curve for the silica nanoparticle concentration. ....25
Figure 18. Calibration curve for the UV absorption level for the $SiO_2$ nanoparticles at 255 nm. ....25
Figure 19. The peak UV absorption at 255nm is a linear function of TFT concentration. ....26
Figure 20. This figure shows the UV absorption profile for a sample with both $SiO_2$ nanoparticles and TFT present. ....27
Figure 21. UV absorption profile for the chemical tracer TFT only (no silica nanoparticles). ....27
Figure 22. Effluent concentration as a function of time for experiments carried out in HFE (a proxy solvent for supercritical $CO_2$). ....28
Figure 23. Comparison of Effluent TFT and $SiO_2$ Nanoparticle as Function of Time ....30
Figure 24. Diffusion modeling methodology for the laboratory experiments ....32
Figure 25. A single production well (center) receives fluid from 4 surrounding injection wells. ....33
Figure 26. Two well flow in a layer of thickness H. ....34
Figure 27. Conceptual flow of a particle and chemical tracer in a fractured shale. ....34
Figure 28. Fracture porosity in a fractured shale ....35
Figure 29. Injection rate, Q, that meets the design criterion for a single well huff-puff test where fast diffusing tracer extends 5 m from the well. ....37

Figure 30. The injection rate, Q, that meets the design criterion that $T=\tau_{TFT}$ for two well test assuming the wells are separated by 10 m. ....37

Figure 31. Prediction of Relative Tracer Concentration as a Function of Time and Distance From Well....39

Figure 32. Planned Field Test Well Configuration.....40

Figure 33. Prediction of Tracer Arrival Curves at 5 $m^3$/m/day for a Two Well Test ....41

Figure 34. Prediction of Tracer Arrival Curves at 20 $m^3$/m/day for a Two Well Test ....42

Figure 35. Matrix Relaxation Time as Function of Fracture Spacing ....43

Figure 36. Prediction of Tracer Arrival Curves at 5 $m^3$/m/day for a Huff-and-Puff Test....44

# List of Tables

Table 1. Diffusion constants estimated from the Stokes-Einstein equation (Appendix C) for the particles and chemical tracer in the proxy supercritical $CO_2$ solvent HFE. ....29

Table 2. Diffusion constants of our $scCO_2$-philic nanoparticles and TFT chemical tracer in supercritical $CO_2$ (see Appendix C) ....35

Table 3. Estimates of fracture porosity and ratio of matrix to fracture porosity ....40

Table 4. Diffusional Relaxation Time of the Shale Matrix Computed for Supercritical $CO_2$....43

# 1. INTRODUCTION

Fractures are a principal factor controlling both the amount of gas that can be stored in shale and the risk associated with that storage. Shales are comprised of thin laminations of sediment with slightly different grain size and different proportions of carbonate, sand, clay, and organic carbon. The shales are faulted and jointed both on a large (meters to tens of meters) and small (single strata) scale. Different lamina can be fractured to very different degrees. Shale permeability is low, but complex connections of the most permeable lamina and fractures provide some permeability. This permeability increases strongly with fluid pressure and deformation, an extreme case being when the shale is hydraulically fractured.

The nature of a shale's high permeability network controls how uniformly gas can be injected and how securely it can be retained. If the permeable network is dense and uniform, injected gas can diffuse into the full pore space and nearly the full porosity of the shale can be utilized for storage. The volume available for carbon dioxide ($CO_2$) storage could be 10% to 15% of the shale volume. On the other hand, if injected gas moves through more widely spaced strata and fractures, the storage volume might be one or even two orders of magnitude smaller. If the injected gas moved along only a small fraction of the most permeable pathways (faults or major fractures), the storage volume would be effectively zero. Even supposing the permeable network of the shale was dense (or could be made so by fracturing), the most permeable pathways could nonetheless be of concern, because gas injected into them could break out into the water-saturated zones surrounding a gas-filled shale. Thus, even though the fine grained and laminated nature of shales allows them to form very durable capillary seals and retain gas generated internally for hundreds of millions of years, it is not clear that gas can be injected into the shales in a fashion that results in a high storage capacity and is safe from breakout.

The key to determining whether gas can be effectively and safely stored is the uniformity and density of the permeable flow network in the shale. This is almost completely unknown and nearly impossible detect and map, but it can be inferred by examining the mixing of injected $CO_2$ and methane ($CH_4$), and this inference can be confirmed in a number of ways which we have investigated in this study.

The first and most basic method we investigated can be understood as follows: Suppose the shale has a porosity of 10% and is gas saturated, as it is at test sites where tests were originally proposed to be carried out under the project in which this work is a part (see Volume 6). The unknown is the flowing pore volume, but we know that when this pore volume is displaced once by injected $CO_2$, the production well will deliver a 50 volume percent (vol %) mix of methane and $CO_2$. If this mixing ratio occurs when the injected volume of $CO_2$ approximately equals the total pore volume in the shale through which flow is thought (from the geology and reservoir simulations) to have occurred, we would infer that the flow through the

shale was uniform and the storage potential high. If on the other hand the compositional mix at the producing well reached 50 vol% methane and $CO_2$ when the injected volume of $CO_2$ was 1% of the total accessed pore volume, we would infer that flow was highly channelized and the storage capacity of the shale very low.

Confidence in these inferences can be increased if a trace gas not in the shale (such as argon or nitrogen) is added to the injected $CO_2$. The loss of this gas to the pore volume accessed by diffusion should equal the methane contributed from that volume. Furthermore if a particle tracer with a diffusion constant in supercritical $CO_2$ very much greater than methane or argon were added, the diffusive loss of this tracer would be very much smaller than the diffusing gases and it would consequently measure the flowing volume of the fractures and connected pathways alone. In actual applications there will, of course, be numerous uncertainties. We will not know the volume of shale through which flow occurs accurately, for example. The tracer particles may be retained for a variety of reasons, and this will complicate interpretation of their arrival. Pressures could fall below supercritical. Nevertheless, it is clear that to evaluate the storage potential of a shale we must assess the uniformity of flow through it, and the methods outlined are one of the very few ways we have to do this.

The tasks we originally proposed to carry out under this proposal were as follows:

1. *Develop a streamline-based interpretive framework*. The model assumes that flow in a single fracture represents the flow path from injection to production well through one pathway (streamline) of high permeability fractures and lamina. Gas diffuses from this path into adjacent gas-filled shale. By specifying the diffusion constant of the gas or particle tracer and obliging the flow rate to be compatible with the field injection rate, the change in gas composition along each streamline from the injection to the monitor well can be calculated, and the streamlines entering the production well can be summed to give the composition of the produced gas as a function of time. The change of the $CO_2/CH_4$ volume ratio compared to that expected from this completely uniform flow will indicate the volume actually accessed. For different diffusion constants the model will also predict the relative times of arrival of supercritical $CO_2$-compatible nanoparticles and chemical tracers in the supercritical $CO_2$.

2. *Carry out bench tests that demonstrate the methodology.* Laboratory experiments were to be carried out at atmospheric pressure to demonstrate the streamline model and its field application. A Hele Shaw style diffusion cell was proposed to be constructed to simulate flow in a fracture (core channel) and diffusion into the shale matrix (attached diffusion slit) adjacent to the fracture. The baffles in the diffusion slit will block the flow of gas. Initially the entire apparatus will be filled with methane gas. Then $CO_2$ will be passed through the base. The $CO_2$ will be at the bottom to prevent gravity drain into the compartments (we aim to test diffusion). If the flow is fast, a 50 vol% mix of methane and $CO_2$ will exit the tube when one *base* pore volume of $CO_2$ has passed through the tube. If the flow is slow, this transition will be achieved

when one *total* pore volume of $CO_2$ (the pore volume of the base plus the overlying fine-pack) has passed through the tube. The flow rates for these two circumstances will be predicted by the streamline model developed in the first task. The laboratory experiment will demonstrate how the gas ratios can be used to measure the fraction of the porosity that is accessed by the injected $CO_2$.

3. *Develop $CO_2$-compatible particles small enough to be carried in supercritical $CO_2$ but large enough to have a very large diffusion constant compared to gas.* We proposed to manufacture particles with attached polymer corona compatible with supercritical $CO_2$ based on fluorinated oligomeric coronas. The particles will be between 5 and 100 nm in diameter. We planned to test these particles for stability and inertness in the supercritical $CO_2$-shale environment in pressure vessels, and verify that the particles can be transported in supercritical $CO_2$ by passing them through a Hele Shaw style diffusion cell dispersed in a supercritical $CO_2$ chemical analogue.

4. *Interpret field tests.* The final task planned was to work with Advanced Resources and those carrying out the field tests to collect gas samples, analyze them, and interpret the results in terms of the uniformity of flow access and the storage potential of shale at the two field sites, and also to carry out tests with the supercritical $CO_2$-compatible nanoparticles designed in Task 3. When it became clear that these field tests would not be carried out within the time period of the funding, this objective changed to using the insights and methods developed to plan field tests that were optimal for inferring the viability of storing $CO_2$ in shale. Designs were planned for two-well flow tests and for single well huff-puff tests.

The successful completion of these tasks is reported here. Specifically:

1. Two supercritical $CO_2$-philic nanoparticles were successfully synthesized. One of the particles is silica-cored, the other iron oxide-cored. The particles were decorated with fluoropolymer to make them dispersible in supercritical $CO_2$. Highly fluorescent fluorophore molecules were incorporated into the polymer decoration, allowing the concentration of the particles to be measured with fluorescent techniques. The particles are of uniform ~40 nm diameter, which is nearly the ideal size for the sequestration measurements in shale.

2. Gas diffusion experiments in a Hele Shaw style cell with an attached diffusion slit which explored the potential impact of gravity settling and demonstrated the methods for inferring sequestration from the diffusional mixing of injected $CO_2$ with $CH_4$ in the shale were carried out. These results were reported in a previous report and summarized here.

3. Laboratory experiments using a supercritical $CO_2$ proxy were successfully carried out in Hele Shaw style apparatus of our own design. The supercritical analogue experiments show how nanoparticles tracers can complement the conclusions reached from gas inter-diffusion. The particles designed in Task 2 performed successfully in the laboratory experiments. They were stable and were not retained in the laboratory apparatus. The successful testing of the particles on the laboratory scale paves the way for future field experiments.

4. Both sets of experiments (gas and supercritical ($scCO_2$) analogue) were interpreted by diffusion models. The models were then simplified with a reasonable approximation and coupled to a flow model simulating flow between wells in a field of up to 7 producers and 7 injection wells. This coupled model was used to design field experiments that could determine the viability of sequestering $CO_2$ in shale in an optimum fashion.

The remainder of this report documents: (1) the methods of particle synthesis we developed to manufacture capable $scCO_2$-philic particles, (2) the proxy $scCO_2$ laboratory experiments we carried out to demonstrate the potential utility of these particles and our model interpretation of those experiments, and (3) the models we developed to plan and interpret field experiments and the use of those models to plan field experiments that might be carried out in the future.

# 2. SYNTHESIS OF $SCCO_2$-PHILIC NANOPARTICLE TRACERS

## a. Introduction

The synthesis of nanoparticles that are stably dispersible in $scCO_2$ and easily detectable at low concentrations is challenging. Our basic strategy was to graft a $scCO_2$-phylic polymer to the particles and add fluorophore molecules to make the polymer corona fluorescent. Initial attempts were disappointing. The $scCO_2$-philic, UV scattering, $SiO_2$-cored, polymer-decorated particles we initially synthesized were poly-dispersed, only moderately stable, detectible only with UV absorption/scattering, and too large (~300 nm in diameter) for tracer tests in shale. The methods reported below produce polymerized, mono-dispersed batches of $SiO_2$ and $Fe_2O_3$ cored nanoparticles which show little tendency to agglomerate, have good stability, are highly fluorescent, and are small (~40 nm) and uniform in size. The key to success proved to be to pay great attention to the polymer grafting process and to keep the particles dispersed throughout this process.

In what follows, we first report the materials, methods and equipment used, second describe the steps taken to synthesize the silica and iron oxide particles, and finally report the properties of the nanoparticles (NPs) and some of their precursors. The methods section provides the recipes for manufacture of the particles. The synthesis is carried out in three steps: Production of the bare particles, attaching a Br initiator onto the particles, and finally, with the

help of this initiator, grafting the polymer to the particles. The $Fe_3O_4$ particles are more challenging to make, but have a higher fluorescence. The $SiO_2$ particles have a greater tendency to aggregate during synthesis. Both particles perform very well in the laboratory diffusion experiments.

## b. Materials

The chemicals used in the synthesis were purchased from the following sources:

From Sigma Aldrich:
- Ferrous sulfate deptahydrate ($FeSO_4 \cdot 7H_2O$)
- ferric chloride hexahydrate ($FeCl_3 \cdot 6H_2O$)
- oleic acid (OA)
- (3-Aminopropyl) trimethoxysilane
- α-Bromoisobutyryl bromide
- copper (I) bromide,
- N, N, N′, N″, N″-Pentamethyldiethylenetriamine (PMDETA) (99%)
- 3,3,4,4,5,5,6,6,7,7,8,8,9,9,10,10,10 - Heptadecafluorodecyl methacrylate (97%)
- triethylamine (TEA)
- toluene anhydrous (99.8%)
- Ludox SM30 silica NP

From Polysciences:
- 1-Pyrenylmethyl methacrylate

From 3M:
- ethoxy-nonafluorobutane (HFE 7200)

The heptadecafluorodecyl methacrylate was passed through an alumina column to remove inhibitor. The 1-Pyrenylmethyl methacrylate dissolved in THF was passed through a silica column to remove inhibitor. All other solvents and reagents were used as received without further purifications.

## c. Methods

**Synthesis of 2-bromo-2-methyl-N-(3-(trimethoxysilyl) propyl) propanamide (BMTP):**

1. α-Bromoisobutyryl bromide (6.72 mL, 0.053 mol) dissolved into 20 mL methylene chloride was added dropwise into 60 mL the mixture of (3-Aminopropyl) trimethoxysilane (12 mL, 0.067 mol) and PMDETA (14 mL, 0.1 mol) at 0 ºC, and the reaction was then kept at room temperature.

2. After 4 hours of reaction, a white precipitate was removed by vacuum filtration.

3. The filtrate was washed with HCl (pH 2-3), NaCl, and distilled water respectively, and dried over anhydrous magnesium sulfate.

4. The final product was obtained after rotary vaporization.

**Synthesis of mono-dispersed $Fe_3O_4$-NPs:**

The synthetic procedure was followed by the method described by Sun et al.[2007]:

1. 2.35 g $FeSO_4 \cdot 7H_2O$ and 4.1 g $FeCl_3 \cdot 6H_2O$ were dissolved into 100 mL distilled water in a 250 mL flask.

2. Iron oxide NPs were prepared by quickly adding 25 mL of 27 weight percent ammonium hydroxide under vigorous stirring at room temperature.

3. 1 mL OA was then added to the black NP solution and reacted at 80 ºC for 1 hour. These steps were carried out under nitrogen atmosphere.

4. The OA functionalized NPs were then extracted twice with 25 mL toluene in the presence of small amount of sodium chloride in order to disperse the NP into organic solvent.

5. Finally, the NP dispersion was dried over anhydrous sodium sulfate and the concentration of the NP dispersion was determined to be 15 mg/mL.

**Preparation of initiator modified $Fe_3O_4$-NPs:**

1. BMTP (1.19 g), 20 mL 2 M TEA in toluene, and 30 mL magnetic NPs were mixed together in a round flask.

2. The mixture was allowed to react under nitrogen for hours.

3. After reaction, 20 mL petroleum ether was added to precipitate the NPs followed by magnetic separation of NPs.

4. The NPs then were re-dispersed in 15 mL toluene. Such process was repeated 3 times to remove the unreacted BMTP and remaining OA.

5. The NPs were finally vacuum dried and ready for polymerization.

6. TGA analysis shows the initiator immobilized on $Fe_3O_4$ is ~ 22 weight percent of total mass.

**Surface polymerization on initiator modified $Fe_3O_4$-NPs:**

1. 10 mg of initiator modified $Fe_3O_4$-NP was dissolved with cosolvent of DMF and TFT (50 : 50 volume percent) in a Schlenk flask followed by 30 minutes purge with argon.

2. In another flask, CuBr (4.7 mg, 0.03 mmol), PMDETA (8 µL, 0.038 mmol), Heptadecafluorodecyl methacrylate (0.67 mL, 2 mmol), and 1-Pyrenylmethyl methacrylate (20 mg, 0.07 mmol) were dissolved in 3 mL cosolvent of DMF and TFT (50 : 50 volume percent). The mixture was freeze thawed three times to remove oxygen.

3. The mixture was then transferred into the NP solution under argon atmosphere and reacted at 70 ºC for 7 hours.

4. The resulting precipitate of polymer functionalized NPs was collected by vacuum filtration.

5. To remove the CuBr residue, the solid was stirred in methanol overnight and the polymer modified NP powder was collected.

**Preparation of initiator modified $SiO_2$-NPs:**

1. Ludox SM 30 particles were first passed through cation exchange resin to protonate the NP solution.

2. The solution was then dialyzed against DMF by using a cellulose membrane (MW cutoff: 7 K) for 48 hours with 1 change of DMF.

3. The $SiO_2$ NPs was precipitated by HFE followed by centrifugation and the product was dried.

4. The concentration of such NP solution was determined to be 115 mg/mL.

5. 1 mL of $SiO_2$ solution was further dispersed into 9 mL DMF followed by adding 11.45 g initiator.

6. The solution was stirred at room temperature for 24 hours.

7. The excess initiator was removed by dialysis against DMF for 96 hours changing DMF 4 times.

8. The content of $SiO_2$ was finally determined to be 8 mg/mL by the same precipitation method described above.

9. TGA analysis shows the initiator immobilized on $SiO_2$ is ~ 25 weight percent of total mass.

**Surface polymerization on initiator modified $SiO_2$-NPs:**

1. 1 mL of initiator modified $SiO_2$-NP solution was added in a Schlenk flask followed by 30 minutes purge with argon.

2. In another flask, CuBr (5.7 mg, 0.04 mmol), PMDETA (10 µL, 0.048 mmol), Heptadecafluorodecyl methacrylate (0.59 mL, 1.8 mmol), and 1-Pyrenylmethyl methacrylate (10 mg, 0.035 mmol) were dissolved in 3 mL DMF. The mixture was freeze thawed three times to remove oxygen.

3. The mixture was then transferred into the NP solution under argon atmosphere and the reaction was carried out at 70 ºC for 7 hours.

4. The resulted precipitate polymer functionalized NPs were collected through vacuum filtration.

5. To remove the CuBr residue, the solid was stirred in methanol overnight and the polymer modified NP powder was collected.

## d. Equipment

### i. Measuring particle size

Dynamic light scattering (DLS) was carried out at 25 ºC with a Malvern Zetasizer Nano ZS instrument equipped with a temperature control and using a 633 nm He-Ne laser for backscattering at 173º. The measurement duration was 15 seconds, and 11 measurements were averaged for each analysis. The distributions of the mean apparent translational diffusion coefficients ($D_T$) were determined by fitting the DLS autocorrelation functions using nonnegative constrained least squares (NNLS). The distribution of apparent sizes $D_h$ was obtained from the distribution of mean apparent translational diffusion coefficients ($D_T$) via

$$D_h = kT/(6\pi\eta D_T),$$

where $k$ is the Boltzmann constant, and $\eta$ is the solvent viscosity which was assumed to be that of HFE.

### ii. Particle images:

NP samples were dissolved in HFE and sonicated for 5 minutes followed by filtering with 0.2 µm filter. TEM was performed with a LEO 1550 FESEM under TEM mode at 30 kV. The sample was prepared by pipetting a drop of NP solution onto a carbon-coated Cu grid and dried in the air.

### iii. Thermogravimetric analysis

TGA was carried out by using the TGA-Q500 (TA Instruments). 3-7 mg of sample was used at a heating rate of 10 ºC/min from room temperature to 600 ºC. Attenuated total reflection infrared spectroscopy (ATR-IR) was recorded on a Nicolet iz10 (Thermo Scientific).

### iv. Determining particle concentration

UV and Fluorescence were measured by SpectraMaz M2e (Molecular Devices) in HFE. The excitation wavelength 340 nm was used for fluorescence measurements.

### v. Solubility

Finally, $scCO_2$ solubility tests were performed in a supercritical fluid phase monitor (SFT-phase monitor II) equipped with a 30 mL cell in which 20 mg of NP was tested. The test was performed at 21 ºC under 1500 psi where $CO_2$ is in its liquid state.

## e. Particle Synthesis

### i. Particle preparation

The bare $Fe_2O_3$ nanoparticles were prepared by adding ammonium hydroxide to a ferrous sulfate solution and reacting in the presence of oxalic acid (OA) for an hour at 80°C under a nitrogen atmosphere. As illustrated in the upper section of **Figure 1** the bare particles were then extracted with toluene and dried over anhydrous sodium sulfate. The separately-prepared BMTP initiator solution is then mixed with the bare nanoparticles and allowed to react under a nitrogen atmosphere for hours, with the result that Br ions are covalently attached to the particles by ligand exchange with the surfactant OA, as illustrated. Petroleum is then added to precipitate the particles which are then separated and re-dispersed in toluene several times to remove the unreacted BMTP and remaining OA. The initiated particles are then dried under vacuum. A polymer corona is then added to the particles by mixing them in DMF and TFT solution, adding PMDETA and other ingredients as described in the Methods section, and reacting at 70°C for 7 hours. The NPs the can be easily mono-dispersed in dimethylformamide (DMF) allowing atom-transfer radical-polymerization (ATRP) processing. DMF is a good solvent for ATRP since the monomer is soluble while polymer is insoluble. Thus the product precipitates upon polymerization (bottom right section of Figure 1). Once the polymer coating process is complete, the particles are collected by vacuum filtration and stirred in methanol to remove the CuBr residue. Aspects of this ligand exchange method is described by Sun et al.[2007].

Figure 1. Synthetic scheme of fluorescent fluoro-polymer functionalized nanoparticles.

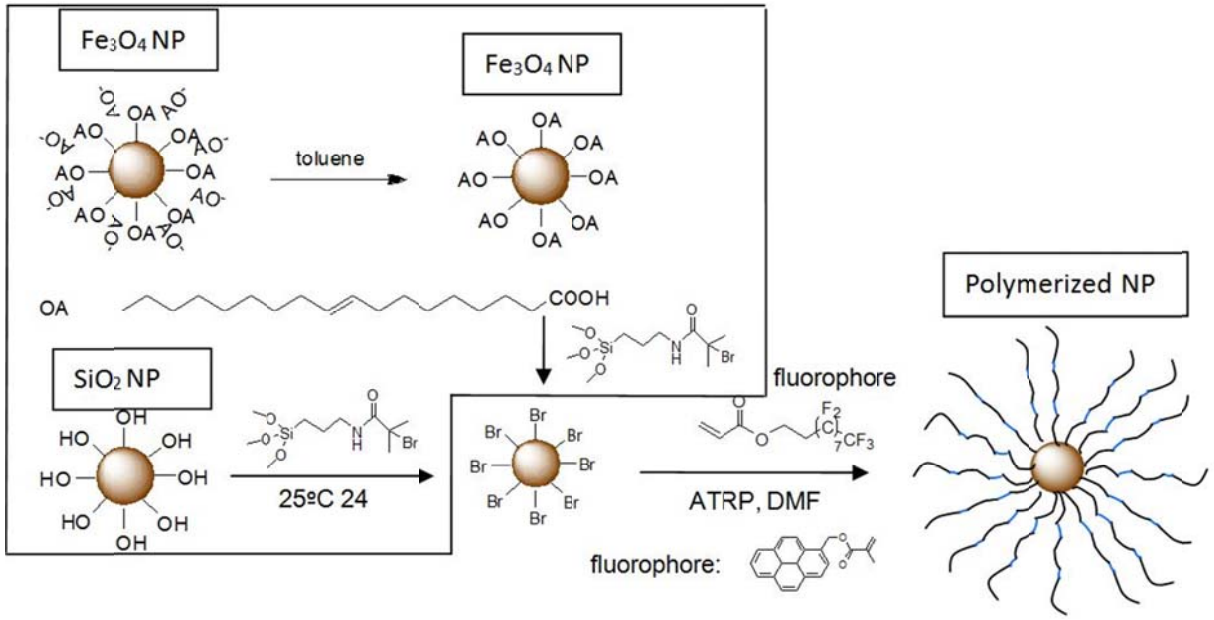

The $Fe_3O_4$ NPs polymerized in DMF are not soluble in Hydrofluoroether (HFE), a chemical proxy for supercritical $CO_2$ ($scCO_2$), or $scCO_2$, and sedimentation was observed to occur in minutes. This is because not enough polymer has been attached to the particle surfaces. The strategy we used to resolve this issue was to add Trifluorotoluene (TFT) to delay polymer precipitation. Adding 10 volume percent of TFT as cosolvent in DMF was not sufficient and infrared spectroscopy shows that very little polymerization had taken place on the NPs. The carbonyl peak 1728 of the fluoro-monomer is almost negligibly small. Low grafting was confirmed by TGA measurements which showed that the polymerized NPs had a similar mass loss ratio to the initiator-modified NPs. Increasing the TFT volume ratio to 50% led to successful polymer grafting. The NPs produced were soluble in HFE and $scCO_2$, and had a hydrodynamic diameter of 43 nm. IR analysis shows a significant increase of peak ratio of acrylate carbonyl peak over the amide I peak of initiator, and TGA data shows 90% of mass loss at 600 ºC is due to the loss of attached polymer.

The polymerization on the $SiO_2$-NP surface was performed in a similar fashion. However, the silica NPs are much more likely to aggregate. Therefore the mono-dispersed state of silica particle needs to be maintained throughout the entire modification procedure. In order to achieve mono-dispersed NPs, Ludox particles in aqueous solution were initially solvent exchanged with DMF instead of fumed silica NPs. The Ludox particles are a colloidal suspension in water. In contrast to the $Fe_3O_4$-NPs, the $SiO_2$-NPs polymerized in DMF are soluble in HFE and $scCO_2$. This might be due to a higher grafting density of polymer on the silica NPs.

### ii. Making the particles fluorescent

**Figure 2a** shows the UV spectrum of $Fe_3O_4$-NP when 3.5% (mol) fluorescent monomer 1-Pyrenylmethyl methacrylate was incorporated in the polymerization process. The peak at 340 nm corresponds to the characteristic peak of 1-Pyrenylmethyl methacrylate and the peak at 445 nm arises from the absorption of $Fe_3O_4$ core. Such NPs show very intense fluorescence (**Figure 2b**). The fluorescence intensity is linear with NP concentration, provided the concentration is less than ~400 ppm. This is probably because the $Fe_3O_4$-NPs have a strong background absorption, which reduces light penetration and fluorophore excitation. At low concentration, the background absorption of $Fe_3O_4$ is greatly reduced, and thus the incident light is exclusively absorbed by fluorophore molecules.

Figure 2. Fluorescent intensity versus concentration for $Fe_3O_4$ nanoparticle.

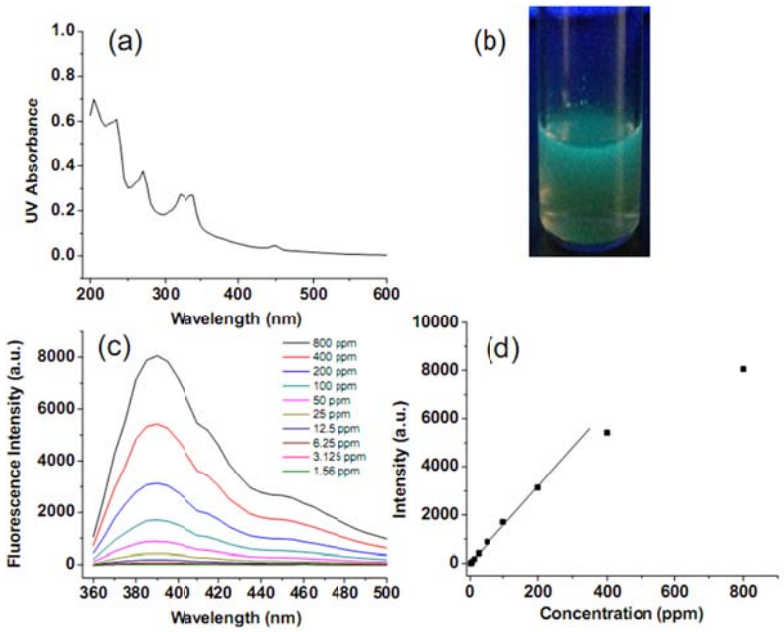


The UV spectrum of $SiO_2$-NPs in **Figure 3** also shows the characteristic $\lambda_{max}$ of 1-Pyrenylmethyl methacrylate at 340 nm. However, the additional peak at 445 nm and the strong baseline absorption corresponding to the absorption of $Fe_3O_4$ is missing for the $SiO_2$-NPs. Therefore, the $SiO_2$-NPs show a uniformly fluorescent emission from the top to the bottom of the sample illuminated from the top, as shown in Figure 3. This is in contrast for the case of $Fe_3O_4$-NPs in Figure 2b, where only the top portion of the solution under excitation is fluorescent, and the bottom portion exhibits the brown characteristic color of the $Fe_3O_4$-NPs. The absence of UV absorption from the bottom portion of the $Fe_3O_4$ sample allows the fluorescence calibration curve to remain linear to high particle concentrations. This advantage is offset to some degree by the fact that the fluorescence of $SiO_2$-NPs is much lower than that of $Fe_3O_4$-NPs at the same concentration.

Figure 3. Fluorescent intensity versus concentration for $SiO_2$ nanoparticles.

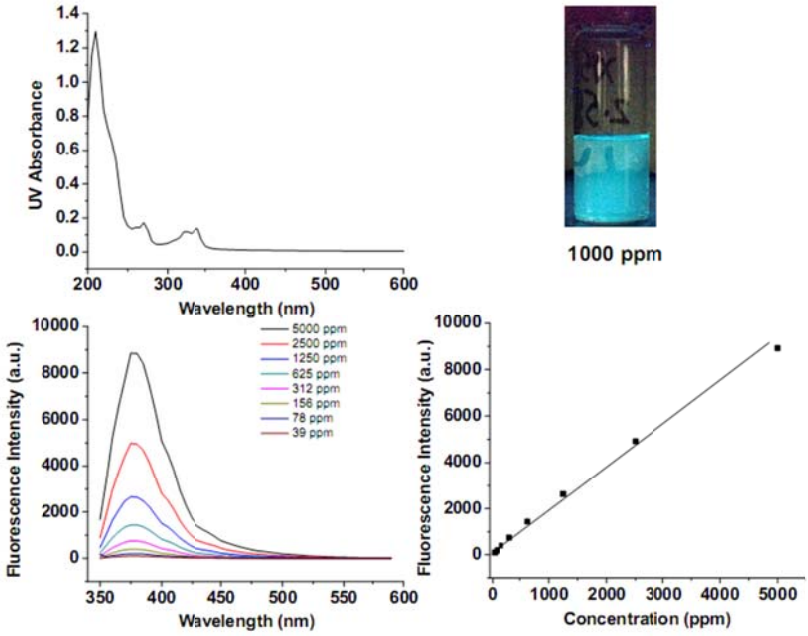


## f. Characterization

Dynamic light scattering (DLS) was used to follow the size distributions of NPs at different synthetic steps as shown in **Figure 4**. OA, initiator, and polymer functionalized NPs can all be dispersed well in their corresponding solvents and have hydrodynamic diameters of 9, 10, and 43 nm, respectively. In general, very little aggregation or clustering was observed from DLS during each step.

The DLS results show that the hydrodynamic diameter of hydroxyl functionalized silica NP is maintained at ~ 6 nm before polymerization with little aggregation. Attachment of initiator onto the NP surface slightly increases the size to ~ 7 nm. The polymerization on NPs leads to a diameter of 39 nm, which is comparable to that of $Fe_3O_4$-NPs. The use of solid-fumed silica NP as starting material resulted in a much larger size particle, probably corresponding to aggregates or clusters in HFE (data not shown). This suggests it is important to keep the $SiO_2$-NP mono-dispersed through each modification step.

The DLS results are consistent with the transmission electron microscope (TEM) analyses indicated in **Figure 5**. Due to the low contrast of the polymeric corona, only the $Fe_3O_4$ core can be observed with TEM. Nevertheless, the spacing between pairs of NPs suggests the existence of a polymer corona on $Fe_3O_4$-NPs and contrasts with the closely packed structures observed for bare NPs.

Figure 4. Hydrodynamic size distributions of $Fe_3O_4$ and $SiO_2$ NPs as measured by DLS.

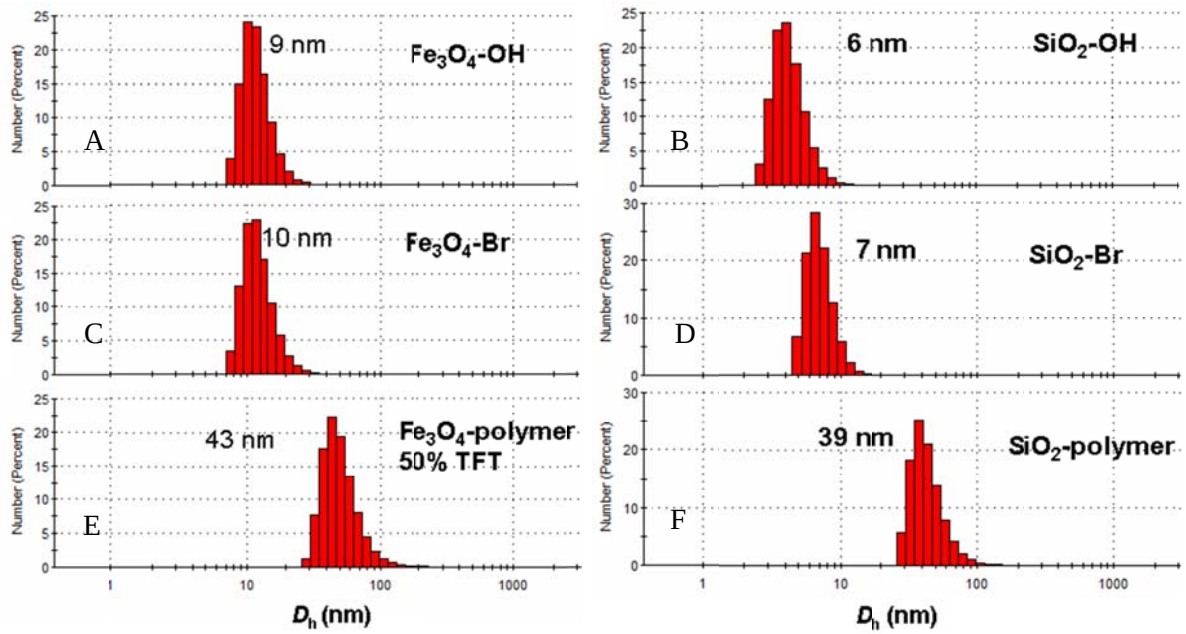


(A) bare $Fe_3O_4$ particle; (B) bare $SiO_2$ particle; (C) $Fe_3O_4$ nanoparticle with attached initiator; (D) $SiO_2$ nanoparticle with attached initiator; (E) $Fe_3O_4$ nanoparticle after polymerization; (F) $SiO_2$ nanoparticle after polymerization.

Figure 5. TEM images of $Fe_3O_4$ and $SiO_2$ NPs

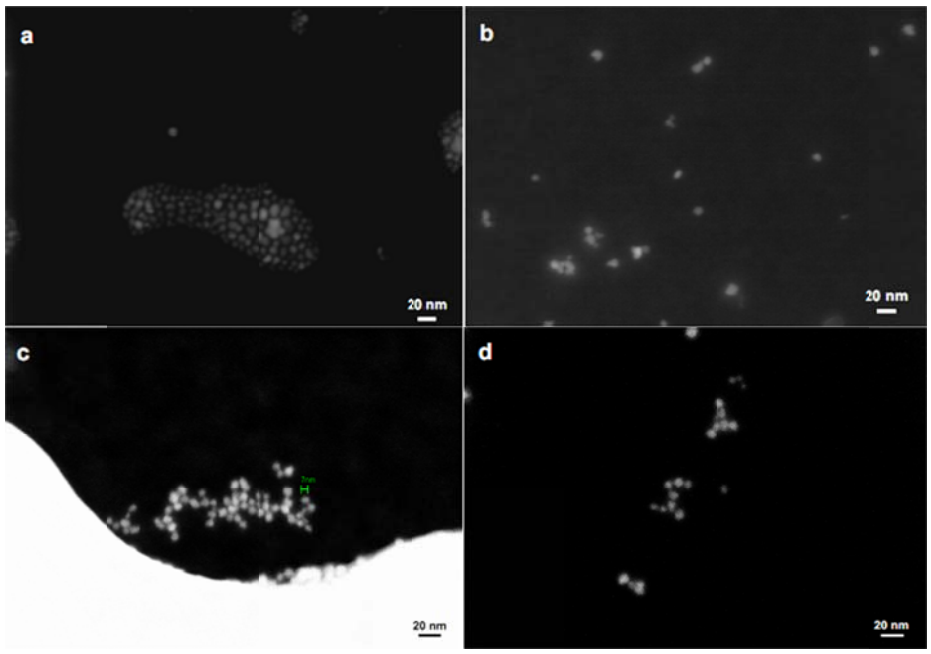


(a) shows the bare $Fe_3O_4$ NP, (b) the polymerized $Fe_3O_4$ NP, (c) the bare $SiO_2$ NP, and (d) the polymerized $SiO_2$ NP. Separation of the polymerized particles by their corona is evident in (b) and (d).

Thermogravimetric analysis (TGA) was also performed to determine the grafting density of initiator coated NPs, **Figures 6 and 7**. Since the mass loss for initiator-NP is about 25% of the total mass of the Br-NP, the content of the initiator on the NP is about 1.05 mmol/g. The grafting density of initiator can be estimated by the following equation, as reported by Liu et al.[2011]

$$GD = \frac{a_{Br} N_A}{\frac{S}{\rho V}},$$

where *GD* is grafting density, $a_{Br}$ is moles of initiator per gram of NP, $N_A$ is Avogadro's number, *S* is the surface area of the NP, *V* is the volume of the NP, and $\rho$ is the density of the NP. Therefore, the grafting density of initiator can be estimated to be 5 initiators per $nm^2$ for $Fe_3O_4$ NP, and 4 initiators per $nm^2$ for $SiO_2$ NP.

Infrared spectroscopy (IR) was also used to confirm the functionalization process, **Figure 8**. The stretching modes of alkyl moieties from OA were clearly seen between 2800 and 3000 $cm^{-1}$ and the carboxylate group of OA was seen at 1701 $cm^{-1}$. After ligand exchange, amide I and II peaks were observed at 1645 and 1534 $cm^{-1}$, respectively, indicating successful attachment of imitator. The disappearance of high frequency stretching peaks and carboxylate peak at 1701 $cm^{-1}$ further suggests the completeness of ligand exchange without OA molecules residing on NPs. When polymerization take place in a Trifluorotoluene – DMF solvent mixture with TFT/DMF=1:9, very little carbonyl stretching at 1728 $cm^{-1}$ was noticed, and the entire spectrum is very similar to that for initiator NPs. However, increasing the TFT/DMF ratio to 1 dramatically increases the 1728 peak, indicating large amounts of polymer brushes have grown on the NP surface. The modifications of initiator and polymer, as monitored by IR, are quite similar to those for $Fe_3O_4$-NP functionalization as shown in Figure 7.

Figure 6. SEM images of $Fe_3O_4$ NPs. (a) shows the bare $Fe_3O_4$ NPs, and (b) the polymerized $Fe_3O_4$ NPs

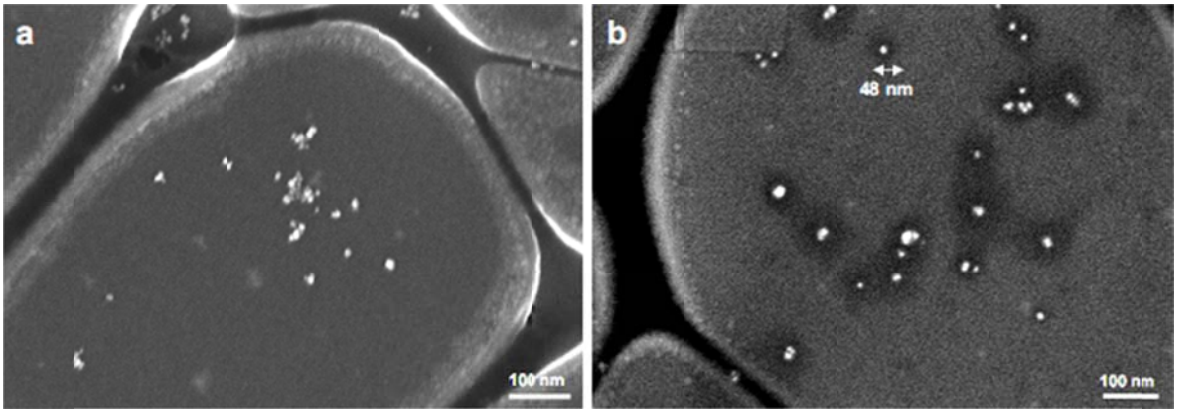


SEM images of $SiO_2$ NP are not shown because SEM technique does not capture $SiO_2$ NP well. The separation of the polymerized particles by their corona is very evident in (b).

Figure 7. TGA images for $Fe_3O_4$ (left) and $SiO_2$ (right) nanoparticles.

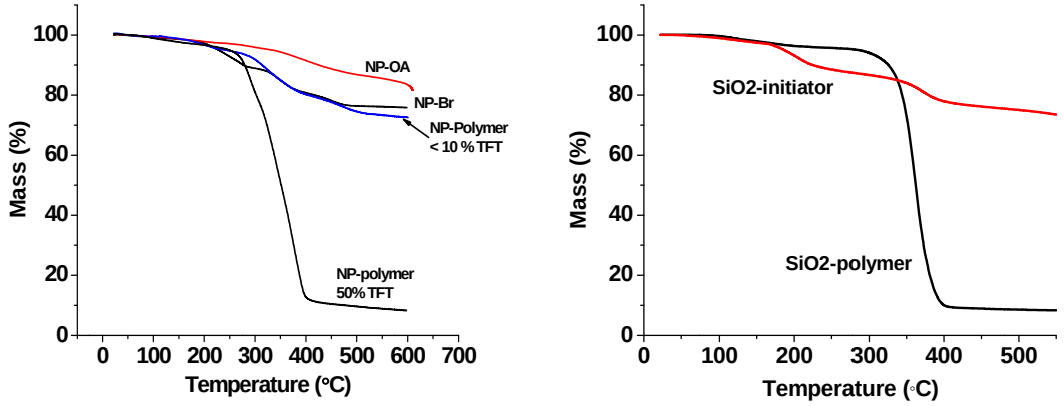

Figure 8. IR characterizations of $Fe_3O_4$ (left) and $SiO_2$ (right) NPs coated at different steps.

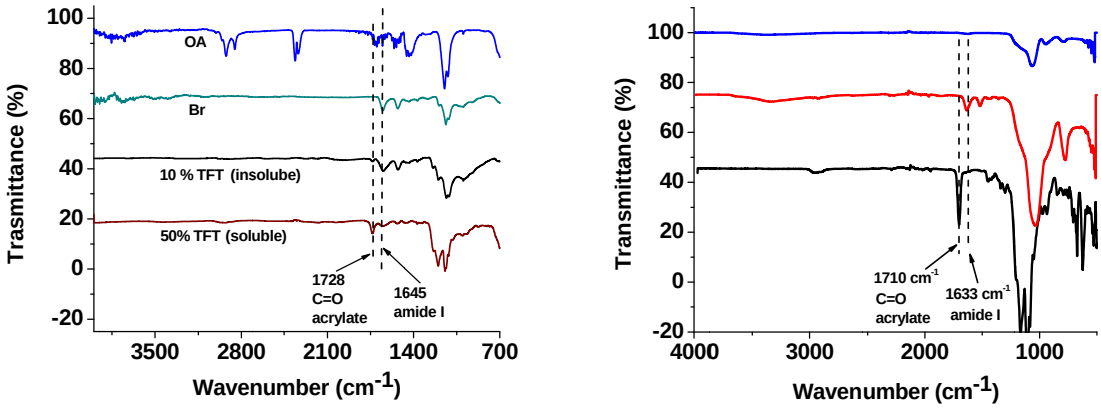


**Figure 9** shows the most critical property of the particles: their dispersibility in supercritical $CO_2$. General speaking, in the development of $CO_2$-philic nanoparticles, liquid $CO_2$ is not as good of a solvent as $scCO_2$ (Hyatt, 1984). The solubility of two types of NPs was tested as shown in Figure 9 in a high pressure chamber with a glass window. Both iron oxide and silica NPs are dispersible in supercritical $CO_2$, but not in liquid $CO_2$ (Figure 9a and a'). The cell has a vertical bar that is clearly visible in c and c' and partly visible in b and b'. A clear solution indicates the uniform dispersion of small particles.

The lack of dispersibility of our nanoparticles in liquid $CO_2$ is not an issue. The vertical depth of a typical gas shale gas is 5,000 to 8,500 feet (1.5 to 2.5 km). For a temperature gradient of 25°C per km and an average surface temperature of 20°C, the temperature at 1.5 km is ~50°C and the pressure will be greater than 150 bars. The critical temperature and pressure of $CO_2$ are 31°C and 73 bars, so in sequestration operations $CO_2$ will be well into the supercritical field (see Figure C4 in the Appendices). The particles are not likely to encounter liquid $CO_2$ in normal field conditions.

Figure 9. Twenty milligrams of nanoparticles are dispersed in a 30mL pressure cell containing, depending on pressure and temperature, different phases of $CO_2$.

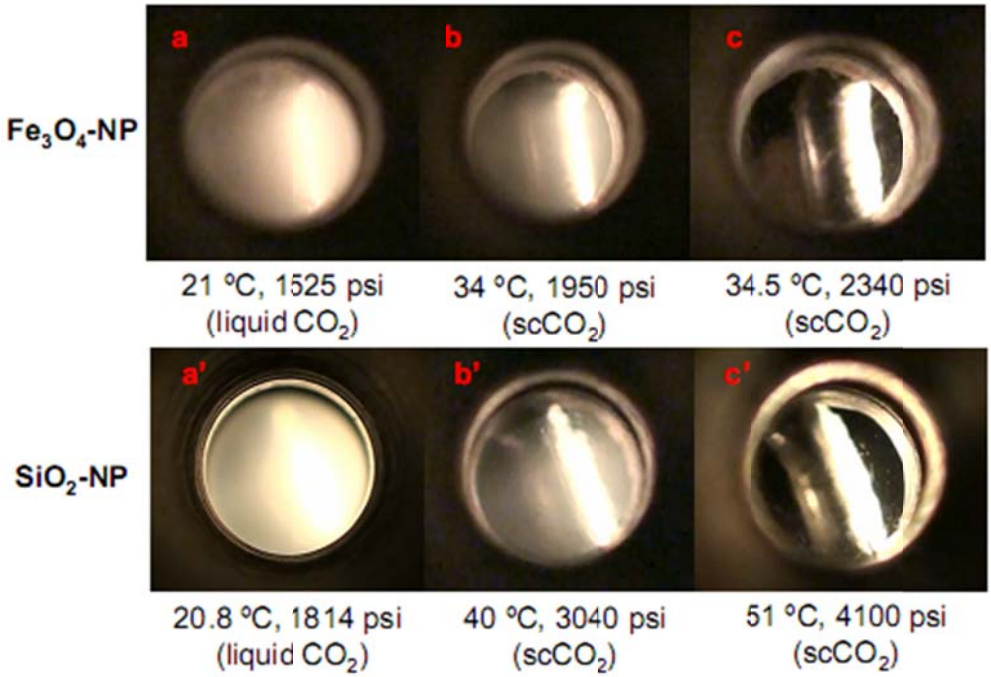


Fluid clarity (where you can clearly see the dividing bar of the cell) indicates the uniform dispersion of small nanoparticles. Cloudiness indicates the particles have clumped together to form clusters large enough to occlude light. The images indicate the nanoparticles are not dispersible in liquid $CO_2$ (not surprising as discussed in the text) but disperse well in supercritical $CO_2$.

# 3. DUAL TRACER DIFFUSION EXPERIMENTS

## a. Introduction

The laboratory experiments had three purposes: (1) to demonstrate in a controlled system how the storage of $CO_2$ in shale could be measured by experiments that could be carried out from wells, (2) to test the nanoparticles we synthesized in a supercritical $CO_2$ proxy, and (3) to test and refine the interpretive models that will be applied, in different form, to both the laboratory and field experiments.

We carried out two different kinds of laboratory experiments. The first set of experiments involved the inter-diffusion of air, methane and carbon dioxide at atmospheric pressure. This set of experiments was reported to Advanced Resources in a report titled "Preliminary laboratory assessment of a smart particle early warning system" by Russell Zhao and Lawrence M. Cathles III. The experiments are also the subject of Russell Zhao's Cornell master's thesis (Appendix A). The essential aspects of this work are summarized briefly in the next section.

The second set of experiments dispersed the nanoparticles we synthesized in a supercritical $CO_2$ fluid analogue, and passed them, together with an inert chemical tracer, through a Hele Shaw style diffusion cell. The purpose was to demonstrate how dual tracers of this kind could be used to assess $CO_2$ sequestration in shale. It is this set of experiments that we mainly describe in this section of this report.

## b. Gas diffusion experiments

The gas diffusion experiments were carried out in a Hele Shaw style flow cell consisting of a 1 cm x 1 cm x 1 m long core channel with an attached diffusional slit 0.2 cm thick and 28.5 cm wide. The apparatus is shown in **Figure 10**. The apparatus is initially filled with one gas (e.g., methane), and then another gas (e.g., $CO_2$) is injected into the core channel. The channel gas diffuses into the slit and is stored there. The storage of the injected gas is assessed by measuring the composition of the effluent gas.

Figure 10. Hele-Shaw modified flow cell used for gaseous diffusion experiments.

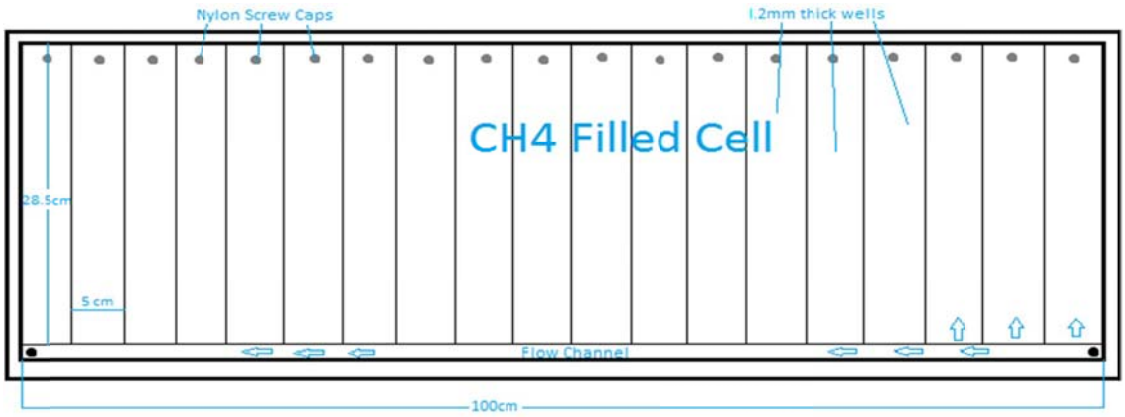


The conclusions reported in Zhao's thesis are: (1) A Hele Shaw-style apparatus can simulate the diffusional sequestration of $CO_2$ into stagnant methane-filled volumes of the shale; (2) The Hele Shaw system experiments can be successfully modeled using gas inter-diffusion constants experimentally measured by others for the pairs of gases involved in our experiments of ~0.18$cm^2$/s; (3) A second order correction of the diffusion constant improves the model fit to the measured data for experiments involving the lightest and most dense gas pairs ($CH_4$ and $CO_2$) when the lightest gas is the injected gas; although the correction required is a bit larger than that suggested by non-linear gas diffusion theories; (4) Gravity drainage and perhaps density stratification of the gases are important in the laboratory experiments, but will not be important in field applications; and (5) Compartment flow is very small, and account need not be made of it in the modeling.

Inter-diffusion of gases is the key to $CO_2$ storage in shale. The implications of the laboratory experiments for the sequestration of $CO_2$ in shale are: (1) The experiments show, by analogy, how the inter-diffusion of injected $CO_2$ and ambient $CH_4$ in a gas shale can be modeled from the fracture spacing and porosity of the shale matrix; (2) The storage fraction plots illustrated provide an effective, easy, and early way to judge the viability of $CO_2$ storage from well tests; and (3) The storage of $CO_2$ in gas shale could be feasible if the fracture spacing is small (<10 cm).

## c. Analogue supercritical $CO_2$ dual tracer diffusion experiments

The gas diffusion experiments show the potential for gas inter-diffusion to provide an early indication of the viability of $CO_2$ sequestration in shale. This assessment can be confirmed with well tests that, in addition, take advantage of the contrasting diffusional properties of a particle and chemical tracers. This section of this report discusses experiments we have performed and analyzed that demonstrate how this might be done.

Flow bypass fluid diffusion experiments were carried out using a $scCO_2$ analogue solvent containing both chemical and nanoparticle tracers. The nanoparticle tracers are those documented in the previous section. Two experiments in two different diffusion cells are reported. Not reported are some initial diffusion experiments that were carried out with earlier prototypes of the particles in a diffusion cell of similar design. These experiments were not successful because of the fact that the nanoparticles were unstable, and because the cell diffusion slit was too wide relative to the core channel and carried too much of the flow. From this experience, two new glass Hele-Shaw diffusion cells were designed and constructed. The experiments described below were carried out in these cells with nanoparticles which performed well.

### i. Experimental materials

Experiments using $scCO_2$ similar to those reported here would have involved keeping the entire apparatus from injection to detection at high pressure. This would have been difficult. Using a $scCO_2$ analog solvent instead of $scCO_2$ avoids these challenges because the experiments can be conducted under ambient conditions of temperature and pressure.

The carrier fluid we chose is a commercial product of 3M: Hydrofluoroether 7200 (HFE). HFE 7200 is chemically similar to $scCO_2$. Chemicals and particles that dissolve or disperse $scCO_2$ will also do so in this HFE solvent. HFE is not fluorescent, so detection of fluorescent nanoparticles is not complicated by interference from the fluorescence of the solvent. The chemical tracer accompanying our nanoparticles is Trifluorotoluene (TFT). The structure of TFT molecule is a benzene ring with three attached fluorine atoms (see Figure C1 in the Appendices).

### ii. Apparatus design

The glass HeleShaw diffusion cells were designed with the diffusion properties of the nanoparticles and TFT in mind. The first glass cell has a core channel with dimensions of 8mm x 8mm x 100mm. The core channel is attached to a 2mm X 80mm X 100mm diffusion slit. The second cell has different core channel dimensions (12mm x 12mm x 100mm), but the diffusion slit is the same. The cores of both cells are larger and the slits apertures are thinner than in the initial, failed, cell design.

The TFT tracer and the $SiO_2$ or $Fe_3O_4$ nanoparticles are premixed at a known concentration in the Hydrofluoroether (HFE). As shown in **Figure 11**, the solvent is held in a 50ml glass syringe mounted on a high precision syringe pump. The injection rate is controlled at 1.44 cc/day in both experiments.

Figure 11. Experiment schematic.

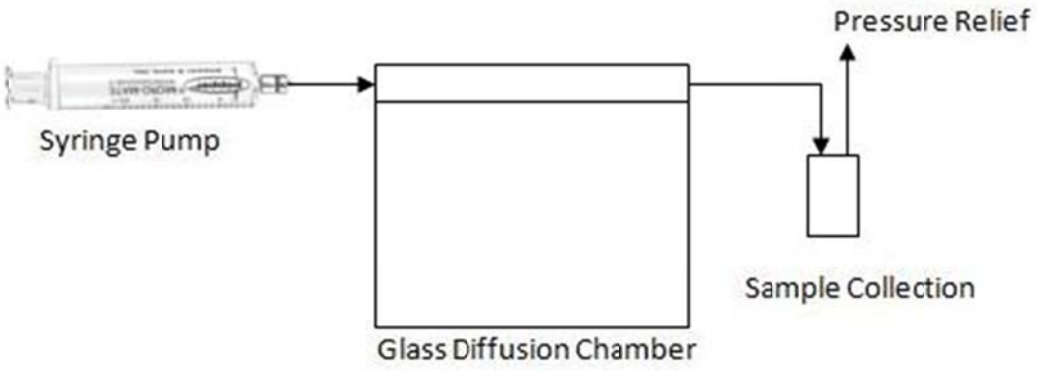


### iii. Fabrication

We chose to construct the apparatus from glass and use stainless steel fittings and tubing to avoid the chemical reactions and swelling that polycarbonate materials in contact with an organic solvent HFE 7200 would have. Glass is difficult to machine and the machining and construction was carried out to our design specifications by Special Glass Products Inc.

The cells consist of a machined/etched glass plate covered with a second glass plate, as shown in **Figure 12**. The inlets and outlets were drilled before sealing the top cover glass. The glass was polished before shipping to us. The brittleness of the glass precluded the installation of glass nipples extending out of the apparatus, and it proved not to be trivial matter to attach a stainless tubing to the small holes drilled in the glass. We used Polydimethylsiloxane (PDMS) with a 1:8 hardener/base ratio as an intermediate elastic material to hold our stainless steel tubing tight while it was chemically bonded to the glass to create a tight seal (**Figure 13**). We further secured the tubing with a thin layer of Corning silicon glass sealant to minimize damage during transportation and usage. Finally, we enclosed the entire apparatus in PDMS to create a pressure-tight, rigid system, and eliminate any potential evaporation of our carrier solvent HFE 7200 (**Figures 14 and 15**). Vacuum grease was applied to the connections to prevent any potential evaporation. PDMS is very inert, it is not soluble in HFE 7200 or water, and HFE 7200 is highly evaporative.

Figure 12. A: Glass cell 1 before bonding. B: Glass cell 2 before bonding. See figure 11, 12 for dimensions.

Figure 13. A. Protection of tubing after it is bonded with the glass cell. B. Close up of the clean bonding between polished glass surface and PDMS.

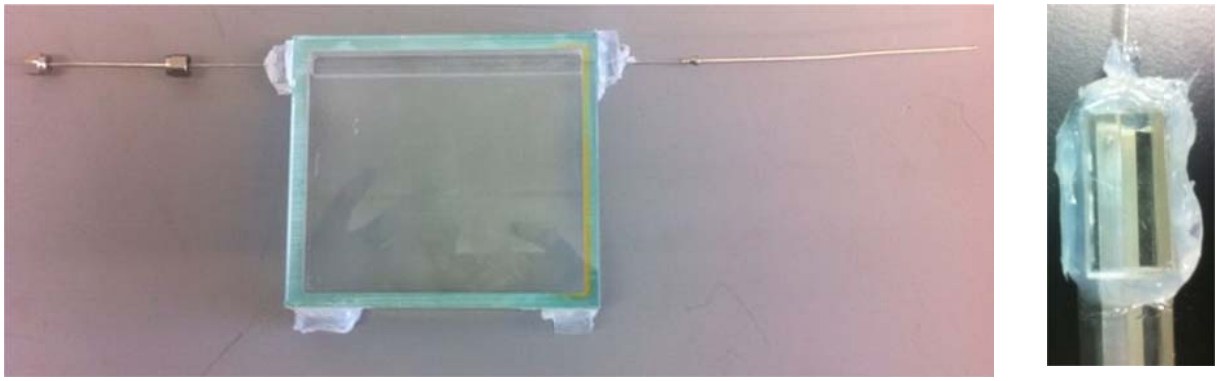

Figure 14. Glass apparatus encased in PDMS. Vacuum grease is applied at each connection to prevent any potential evaporation.

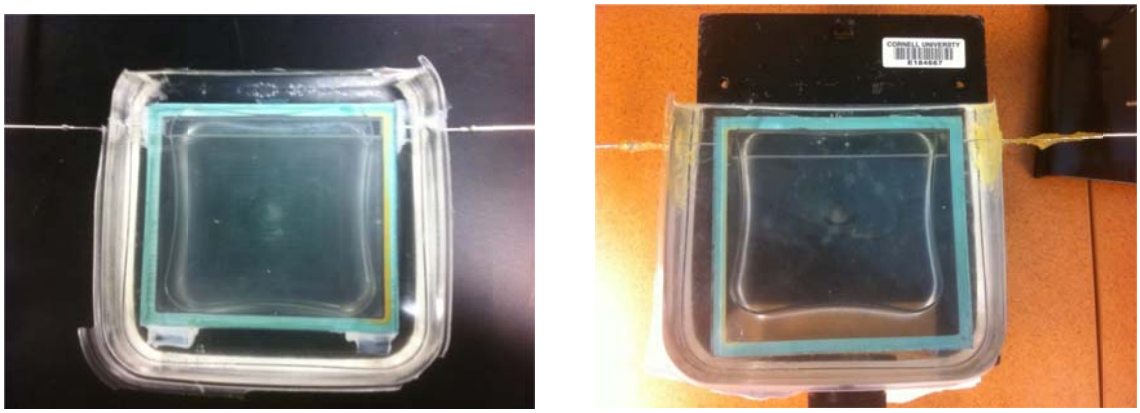

Figure 15. The glass diffusion system in operation in the lab.

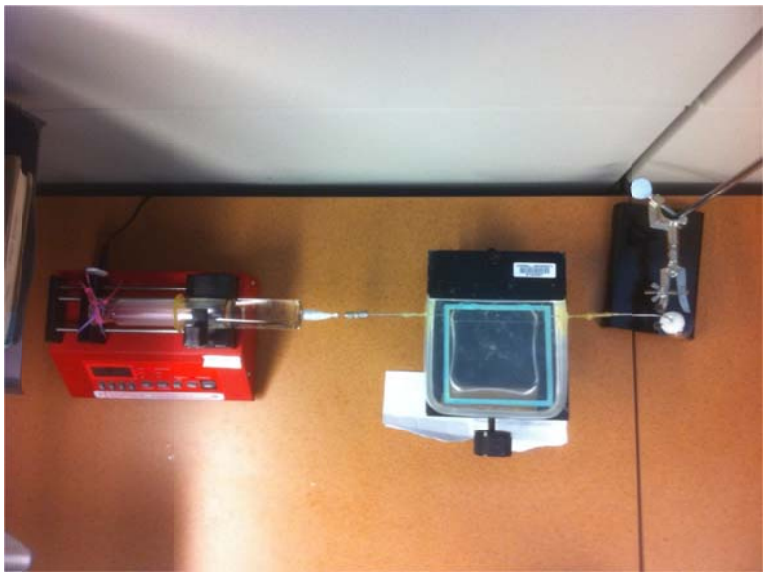

### iv. Tracer Detection

Ultraviolet absorption spectroscopy is used to measure the concentration of the TFT chemical tracer. TFT has a benzene ring UV absorption peak at 255 nm wavelength. The concentration of the $SiO_2$ and $Fe_3O_4$ nanoparticle tracers are measured mainly by the fluorescence of fluorophore molecules imbedded in the polymer coronae. Both of these particles have the same excitation and emission peaks, but the $Fe_3O_4$ nanoparticles are more fluorescent for the same particle concentration. Because TFT has no UV absorption beyond a 300 nm wavelength, both fluorescence and ultraviolet absorption spectroscopy could have been used to determine the concentration of nanoparticles particles, but we did not do this here.

The fluorescence and UV absorption profile of the HFE solvent is considered a constant background and subtracted from every measurement. We also made sure that there was no interaction between our chemical and nanoparticle tracers by measuring the fluorescence and UV absorption at a few known concentrations and verifying that the individual concentration-fluorescent intensity and UV absorption calibration curves remained valid.

Data were collected at time intervals that yield the minimal sample size required for analysis. To minimize the evaporation during the measurements, the fluid sample was withdrawn from the sample collection vial with a glass syringe and quickly injected to a clean glass cuvette with its top sealed. The software program Proview was used to interpret the output from the SpectraMax spectrophotometer built by Molecular Devices Company. Glass cuvettes and glass syringes were cleaned thoroughly, dried completely, and reused for the next sample measurement.

### v. Data Interpretation

**Figures 16 through 21** document the interpretation methods used. The methods for $SiO_2$ and $Fe_3O_4$ nanoparticles are the same. The effluent concentration of nanoparticle tracers is calculated by measuring the effluent fluid's fluorescence. Figure 16 shows a typical sample fluorescence spectra. The fluorescent peak at 390 nm indicates (Figure 17) a silica nanoparticle concentration of ~3400 ppm.

Once the concentration of the particles has been determined from their fluorescence, their UV absorption can be subtracted from the UV absorption spectra for the solution. Figure 18 shows that the UV absorption expected for a 3400 ppm silica solution is ~0.17. When a UV silica absorption spectra with a peak height at 255 nm of 0.17 is subtracted from the total spectra, the residual 255 nm peak height can be used to determine the TFT concentration from the calibration curve in Figure 19.

Figure 16. Measured fluorescence of silica nanoparticles dispersed in HFE together with TFT.

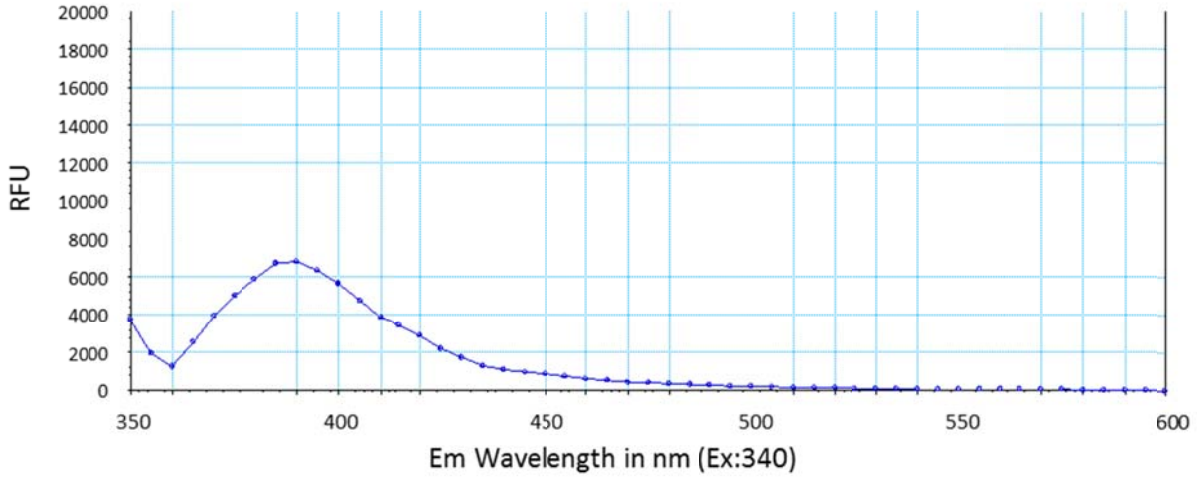


Solution and tracers are excited at 340 nm. The TFT is not fluorescent. The peak emission is at 390 nm. X axis is the wavelength in nm, Y axis is the intensity level.

Figure 17. Fluorescence calibration curve for the silica nanoparticle concentration.

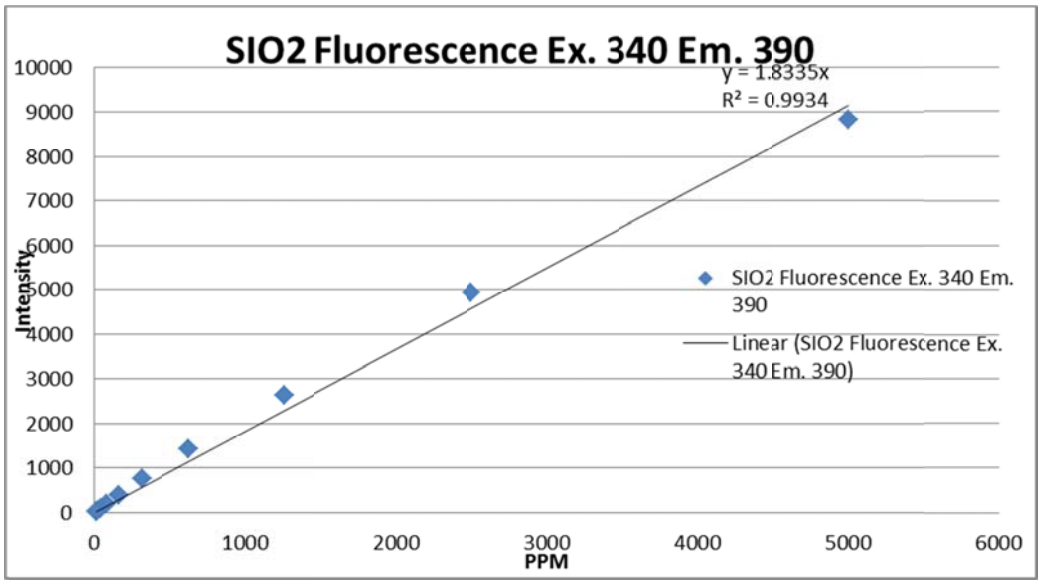


The relationship between the emission intensity (excited at 340 nm and measured at 390 nm) and the nanoparticle concentration is linear. The concentration of silica nanoparticles in Figure 18 is ~3700 ppm $SiO_2$ according to this calibration curve.

Figure 18. Calibration curve for the UV absorption level for the $SiO_2$ nanoparticles at 255 nm.

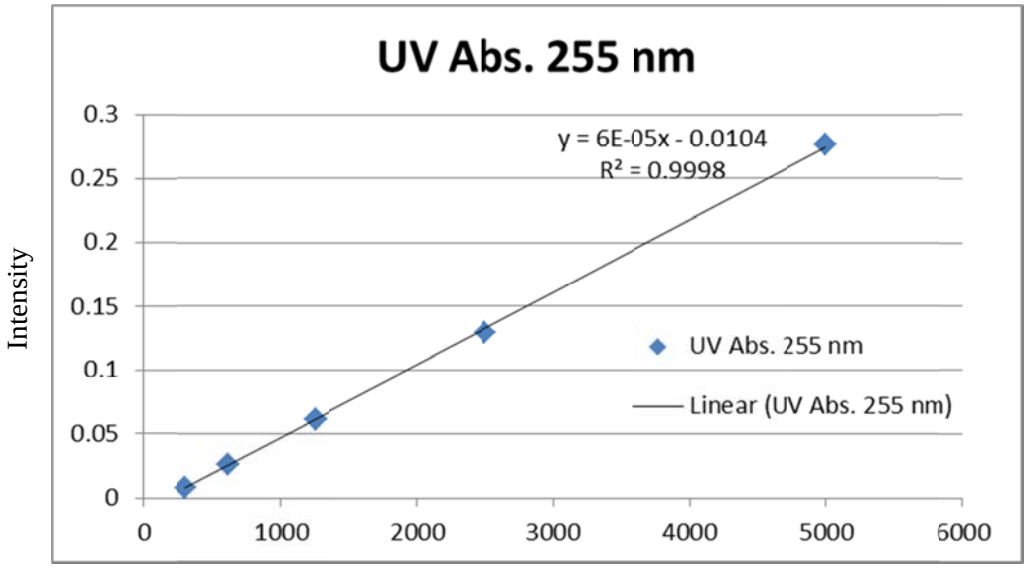

Figure 19. The peak UV absorption at 255nm is a linear function of TFT concentration.

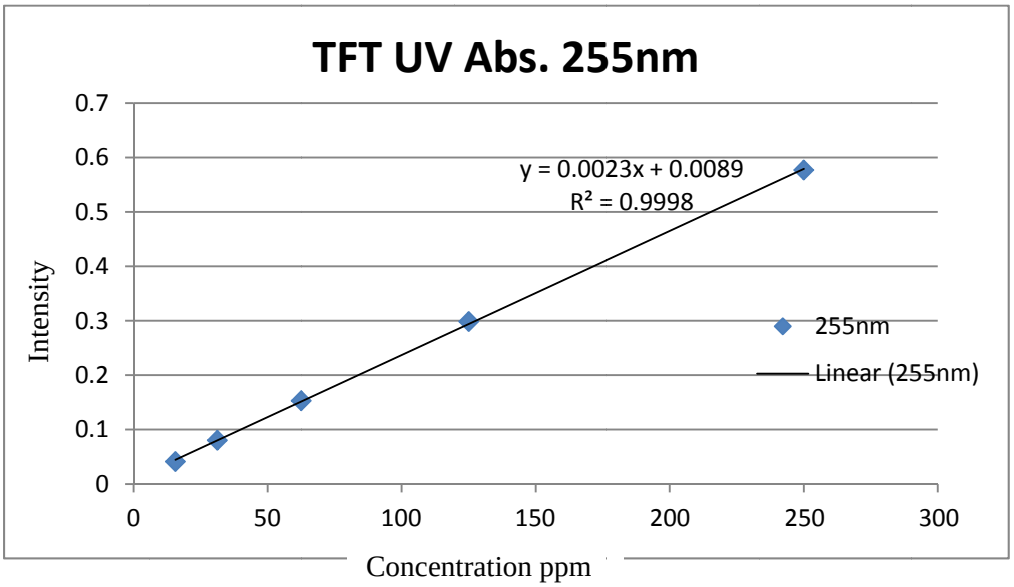


Figure 20 shows the UV absorption for $SiO_2$ nanoparticles and TFT, Figure 21 shows the UV absorption with the $SiO_2$ UV absorption subtracted out. The benzene peak height of ~2.6 in this figure indicates, via the calibration curve in Figure 19, that the TFT concentration of a little over 100 ppm.

Figure 20. This figure shows the UV absorption profile for a sample with both $SiO_2$ nanoparticles and TFT present.

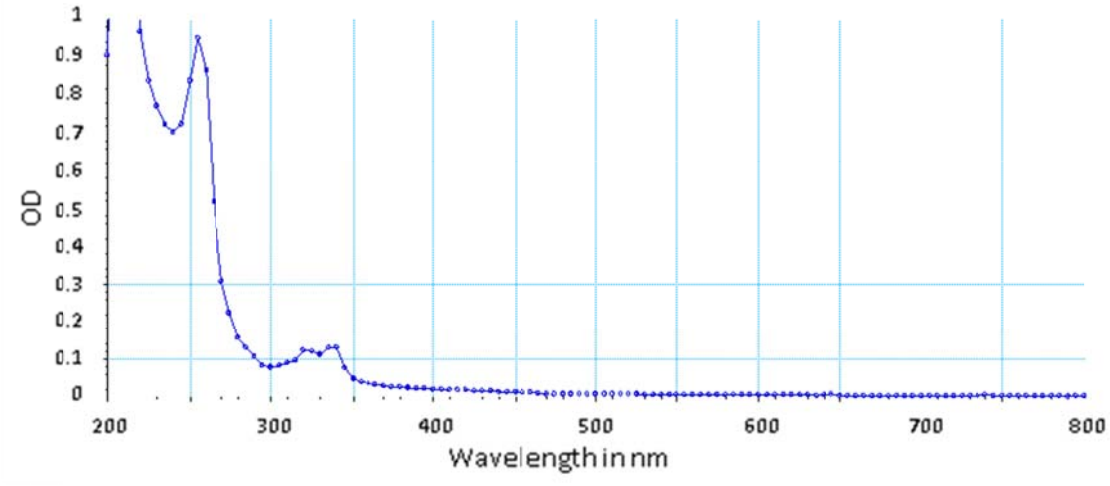


Figure 21. UV absorption profile for the chemical tracer TFT only (no silica nanoparticles).

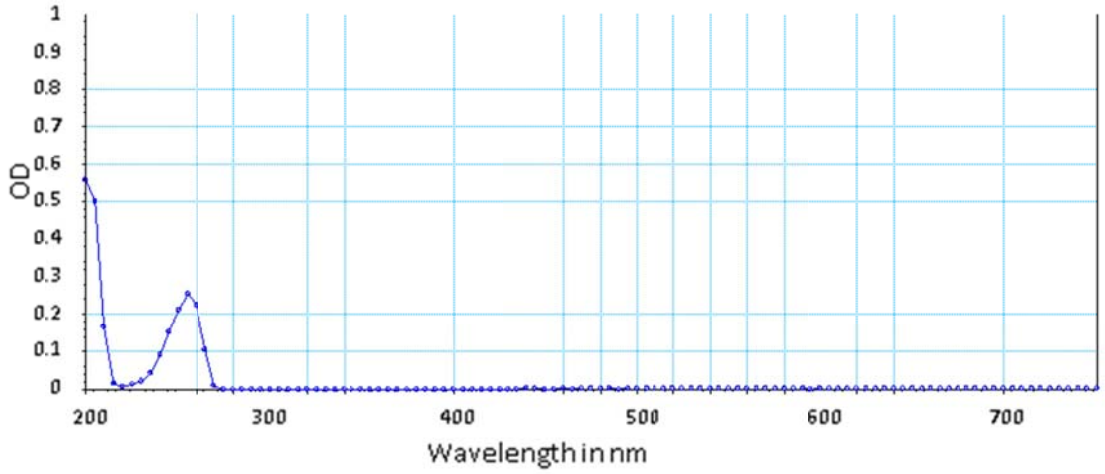


The UV absorption peak of benzene ring is at 255nm. There is no UV absorption after 280nm.

### vi. Experimental Results and interpretation

**Figure 22** shows the effluent tracer concentration as a function of time for the two experiments. Each experiment lasted about a month. At the common injection rate of 1.44 cc/day, 1 core pore volume was injected in ~4.4 days in the first apparatus hosting the $SiO_2$ nanoparticle experiment, and 1 core pore volume was injected in 10 days in the second apparatus hosting the $Fe_2O_3$ nanoparticle experiment. One total pore volume (matrix plus core) was injected into the first apparatus in 22.4 days and into the second apparatus in 30.4 days.

Figure 22. Effluent concentration as a function of time for experiments carried out in HFE (a proxy solvent for supercritical $CO_2$).

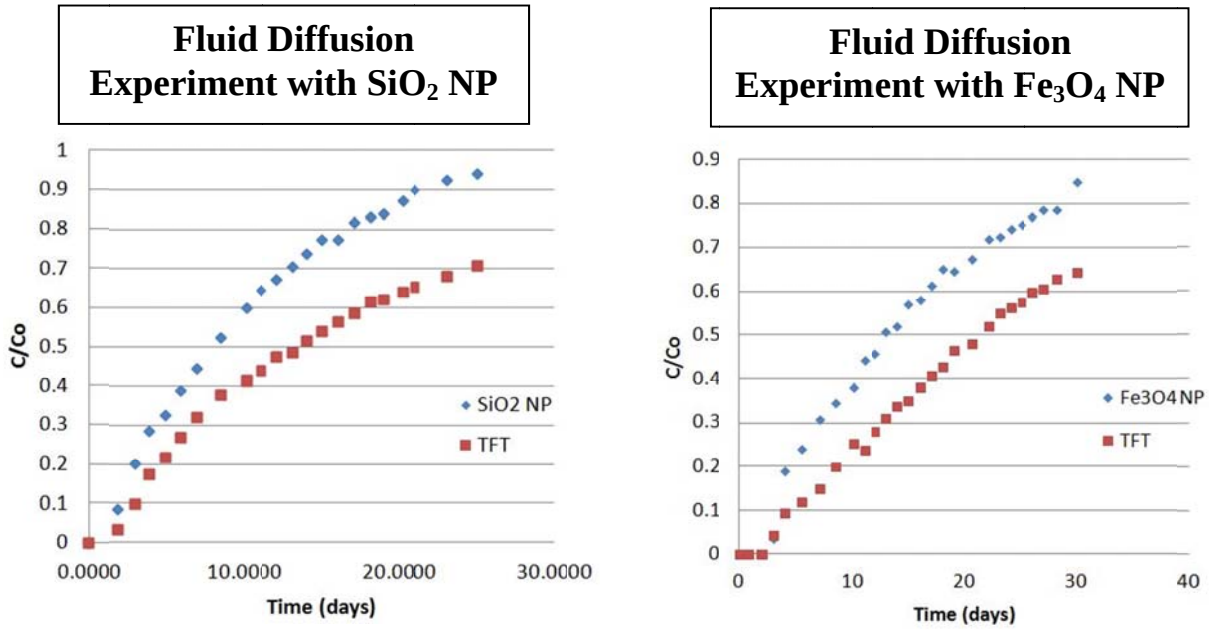


**Table 1** gives the diffusion constants we estimate from the Stokes-Einstein equation for the chemical and nanoparticle tracers used. The distance the TFT and particles would diffuse in one day are estimated in the last column of the table. This column shows that diffusion in the core channel will be important. At face value, diffusion in the core channel would appear to be less important for the nanoparticles, but dispersion in the channel is important, as we discuss below.

Table 1. Diffusion constants estimated from the Stokes-Einstein equation (Appendix C) for the particles and chemical tracer in the proxy supercritical $CO_2$ solvent HFE.

| | $D_o$[cm$^2$/s] x $10^5$ | $D_o$[cm$^2$/day] | $x$[1 day]= $2\sqrt{D_o t}$ |
|---|---|---|---|
| **TFT** | 1.4 -**2.5**- 3.55 | 2.16 | 2.9 cm |
| **$SiO_2$ NPs** | 0.0182 | 0.015 | 0.25 |
| **$Fe_2O_3$ NPs** | 0.0165 | 0.014 | 0.24 |

The range in Do for TFT reflects the maximum and minimum dimensions of the molecule with the middle value representing the best-fitting value to our experiments.

Figure 22 shows plots the concentrations of the tracers in the two experiments as a function of time. The effluent concentrations of the nanoparticles and TFT chemical tracer were determined as described above. After a month of injection, the nanoparticle tracer reaches more than 90% of its injected concentration in both cases. The TFT tracer achieves between 60% and 70% of its injected concentration. The results of the two experiments are similar even though they were carried out in apparatus of slightly different design and used nanoparticles of similar sized but different core material. In both cases, the nanoparticles arrived before the chemical tracer in both experiments. This reflects the fact that the chemical tracer diffuses more in the slit adjacent to the core flow channel than do the nanoparticles.

**Figure 23** shows our model interpretation of the experimental data in Figure 22. We achieve an excellent fit between the effluent concentrations of TFT and our model predictions using a TFT diffusion constant of $2.5 \times 10^{-5}$ cm$^2$/s. As shown in Table 1, this diffusion constant has a value intermediate between the values calculated for the maximum and minimum dimensions of the TFT molecule using the Stokes-Einstein equation. The TFT molecule is elliptical with radii of 100 and 250 μm. The diffusion constants expected for spherical particles of 100 and 250 μm radius are $3.6 \times 10^{-5}$ and $1.4 \times 10^{-5}$, respectively. The TFT diffusion constant that best fits our experimental results lies between these two values and is therefore of a reasonable and expected magnitude.

The model prediction for the nanoparticle effluent concentration curves shown in Figure 23 uses the diffusion constants estimated for these particles indicated in Table 1 ($1.82 \times 10^{-7}$ and $1.65 \times 10^{-7}$ cm$^2$/s for $SiO_2$ and $Fe_2O_3$, respectively) and a dispersion constant of 2 cm. The dispersion constant of a channel should be similar to the dimensions of the channel, which in our experiments is ~1 cm. A dispersion constant of 2 cm is thus very reasonable. We conclude that both the chemical and nanoparticle tracers behave as expected in our experiments. The experiments show the nanoparticles we have synthesized do not clump or stick in the glass apparatus used, and the chemical-nanoparticle tracers clearly have the potential to measure matrix (slit) diffusion.

Figure 23. Comparison of Effluent TFT and $SiO_2$ Nanoparticle as Function of Time

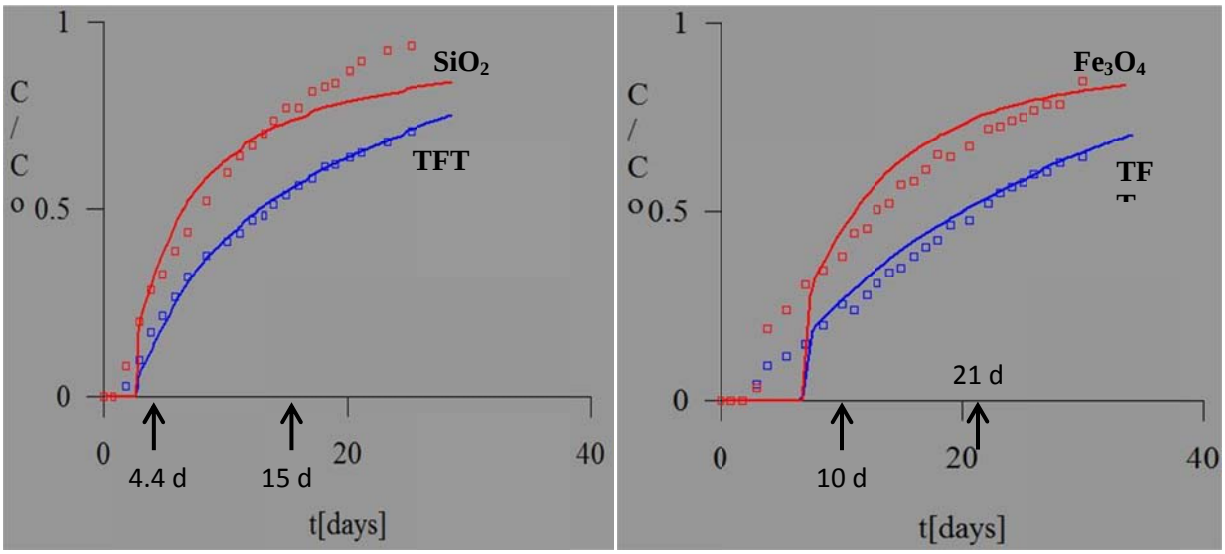


A) Comparison of the effluent TFT (blue) and $SiO_2$ nanoparticle (red) concentration as a function of time (square data points) to the concentrations predicted by the advection-diffusion model described above. B) Gives a similar comparison for the $Fe_2O_3$ nanoparticles. In both cases the diffusion coefficient used to model TFT chemical tracer is $2.5 \times 10^{-5}$ $cm^2/s$. The diffusion coefficient used for the $SiO_2$ and $Fe_3O_4$ nanoparticles are as indicated in Table 1. A dispersion coefficient of 2 cm provides the best fit between experimental data and the model. Arrows indicate one core channel pore volume and 1 total pore volume on each diagram.

### vii. Conclusion

The analogue supercritical $CO_2$ experiments show a clear arrival delay of the chemical TFT tracer compared to the nanoparticles. The TFT arrival can be predicted with a reasonable diffusion constant. The particle arrival observed agrees very well with model predictions provided dispersion in the core channel is taken into account. Dispersion is not likely to be important in field experiments because the dimensions of the fractures will be ~0.05 mm rather than ~1 cm. The particles we have synthesized are not retained in the apparatus and perform well in the tests as far as we can tell. They do not clump, stick, or become otherwise entrained in the apparatus. The clear separation in arrival time between chemical and particle tracers in Figures 22 and 23 indicates that particle tracers could provide important constraints on matrix sequestration of supercritical $CO_2$ in shale.

# 4. STREAMLINE MODELING

The laboratory experiments discussed above demonstrate how storage of an injected gas might be inferred from the intermixing of the injected gas with gas already in a shale, and how this inference might be confirmed with dual (particle and chemical) tracer tests. Here we discuss how models can be used to translate the laboratory results to the design of field experiments. Both laboratory experiments were interpreted using a finite element flow-diffusion model, but the models needed to plan well tests in the field must encompass additional factors. This section of this report: (1) reviews the model used to interpret the experiments; (2) shows how a rule-of-thumb inferred from the experiments can be used to design field tests that are optimal for inferring $CO_2$ storage effectiveness; (3) describes the integration of a diffusion model with a multi-well flow model; and (4) discusses the application of this integrated model to field test planning.

## a. Modeling laboratory experiments

In the experimental models, the advection of tracer along the core channel and the diffusion of tracer into the slit are calculated separately using operator splitting methods. As shown in **Figure 24**, the core channel fluid is advanced in discrete time steps, after which the diffusion into the matrix is calculated using finite element methods. The longitudinal dispersion is calculated by multiplying the longitudinal coefficient $a_L$ by the longitudinal (channel parallel) velocity in the slit $v_c$. The transverse dispersion in the slit is $\left(\frac{a_T}{a_L}\right) a_L v_c$, where $\frac{a_T}{a_L}$ is the ratio of transverse to longitudinal dispersion, usually around 0.1, and $v_c$ is the horizontal velocity in the slit calculated as described below.

We found that even if diffusion slit was divided into many segments by thin baffles, significant flow still occurred in each compartment. The flow expected in the slit compartments is shown in the Figure 24. There is a linear pressure drop across the core channel, and within each slit compartment this drives a circulation similar to that illustrated. We can calculate this flow using the methods of Toth (1959) as described in Subramanian et al. (2012). The gas or HFE flowing into each compartment of the slit will carry injected tracers, but the fluid exiting the compartment will, for a while, contain none of the injected tracers. Thus the circulation loops in each slit compartment dilute the gas moving through the core channel. We take this effect into account in our model. We calculated multiple streamlines in each compartment and track the flow along each one, diluting the channel until the flow along the streamline completes a loop from its entry to its exit from the compartment.

Figure 24. Diffusion modeling methodology for the laboratory experiments

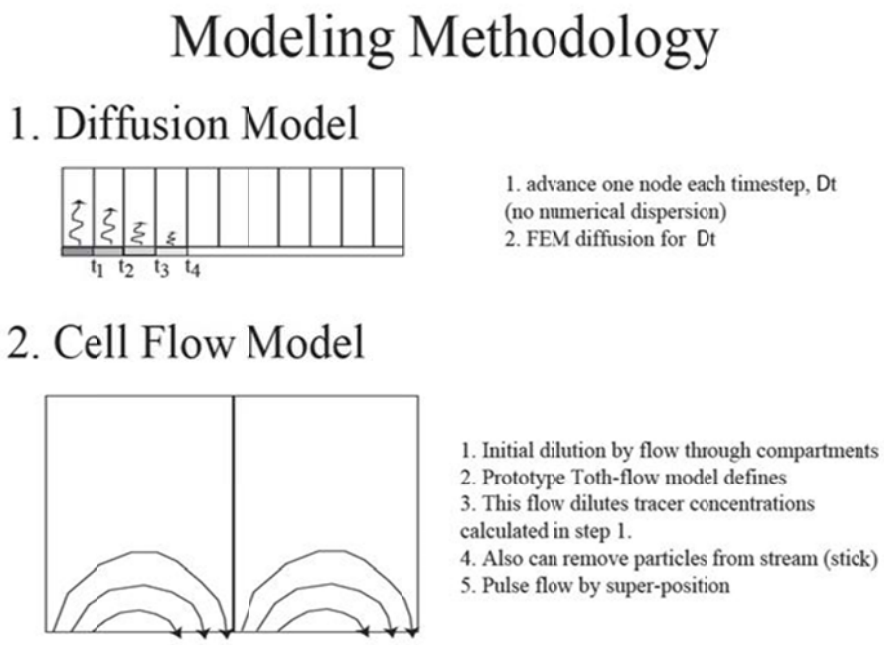


## b. Modeling field tests

The field situation of course differs from the laboratory situation. In the field, tests will be carried out by injecting into a perforated interval of a well and then either retrieving the injected fluids in that same well, or retrieving them from a nearby well. There may be several operational wells in an area, and this will complicate tracer interpretation. For example, a production well that is surrounded by 4 injection wells will have only a fraction of its production coming from any one of these injection wells. For the situation shown in **Figure 25**, fluid injected into well A will contribute at most ~25% of the fluid produced from the central production well, and thus any tracer injected into A could only produce a tracer concentration ~25% of the injected concentration.

Figure 25. A single production well (center) receives fluid from 4 surrounding injection wells.

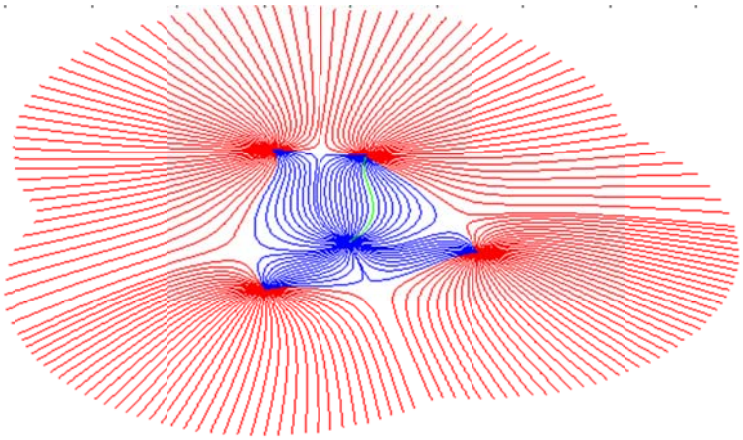

The red lines are streamlines emanating from the injection wells that do not connect to the production well; the blue streamlines are those that do connect to the production well. The streamlines were generated with the Gao matlab program developed for this project which is described in detail on Appendix B.

We use potential field theory to model the flow caused by injection and production from wells in a layer (confined aquifer) of defined thickness. The flow of all wells is just the sum of the flows in individual wells:

$$\vec{u}(\vec{x}) = \sum_i \frac{Q_i}{2\pi H \phi} \frac{\vec{x} - \vec{x}_i}{|\vec{x} - \vec{x}_i|^2} . \quad (1)$$

Here $H$ is the thickness of the flow layer (aquifer) as illustrated in Figure 26, $Q_i$ is the injection rate into the subject well in $m^3$/day, $\phi$ is the porosity through which flow takes place in the flow layer, $\vec{x}_i$ is the location of the well, and $\vec{u}(\vec{x})$ is the true velocity of the fluid at location $\vec{x}$. The superscript arrow indicates the quantities are vectors, so the location of the well is at position $x_i$, $y_i$, and the fluid velocity has a direction as well as a magnitude. The streamlines in Figure 27 were generated using equation (1).

Figure 26. Two well flow in a layer of thickness H.

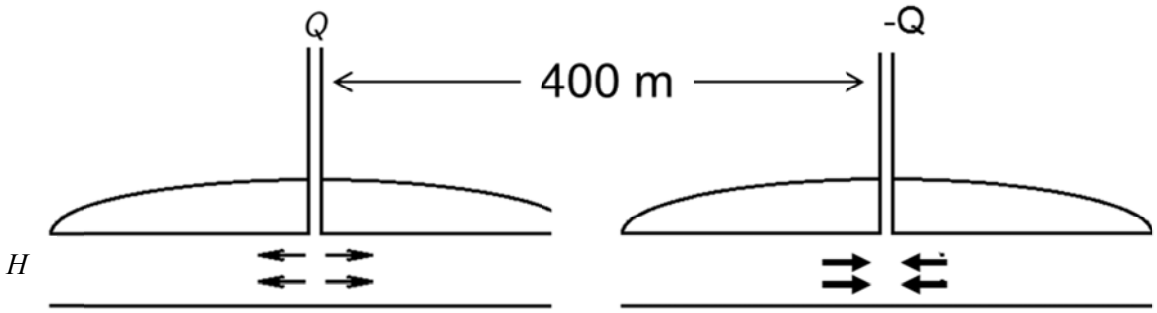


**Figure 27** shows how we conceptualize the movements of particle and chemical tracers in a fractured shale. In the limit that the particles (small red dots in Figure 27) do not diffuse at all, particles will travel through the fractures only, and not diffuse at all into the matrix shale surrounding the fractures. A diffusing chemical tracer, on the other hand, will diffuse into the shale matrix as it moves along the fracture as shown by the pink shading in Figure 27. In the limit of very fast diffusion, a chemical tracer will advance as it fills the entire porosity of the shale. The true velocity of a perfectly non-diffusing particle tracer will be given by equation (1) with $\phi=\phi_f$, where $\phi_f$ is the porosity of the fractures only. The true velocity of a very rapidly diffusing chemical tracer will be given by equation (1) with $\phi = \phi_{tot}$, where $\phi_{tot}$ is the total porosity of the shale (the matrix porosity plus the fracture porosity).

Figure 27. Conceptual flow of a particle and chemical tracer in a fractured shale.

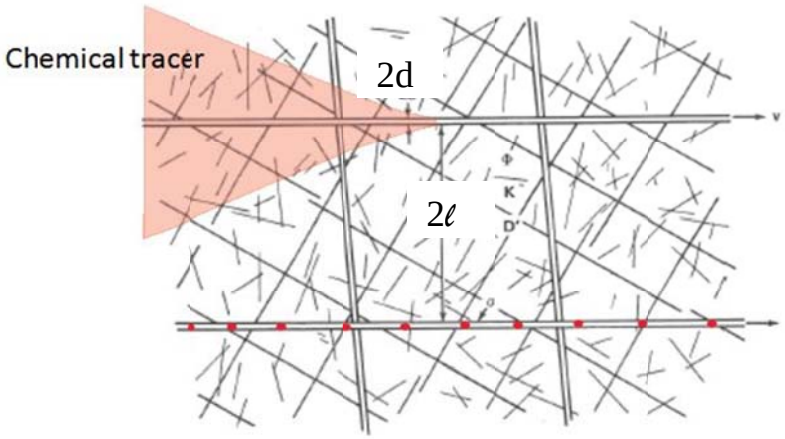

Real tracers will have diffusion constants that are neither 0 nor infinite, but something in between. Table 2 gives the diffusion constants for our chemical and particle tracers in $scCO_2$. Appendix C describes how the diffusion constants are calculated from the Stokes-Einstein equation.

Table 2. Diffusion constants of our $scCO_2$-philic nanoparticles and TFT chemical tracer in supercritical $CO_2$ (see Appendix C)

| | | $D_o$[cm$^2$/s] x $10^5$ | $D_o$[cm$^2$/day] |
|---|---|---|---|
| **Diffusion in Supercritical $CO_2$** | **40 nm diameter np** | 0.545 | 0.47 |
| | **Trifluorotoluene (TFT)** | 36.4 | 31.5 |
| **Inter-diffusion** | **$scCO_2$ and $CH_4$** | 88.7 | 76.6 |

Whether a tracer will arrive as if it moves through the total porosity, as a fast-diffusing chemical might, or as if it moves through the fractures only (as a particle tracer might), depends on the rate at which the tracer can diffuse into the matrix compared to the duration of the test. How much sooner the slow-diffusing tracer could arrive depends on the ratio of the matrix to fracture porosity. The two fundamental design parameters are thus the **diffusional relaxation time of the matrix** and the **ratio of matrix to fracture porosity**.

Figure 28 shows that the ratio of the matrix to fracture porosity in fractured shale equals the matrix porosity times the separation between fractures divided by the aperture of the fracture. Equation (2) gives the diffusional relaxation time of the matrix.

Figure 28. Fracture porosity in a fractured shale

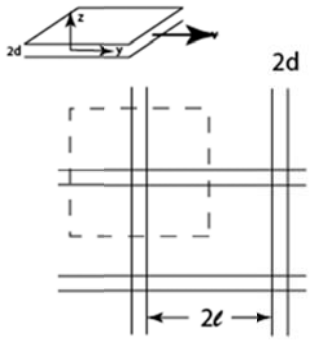


$$\phi_f^{1D} = \frac{d}{\ell}, \quad \phi_f^{2D} = \frac{2d}{\ell}, \quad \phi_f^{3D} = \frac{3d}{\ell}$$

$$\phi_{tot} = \phi_m + (1-\phi_m)\phi_f \cong \phi_m + \phi_f$$

$$\frac{\phi_m}{\phi_f^{1D}} = \frac{\phi_m \ell}{d}$$

$$\tau = \frac{\tau_m \ell^2}{4D_o} \qquad (2)$$

In equation (2), $\tau_m$ is the tortuosity of the pores in the matrix (approximately 3), $\ell$ is ~ ½ the separation of the fractures (approximate because this statement neglects the fracture aperture), and $D_o$ is the tracer diffusion constant from Table 2.

## c. Field test design

### i. Test design based on a simple rule-of-thumb

From all the Hele-Shaw style diffusional experiments we have carried out (see, for example, the inverse Peclet number discussion in Subramanian et al., 2012), and also from theoretical considerations, we know that the transition from non-diffusing to fully diffusing (into the matrix) tracer behavior occurs when the full-porosity transit time equals the diffusional relaxation time of the matrix. This observation is the basis of a very simple "back-of-the envelope" method of designing dual tracer field tests that are optimal for assessing how well $CO_2$ might be diffusively sequestered in fractured shale**. The design criterion is simply that the total-porosity-fluid-transit-time is equal to the diffusional relaxation time of the chemical tracer in the shale matrix.** Under this criterion, the chemical tracer should diffuse substantially into the matrix, but the particle tracer, with its much smaller diffusion constant, will not. The difference between the return (to a single well) or transmission (to a second well) of the particle and chemical tracers should be close to maximum with this design criterion, and the field test designed on this basis should stand the greatest probability of successfully assessing the potential to store $CO_2$ in a fractured shale.

The shales considered for field testing in this project have total porosities of ~10%. **Figure 29** applies the above rule-of-thumb-design-criteria to a huff-puff single well experiment, and **Figure 30** applies the design rule-of-thumb to a two-well test.

Figure 29 shows that if we wish the fast-diffusing tracer to extend 5 m from the well bore, and the fractures are spaced 10 to 20 cm apart, the tracer should be injected at 13 $m^3$/m/day for 0.6 days, or 3.3 $m^3$/m/day for 3.3 days, respectively. After injection, the fluid would be produced back at the same rate for the same periods of time. How far the non-diffusing tracer could extend from the well bore depends on the ratio of the matrix to fracture porosity. For example, if d=0.5mm (see discussion below), the ratio of the matrix to fracture porosity ($\phi_m / \phi_f = \phi_m \ell / d$) is between 10 and 20, and the particle tracer could extend 50 to 100 m from the injection well.

Figure 29. Injection rate, Q, that meets the design criterion for a single well huff-puff test where fast diffusing tracer extends 5 m from the well.

$$\text{design criterion} \quad t = \frac{\pi r^2 \phi_{tot}}{Q} = \tau_{TFT}$$

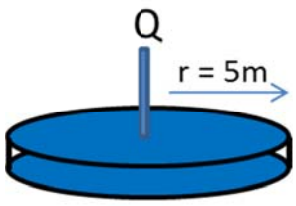


| | $D_o^{TFT}$ = 31.5 [cm²/day] $\tau_m$=3, $\phi_m$=0.1 | |
|---|---|---|
| $\ell$ [cm] | 5 | 10 |
| τ[days] | 0.6 | 2.4 |
| $Q_{r=5m}$[m³/m/d] | 13 | 3.3 |

The matrix relaxation time, [days], is calculated from equation (2) using $D_o^{TFT}$ = 31.5 cm²/day (Table 2) and a matrix tortuosity, $_m$=3.

Figure 30. The injection rate, Q, that meets the design criterion that T=$\tau_{TFT}$ for two well test assuming the wells are separated by 10 m.

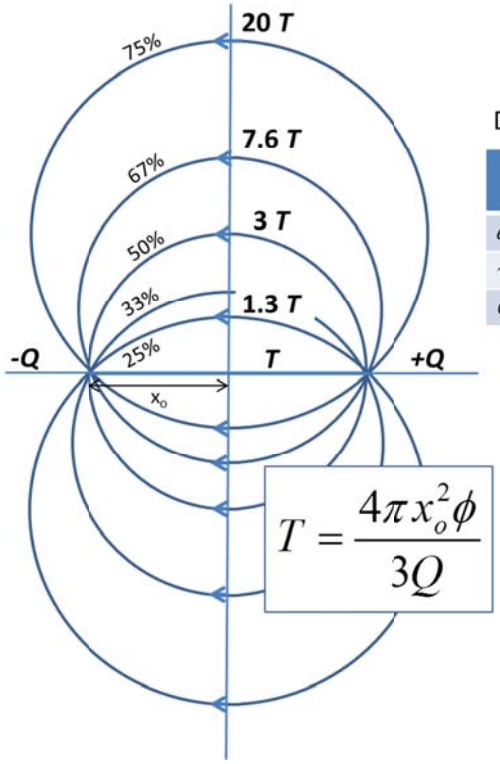


Design criterion: $T = \tau_{TFT}$

| | $D_o^{TFT}$ = 31.5 [cm²/day] $\tau_m$=3, $\phi_m$=0.1 | |
|---|---|---|
| $\ell$ [cm] | 5 | 10 |
| τ[days] | 0.6 | 2.4 |
| $Q_{x_o=5m}$[m³/m/d] | 17.4 | 4.3 |

The matrix relaxation time, $_{TFT}$[days], is calculated from equation (2) using $D_o^{TFT}$ = 31.5 cm²/day (Table 2) and a matrix tortuosity, $_m$=3.

Figure 30 applies this optimum design procedure to a two well test similar to the single well test in Figure 29. It assumes the same shale properties. In this case, the design criterion is based on the fastest transit time between the two wells. For two wells, where one well is injecting and the other producing at the same rate, the streamlines between wells are circular, and integration of the transit times is easy. The transit time for the streamlines can be expressed as multiples of the direct (shortest distance and fastest) transit time T, and the fraction of the injected fluid captured by the production well can be inferred from the fraction of its well bore receiving streamlines from the injection well.

The design criterion we assume in the 2-well case is that the direct transit time equals the matrix diffusion time for the TFT tracer. For wells spaced 10 meters apart and assuming 10 cm fracture spacing, the optimum injection rate should be 17.4 $m^3$/m/day and the injection should be maintained for about 1.8 days. Note that 50% arrival is expected in this period of time if the diffusion into the matrix is fast. The first TFT tracer could be anticipated in 0.6 days if the diffusion into the matrix is very fast, and sooner if the diffusion is slower or the fractures further apart. If the fracture spacing is 20 cm, the injection should be at 4.3 $m^3$/m/day for ~7.2 days. For a matrix/ fracture porosity ratio of 10, the *particle tracer* could be expected to reach 50% injected concentration in one-tenth the time required by the TFT tracer, or between ~4 and 17 hours (rather than 1.8 and 7.2 days) for fracture spacings between 10 and 20 centimeters.

## d. Test design based on a model that integrates flow and matrix diffusion

The simple rule-of-thumb design discussed in the previous section is useful but it does not predict the actual tracer arrivals; it only expresses a design criteria. Models that compute the dynamic diffusive filling of the matrix provide further insight and will be needed to interpret actual field tests. This section shows: (1) how we have coupled the flow patterns shown in Figure 25 to a matrix diffusion model that is based on a simplifying but useful assumption, and then (2) shows how this model can be used to design field tests.

### i. The simplifying assumption of the coupled model

Conceptually it is easy to see how the diffusion of tracers moving with a fluid through fractures might be simulated. One could simply advance the fracture fluid in small steps, and at each step calculate the diffusion into the adjacent matrix, much as was done in the models we developed for interpreting the laboratory experiments that we discussed above (see Figures 24 and 27). When a large number of steamlines (flow paths) must be considered (as illustrated in Figure 25), however, this conceptual approach becomes cumbersome because, to compute the increment of diffusion into the matrix one would need to have stored at all locations along the streamline information on how much tracer had already been sequestered in the matrix as well as information on the distribution of that tracer in the matrix.

One way around this challenge is to make the simplifying assumption that, at any time, the flux of tracer from the fracture into the matrix is the maximum flux possible times the difference between the concentration of tracer in the fracture and the average concentration of tracer already in the matrix at that locality. With this assumption, one need only store the average concentration of the tracer in the matrix, and the change in tracer concentration in the fracture can be calculated implicitly (e.g., using a method which solves for the composition at the end of the timestep and is computationally unconditionally stable). As shown in **Figure 31**, it predicts tracer concentrations within about a factor of 2 of their proper values. Better computational methods could be implemented, and we will do this, but for now and in the rest of this report we will use this simplifying sequestration assumption.

Figure 31. Prediction of Relative Tracer Concentration as a Function of Time and Distance From Well

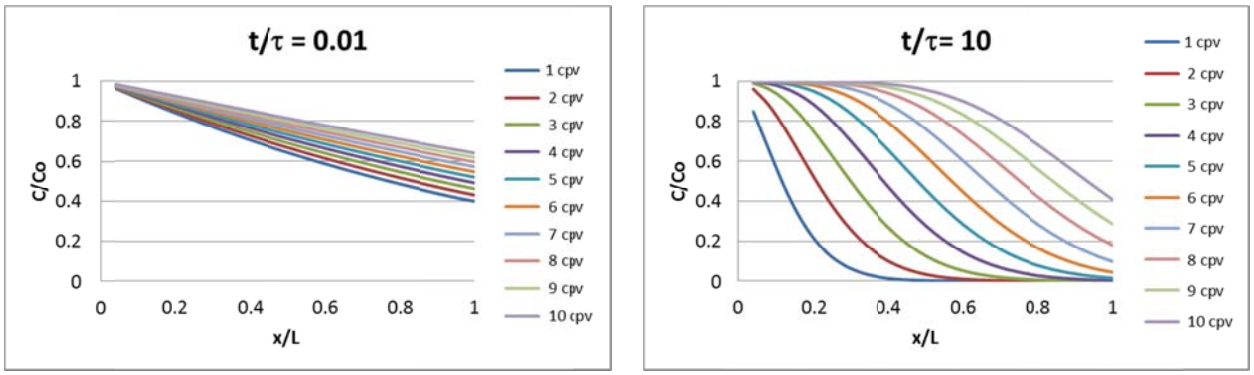


Simulation of planar flow for a period of time t, matrix diffusional relaxation time , and $_m/_{fx}$ = 10, so ten core pore volumes (cpv) equals the total porosity of the system. The solution at t/ = 0.1 should be close to C/Co=1 from x/L =0 to 1 (a non-diffusing tracer should transit the system in one core pore volume). The solution at t/ = 10 is perhaps a bit more smeared out than it should be but nevertheless is quite reasonable. The tracer front advances as it fills the matrix porosity, and at one total pore volume, the injected tracer concentration is 0.5 as it should be.

### ii. Shale properties

The operational aspects of shale sequestration of $CO_2$ are envisioned to be similar to the recovery of $CH_4$ from tight gas shale. As shown in **Figure 32**, there will be about 8 wells from a pad serving a square mile of subsurface shale. Each well will tap 80 acres and lie about 200m from its neighbors. The injection interval for the planned huff-puff test was 46 m (150 ft).

Figure 32. Planned Field Test Well Configuration.

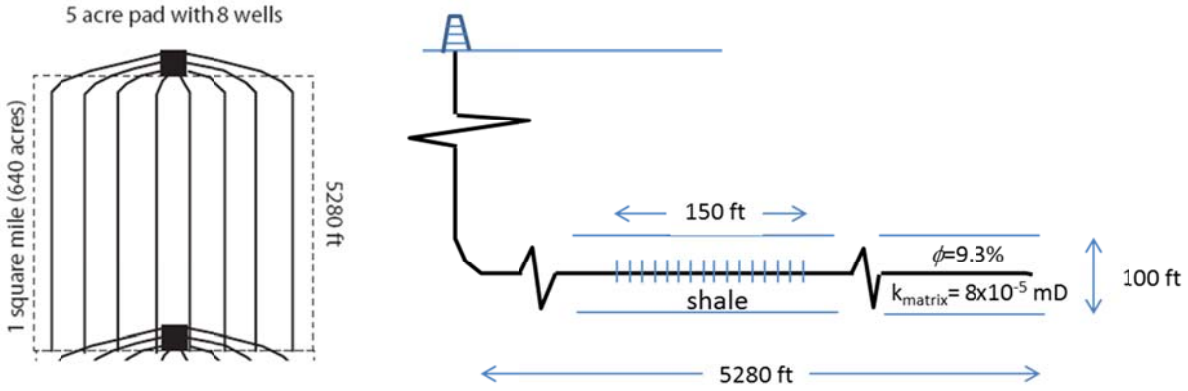


Information from Mike Godec for the Union Springs shale in Pennsylvania. We assume the shale thickness is 100 ft.

The fracture aperture depends on the injection rate. Assuming that 50 mesh sand is carried into the fractures created in a fracturing operation, the fracture aperture under flowing conditions is ~0.5 mm. A fracturing operation typically injects a fluid volume of 10 $m^3$/m-treated over a period of about ½ an day at an injection rate of ~20$m^3$/m/day. For these numbers, 4 million gallons of water is used to treat eight 200 meter long segments of a mile long well. Once the fractures are propped open with sand, injection and production could be a much slower rates. So we do not use the fracture injection rates as a flow rate constraint, but simply adopt the fracture aperture of 0.5 mm.

The fracture spacing is perhaps the most uncertain parameter. Fractures could be as close as 5 cm or close, or as distant as 100 cm. As shown in **Table 3**, a reasonable estimate for fracture porosity is ~1%, and a reasonable ratio of matrix to fracture porosity is 10.

Table 3. Estimates of fracture porosity and ratio of matrix to fracture porosity

| d=0.5 mm, $\phi_m$=0.1 | | | |
|---|---|---|---|
| $2\ell$ [cm] | 5 | **10** | 100 |
| $\phi_f^{1D} = d/\ell$ | 2% | **1%** | 0.1% |
| $\phi_f^{2D} = d/\ell$ | 4% | 2% | 0.2% |
| $\phi_m / \phi_f^{1D}$ | 5 | 10 | 100 |

### iii. Results

**Figure 33** shows arrival curves for a 2-well test where the well separation is 10 m and the injection and production rates are 5 $m^3$/m/day, the same case as indicated by the design criterion in Figure 29.

Figure 33. Prediction of Tracer Arrival Curves at 5 $m^3$/m/day for a Two Well Test

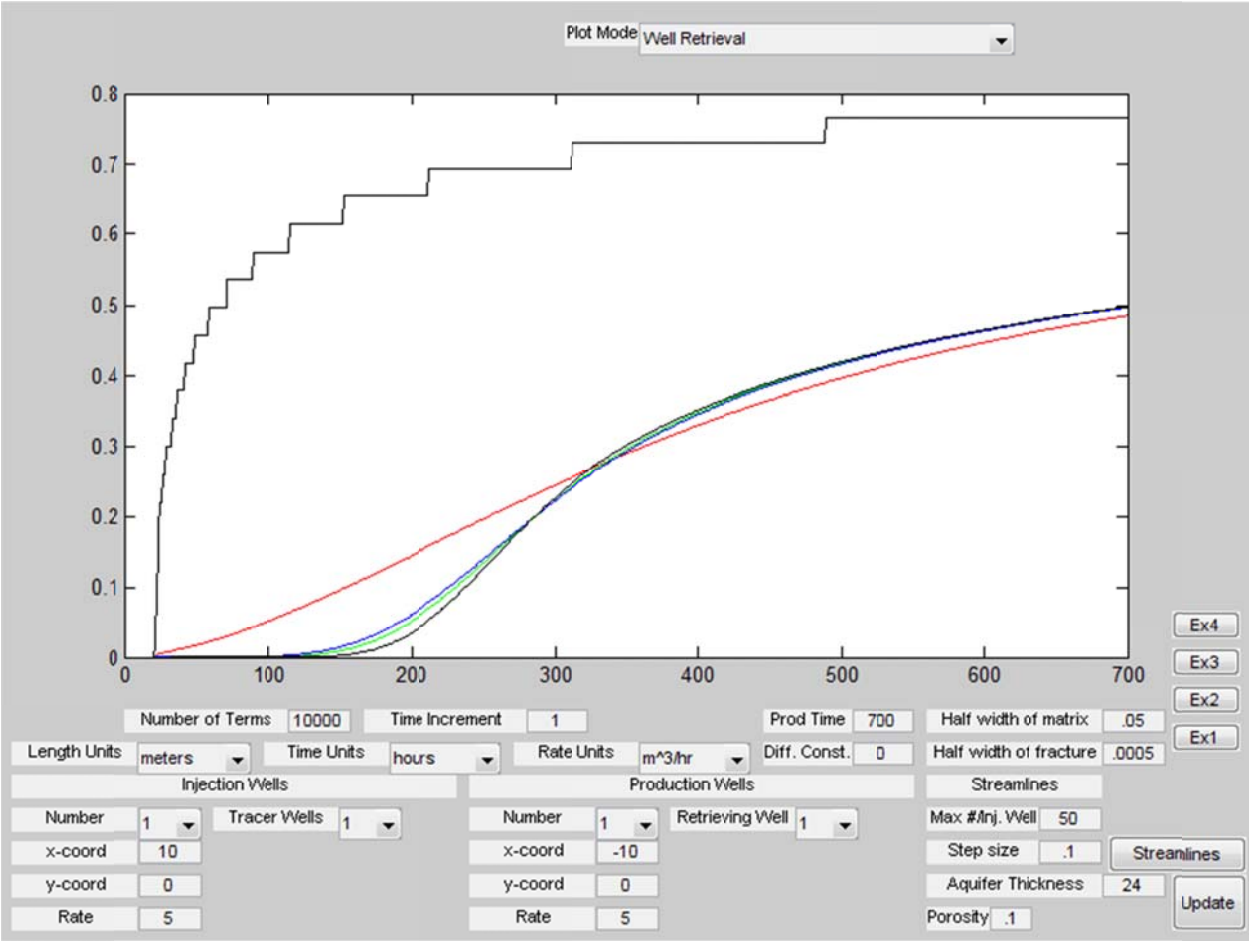


Tracer arrival curves for nanoparticles (red), TFT (blue), and $CO_2$ (green) for supercritical $CO_2$ injected and produced at 5$m^3$/m/day (equivalent to 5 $m^3$/hour over a 24 m interval in each well) from wells separated by 20 m. The diffusion constant of the tracers are as indicated in Table 2, the tortuosity of the pores in the matrix is 3, the fracture spacing is 10 cm, and the matrix porosity is 10%. There is good separation of the tracers for the first 240 hours (10 days) of the experiment.

Under operational conditions, the well spacing would be about 200 m and supercritical $CO_2$ would be injected steadily into one of the wells at ~20 $m^3$/m/day and the neighbor wells might be producing methane at about the same rate. Under these circumstances, by the equation in Figure 30, the direct transit time for full-fill of the 10% shale porosity would be 0.6 years. For a fracture spacing of 10 cm, as shown in Table 4, this transit time is long compared to the diffusional relaxation time in supercritical $CO_2$ of either TFT or our 40 nm diameter nanoparticles (0.6 and 40 days respectively). Thus, we would expect both the nanoparticles and the chemical tracer to fill the matrix as they move from the injection to the production well, and we would expect all the tracers to arrive at the production well at the same time with no diffusion-measuring separation. **Figure 34** shows this is in fact the case.

Figure 34. Prediction of Tracer Arrival Curves at 20 $m^3$/m/day for a Two Well Test

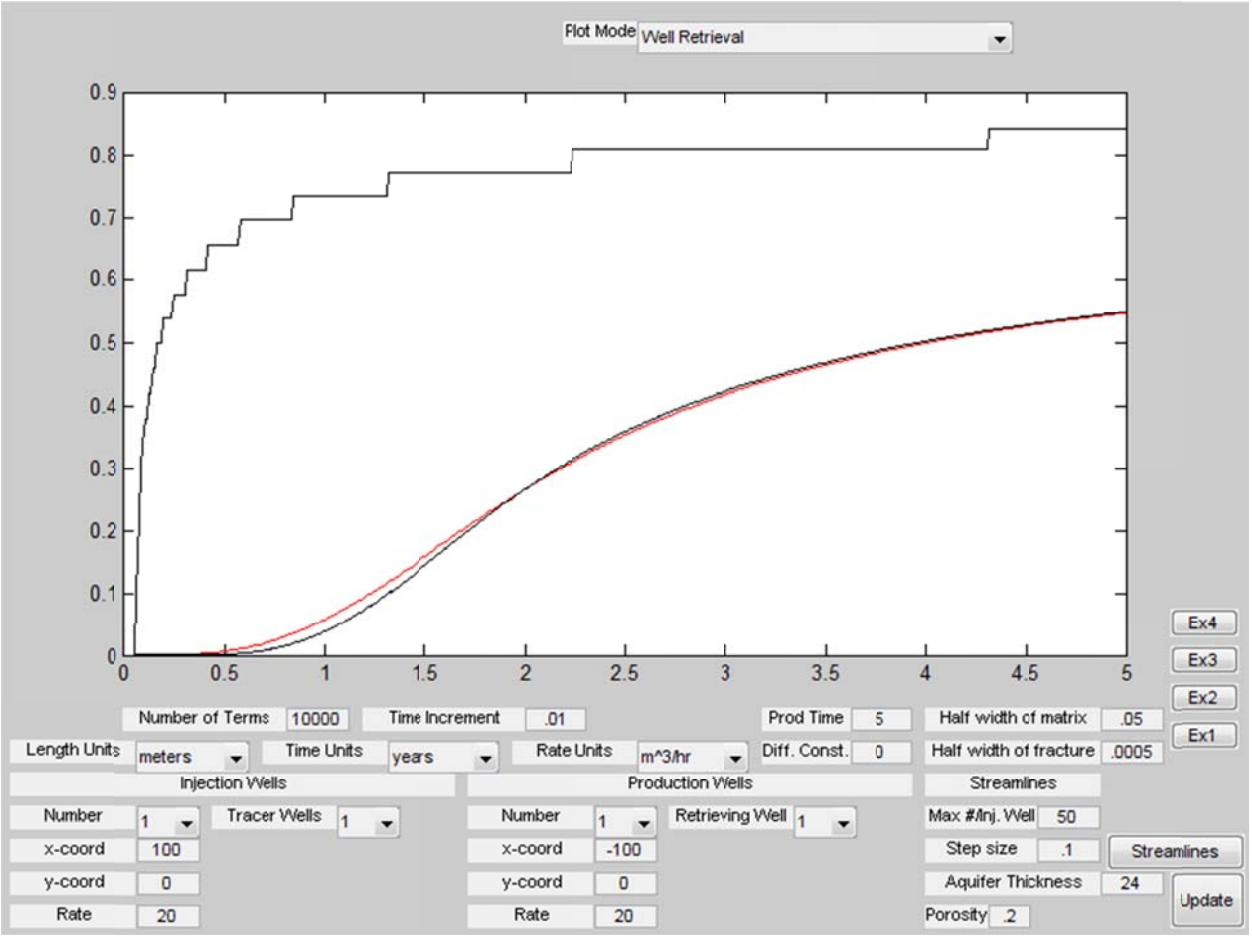


Tracer arrival curves for nanoparticles and TFT in supercritical $CO_2$ injected and produced at 20$m^3$/m/day (equivalently 20 $m^3$/hr over 24 m interval) from wells separated by 200 m. The diffusion constants for the tracers are as indicated in Table 2, the tortuosity of the pores in the matrix is 3, the fracture spacing is 10 cm, and the matrix porosity is 10%.

Figures 33 and 34 together make the important point that dual porosity methods for assessing the $CO_2$ sequestration potential of shale need to be carried out at a much smaller well separation than will be afforded by the operational well spacing of ~200 m. Test wells well need to be drilled or experiments carried out in huff-puff mode from a single well.

**Figure 35** and **Table 4** illustrate this point further. Table 4 computes the diffusional relaxation time of the matrix assuming fractures are spaced 10cm and 1m apart.

Table 4. Diffusional Relaxation Time of the Shale Matrix Computed for Supercritical $CO_2$

| | Aqueous | | Supercritical | |
|---|---|---|---|---|
| **½ fracture spacing [cm],ℓ** | **5** | **50** | **5** | **50** |
| **Chemical** | 11 days | 3 years | 0.6 days | 60 days |
| **Nanoparticle** | 144 days | 40 years | 40 days | 11 years |
| Diffusional relaxation time of the shale matrix computed for supercritical $CO_2$ from $\tau = \frac{\tau_m \ell^2}{4D_o}$, assuming $D_o$=36.4 $cm^2/s$ for TFT, and $D_o$=0.545 $cm^2/s$ for 40 nm diameter nanoparticles. The matrix pore tortuosity $\tau_m$ =3. | | | | |

Figure 35. Matrix Relaxation Time as Function of Fracture Spacing

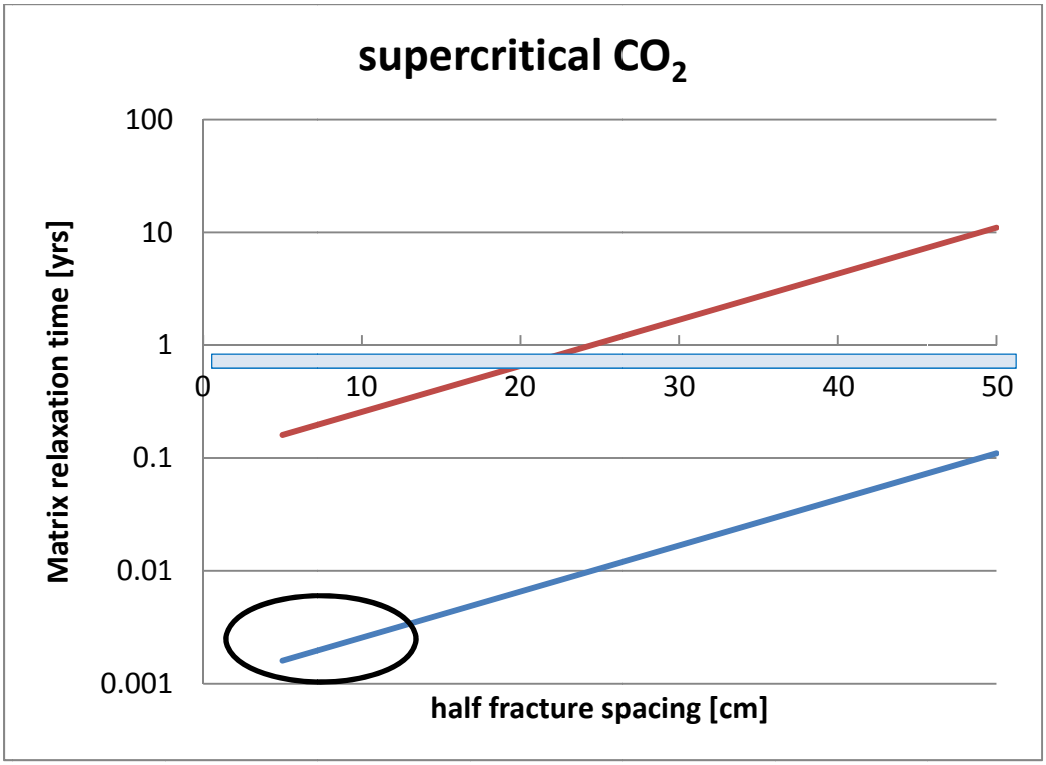


Under operational conditions in a $CO_2$ sequestration in shale operation, the porosity-fill transit time between wells spaces ~200m apart will be between 0.5 and 1 year (blue bar). The matrix relaxation times for TFT and 40 nm diameter nanoparticles are shown by the blue and red lines, respectively. The black oval indicates the conditions optimal for inferring the viability of sequestering $CO_2$ in shale assuming that the fracture spacing is between 10 and 30 cm. The fact the chemical tracer relaxation time is much shorter than the porosity-full transit time means that the test well spacing must be much shorter than the operational spacing.

Testing in huff-puff mode would be a way to carry out the tests on the time scale needed to accommodate rapid matrix diffusional relaxation times without having to drill additional wells. **Figure 36** predicts the result of such and experiment. The prediction is somewhat counter-intuitive. For very fast diffusing or very slow diffusing tracers, the tracer will move out from the huff-puff well and then be retrieved with only dispersive dilution. In the limits, a huff-puff test will therefore tell us noting about the ability to diffusively sequester $CO_2$. However, a tracer that diffuses just a bit into the matrix, but moves a great distance into the formation, will lose tracer to the matrix and be retrieved at lower concentration than a more rapidly diffusing tracer. This is what is shown in Figure 36. The nanoparticle tracer is retrieved at much lower concentration than the highly diffusing $CO_2$ or TFT tracers.

Figure 36. Prediction of Tracer Arrival Curves at 5 $m^3$/m/day for a Huff-and-Puff Test

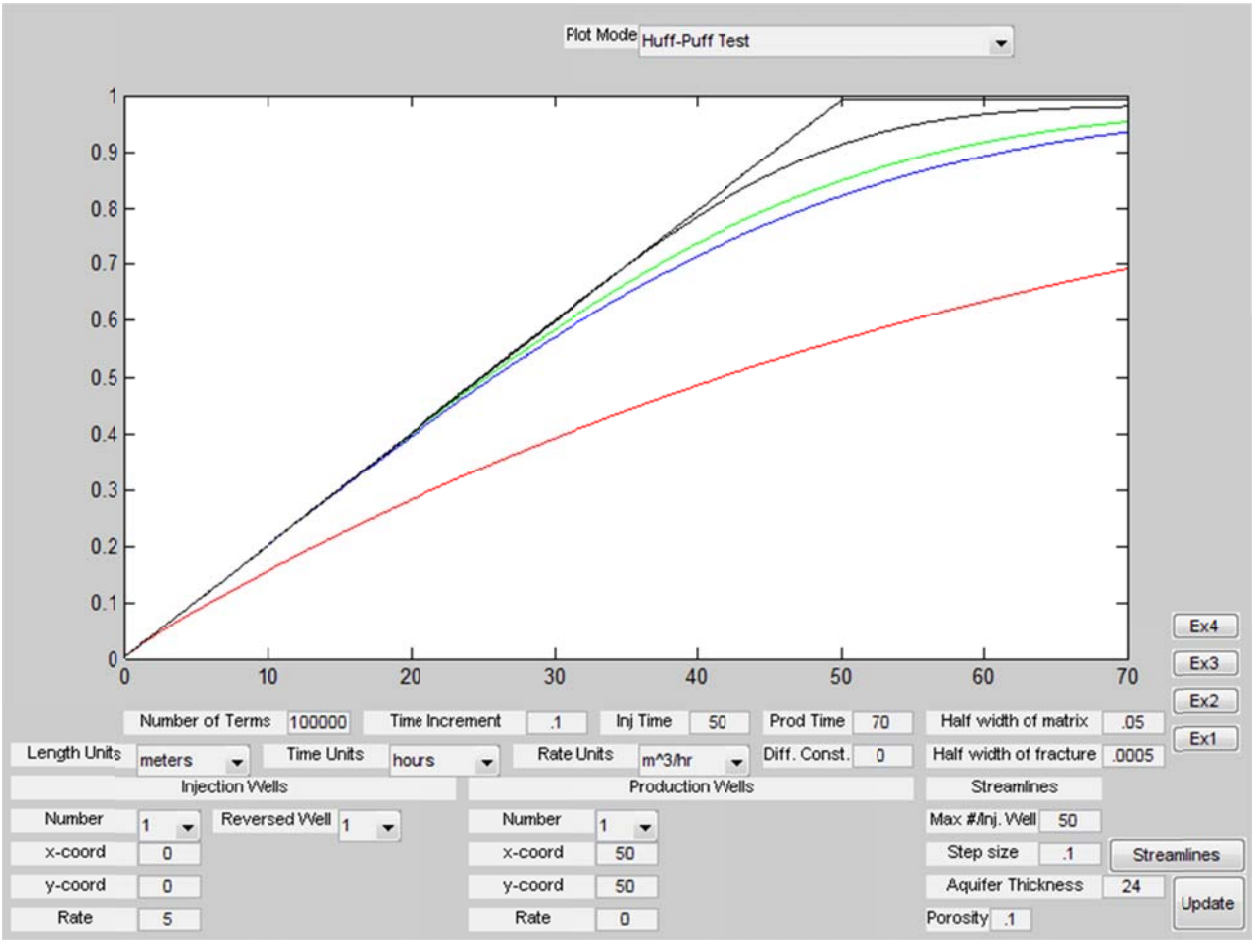


Tracer retrieval curves for nanoparticles (red), TFT (blue), and methane (green) in supercritical $CO_2$ injected and produced at 5$m^3$/m/day (equivalently 5 $m^3$/hr over 24 m interval) for 50 hours from a huff-and-puff test. The diffusion constant of the chemical TFT tracer is $36.4 \times 10^{-5}$ $cm^2$/s, the diffusion constant for the nanoparticles is $0.545 \times 10^{-5}$ $cm^2$/s, the diffusion constant for methane is $8.9 \times 10^{-4}$ $cm^2$/s, the tortuosity of the pores in the matrix is 3, the fracture spacing is 10 cm, and the matrix porosity is 10%.

We are not fully confident of this result because the approximations we have made in coupling the flow and diffusion affect the initial diffusion markedly. The predictions in Figure 36 should be re-evaluated based on more accurate diffusion modeling and tests should not be designed until this is done.

## e. Summary and Discussion

We have synthesized super-critical $CO_2$-philic nanoparticles and shown that they can be used in laboratory experiments to measure diffusional $CO_2$ sequestration into a matrix slit. We have shown that these experiments can be successfully modeled. We have shown how field tests can be designed using the simple rule of thumb that the most information will be obtained for tests where the diffusional relaxation time of the fast-diffusing chemical tracer is approximately equal to the residence time of the injected fluid in the formation. We have shown that the well spacing that is optimal for the kind of testing that could assess the potential for $CO_2$ sequestration is much smaller than the operational well separation. Based on a simplifying assumption we have modeled a simple two-well test and a huff-puff test. However, we have also warned that the huff-puff test simulation must be considered tentative in light of the simplifying model assumption we have made. The laboratory experiments and the models we have constructed show that field tests could provide a very useful early indication of the potential viability of sequestering $CO_2$ in shale.

# 5. DISCUSSION AND OVERALL CONCLUSIONS

The particles we have synthesized, the laboratory experiments we have performed, and the modeling and field test designs show how gas-interdiffusion and chemical and nanoparticles tracers in supercritical $CO_2$ could provide an early indication of the viability of sequestering $CO_2$ in shale. However, we have not demonstrated that the nanoparticles or TFT will be inert tracers in shale, and the approximations made in the modeling may undermine some of the field test predictions. The laboratory experiments are subject to deficiencies that will not be present in field tests. For example, the flow in the forced and gravitational flow in the diffusion slit in the gas diffusion experiments will not be important in the field situation. Also, the dispersion in the HFE analogue supercritical $CO_2$ experiments will not be a factor in the field. However, the nanoparticle could well stick in shale even though they do not stick or clump in the glass laboratory experiments.

Our conclusion is that the laboratory experiments that we have carried out adequately support the viability of the methods we propose. Further laboratory diffusion experiments are not needed. On the other hand, experiments are needed to show that the particles we have synthesized do not stick to shale. Simple column experiments where our nanoparticles are dispersed in HFR and passed through a column of crushed shale could investigate this issue. Second, a dual diffusion model that is not subject to the simplifying approximation we have made here is needed. We know how to construct these models and will do so in the next months.

If our nanoparticles can be demonstrated not to stick in shale, and the improved models lead to fully confident field test designs, the next steps forward will be to carry out laboratory experiments using particle and TFE tracers in supercritical $CO_2$ experiments in the laboratory, and then design and carry out field experiments.

# 6. ACKNOWLEDGEMENTS

We are grateful for the support of the Cornell KAUST Center for Sustainable Energy Development for making available the laboratory space and analytical equipment that made this project possible. We are grateful to Mike Godec of ARI for project advice and guidance. We are grateful for the funding from ARI and DOE that supported this project under DOE Project No. DE-FE0004633.

# 7. REFERENCES

Cathles, L.M., R. Shannon. 2007. How potassium silicate alteration suggests the formation of porphyry ore deposits begins with the nearly explosive but barren expulsion of large volumes of magmatic water. Earth and Planetary Science Letters 262, 92-108

Cathles, L., H. Spedden, and E. Malouf, A tracer technique to measure the diffusional accessibility of matrix block mineralization. American Institute of Mining, 1974. 103rd Annual Meeting.

Hwang, H. S., Lee, J., Zakhidov, A., DeFranco, J. A., Fong, H. H., Holmes, A. B., Malliaras, G. G., Ober, C. K., Dry photolithographic patterning process for organic electronic devices using supercritical carbon dioxide as a solvent. J. Mater. Chem., 2008, 18, 3087-3090. DOI: 10.1039/b802713g

Hyatt, J. A. 1984. Liquid and Supercritical Carbon Dioxide as Organic Solvents. J. Org. Chem. 1984, 49, 5097-5101

J. Liu, W. He, L. Zhang, Z. Zhang, J. Zhu, L. Yuan, H. Chen, Z. Cheng and X. Zhu, Langmuir 2011, 27, 12684-12692.

Krysmann, M. J., Kelarakis, A., Dallas, P., Giannelis, E. P., Formation Mechanism of Carbogenic Nanoparticles with Dual Photoluminescence Emission. J. Am. Chem.Soc. 2012, 134, 747-750

R. C. Reid and T. K. Sherwood. The Properties of Gases and Liquids, pages 2nd ed: 520–543, 632–633 4th ed: 577–597. McGraw-Hill Book Company, 1966, 1987.

Subramanian, S. K., Li, Y., Cathles, L. M., Assessing Preferential Flow by Simultaneously Injecting Nanoparticles and Chemical Tracers. Water Resources Research, 2012, doi:10.1029/2012WR012148, in press.

Y. Sun, X. Ding, Z. Zheng, X. Cheng, X. Hu and Y. Peng, European Polymer Journal 2007, 43, 762-772.

Toth, J., A Theory of Groundwater Motion in Small Drainage Basins in Central Alberta, Canada. Journal of Geophusical Research, 1962. 67(11).

# APPENDIX A:

*Flow Meter Operating Instructions*:

1): Flow meter must always be oriented vertically to function correctly.

2): Close the valve by turning it clockwise - Do not over tighten

3): Pressurize the system (Do not exceed inlet pressure of 200psi. 15-20psi is adequate for this meter)

4): Open the valve until the float rises to the desired flow rate (note: flow meter may need to be adjusted periodically for the first 5-10 minutes until flow rate stabilizes.)

**Fig. A1 – Correlated Flow Meter**

*Calibration Data* – For STP: 1 atm @ 70°F

This information can be obtained by request through a Cole-Parmer representative.

Email requests can be sent to techinfo@coleparmer.com

| Scale Reading | $CO_2$ Flow Rate (ml/min) | $CH_4$ Flow Rate (ml/min) |
|---|---|---|
| 65 | 6.57 | 8.67 |
| 60 | 5.92 | 7.58 |
| 55 | 5.28 | 6.59 |
| 50 | 4.65 | 5.82 |
| 45 | 4.05 | 5.16 |
| 40 | 3.47 | 4.61 |
| 35 | 2.95 | 3.95 |
| 30 | 2.44 | 3.40 |
| 25 | 1.95 | 2.64 |
| 20 | 1.52 | 2.20 |
| 15 | 1.14 | 1.54 |
| 10 | .840 | 1.10 |
| 5 | .580 | .439 |

Table A.1: Flow rate of injecting gas.

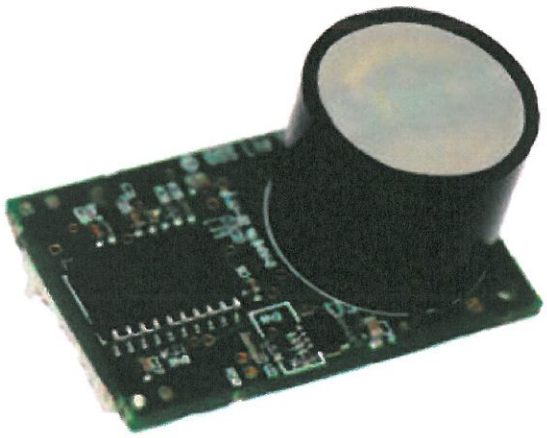

**Fig. A2 – C20 $CO_2$ Sensor**

The carbon dioxide sensor used for these experiments was obtained from CO2Meter.com. It is manufactured by Gas Sensing Solutions. The C20 is a real time sensor that can detect $CO_2$ concentrations from 0%-100%. It uses Aluminum Indium Antimonde NDIR (non dispersive infrared) LED technology. The sensor can be fitted with a tube cap that allows fluid to be injected across the sensor. The sensor is powered through a standard outlet and connects to a computer via USB. The software used to collect the data is called DAS100 and can be downloaded for free from the manufacturer's website.

A set of instructions along with a video for the DAS software can be found on the manufacturer's website.

## REFERENCES

Busch, Andreas. Sascha Alles, Yves Gensterblum, Dirk Prinz, David N. Dewhurst, Mark D. Raven, Helge Stanjek, Bernhard M. Krooss. 2008. *Carbon dioxide storage potential of shales*. International Journal of Greenhouse Gas Control 2, 297-308

Carslaw, H. S., Jaeger, J. C., *Conduction of Heat in Solids*. Oxford at the Clarendon Press, Second Edition, 1959. ISBN 0198533683.

Cathles, L.M., R. Shannon. 2007. *How potassium silicate alteration suggests the formation of porphyry ore deposits begins with the nearly explosive but barren expulsion of large volumes of magmatic water.* Earth and Planetary Science Letters 262, 92-108

Cathles, L., H. Spedden, and E. Malouf, *A tracer technique to measure the diffusional accessibility of matrix block mineralization.* American Institute of Mining, 1974. 103rd Annual Meeting.

Chapman, S., and T. G. Cowling: "The Mathematical Theory of Non-Uniform Gases. An Account of the Kinetic Theory of Viscosity, Thermal Conduction and Diffusion in Gases", (3rd ed.), Cambridge University Press. 1970

Chen, N. H. and D. F. Othmer, *New Generalized Equation for Gas Diffusion Coefficient J. Chem. Eng. Data*, **1962**, *7* (1), pp 37–41. DOI: 10.1021/je60012a011

E. V. Evans and C. N. Kenney, *Gaseous Dispersion in Laminar Flow Through a Circular Tube Proc. R. Soc. Lond. A* 1965 **284**, 540-550. doi: 10.1098/rspa.1965.0079

Fong, H. H., Lee, J., Lim, Y., Zakhidov, A. A., Wong, W. H., Holmes, A. B., Ober, C. K., and Malliaras, G. G., *Orthogonal Processing and Patterning Enabled by Highly Fluorinated Light-Emitting Polymers*. Advanced Materials 2011, 23, p. 735-739. DOI: 10.1002/adma.201002986

Ghesmat, K., Hassanzadeh, H., Abedi, J., Chen, Z., *Influence of Nanoparticles on the Dynamics of Miscible Hele-Shaw Flows*. J. Appl. Phys. **109**, 104907 (2011); doi: 10.1063/1.3592228

Hirschfelder, J. O., C. F. Curtiss, and R. B. Bird: "Molecular Theory of Gases and Liquids," Wiley, New York, 1964.

Hudson, T. L., *PhD Thesis*, California Institute of Technology, 2008. Web only: http://resolver.caltech.edu/CaltechETD:etd-05022008-154254

Hwang, H. S., Lee, J., Zakhidov, A., DeFranco, J. A., Fong, H. H., Holmes, A. B., Malliaras, G. G., Ober, C. K., *Dry photolithographic patterning process for organic electronic devices using supercritical carbon dioxide as a solvent.* J. Mater. Chem., 2008, **18**, 3087-3090. DOI: 10.1039/b802713g

Krysmann, M. J., Kelarakis, A., Dallas, P., Giannelis, E. P., *Formation Mechanism of Carbogenic Nanoparticles with Dual Photoluminescence Emission.* J. Am. Chem.Soc. 2012, 134, 747-750

Marrero, T. R. and E. A. Mason, *Gaseous Diffusion Coefficient,* J. Phys. Ref. Data. Vol. 1, No. 1, 1972

McDowell-Boyer, L.M., J.R. Hunt, and N. Sitar, *Particle transport through porous media.* Water Resources Research, 1986. **22**(Copyright 1987, IEE): p. 1901-1921.

Nuttall, Brandon C. Cortland F. Eble, James A. Drahovzal. 2005. *Analysis of Devonian black shales in Kentucky for potential carbon dioxide sequestration and enhanced natural gas production.* Kentucky Geological Survey. Final Report DE-FC26-02NT41442

Paterson, Lincoln. 1981. *Radial fingering in a Hele Shaw cell.* Journal of Fluid Mechanics 113, 513-529

Pritchard, D.T., J.A. Currie. 1982. *Diffusion of coefficients of carbon dioxide, nitrous oxide, ethylene and ethane in air and their measurement.* Journal of Soil Science 33, 175-184

R. C. Reid and T. K. Sherwood. *The Properties of Gases and Liquids*, pages 2nd ed: 520–543, 632–633 4th ed: 577–597. McGraw-Hill Book Company, 1966, 1987.

Renner, T. A., *Measurement and Correlation of Diffusion Coefficients for $CO_2$ and Rich-Gas Applications.* SPE Reservoir Engineering. May 1988. p. 517-523

Saffman, P.G. and G. Taylor, *The Penetration of a fluid into a Porous Medium or Hele-Shaw Cell Containing a More Viscous Liquid.* Proceedings of the Royal Society A: Mathematical, Physical and Engineering Sciences, 1958. **245**(1242): p. 312-329.

Shapiro, A.M., *Effective matrix diffusion in kilometer-scale transport in fractured crystalline rock.* Water Resources Research, 2001. **37**(Compendex): p. 507-522.

Sherwood, T. K., Pigford, R. L., and C. R. Wilke: "Mass Transfer". McGraw-Hill Chemical Engineering Series. 1975, ISBN: 0070566925.

Silliman, S.E., *Particle transport through two-dimensional, saturated porous media: influence of physical structure of the medium.* Journal of Hydrology, 1995. **167**(1-4): p. 79-98.

Solomon, S., D. Qin, M. Manning, Z. Chen, M. Marquis, K.B. Averyt, M.Tignor and H.L. Miller. IPCC, 2007: *Climate Change 2007: The Physical Science Basis. Contribution of Working Group I to the Fourth Assessment Report of the Intergovernmental Panel on Climate Change.* Cambridge University Press, Cambridge, United Kingdom and New York, NY, USA.
S. K. R. Subramanian. *M.S. thesis*, Cornell University, 2011.

Subramanian, S. K., Li, Y., Cathles, L. M., *Assessing Preferential Flow by Simultaneously Injecting Nanoparticles and Chemical Tracers.* Water Resources Research, 2012, doi:10.1029/2012WR012148, in press.

Toth, J., *A Theory of Groundwater Motion in Small Drainage Basins in Central Alberta, Canada.* Journal of Geophusical Research, 1962. **67**(11).

Weissman, S., and G. A. DuBro, *Diffusion Coefficient for $CO_2$ -- $CH_4$.* J. Chem. Phys. **54**, 1881(1971); doi: 10.1063/1.1675111.

# Appendix B: A manual for a Matlab model of the movement of tracers in a well field

Timothy Gao

# A Model of Fluid Flow Through Porous Media

**Timothy K. Gao**
College of Engineering, Cornell University, Ithaca, NY 14853, USA. E-mail: tkg24@cornell.edu

**Abstract**

In this paper, a model is developed using MATLAB that semianalytically simulates fluid flow through the fractures of a porous medium, with diffusion of heat or tracer solutes into the matrix material between fractures. The fractures are assumed to be a constant distance apart and a constant width, both of which can be defined by the user. Calculations are done along individual streamlines from a number of injection and production wells. The model is composed of a streamline plotter that assumes a potential due solely to injection or production from the set of wells, and a concentration calculator that uses Carslaw and Jaeger's diffusion equations. Each part is subdivided into several submodes: the streamline plotter can be set to plot either streamlines or contours based on the age of water along each streamline, and the concentration calculator can be used to plot concentration versus either time or position along a particular streamline. Streamlines generated by the plotter can be stored, and the model is capable of running "huff and puff" tests.

## 1 Introduction

Understanding subterranean fluid flow is important in any context that involves injection or extraction of material from the subsurface. Because of the inherent difficulties in performing a field test, it is useful to have a model that predicts the flow of tracers injected underground. The attached code uses MATLAB to implement a GUI (graphical user interface) that allows the user to model fluid flow between injection wells, where fluid is injected underground, and production wells, where fluid is extracted. In addition, it allows the user to save generated streamlines in data files for later use and to read data from previously saved files to either plot the saved streamlines or to calculate the concentration of an injected fluid along any saved streamline. Finally, it allows the user to simulate huff and puff tests, where a particular well injects fluid for a certain amount of time and produces fluid afterwards. All calculations are done in length units of meters, time units of hours, and the corresponding derived units, although the user is allowed some flexibility in the units of inputted quantities.

The model given by the attached code allows the user to control the positions and injection/production rates of up to five injection wells and five production wells in a two-dimensional cartesian coordinate system. It has several plot modes which allow the user to view either the streamlines that terminate at a production well (with markers that give either the furthest extent of injected fluid (the fluid front) at certain times or the position of the temperature front at those times), age contours that show the distance that injected fluid has travelled from an injection well at various times, all streamlines regardless of where they end (those going to infinity are truncated at a certain distance away from the wells), the concentration versus time or distance for a specific streamline, or the fraction of injected fluid retrieved versus time in a huff and puff test.

# 2 Methods

## 2.1 Streamline Model

The mathematical model used to generate the streamlines is outlined in Section 3.1.2 of *Groundwater Transport*[3]. It assumes that fluid occupies an aquifer with uniform thickness $b$ and uniform porosity $\phi$, and that the fluid velocity has the form

$$\bar{u}(\bar{x}) = \bar{u}(x,y) = u(x,y)\hat{x} + v(x,y)\hat{y} = -\nabla\Phi. \tag{1}$$

The complex velocity potential $\tilde{W}$ is given by

$$\tilde{W}(\tilde{Z}) = \Phi + i\Psi = \sum_j \frac{-Q_j}{2\pi b\phi} \ln(\tilde{Z} - \tilde{Z}_j), \tag{2}$$

where the sum is over all injection and production wells, $Q_j$ is the rate at which fluid enters the region at well $j$ ($Q_j > 0$ if fluid is injected at well j), and $\tilde{Z}_j = x_j + iy_j$, where $(x_j, y_j) = \bar{x}_j$ is the position of well $j$. Plugging the real part of (2) into (1) gives

$$\bar{u}(\bar{x}) = \sum_j \frac{Q_j}{2\pi b\phi} \frac{\bar{x} - \bar{x}_j}{|\bar{x} - \bar{x}_j|^2}. \tag{3}$$

To draw a single streamline, the model starts a distance 0.1m in a specified direction from a particular injection well and steps a constant distance in the direction of the velocity until the streamline either reaches a production well or exceeds a defined distance away from the nearest well. The times that injected fluid would take to reach each step are used to calculate the positions of either the fluid front or the temperature front. It is assumed that the temperature front moves at the speed of the fluid front multiplied by the porosity and by a thermal velocity coefficient, given by

$$\phi_{therm} = \frac{1}{\phi_m} \frac{\rho_m c_m}{\rho_f c_f},$$

where $\phi_m$ is the porosity of the rock matrix, $\rho_m$ is the density of the rock matrix, $c_m$ is the heat capacity of the rock matrix, and $\rho_f$ and $c_f$ are the density and heat capacity of the fluid in the fracture.

## 2.2 Concentration Model

To calculate the concentration of injected fluid for a specific streamline and a particular time and distance along the streamline, the model uses diffusion formulas derived in Carslaw and Jaeger[1].

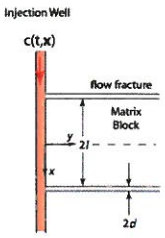


Figure 1: Assumed Geometry of Subsurface. Flow (in the y-direction) occurs from a source (red vertical bar) along fractures of width $2d$ separated a distance $2l$ apart.

Assuming the planar fractures through which the fluid flows have the geometry shown in Fig. 1 (adapted from Cathles[2]), the concentration at position $x$ and time $t$ expressed as a fraction of concentration $C_0$ in the streamline is

$$\frac{C(x,t)}{C_0} = 1 - \frac{4}{\pi}\sum_{n=0}^{\infty}\frac{(-1)^n}{2n+1}\cos\left(\frac{(2n+1)\pi\xi}{2}\right)\exp\left(-\frac{(2n+1)^2\pi^2 T}{16}\right), \tag{4}$$

where

$$\xi = \frac{x}{l}, \quad T = \frac{4Dt}{l^2},$$

$l$ is the half-width of the matrix, and $D$ is an effective diffusion constant. The effective diffusion constant is the diffusion constant of the tracer in water at the ambient temperature divided by the tortuosity of the matrix pore space (e.g., $D = D_o/\tau$, where $D_o$ is the aqueous diffusion constant and $\tau$ is the tortuosity). For heat, $T = 4\kappa/l^2$, where $\kappa = K_m/\rho_m c_m$ is the thermal diffusivity of the matrix, $\rho_m$ is the density of the matrix, and $c_m$ is the heat capacity of the matrix. Thus, if the half-width of the fracture is $d$, the flux of concentration out of the fracture at some position along a streamline is

$$J = \frac{D}{d}\frac{\partial}{\partial x}\left[\frac{C(x=l,t)}{C_0}\right] = \frac{2D}{dl}\sum_{n=0}^{\infty}\exp\left(-\frac{(2n+1)^2\pi^2 T}{16}\right). \tag{5}$$

Integration of this equation can be used to find the fraction of concentration $C_0$ that diffuses out from the streamline between times $t_a$ and $t_b$,

$$\begin{aligned}\frac{\Delta C_0}{C_0} &= \int_{t_a}^{t_b} J dt \\ &= \frac{8l}{\pi^2 d}\sum_{n=0}^{\infty}\frac{\left[\exp\left(-\frac{(2n+1)^2\pi^2 D t_a}{4l^2}\right) - \exp\left(-\frac{(2n+1)^2\pi^2 D t_b}{4l^2}\right)\right]}{(2n+1)^2}\end{aligned} \tag{6}$$

Equation (6) assumes the step change in concentration that occurs at t=0 is maintained at all later times. As the concentration in the fracture at location y along the streamline changes, the changes are captured by additional step changes and their consequences captured by equation (6). The step changes can be positive or negative, and the results are summed to give the total average concentration of solute (or temperature) in the matrix at any particular time. The loss of solute (or heat) to the matrix is balanced by a drop in solute concentration (or heat) in the fracture fluid. The model creates a matrix $\mathbf{C}$ of fracture concentration values, with $\mathbf{C}_{ij}$ giving the concentration of solute or heat in the fracture at time $t_j$ and position $x_i$ along the streamline. $\mathbf{C}_{ij}$ equals the non-diffused fraction of fracture solute or heat at the previous position and time, $x_{i-1}$ and $t_{j-1}$. This is calculated by summing the non-diffused fractions reaching $x_{i-1}$ at all previous times, $\mathbf{C}_{(i-1)k}$, where $0 \le k \le j-1$ and the non-diffused fractions are given by (6) with the appropriate start and end times. The GUI allows the user to select how many terms of the infinite sum are calculated.

## 2.3 GUI Modes

### 2.3.1 Streamline Calculating Mode

In the streamline calculating mode, the code evenly spaces the streamlines that start around each injection well, determining the starting positions based on the user-specified number of streamlines per injection well. Fig. 2 shows the model running in a streamline calculating mode.

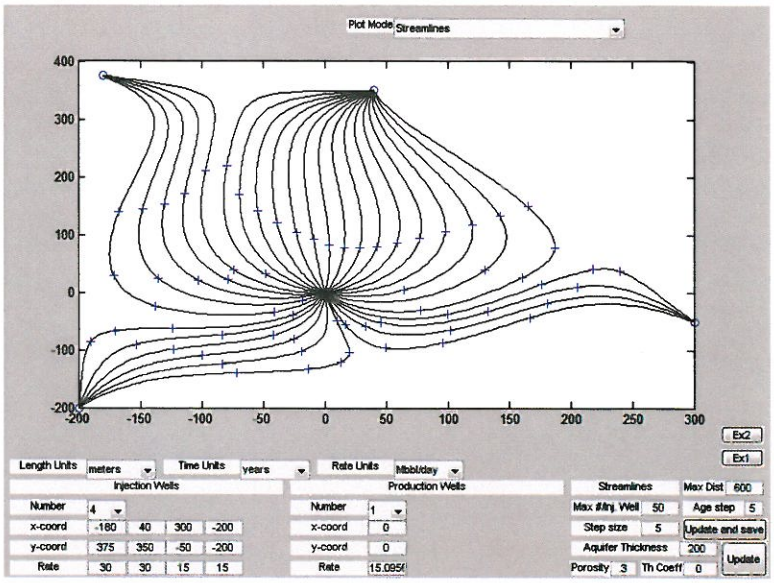


Figure 2: Example of the GUI running in streamline calculating mode

As can be seen, the production well controls are at the bottom middle and the injection well controls are at the bottom left, with unused well controls hidden. Above the well controls are dropdown menus that allow the user some leeway in determining the units of input parameters. Distance or position parameters can either be in meters or feet, time parameters can be in years or hours, and rate parameters can either be in $m^3/s$, $m^3/hour$, or Mbbl/day. To the bottom right are streamline and environment controls that determine the number of streamlines to calculate for each injection well, the step size to use between adjacent points along a streamline, the porosity $\phi$, the maximum distance away from the nearest well that a streamline is allowed to be before it is truncated, the time interval (age step) between successive markers (blue crosses) indicating either the position of the temperature front or the fluid front (calculated assuming the fluid fills the full porosity in moving from one position to another), and the thermal velocity coefficient that determines the speed of the temperature front relative to the fluid front. If the thermal coefficient is set to 0, then the markers indicate the position of the fluid front. Otherwise, they indicate the position of the temperature front. Additionally, there are buttons that allow the user to update the figure using current values of the input parameters and to save the generated streamlines and environmental data in data files. Finally, at the top of the GUI, there is a drop-down menu that allows the user to change the plot mode.

### 2.3.2 Storing Data

When the "Update and save" button is clicked in a streamline calculating mode, the GUI both displays the streamlines and saves their information in .dat files. Each file stores one piece of information for streamlines emanating from one injection well. In total, there are five pieces of information stored for each streamline: the x- and y-positions of each point along the streamline, the times that injected fluid initially reaches each point, the magnitudes of the Darcy velocity at each point, and whether the streamline reaches a production well or not. For the files storing position or time information, columns correspond to streamlines and rows correspond to points along a streamline. In addition,

environmental data (the aquifer thickness, porosity, thermal velocity coefficient, and step size) is stored in a separate file. Thus, 26 data files are generated; files corresponding to an unused injection well are left blank.

### 2.3.3 Contour plotting mode

In the Contour plotting mode, the code stores the positions reached by the fluid front (fluid filling the total porosity) or the temperature front (rock fully heated to the injected temperature upstream of the front, unheated downstream of the front) at user-specified times by four initial streamlines from each injection well and, while the distance between adjacent points on each contour exceeds a maximum distance, calculates and stores the positions reached by a streamline emitted at an angle halfway between the two bounding streamlines. Thus, it guarantees that each contour is drawn using points that are at most a certain distance apart. Fig. 3 shows the model running in age contour plotting mode.

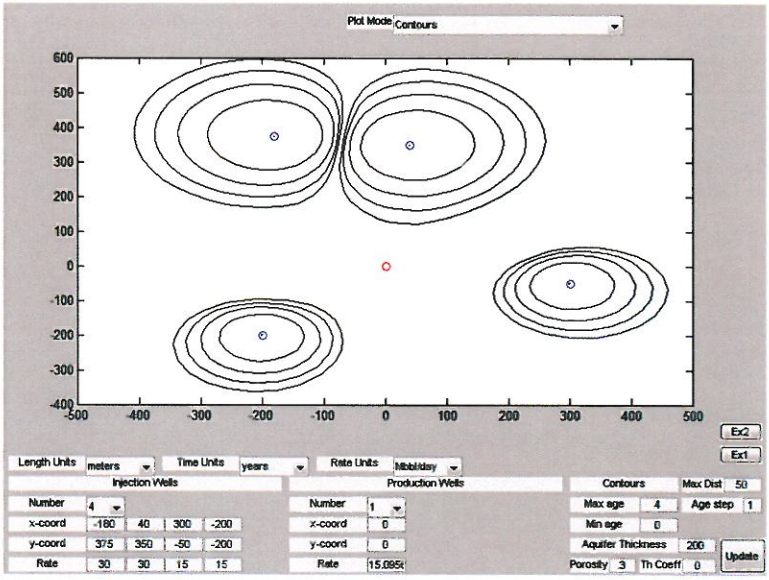


Figure 3: Example of the GUI running in age contour plotting mode

Most of the controls are the same as in the streamline plotting mode, but the controls that deal specifically with streamlines are replaced by ones for age contours, such as the minimum and maximum ages to plot contours for. The age step control is carried over from the streamline mode and it determines the age interval between successive contours. The maximum distance control is repurposed to give the maximum allowed distance between adjacent points on the same contour.

## 2.4 Well Retrieval mode

In the Well retrieval mode, the program simulates the results of a well retrieval test. Multiple injection wells and production wells are allowed, with tracer injected from at least one injection well. The GUI either plots the streamlines going into the retrieving well, or the concentration of tracer in retrieved fluid versus time. Fig. 4 shows the GUI running in Well Retrieval mode and displaying the concentration of tracer in retrieved fluid.

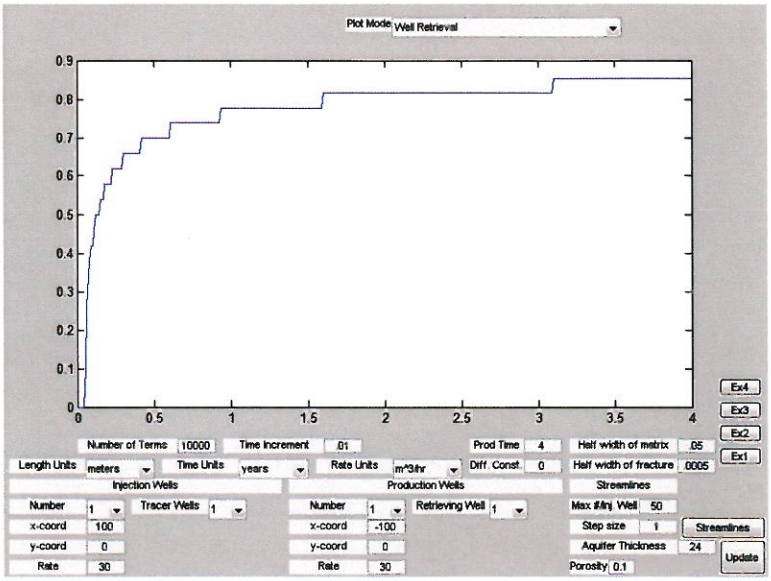


Figure 4: Example of the GUI running in well retrieval mode

Again, most controls are the same as in the streamline plotting mode, but controls for the fracture width and spacing, as well as the diffusion constant (in $m^2/hr$), timespan of the test, and the time increment used, are immediately below the graph. Also, controls for the retrieving well and the number of injection wells that inject tracer are present.

### 2.4.1 Streamline reading mode

In the streamline reading mode ("Streamlines from file"), the GUI reads the streamlines stored in the data files and plots streamlines selected by the user. Fig. 5 shows the GUI model running in a streamline reading mode.

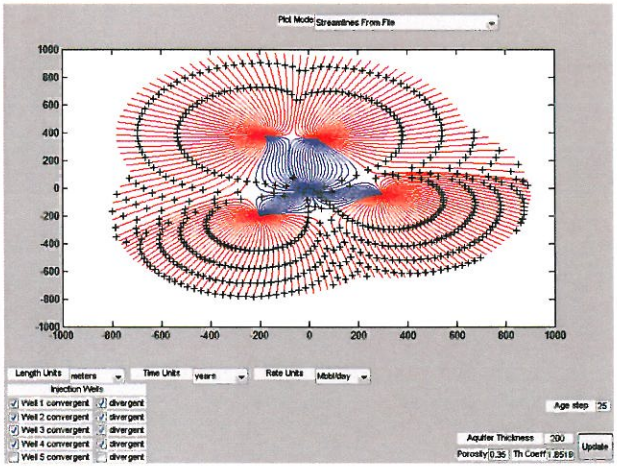


Figure 5: Example of the GUI running in a streamline reading mode

As can be seen, the well controls are replaced by checkboxes that allow the user to plot streamlines from any combination of injection wells. In addition, the user can decide whether or not to plot

streamlines that diverge to infinity instead of converging to a production well. Since these modes include markers which denote the position of either the fluid front or temperature front, the environmental controls are still present, as well as the age increment between markers along the same streamline.

### 2.4.2 Concentration calculating mode

In the concentration calculating mode ("Concentrations along Streamline from file"), the GUI allows the user to plot the concentration of injected fluid versus either time or position along a specific streamline. As a result, there are three submodes in this particular mode. Fig. 6 shows the GUI running in one of the concentration calculating modes.

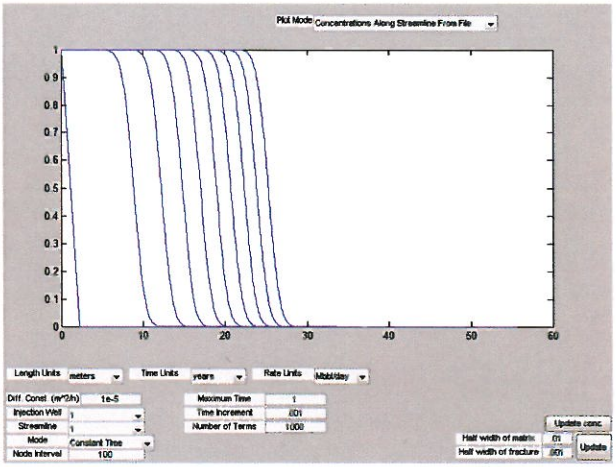


Figure 6: Example of the GUI running in a concentration plotting mode

The graph shows concentration versus time for multiple position nodes along the streamline, with each curve corresponding to a different node. The main controls are in the bottom left and allow the user to set the effective diffusion coefficient $D = D_0/\tau$ (units of square meters per hour, $D_o$ being the aqueous diffusion constant and $\tau$ being the tortuosity of the pores in the matrix), the specific streamline to use, the subplot mode (streamline, constant time, or constant position), and the interval between nodes to plot concentrations for (either time or position, depending on the subplot mode). There are also controls that set the value of $l$ (the half-width of the rock matrix), that update the calculated concentration values, and that update the plot. For temperature calculations the porosity should be set to 1, the diffusion constant set to the thermal diffusivity of the matrix, $\kappa/(\rho_f c_f)$, and the thermal coefficient set to $\rho_m c_m/\rho_f c_f$. The thermal coefficient is 0 for solute calculations. The porosity in this mode is the porosity of the matrix only.

### 2.4.3 Huff and Puff Mode

In the Huff and Puff mode, the GUI allows the user to select an injection well and change it to a production well. It can either graph the streamlines put out by the selected well during the injection period or it can graph the fraction of the total injected fluid retrieved versus time. Fig. 7 shows the

GUI running in the Huff and Puff Mode and displaying the fraction of injected tracer retrieved versus time.

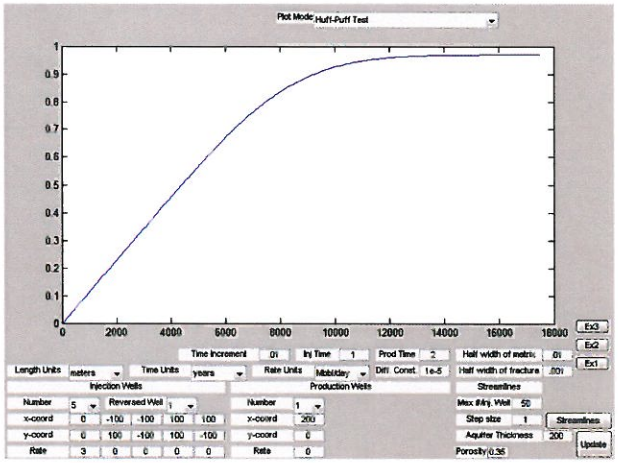


Figure 7: Example of the GUI running in Huff and Puff Mode

In this mode, the user can set the time that fluid is injected using "Inj Time" and the time that fluid is retrieved using "Prod Time." The increment between successive times at which concentrations are calculated can also be set. For the injection period, stored streamline data is used. However, new streamlines are calculated for the production period, using the well controls at the bottom. The reversed well is chosen from the injection wells and has its injection rate converted to a production rate. At the bottom right are the controls for the fracture and matrix half-widths, as well as the number of streamlines to plot out from the reversed injection well and the aquifer thickness and matrix porosity.

# 3 Results

## 3.1 Simulation of flow using realistic well data

We assume a well configuration like the one shown in Fig. 8.

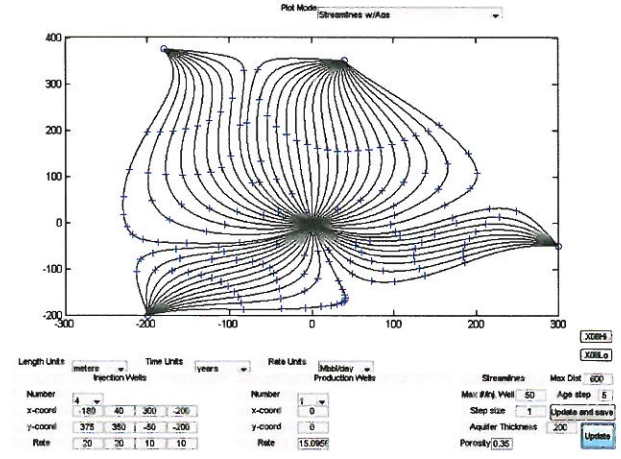

Figure 8: Simulated flow with a realistic well configuration and rates.

If the injection well rates are increased by 50%, the streamline pattern is instead given by Fig. 9.

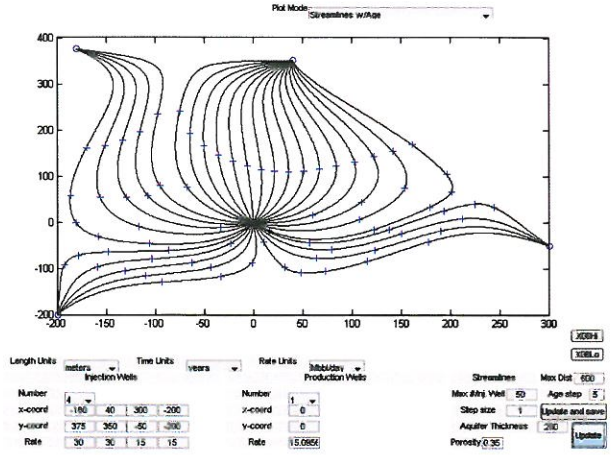


Figure 9: Simulated flow with same well configuration but higher injection rates

In both cases, the production well rate is kept at $100 m^3$/hour. Results of the concentration calculator for the higher injection rates are shown in Fig. 10, which plots the concentration versus time for specific distances along the streamline.

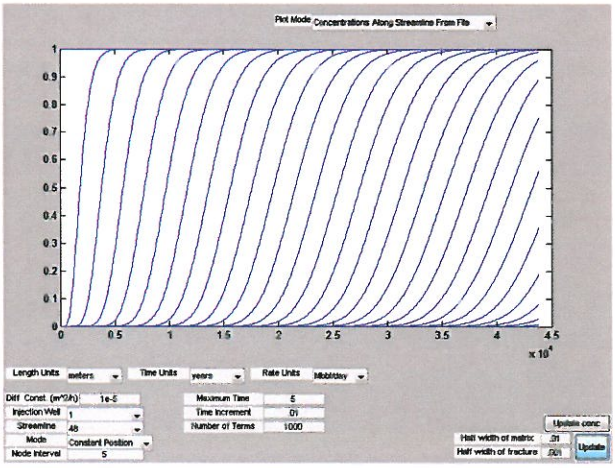


Figure 10: Concentration versus time (in hours) for every 5th node along streamline 58 (the green streamline in Figure 11). for a streamline ending at the production well. The left side of the diagram starts at the 1st node from the injection well, with each subsequent line to the right corresponding to the concentration versus time for a position 5 more nodes down the streamline. The number of node profiles plotted is determined by the node interval. If a streamline not terminating at a production well is selected, the nodes plotted are those along the red streamlines in Figure 11, culled by the node interval selected.

The streamline that the concentrations were calculated for is shown in Fig. 11.

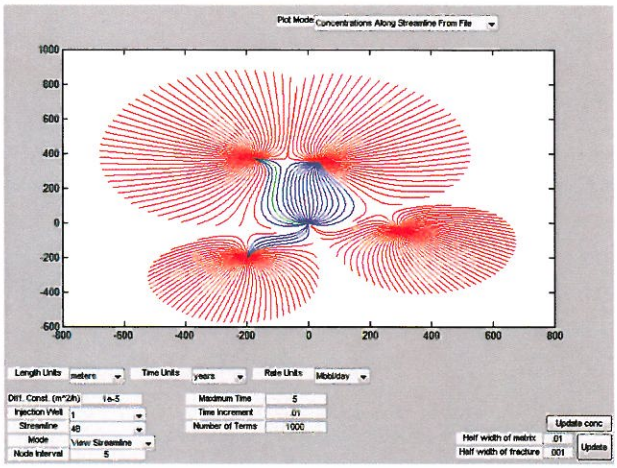


Figure 11: Streamline configuration: streamlines that don't reach a production well are shown in red, while streamlines that do are shown in blue and the streamline that concentrations were calculated for is shown in green

As expected, the concentration curve is sharper for points closer to the injection well.

## 3.2 Huff and Puff Test

Using the well configuration below, we can see that the flow pattern is that of a single well.

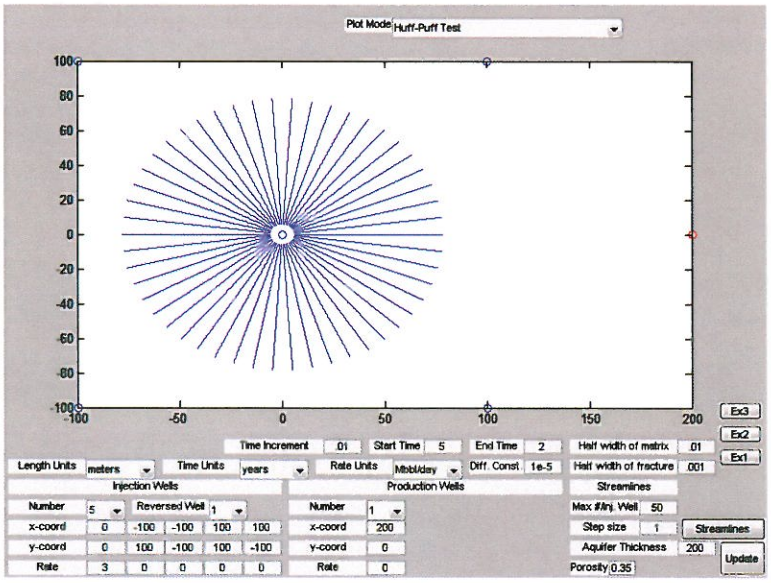


Figure 12: Well configuration for huff and puff test.

If we set the diffusion constant equal to 0, we would expect the fraction retrieved to increase linearly until the "huff" and "puff" portions of the test have been going for the same amount of time, at which point the fraction retrieved would be 1. Running the simulation gives Fig. 13, which shows that it gives the expected result.

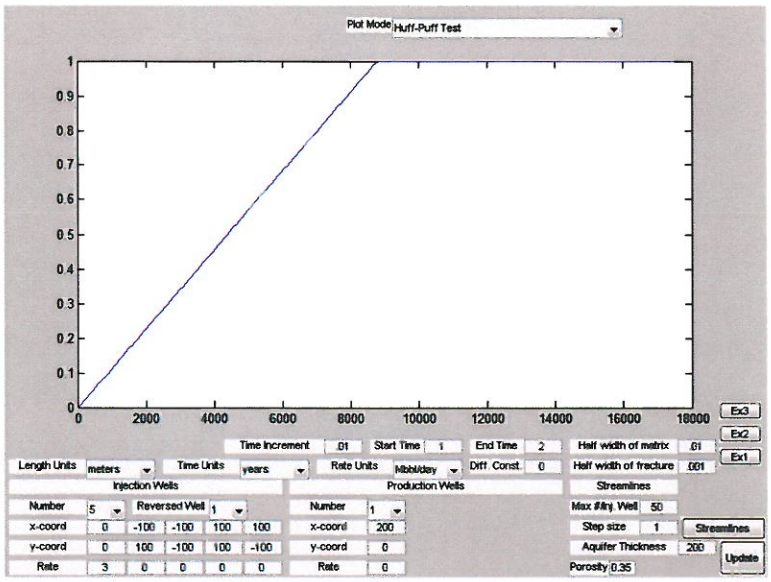


Figure 13: Fraction of injected fluid retrieved versus time in huff and puff test. Graph time units are hours.

Running the simulation again with a diffusion constant of $2.8\text{cm}^2/\text{s}$ gives a curve that has less of a kink, as shown in Fig. 14.

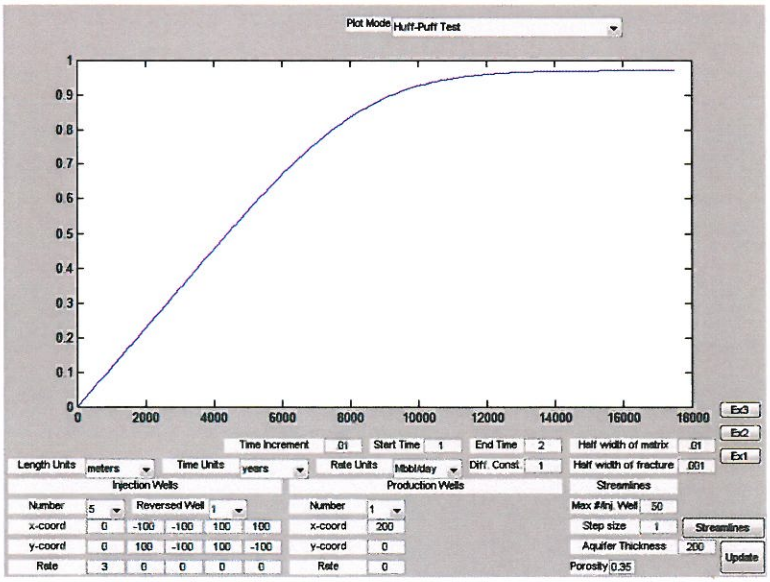


Figure 14: Fraction of injected fluid retrieved versus time in huff and puff test. Graph time units are hours.

Since this is the high-diffusion limit, the retrieved fraction of injected fluid should be greater than that with an intermediate diffusion constant since in this limit, the limiting factor on retrieving injected fluid is the production rate, not the diffusion. Fig. 15 shows the retrieval curve for a diffusion constant of $2.8 \times 10^{-9}\text{cm}^2/\text{s}$.

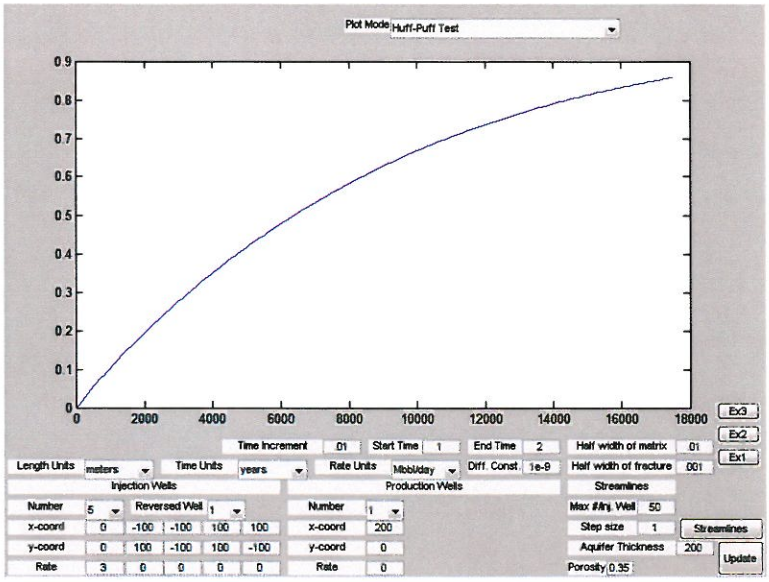


Figure 15: Fraction of injected fluid retrieved versus time in huff and puff test. Graph time units are hours.

As can be seen, the fraction retrieved is below both the low- and high-diffusion limits for a given time.

# 4 Conclusions

The simulations contained in this GUI give results that make intuitive sense, although they haven't been tested against data.

# References

[1] Carslaw, H. S. and Jaeger, J. C., 1959. *Conduction of Heat in Solids 2nd edit.*, Oxford University Press, 510 p.

[2] Cathles, L. "Tracers in Fractured Rock." Earth Science Fundamentals Module. IGERT. Ithaca, 13 February 2012.

[3] I. Javandel, C. Doughty, and C. F. Tsang, *Groundwater Transport: Handbook of Mathematical Models*, American Geophysical Union, 1984.

# Appendix C: Methods for estimating diffusion constants

Yushi Zhao

# Appendix C: Diffusion Coefficients

Diffusion constants for the solvents, solutes and particles discussed in the body of the ARI report are calculated here using the Stokes Einstein equation. The calculations are summarized in Table C1.

**Table C1. Summary of calculated diffusion constants**

| Solvent | Viscosity | Solute | Radius | $D_o[cm^2/s] \times 10^5$ |
|---|---|---|---|---|
| **HFE** | 600 PaS (3M, 2009) | TFT | 0.25 nm maximum | 1.42 |
| | | | 0.1 nm minimum | 3.55 |
| | | nanoparticles | 40 nm | 0.017 |
| **$scCO_2$** | 20 μPaS | TFT | 0.3 nm maximum | 36.4 |
| | | nanoparticles | 40 nm | 0.545 |
| **Methane-supercritical $CO_2$ interdiffusion** (Wilke-Chang's estimation method) | | | | 88.7 |

## The Stokes-Einstein's Equation

Assumptions: Diffusing entities dispersed or dissolved in a liquid, the entities are spherical, and the Reynolds number is low (no turbulence). Under these circumstances, the diffusion constant of the entities (molecules or particles) can be estimated from equation C1 (Poling, et al. 2001).

$$D = \frac{KT}{6\pi\mu r} \qquad \text{(C1)}$$

where,

K = Boltzmann's Constant ($1.38065 \times 10^{-23}$ J/K)
T = Absolute Temperature in K (297 K)
$\mu$ = kinematic viscosity 0.43 cSt
r = radius of the particle

## Chemical Tracer - Trifluorotoluene (TFT)

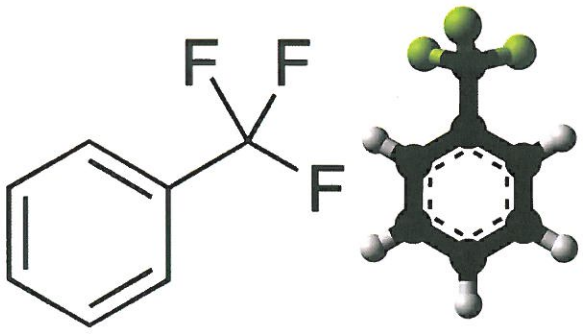


**Figure C1. Trifluorotoluene molecule.**

The TFT molecule is elliptical. We can estimate the diameter of the of the major axis of this ellipse from the molecular bond lengths. Adding (1 x H-C bond length) + (3 x C-C bond length) + (1 x C-F bond length) we find a major axis diameter of between 480 and 560 picometers. A radius of 250 pm as gives us 1.42 x $10^{-9}$ $m^2/s$ or 1.42 x $10^{-5}$ $cm^2/s$ for TFT in Hydrofluoroether (HFE) in ambient conditions.

The same calculation with the minor molecular ellipse dimension gives a diameter of ~ 200 pm, and this suggests a diffusion constant of 3.55 x $10^{-9}$ $m^2/s$ or 3.55 x $10^{-5}$ $cm^2/s$. The best fit diffusion constant for our interpretation of the TFT tracer in HFE is 2.5 x $10^{-9}$ $m^2/s$ or 2.5 x $10^{-5}$ $cm^2/s$. Since this diffusion constant lies between these diffusion coefficient estimates for TFT , our best fit model diffusion constant is very reasonable.

To find a value for the viscosity of $scCO_2$, generally, people refer to 1/10 of that of the water at 20C, or 40% less than that of the liquid $CO_2$. But it is really a function of temperature pressure.

Using the dynamic viscosity of $scCO_2$ and assuming $scCO_2$ carries all fluid diffusional properties near the critical point (304K, 7mPa or 73 atm) of $CO_2$ 20 $\mu$Pa s (Fenghour, Wakeham 1997), the diffusion coefficient based on Stokes-Einstein's equation for molecule with 300 pm radius is 3.64 x $10^{8}$ $m^2/s$ or 3.64 x $10^{4}$ $cm^2/s$. The viscosity further reduces with the increase in reservoir temperature, however it increases with pressure increase.

## Nanoparticle Tracers

### SiO2 nanoparticle by Yisheng

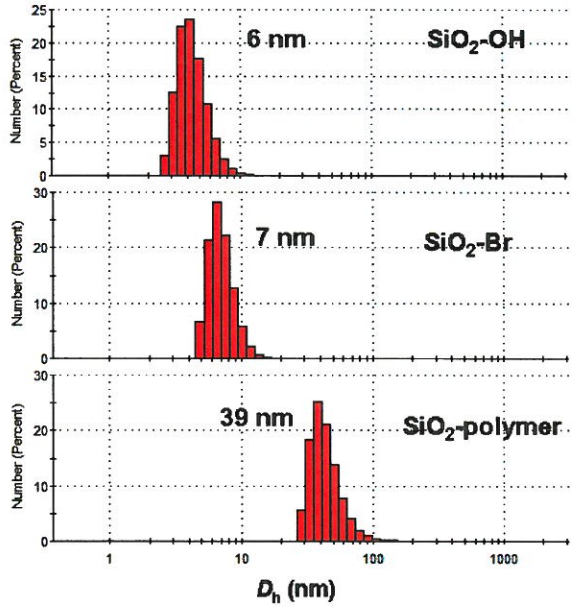


**Figure C2. Size distribution of $SiO_2$ nanoparticle before and after polymerization.**

Calculated Diffusion Coefficient based on Stokes-Einstein's equation considering a solid elastic sphere with 19.5 nanometer as radius gives us 1.82 x $10^{-11}$ $m^2/s$ or 1.82 x $10^{-7}$ $cm^2/s$ for this kind of $SiO_2$ nanoparticle in Hydrofluoroether (HFE) in ambient conditions.

Using the dynamic viscosity of $scCO_2$ and assuming $scCO_2$ carries all fluid diffusional properties near the critical point (304K, 7mPa or 73 atm) of $CO_2$ (20 $\mu$Pa s ~ 0.00002 P) and assuming uniformity in sizes, the diffusion coefficient based on Stokes-Einstein's equation for molecule with 19.5 nm radius is $5.6 \times 10^{-10}$ $m^2/s$ or $5.6 \times 10^{-6}$ $cm^2/s$.

### $Fe_3O_4$ nanoparticle by Yisheng

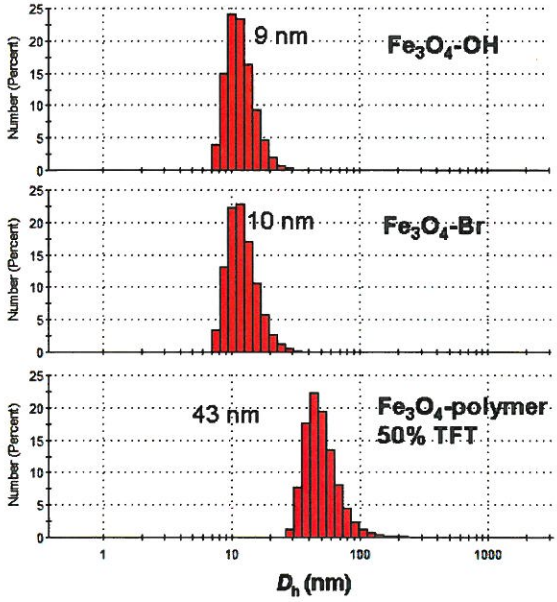


**Figure C3. Size distribution for the $Fe_3O_4$ nanoparticle before and after polymerization.**

Calculated Diffusion Coefficient based on Stokes-Einstein's equation considering a solid elastic sphere with a radius of 21.5 nanometers gives $1.65 \times 10^{-11}$ $m^2/s$ or $1.65 \times 10^{-7}$ $cm^2/s$ for this kind of $Fe_3O_4$ nanoparticle in Hydrofluoroether (HFE) in ambient conditions.

Using the dynamic viscosity of $scCO_2$ and assuming $scCO_2$ carries all fluid diffusional properties near the critical point (304K, 7mPa or 73 atm) of $CO_2$ (20 $\mu$Pa s ~ 0.00002 P s) and assuming uniformity in sizes, the diffusion coefficient based on Stokes-Einstein's equation for molecule with 21.5 nm radius is $5.08 \times 10^{-10}$ $m^2/s$ or $5.08 \times 10^{-6}$ $cm^2/s$.

Table C2. Diffusion constants in scCO2 for spherical particles of different diameter.

| Diameter (nm) | Diffusion Coefficient (cm2/s) |
|---|---|
| 0.1 | 2.18E-03 |
| 1 | 2.18E-04 |
| 10 | 2.18E-05 |
| 20 | 1.09E-05 |
| 30 | 7.27E-06 |
| 40 | 5.45E-06 |
| 50 | 4.36E-06 |
| 100 | 2.18E-06 |
| 200 | 1.09E-06 |
| 300 | 7.27E-07 |
| 400 | 5.45E-07 |
| 500 | 4.36E-07 |
| 1000 | 2.18E-07 |

## Estimation of Interdiffusion Coefficient of $scCO_2$ and Methane

$CO_2$ has a critical temperature of 304.25 K and critical pressure of 72.9 atm/7.39MPa. At supercritical phase, it tries to expand to fill its container like a gas but with a density like that of a liquid.

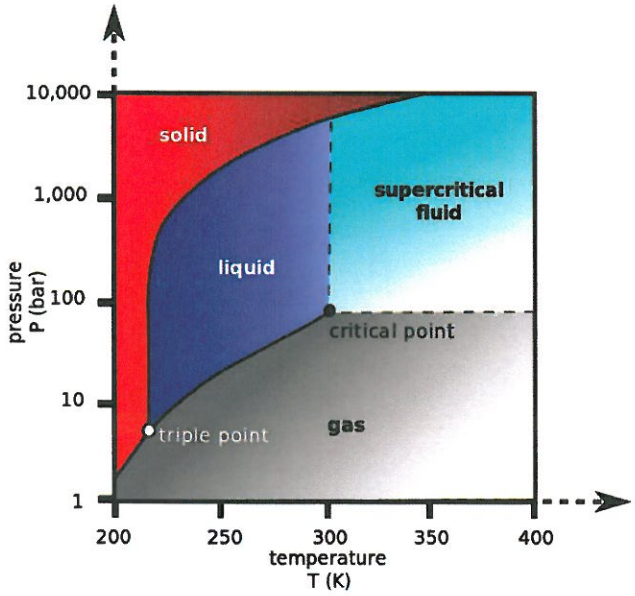


Figure C4. Carbon dioxide pressure-temperature phase diagram (Carbon Dioxide).
http://commons.wikimedia.org/wiki/File:Carbon_dioxide_pressure-temperature_phase_diagram.svg

There are several ways to estimate the interdiffusion coefficient of $scCO_2$ and methane, namely Stokes-Einstein-based correlations, Dymond free-volume type expression, Catchpole-King correlation, and Tracer Liu-Silva-Macedo Equation. Here used Stokes-Einstein based correlations

(Wilke-Chang's) estimation method because it is thought to be a better estimation of diffusion coefficients for $scCO_2$.

$$D_{12} = 7.4 * 10^{-8} \frac{(\phi M_1)^{1/2} T}{\eta_1 V_{2,eb}^{0.6}}$$

1: solvent ($CO_2$)
2: solute ($CH_4$)
$\phi$: association factor for $M_1$, for unassociated $CO_2$ its 1
eb: normal boiling point
M: molecular weight
T: temperature in K
η: viscosity in cP
V: molar volume in $cm^3/mol$

The estimation based on the above equation yields 8.87 x $10^{-4}$ $cm^2/s$

## References

3M. (2009, September 9). 3M™ Novec™ 7200 Engineered Fluid[Material Safety Data Sheet]. Retrieved from http://multimedia.3m.com/mws/mediawebserver?mwsId=SSSSSufSevTsZxtU4Y_G5x_GevUqevTSevTSevTSeSSSSSS--&fn=prodinfo_nvc7200.pdf

Bruce E. Poling, John M. Prausnitz, and John P. O'Connell. *The Properties of Gases and Liquids, Fifth Edition.* The McGraw-Hill Companies, Inc. 2001, **DOI: 10.1036/0070116822**

Fenghour, A., Wakeham, W. A. *The Viscosity of Carbon Dioxide.* J. Phys. Chem. Ref. Data, Vol. 27, No. 1, 1998

Wilke, C. R., Chang, P. *Correlation of Diffusion Coefficients in Dilute Solutions.* A.I.Ch.E Journal. June 1955, 264-270

Wikipedia contributors. "Carbon dioxide." *Wikipedia, The Free Encyclopedia*. Wikipedia, The Free Encyclopedia, 21 May. 2013. Web. 21 May. 2013.

# Appendix D: An approximate method for calculating diffusion from a fluid moving in fractures into an adjacent matrix

Timothy Gao

# Using the Carslaw & Jaeger diffusion equation and material conservation to calculate fracture and matrix concentrations as a funtion of time

## Concentrations in the fracture and matrix as a function of time

Given a rock matrix penetrated every $2l$ by fractures $2d$ wide, the Carslaw & Jaeger diffusion equation that gives the concentration in the matrix of a fluid (that travels in the fractures and diffuses into the matrix) as a function of time and position from the nearest fracture is

$$C(y,t) = C_0 \left\{ 1 - \frac{4}{\pi} \sum_{n=0}^{\infty} \frac{(-1)^n}{2n+1} \cos\left[ \frac{(2n+1)\pi\xi}{2} \right] \exp\left[ -\frac{(2n+1)^2\pi^2 T}{16} \right] \right\}, \tag{1}$$

where

$$\xi = \frac{y}{l}, \quad T = \frac{4Dt}{l^2}, \tag{2}$$

and $D$ is the diffusion constant of the fluid that travels through the fractures. Integrating this equation over width $l$ gives us the average concentration of the fluid in the matrix, $C_{avg}(t)$:

$$\begin{aligned} C_{avg}(t) &= \frac{\int_0^l C(y,t)dy}{l} \\ &= \frac{C_0}{l} \left\{ l - \frac{4}{\pi} \sum_{n=0}^{\infty} \frac{(-1)^n}{2n+1} \frac{2l}{(2n+1)\pi} \sin\left[ \frac{(2n+1)\pi\xi}{2} \right] \exp\left[ -\frac{(2n+1)^2\pi^2 T}{16} \right] \Bigg|_0^l \right\} \\ C_{avg} &= C_0 \left\{ 1 - \frac{8}{\pi^2} \sum_{n=0}^{\infty} \frac{\exp\left[ -\frac{(2n+1)^2\pi^2 T}{16} \right]}{(2n+1)^2} \right\}. \end{aligned} \tag{3}$$

This equation assumes that the concentration in the fracture, $C_{frac}(t)$, stays at $C_{frac} = C_0$ for all time, and that the starting concentration of the matrix concentration is $C_{avg}(0) = 0$. If, instead, we assume that $C_{frac}(t)$ can vary with time and that $C_{avg}(0) \neq 0$, we can use the approximation $C_0 \approx C_{frac}(t) - C_{avg}(0)$ to get the equation

$$C_{avg}(t) = \Big[ C_{frac}(t) - C_{avg}(0) \Big] \left\{ 1 - \frac{8}{\pi^2} \sum_{n=0}^{\infty} \frac{\exp\left[ -\frac{(2n+1)^2\pi^2 T}{16} \right]}{(2n+1)^2} \right\} + C_{avg}(0). \tag{4}$$

Assuming the fluid moves in discrete steps, we can use conservation of solute mass to obtain another relation between $C_{frac}(t)$ and $C_{avg}(t)$:

$$\phi l C_{avg}(t) + d C_{frac}(t) = \phi l C_{avg}(0) + d C_{frac}(0), \tag{5}$$

where $\phi$ is the porosity of the rock in the matrix. Note that this equation assumes the fluid in the fractures is static over the time step.

Using these two equations to solve for $C_{frac}$ gives

$$C_{frac}(t) = \frac{C_{frac}(0) + \frac{\phi l}{d} C_{avg}(0) \left\{ 1 - \frac{8}{\pi^2} \sum_{n=0}^{\infty} \frac{\exp\left[ -\frac{(2n+1)^2 \pi^2 T}{16} \right]}{(2n+1)^2} \right\}}{1 + \frac{\phi l}{d} \left\{ 1 - \frac{8}{\pi^2} \sum_{n=0}^{\infty} \frac{\exp\left[ -\frac{(2n+1)^2 \pi^2 T}{16} \right]}{(2n+1)^2} \right\}}. \tag{6}$$

In the limit $t \to \infty$, the matrix and fracture concentrations approach the same value $C_\infty$. Setting $C_{avg}(t) = C_{frac}(t) = C_\infty$ in equation (5) yields

$$C_\infty = \frac{C_{frac}(0) + \frac{\phi l}{d} C_{avg}(0)}{1 + \frac{\phi l}{d}}.$$

In equation (6), the sum of exponentials disappears at large values of $t$. Thus, (6) predicts that at large times,

$$\lim_{t \to \infty} C_{frac}(t) = \frac{C_{frac}(0) + \frac{\phi l}{d} C_{avg}(0)}{1 + \frac{\phi l}{d}} = C_\infty.$$

Over each timestep, the fracture concentration for large $\Delta t$ reaches the correct mass balance limit.

We can also verify that the fracture and matrix concentrations never cross by setting $C_{avg}(t) = C_{frac}(t)$ in equation (4):

$$\begin{aligned} C_{frac}(t) &= \left[ C_{frac}(t) - C_{avg}(0) \right] \left\{ 1 - \frac{8}{\pi^2} \sum_{n=0}^{\infty} \frac{\exp\left[ -\frac{(2n+1)^2 \pi^2 T}{16} \right]}{(2n+1)^2} \right\} + C_{avg}(0) \\ 0 &= \left[ C_{frac}(t) - C_{avg}(0) \right] \frac{8}{\pi^2} \sum_{n=0}^{\infty} \frac{\exp\left[ -\frac{(2n+1)^2 \pi^2 T}{16} \right]}{(2n+1)^2} \end{aligned} \tag{7}$$

This equation can be satisfied if either $C_{frac}(t) - C_{avg}(t) = 0$ or if sum of exponentials equals 0. The latter is the case as $t \to \infty$. We can simplify equation (6) by letting $f(t) = 1 - \frac{8}{\pi^2} \sum(...)$ to get

$$C_{frac}(t) = \frac{C_{frac}(0) + \frac{\phi l}{d} C_{avg}(0) f(t)}{1 + \frac{\phi l}{d} f(t)}. \tag{8}$$

If $C_{avg}(0) = C_{frac}(t)$, then equation (7) is satisfied. Replacing $C_{frac}(t)$ with $C_{avg}(0)$ in equation (8) gives

$$\begin{aligned} C_{avg}(0) &= \frac{C_{frac}(0) + \frac{\phi l}{d} C_{avg}(0) f(t)}{1 + \frac{\phi l}{d} f(t)} \\ \left[ 1 + \frac{\phi l}{d} f(t) \right] C_{avg}(0) &= C_{frac}(0) + \frac{\phi l}{d} C_{avg}(0) f(t) \\ C_{avg}(0) &= C_{frac}(0) \end{aligned}$$

Clearly, the concentrations can never cross, since this result indicates that $C_{avg}(t) = C_{frac}(t)$ for finite $t$ only if the initial fracture and matrix concentrations are equal, in which case no net diffusion occurs. Thus, the absolute value of the difference between the matrix and fracture concentrations decreases monotonically with time to an equilibrium value of 0, as is expected.

## Use of equations to create concentration matrices

These equations can be used to calculate the fracture and rock matrix concentration at each time and position along a specific streamline. We can build up matrices for both the fracture and rock matrix concentrations by calculating all concentrations at a certain time and using those to calculate concentrations at the next time. Since the fluid in the fracture flows down from node to node as time progresses, we can assume that $C^f_{i,j}$, the fracture concentration at $(x_i, t_j)$, is the non-diffused portion of the fracture concentration at the previous node and previous time, $C^f_{i-1,j-1}$. The diffused portion of $C^f_{i-1,j-1}$ goes into the rock matrix at position $x_{j-1}$, since the fluid in the rock matrix stays put. Thus, $C^m_{x_i,t_j}$, the rock matrix concentration at $(x_i, t_i)$, is given by $C^m_{x_i,t_{j-1}}$ plus the diffused portion of $C^f_{i-1,j-1}$.

## Advantages of the method

Our approximation that, over a timestep (when the fracture fluid is static), the flux into the matrix can be considered to be driven by the difference between the average solute concentration in the matrix and the concentration in the fracture has several advantages over a sum of concentration step functions which is a less approximate alternative method of solution to which we will compare our results below. Firstly, the computations are much faster using this approximation because the matrix and fracture concentrations at a particular time and position are determined by the concentrations at the previous time and position only (not the entire history of the concentrations at the previous position). Secondly, the method is ideally suited for cases where the concentration time series reverses, as happens in huff-puff tests, since it doesn't require storage of the concentration history for each position. Thirdly, the method seems to be more accurate in the limit of very high diffusion constants.

## Verification of the method

We verify the method described above by showing it gives correct results when diffusion constants are very high and very low, and showing that it gives results similar to (but more accurate than) a method which does not approximate the driving concentration difference as that between the fracture and average matrix concentrations.

Consider first the case of radial flow from an injection well where the tracer diffusion constant is so high and the fractures so closely spaced that the solute will fill the matrix quickly and the concentration front will proceed at the rate at which it fills the matrix completely as it moves along. An effective diffusion constant of 2.8 $cm^2/s$ is such a case. For a fracture half-spacing of $l = 1$cm, the diffusional relaxation time is around 0.5 seconds. The fracture fluid is advanced 1m each timestep, and each timestep is 1 hour long. The injection rate into a 200m thick aquifer is 19.9 $m^3/hr$. The other parameters are $d = 0.1$cm and $\phi = 0.35$. The predicted rock and fracture concentration matrices for this case are given below.

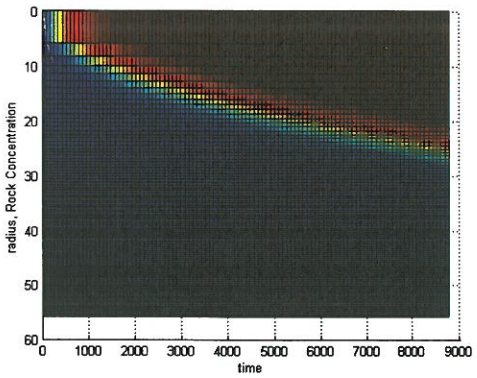


Figure 1: Rock matrix concentration for all time and position nodes. Diffusion constant of 2.8 $\mathrm{cm}^2/\mathrm{s}$

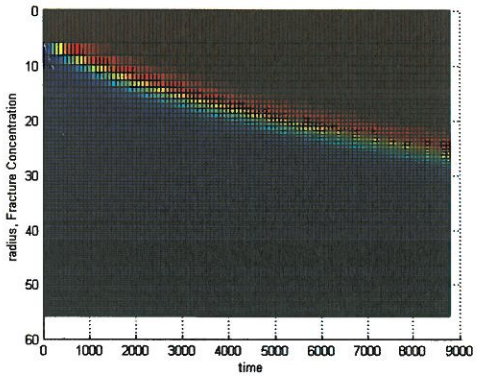


Figure 2: Fracture concentration for all time and position nodes. Diffusion constant of 2.8 $\mathrm{cm}^2/\mathrm{s}$

As expected the rock and fracture concentration are the same, and both fill the 200m thick aquifer in a fashion which forms a disc with unit concentration to a radius of around 26m after 8760 hours of injection. We can easily verify that this solution is reasonable. The total porosity is given by equation (9). Taking $d = 0.1\mathrm{cm}$, $l = 1\mathrm{cm}$, $\phi = 0.35$, the total effective porosity is

$$\phi_{eff} = \frac{d}{d+l} + \left(1 - \frac{d}{d+l}\right)\phi = 0.409. \tag{9}$$

For an aquifer thickness of 200m, the total volume of fluid injected should be

$$V_{tot} = 200\pi(26)^2\phi_{eff} = 1.7 \times 10^5 \mathrm{m}^3$$

Dividing this by the time at the end of the test, 8760 hours, gives us a rate of

$$Q_{approx} = 20.\ \mathrm{m}^3/\mathrm{hr},$$

which agrees very well with the actual rate in this test, $3\mathrm{Mbb/day} = 19.9\mathrm{m}^3/\mathrm{hr}$.

## Comparison to a more physically based alternative method of computation

Timewise, the approximate method described here is much faster than a more physically-based alternative method of computation, which uses a superposition of step function concentration changes in the injected fluid at any node. We show here that the new method also provides more reasonable results for at huff-puff test and for high-diffusivity flow.

Figure 3 shows the advance of a tracer concentration front with time, but in contrast to Figure 2 the flow is now planar rather than radial. The top row of diagrams show the advance for a non-diffusive tracer (D=0) and the bottom row of figures shows the advance for a very diffusive (D=2.8 $m^2$/hr) tracer. The first column of panels shows the tracer concentration in the fractures for our original or "old" method of computation which superimposed step function increases in fracture concentration calculating the diffusion into the matrix at all times from this step change. The second column shows the fracture concentrations for the new, approximate method described here. The right column shows the average matrix concentration for the new method.

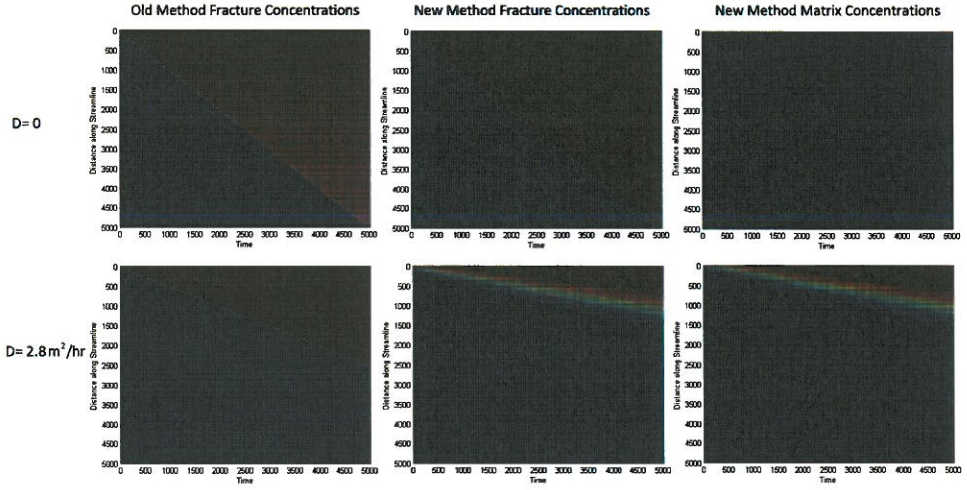


Figure 3: Fluid velocity tests for low-diffusion and high-diffusion. All graphs have the same color scale. Time units are hours and distance units are meters.

Clearly, the two methods give identical results in the zero-diffusion limit. The accuracy of the new method is better that the old in the high diffusivity limit. As before, $d = 0.1$cm, $l = 1$cm, $\phi = 0.35$, the fracture porosity is

$$\phi_{frac} = \frac{1}{11} = 0.091$$

and the effective porosity is

$$\phi_{eff} = 0.409.$$

The test was set up so that fluid moving entirely in the fracture would travel a distance of 1m down the streamline in one hour. Thus, at a time $t_{end}$ =5000 hours, the fluid front in the zero-diffusion limit would be a distance $x_{low} = 5000$m from the injection point. Using this distance, as well as the

ratio between the two porosities $\phi_{frac}$ and $\phi_{eff}$, it is possible to predict the position of the fluid front at $t_{end}$ in the high-diffusion limit. Since the highly diffusing fluid would travel throughout the whole geometry instead of sticking in the fractures, it would travel more slowly down the streamline. The distance down the streamline, $x_{high}$, that it would reach in 5000 hours is given by the equation

$$x_{high} = \frac{\phi_{frac}}{\phi_{eff}} x_{low} = \left(\frac{0.091}{0.409}\right) 5000 = 1111\text{m}.$$

From the figure, we can see that the new method is much more consistent with this result.

# Volume 8
# Assessment of Technical and Economic Potential of Recovering Methane and Storing $CO_2$ in Eastern Gas Shales

## Assessment of Factors Influencing Effective $CO_2$ Storage Capacity and Injectivity in Eastern Gas Shales

Prepared for:
U.S. Department of Energy
National Energy Technology Laboratory
DOE Award Number: DE-FE0004633

Prepared by:
Michael Godec, Principal Investigator
Advanced Resources International, Inc.
4501 Fairfax Drive ▪ Suite 910 ▪ Arlington, Virginia 22203

Date:
October 23, 2013


4501 Fairfax Drive ▪ Suite 910 ▪ Arlington, Virginia 22203 ▪ Phone: (703) 528-8420 ▪ web: www.adv-res.com

## Advanced Resources International, Inc.

# Table of Contents

**1.** INTRODUCTION ..... 1
**2.** ECONOMIC ANALYSES – OVERVIEW OF APPROACH ..... 3
a. Engineering Costing Model for Shale Gas Development ..... 3
b. Engineering Costing Model for $CO_2$ Injection ..... 8
c. Economic/Cash Flow Analyses for Enhanced Shale Gas Development with $CO_2$ Injection ..... 10
**3.** MARCELLUS SHALE ..... 13
a. Reservoir Simulation Analyses ..... 13
b. Approach for History Matching ..... 13
c. Results of History Matching ..... 16
d. $CO_2$ Injection Scenarios -- Simulation Results and Interpretation ..... 18
e. Development of Input Data for Basin Assessment ..... 31
f. Simulation Results for Basin Assessment ..... 31
g. Potential for Enhanced Gas Recovery and $CO_2$ Storage ..... 38
**4.** UTICA SHALE ..... 40
a. Development of Input Data ..... 40
b. Simulation Results ..... 49
c. Economic Analyses ..... 53
d. Potential for Enhanced Gas Recovery and $CO_2$ Storage ..... 56
**5.** ANTRIM SHALE ..... 58
a. Approach for and Results from History Matching ..... 58
b. Development of Input Data for $CO_2$-EGR and Storage Cases ..... 61
c. Development of Simulation Scenarios for $CO_2$-EGR/Storage Cases ..... 66
d. Potential for $CO_2$ Storage ..... 70
**6.** REFERENCES ..... 72

# List of Figures

Figure 1: Representation of Methodology for Estimating Gas Gathering System Costs ..... 6
Figure 2: Representation of Methodology for Estimating Gas Gathering System Costs ..... 7
Figure 3: Example of Summary Output from the Cash Flow Model ..... 12
Figure 4: Marcellus Methane and $CO_2$ Adsorption Isotherms ..... 15
Figure 5: Gas Rate History Match ..... 17
Figure 6: Water Rate History-Match ..... 17
Figure 7: Line Drive Pattern Representation ..... 19
Figure 8: Grid Block Representation of Line Drive Pattern ..... 19
Figure 9: Methane Production Results from Simulation Runs for Alternative Injection Timing Scenarios --- Case 1 – Marcellus Area 5 ..... 25
Figure 10: Methane Production Results from Simulation Runs for Alternative Injection Timing Scenarios --- Case 2 – Marcellus Area 5 ..... 26
Figure 11: Methane Production Results from Simulation Runs for Alternative Injection Timing Scenarios --- Case 3 – Marcellus Area 5 ..... 26
Figure 12: Marcellus Model Areas for Simulating Potential CO2 Storage and Enhanced Gas Recovery ..... 32
Figure 13. Utica/ Point Pleasant Study Area with Model Area Sub-Divisions ..... 40
Figure 14. Methane Adsorption Isotherms for the Utica/ Point Pleasant ..... 48
Figure 15. $CO_2$ Adsorption Isotherms for the Utica/ Point Pleasant ..... 48
Figure 16. Permeability Decay Correlation used for Estimating Matrix Permeability ..... 50
Figure 17: "Typical" Antrim Shale Gas Well – Gas Production Rate ..... 58
Figure 18: "Typical" Antrim Shale Gas Well – Water Production Rate ..... 59
Figure 19: Methane and Carbone Dioxide Isotherms ..... 60
Figure 20: Gas and Water Rate History-Match for Typical Antrim Well ..... 61
Figure 21: Antrim Shale Cross-Sections and Model Areas ..... 62

# List of Tables

Table 1: Summary of Well Costs for a 10,000 Foot Shale Gas Well ..... 5
Table 2: Elevation, Thickness and Well Length ..... 14
Table 3: History-Match Input Parameters ..... 16
Table 4: Enhanced Gas Recovery and $CO_2$ Storage as a Function of Distance between the Injection and Production Wells for a 50 Foot Cross-Section of Horizontal Well – Marcellus Area 5 ..... 20
Table 5: Methane Recovery and $CO_2$ Storage for Three Completion and Several Injection Timing Scenarios – Marcellus Area 5 ..... 24
Table 6: Economics of Methane Recovery and $CO_2$ Storage for Several Injection Timing Scenarios – Marcellus Area 5 – Case 2 – Three Wellhead Gas Prices ..... 28
Table 7: Economics of Methane Recovery and $CO_2$ Storage for Several Injection Timing Scenarios – Marcellus Area 5 – All 3 Cases -- $5.00/Mcf Wellhead Gas Price ..... 30
Table 8. Summary and Description of Marcellus Model Areas ..... 33

Table 9. Model Layer Attributes for Upper Marcellus (Oatka Creek).....34
Table 10. Model Layer Attributes for Purcell/ Cherry Valley Limestone .....35
Table 11. Model Layer Attributes for Lower Marcellus (Union Springs) .....36
Table 12: Methane Recovery and $CO_2$ Storage for Case 2 Completion Strategy for Alternative Injection Timing Scenarios – All Marcellus Areas .....37
Table 13: Methane Recovery and $CO_2$ Storage Potential for the Marcellus Shale .....39
Table 14. Description and Summary of Utica Shale/ Point Pleasant Model Areas .....42
Table 15. Model Layer Attributes for Upper Utica Shale– Archie Water Saturation .....43
Table 16. Model Layer Attributes for Organic-Rich Basal Utica Shale – Simandoux Water Saturation .....44
Table 17. Model Layer Attributes for Shale - Rich Point Pleasant (Upper Point Pleasant) and Equivalent Formations – Simandoux Water Saturation .....45
Table 18. Model Layer Attributes for Carbonate - Rich Point Pleasant (Lower Point Pleasant) and Equivalent Formations – Archie Water Saturation .....46
Table 19. Key Parameters by Layer and Model Area used in the Simulation Runs.....47
Table 20. Impact of Assumed Matrix Permeability on the Results of the Simulation Runs for the Utica Shale Model Areas.....51
Table 21. Methane Recovery and $CO_2$ Storage for Case 2 Completion Strategy for Alternative Injection Timing Scenarios – All Utica Areas.....52
Table 22: Economics of Methane Recovery and $CO_2$ Storage for Several Injection Timing Scenarios – Utica Area 5 – Case 2 – Three Wellhead Gas Prices.....54
Table 23: Economics of Methane Recovery and $CO_2$ Storage for Several Injection Timing Scenarios – Utica Area 3 – Case 2 - Two Wellhead Gas Prices .....55
Table 24: Methane Recovery and $CO_2$ Storage Potential for the Utica Shale .....57
Table 25. Antrim Shale Reservoir Properties Used to Obtain Match for "Typical" Well .....60
Table 26. Summary of Methane Adsorption Isotherm Data for the Antrim Shale.....63
Table 27. Description and Summary of Antrim Shale Model Areas .....64
Table 28. Model Layer Attributes for the Lachine and Norwood Members of the Antrim Shale .....65
Table 29: Economics of Methane Recovery and $CO_2$ Storage for Several Injection Timing Scenarios – Antrim Shale, Area 1 - Three Wellhead Gas Prices – 80-Acre Spacing .....68
Table 30: Comparison of Economics of Methane Recovery and $CO_2$ Storage for Antrim Shale, Area 1 - Three Wellhead Gas Prices – 80-Acre vs. 40-Acre Spacing .....69
Table 31: Methane Recovery and $CO_2$ Storage Potential for the Antrim Shale .....71

# 1. INTRODUCTION

Assessments of the potential technical and economic implications of $CO_2$ storage in gas shales is quite limited; though several studies and field-test experience regarding $CO_2$ storage in coal seams can serve as a source of some guidance and insights. Even then, such site-specific economic assessments of $CO_2$ storage in coal seams have focused on hypothetical case studies (Bromhal, et al., 2004; Davis, et al., 2004), which may not necessarily reflect "real-world" conditions.

Several high level assessments of the economics of $CO_2$ storage in coal seams have been conducted. Based on costs and performance experience over ten years ago, Gale and Freund (2001) concluded that $CO_2$-enhanced coal bed methane (ECBM) recovery might be profitable in the United States at wellhead natural gas prices of U.S. $1.75 to $2.00/Mcf. Reeves (2003) estimated that between 25 and 30 billion metric tons, or Gigatonnes (Gt), of $CO_2$ was economical to store (assuming wellhead natural gas prices of $3.00/Mcf), and 80 to 85 Gt of storage potential was estimated at costs of less than $5 per metric ton. These estimates did not include any costs associated with $CO_2$ capture and transportation, only representing the costs associated with geologic storage.

The same engineering techniques used to achieve commercial gas production from gas shales – dense well spacing, horizontal drilling, and/or hydraulic fracturing – will also likely be needed to enhance $CO_2$ injectivity and storage in these formations. This conclusion is supported by small scale field tests and associated simulation work, but no large scale tests have yet to be conducted in either coal or shales, and with the only moderately sized injection test in coal seams being the Pump Canyon demonstration project in the San Juan basin in the south western United States, where about 18,000 tons of $CO_2$ were injected over a 12-month period (Koperna, et al., 2009).

Some critical questions that need to be addressed when understanding the economic potential for enhanced gas recovery (EGR) from and $CO_2$ storage in gas shales include:

- What impact does the phasing of primary and EGR have on the effectiveness of $CO_2$ storage?
- What shale reservoir environment provides the best economics (e.g. permeability, depth, TOC, rate, spacing, etc.)?
- Are greenfield or brownfield projects better?
- How sensitive are results to natural gas prices?
- How might $CO_2$ emission reduction credits impact the results?

In this assessment, the objective was to develop preliminary reservoir models and simulations to characterize the potential for both $CO_2$ storage and EGR for each of the target gas shale formations. Based on that, engineering costing and cash flow analyses were used to estimate economic potential based on natural gas prices and possible $CO_2$ emission reduction credits or carbon taxes.

Based on the results in Volumes 2 through 4, input parameters were developed for reservoir modelling. Based on the reservoir models, reservoir simulations were performed using ARI's proprietary COMET3 reservoir simulator. These reservoir simulations allowed for the estimation of $CO_2$ injection rates into gas shale reservoirs, the rate at which adsorbed methane is displaced from the shale by $CO_2$, the total volume of $CO_2$ stored, the initial dimensions of the $CO_2$ plume, and the disposition of the $CO_2$ in the reservoir over time. Potential constraints to economic EGR and $CO_2$ storage in gas shales were assessed -- particularly the low permeability and porosity -- with potential development and production options proposed that may help overcome these constraints. Engineering costing and cash flow analyses were performed to determine the impact on economic viability of the phasing of primary and EGR, natural gas prices, and potential $CO_2$ emission reduction credits or carbon taxes.

Finally, the results of these assessments were used to estimate the technical potential for EGR and $CO_2$ storage in the Marcellus, Utica and Antrim gas shales.

# 2. ECONOMIC ANALYSES – OVERVIEW OF APPROACH

Ultimately, from the perspective of a shale gas producer, the optimization of $CO_2$ injection in shales will be based on economics. Important factors to consider include the wellhead price for produced gas, the cost for purchased $CO_2$, the cost of processing produced/recycled $CO_2$, and the extent that any value is placed on $CO_2$ stored, say in the form of an emission reduction credit or carbon tax.

The objective of the economic analyses is to evaluate the impact of the potential constraints to economic $CO_2$ storage in gas shales, particularly the low permeability and porosity, and identify potential development and production options that may help overcome these constraints. This involves characterizing the critical performance factors for $CO_2$ injection and storage, reservoir properties (e.g., permeability, porosity,), and the timing of $CO_2$ injection.

## a. Engineering Costing Model for Shale Gas Development

The cost model for primary shale gas development specifically incorporates recent (unpublished) work by Advanced Resources for the Energy Information Administration (EIA) to develop a component-based cost model for shale gas development. This model estimates vertical and horizontal shale gas well drilling costs, completion and stimulation costs; gas gathering and compression costs, and shale gas well operating costs. Costs are estimated as a function of vertical well depth, lateral length, steel costs, labor costs, fuel costs, and variations in regional construction costs.

Specifically, the following steps were pursued to develop these costs:

- Detailed, component-specific capital cost data were assembled for well drilling and completion, fracture stimulation, surface equipment, gas gathering, gas treating, and compression.
- Detailed, component-specific cost data were assembled for well operations, with special attention given to key environmental control costs, such as water treatment and disposal and site maintenance.
- The component costs for each of the cost categories were characterized to enable accurate representation of the linkages between the cost of steel, fuel, and labor for each area.
- The component costs for each were also assessed to establish relationships between cost and well depth, geographic areas and special environmental settings.

To develop the cost data, all line items from the AFEs were grouped into four cost types: “steel”, “labor”, “other drilling and completion”, and “hybrid”. Hybrid line items were deemed to include some portion of both labor and other drilling and completion cost as a part of the total

line item cost. Each line item was assigned a subcategory, representing common cost items incurred in drilling horizontal shale wells.

Additionally, each line item was then identified as either a fixed or a variable cost type. Fixed costs remain constant, regardless of well depth (i.e. well site development and road construction). Variable costs fluctuate according to vertical depth or measured depth, as appropriate, (i.e. drilling services, drilling equipment, etc.). Similar categories of expenses were then averaged to provide a representative estimate of costs for each subcategory.

**Table 1** summarizes well drilling and completion costs, fracturing costs, steel costs, and labor costs for an example well at a depth of 10,000 feet. Based on the available data, cost per fracturing stage relationships were developed for fracturing materials, perforation materials, and fracturing water usage.

The gas gathering component costs for shale gas well development was established using data provided by industry experts. The gas gathering component cost is divided into three main systems:

- The low pressure delivery (or suction) pipe, which delivers gas from the well to the compressor phase
- The compressor station (four compressor units), which includes all associated dehydrators, separators, meters, water containment units, compressor housing and noise abatement structures.
- The high pressure discharge pipe, which carries the compressed gas to the main gas pipeline.

The gas gathering model employs several further assumptions:

- Gas enters the delivery pipeline at 90 psi, and is delivered to the compressor station at 35 psi.
- Gas is compressed to 1,200 psi and is delivered to the main pipeline at 1,100 psi.
- The compressors utilize 4.5 percent of the delivered gas as fuel.
- Annual gas gathering and compression operating costs amount to $2.4 million per year
- The gas gathering component provides gathering costs for four different initial well production rates: 1.0 MMcfd, 3.0 MMcfd, 5.0 MMcfd, and 10.0 MMcfd.

Table 1: Summary of Well Costs for a 10,000 Foot Shale Gas Well

| Other Drilling & Completion Costs | | |
|---|---|---|
| | | **Cost** |
| **Equipment Costs** | | |
| Drilling/Completion | $ | 1,673,649 |
| Misc./Rentals | $ | 556,697 |
| TOTAL EQUIPMENT COSTS | $ | 2,230,345 |
| **Materials/Overhead Costs** | | |
| Cement | $ | 98,289 |
| Chemicals/Fluids | $ | 360,912 |
| Water | $ | 27,295 |
| Fuel | $ | 207,044 |
| Environmental/Safety | $ | 28,661 |
| Water Pit/Location | $ | 151,739 |
| Overhead/Permits | $ | 150,520 |
| TOTAL MATERIALS/OVERHEAD COSTS | $ | 1,024,459 |
| **Fracturing Costs** | | |
| Fracturing | $ | 1,402,091 |
| Perforation | $ | 150,762 |
| Frac Water | $ | 384,444 |
| TOTAL FRACTURING COSTS | $ | 1,937,297 |
| **TOTAL OTHER DRILLING & COMPLETION COSTS** | **$** | **5,192,102** |

| Steel Costs | | |
|---|---|---|
| | | **Cost** |
| Casing Head (Fixed Cost) | $ | 25,500 |
| Conductor | $ | 4,031 |
| Surface Casing | $ | 41,740 |
| Intermediate Casing | $ | 238,000 |
| Production Casing | $ | 433,020 |
| Tubing | $ | 70,000 |
| **TOTAL STEEL COSTS** | **$** | **812,291** |

| Labor Costs | | |
|---|---|---|
| | | **Cost** |
| Consulting/Supervision | $ | 112,149 |
| Drilling/Completion | $ | 223,529 |
| Contract Labor | $ | 211,219 |
| Fracturing | $ | 174,851 |
| **TOTAL LABOR COSTS** | **$** | **721,747** |

| **Total Well CAPEX** | **$ 6,726,140** |
|---|---|

The amount of gathering infrastructure needed to develop a given area was established by using data from mature field development gathering systems. These data allowed for the determination of a "steady state" relationship between wells drilled and gas gathering infrastructure that represents a realistic estimate of the gathering requirements of a field-scale development. This "steady-state" ratio is used to determine the number of compressor units required for a given field. The number of gathering stations is based on the number of total compressors needed, assuming four compressor units per gathering station.

**Figure 1** represents the gas gathering model used to calculate total gathering costs, which are then scaled based on a determined well spacing and total field acreage.

Figure 1: Representation of Methodology for Estimating Gas Gathering System Costs

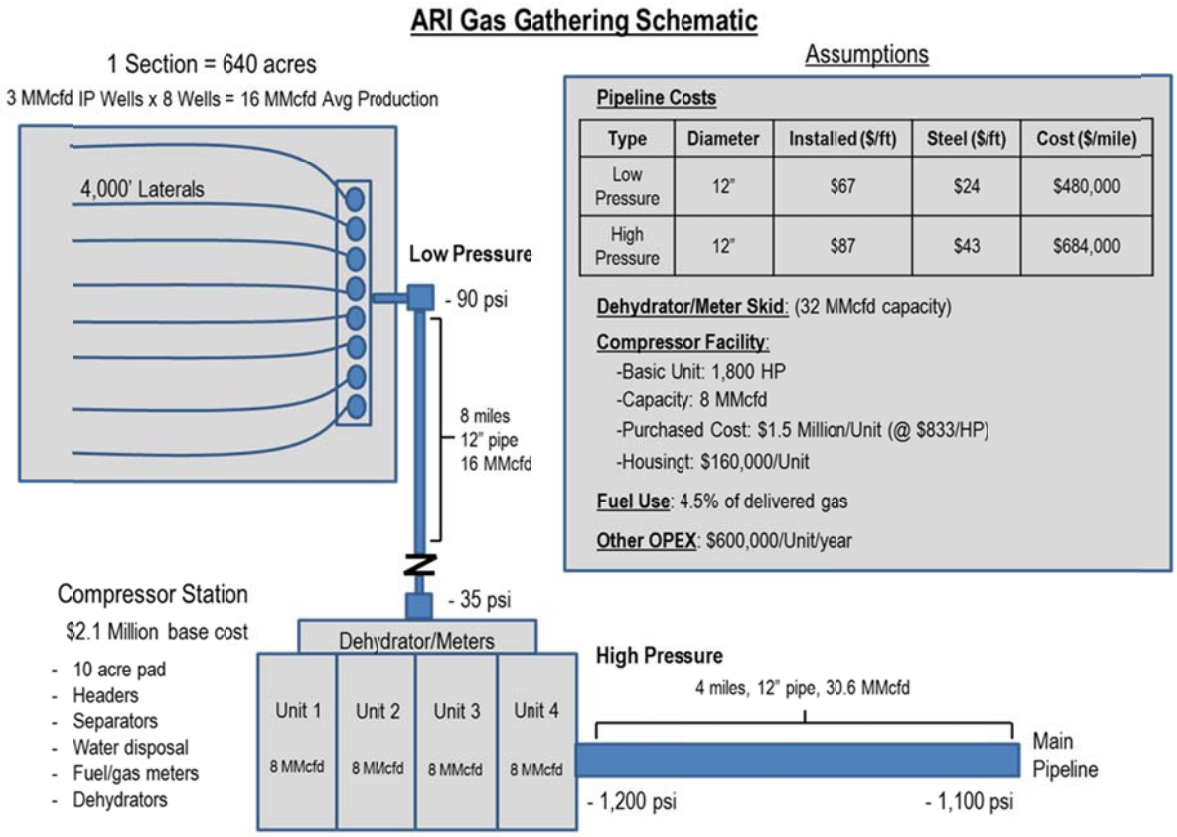

Annual shale gas well operating costs are derived from the EIA Oil and Gas Lease Equipment and Operating Costs 1994 through 2009 report (EIA, 2010). Operating costs data were assembled for wells varying by depth and production, which produced a linear cost curve. Since the EIA figures provided cost data in 2009 dollar amounts, the data was first normalized to 2011 dollars using a producer price index for natural gas extraction provided by the Bureau of Labor Statistics (http://data.bls.gov/cgi-bin/dsrv?pc). The overall annual operating cost is further divided into labor and non-labor costs. Labor costs are assumed to be 80 percent of the total operating cost, while non-labor costs are assumed to be 20 percent of the total operating cost.

**Figure 2** illustrates how average operating costs (in 2010 dollars) are estimated.

Figure 2: Representation of Methodology for Estimating Gas Gathering System Costs

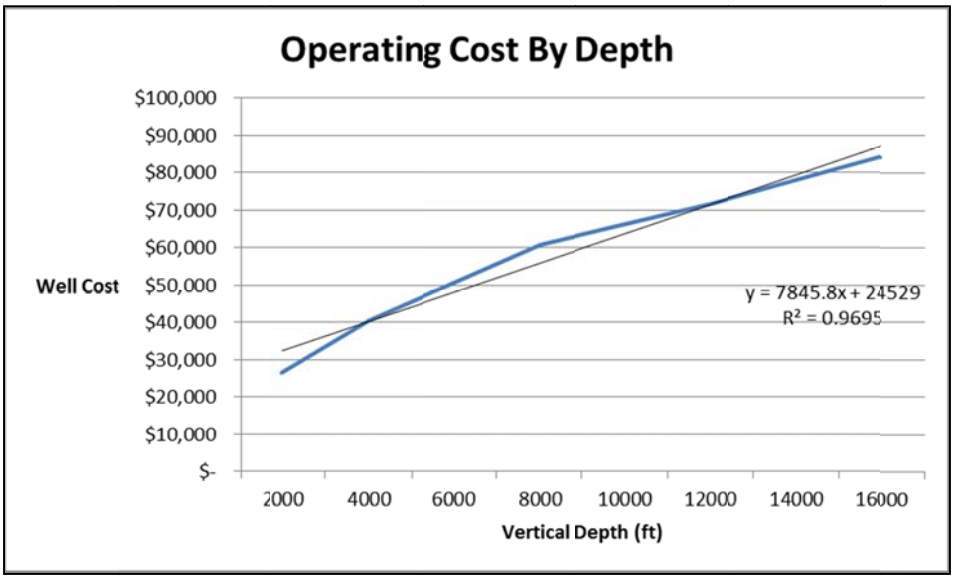


| | MMcfd | | | | | | | |
|---|---|---|---|---|---|---|---|---|
| **Depth** | **0.25** | **0.5** | **1** | **5** | **10** | **Average Cost** | **Cost Per Depth** | **Operating Cost By Depth*** |
| **2,000** | $ 22,400 | | | | | $ 22,400 | $ 11.20 | $ 26,656 |
| **4,000** | $ 33,500 | $ 34,500 | | | | $ 34,000 | $ 8.50 | $ 40,460 |
| **8,000** | $ 55,400 | $ 40,400 | $ 57,600 | | | $ 51,133 | $ 6.39 | $ 60,849 |
| **12,000** | $ 69,800 | $ 49,600 | $ 63,700 | $ 57,600 | | $ 60,175 | $ 5.01 | $ 71,608 |
| **16,000** | | $ 51,500 | $ 67,900 | $ 69,600 | $ 94,300 | $ 70,825 | $ 4.43 | $ 84,282 |
| * Average cost * 19% cost adjustment factor (BLS Cost Adjustment 2009 to 2011 Gas Extraction Factor) | | | | | | | | |

## b. Engineering Costing Model for $CO_2$ Injection

The $CO_2$ injection cost model features updated cost estimation procedures developed by Advanced Resources for NETL (USDOE/NETL, 2011). The adapted cost model includes costs for: (1) drilling new wells or reworking existing wells; (2) providing surface equipment for new wells; (3) installing the $CO_2$ recycle plant; (4) constructing a $CO_2$ spur-line from the main $CO_2$ trunk line to the shale gas EGR prospects; and (5) other capital investment costs. The cost model accounts for normal well operation and maintenance (O&M), for lifting costs of the produced gases, and for costs of capturing, separating and reinjecting the produced $CO_2$.

The costs associated with $CO_2$ injection wells can be assumed to be equivalent to the costs associated with gas production wells.

$CO_2$ Recycle Plant Investment Cost. Operation of an EGR project requires a recycling plant to capture and reinject the produced $CO_2$. Although different $CO_2$ injection designs require different specifications for a $CO_2$ plant, they all generally require some or all of the following: gas/liquid separation, water/oil separation, dehydration, $CO_2$/hydrocarbon gas separation (including possibly $H_2S$ removal), and $CO_2$ compression for reinjection. For purposes of this assessment, these are all included in the estimated $CO_2$ recycle plant cost estimate. This estimate does not include the costs associated with natural gas liquids (NGLs) recovery.

The size of the recycle plant is based on peak $CO_2$ recycling requirements and the costs are based on the size of the plant. If the peak rate is less than 30 million cubic feet per day (MMcf/d), then:

Capital cost (in 1,000 $) = 1,200 * Peak Rate (in MMcfd of $CO_2$ throughput)

If peak rate is greater than 30 MMcf/d, then

Capital cost (in 1,000 $) = 36,000 + (Peak Rate – 30) * 750

Again, the peak rate is expressed in MMcfd of $CO_2$ throughput.

Approximately half of the total costs for the recycle plant correspond to the costs of compression. The full cost of the plant can be assumed to be incurred at the start of the project.

$CO_2$ Recycle O&M Costs. The O&M costs of $CO_2$ recycling (in $ per Mcf of $CO_2$ processed) are indexed to energy costs and set at 6 percent of the gas price (e.g. $0.30 per Mcf at a $5.00 per Mcf wellhead natural gas price).

$CO_2$ Distribution System Costs. The $CO_2$ distribution system is similar to the gathering systems used for natural gas; consisting of all manifolds and distribution lines on the site, both from the production wells to the recycle plant, and from the recycle plant to the injection wells. It consists of all manifolds and distribution lines from the $CO_2$ source at the lease line to the $CO_2$ injection/storage wells.

A distribution "hub" is constructed with smaller pipelines delivering $CO_2$ to the project site. The distribution pipeline cost is dependent on the injection requirements for the project. The fixed component is $200,000. The variable cost component ($C_D$) accounts for increasing piping diameters associated with increasing $CO_2$ injection requirements, specifically:

- $360,000 per mile for 4-inch pipe ($CO_2$ rate less than 15 MMcf/d)
- $540,000 per mile for 6-inch pipe ($CO_2$ rate of 15 to 35 MMcf/d)
- $720,000 per mile for 8-inch pipe ($CO_2$ rate of 35 to 60 MMcf/d)
- $900,000 per mile for pipe greater than 8 inches in diameter ($CO_2$ rate greater than 60 MMcf/d).

Aside from the injection volume, costs also depend on the distance from the $CO_2$ "hub" (transfer point) to the shale field. Therefore, the equation for representing the costs of the $CO_2$ distribution system is as follows:

Pipeline Construction Costs = $200,000 + $C_D$*Distance (in miles)

Where: $C_D$ is the cost per mile of the necessary pipe diameter (based on the $CO_2$ injection rate)

For purposes of this study, this distance is assumed to be 10 miles.

Onsite $CO_2$ Booster Compression. Boost compression may be required for both new $CO_2$ sources (unless those sources are already delivered at injection pressure, which is generally the case today) and recycled $CO_2$ being produced from the reservoir. Costs associated with compressing $CO_2$ are included in the recycling plant costs.

However, it may be necessary to assess additional compression costs if the $CO_2$ is not assumed to be delivered at injection pressure. $CO_2$ compression power requirements depend on the differential between the pressure of the $CO_2$ delivered to the site (recall that compression costs are already included in cases where the source of the $CO_2$ is the recycle plant) and the required field injection pressure. This range is directly affected by the pressure of the source (or recycled) $CO_2$ and the characteristics of the reservoir that dictate the injection pressure (porosity, permeability, thickness, etc.) In general, the higher the pressure of the source $CO_2$, the lower the compression energy requirements.

Compressor Capital Costs. To calculate the pumping power requirement ($W_p$, in horsepower (hp)) for boosting the $CO_2$ pressure from the source ($P_{source}$) to the required injection pressure ($P_{inj}$) (in MPa), the following equation can be assumed (McCollum and Ogden, 2006):

$$W_p = 1.341*((1000*10)/(36*24))*((m*(P_{inj}-P_{source}))/(\rho*\eta_p))$$

Where m is the $CO_2$ mass flow rate (in tonnes/day), and assuming the following values:

$\rho$ = 630 kg/$m^3$
$\eta_p$ = 0.75
1.341 = hp/kW
1,000 = kilograms per tonne
24 = hours per day
10 = bar/MPa
36 = $m^3$*bar/hour per kW.

For purposes of this assessment, a capital cost of $2,000 per hp can be assumed, based on the assessment of Jablonowski and Singh (2010).

The annual energy required for compression is estimated by multiplying $W_p$ by the period of time over which the power is used. For example, if the compressors run 60 percent of the time over the course of the year, $W_p$ would be multiplied by 5,256 (0.60 * 365 days/year * 24 hours/day) to get to kWh.

The costs of power for compression can be calculated assuming the U.S. average cost of purchased electricity, all sectors, in November 2012 of $0.0958/kWh[1] multiplied by the power requirements in kWh.

## c. Economic/Cash Flow Analyses for Enhanced Shale Gas Development with $CO_2$ Injection

Economic analyses were performed using an industry standard cash flow model. The key inputs and assumptions of the economic model include natural gas prices; $CO_2$ purchase costs, $CO_2$ credit or carbon tax values (if any), the financial hurdle rate, rates for royalties, state severance/ad valorem taxes, and state and federal income taxes. This is in addition to all the costs associated with shale gas production and $CO_2$ injection for EGR, including all CAPEX and OPEX costs explicit to an EGR project.

Recall that the preferred cases from the simulations assumed three wells (two half production wells on the edge and one full well in the middle, with this well a production well at first but later converted to an injection well). In these simulations, the two outside (half) wells

[1] http://www.eia.gov/electricity/monthly/epm_table_grapher.cfm?t=epmt_5_6_a

were assumed to be completed only in the Union Springs formation. The middle well was completed either in the Union Springs (Marcellus) formation or the top (Devonian) shales. Thus, for purposes of the economic analyses, two wells were assumed in the engineering costing and the cash flow analysis modeling.

An example of summary output from the cash flow model is shown in **Figure 3**.

# Figure 3: Example of Summary Output from the Cash Flow Model

**SIMPLIFIED UNCONVENTIONAL GAS CASH FLOW MODEL -- INDIVIDUAL "PATTERN" INCREMENTAL SECONDARY RECOVERY + CO2 STORAGE**

| | | | | | | | | | | | | | | | | | | | | | | | |
|---|---|---|---|---|---|---|---|---|---|---|---|---|---|---|---|---|---|---|---|---|---|---|---|
| G&A Rate on Investment | 10% | Discount Rate | 10% | | EUR/well (Mcf) | | 2,877,987 | | | | | | | | | | | | | | | | |
| Fed Tax Rate | 34% | Fed ITC Period | 0 | years | NPV | -$1,452,345 | | | | | | | | | | | | | | | | | |
| Discount Factor | | State ITC Period | 0 | years | IRR | 9% | | | | | | | | | | | | | | | | | |
| R/P Ratio | 10 | State ITC Rate | 15.0% | | | | | | | | | | | | | | | | | | | | |
| Royalty Rate | 12.5% | Fed ITC Rate | 15.0% | | Max. CO2 Injection Rate (Mcf/d) | | 567 | | | | | | | | | | | | | | | | |
| Sev. Tax Rate | 5.0% | Sev Tax Relief Period | 0 | years | Avg. CO2 Injection Rate (Mcf/d) | | 420 | | | | | | | | | | | | | | | | |
| State Inc. Tax Rate | 5.00% | G&A Rate on O&M | 20% | | | | | | | | | | | | | | | | | | | | |
| % Tangible CapEx | 40% | | | | | | | | | | | | | | | | | | | | | | |
| Item | Year | 0 | 1 | 2 | 3 | 4 | 5 | 6 | 7 | 8 | 9 | 10 | 11 | 12 | 13 | 14 | 15 | 16 | 17 | 18 | 19 | 20 | 21 |
| Estimated Res. /Well (Mcf) | | | 2,877,987 | 1,858,538 | 1,630,439 | 1,467,867 | 1,338,093 | 1,226,729 | 1,126,760 | 1,034,242 | 946,911 | 863,378 | 782,694 | 704,312 | 627,828 | 552,989 | 479,646 | 407,619 | 336,834 | 267,253 | 198,879 | 131,636 | 65,453 |
| Gas Production (Mcf) | | | 1,019,449 | 228,099 | 162,573 | 129,773 | 111,365 | 99,969 | 92,518 | 87,331 | 83,533 | 80,684 | 78,383 | 76,483 | 74,840 | 73,342 | 72,027 | 70,785 | 69,580 | 68,375 | 67,243 | 66,183 | 65,453 |
| Production (Mcf/month) | | | 33,982 | 7,603 | 5,419 | 4,326 | 3,712 | 3,332 | 3,084 | 2,911 | 2,784 | 2,689 | 2,613 | 2,549 | 2,495 | 2,445 | 2,401 | 2,360 | 2,319 | 2,279 | 2,241 | 2,206 | 2,182 |
| Production (Mcf/day) | | | 2,791 | 625 | 445 | 355 | 305 | 274 | 253 | 239 | 229 | 221 | 215 | 209 | 205 | 201 | 197 | 194 | 191 | 187 | 184 | 181 | 179 |
| $CO_2$ Injection (Mcf/d) | | | 7 | 567 | 504 | 478 | 462 | 450 | 441 | 433 | 427 | 422 | 419 | 417 | 417 | 417 | 418 | 420 | 422 | 426 | 429 | 433 | 436 |
| $CO_2$ Injection (Mcf/year) | | | 2,519 | 206,809 | 183,997 | 174,397 | 168,703 | 164,396 | 160,856 | 157,972 | 155,673 | 153,994 | 152,862 | 152,242 | 152,023 | 152,169 | 152,607 | 153,264 | 154,176 | 155,308 | 156,585 | 157,972 | 158,958 |
| $CO_2$ Injection (tonnes/year) | | | 133 | 10,942 | 9,735 | 9,227 | 8,926 | 8,698 | 8,511 | 8,358 | 8,237 | 8,148 | 8,088 | 8,055 | 8,044 | 8,051 | 8,074 | 8,109 | 8,157 | 8,217 | 8,285 | 8,358 | 8,410 |
| $CO_2$ Production/Recycle (Mcf/d) | | | 0 | 0 | 0 | 0 | 0 | 0 | 0 | 0 | 0 | 0 | 0 | 0 | 0 | 0 | 0 | 0 | 0 | 0 | 0 | 0 | 0 |
| $CO_2$ Production/Recycle (Mcf/year) | | | 0 | 0 | 0 | 0 | 0 | 0 | 0 | 0 | 0 | 0 | 0 | 0 | 0 | 0 | 0 | 0 | 0 | 0 | 0 | 0 | 0 |
| $CO_2$ Production/Recycle (tons/year) | | | 0 | 0 | 0 | 0 | 0 | 0 | 0 | 0 | 0 | 0 | 0 | 0 | 0 | 0 | 0 | 0 | 0 | 0 | 0 | 0 | 0 |
| $CO_2$ Purchase (Mcf/year) | | | 2,519 | 206,809 | 183,997 | 174,397 | 168,703 | 164,396 | 160,856 | 157,972 | 155,673 | 153,994 | 152,862 | 152,242 | 152,023 | 152,169 | 152,607 | 153,264 | 154,176 | 155,308 | 156,585 | 157,972 | 158,958 |
| $CO_2$ Purchase (tons/year) | | | 133 | 10,942 | 9,735 | 9,227 | 8,926 | 8,698 | 8,511 | 8,358 | 8,237 | 8,148 | 8,088 | 8,055 | 8,044 | 8,051 | 8,074 | 8,109 | 8,157 | 8,217 | 8,285 | 8,358 | 8,410 |
| Gas Price ($/Mcf) | | $5.00 | $5.00 | $5.00 | $5.00 | $5.00 | $5.00 | $5.00 | $5.00 | $5.00 | $5.00 | $5.00 | $5.00 | $5.00 | $5.00 | $5.00 | $5.00 | $5.00 | $5.00 | $5.00 | $5.00 | $5.00 | $5.00 |
| *Purchased $CO_2$ Price ($/Mcf)* | | ***$0.00*** | ***$0.00*** | ***$0.00*** | ***$0.00*** | ***$0.00*** | ***$0.00*** | ***$0.00*** | ***$0.00*** | ***$0.00*** | ***$0.00*** | ***$0.00*** | ***$0.00*** | ***$0.00*** | ***$0.00*** | ***$0.00*** | ***$0.00*** | ***$0.00*** | ***$0.00*** | ***$0.00*** | ***$0.00*** | ***$0.00*** | ***$0.00*** |
| *Purchased $CO_2$ Price ($/tonne)* | | ***$0.00*** | ***$0.00*** | ***$0.00*** | ***$0.00*** | ***$0.00*** | ***$0.00*** | ***$0.00*** | ***$0.00*** | ***$0.00*** | ***$0.00*** | ***$0.00*** | ***$0.00*** | ***$0.00*** | ***$0.00*** | ***$0.00*** | ***$0.00*** | ***$0.00*** | ***$0.00*** | ***$0.00*** | ***$0.00*** | ***$0.00*** | ***$0.00*** |
| *$CO_2$ Credit ($/ton)* | | ***$5.00*** | ***$5.00*** | ***$5.00*** | ***$5.00*** | ***$5.00*** | ***$5.00*** | ***$5.00*** | ***$5.00*** | ***$5.00*** | ***$5.00*** | ***$5.00*** | ***$5.00*** | ***$5.00*** | ***$5.00*** | ***$5.00*** | ***$5.00*** | ***$5.00*** | ***$5.00*** | ***$5.00*** | ***$5.00*** | ***$5.00*** | ***$5.00*** |
| *$CO_2$ Credit ($/Mcf)* | | ***$0.26*** | ***$0.26*** | ***$0.26*** | ***$0.26*** | ***$0.26*** | ***$0.26*** | ***$0.26*** | ***$0.26*** | ***$0.26*** | ***$0.26*** | ***$0.26*** | ***$0.26*** | ***$0.26*** | ***$0.26*** | ***$0.26*** | ***$0.26*** | ***$0.26*** | ***$0.26*** | ***$0.26*** | ***$0.26*** | ***$0.26*** | ***$0.26*** |
| Revenue from Gas Production ($) | | | $5,097,246 | $1,140,493 | $812,864 | $648,867 | $556,824 | $499,845 | $462,589 | $436,656 | $417,663 | $403,419 | $391,913 | $382,417 | $374,199 | $366,711 | $360,137 | $353,927 | $347,901 | $341,874 | $336,213 | $330,917 | $327,264 |
| Revenue from $CO_2$ Credit ($) | | | $12,593 | $1,034,045 | $919,983 | $871,985 | $843,515 | $821,980 | $804,278 | $789,860 | $778,363 | $769,968 | $764,310 | $761,208 | $760,113 | $760,843 | $763,033 | $766,318 | $770,880 | $776,538 | $782,925 | $789,860 | $794,788 |
| Royalty ($) | | | ($637,156) | ($142,562) | ($101,608) | ($81,108) | ($69,603) | ($62,481) | ($57,824) | ($54,582) | ($52,208) | ($50,427) | ($48,989) | ($47,802) | ($46,775) | ($45,839) | ($45,017) | ($44,241) | ($43,488) | ($42,734) | ($42,027) | ($41,365) | ($40,908) |
| Severance Tax | | | ($223,005) | ($49,897) | ($35,563) | ($28,388) | ($24,361) | ($21,868) | ($20,238) | ($19,104) | ($18,273) | ($17,650) | ($17,146) | ($16,731) | ($16,371) | ($16,044) | ($15,756) | ($15,484) | ($15,221) | ($14,957) | ($14,709) | ($14,478) | ($14,318) |
| Royalty Relief ($) | | | | | | | | | | | | | | | | | | | | | | | |
| Net Revenues ($) | | | $4,249,679 | $1,982,080 | $1,595,676 | $1,411,355 | $1,306,375 | $1,237,476 | $1,188,805 | $1,152,831 | $1,125,545 | $1,105,309 | $1,090,088 | $1,079,091 | $1,071,165 | $1,065,671 | $1,062,396 | $1,060,520 | ######### | $1,060,720 | $1,062,402 | $1,064,934 | ######## |
| Capital Investment ($) -- Gas Production | | $5,789,814 | | | | | | | | | | | | | | | | | | | | | |
| Tangible Capital | | $2,315,925 | | | | | | | | | | | | | | | | | | | | | |
| Intangible Capital | | $3,473,888 | | | | | | | | | | | | | | | | | | | | | |
| Capital Investment ($) -- $CO_2$ Injection | | $5,201,838 | $0 | $0 | $0 | $0 | $0 | $0 | $0 | $0 | $0 | $0 | $0 | $0 | $0 | $0 | $0 | $0 | $0 | $0 | $0 | $0 | $0 |
| Tangible Capital | | $2,080,735 | $0 | $0 | $0 | $0 | $0 | $0 | $0 | $0 | $0 | $0 | $0 | $0 | $0 | $0 | $0 | $0 | $0 | $0 | $0 | $0 | $0 |
| Intangible Capital | | $3,121,103 | $0 | $0 | $0 | $0 | $0 | $0 | $0 | $0 | $0 | $0 | $0 | $0 | $0 | $0 | $0 | $0 | $0 | $0 | $0 | $0 | $0 |
| Gas Production O&M Costs ($) | | | $47,282 | $47,282 | $47,282 | $47,282 | $47,282 | $47,282 | $47,282 | $47,282 | $47,282 | $47,282 | $47,282 | $47,282 | $47,282 | $47,282 | $47,282 | $47,282 | $47,282 | $47,282 | $47,282 | $47,282 | $47,282 |
| $CO_2$ Injection O&M Costs ($) | | | $82 | $6,769 | $6,022 | $5,708 | $5,522 | $5,381 | $5,265 | $5,171 | $5,095 | $5,040 | $5,003 | $4,983 | $4,976 | $4,981 | $4,995 | $5,016 | $5,046 | $5,083 | $5,125 | $5,171 | $5,203 |
| Purchased $CO_2$ Costs ($) | | | $0 | $0 | $0 | $0 | $0 | $0 | $0 | $0 | $0 | $0 | $0 | $0 | $0 | $0 | $0 | $0 | $0 | $0 | $0 | $0 | $0 |
| G&A on O&M | | $0 | $9,456 | $9,456 | $9,456 | $9,456 | $9,456 | $9,456 | $9,456 | $9,456 | $9,456 | $9,456 | $9,456 | $9,456 | $9,456 | $9,456 | $9,456 | $9,456 | $9,456 | $9,456 | $9,456 | $9,456 | $9,456 |
| Operating Profits ($) | | ($21,983,303) | $4,192,858 | $1,918,573 | $1,532,915 | $1,348,909 | $1,244,115 | $1,175,357 | $1,126,802 | $1,090,922 | $1,063,712 | $1,043,531 | $1,028,346 | $1,017,370 | $1,009,451 | $1,003,952 | $1,000,663 | $998,765 | $998,288 | $998,899 | $1,000,538 | $1,003,026 | ######## |
| Intangible Expenses | | $6,594,991 | $0 | $0 | $0 | $0 | $0 | $0 | $0 | $0 | $0 | $0 | $0 | $0 | $0 | $0 | $0 | $0 | $0 | $0 | $0 | $0 | $0 |
| Depreciation (Producer) | | $0 | $330,846 | $330,846 | $330,846 | $330,846 | $330,846 | $330,846 | $330,846 | $0 | $0 | $0 | $0 | $0 | $0 | $0 | $0 | $0 | $0 | $0 | $0 | $0 | $0 |
| Depreciation (Injector) | | $0 | $297,248 | $297,248 | $297,248 | $297,248 | $297,248 | $297,248 | $297,248 | $0 | $0 | $0 | $0 | $0 | $0 | $0 | $0 | $0 | $0 | $0 | $0 | $0 | $0 |
| Taxable Income | | ($28,578,294) | $3,564,764 | $1,290,478 | $904,821 | $720,815 | $616,020 | $547,262 | $498,707 | $1,090,922 | $1,063,712 | $1,043,531 | $1,028,346 | $1,017,370 | $1,009,451 | $1,003,952 | $1,000,663 | $998,765 | $998,288 | $998,899 | $1,000,538 | $1,003,026 | ######## |
| Federal Taxes | | ($9,716,620) | $1,212,020 | $438,763 | $307,639 | $245,077 | $209,447 | $186,069 | $169,560 | $370,913 | $361,662 | $354,800 | $349,638 | $345,906 | $343,213 | $341,344 | $340,225 | $339,580 | $339,418 | $339,626 | $340,183 | $341,029 | $341,661 |
| Federal Investment Tax Credit | | $0 | $0 | $0 | $0 | $0 | $0 | $0 | $0 | $0 | $0 | $0 | $0 | $0 | $0 | $0 | $0 | $0 | $0 | $0 | $0 | $0 | $0 |
| State Investment Tax Credit | | $868,472 | $0 | $0 | $0 | $0 | $0 | $0 | $0 | $0 | $0 | $0 | $0 | $0 | $0 | $0 | $0 | $0 | $0 | $0 | $0 | $0 | $0 |
| State Taxes | | ($986,507) | $117,637 | $42,586 | $29,859 | $23,787 | $20,329 | $18,060 | $16,457 | $36,000 | $35,102 | $34,437 | $33,935 | $33,573 | $33,312 | $33,130 | $33,022 | $32,959 | $32,943 | $32,964 | $33,018 | $33,100 | $33,161 |
| After Tax Profit ($) | | ($17,006,695) | $2,235,107 | $809,130 | $567,323 | $451,951 | $386,245 | $343,134 | $312,689 | $684,008 | $666,947 | $654,294 | $644,773 | $637,891 | $632,926 | $629,478 | $627,416 | $626,226 | $625,926 | $626,309 | $627,338 | $628,897 | $630,063 |
| Add Back Intangibles | | $6,594,991 | $0 | $0 | $0 | $0 | $0 | $0 | $0 | $0 | $0 | $0 | $0 | $0 | $0 | $0 | $0 | $0 | $0 | $0 | $0 | $0 | $0 |
| Add Back Depreciation | | $0 | $628,094 | $628,094 | $628,094 | $628,094 | $628,094 | $628,094 | $628,094 | $0 | $0 | $0 | $0 | $0 | $0 | $0 | $0 | $0 | $0 | $0 | $0 | $0 | $0 |
| After Tax Cash Flow ($) | | ($10,411,704) | $2,863,201 | $1,437,224 | $1,195,417 | $1,080,045 | $1,014,339 | $971,228 | $940,784 | $684,008 | $666,947 | $654,294 | $644,773 | $637,891 | $632,926 | $629,478 | $627,416 | $626,226 | $625,926 | $626,309 | $627,338 | $628,897 | $630,063 |
| Discounted Cash Flow | | ($10,411,704) | $2,576,881 | $1,164,152 | $871,459 | $708,618 | $598,957 | $516,150 | $449,974 | $294,443 | $258,389 | $228,138 | $202,337 | $180,159 | $160,881 | $144,004 | $129,179 | $116,041 | $104,387 | $94,006 | $84,744 | $76,459 | $68,941 |
| Cum. Disc. Cash Flow | | ($10,411,704) | ($7,834,823) | ($6,670,671) | ($5,799,212) | ($5,090,594) | ($4,491,637) | ($3,975,487) | ($3,525,513) | ($3,231,070) | ($2,972,681) | ($2,744,543) | ($2,542,206) | ($2,362,047) | ($2,201,166) | ($2,057,161) | ($1,927,982) | ########## | ########## | ########## | ########## | ########## | ######## |

# 3. MARCELLUS SHALE

## a. Reservoir Simulation Analyses

The intent of reservoir simulation is to estimate $CO_2$ injection rates into a gas shale reservoir, the rate at which adsorbed methane is displaced from the shale by $CO_2$, the total volume of methane produced (by both traditional primary production and as enhanced by the injection of $CO_2$), the total volume of $CO_2$ stored, and the disposition of the $CO_2$ in the reservoir over time. These estimates are made under alternative development strategies.

## b. Approach for History Matching

Data was provided by a Marcellus Shale operator in Northwest Pennsylvania, which corresponded to the Marcellus shale "Area 5" in Volume 2. The subject horizontal well was drilled to a depth of nearly 5,800 feet (1,770 meters), with an approximately 2,300 feet (700 meters) lateral in the primary target, the Union Springs shale formation. The well was fractured with a 20-stage treatment; the main fracturing fluid used for all the stages was slick water fluid with 40/70 mesh proppant. When the history-match exercise was started, the well had been on production for almost a year.

The reservoir simulator used for the study was Advanced Resources' proprietary *COMET3* simulator. A triple porosity model was constructed in order to adequately represent the release and transport mechanism for gas-bearing shales. Details on the model theory are provided in Sawyer, et al. (1990).

A gas-bearing shale reservoir consists of a "triple porosity" gas storage system: (1) the micro-pore matrix system within the shale, (2) molecular adsorption within micro-pore matrix system, and (3) the natural fractures or cleats within the shale. In COMET3, two distinct systems are represented: the micro-pore matrix system and the fracture/cleat system. To take into account the micro-porosity system, each matrix block is sub-divided into smaller grid blocks. The release and transport mechanisms for this type of reservoir system are characterized by a combination of desorption, diffusion (within the matrix), and Darcy flow through a dual permeability system. The triple porosity/dual permeability system assumes that there are two parallel hydro-dynamic systems (fracture and matrix) in the reservoir and desorption and diffusion of gas occurs within the matrix.

A cross-section of the zones encountered during the well drilling was provided by the operator and thus allowed to precisely model the various shale layers encountered, as well as represent the appropriate well length in each zone.

Four different shale zones from the Middle Devonian were modeled (top to bottom):

- Aggregation of several minor shale layers (Stafford, Levanna and Skateaneles)
- Oatka Creek
- Cherry Valley
- Union Springs (main pay zone).

Elevation and thicknesses for each layer are summarized in **Table 2**. Included in the last column is the modeled length of the well in each shale zone encountered (with the reported length in parentheses). No dip was assumed, as the surface in the area of interest for the simulation is relatively flat. However, the existence of a syncline is known and was implemented in the model by a localized elevation change.

Table 2: Elevation, Thickness and Well Length

| Shale | Elevation (feet below ground level) | Thickness (ft) | Well Length (feet) |
|---|---|---|---|
| Top Shales | 5,667 | 85 | 400 (411) |
| Oatka Creek | 5,752 | 22 | 1,300 (1,330) |
| Cherry Valley | 5,774 | 3 | 500 (458) |
| Union Springs | 5,777 | 15 | 2,300 (2,343) |

Three methane isotherms were available from a vertical well in the vicinity of the studied horizontal well, each taken from different depths within the productive section in the Marcellus. An average methane isotherm based on the three was used in the simulator (**Figure 4**). Also shown is the one $CO_2$ isotherm acquired as part of this effort in the Marcellus.

An initial pressure gradient of 0.58 pounds per square inch (psia) (7.6 kilopascals (kPA) per meter of depth) per foot depth was assumed in the simulator based on communication with the operator.

Matrix permeability encountered along the well was assumed to vary between 100 nanodarcies (nD) and 1,000 nD (data reported by the operator), and averages 520 nD. Permeability was assumed to be isotropic in all directions (horizontal and vertical), since no data were available to support an alternative assumption. Gas-filled porosity in the area of interest averages 7 percent and varies between 5 percent and 10 percent along the well. Both sets of relative permeability curves (matrix and fracture) were assumed to be straight lines for lack of better information.

Figure 4: Marcellus Methane and $CO_2$ Adsorption Isotherms

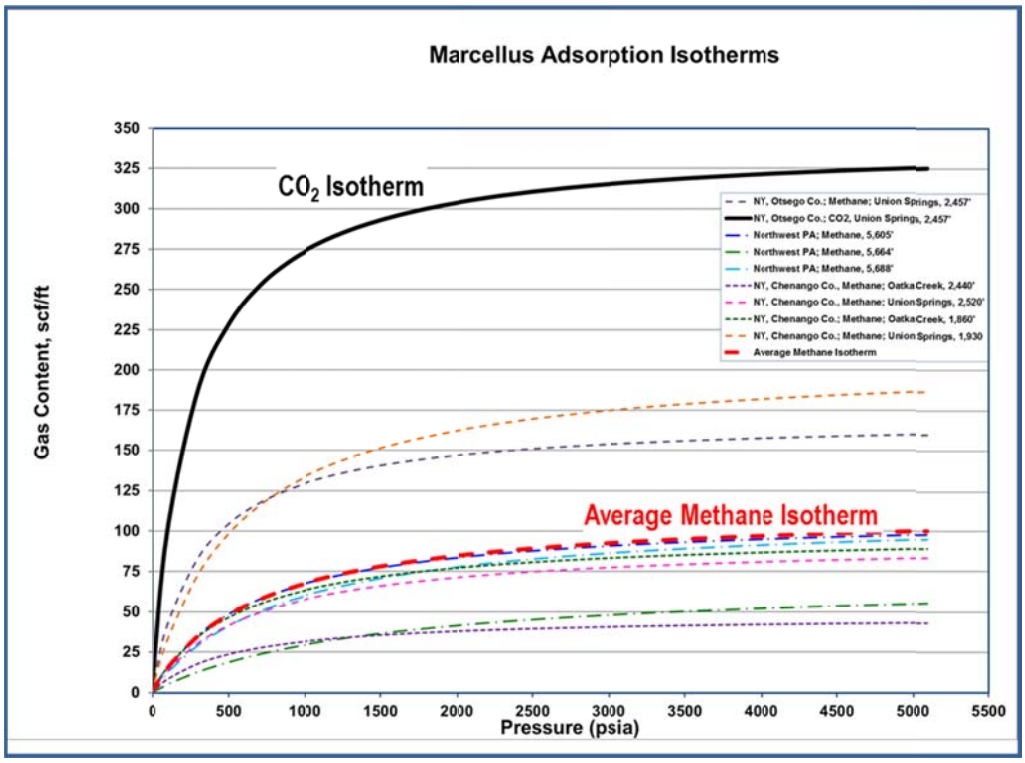


The initial model assumed coverage of an area of 1,170 acres (4.7 $km^2$) with the boundaries based upon the existence of another producing branch from the horizontal well. Each grid block was 100 by 100 feet (30 by 30 meters), for a total of 20,400 grid blocks, all active.

The well was fractured with a 20-stage treatment (slick water fluid with proppant). The micro-seismic data obtained during the treatment were analyzed. A detailed micro-seismic report was available and used as a guide to define a fractured area around the horizontal well in the model.

To represent the fractured zone in the model, a smaller 'matrix block size' area was implemented. By decreasing the size of the sub-blocks, the intensity of the fractures inside the matrix is increased. To account for the water injected during the stimulation work, increased water saturation in the fractured area was assumed. (A scenario of water injection was tried first, but with very low permeability values, run time was excessive.) From communication with the operator, initial water saturation was set at 35 percent and increased to 70 percent in the fractured area (water volumes were checked to make sure the increased water saturation contributed correctly to the additional volume of water from fracturing).

## c. Results of History Matching

The results were compared to actual production data for the well with the objective of obtaining an acceptable match to historical production. During the history-matching process, the simulations were run with the well producing on wellhead pressure while matching the well's producing gas and water rates. **Table 3** shows the list of the main parameters that were kept constant during the history-matching exercise and their corresponding values. **Figures 5** and **6** illustrate the history-match results for gas and water production rates, respectively. The simulated gas rates (orange curve) are compared to the actual production gas data (red dots). Simulated water production rates (yellow curve) are also compared to actual water production rates (blue dots).

Table 3: History-Match Input Parameters

| | | |
|---|---|---|
| **Shale Depth** | 5,670 | ft |
| **Shale Thickness** | 125 | ft |
| **Pay Zone Thickness** | 15 | ft |
| **Matrix Permeability** | 100 | nD |
| **Matrix Porosity** | 7 | % |
| **Water Saturation** | 35 | % |
| **Initial Pressure Gradient** | 0.58 | psia/ft |
| **$CH_4$ Langmuir Volume** | 90 | scf/ton |
| **$CH_4$ Langmuir Pressure** | 1,000 | psia |
| **$CO_2$ Langmuir Volume** | 172 | scf/ton |
| **$CO_2$ Langmuir Pressure** | 416 | psia |

Figure 5: Gas Rate History Match

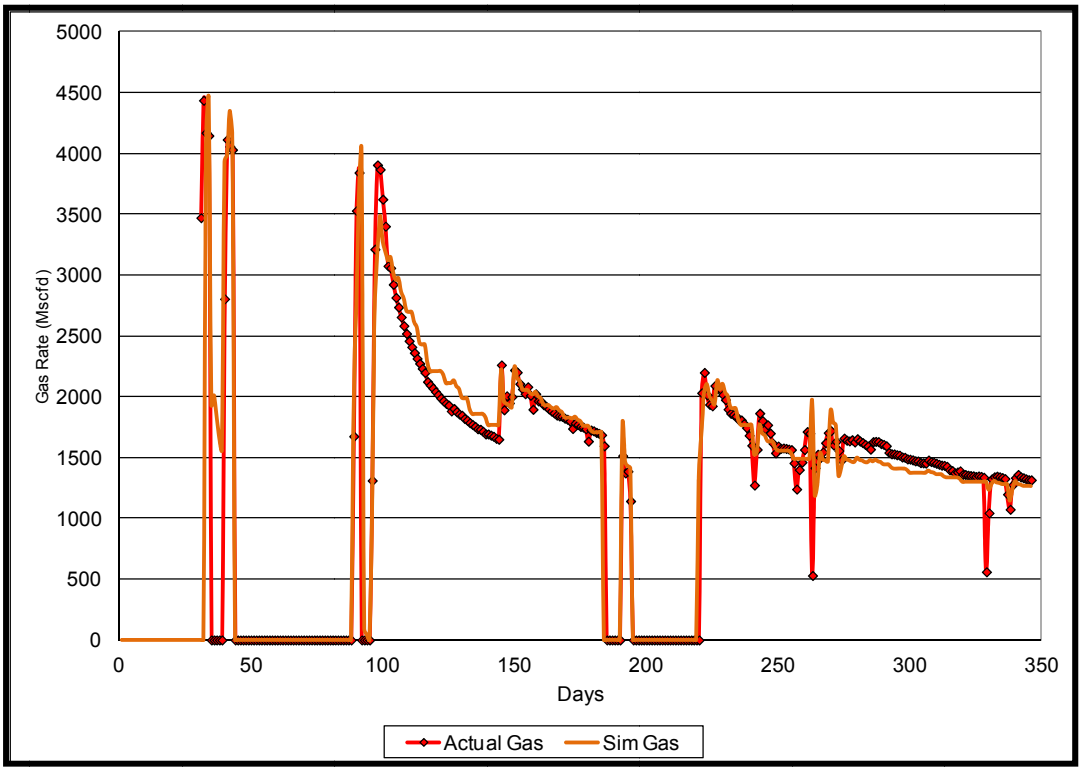


Figure 6: Water Rate History-Match

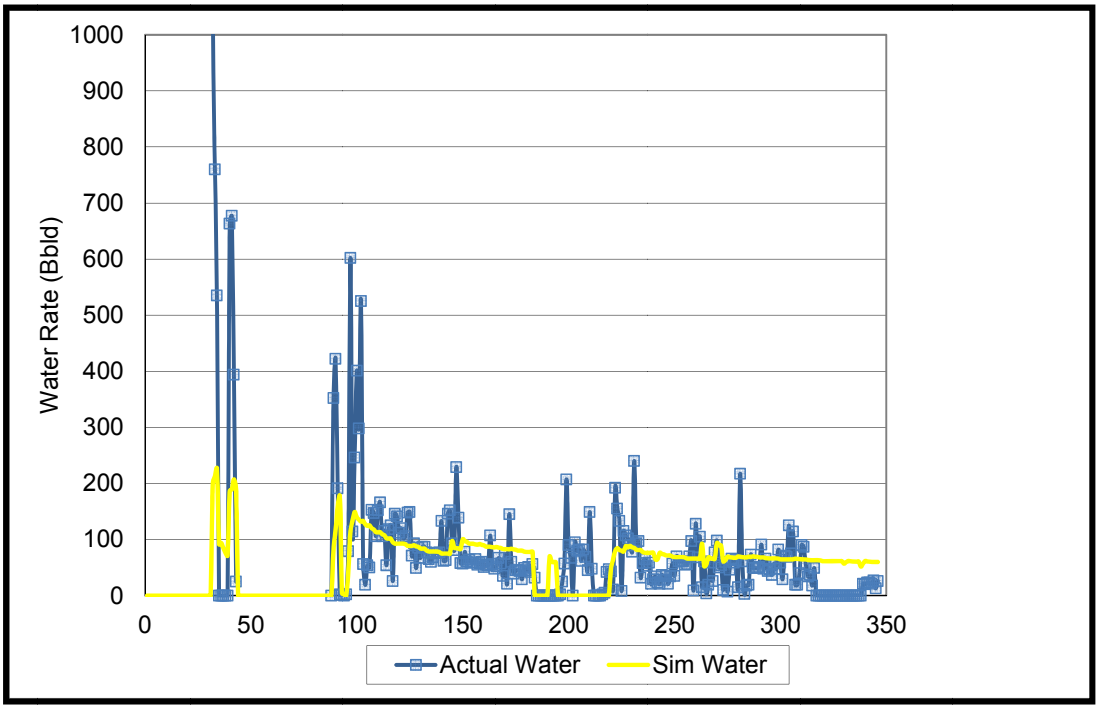

## d. $CO_2$ Injection Scenarios -- Simulation Results and Interpretation

A number of different simulation scenarios were evaluated and considered based on the information provided by an operator for a proprietary Marcellus well.

However, a limitation due to the sheer number of unknowns and generation of solution equations of the triple-porosity model in *COMET3* is the inability to model and track the multiple components associated with $CO_2$ injection/enhanced gas recovery scenarios. As such, the triple-porosity model was reduced to a dual-porosity history-match. Since water production from the shale is primarily coming from the micro-porosity network, the matrix porosity value of 7 percent was assumed in the dual-porosity model. Similarly, as gas flow is primarily governed by Darcy's flow through the cleat system, the fracture permeability value of 0.0025 millidarcies (mD) was assumed in the dual-porosity model.

To account for the volume of water injected during the fracturing job, an average water saturation of 55 percent was assumed. (In the triple-porosity model, values of 70 percent in the fractured zone and 35 percent in the rest of the model were assumed.) Given these assumptions, except for early peaks, history matches were satisfactory. Cumulative gas production for both cases were compared and found to agree within 5 percent, confirming the adequacy of the dual-porosity model characterization.

Most reservoir characteristics from the triple-porosity model were kept identical for the $CO_2$ injection/enhanced gas recovery scenarios except for two main differences:

- Instead of producing from the four shale zones, the well was assumed to be only completed in the main pay zone (Union Springs, bottom layer), since that was the primary target of the operator's well completion (see **Table 2**).
- The well was stimulated with the addition of a negative skin factor (instead of decreasing the matrix block size, an option not available in the dual porosity model). This compliments the assumptions regarding the hydraulic fractures by representing the stimulation near the wellbore, but may artificially keep the plume closer to the wellbore than may actually be occurring based on the dispersion of the fractures.

Injection/Production Optimization. A line-drive injection pattern was designed (**Figure 7**) to maximize the sweep efficiency between horizontal producers and horizontal injectors in such a low permeability environment. The grid block representation of this line drive pattern is shown in **Figure 8**. Taking advantage of the symmetry, and to be able to apply the results to any well length, the model was simplified with a 15-meter cross-section of the horizontal well. The results can then be scaled up to represent the full well recoveries.

Figure 7: Line Drive Pattern Representation

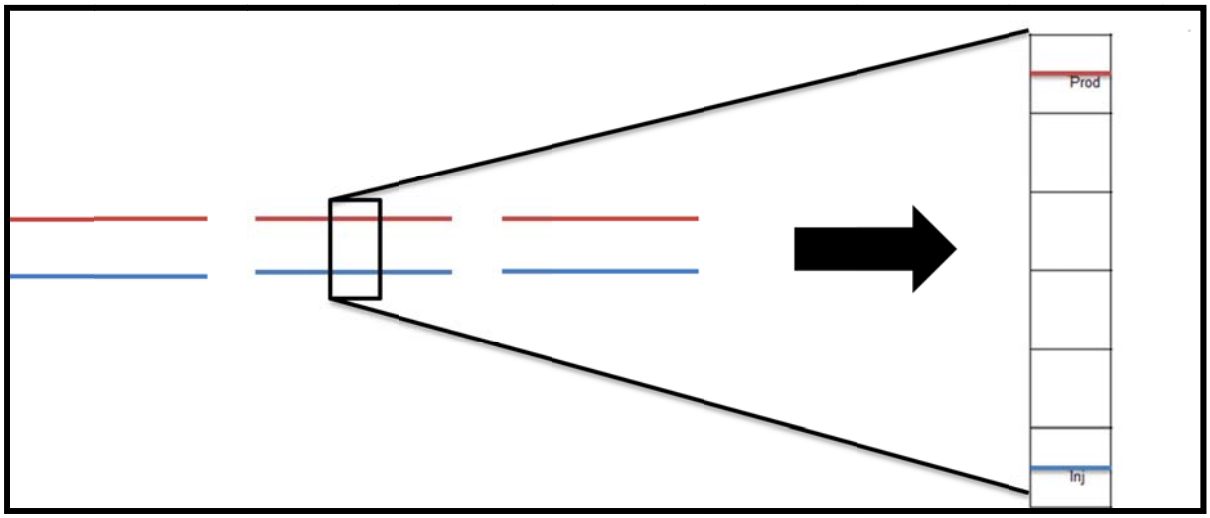


Figure 8: Grid Block Representation of Line Drive Pattern

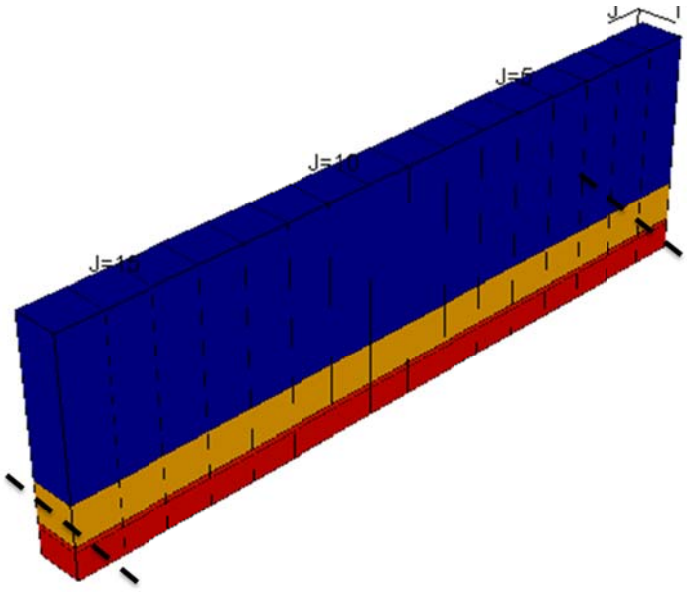

Both the production well and the well that will eventually be used for $CO_2$ injection are assumed to be produced at 150 psia (1.0 kPa) wellhead pressure for 10 years before $CO_2$ injection starts. At that time, it was assumed that one of the two wells would be recompleted as an injection well, and injection will begin, with 100 percent $CO_2$ injected for the following 10 years at an injection pressure based on the assumed pressure gradient.

Various distances between the injector and the producer were tested to determine the distance between the injector and the producer for optimum $CO_2$ storage and/or enhanced gas production. Results are presented in **Table** 4. These results are limited to the assumption that primary production from both wells occurs for 10 years, and then one well is converted to an injector, and $CO_2$ injection and enhanced gas recovery occur for 10 years. Different schemes would result in different results.

Table 4: Enhanced Gas Recovery and $CO_2$ Storage as a Function of Distance between the Injection and Production Wells for a 50 Foot Cross-Section of Horizontal Well – Marcellus Area 5

| Distance between wells | No Injection (MMscf) | Injection (MMscf) | | | |
|---|---|---|---|---|---|
| | Cum CH4 Produced | Cum CH4 Produced | Cum CO2 Injected | Cum CO2 Produced | Stored CO2 |
| 50 ft | 6.4 (85.1%) | 7.2 (95.3%) | 38.6 | 25.5 | 13.1 |
| 100ft | 9.4 (83.0%) | 10.6 (93.3%) | 28.0 | 9.9 | 18.1 |
| 150ft | 12.2 (80.4%) | 13.6 (89.5%) | 25.4 | 3.9 | 21.5 |
| 200ft | 14.7 (77.5%) | 16.1 (85.0%) | 24.3 | 1.2 | 23.1 |
| 250ft | 16.9 (74.5%) | 18.3 (80.3%) | 23.6 | 0.2 | 23.4 |
| 300ft | 19.0 (71.5%) | 20.0 (75.2%) | 22.6 | 0.0 | 22.6 |
| 400ft | 22.4 (65.6%) | 22.9 (67.1%) | 21.2 | 0.0 | 21.2 |
| 500ft | 25.0 (60.1%) | 25.3 (60.7%) | 19.7 | 0.0 | 19.7 |
| 750ft | 29.3 (48.3%) | 29.3 (48.4%) | 16.6 | 0.0 | 16.6 |

Given this time frame for production and subsequent injection, the results indicate that an average distance of 200 to 250 feet between the injection and production wells appears to be the most favorable - providing 7 percent incremental gas production due to $CO_2$ injection, a net $CO_2$ storage volume of 23 to 24 MMcf for the 50 foot cross-section that was the focus of the simulation. This case also resulted in low volumes of recycled $CO_2$.

A very short distance between injector and producer (the 50 foot case, for example) provides both high injection volumes due to highly depleted conditions from the primary production and the greatest amounts of incremental gas production, up to 10 percent. However, very little $CO_2$ storage occurs as most of the $CO_2$ is being reproduced.

When the distance between wells is large (the 750 foot case, for example) $CO_2$ injection volumes are lower because there is relatively little depleted pore volume available to accept the injected $CO_2$. There is no $CO_2$ reproduced as most of the $CO_2$ does not even reach the production well. Consequently no incremental gas production is noticeable, although moderate volumes of the injected $CO_2$ are stored.

When the distance between wells is large (the 750 foot case, for example), $CO_2$ injection volumes are lower because there is relatively little depleted pore volume available to accept the injected $CO_2$. There is no $CO_2$ reproduced as most of the $CO_2$ does not even reach the production well. Consequently, no incremental gas production is noticeable, although moderate volumes of the injected $CO_2$ are stored.

Potential for Current Development Practices. Most wells in the Marcellus shale are currently horizontal wells completed on 80-acre spacing, which means the spacing between wells is at the higher end of the distances considered (580 feet) in the above optimization example. Therefore, the most reasonable basis for assessing potential incremental gas production and $CO_2$ storage potential in the Marcellus should be assuming traditional pattern spacing in the play. This approach assumes that any shale gas wells considered for use for $CO_2$ storage will be wells first considered and developed using traditional development practices.

The first scenario considered in the reservoir simulations assumed two (half) horizontal wells completed in the lowermost Union Springs formation (the target zone for the well that was used in the history match) on the edge of the model, again with the configuration shown in **Figure 4**. Like that for the history match case, each well was fractured with a 20-stage treatment (slick water fluid with proppant). For this case, the fracture permeability was assumed to be 250 times greater than the matrix permeability as a result of the fracture stimulation. Both wells were assumed to produce at 25 psia for 10 years, before one was switched to an injector. This injector was assumed to inject at a pressure corresponding to 0.58 psia per foot (7.6 kPA per meter) of depth for an additional 10 years.

Results directly from the simulator concluded that cumulative gas production with $CO_2$ injection was 2.95 Bcf, compared with production without injection of 2.93 Bcf (34 percent recovery efficiency of estimated gas in place). Thus, very little incremental gas production resulted from $CO_2$ injection in this scenario, but a large volume of $CO_2$ was injected (3.4 Bcf), of which, nearly all was stored.

Another scenario was considered where in the two-well case, vertical permeability in the fractured area was assumed to be improved by a factor of 4, under the assumption that hydraulic fracturing technology in the future would perform considerably better than today. In

this case, cumulative incremental gas production without injection was 4.1 Bcf, and with injection was 4.24 Bcf. About 4.1 Bcf of $CO_2$ was injected, of which nearly all was stored.

In all of these cases, while effective $CO_2$ storage was realized, incremental gas production due to $CO_2$ injection was modest. Injected $CO_2$ appears to just fill up the pore space already depleted, but little of the $CO_2$ penetrates the unproduced areas of the matrix to encourage additional methane desorption and $CO_2$ re-adsorption. Therefore, these cases indicate that one can optimize for incremental gas production, or optimize for $CO_2$ storage, but not both.

Another reason that EGR due to $CO_2$ injection was so modest was the relative productivity of the Union Springs formation was much better compared to the other three formations. The top Devonian-age Shales, the Oatka Creek, and the Cherry Valley formations had lower permeability and porosity than the Union Springs. As a result, with two wells completed in the Union Springs formation, nearly all of the methane produced (both primary and incremental due to $CO_2$ injection) is from the Union Springs and all of the $CO_2$ injected stays within this formation. Very little makes it into the other three formations, so little incremental gas is produced from or $CO_2$ stored in the other three formations.

Since incremental gas production was so modest, a second set of scenarios was considered which assumed three wells (two halves on the edge and one full well in the middle). In these simulations, the two outside (half) wells were assumed to be completed only in the Union Springs formation. The middle well was completed either in the Union Springs (Marcellus) formation or the top (Devonian) shales.

Several cases were considered and compared:

- Case 1 assumes the middle well is completed in the Devonian formation, with vertical permeability enhanced.
- Case 2 assumes the middle well is completed in the Devonian formation, with vertical permeability not enhanced.
- Case 3 assumes the middle well is completed in the Union Springs (Marcellus) formation, with vertical permeability not enhanced.

In all of these cases, four timing scenarios were considered; with scenarios for $CO_2$ injection starting at 1, 5, 10, and 15 years of primary production in the two, outside (half) wells. In addition, the middle well produces until it is converted to injection. In all cases, production lasts 20 years after $CO_2$ injection starts. In addition, the middle well produces until it is converted to injection.

The wells (producers and injector) were considered to be either standard completions or completions where the vertical permeability in the fractured area was assumed to be improved by the factor of 4. Specifically, instead of the normal ratio of 250 between the matrix permeability and the fracture permeability, the ratio is assumed to be 1,000 for the horizontal permeability ($K_x$ and Ky) for the Devonian shale completion only. In addition, the vertical permeability is enhanced for all the layers -- by a factor of 2,500 between the matrix permeability and the fracture permeability, instead of 250.

These results are shown in **Table 5**. As would be expected, cumulative methane production (7 to 8 Bcf per well) is greatest with the enhanced permeability injection well completed in the Devonian shales (Case 1); this case also stores the most $CO_2$ (from 19 to 22 Bcf), with minimal $CO_2$ reproduced. Moreover, of the three cases considered, it's the only one where $CO_2$ injection results in greater recovery that would occur for the same period of time without $CO_2$ injection; though this incremental recovery is quite modest – ranging from 0.6 to 0.8 Bcf. However, one could argue about the feasibility of achieving the level of technological performance assumed in Case 1, at least given today's technology.

Case 2, which assumes the middle well is completed in the Devonian formation with vertical permeability not enhanced, is perhaps the most realistic scenario in terms of today's technology. Reasonable methane recovery results from $CO_2$ injection, though somewhat less than would otherwise occur without $CO_2$ injection. Nonetheless, all $CO_2$ injected (from 3.3 to 6.5 Bcf) is stored; none is re-produced.

Case 3, with all wells completed in the Union Springs formation, results in the lowest recovery (both with and without $CO_2$ injection), and the least $CO_2$ stored. In this case, injected $CO_2$ is just recycling through the system, and not contacting much incremental adsorbed methane and/or pore space where the $CO_2$ can be stored.

Also shown in **Table 5** is that the later $CO_2$ injection is initiated and the longer the system is producing, the more methane gets produced, and more $CO_2$ that gets stored. Moreover, in two of the three cases, the results show that injecting $CO_2$ does not result in increased production relative to the no-injection case. However, in these cases, the injection of $CO_2$ results in greater gas production earlier, which could be economically beneficial. However, this is not always the case.

For example, as shown in **Figure 9**, for the Case 1 set of runs, the initiation of $CO_2$ injection results in a short period of production fall off, but then a spike in production due to the start of $CO_2$ injection, relative to when no injection takes place, regardless of the point in time that injection is initiated.

Table 5: Methane Recovery and $CO_2$ Storage for Three Completion and Several Injection Timing Scenarios – Marcellus Area 5

| | Case 1 - Middle Well in Devonian with Enhanced Permeability | | | | Case 2 - Middle Well in Devonian without Permeability Enhancement | | | | Case 3 - Middle Well in Union Springs without Permeability Enhancement | | | |
|---|---|---|---|---|---|---|---|---|---|---|---|---|
| | Cum $CH_4$ Production (Bcf) | Recovery (%) | Cum $CO_2$ Injection (Bcf) | Cum $CO_2$ Production (Bcf) | Cum $CH_4$ Production (Bcf) | Recovery (%) | Cum $CO_2$ Injection (Bcf) | Cum $CO_2$ Production (Bcf) | Cum $CH_4$ Production (Bcf) | Recovery (%) | Cum $CO_2$ Injection (Bcf) | Cum $CO_2$ Production (Bcf) |
| Primary Prod. for 21 years | 6.7 | 77.9 | - | - | 5.4 | 62.8 | - | - | 3.3 | 38.4 | - | - |
| Primary Prod. for 26 years | 6.8 | 79.1 | - | - | 5.6 | 65.1 | - | - | 3.5 | 40.7 | - | - |
| Primary Prod. for 31 years | 7.0 | 81.4 | - | - | 5.8 | 67.4 | - | - | 3.7 | 43.0 | - | - |
| Primary Prod. for 36 years | 7.1 | 82.6 | - | - | 6.0 | 69.8 | - | - | 3.9 | 45.3 | - | - |
| Primary 1 year, EGR 20 years | 7.4 | 86.2 | 19.1 | 1.8 | 3.6 | 41.5 | 3.3 | - | 2.8 | 32.4 | 14.3 | 9.9 |
| Primary 5 years, EGR 20 years | 7.6 | 88.7 | 21.2 | 2.9 | 4.5 | 52.2 | 5.0 | - | 3.0 | 35.1 | 15.1 | 10.6 |
| Primary 10 years, EGR 20 years | 7.7 | 89.8 | 22.0 | 3.2 | 5.1 | 59.0 | 6.0 | - | 3.3 | 38.4 | 15.7 | 11.0 |
| Primary 15 years, EGR 20 years | 7.8 | 90.4 | 22.4 | 3.3 | 5.4 | 63.1 | 6.5 | - | 3.6 | 41.4 | 16.1 | 11.3 |

Figure 9: Methane Production Results from Simulation Runs for Alternative Injection Timing Scenarios --- Case 1 – Marcellus Area 5

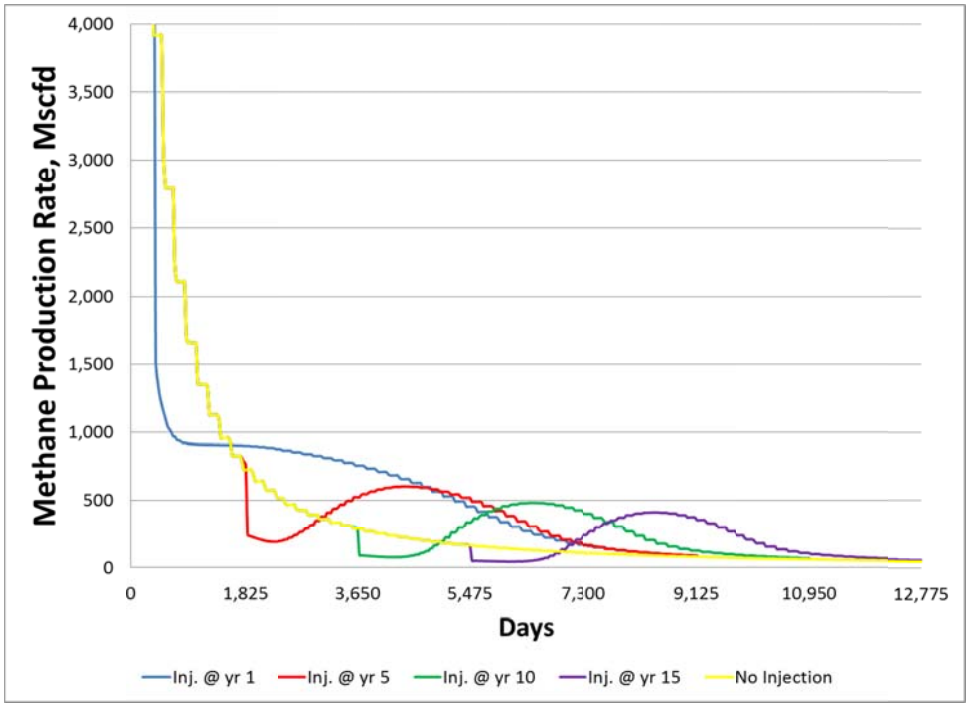


However, in Case 2, no incremental spike in production occurs when $CO_2$ is injected, relative to when no injection occurs, as shown in **Figure 10**. This is because without permeability enhancement due to advanced stimulation technology, most of the $CO_2$ injected remains in the upper, relatively thick and permeable Devonian shale layers. As a result, the injected $CO_2$ has relatively little influence on increasing production in the entire stratigraphic sequence, since it never makes it to the production wells. However, no $CO_2$ in produced, i.e., all injected $CO_2$ is stored. Moreover, while not explicitly modeled, one should expect that substantial additional amounts of $CO_2$ could be stored in this scenario if injection continued for a longer period of time.

Finally, in Case 3, where injection takes place in the Union Springs formation, rather than in the Devonian formations, a production spike is again seen, though this spike is not as pronounced as in Case 1 (**Figure 11)**. Injection and production wells are completed in the Union Springs formation, resulting in increased production due to $CO_2$ injection, but mostly from the Union Springs. In Cases 1 and 2, much greater production is realized from the other formations, which also contributes to much greater $CO_2$ storage potential, since $CO_2$ recycling through the system is substantially less.

Figure 10: Methane Production Results from Simulation Runs for Alternative Injection Timing Scenarios --- Case 2 – Marcellus Area 5

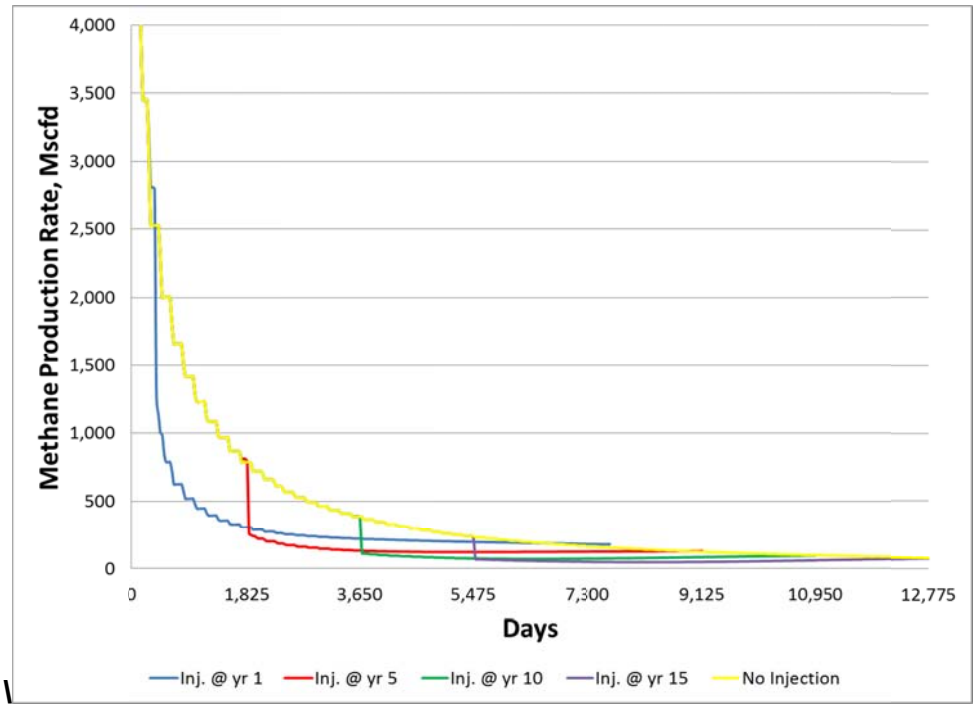


Figure 11: Methane Production Results from Simulation Runs for Alternative Injection Timing Scenarios --- Case 3 – Marcellus Area 5

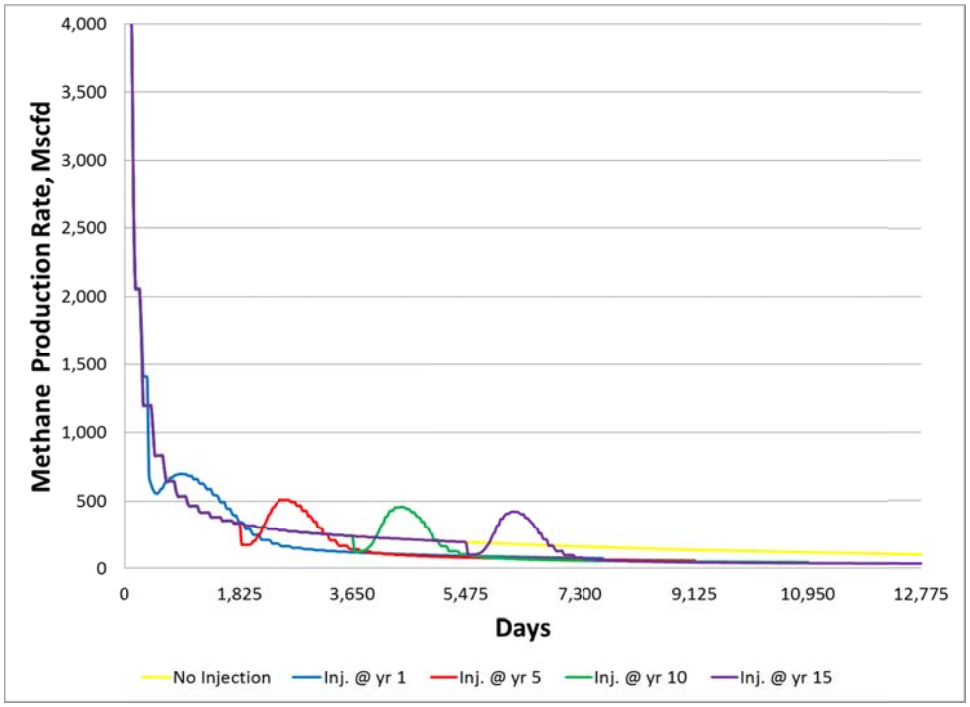

All three cases show that the timing of when $CO_2$ injection commences is important, and can affect three different outcomes that may impact project decision-making: (1) the amount of incremental gas production, (2) the amount of $CO_2$ stored, and (3) the amount of $CO_2$ recycled (that would need to be processed, increasing project costs).

Economic Analyses. An initial set of cash flow analyses were performed for Case 2, which assumes the middle well is completed in the Devonian formation, with vertical permeability not enhanced. The analyses were performed for three assumed wellhead natural gas prices:

- $5.00 per Mcf, which is the average wellhead price forecast for the next 20 years in the Energy Information Administration's Reference Case in their 2013 Annual Energy Outlook (AEO) (EIA, 2013).
- $6.00 per Mcf, which is the average wellhead price forecast for the next 20 years in the EIA's High Oil Price Scenario in the 2013 AEO.
- $3.60 per Mcf, representative of the spot market prices for natural gas contracts in early July, 2013 for the following month.[2]

Five cases were considered, one with no $CO_2$ injection, and four timing scenarios with $CO_2$ injection starting at 1, 5, 10, and 15 years in the middle well. In all cases, production lasts 20 years after $CO_2$ injection starts. In addition, the middle well produces natural gas until it is converted to $CO_2$ injection. In all cases for this assessment, it was assumed that $CO_2$ provided to the shale gas operator for injection is provided at no cost.

Economic results (**Table 6**) show the internal rate of return (IRR) and net present value (NPV) realized for each gas price case. Also shown for the four injection scenarios is a $CO_2$ emission reduction credit or carbon tax value, in dollars per metric ton (tonne) of $CO_2$ that would be necessary for the project to yield a 10 percent IRR. As shown, while this case is economic without $CO_2$ injection at all prices considered (though just barely at $3.60 per Mcf), the EGR cases are not economic except when primary production takes place for more than 10 years (except for the $3.60 per Mcf price case) before $CO_2$ injection is initiated. Again depending on wellhead gas prices, carbon credits or emission reduction credit values as high as $7.50 per tonne may be required to ensure economic viability of $CO_2$ injection.

[2] http://www.bloomberg.com/energy/

Table 6: Economics of Methane Recovery and $CO_2$ Storage for Several Injection Timing Scenarios – Marcellus Area 5 – Case 2 – Three Wellhead Gas Prices

| | $5.00 /Mcf Wellhead Gas Price | | |
|---|---|---|---|
| | IRR (%) | NPV ($MM) | Credit Price to achieve 10% IRR ($/tonne) |
| No Injection | 11 | 2.60 | NA |
| $CO_2$ Injection for 20 years | | | |
| 1 yr Primary + 20 (EGR 21) | 9 | -4.34 | $5.80 |
| 5 yrs Primary + 20 (EGR 25) | 9 | -1.46 | $1.90 |
| 10 yrs Primary + 20 (EGR 30) | 10 | 0.40 | none |
| 15 yrs Primary + 20 (EGR 35) | 10 | 1.23 | none |

| | $3.60 /Mcf Wellhead Gas Price | | |
|---|---|---|---|
| | IRR (%) | NPV ($MM) | Credit Price to achieve 10% IRR ($/tonne) |
| No Injection | 10 | 0.63 | NA |
| $CO_2$ Injection for 20 years | | | |
| 1 yr Primary + 20 (EGR 21) | 8 | -5.59 | $7.50 |
| 5 yrs Primary + 20 (EGR 25) | 9 | -3.13 | $4.10 |
| 10 yrs Primary + 20 (EGR 30) | 9 | -1.45 | $2.70 |
| 15 yrs Primary + 20 (EGR 35) | <10 | -0.73 | $0.90 |

| | $6.00 /Mcf Wellhead Gas Price | | |
|---|---|---|---|
| | IRR (%) | NPV ($MM) | Credit Price to achieve 10% IRR ($/tonne) |
| No Injection | 12 | 4.00 | NA |
| $CO_2$ Injection for 20 years | | | |
| 1 yr Primary + 20 (EGR 21) | 9 | -3.44 | $4.60 |
| 5 yrs Primary + 20 (EGR 25) | <10 | -0.26 | $0.40 |
| 10 yrs Primary + 20 (EGR 30) | 11 | 1.70 | none |
| 15 yrs Primary + 20 (EGR 35) | 11 | 2.64 | none |

**Table 7** shows similar results for just one wellhead gas price, but for the three different cases. For Case 1, which assumes the middle well is completed in the Devonian formation, with vertical permeability enhanced, at least 10 years of production before initiation of $CO_2$ injection is required to achieve a positive NPV at a 10 percent IRR. Otherwise, carbon credits or emission reduction credit values of $0.30 per tonne may be required to ensure economic viability. For Case 2, which assumes the middle well is completed in the Devonian formation, with vertical permeability not enhanced, at least 10 years of production before initiation of $CO_2$ injection is required to achieve a positive NPV; otherwise, carbon credits or emission reduction credit values of as much as $5.80 per tonne may be required. Finally, for Case 3, which assumes the middle well is completed in the Union Springs (Marcellus) formation with vertical permeability not enhanced, economic viability requires carbon credits or emission reduction credit values on the order of $2.20 to $4.60 per tonne to ensure economic viability.

Table 7: Economics of Methane Recovery and $CO_2$ Storage for Several Injection Timing Scenarios – Marcellus Area 5 – All 3 Cases -- $5.00/Mcf Wellhead Gas Price

| CASE 1 | | | |
|---|---|---|---|
| | $5.00 | /Mcf Wellhead Gas Price | |
| | IRR (%) | NPV ($MM) | Credit Price to achieve 10% IRR ($/tonne) |
| No Injection | 12 | 3.80 | NA |
| $CO_2$ Injection for 20 years | | | |
| 1 yr Primary + 20 (EGR 21) | <10 | -1.18 | $0.30 |
| 5 yrs Primary + 20 (EGR 25) | <10 | -1.10 | $0.30 |
| 10 yrs Primary + 20 (EGR 30) | 10 | 0.72 | none |
| 15 yrs Primary + 20 (EGR 35) | 11 | 2.03 | none |
| CASE 2 | | | |
| | $5.00 | /Mcf Wellhead Gas Price | |
| | IRR (%) | NPV ($MM) | Credit Price to achieve 10% IRR ($/tonne) |
| No Injection | 11 | 2.60 | NA |
| $CO_2$ Injection for 20 years | | | |
| 1 yr Primary + 20 (EGR 21) | 9 | -4.34 | $5.80 |
| 5 yrs Primary + 20 (EGR 25) | 9 | -1.46 | $1.90 |
| 10 yrs Primary + 20 (EGR 30) | 10 | 0.40 | none |
| 15 yrs Primary + 20 (EGR 35) | 10 | 1.23 | none |
| CASE 3 | | | |
| | $5.00 | /Mcf Wellhead Gas Price | |
| | IRR (%) | NPV ($MM) | Credit Price to achieve 10% IRR ($/tonne) |
| No Injection | 9 | -1.09 | NA |
| $CO_2$ Injection for 20 years | | | |
| 1 yr Primary + 20 (EGR 21) | 8 | -3.02 | $2.20 |
| 5 yrs Primary + 20 (EGR 25) | 8 | -2.70 | $2.80 |
| 10 yrs Primary + 20 (EGR 30) | 9 | -2.09 | $3.50 |
| 15 yrs Primary + 20 (EGR 35) | 9 | -1.69 | $4.60 |

## e. Development of Input Data for Basin Assessment

To this point, all of the analyses presented were based on reservoir and performance characteristics of the Marcellus Shale in Area 5 (**Figure 12**), as originally presented in Volume 2. In terms of characterizing the overall methane production and $CO_2$ storage potential of the Marcellus shale play, the results of Case 2 were applied all of the areas in the Marcellus.

For each of the nine areas in Figure 12, separate attributes for key parameters were specified for each of the four reservoir layers modeled (from upper to lower) – the Upper Devonian, the Upper Marcellus/ Oatka Creek, the Purcell/ Cherry Valley, and the Lower Marcellus/ Union Springs. Selected maps of calculated values are included in the Appendix of Volume 2. **Table 8** provides a description and summary of the nine model areas. **Tables 9, 10, 11,** summarize the model layer attributes that were incorporated into the reservoir simulations for the Upper Marcellus/ Oatka Creek, the Purcell/ Cherry Valley, and the Lower Marcellus/ Union Springs formations, respectively. For the Top Shales (Devonian), based on available logs, it was assumed that the layer was 100 feet thick, directly lying on top of the Upper Marcellus (Oatka Creek) with a porosity of 8 percent and a matrix permeability of $1.8 \times 10^{-5}$ millidarcies.

## f. Simulation Results for Basin Assessment

Again, for each area, the Case 2 development scenario was considered with no $CO_2$ injection (with production for 21, 25, 30, and 35 years), along with four timing scenarios with $CO_2$ injection starting at 1, 5, 10, and 15 years in the middle well. In all cases, production lasts 20 years after $CO_2$ injection starts. In addition, the middle well produces natural gas until it is converted to $CO_2$ injection.

The results are summarized in **Table 12**. As shown, average methane recovery per 80 acre unit ranges from 1.26 to 9.49 Bcf, and average cumulative volumes of $CO_2$ injected/ stored for the 80 acre unit range from 2.05 to 9.65 Bcf. Little or no $CO_2$ breakthrough was experienced in the scenarios considered.

Figure 12: Marcellus Model Areas for Simulating Potential CO2 Storage and Enhanced Gas Recovery

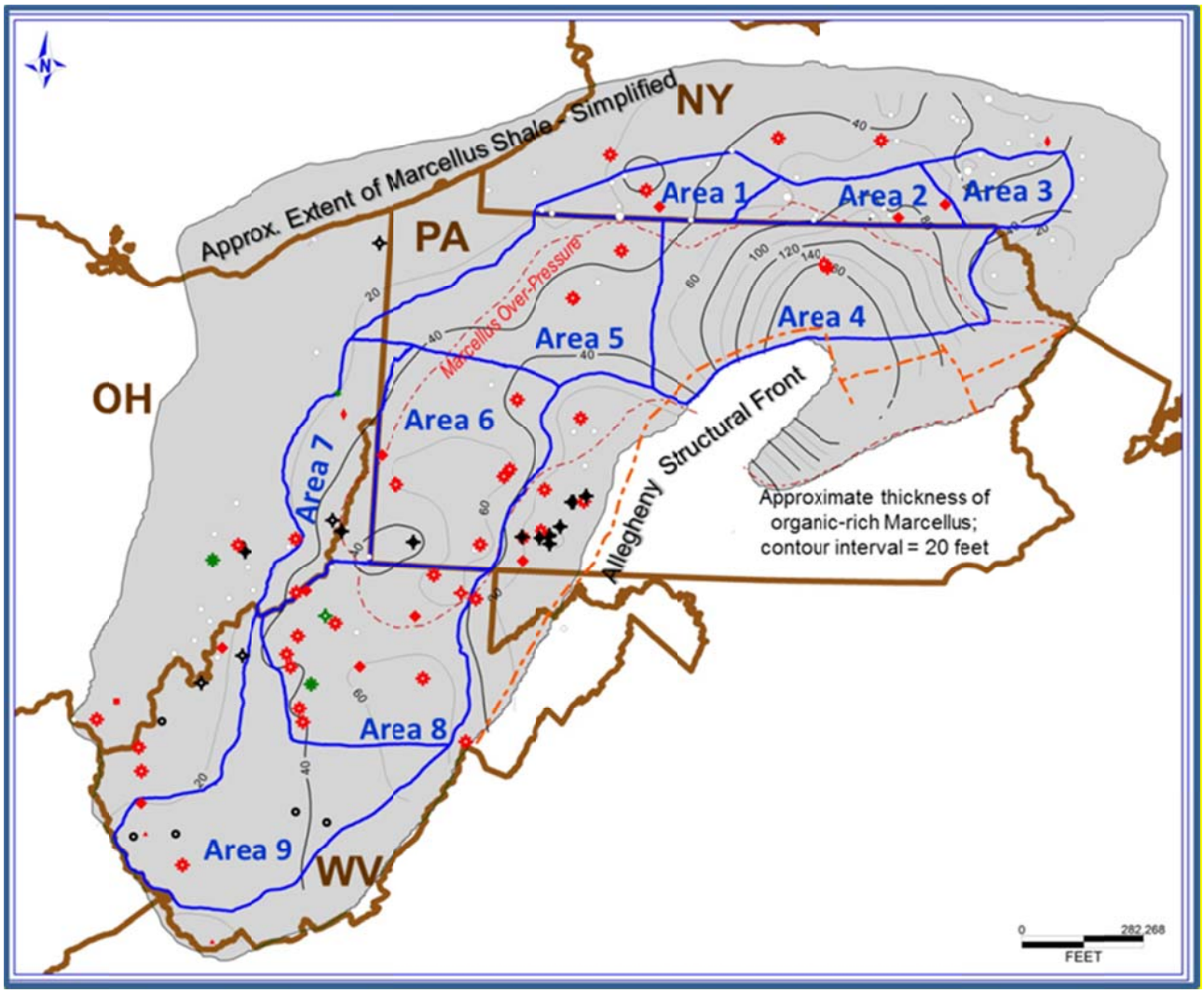

Table 8. Summary and Description of Marcellus Model Areas

| MODEL AREA | Area Description | Composite Model Well | Total Area, Acres | Total Area, miles$^2$ | Reservoir Pressure Gradient, psi/ft | Mean Reservoir Pressure, psia | Mean Reservoir Temperature, $^0$F | FVF for Methane, ft$^3$/ scf | FVF for $CO_2$, ft$^3$/ scf |
|---|---|---|---|---|---|---|---|---|---|
| AREA 1 | West Central NY; Normal Pressure | Allegany Co | 1,257,845 | 1,965 | 0.42 | 1,836 | 108.9 | 0.00719 | 0.00268 |
| AREA 2 | South Central NY; Normal Pressure | Tioga/ Broome Cos. | 1,164,491 | 1,820 | 0.45 | 2,023 | 111.4 | 0.00635 | 0.00248 |
| AREA 3 | East Central NY; Under Pressured | Chenango/ Otsego Cos. | 1,074,462 | 1,679 | 0.33 | 992 | 80.3 | 0.013525 | 0.00796 |
| AREA 4 | Northeast PA; Over Pressured | Bradford Co. | 5,007,988 | 7,825 | 0.64 | 4,053 | 138 | 0.003796 | 0.002286 |
| AREA 5 | NW - North Central PA; Over Pressured | Elk Co. | 3,651,027 | 5,705 | 0.56 | 3,197 | 128.5 | 0.004443 | 0.002275 |
| AREA 6 | SW - South Central PA; Normal to Over Pressured | Washington/ Fayette Cos. | 3,565,689 | 5,571 | 0.50 | 3,370 | 137 | 0.004358 | 0.002406 |
| AREA 7 | Eastern OH & WV Panhandle; Normal to Under-Pressured | Columbiana, OH; Tyler, WV | 2,250,702 | 3,517 | 0.41 | 2,079 | 120.9 | 0.006541 | 0.00267 |
| AREA 8 | North & Central WV; Normal to Under-Pressured | Tyler, Taylor, Lewis Cos. | 4,035,195 | 6,305 | 0.42 | 2,917 | 128.9 | 0.004977 | 0.002565 |
| AREA 9 | South & Southwest WV; Under Pressured | Lincoln Co. | 4,407,607 | 6,887 | 0.30 | 1,290 | 95 | 0.010223 | 0.002968 |
| Total Marcellus Study Area | | | 26,415,006 | 41,274 | | | | | |

Table 9. Model Layer Attributes for Upper Marcellus (Oatka Creek)

| Model Area | Area Description | Average Depth, ft. | Thickness, ft. | Total Porosity, fraction | Matrix Permeability, md | Water Saturation, fraction | Calculated TOC, wt. % | Mean Adsorbed Gas Content, scf/ ton | Theoretical Max. Adsorbed $CO_2$, scf/ ton |
|---|---|---|---|---|---|---|---|---|---|
| AREA 1 | West Central NY; Normal Pressure | 3,636 | 9 | 0.059 | 1.18E-06 | 0.10 | 5.1 | 81.4 | 297.8 |
| AREA 2 | South Central NY; Normal Pressure | 4,640 | 52 | 0.060 | 1.38E-06 | 0.57 | 4.7 | 74.5 | 278.1 |
| AREA 3 | East Central NY; Under Pressured | 2,995 | 10 | 0.070 | 5.74E-06 | 0.24 | 3.9 | 50.4 | 208.9 |
| AREA 4 | Northeast PA; Over Pressured | 6,281 | 43 | 0.074 | 9.58E-06 | 0.41 | 3.7 | 72.0 | 234.0 |
| AREA 5 | NW - North Central PA; Over Pressured | 5,696 | 11 | 0.058 | 1.09E-06 | 0.33 | 4.3 | 81.0 | 268.9 |
| AREA 6 | SW - South Central PA; Normal to Over Pressured | 6,714 | 29 | 0.07 | 5.74E-06 | 0.28 | 4.6 | 84.5 | 286.7 |
| AREA 7 | Eastern OH & WV Panhandle; Normal to Under-Pressured | 5,051 | 20 | 0.104 | 2.22E-04 | 0.26 | 7.1 | 118.8 | 426.9 |
| AREA 8 | North & Central WV; Normal to Under-Pressured | 6,933 | 13 | 0.074 | 9.58E-06 | 0.32 | 5.7 | 102.1 | 351.6 |
| AREA 9 | South & Southwest WV; Under Pressured | Absent | | | | | | | |

Table 10. Model Layer Attributes for Purcell/ Cherry Valley Limestone

| Model Area | Area Description | Average Depth, ft. | Thickness, ft. | Total Porosity, fraction | Matrix Permeability, md | Water Saturation, fraction | Calculated TOC, wt. % | Mean Adsorbed Gas Content, scf/ ton | Theoretical Max. Adsorbed $CO_2$, scf/ ton |
|---|---|---|---|---|---|---|---|---|---|
| AREA 1 | West Central NY; Normal Pressure | 3,645 | 4 | 0.061 | 1.60E-06 | 0.16 | 2.5 | 40.3 | 147.4 |
| AREA 2 | South Central NY; Normal Pressure | 4,692 | 3 | 0.040 | 3.27E-08 | 0.53 | 3.4 | 58.3 | 200.4 |
| AREA 3 | East Central NY; Under Pressured | Absent | | | | | | | |
| AREA 4 | Northeast PA; Over Pressured | 6,324 | 89 | 0.065 | 2.89E-06 | 0.46 | 3.3 | 63.0 | 204.9 |
| AREA 5 | NW - North Central PA; Over Pressured | 5,707 | 12 | 0.043 | 6.00E-08 | 0.51 | 3.3 | 61.3 | 202.5 |
| AREA 6 | SW - South Central PA; Normal to Over Pressured | 6,743 | 20 | 0.051 | 3.08E-07 | 0.78 | 2.5 | 46.7 | 152.7 |
| AREA 7 | Eastern OH & WV Panhandle; Normal to Under-Pressured | 5,071 | 9 | 0.088 | 5.00E-05 | 0.44 | 4.9 | 83.1 | 291.5 |
| AREA 8 | North & Central WV; Normal to Under-Pressured | 6,946 | 20 | 0.065 | 2.89E-06 | 0.49 | 5.2 | 97.9 | 320.7 |
| AREA 9 | South & Southwest WV; Under Pressured | Absent | | | | | | | |

Table 11. Model Layer Attributes for Lower Marcellus (Union Springs)

| Model Area | Area Description | Average Depth, ft. | Thickness, ft. | Total Porosity, fraction | Matrix Permeability, md | Water Saturation, fraction | Calculated TOC, wt. % | Mean Adsorbed Gas Content, scf/ ton | Theoretical Max. Adsorbed $CO_2$, scf/ ton |
|---|---|---|---|---|---|---|---|---|---|
| AREA 1 | West Central NY; Normal Pressure | 3,649 | 15 | 0.072 | 7.40E-06 | 0.21 | 5.6 | 93.3 | 330.2 |
| AREA 2 | South Central NY; Normal Pressure | 4,695 | 33 | 0.079 | 1.97E-05 | 0.22 | 6.3 | 106.2 | 376.8 |
| AREA 3 | East Central NY; Under Pressured | 3,005 | 50 | 0.070 | 5.74E-06 | 0.26 | 5.5 | 75.3 | 294.6 |
| AREA 4 | Northeast PA; Over Pressured | 6,413 | 34 | 0.087 | 4.30E-05 | 0.19 | 5.6 | 107.0 | 353.1 |
| AREA 5 | NW - North Central PA; Over Pressured | 5,719 | 34 | 0.093 | 8.00E-05 | 0.18 | 6.8 | 123.6 | 422.3 |
| AREA 6 | SW - South Central PA; Normal to Over Pressured | 6,763 | 36 | 0.080 | 1.97E-05 | 0.51 | 4.1 | 77.9 | 261.8 |
| AREA 7 | Eastern OH & WV Panhandle; Normal to Under-Pressured | 5,080 | 9 | 0.115 | 5.62E-04 | 0.19 | 9.2 | 148.7 | 547.2 |
| AREA 8 | North & Central WV; Normal to Under-Pressured | 6,966 | 31 | 0.087 | 4.37E-05 | 0.24 | 6.7 | 120.0 | 413.3 |
| AREA 9 | South & Southwest WV; Under Pressured | 4,022 | 21 (Total Marcellus) | 0.084 | 3.10E-07 | 0.21 | 6.0 | 93.6 | 339.2 |

Table 12: Methane Recovery and $CO_2$ Storage for Case 2 Completion Strategy for Alternative Injection Timing Scenarios – All Marcellus Areas

| | Area 1 | | | | Area 2 | | | | Area 3 | | | |
|---|---|---|---|---|---|---|---|---|---|---|---|---|
| | Cum $CH_4$ Prod (Bcf) | Recovery (%) | Cum $CO_2$ Inj (Bcf) | Cum $CO_2$ Prod (Bcf) | Cum $CH_4$ Prod (Bcf) | Recovery (%) | Cum $CO_2$ Inj (Bcf) | Cum $CO_2$ Prod (Bcf) | Cum $CH_4$ Prod (Bcf) | Recovery (%) | Cum $CO_2$ Inj (Bcf) | Cum $CO_2$ Prod (Bcf) |
| **No Inj 21** | 1.66 | 42.9 | - | - | 3.89 | 48.6 | - | - | 1.59 | 36.2 | - | - |
| **No Inj 25** | 1.78 | 46.0 | - | - | 4.12 | 51.5 | - | - | 1.73 | 39.4 | - | - |
| **No Inj 30** | 1.90 | 49.1 | - | - | 4.36 | 54.5 | - | - | 1.87 | 42.6 | - | - |
| **No Inj 35** | 2.00 | 51.7 | - | - | 4.55 | 56.9 | - | - | 2.00 | 45.6 | - | - |
| **EGR 21** | 0.95 | 24.5 | 2.53 | 0 | 2.06 | 25.8 | 2.72 | 0 | 0.72 | 16.4 | 1.49 | 0 |
| **EGR 25** | 1.25 | 32.1 | 2.74 | 0 | 2.83 | 35.3 | 3.71 | 0 | 1.06 | 24.2 | 2.19 | 0 |
| **EGR 30** | 1.49 | 38.4 | 2.79 | 0 | 3.42 | 42.7 | 4.46 | 0 | 1.35 | 30.7 | 2.26 | 0 |
| **EGR 35** | 1.68 | 43.4 | 2.62 | 0 | 3.86 | 48.3 | 4.73 | 0 | 1.56 | 35.5 | 2.25 | 0 |
| **Average per 80 acres** | **1.59** | | **2.67** | | **3.64** | | **3.91** | | **1.49** | | **2.05** | |

| | Area 4 | | | | Area 5 | | | | Area 6 | | | |
|---|---|---|---|---|---|---|---|---|---|---|---|---|
| | Cum $CH_4$ Prod (Bcf) | Recovery (%) | Cum $CO_2$ Inj (Bcf) | Cum $CO_2$ Prod (Bcf) | Cum $CH_4$ Prod (Bcf) | Recovery (%) | Cum $CO_2$ Inj (Bcf) | Cum $CO_2$ Prod (Bcf) | Cum $CH_4$ Prod (Bcf) | Recovery (%) | Cum $CO_2$ Inj (Bcf) | Cum $CO_2$ Prod (Bcf) |
| **No Inj 21** | 9.42 | 59.5 | - | - | 5.4 | 62.8 | - | - | 5.85 | 58.0 | - | - |
| **No Inj 25** | 9.82 | 62.0 | - | - | 5.6 | 65.1 | - | - | 6.12 | 60.7 | - | - |
| **No Inj 30** | 10.20 | 64.4 | - | - | 5.8 | 67.4 | - | - | 6.38 | 63.2 | - | - |
| **No Inj 35** | 10.50 | 66.3 | - | - | 6.0 | 69.8 | - | - | 6.59 | 65.3 | - | - |
| **EGR 21** | 7.69 | 48.6 | 4.83 | 0 | 3.6 | 41.5 | 3.3 | 0 | 4.12 | 40.9 | 4.93 | 0 |
| **EGR 25** | 8.76 | 55.3 | 6.70 | 0 | 4.5 | 52.2 | 5.0 | 0 | 5.05 | 50.0 | 6.72 | 0 |
| **EGR 30** | 9.52 | 60.1 | 7.81 | 0 | 5.1 | 59.0 | 6.0 | 0 | 5.67 | 56.2 | 7.81 | 0 |
| **EGR 35** | 10.00 | 63.2 | 8.37 | 0 | 5.4 | 63.1 | 6.5 | 0 | 6.06 | 60.1 | 8.4 | 0 |
| **Average per 80 acres** | **9.49** | | **6.93** | | **5.18** | | **5.20** | | **5.73** | | **6.97** | |

| | Area 7 | | | | Area 8 | | | | Area 9 | | | |
|---|---|---|---|---|---|---|---|---|---|---|---|---|
| | Cum $CH_4$ Prod (Bcf) | Recovery (%) | Cum $CO_2$ Inj (Bcf) | Cum $CO_2$ Prod (Bcf) | Cum $CH_4$ Prod (Bcf) | Recovery (%) | Cum $CO_2$ Inj (Bcf) | Cum $CO_2$ Prod (Bcf) | Cum $CH_4$ Prod (Bcf) | Recovery (%) | Cum $CO_2$ Inj (Bcf) | Cum $CO_2$ Prod (Bcf) |
| **No Inj 21** | 4.68 | 75.9 | - | - | 5.68 | 65.4 | - | - | 1.49 | 38.5 | - | - |
| **No Inj 25** | 4.79 | 77.6 | - | - | 5.88 | 67.7 | - | - | 1.61 | 41.6 | - | - |
| **No Inj 30** | 4.89 | 79.3 | - | - | 6.08 | 70.0 | - | - | 1.74 | 45.0 | - | - |
| **No Inj 35** | 4.97 | 80.6 | - | - | 6.24 | 71.8 | - | - | 1.85 | 47.8 | - | - |
| **EGR 21** | 4.87 | 79.1 | 4.75 | 0.17 | 5.83 | 67.2 | 8.5 | 0.00 | 0.32 | 8.3 | 2.9 | 0.0 |
| **EGR 25** | 4.93 | 80.0 | 4.31 | 0.06 | 6.23 | 71.7 | 9.7 | 0.01 | 0.69 | 17.9 | 2.3 | 0.0 |
| **EGR 30** | 4.98 | 80.9 | 3.83 | 0.02 | 6.45 | 74.3 | 10.1 | 0.01 | 1.06 | 27.4 | 1.7 | 0.0 |
| **EGR 35** | 5.03 | 80.7 | 3.49 | 0.00 | 6.59 | 75.9 | 10.3 | 0.01 | 1.30 | 33.7 | 2.2 | 0.0 |
| **Average per 80 acres** | **4.89** | | **4.10** | | **6.12** | | **9.65** | | **1.26** | | **2.28** | |

The next step in the assessment was to determine what portion of the estimated total methane gas in place and the theoretical maximum $CO_2$ storage capacity in the Marcellus shale would actually be accessible. For this, the following steps were pursued:

- The total area of each of the areas was divided by 80 acres (the assumption for the recoveries per well in Table 12) to determine the number of wells would be required to develop all of the acreage in each of the nine study areas.
- An estimate of the number of accessible well sites was made based on the assumption that only half of the total number of well sites in each area would be accessible for development.
- Based on the results summarized in Tables 6 and 7, it was assumed that only areas with estimated cumulative production per well better than those associated with Area 5 would likely be economic to develop under primary methane recovery. The assumption is only those areas that are determined to be economic to pursue at prices of $5.00 per Mcf would be a likely candidate for subsequent enhanced recovery via $CO_2$ injection. Only areas 4, 5, 6, and 8 met this condition.
- For these areas, it was assumed that only half of the area would have properties as good as or better than that assumed in the simulation runs. Based on that, only half of the accessible well sites would be economically feasible to pursue.

## g. Potential for Enhanced Gas Recovery and $CO_2$ Storage

The results of the application of this approach are shown in **Table 13** (those areas expected to be economic at $5.00 per Mcf are highlighted in yellow). In summary, the results indicate that about 349 Tcf of methane is recoverable in the Marcellus Shale at natural gas prices of $5.00 per Mcf, out of about 697 Tcf that could be considered technically recoverable and accessible. This potential amounts the potential for storing 734 Tcf (or 39 billion metric tonnes, or Gt) of $CO_2$. This compares to earlier DOE/NETL efforts that developed a preliminary estimate that the Marcellus shale has the potential to store from 17 to 166 Gt of $CO_2$ (DOE/NETL, 2010).

Table 13: Methane Recovery and $CO_2$ Storage Potential for the Marcellus Shale

| | Total Area, Acres | Total Area, miles$^2$ | Estimated Total Gas In-Place, Bcf | Estimated Theoretical Maximum $CO_2$ Storage, Bcf | No. of Wells at 80-Acre Spacing | No. of Accessible, Feasible Well Sites | $CH_4$ Production per Well (Bcf) | $CO_2$ Stored per Well (Bcf) | Technical $CH_4$ Production Potential (Bcf) | Technical $CH_4$ Production Potential Better than Average(Bcf) | $CO_2$ Storage Potential (Bcf) | $CO_2$ Storage Potential (MMtonne) |
|---|---|---|---|---|---|---|---|---|---|---|---|---|
| Area 1 | 1,257,845 | 1,965 | 21,186 | 66,001 | 15,723 | 7,862 | 1.59 | 2.67 | 12,490 | 6,245 | 20,990 | 1,111 |
| Area 2 | 1,164,491 | 1,820 | 59,665 | 190,467 | 14,556 | 7,278 | 3.64 | 3.91 | 26,465 | 13,232 | 28,421 | 1,504 |
| Area 3 | 1,074,462 | 1,679 | 22,631 | 80,530 | 13,431 | 6,715 | 1.49 | 2.05 | 9,972 | 4,986 | 13,750 | 728 |
| Area 4 | 5,007,988 | 7,825 | 505,393 | 1,184,168 | 62,600 | 31,300 | 9.49 | 6.93 | 296,997 | 148,499 | 216,830 | 11,472 |
| Area 5 | 3,651,027 | 5,705 | 190,482 | 476,823 | 45,638 | 22,819 | 5.18 | 5.20 | 118,088 | 59,044 | 118,658 | 6,278 |
| Area 6 | 3,565,689 | 5,571 | 148,094 | 368,350 | 44,571 | 22,286 | 5.73 | 6.97 | 127,696 | 63,848 | 155,219 | 8,213 |
| Area 7 | 2,250,702 | 3,517 | 75,300 | 225,713 | 28,134 | 14,067 | 4.89 | 4.10 | 68,822 | 34,411 | 57,604 | 3,048 |
| Area 8 | 4,035,195 | 6,305 | 219,554 | 565,895 | 50,440 | 25,220 | 6.12 | 9.65 | 154,409 | 77,205 | 243,247 | 12,870 |
| Area 9 | 4,407,607 | 6,887 | 56,612 | 198,147 | 55,095 | 27,548 | 1.26 | 2.28 | 34,641 | 17,321 | 62,671 | 3,316 |
| | 26,415,006 | 41,274 | 1,298,917 | 3,356,094 | 330,188 | 165,094 | | | 849,581 | 424,791 | 917,390 | 48,539 |
| Economic Areas @ $5.00/Mcf -- 4, 5, 6, & 8 | | | | | | | | | 697,191 | 348,595 | 733,954 | 38,834 |
| | Assumes | 50% | of well sites are accessible | | | | | | | | | |
| | | 50% | of the accessible well sites are better than average | | | | | | | | | |

# 4. UTICA SHALE

No historical production data were available to provide the basis for history matching production in the Utica shale. Therefore, no history matching analyses comparable to that performed for the Marcellus Shale was possible in the Utica shale.

## a. Development of Input Data

The well log analyses for individual study wells were aggregated to create a composite model well for each of eleven model areas, as shown in **Figure 13**, from which estimated total gas in-place and theoretically maximum $CO_2$ storage capacity were developed.

Figure 13. Utica/ Point Pleasant Study Area with Model Area Sub-Divisions

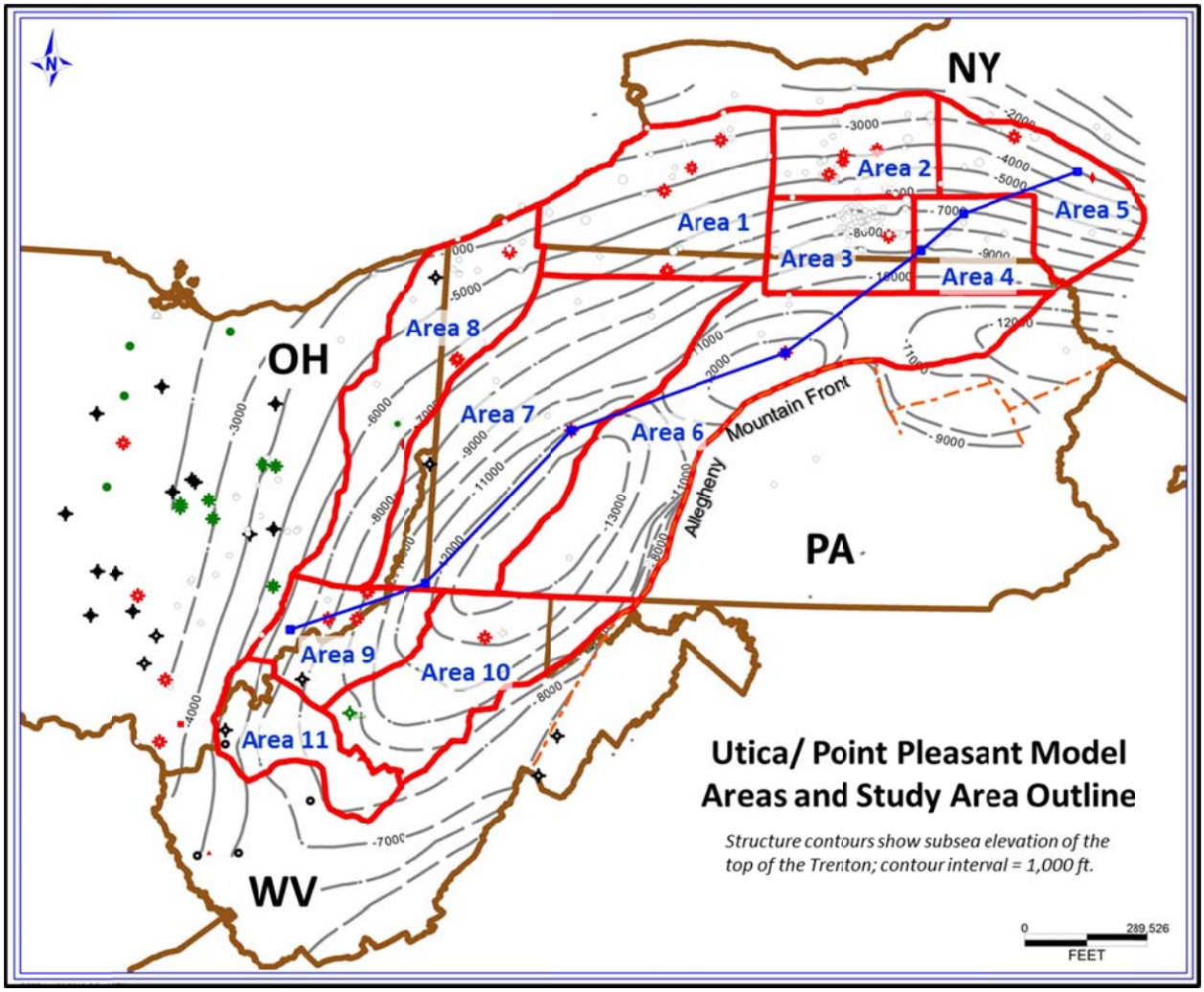

The rationale for the development of model areas was described in detail in Volume 3. In addition, also described in Volume 3 is the approach taken to simplify the representation of the complex stratigraphy of the Utica Shale and the underlying Point Pleasant Formation. The Utica was divided into two model layers, the "Upper Utica" and the "Basal Utica Shale", a high gamma ray, low bulk density zone at the base for the Utica immediately overlying the Trenton Limestone or Trenton- equivalent formations. The Point Pleasant was also divided into two reservoir model layers, the "Upper (Shaley) Point Pleasant" and the carbonate-rich "Lower Point Pleasant".

**Table 14** provides a description of the Utica/ Point Pleasant model areas and a summary of estimated model area parameters for calculating gas in-place and maximum $CO_2$ storage capacity, including estimated reservoir pressure gradient, extrapolated mean reservoir pressure and temperature, and estimated formation volume factor for methane and $CO_2$. Model well attributes for each model area and each layer were developed for incorporation into the reservoir simulation. These model well attributes include the average depth of the layer, thickness, average total porosity, average permeability, average calculated water saturation, average TOC, adsorbed gas content (scf/ton) and maximum adsorbed $CO_2$ storage capacity (scf/ton).

**Table 15** summarizes the model well attributes for the Upper Utica reservoir layer. The model well attributes for the Basal Utica Shale are summarized in **Table 16**. **Table 17** contains the model well attributes for the Upper Point Pleasant layer (shale-rich Point Pleasant) and **Table 18** contains the model well attributes for the Lower Point Pleasant reservoir layer, the carbonate-rich Point Pleasant.

The key parameters used for the simulation are summarized in **Table 19**.

For areas 1 to 5, isotherms for the Ross # 1 were used. Two isotherms were available, one for the Utica shale (isotherm 1) and one for the Point Pleasant equivalent (isotherm 2). Isotherm 1 was applied to layers 1 and 2 of the model while isotherm 2 was applied to layers 3 and 4. For areas 6 to 11, isotherms for the Beardmore #1 well were available. These were averaged and the same isotherm used in all four layers.

These isotherms are shown in **Figures 14** (for methane) and **Figure 15** (for $CO_2$).

Table 14. Description and Summary of Utica Shale/ Point Pleasant Model Areas

| MODEL AREA | Area Description | Total Area, Acres | Total Area, miles$^2$ | Estimated Reservoir Pressure Gradient, psi/ft | Mean Reservoir Pressure, psia | Mean Reservoir Temperature, $^0$F | FVF for Methane, ft$^3$/ scf | FVF for $CO_2$, ft$^3$/ scf |
|---|---|---|---|---|---|---|---|---|
| AREA 1 | Western NY & Northwest PA | 4,050,794 | 6,329 | 0.46 | 2,720 | 131 | 0.00458 | 0.00237 |
| AREA 2 | North Central NY | 1,992,915 | 3,114 | 0.53 | 2,928 | 126 | 0.00476 | 0.00234 |
| AREA 3 | South Central NY; North Central PA | 1,793,827 | 2,803 | 0.53 | 4,812 | 178 | 0.00370 | 0.00227 |
| AREA 4 | Southeast Central NY (Broome & Tioga Cos.) | 1,572,025 | 2,456 | 0.63 | 5,968 | 184 | 0.00328 | 0.00216 |
| AREA 5 | Northeast NY (Cortland, Madison, Otsego Cos.) | 2,451,694 | 3,831 | 0.44 | 2,224 | 119 | 0.00505 | 0.00239 |
| AREA 6 | Northeast PA; East Central PA | 6,777,578 | 10,590 | 0.63 | 7,717 | 250 | 0.00316 | 0.00203 |
| AREA 7 | West PA; WV Panhandle; East Central OH | 7,170,236 | 11,204 | 0.60 | 6,621 | 208 | 0.00313 | 0.00208 |
| AREA 8 | Northwest PA; Eastern OH | 4,133,518 | 6,459 | 0.53 | 3,547 | 143 | 0.00425 | 0.00238 |
| AREA 9 | Northwest WV; Southeast OH | 1,948,414 | 3,044 | 0.53 | 4,738 | 176 | 0.00373 | 0.00230 |
| AREA 10 | Central WV | 3,421,544 | 5,346 | 0.53 | 6,406 | 222 | 0.00306 | 0.00203 |
| AREA 11 | Southwest- South Central WV | 1,751,393 | 2,737 | 0.53 | 4,083 | 158 | 0.00397 | 0.00244 |
| Utica/ Point Pleasant Study Area Total | | 37,063,938 | 57,913 | | | | | |

Table 15. Model Layer Attributes for Upper Utica Shale– Archie Water Saturation

| Model Area | Area Description | Average Depth, ft. | Thickness, ft. | Total Porosity, fraction | Matrix Permeability, md | Water Saturation, fraction* | Calculated TOC, wt. % | Mean Adsorbed Gas Content, scf/ ton | Theoretical Max. Adsorbed $CO_2$, scf/ ton |
|---|---|---|---|---|---|---|---|---|---|
| AREA 1 | Western NY & Northwest PA | 5,710 | 172 | 0.029 | 5.18E-06 | 0.65 | 0.9 | 13.6 | 26.8 |
| AREA 2 | North Central NY | 5,421 | 104 | 0.027 | 4.62E-06 | 0.87 | 0.6 | 9.3 | 18.3 |
| AREA 3 | South Central NY; North Central PA | 8,953 | 127 | 0.026 | 4.37E-06 | 0.80 | 0.5 | 8.5 | 15.7 |
| AREA 4 | Southeast Central NY (Broome & Tioga Cos.) | 9,297 | 116 | 0.020 | 3.11E-06 | 0.54 | 0.4 | 7.5 | 13.7 |
| AREA 5 | Northeast NY (Cortland, Madison, Otsego Cos.) | 4,734 | 199 | 0.031 | 5.80E-06 | 0.68 | 1.1 | 16.6 | 33.7 |
| AREA 6 | Northeast PA; East Central PA | 12,077 | 137 | 0.027 | 4.62E-06 | 0.73 | 0.8 | 14.9 | 26.8 |
| AREA 7 | West PA; WV Panhandle; East Central OH | 10,907 | 155 | 0.025 | 8.15E-05 | 0.73 | 0.70 | 9.4 | 24.1 |
| AREA 8 | Northwest PA; Eastern OH | 6,544 | 107 | 0.031 | 9.17E-05 | 0.73 | 1.3 | 15.0 | 42.1 |
| AREA 9 | Northwest WV; Southeast OH | 8,807 | 105 | 0.023 | 7.84E-05 | 0.96 | 0.5 | 5.8 | 15.5 |
| AREA 10 | Central WV | 11,991 | 84 | 0.020 | 7.39E-05 | 0.73 | 1.0 | 13.0 | 33.6 |
| AREA 11 | Southwest- South Central WV | 7,661 | 43 | 0.033 | 9.53E-05 | 0.60 | 0.8 | 10.1 | 27.7 |

** Archie water saturation algorithm used to compute water saturation for the Upper Utica Shale model layer.*

Table 16. Model Layer Attributes for Organic-Rich Basal Utica Shale – Simandoux Water Saturation

| Model Area | Area Description | Average Depth, ft. | Thickness, ft. | Total Porosity, fraction | Matrix Permeability, md | Water Saturation, fraction* | Calculated TOC, wt. % | Mean Adsorbed Gas Content, scf/ ton | Theoretical Max. Adsorbed $CO_2$, scf/ ton |
|---|---|---|---|---|---|---|---|---|---|
| AREA 1 | Western NY & Northwest PA | 5,882 | 45 | 0.038 | 8.63E-06 | 0.25 | 1.0 | 15.7 | 31.0 |
| AREA 2 | North Central NY | 5,525 | 10 | 0.033 | 6.50E-06 | 0.28 | 1.1 | 17.3 | 33.9 |
| AREA 3 | South Central NY; North Central PA | 9,080 | 36 | 0.032 | 6.14E-06 | 0.29 | 1.2 | 22.1 | 41.1 |
| AREA 4 | Southeast Central NY (Broome & Tioga Cos.) | 9,413 | 60 | 0.052 | 1.91E-05 | 0.22 | 2.4 | 45.6 | 83.2 |
| AREA 5 | Northeast NY (Cortland, Madison, Otsego Cos.) | 4,933 | 121 | 0.047 | 1.44E-05 | 0.32 | 2.1 | 30.8 | 62.5 |
| AREA 6 | Northeast PA; East Central PA | 12,214 | 35 | 0.041 | 1.02E-05 | 0.25 | 1.8 | 34.7 | 62.3 |
| AREA 7 | West PA; WV Panhandle; East Central OH | 11,062 | 34 | 0.038 | 1.05E-04 | 0.25 | 1.7 | 23.2 | 59.9 |
| AREA 8 | Northwest PA; Eastern OH | 6,651 | 41 | 0.043 | 1.16E-04 | 0.27 | 2.3 | 26.8 | 74.9 |
| AREA 9 | Northwest WV; Southeast OH | 8,912 | 28 | 0.032 | 9.35E-05 | 0.35 | 1.1 | 13.2 | 35.3 |
| AREA 10 | Central WV | 12,075 | 12 | 0.024 | 7.99E-05 | 0.38 | 0.7 | 9.7 | 25.1 |
| AREA 11 | Southwest- South Central WV | Absent | | | | | | | |

**Simandoux water saturation algorithm used for the basal Utica Shale model layer; corrects the Archie equation for shale.*

Table 17. Model Layer Attributes for Shale - Rich Point Pleasant (Upper Point Pleasant) and Equivalent Formations – Simandoux Water Saturation

| Model Area | Area Description | Average Depth, ft. | Thickness, ft. | Total Porosity, fraction | Matrix Permeability, md | Water Saturation, fraction* | Calculated TOC, wt. % | Mean Adsorbed Gas Content, scf/ ton | Theoretical Max. Adsorbed $CO_2$, scf/ ton |
|---|---|---|---|---|---|---|---|---|---|
| AREA 1 | Western NY & Northwest PA | Absent | | | | | | | |
| AREA 2 | North Central NY | Absent | | | | | | | |
| AREA 3 | South Central NY; North Central PA | 9,116 | 109 | 0.041 | 1.02E-05 | 0.34 | 1.7 | 31.4 | 58.4 |
| AREA 4 | Southeast Central NY (Broome & Tioga Cos.) | 9,473 | 109 | 0.040 | 9.66E-06 | 0.23 | 1.8 | 33.1 | 60.4 |
| AREA 5 | Northeast NY (Cortland, Madison, Otsego Cos.) | 5,054 | 104 | 0.042 | 1.08E-05 | 0.29 | 1.5 | 22.9 | 46.5 |
| AREA 6 | Northeast PA; East Central PA | 12,249 | 130 | 0.040 | 9.66E-06 | 0.26 | 1.6 | 30.8 | 55.3 |
| AREA 7 | West PA; WV Panhandle; East Central OH | 11,096 | 113 | 0.045 | 1.20E-04 | 0.26 | 1.8 | 24.6 | 63.4 |
| AREA 8 | Northwest PA; Eastern OH | 6,692 | 59 | 0.048 | 1.28E-04 | 0.20 | 2.1 | 24.6 | 68.9 |
| AREA 9 | Northwest WV; Southeast OH | 8,940 | 61 | 0.055 | 1.47E-04 | 0.28 | 2.9 | 36.6 | 98.2 |
| AREA 10 | Central WV | 12,087 | 45 | 0.043 | 1.16E-04 | 0.24 | 1.4 | 18.5 | 47.8 |
| AREA 11 | Southwest-South Central WV | 7,704 | 87 | 0.049 | 1.30E-04 | 0.52 | 1.6 | 19.6 | 53.5 |

**Simandoux water saturation algorithm for the Upper (shaley) Point Pleasant model layer; corrects the Archie equation for shale.*

Table 18. Model Layer Attributes for Carbonate - Rich Point Pleasant (Lower Point Pleasant) and Equivalent Formations – Archie Water Saturation

| Model Area | Area Description | Average Depth, ft. | Thickness, ft. | Total Porosity, fraction | Matrix Permeability, md | Water Saturation, fraction* | Calculated TOC, wt. % | Mean Adsorbed Gas Content, scf/ ton | Theoretical Max. Adsorbed $CO_2$, scf/ ton |
|---|---|---|---|---|---|---|---|---|---|
| AREA 1 | Western NY & Northwest PA | Absent | | | | | | | |
| AREA 2 | North Central NY | Absent | | | | | | | |
| AREA 3 | South Central NY; North Central PA | 9,225 | 51 | 0.037 | 8.15E-06 | 0.52 | 1.4 | 24.4 | 45.3 |
| AREA 4 | Southeast Central NY (Broome & Tioga Cos.) | 9,582 | 107 | 0.037 | 8.15E-06 | 0.37 | 1.7 | 31.8 | 58.0 |
| AREA 5 | Northeast NY (Cortland, Madison, Otsego Cos.) | 5,158 | 89 | 0.034 | 6.88E-06 | 0.54 | 1.0 | 15.2 | 30.8 |
| AREA 6 | Northeast PA; East Central PA | 12,379 | 99 | 0.045 | 1.28E-05 | 0.43 | 1.9 | 36.3 | 65.1 |
| AREA 7 | West PA; WV Panhandle; East Central OH | 11,209 | 87 | 0.046 | 1.23E-04 | 0.43 | 1.5 | 19.6 | 50.6 |
| AREA 8 | Northwest PA; Eastern OH | 6,751 | 79 | 0.046 | 1.23E-04 | 0.43 | 1.5 | 17.0 | 47.7 |
| AREA 9 | Northwest WV; Southeast OH | 9,001 | 53 | 0.044 | 1.18E-04 | 0.42 | 1.6 | 20.5 | 55.0 |
| AREA 10 | Central WV | 12,132 | 34 | 0.035 | 9.91E-05 | 0.33 | 0.4 | 5.2 | 13.4 |
| AREA 11 | Southwest- South Central WV | Absent | | | | | | | |

** Archie water saturation algorithm used for the Lower Point Pleasant model layer.*

Table 19. Key Parameters by Layer and Model Area used in the Simulation Runs

| | Model Area 1 Western NY & NW Pennsylvania | Model Area 2 North Central NY | Model Area 3 S Central NY & N Central PA | Model Area 4 East NY (mainly Broome & Tioga Co) | Model Area 5 - A Northeast NY | Model Area 6 NE PA & E-Central PA | Model Area 7 West PA, WV Panhandle, E Central OH | Model Area 8 NW PA, Eastern OH | Model Area 9 Northwest WV, Southeast OH | Model Area 10 Central WV | Model Area 11 Southwest-South Central WV |
|---|---|---|---|---|---|---|---|---|---|---|---|
| Estimated Reservoir Pressure Gradient, psi/ft | 0.46 | 0.53 | 0.53 | 0.63 | 0.44 | 0.63 | 0.60 | 0.53 | 0.53 | 0.53 | 0.53 |
| Estimated Mean Reservoir Temperature, °F | 131.1 | 125.8 | 178.1 | 183.8 | 118.9 | 250.0 | 207.7 | 143.0 | 176.0 | 222.3 | 157.9 |
| **Upper Utica Shale** | | | | | | | | | | | |
| Depth, ft. | 5,710 | 5,421 | 8,953 | 9,297 | 4,734 | 12,077 | 10,907 | 6,544 | 8,807 | 11,991 | 7,661 |
| Gross Thickness, ft. | 172 | 104 | 127 | 116 | 199 | 137 | 155 | 107 | 105 | 84 | 43 |
| Average Total Porosity, fraction | 0.029 | 0.027 | 0.026 | 0.020 | 0.031 | 0.027 | 0.025 | 0.031 | 0.023 | 0.020 | 0.033 |
| Average Matrix Permeability of Net Pay, md | 8.815E-05 | 8.477E-05 | 8.313E-05 | 7.393E-05 | 9.166E-05 | 8.477E-05 | 4.128E-06 | 5.801E-06 | 3.685E-06 | 3.109E-06 | 6.498E-06 |
| **Basal Utica Shale (High TOC)** | | | | | | | | | | | |
| Depth, ft. | 5,882 | 5,525 | 9,080 | 9,413 | 4,933 | 12,214 | 11,062 | 6,651 | 8,912 | 12,075 | Absent |
| Gross Thickness, ft. | 45 | 10 | 36 | 60 | 121 | 35 | 34 | 41 | 28 | 12 | |
| Average Total Porosity, fraction | 0.038 | 0.033 | 0.032 | 0.052 | 0.047 | 0.041 | 0.038 | 0.043 | 0.032 | 0.024 | |
| Average Matrix Permeability, md | 1.051E-04 | 9.532E-05 | 9.347E-05 | 1.382E-04 | 1.253E-04 | 1.115E-04 | 8.628E-06 | 1.146E-05 | 6.140E-06 | 3.900E-06 | |
| **Point Pleasant/ Pt. Pleasant Equivalents Shale-Rich** | | | | | | | | | | | |
| Depth, ft. | Absent | Absent | 9,116 | 9,473 | 5,054 | 12,249 | 11,096 | 6,692 | 8,940 | 12,087 | 7,704 |
| Gross Thickness, ft. | | | 109 | 109 | 104 | 130 | 113 | 59 | 61 | 45 | 87 |
| Average Total Porosity, fraction | | | 0.041 | 0.040 | 0.042 | 0.040 | *0.045* | 0.048 | 0.055 | 0.043 | 0.049 |
| Average Matrix Permeability, md | | | 1.115E-04 | 1.093E-04 | 1.137E-04 | 1.093E-04 | 1.283E-05 | 1.521E-05 | 2.263E-05 | 1.146E-05 | 1.610E-05 |
| **Total Point Pleasant/ Pt. Pleasant Equivalents - Carbonate-Rich** | | | | | | | | | | | |
| Depth, ft. | Absent | Absent | 9,225 | 9,582 | 5,158 | 12,379 | 11,209 | 6,751 | 9,001 | 12,132 | Absent |
| Gross Thickness, ft. | | | 51 | 107 | 89 | 99 | 87 | 79 | 53 | 34 | |
| Average Total Porosity, fraction | | | 0.037 | 0.037 | 0.034 | 0.045 | 0.040 | 0.046 | 0.044 | 0.035 | |
| Average Matrix Permeability, md | | | 1.031E-04 | 1.031E-04 | 9.720E-05 | 1.205E-04 | 9.664E-06 | 1.358E-05 | 1.213E-05 | 7.278E-06 | |

Figure 14. Methane Adsorption Isotherms for the Utica/ Point Pleasant

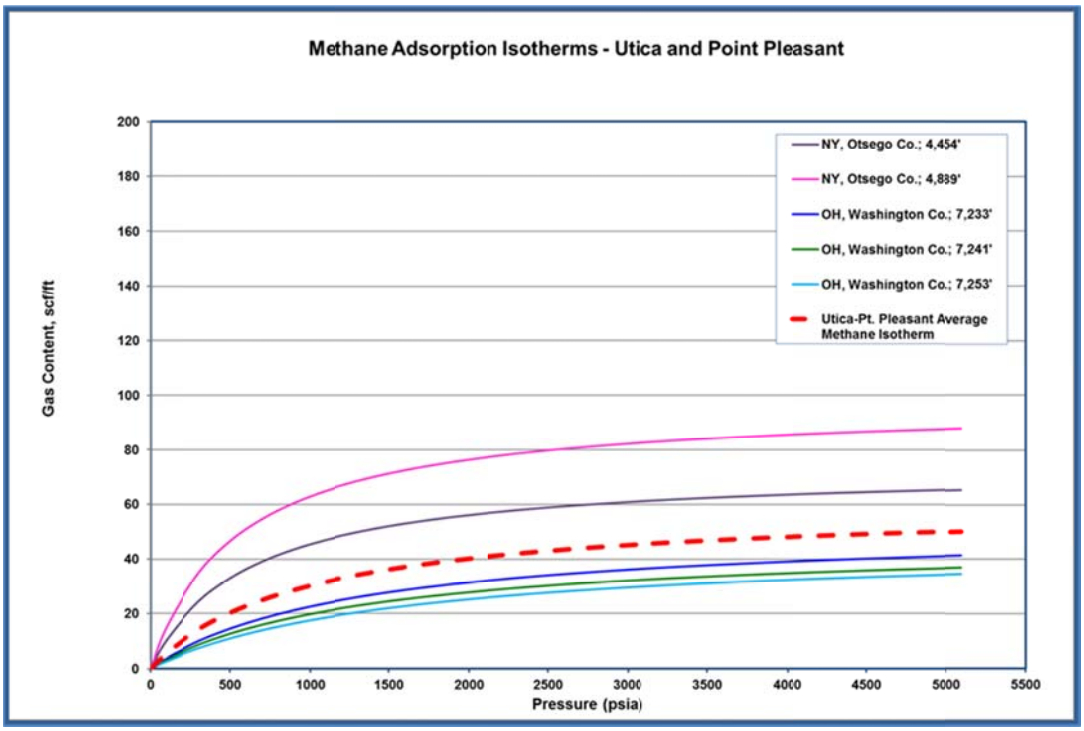


Figure 15. $CO_2$ Adsorption Isotherms for the Utica/ Point Pleasant

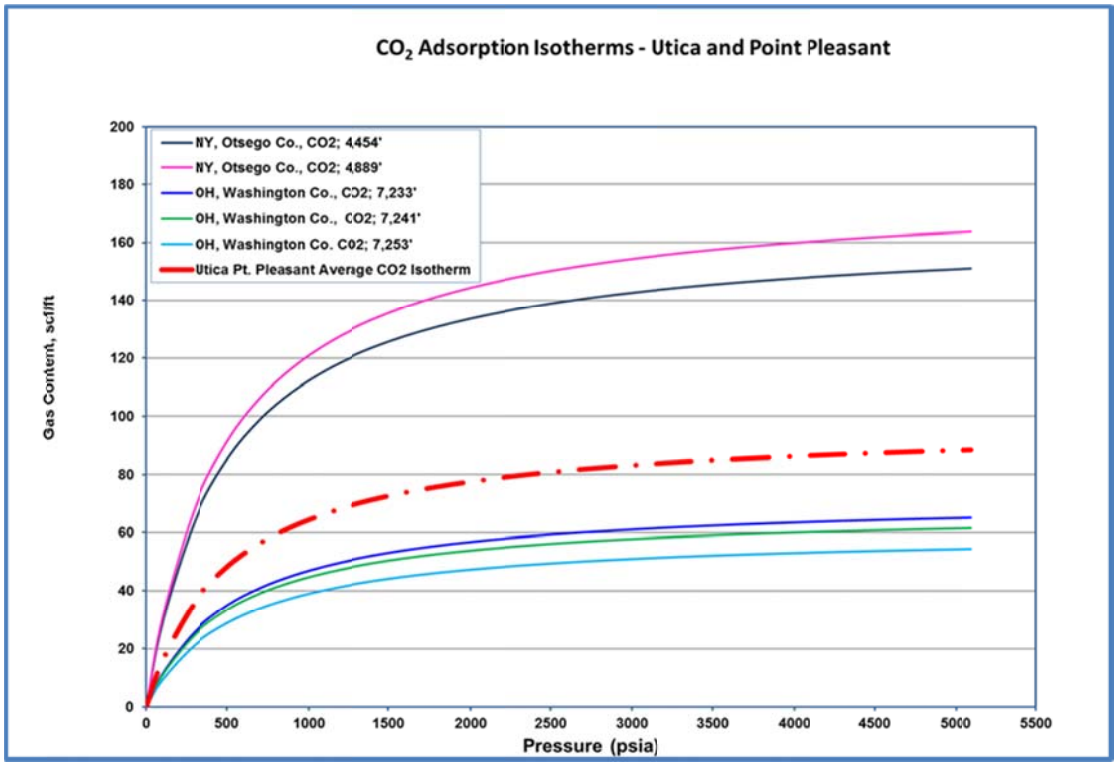

## b. Simulation Results

The reservoir simulation approach described above for the Marcellus Shale was comparably applied to the Utica. Similar to that performed for the Marcellus shale, simulations for the Utica shale were also run on 80-acre spacing with one half 5,000 foot long horizontal well on each side of the model. Each well was assumed to produce at 25 psia wellhead pressure for 20 years. The area between the 2 wells was considered fractured and with fracture permeability 250 times the matrix permeability.

For areas 1 to 5, the wells were assumed to be completed in the Basal Utica Shale (layer 2), whereas for areas 6 to 11, they are completed in the Point Pleasant shale rich zone (layer 3).

An initial set of simulation runs were performed, with recovery rates per well and recovery efficiency (relative to estimated gas in place) that are currently considerably higher than indicated by the results from recently drilled Utica wells. It was postulated that one reason for this was that the actually values for matrix permeability were probably substantially lower than the permeability values estimated based on the well logs.

To adjust matrix permeability values, we assumed a permeability decay correlation as shown in **Figure 16** to estimate pressure decay matrix permeability values as a function of pressure. The data used in this correlation were based on the results of pressure decay tests on a crushed sample from the Beardmore #1 well provided by an operator in the Utica shale in Ohio. These were used to adjust permeability relative to the estimates obtained from well logs.

Using the correlation above, the matrix permeability, K, was re-estimated as a function of pressure using the equation:

$$K = K_0 * \exp(-8.62e^{-4} * P)$$

where $K_0$ is the original permeability value estimated from the log data and P is the estimated pressure for the corresponding layer.

**Table 20** shows the impact of adjusting this matrix permeability value on cumulative methane production and recovery efficiency. As shown, adjusting the value of matrix permeability resulted in recovery efficiencies and per well recoveries more in line with that currently being realized by operators in the Utica.

Figure 16. Permeability Decay Correlation used for Estimating Matrix Permeability

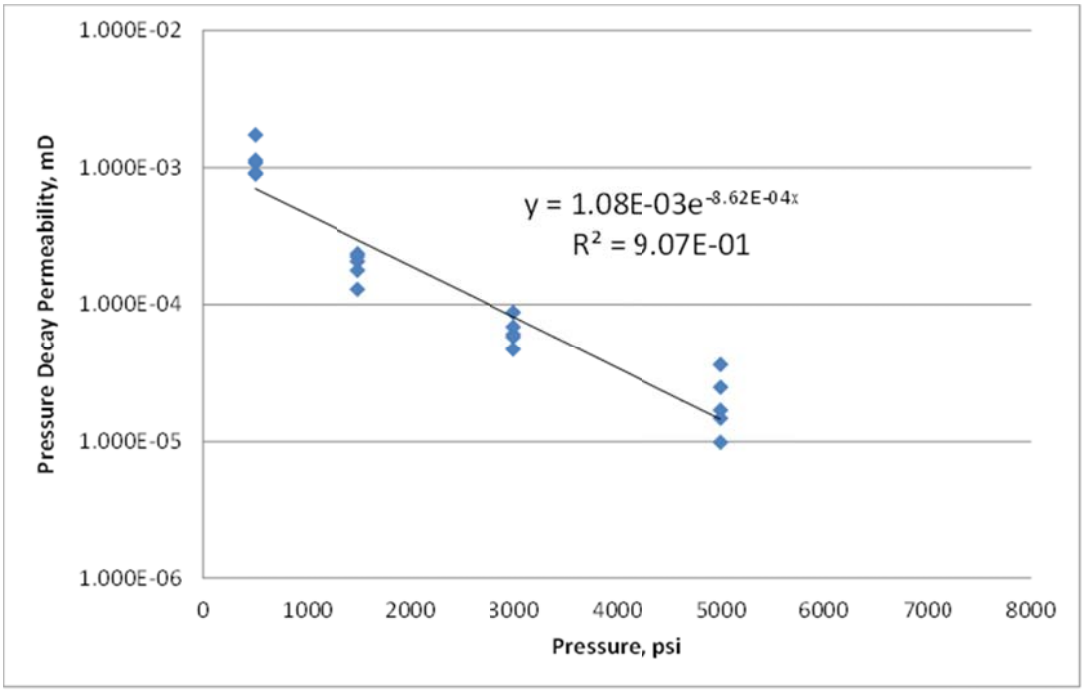


The adjusted matrix permeability values were used for all of the areas. Again, five cases were considered, one with no $CO_2$ injection, and four timing scenarios with $CO_2$ injection starting at 1, 5, 10, and 15 in the middle well. In all cases, production lasts 20 years after $CO_2$ injection starts. For these runs, for Areas 1 through 5, the producers are still completed in the Basal Utica Shale (layer 2), whereas the injector was assumed to be completed in the Upper Utica Shale (Layer 1). For areas 6 through 11, the producers are still completed in the Point Pleasant Shale Rich Zone (layer 3) and the injector is assumed to be completed in the Upper Utica Shale (Layer 1).

The results are summarized in **Table 21**. As shown, average methane recovery per 80 acre unit ranges 0.17 to 6.5 Bcf, and average cumulative volumes of $CO_2$ injected/ stored for the 80 acre unit range from minimal levels to as much as 4.29 Bcf. Little or no $CO_2$ breakthrough was experienced in the scenarios considered. However, in a number of scenarios, very low permeability and other factors contributed to minimal cumulative production volumes, as well as minimal volumes of $CO_2$ that could be stored.

Table 20. Impact of Assumed Matrix Permeability on the Results of the Simulation Runs for the Utica Shale Model Areas

| | | Area 1 | Area 2 | Area 3 | Area 4 | Area 5 | Area 6 | Area 7 | Area 8 | Area 9 | Area 10 | Area 11 |
|---|---|---|---|---|---|---|---|---|---|---|---|---|
| From Log Data | Cum $CH_4$ Production (Bcf) | 3.7 | 1.98 | 8.3 | 8.4 | 8.8 | 7.5 | 6.68 | 4.42 | 3.57 | 2.37 | 2.67 |
| | Recovery (%) | 68.6 | 71.6 | 69.2 | 52.7 | 59.9 | 59.6 | 57.4 | 59.8 | 54 | 52.3 | 71.3 |
| Permeability Decay Correlation | Cum $CH_4$ Production (Bcf) | 2.1 | 1.23 | 1.74 | 1.34 | 4.6 | 0.36 | 0.1 | 0.74 | 0.48 | 0.1 | 0.5 |
| | Recovery (%) | 38.4 | 44.6 | 14.6 | 8.4 | 31.3 | 2.9 | 0.8 | 10 | 7.2 | 2.5 | 13 |

Table 21. Methane Recovery and $CO_2$ Storage for Case 2 Completion Strategy for Alternative Injection Timing Scenarios – All Utica Areas

| | Area 1 | | | | Area 2 | | | | Area 3 | | | |
|---|---|---|---|---|---|---|---|---|---|---|---|---|
| | Cum $CH_4$ Prod (Bcf) | Recovery (%) | Cum $CO_2$ Inj (Bcf) | Cum $CO_2$ Prod (Bcf) | Cum $CH_4$ Prod (Bcf) | Recovery (%) | Cum $CO_2$ Inj (Bcf) | Cum $CO_2$ Prod (Bcf) | Cum $CH_4$ Prod (Bcf) | Recovery (%) | Cum $CO_2$ Inj (Bcf) | Cum $CO_2$ Prod (Bcf) |
| **No Inj 21** | 2.88 | 53.0 | - | - | 1.75 | 63.2 | - | - | 2.79 | 23.4 | - | - |
| **No Inj 25** | 3.02 | 55.6 | - | - | 1.82 | 65.7 | - | - | 3.08 | 25.8 | - | - |
| **No Inj 30** | 3.16 | 58.2 | - | - | 1.90 | 68.6 | - | - | 3.39 | 28.4 | - | - |
| **No Inj 35** | 3.28 | 60.4 | - | - | 1.96 | 70.8 | - | - | 3.66 | 30.7 | - | - |
| **EGR 21** | 2.65 | 47.0 | 2.73 | 0 | 1.61 | 52.0 | 1.89 | 0 | 1.91 | 16 | 0.47 | 0 |
| **EGR 25** | 2.91 | 51.7 | 3.12 | 0 | 1.82 | 59.0 | 2.39 | 0.01 | 2.35 | 19.7 | 0.61 | 0 |
| **EGR 30** | 3.08 | 54.7 | 3.21 | 0 | 1.93 | 62.3 | 2.57 | 0.03 | 2.78 | 23.3 | 0.71 | 0 |
| **EGR 35** | 3.2 | 56.9 | 3.19 | 0 | 1.99 | 64.4 | 2.66 | 0.01 | 3.15 | 26.4 | 0.79 | 0 |
| **Average per 80 acres** | **3.02** | | **3.06** | | **1.85** | | **2.38** | | **2.89** | | **0.65** | |

| | Area 4 | | | | Area 5 | | | | Area 6 | | | |
|---|---|---|---|---|---|---|---|---|---|---|---|---|
| | Cum $CH_4$ Prod (Bcf) | Recovery (%) | Cum $CO_2$ Inj (Bcf) | Cum $CO_2$ Prod (Bcf) | Cum $CH_4$ Prod (Bcf) | Recovery (%) | Cum $CO_2$ Inj (Bcf) | Cum $CO_2$ Prod (Bcf) | Cum $CH_4$ Prod (Bcf) | Recovery (%) | Cum $CO_2$ Inj (Bcf) | Cum $CO_2$ Prod (Bcf) |
| **No Inj 21** | 2.00 | 12.6 | - | - | 6.17 | 42.0 | - | - | 0.7 | 5.6 | - | - |
| **No Inj 25** | 2.23 | 14.0 | - | - | 6.58 | 44.8 | - | - | 0.81 | 6.4 | - | - |
| **No Inj 30** | 2.50 | 15.7 | - | - | 7.00 | 47.6 | - | - | 0.95 | 7.6 | - | - |
| **No Inj 35** | 2.73 | 17.2 | - | - | 7.35 | 50.0 | - | - | 1.08 | 8.6 | - | - |
| **EGR 21** | 1.43 | 9.0 | 0.08 | 0 | 5.31 | 36.1 | 3.60 | 0 | 0.4 | 3.2 | 0.0003 | 0 |
| **EGR 25** | 1.74 | 10.9 | 0.14 | 0 | 6.00 | 40.9 | 4.27 | 0 | 0.54 | 4.3 | 0.0090 | 0 |
| **EGR 30** | 2.06 | 13.0 | 0.19 | 0 | 6.59 | 44.9 | 4.60 | 0 | 0.69 | 5.5 | 0.0200 | 0 |
| **EGR 35** | 2.35 | 14.8 | 0.23 | 0 | 7.02 | 47.8 | 4.69 | 0 | 0.83 | 6.6 | 0.0300 | 0 |
| **Average per 80 acres** | **2.13** | | **0.16** | | **6.50** | | **4.29** | | **0.75** | | **0.01** | |

| | Area 7 | | | | Area 8 | | | | Area 9 | | | |
|---|---|---|---|---|---|---|---|---|---|---|---|---|
| | Cum $CH_4$ Prod (Bcf) | Recovery (%) | Cum $CO_2$ Inj (Bcf) | Cum $CO_2$ Prod (Bcf) | Cum $CH_4$ Prod (Bcf) | Recovery (%) | Cum $CO_2$ Inj (Bcf) | Cum $CO_2$ Prod (Bcf) | Cum $CH_4$ Prod (Bcf) | Recovery (%) | Cum $CO_2$ Inj (Bcf) | Cum $CO_2$ Prod (Bcf) |
| **No Inj 21** | 0.15 | 1.3 | - | - | 1.09 | 14.7 | - | - | 0.61 | 9.2 | - | - |
| **No Inj 25** | 0.17 | 1.5 | - | - | 1.25 | 16.9 | - | - | 0.69 | 10.4 | - | - |
| **No Inj 30** | 0.20 | 1.7 | - | - | 1.43 | 19.4 | - | - | 0.79 | 12.0 | - | - |
| **No Inj 35** | 0.23 | 2.0 | - | - | 1.60 | 21.7 | - | - | 0.88 | 13.3 | - | - |
| **EGR 21** | 0.11 | 0.9 | 0.000 | 0.00 | 0.79 | 10.7 | 0.040 | 0 | 0.50 | 7.6 | 0.010 | 0 |
| **EGR 25** | 0.13 | 1.1 | 0.000 | 0.00 | 0.97 | 13.2 | 0.060 | 0 | 0.59 | 9.0 | 0.016 | 0 |
| **EGR 30** | 0.17 | 1.4 | 0.001 | 0.00 | 1.18 | 16.0 | 0.067 | 0 | 0.70 | 10.5 | 0.020 | 0 |
| **EGR 35** | 0.20 | 1.7 | 0.002 | 0.00 | 1.37 | 18.5 | 0.077 | 0 | 0.79 | 12.0 | 0.023 | 0 |
| **Average per 80 acres** | **0.17** | | **0.00** | | **1.21** | | **0.06** | | **0.69** | | **0.02** | |

| | Area 10 | | | | Area 11 | | | |
|---|---|---|---|---|---|---|---|---|
| | Cum $CH_4$ Prod (Bcf) | Recovery (%) | Cum $CO_2$ Inj (Bcf) | Cum $CO_2$ Prod (Bcf) | Cum $CH_4$ Prod (Bcf) | Recovery (%) | Cum $CO_2$ Inj (Bcf) | Cum $CO_2$ Prod (Bcf) |
| **No Inj 21** | 0.15 | 3.3 | - | - | 0.75 | 20.0 | - | - |
| **No Inj 25** | 0.17 | 3.8 | - | - | 0.85 | 22.7 | - | - |
| **No Inj 30** | 0.20 | 4.4 | - | - | 0.96 | 25.6 | - | - |
| **No Inj 35** | 0.23 | 5.1 | - | - | 1.06 | 28.3 | - | - |
| **EGR 21** | 0.12 | 2.6 | 0.003 | 0 | 0.52 | 14.0 | 0.040 | 0 |
| **EGR 25** | 0.14 | 3.1 | 0.004 | 0 | 0.6 | 17.2 | 0.054 | 0 |
| **EGR 30** | 0.17 | 3.7 | 0.005 | 0 | 0.78 | 20.7 | 0.066 | 0 |
| **EGR 35** | 0.19 | 4.3 | 0.006 | 0 | 0.89 | 23.9 | 0.076 | 0 |
| **Average per 80 acres** | **0.17** | | **0.00** | | **0.81** | | **0.06** | |

## c. Economic Analyses

The engineering costing and cash flow analysis approach described above for the Marcellus Shale was also comparably applied to the Utica. For the Utica, economics were initially run on two areas -- Area 3 and Area 5.

Economic results for these analyses are shown in **Table 22** and **23**. Table 23 shows the results for Area 5, with the highest level of production and injection of all the areas in the Utica Shale. Again shown are the IRR and NPV realized for three wellhead gas prices ($5.00, $3.60 and $6.00 per Mcf). Also shown for the four injection scenarios is a $CO_2$ emission reduction credit or carbon tax value (in $/tonne of $CO_2$) that would be necessary for the project to yield a 10 percent IRR. While this case is economic without $CO_2$ injection at prices of $5.00 and $6.00 per Mcf, the EGR cases are not always economic except when primary production takes place for 5 to 10 years (depending on gas price) before $CO_2$ injection is initiated. Again depending on wellhead gas prices, carbon credits or emission reduction credit values as high as $5.40 per tonne may be required to ensure economic viability of $CO_2$ injection.

**Table 23** shows similar results for Area 3. However, in this case, the well productivities are considerably lower than for Area 5. As a result, higher gas prices are necessary to achieve economic viability with just traditional production. In fact, prices of at least $7.50 per Mcf may be required even to achieve economic viability with traditional production. Assuming natural gas prices of $7.50 and $9.00 per Mcf, almost all of the EGR cases are not economic without credits. Again depending on wellhead gas prices, credit values will need to be much higher than those required for Area 5 to ensure economic viability for EGR, ranging from $10 to $54 per tonne.

Finally, all of the areas in the Utica have well productivities lower that Area 3 except for Areas 1 and 5. Thus, at these prices, the achieving commercial viability for EGR and $CO_2$ storage in the Utica is likely to be challenging without incentives.

Table 22: Economics of Methane Recovery and $CO_2$ Storage for Several Injection Timing Scenarios – Utica Area 5 – Case 2 – Three Wellhead Gas Prices

| | $5.00 /Mcf Wellhead Gas Price | | |
|---|---|---|---|
| | IRR (%) | NPV ($MM) | Credit Price to achieve 10% IRR ($/tonne) |
| No Injection | 12 | 4.33 | NA |
| $CO_2$ Injection for 20 years | | | |
| 1 yr Primary + 20 (EGR 21) | <10 | -1.95 | $2.70 |
| 5 yrs Primary + 20 (EGR 25) | 10 | 0.62 | none |
| 10 yrs Primary + 20 (EGR 30) | 11 | 2.91 | none |
| 15 yrs Primary + 20 (EGR 35) | 11 | 3.19 | none |

| | $3.60 /Mcf Wellhead Gas Price | | |
|---|---|---|---|
| | IRR (%) | NPV ($MM) | Credit Price to achieve 10% IRR ($/tonne) |
| No Injection | 11 | 1.87 | NA |
| $CO_2$ Injection for 20 years | | | |
| 1 yr Primary + 20 (EGR 21) | 9 | -3.87 | $5.40 |
| 5 yrs Primary + 20 (EGR 25) | 9 | -1.61 | $2.80 |
| 10 yrs Primary + 20 (EGR 30) | <10 | -0.07 | $0.20 |
| 15 yrs Primary + 20 (EGR 35) | 10 | 0.08 | none |

| | $6.00 /Mcf Wellhead Gas Price | | |
|---|---|---|---|
| | IRR (%) | NPV ($MM) | Credit Price to achieve 10% IRR ($/tonne) |
| No Injection | 12 | 6.08 | NA |
| $CO_2$ Injection for 20 years | | | |
| 1 yr Primary + 20 (EGR 21) | <10 | -0.57 | $0.80 |
| 5 yrs Primary + 20 (EGR 25) | 11 | 2.20 | none |
| 10 yrs Primary + 20 (EGR 30) | 11 | 3.98 | none |
| 15 yrs Primary + 20 (EGR 35) | 12 | 4.91 | none |

Table 23: Economics of Methane Recovery and $CO_2$ Storage for Several Injection Timing Scenarios – Utica Area 3 – Case 2 - Two Wellhead Gas Prices

| | $7.50 /Mcf Wellhead Gas Price | | |
|---|---|---|---|
| | IRR (%) | NPV ($MM) | Credit Price to achieve 10% IRR ($/tonne) |
| No Injection | 10 | 0.37 | NA |
| $CO_2$ Injection for 20 years | | | |
| 1 yr Primary + 20 (EGR 21) | 8 | -5.24 | $54 |
| 5 yrs Primary + 20 (EGR 25) | 9 | -3.08 | $35 |
| 10 yrs Primary + 20 (EGR 30) | 9 | -1.55 | $25 |
| 15 yrs Primary + 20 (EGR 35) | <10 | -0.71 | $18 |

| | $9.00 /Mcf Wellhead Gas Price | | |
|---|---|---|---|
| | IRR (%) | NPV ($MM) | Credit Price to achieve 10% IRR ($/tonne) |
| No Injection | 11 | 1.42 | NA |
| $CO_2$ Injection for 20 years | | | |
| 1 yr Primary + 20 (EGR 21) | 8 | -4.55 | $47 |
| 5 yrs Primary + 20 (EGR 25) | 9 | -2.22 | $25 |
| 10 yrs Primary + 20 (EGR 30) | <10 | -0.59 | $10 |
| 15 yrs Primary + 20 (EGR 35) | 10 | 0.30 | none |

## d. Potential for Enhanced Gas Recovery and $CO_2$ Storage

Like that for the Marcellus, the same steps were pursued to determine what portion of the estimated total methane gas in place and the theoretical maximum $CO_2$ storage capacity in the Utica shale would actually be accessible. For this, the following was assumed:

- The total area of each of the areas was divided by 80 acres (the assumption for the recoveries per well in Table 21) to determine the number of wells would be required to develop all of the acreage in each of the nine study areas.
- An estimate of the number of accessible well sites was made based on the assumption that only half of the total number of well sites in each area would be accessible for development.
- Based on the results summarized in Tables 22 and 23, it was assumed that only areas with estimated cumulative production per well better than those associated with Area 3 would likely be economic to develop under primary methane recovery. The assumption is only those areas that are determined to be economic to pursue at prices of $7.50 per Mcf would be a likely candidate for subsequent enhanced recovery via $CO_2$ injection. This is a somewhat higher price than that assumed for the Marcellus. Only areas 1, 3, and 5 meet this condition.
- For these areas, it was assumed that only half of the area would have properties as good as or better than that assumed in the simulation runs. Based on that, only half of the accessible well sites would be economically feasible to pursue.

The results of the application of this approach are shown in **Table 24** (those areas expected to be economic at $7.50 per Mcf are highlighted in yellow). In summary, the results indicate that about 104 Bcf of methane is recoverable in the Utica Shale at natural gas prices of $7.50 per Mcf, out of about 208 Tcf that could be considered technically recoverable and reasonably accessible. This potential amounts the potential for storing 150 Tcf (or 8 Gt) of $CO_2$.

Table 24: Methane Recovery and $CO_2$ Storage Potential for the Utica Shale

| | Total Area, Acres | Total Area, miles$^2$ | Estimated Total Gas In-Place, Bcf | Estimated Theoretical Maximum $CO_2$ Storage, Bcf | No. of Wells at 80-Acre Spacing | No. of Accessible, Feasible Well Sites | $CH_4$ Production per Well (Bcf) | $CO_2$ Stored per Well (Bcf) | Technical $CH_4$ Production Potential (Bcf) | Technical $CH_4$ Production Potential Better than Average(Bcf) | $CO_2$ Storage Potential (Bcf) | $CO_2$ Storage Potential (MMtonne) |
|---|---|---|---|---|---|---|---|---|---|---|---|---|
| Area 1 | 4,050,794 | 6,329 | 159,900 | 16,150 | 50,635 | 25,317 | 3.02 | 3.06 | 76,522 | 38,261 | 77,535 | 4,102 |
| Area 2 | 1,992,915 | 3,114 | 19,100 | 1,990 | 24,911 | 12,456 | 1.85 | 2.38 | 23,012 | 11,506 | 29,613 | 1,567 |
| Area 3 | 1,793,827 | 2,803 | 154,900 | 13,910 | 22,423 | 11,211 | 2.89 | 0.65 | 32,387 | 16,193 | 7,231 | 383 |
| Area 4 | 1,572,025 | 2,456 | 254,100 | 21,510 | 19,650 | 9,825 | 2.13 | 0.16 | 20,928 | 10,464 | 1,572 | 83 |
| Area 5 | 2,451,694 | 3,831 | 312,800 | 33,890 | 30,646 | 15,323 | 6.50 | 4.29 | 99,638 | 49,819 | 65,736 | 3,478 |
| Area 6 | 6,777,578 | 10,590 | 1,046,300 | 92,800 | 84,720 | 42,360 | 0.75 | 0.01 | 31,770 | 15,885 | 628 | 33 |
| Area 7 | 7,170,236 | 11,204 | 946,100 | 86,450 | 89,628 | 44,814 | 0.17 | 0.00 | 7,618 | 3,809 | 34 | 2 |
| Area 8 | 4,133,518 | 6,459 | 358,700 | 39,100 | 51,669 | 25,834 | 1.21 | 0.06 | 31,260 | 15,630 | 1,576 | 83 |
| Area 9 | 1,948,414 | 3,044 | 131,700 | 13,190 | 24,355 | 12,178 | 0.69 | 0.02 | 8,448 | 4,224 | 210 | 11 |
| Area 11 | 3,421,544 | 5,346 | 170,500 | 15,280 | 42,769 | 21,385 | 0.17 | 0.00 | 3,662 | 1,831 | 96 | 5 |
| Area 12 | 1,751,393 | 2,737 | 63,600 | 6,160 | 21,892 | 10,946 | 0.81 | 0.06 | 8,825 | 4,413 | 646 | 34 |
| | 37,063,938 | 57,913 | 3,617,700 | 340,430 | 463,299 | 231,650 | | | 344,071 | 172,035 | 184,877 | 9,782 |
| | | | | | | | | | | | | |
| Economic Areas @ $7.50/Mcf -- 1,3,5 | | | | | | | | | 208,547 | 104,274 | 150,502 | 7,963 |
| | | | | | | | | | | | | |
| | Assumes | 50% | of well sites are accessible | | | | | | | | | |
| | | 50% | of the accessible well sites are better than average | | | | | | | | | |

# 5. ANTRIM SHALE

## a. Approach for and Results from History Matching

Relative to the Utica shale and to a lesser extent the Marcellus shale, gas production from the Antrim shale has been taking place for some time, and the target wells for EGR and $CO_2$ storage are likely to be mature vertically competed wells. This is unlike the typical horizontal wells that are characteristic of the less-mature Utica and Marcellus shales.

Therefore, history matching of production from Antrim shale gas wells consisted in matching production data from a "typical" vertical Antrim shale gas well. The "typical" Antrim shale gas well is this assessment was assumed to be vertically completed in both the Lachine and the Norwood intervals, and is drilled on 80-acre spacing. Traditionally, relatively small (relative to today's practice), single-stage hydraulic stimulations were performed in the targeted formations. The typical vertical well is consistent with that assumed in the work of Zuber et al. (1994).

After 30 years, the "typical" well is assumed to produce 505 million cubic feet (MMcf) of gas and 185,000 barrels of water. Based on Zuber et al (1994), initial gas in place is assumed to be 1.39 Bcf per 80 acres.

**Figures 17** and **18** below show the "typical" Antrim shale gas well production data for gas and water, respectively.

Figure 17: "Typical" Antrim Shale Gas Well – Gas Production Rate

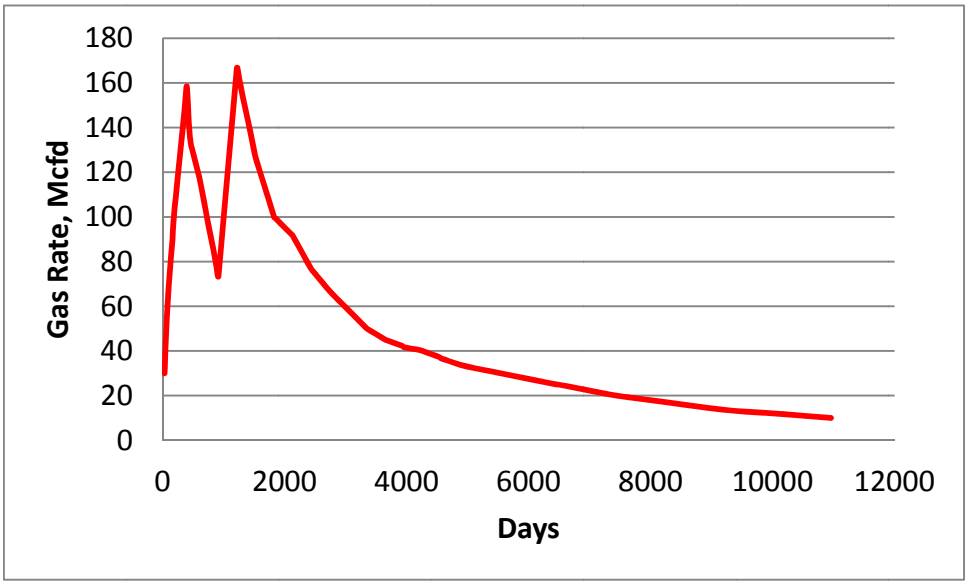

Figure 18: "Typical" Antrim Shale Gas Well – Water Production Rate

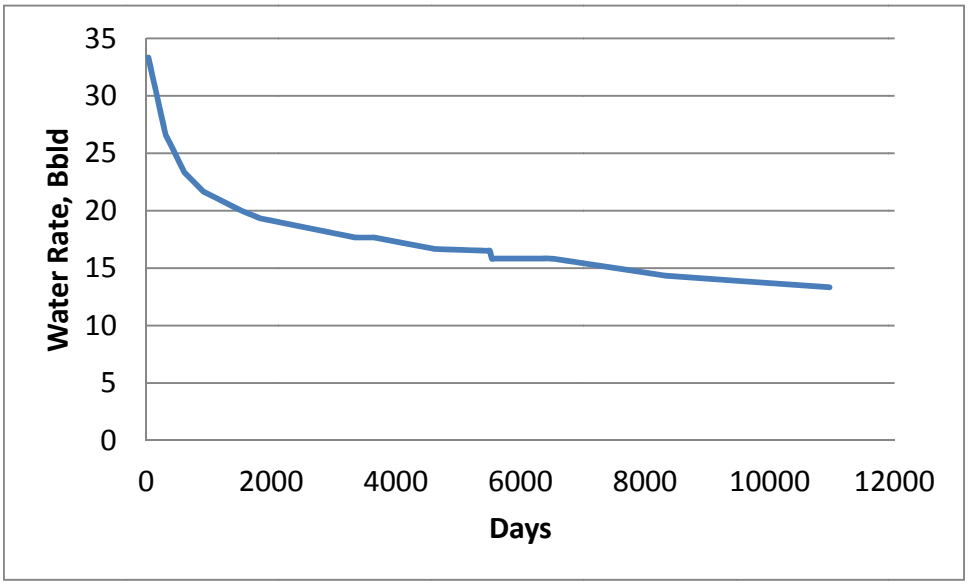


Advanced Resources' COMET3$^{TM}$ dual-porosity model was run on an 80-acre spacing with one vertical well completed and stimulated in both the Lachine and the Norwood shales, and run for 30 years in order to compare cumulative production with the "typical" Antrim well.

The methane isotherms were computed as an average from those reported by Zuber et al. (1994) and those reported by Lancaster and Hill (1993), and are shown in **Figure 19**. These were compared with $CO_2$ isotherms published by the Midwest Regional Carbon Sequestration Partnership, which developed an initial estimate of theoretical $CO_2$ storage capacity for the Antrim and Ohio Shales, by applying $CO_2$ adsorption isotherms obtained for the Ohio Shale in the Appalachian Basin to the Antrim (Wickstrom and others, 2005).

**Table 25** summarizes the Antrim shale reservoir properties used to obtain a match for the "typical" well.

It is worth mentioning the thicknesses for both the Lachine and the Norwood as the Lachine is on average 90 feet thick, whereas the Norwood is on average 30 feet thick. Using the available isotherms to achieve a representative match of the data, thickness had to be reduced. An explanation could be that the full thickness is not contributing to the production. Another possibility would be that the isotherms are too high, or it could be that a combination of the two (isotherms and thickness) needs to be altered. Feeling quite confident with the isotherms, the decision was made to reduce the assumed net thickness contributing to production.

Figure 19: Methane and Carbone Dioxide Isotherms

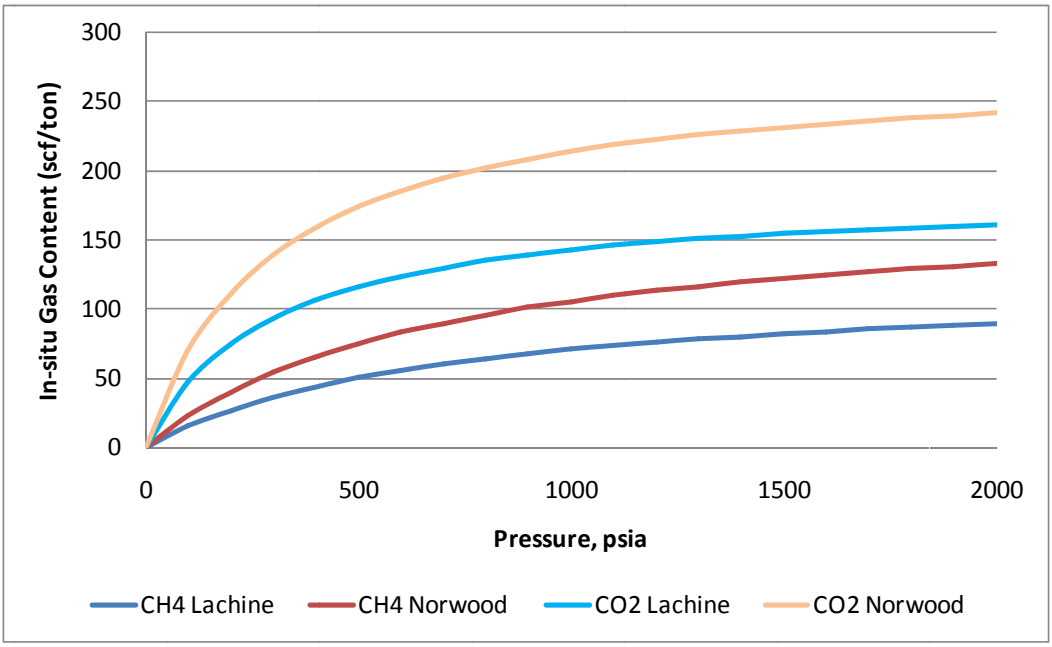


Table 25. Antrim Shale Reservoir Properties Used to Obtain Match for "Typical" Well

| Parameter | Value | Units |
|---|---|---|
| Pattern Area | 80 | Acres |
| Depth | | |
| - Lachine | 1,500 | feet |
| - Norwood | 1,620 | feet |
| Reservoir Pressure Gradient | 0.31 | psig/ft |
| Thickness | | |
| - Lachine | 33 | feet |
| - Norwood | 11 | feet |
| Reservoir Temperature | 76 | deg. Farenheit |
| Initial Water Saturation (Fracture and Matrix) | 50 | % |
| Porosity (Fracture and Matrix) | 1.5 | % |
| Permeability (Fracture and Matrix) | 3.6 | mD |
| Stimulation Effectiveness | -2 | - |
| In-situ Methane Langmuir Volume | | |
| - Lachine | 120 | scf/ton |
| - Norwood | 179 | scf/ton |
| Methane Langmuir Pressure | 700 | psia |

The results from the history-match are shown in **Figure 20**. Cumulative gas production from the history-match is 520 MMcf, in good accordance with the value from the "typical" Antrim well.

Figure 20: Gas and Water Rate History-Match for Typical Antrim Well

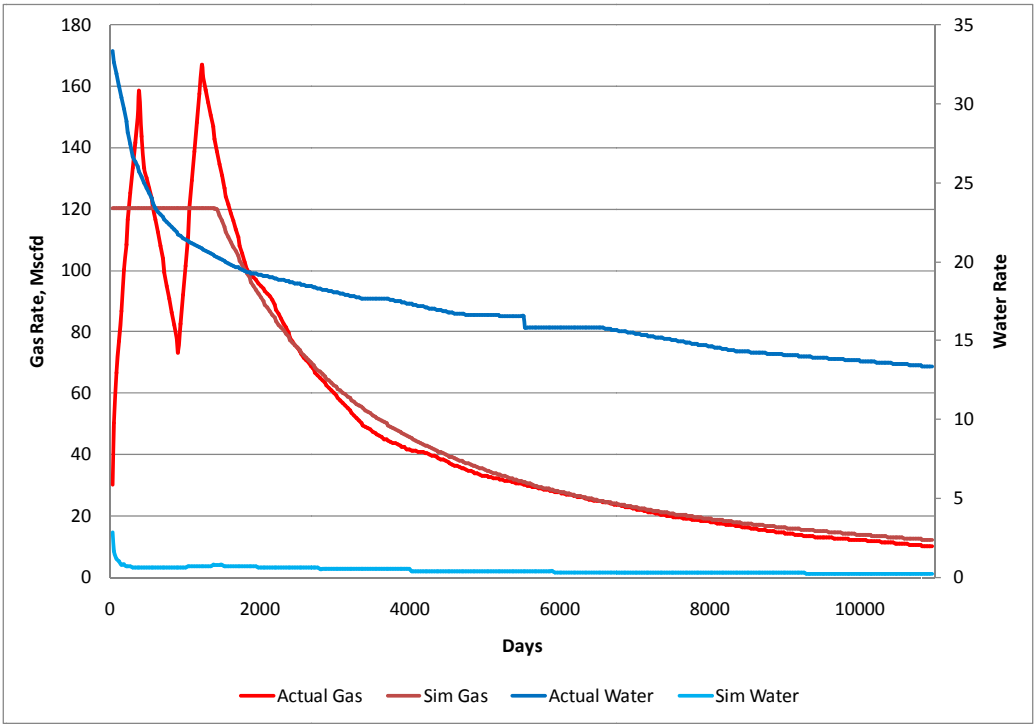


## b. Development of Input Data for $CO_2$-EGR and Storage Cases

Three model areas are proposed for the Antrim Shale: 1) the northern shallow biogenic gas play area; 2) the thermogenic Antrim play area in the central Michigan Basin, and 3) a hypothetical southern shallow biogenic gas play on the southern rim of the basin. The three model areas are shown in **Figure 21**. Model well parameters for reservoir simulation are generalized based on published Antrim data and analyses and previous modeling of the Antrim shallow biogenic gas play conducted by Advanced Resources.

Figure 21: Antrim Shale Cross-Sections and Model Areas

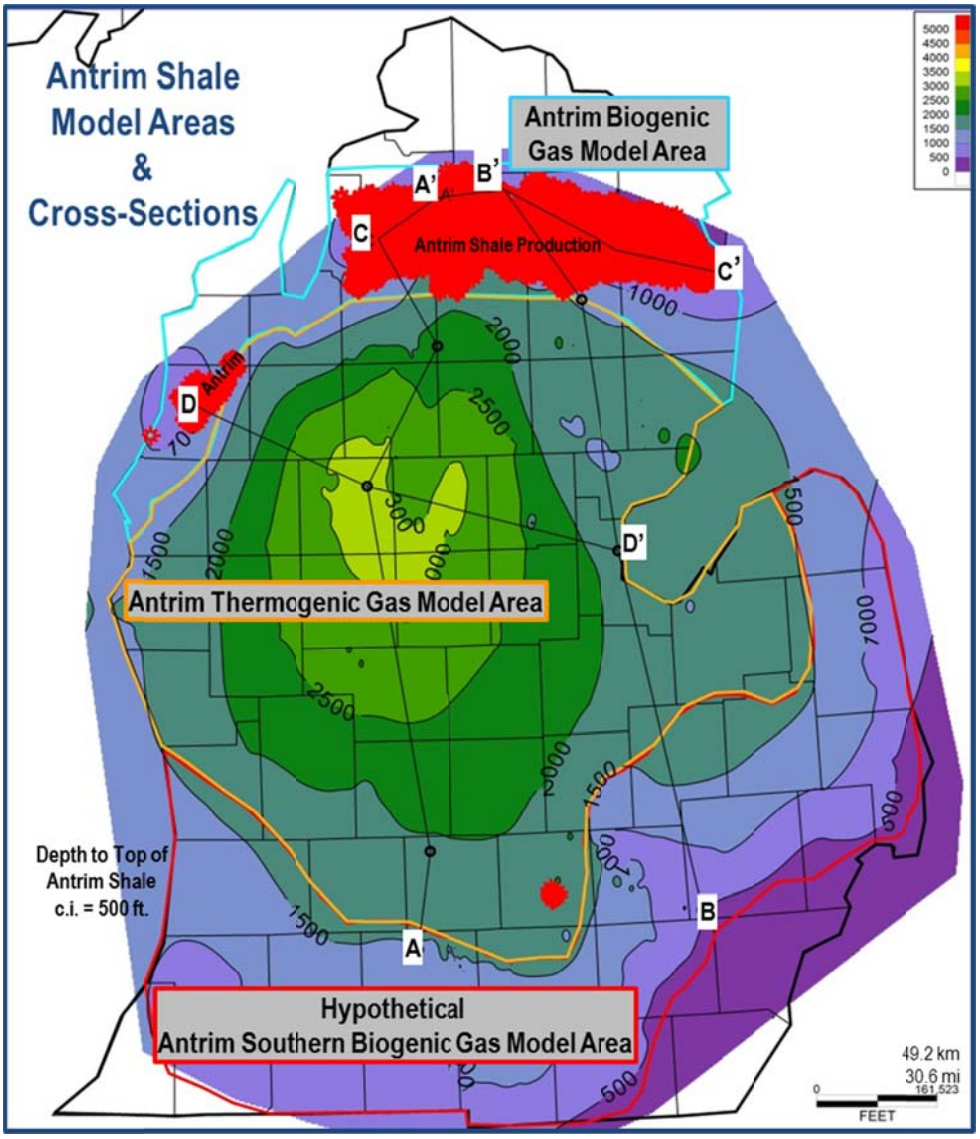


The northern shallow biogenic gas model area is the only model area of the three for which reservoir simulation of EGR and $CO_2$ injection and storage is practical. Therefore, it is the only area for which $CO_2$ injection simulations were performed. Only the northern shallow biogenic gas play has enough Antrim production data and known reservoir parameters to produce meaningful simulation results. The model area for the thermogenic Antrim gas play has very little Antrim production data, and little supporting data to estimate essential input parameters for reservoir simulation.

Very little published methane isotherm data are available for the Antrim Shale in the Michigan Basin. **Table 26** summarizes the available methane adsorption isotherm data obtained for this analysis. The average Langmuir volume for all three samples is 122.1 scf/ton and the average Langmuir pressure is 711.2 psia. The average Langmuir parameters are applied to both the Lachine and Norwood Antrim Shale members to estimate adsorbed gas content.

Table 26. Summary of Methane Adsorption Isotherm Data for the Antrim Shale

| Interval | He Porosity, fraction | Langmuir Volume, VL, (scf/ton) | Langmuir Pressure, PL, (psia) | Source |
|---|---|---|---|---|
| Lachine | 0.074 (total porosity) | 122.8 | 654.8 | Nomeco Bagley East B3-11 Well, Otsego Co., MI Sample depth 1,360.6' – 1,361', reported in Lancaster and Hill, 1993 |
| Lachine | 0.090 (total porosity) | 145.6 | 749.3 | Nomeco Bagley East B3-11 Well, Otsego Co., MI Sample depth 1,360.6' – 1,361', reported in Lancaster and Hill, 1993 |
| Antrim (not differentiated) | 0.03 (gas-filled porosity) | 97.8 | 729.5 | Zuber, Frantz and Gatens, 1994. |
| Average | | 122.1 | 711.2 | |

Since no Antrim $CO_2$ adsorption isotherm data were available for this analysis, it was estimated that $CO_2$ is preferentially adsorbed by a factor of 2, so assumed a Langmuir volume for $CO_2$ that is two times the Langmuir volume for methane. Thus, the average $CO_2$ Langmuir volume assumed is 244.1 scf/ton.

Based on the analyses described in Volume 4, the estimated model area parameters for calculating gas in-place, maximum $CO_2$ storage capacity, and to provide the starting point for reservoir simulation are summarized in **Table 27**. Included are the model areas, estimated reservoir pressure gradient, extrapolated mean reservoir pressure and temperature, and estimated formation volume factor for methane and $CO_2$. **Table 28** summarizes average model well attributes for each model area that are incorporated into the reservoir simulation. The key model well attributes provided in these tables include the average depth of the layer, thickness, average total porosity, average permeability, average calculated water saturation, average TOC, average bulk density, and adsorbed gas content (scf/ton).

Table 27. Description and Summary of Antrim Shale Model Areas

| Description and Summary of Antrim Model Areas | | | | | | | | | |
|---|---|---|---|---|---|---|---|---|---|
| MODEL AREA | Area Description | Total Area, Acres | Total Area, miles$^2$ | Estimated Reservoir Pressure Gradient, psi/ft. | Estimated $CO_2$ Content in Gas Stream, fraction | Est. Reservoir Pressure, psia | Est. Reservoir Temperature, $^0$F | Est. FVF for Methane, ft$^3$/scf | Est. FVF for $CO_2$, ft$^3$/scf |
| AREA 1 | Antrim Shale Shallow Biogenic Gas Play – Northern Basin | 3,462,962 | 5,411 | 0.31 | 0.30 | 500 | 70 | 0.02748 | 0.02353 |
| AREA 2 | Antrim Shale Deep Thermogenic Gas Play – Central Basin | 12,349,068 | 19,295 | 0.43 | 0 | 1,100 | 85 | 0.01686 | 0.01251 |
| AREA 3 | Hypothetical Shallow Biogenic Gas Play in Southern Basin | *7,713,139* | *12,052* | *0.31* | *0.10* | *500* | *70* | *0.02748* | *0.02353* |
| Total for Areas 1 and 2 | | 15,812,030 | 24,706 | | | | | | |

Table 28. Model Layer Attributes for the Lachine and Norwood Members of the Antrim Shale

| Attribute | Lachine | Norwood |
|---|---|---|
| Thickness, ft. | 90 | 30 |
| Total Porosity, fraction | 0.09 | .09 |
| Matrix Permeability, mD | 2.00E-8 | 2.00E-8 |
| Average Total Oil + Water Saturation, fraction | 0.61 | 0.61 |
| Gas- Filled Porosity, Fraction | 0.035 | 0.035 |
| Average Bulk Density, g/cc | 2.36 | 2.27 |
| Average TOC, % | 8.0 | 11.0 |
| Methane Isotherm Average Langmuir Volume, $V_L$, scf/ton | 122.1 | 122.1 |
| $CO_2$ Isotherm Average Langmuir Volume, $V_L$, scf/ton | 244.2 | 244.2 |
| Average Langmuir Pressure, $P_L$, psia | 711.2 | 711.2 |
| Adsorbed Gas Content, scf/ton (Area 1; Biogenic Gas Play, Northern Basin) | 48.3 | 50.5 |
| Adsorbed Gas Content, scf/ton (Area 2; Thermogenic Gas Play, Central Basin) | 73.5 | 74.8 |
| Maximum Adsorbed $CO_2$ Content, scf/ton (Area 1; Biogenic Gas Play, Northern Basin) | 96.5 | 101.1 |
| Maximum Adsorbed $CO_2$ Content, scf/ton (Area 2; Thermogenic Gas Play, Central Basin) | 147.0 | 149.7 |

## c. Development of Simulation Scenarios for $CO_2$-EGR/Storage Cases

As stated above, the reservoir simulation approach for the Antrim shale was different than that performed for the Marcellus and Utica Shales. In the relatively immature (in terms of development) Marcellus and Utica Shales, the standard well drilling practice is a horizontal well, assumed to be at 80 acre spacing. The Antrim Shale, in contrast, is a more mature play, with a long history of development, with most of the older wells (the primary target for EGR with $CO_2$ injection) drilled vertically. Thus, well production simulations for the Antrim were assumed to be vertically completed and stimulated in both the Lachine and Norwood intervals, drilled on 80-acre spacing. Relatively small (relative to today's practice), single-stage hydraulic stimulations were assumed to be performed in both the Lachine and Norwood intervals, consistent with traditional practices in the Antrim shale.

Each well was assumed to produce at 25 psia wellhead pressure for a period of time. When the commencement of $CO_2$ injection was assumed, a new well was assumed to be drilled between the wells on 80-acre spacing, and $CO_2$ was injected into that well. The injection wells were assumed to be drilled and completed in the same way as the production wells. Like the other cases, the area between the injection and production wells was considered fractured, with fracture permeability 250 times the matrix permeability.

Four cases were considered, one with no $CO_2$ injection, and four timing scenarios. In these cases, all 80-acre patterns were assumed to produce for 45 years, with different timing scenarios for when injection commences. The scenarios assumed are as follows:

- Produce well without EGR for 45 years
- Produce well for 15 years, inject $CO_2$ for EGR for 30 years
- Produce well for 20 years, inject $CO_2$ for EGR for 25 years
- Produce well for 25 years, inject $CO_2$ for EGR for 20 years

The cumulative methane recovery, percent recovery, $CO_2$ produced, and $CO_2$ injected for a pair of wells (one producer and one injector) are summarized below:

| | Cum $CH_4$ (Bcf) | Recovery (%) | Produced $CO_2$ (Bcf) | Injected $CO_2$ (Bcf) |
|---|---|---|---|---|
| No injection | 0.56 | 52.9 | 0.10 | - |
| Produce 15 years, inject 30 years | 0.74 | 69.5 | 2.17 | 3.80 |
| Produce 20 years, inject 25 years | 0.74 | 69.4 | 1.64 | 3.26 |
| Produce 25 years, inject 20 years | 0.74 | 69.1 | 1.10 | 2.72 |

As shown, $CO_2$ injection in the Antrim shale shows much more improvement in recovery compared to that seen in the Marcellus and Utica shales. $CO_2$ injection results in enhanced gas recovery of 0.18 Bcf, and can store on the order of 1.5 Bcf per pattern. Also note that the gas from the Antrim shale already contains relatively higher amounts of $CO_2$, even without $CO_2$ injection, than the other shales assessed. In fact, 0.1 Bcf of $CO_2$ is produced even in the no injection case.

This potential was also examined by assuming wells are initially spaced at 40 acres, with similar results.

The engineering costing and cash flow analysis approach described above was applied to the Antrim shale, for just the northern shallow biogenic gas model area – Area 1.

Economic results for these analyses assuming 80-acre well spacing are summarized in **Table 29**. As shown, with traditional development practices, these wells are only marginally economic at natural gas prices of $9.00 per Mcf and higher. However, their economics do not change all that much with deployment of $CO_2$ injection and enhanced gas recovery. The incremental gas produced from $CO_2$ injection is better than that seen in the Marcellus and the Utica shales, and the incremental gas production from EGR offsets the added costs for the injection well, assuming that the $CO_2$ is available at no cost. Nonetheless, when gas prices are at or below $9.00 per Mcf, some incentives will likely be required to stimulate $CO_2$ injection and storage with EGR in the Antrim gas shale.

Developing the EGR project on 40-acre spacing, at least for the case where a well produces for 25 years before EGR begins, shows a slight improvement in economic viability, as shown in **Table 30**.

Table 29: Economics of Methane Recovery and $CO_2$ Storage for Several Injection Timing Scenarios – Antrim Shale, Area 1 - Three Wellhead Gas Prices – 80-Acre Spacing

| | $9.00 /Mcf Wellhead Gas Price | | |
|---|---|---|---|
| | IRR (%) | NPV ($MM) | Credit Price to achieve 10% IRR ($/tonne) |
| No Injection | 10 | 0.04 | NA |
| Produce 15 years, inject 30 years | <10 | -0.10 | $0.20 |
| Produce 20 years, inject 25 years | <10 | -0.20 | $0.30 |
| Produce 25 years, inject 20 years | 10 | 0.03 | none |

| | $10.00 /Mcf Wellhead Gas Price | | |
|---|---|---|---|
| | IRR (%) | NPV ($MM) | Credit Price to achieve 10% IRR ($/tonne) |
| No Injection | 10 | 0.17 | NA |
| Produce 15 years, inject 30 years | 10 | 0.03 | none |
| Produce 20 years, inject 25 years | 10 | 0.11 | none |
| Produce 25 years, inject 20 years | 10 | 0.13 | none |

| | $5.00 /Mcf Wellhead Gas Price | | |
|---|---|---|---|
| | IRR (%) | NPV ($MM) | Credit Price to achieve 10% IRR ($/tonne) |
| No Injection | 9 | -0.46 | NA |
| Produce 15 years, inject 30 years | 8 | -0.64 | $5.40 |
| Produce 20 years, inject 25 years | 8 | -0.54 | $7.40 |
| Produce 25 years, inject 20 years | 8 | -0.51 | $11.60 |

Table 30: Comparison of Economics of Methane Recovery and $CO_2$ Storage for Antrim Shale, Area 1 - Three Wellhead Gas Prices – 80-Acre vs. 40-Acre Spacing

| | $9.00 /Mcf Wellhead Gas Price | | |
|---|---|---|---|
| | IRR (%) | NPV ($MM) | Credit Price to achieve 10% IRR ($/tonne) |
| No Injection - 80 acre spacing | | | |
| 80 acre spacing | 10 | 0.04 | NA |
| 40 acre spacing | 10 | 0.08 | NA |
| Produce 25 years, inject 20 years | | | |
| 80 acre spacing | 10 | 0.03 | none |
| 40 acre spacing | 10 | 0.05 | none |

| | $9.00 /Mcf Wellhead Gas Price | | |
|---|---|---|---|
| | IRR (%) | NPV ($MM) | Credit Price to achieve 10% IRR ($/tonne) |
| No Injection - 80 acre spacing | | | |
| 80 acre spacing | 10 | 0.17 | NA |
| 40 acre spacing | 11 | 0.21 | NA |
| Produce 25 years, inject 20 years | | | |
| 80 acre spacing | 10 | 0.13 | none |
| 40 acre spacing | 10 | 0.19 | none |

| | $9.00 /Mcf Wellhead Gas Price | | |
|---|---|---|---|
| | IRR (%) | NPV ($MM) | Credit Price to achieve 10% IRR ($/tonne) |
| No Injection - 80 acre spacing | | | |
| 80 acre spacing | 9 | -0.46 | NA |
| 40 acre spacing | 9 | -0.44 | NA |
| Produce 25 years, inject 20 years | | | |
| 80 acre spacing | 8 | -0.51 | $11.60 |
| 40 acre spacing | 9 | -0.48 | $6.70 |

However, for a mature area like the Antrim shale, with a long history of development, it is probably more appropriate to assess the potential of $CO_2$ injection and EGR on an incremental basis. That is, the economic assessment should consider only the incremental costs associated with injecting $CO_2$, and the incremental production that results from that injection.

From the perspective of incremental economics, even at natural gas prices as high as $10.00 per Mcf, EGR from $CO_2$ injection is not economic. However, $CO_2$ emission reduction credits ranging from $1.00 to $1.50 per tonne are sufficient to bridge the economic shortfall.

Nonetheless, of the three areas investigated, the Antrim shale probably has the best characteristics for EGR from $CO_2$ injection. The assessments performed here assumed the traditional development practice for each basin. The Marcellus and Utica shales, since they are considerably less mature, are taking advantage of more modern horizontal drilling practices and very large, multi-stage hydraulic fracturing. The Antrim shale, on the other hand, was generally developed using vertical wells and small single-stage fractures in the target horizons. If the Antrim gets further developed for EGR and $CO_2$ injection using practices now pursued in the Marcellus and Utica, its commercial potential could be significantly better.

## d. Potential for $CO_2$ Storage

Like that for the Marcellus and Utica, the same steps were pursued to determine what portion of the estimated total methane gas in place and the theoretical maximum $CO_2$ storage capacity in the Utica shale would actually be accessible. However, for the Antrim, only the potential associated with Area 1 was determined to be accessible.

The results of the application of this approach are shown in **Table 31**. In summary, the results indicate that about 8 Bcf of methane is recoverable in the Antrim Shale at natural gas prices of $9.00 per Mcf, out of about 16 Tcf that could be considered technically recoverable and reasonably accessible today. This amounts to the potential for storing 17 Tcf (or 1 Gt) of $CO_2$.

Table 31: Methane Recovery and $CO_2$ Storage Potential for the Antrim Shale

| | Total Area, Acres | Total Area, miles$^2$ | Estimated Total Gas In-Place, Bcf | Estimated Theoretical Maximum $CO_2$ Storage, Bcf | No. of Wells at 80-Acre Spacing | No. of Accessible, Feasible Well Sites | $CH_4$ Production per Well (Bcf) | $CO_2$ Stored per Well (Bcf) | Technical $CH_4$ Production Potential (Bcf) | Technical $CH_4$ Production Potential Better than Average(Bcf) | $CO_2$ Storage Potential (Bcf) | $CO_2$ Storage Potential (MMtonne) |
|---|---|---|---|---|---|---|---|---|---|---|---|---|
| Area 1 | 3,462,962 | 5,411 | 80,678 | 8,117 | 43,287 | 21,644 | 0.74 | 1.58 | 16,016 | 8,008 | 17,098 | 905 |
| Area 2 | 12,349,068 | 19,295 | 481,989 | 45,537 | 154,363 | 77,182 | n.e. | n.e. | n.e. | n.e. | n.e. | n.e. |
| Area 3 | *7,713,139* | *12,052* | 190,060 | 18,078 | 96,414 | 48,207 | n.e. | n.e. | n.e. | n.e. | n.e. | n.e. |
| | 23,525,169 | 36,758 | 752,727 | 71,732 | 294,065 | 147,032 | | | 16,016 | 8,008 | 17,098 | 905 |

# 6. REFERENCES

Bromhal, Grant S., W. Neal Sams, Sinisha, A. Jikich, Turgay Ertekin, and Duane H. Smith. 2004. "Assessing Economics for Sequestering $CO_2$ in Coal Seams with Horizontal Wells," paper presented at the 3rd Annual Sequestration Conference, Alexandria, VA, May 3-6

Davis, Darrell, Anne Oudinot, and Aiysha Sultana. 2004. "CoalSeqV2.0 Screening Model & Economic Sensitivity Study," paper presented at the Third International Forum on Geologic Sequestration of $CO_2$ in Deep, Unmineable Coalseams, Baltimore, MD, March 25 & 26

Energy Information Administration. 2010. *Oil and Gas Lease Equipment and Operating Costs 1994 Through 2009*. Released September 28, 2010 (http://www.eia.gov/pub/oil_gas/natural_gas/data_publications/cost_indices_equipment_production/current/coststudy.html)

Energy Information Administration. 2013. *Annual Energy Outlook 2013*, DOE/EIA-0383 (2013) April (http://www.eia.gov/forecasts/aeo/)

Gale, John and Paul Freund. 2001. "Coal-Bed Methane Enhancement with $CO_2$ Sequestration Worldwide Potential," *Environmental Geosciences*, Volume 8, Issue 3, pages 210–217, September

Jablonowski, C and A. Singh. 2010. "A Survey of $CO_2$-EOR and $CO_2$ Storage Project Costs," SPE Paper No. 139669-MS presented at the SPE International Conference on $CO_2$ Capture, Storage, and Utilization, New Orleans, Louisiana, USA, 10-12 November

Koperna, George J. Jr., Anne Y. Oudinot, Glenn R. McColpin, Ning Liu, Jason E. Heath, Arthur Wells, and Genevieve B. Young. 2009. "$CO_2$-ECBM/Storage Activities at the San Juan Basin's Pump Canyon Test Site," SPE Paper 124002 presented at the SPE Annual Technical Conference and Exhibition, , New Orleans, Louisiana, 4-7 October

Lancaster, D. E. and D. G. Hill, "A Multi-Laboratory Comparison of Isotherm Measurements on Antrim Shale Samples, Otsego County, MI," 1993 SCA Conference Paper Number 9303, 1993

McCollum, D., and J. Ogden. 2006. *Techno-Economic Models for Carbon Dioxide Compression, Transport and Storage*. Institute of Transportation Studies, University of California, Davis, October (http://publications.its.ucdavis.edu/publication_detail.php?id=1047)

Reeves, S.R. 2003. *Assessment of $CO_2$ Sequestration and ECBM Potential of U.S. Coalbeds*, Topical Report, Prepared for DOE/NETL Contract No. DE-FC26-00NT40924, February

U.S. Department of Energy/National Energy Technology Laboratory (DOE/NETL). 2010. Impact of the Marcellus Shale Gas Play on Current and Future CCS Activities, August 2010

U.S. Department of Energy/National Energy Technology Laboratory. 2011. *Improving Domestic Energy Security and Lowering $CO_2$ Emissions with "Next Generation" $CO_2$-Enhanced Oil Recovery ($CO_2$-EOR),* report DOE/NETL-2011/1504 prepared by Advanced Resources International, June 20, (http://www.netl.doe.gov/energy-analyses/pubs/NextGen_CO2_EOR_06142011.pdf)

Wickstrom, L.H. and 28 others, 2005, Characterization of Geologic Sequestration Opportunities in the MRCSP Region, Phase 1 Task Report for Period of Performance October 2003 – September 2005, Midwest Region Carbon Sequestration Partnership, U.S. Department of Energy Cooperative Agreement DE-PS26-05NT42255, 152 pp.

Zuber, M.D., J. H. Frantz, Jr., and J.M Gatens III, "Reservoir Characterization and Production Forecasting for Antrim Shale Wells: An Integrated Reservoir Analysis Methodology," SPE Paper No. 28606 presented at the SPE 69th Annual Technical Conference and Exhibition, New Orleans, LA, September 25-28, 1994.